Imperial College London

Department of Medicine

National Heart and Lung Institute (NHLI)

Role of CLIC proteins in mitochondrial dysfunction in pulmonary arterial hypertension

Thesis submitted in partial fulfilment of the requirements for the degree of Doctor of Philosophy

By

Mai Meshal Alzaydi

2021

Declaration of originality

I, Mai Alzaydi declare that this thesis is my own work and has not been submitted in any form for another degree or diploma at any university or other institution of tertiary education. Information derived from the published or unpublished work of others has been acknowledged in the text and a list of references is given.

Copyright Declaration

The copyright of this thesis rests with the author and is made available under a Creative Commons Attribution Non-Commercial No Derivatives licence. Researchers are free to copy, distribute or transmit the thesis on the condition that they attribute it, that they do not use it for commercial purposes and that they do not alter, transform or build upon it. For any reuse or redistribution, researchers must make clear to others the licence terms of this work.

Acknowledgements

In the name of Allah the merciful, the beneficent, I am most grateful to the almighty Allah who helped me and enabled me to accomplish this thesis during the ongoing pressures of the Covid-19 pandemic.

First and foremost I would like to express my sincere gratitude to my supervisor, Dr. Beata Wojciak-Stothard, for her invaluable guidance, continuous support, motivation and encouragement throughout my PhD journey. I feel extremely fortunate and proud to have been one of her students, and I truly enjoyed working in a research environment she created, and which stimulated my critical thinking and creativity, inspiration, joy and enthusiasm. Dr. Wojciak-Stothard's patience, courage and care were greatly appreciated throughout my academic research and in my daily life, especially during my pregnancy. Sharing her motherhood experiences motivated me still further, and gave me the strength and power to continue my research and achieve my goals. I would also like to express my sincere thanks to the co-supervisor of my PhD, Professor Lan Zhao.

I would also like to thank all members of Beata's group: Dr. Giusy Russomanno, Dr. Hebah Sindi, Alexander Ainscough, Rehab Alharbi and Dr. Sandro Satta. A big thank you goes to the master's students who worked with me during their research, Angelos Glynos, and Pei Haoyu. I would like to extent my gratitude to Dr. Vahitha Abdul-Salam for her contribution, skilful guidance, insightful comments and unconditional support throughout this project.

I would like to acknowledge the valuable input of Dr. Daria Capece in the Seahorse experiments. She was always willing to help resolve the most difficult experimental issues. I would like to thank Dr. Maria Teresa Cencioni for her guidance in the flow cytometry technique, and my friends Dr. Felwah Alzaid, Dr. Mariam Albahrani, Alaa Ismail, Rean Mohammed, Seham Alshehri, Aseel Alfuhied, and my cousin Fatimah Alshahrani for their unlimited support and for making my study and life in the UK a wonderful experience.

It is my pleasure to acknowledge the Department of Medicine, NHLI, the faculty and its staff members, especially the PH group, Lan's and Martin's groups. It was a great pleasure working with them, and I appreciate their help and positive energy, which helped make this journey such an unforgettable one.

Words cannot express how grateful I am to all my friends in Saudi for being the support system for my life.

I gratefully acknowledge the funding received towards my PhD from King Abdulaziz City for Science and Technology (KACST) and for offering me this opportunity to pursue my PhD.

Being a mother of three means that there are times when I am completely and totally overwhelmed, and without the help of my parents I would not have been able to complete this thesis. I am endlessly grateful for all their help, encouragement and inspiration, I wouldn't be where I am today without their love and support. A huge thank you goes to our lovely nanny Larmie. I can't thank you enough for the care and love you gave to my kids while I was busy with my lab work. I would like to express my sincere gratitude to my sister, brothers, sisters-in-law and every member of my family. Thank you for your endless support and for the love you sent my way during this journey.

Finally, I would like to extend my sincere thanks to my husband Thamer, the driving force behind everything I do. I dedicate everything to you, and I thank you for being my rock; a stable and constant comfort for me. Thank you for being patient during challenging times, and for being encouraging, motivating, selfless and always on board when I ever needed any help. Thank you for your unwavering support and your belief in me. Without your tremendous understanding and encouragement in the past few years, it would have been impossible for me to complete my study.

These acknowledgements would not be complete without mentioning my lovely children, Abdulelah, Lulwah, and Shahad. Thank you for your endless love and joy you filled my life with after all the long working days. Thank you for easing my tiredness with your beautiful smiles. I cannot be more thankful to you for being a part of this unforgettable journey.

Abstract

Background:

Pulmonary arterial hypertension (PAH) is a severe and currently incurable disease characterised by progressive pulmonary vascular remodelling and right heart hypertrophy. PAH bears many hallmarks of cancer, including apoptosis resistance, increased cell proliferation and mitochondrial dysfunction characterised by membrane hyperpolarization, mitochondrial fission and metabolic switch from mitochondrial oxidative phosphorylation to glycolysis. Chloride intracellular channel proteins CLIC1 and CLIC4 are highly expressed in the remodelled pulmonary vasculature in PAH, and these redox-sensitive proteins regulate cell proliferation and angiogenesis. New data suggests that CLIC1, CLIC4 and CLIC5 may also act as structural components of mitochondrial membranes but their role has not been investigated.

Hypothesis:

Increased expression of CLIC proteins induces mitochondrial dysfunction in human pulmonary vascular endothelial cells (HPAECs) *in vitro*, consistent with pathological changes seen in PAH.

Methods:

CLIC1, CLIC4 and CLIC5 expression was manipulated by adenoviral gene transfer. The effects of CLIC expression changes on mitochondrial fission/fusion, mitochondrial membrane potential ($\Delta\psi m$), mitochondrial reactive oxygen species (mtROS) generation, expression of mitochondrial proteins, glycolysis and mitochondrial respiration were studied in human pulmonary artery endothelial cells (HPAECs) and endothelial colony forming cells (ECFCs) derived from PAH patients and healthy individuals. The subcellular localization of CLIC proteins and their effect on mitochondrial structure were studied using transmission electron microscopy. Mitochondrial content, mitochondrial fragmentation, mitochondrial membrane potential, microtubule dynamics and microtubule-mitochondrial interaction were studied using immunofluorescence

and confocal microscopy. Fluorescence-activated cell sorting (FACS) scans were used to detect changes in mitochondrial reactive oxygen species (ROS) generation, while the expression levels of proteins regulating mitochondrial dynamics were analysed by electrophoresis and western blotting. Agilent Seahorse bioenergetics assays were carried out in order to evaluate the potential contribution of CLIC proteins to the Warburg effect. Mitochondrial proteomic analysis of HPAECs overexpressing CLIC proteins was used to identify key signalling pathways. Finally, the effect of CLIC1 and CLIC4 silencing and mitofusin-2 (MFN2) overexpression on CLIC-induced mitochondrial dysfunction in HPAECs, and ECFCs was also investigated.

Results:

CLIC1 and CLIC4 overexpression induced mitochondrial fission, and this effect was accompanied by a significant decrease in the expression of fission regulators MFN2 and optic atrophy 1 (OPA1) and the increased activation of fission regulator DRP1. Mitochondrial fragmentation was accompanied by changes in the ultrastructure of mitochondrial cristae and the reorganization of microtubule cytoskeleton. CLIC proteins significantly reduced mitochondrial respiration, increased mitochondrial membrane potential and mitochondrial reactive oxygen species (ROS) generation and stimulated glycolysis in HPAECs. These changes were partially prevented by the overexpression of MFN2. Endothelial cells from PAH patients showed increased expression of CLIC1 and CLIC4 accompanied by mitochondrial fragmentation, increased mitochondrial membrane potential and reduced expression of MFN2. The disease phenotype was reversed by CLIC1 and CLIC4 silencing or overexpression of MFN2.

Conclusion CLIC proteins are likely to play a contributory role in mitochondrial dysfunction in PAH.

Table of Contents

DECLARATION OF ORIGINALITY ..... **II**

COPYRIGHT DECLARATION ..... **III**

ACKNOWLEDGEMENTS ..... **IV**

ABSTRACT ..... **VI**

TABLE OF CONTENTS ..... **VIII**

LIST OF FIGURES ..... **XII**

LIST OF TABLES ..... **XVII**

ABBREVIATIONS ..... **XIX**

CHAPTER 1: GENERAL INTRODUCTION **1**

1.1. PULMONARY VASCULATURE: STRUCTURE, FUNCTION AND DEVELOPMENT 1

1.2. PULMONARY HYPERTENSION 5

1.2.1. Definition and classification *5*

1.3. PATHOBIOLOGY OF PULMONARY ARTERIAL HYPERTENSION 8

1.3.1. Pulmonary vasoconstriction *9*

1.3.2. Pulmonary vascular remodelling *10*

1.4. ROLE OF ENDOTHELIUM IN PULMONARY HYPERTENSION 15

1.4.1. Vascular endothelial cells *15*

1.4.2. Blood vessel formation and endothelial progenitor cells (EPCs) *16*

1.5. CURRENT THERAPIES IN PULMONARY ARTERIAL HYPERTENSION 21

1.6. ROLE OF MITOCHONDRIA IN PAH 24

1.6.1. Mitochondrial alterations in pulmonary arterial endothelial cells *25*

1.6.2. Metabolism: general overview *25*

1.6.3. Mitochondria and metabolism in PAH *26*

1.6.4. Mitochondrial membrane potential and ROS generation in PAH *29*

1.6.5. Mitochondrial dynamics *31*

1.6.6. Mitochondrial dynamics in PAH *32*

1.6.7. Mitophagy changes in pulmonary arterial hypertension *36*

1.7. THERAPEUTIC DEVELOPMENT OF METABOLIC DRUGS IN PULMONARY HYPERTENSION 40

1.8. CHLORIDE INTRACELLULAR CHANNEL PROTEINS 43

1.8.1. The CLIC protein Family *43*

1.8.2. CLIC structure *44*

1.8.3. CLIC localization *46*

1.8.4. CLIC function *47*

1.8.5. CLIC in PAH *48*

1.8.6. Chloride intracellular channel 1 ..... *49*

1.8.7. Chloride intracellular channel 4 ..... *50*

1.8.8. Chloride intracellular channel 5 ..... *52*

1.9. MAIN HYPOTHESIS AND PROJECT AIMS 55

1.9.1. Hypothesis *55*

1.9.2. Study aims *55*

CHAPTER 2: MATERIALS AND METHODS **58**

2.1 CELL CULTURE TECHNIQUES 58

2.1.1 Cell culture *58*

2.1.2 Sub-culturing cells *62*

2.1.3 Establishment and storage of cells *63*

2.2 MANIPULATION OF PROTEIN EXPRESSION IN CELLS BY ADENOVIRAL GENE TRANSFER 64
2.2.1 Adenoviral constructs 64
2.2.2 Adenoviral multiplication and purification 65
2.2.3 Cell infection 65
2.3 TRANSMISSION ELECTRON MICROSCOPY 66
2.3.1 Preparation of culture dishes, cell culture and fixation 66
2.3.2 Immunogold labelling of mitochondria in CLIC-overexpressing HPAECs 67
2.4 FLUORESCENT LABELLING OF MITOCHONDRIA AND MEASUREMENT OF MITOCHONDRIAL FRAGMENTATION 69
2.5 MICROTUBULE STAINING 70
2.6 EVALUATION OF MITOCHONDRIAL FUNCTION 72
2.6.1 Measurement of mitochondrial membrane potential by TMRE staining 72
2.6.2 Measurement of mitochondrial reactive oxygen species (mtROS) 72
2.6.3 Mitochondrial bioenergetic profile 73
2.7 ISOLATION OF MITOCHONDRIA 78
2.7.1 Isolation of mitochondria from HPAECs 78
2.7.2 Mitochondrial proteomic analysis 81
2.8 PROTEIN IDENTIFICATION METHODS 83
2.8.1 Western blotting 83
2.9 RNA EXTRACTION, PURIFICATION AND QUANTIFICATION 89
2.9.1 RNA extraction from cultured cells 89
2.9.2 RNA quality assessment 91
2.9.3 Real-time quantitative PCR (qPCR) for gene expression 93
2.9.4 PCR data analysis 95
2.10 STATISTICAL ANALYSIS 96

CHAPTER 3 RESULTS: EFFECTS OF CLIC PROTEIN EXPRESSION CHANGES ON MITOCHONDRIAL STRUCTURE AND DYNAMICS IN HPAECS 98

3.1 INTRODUCTION 98
3.2 EXPERIMENTAL AIMS 103
3.3 EXPERIMENTAL OUTLINE 104
3.3.1 Manipulation of CLIC expression in HPAECs 105
3.3.2 Measurement of mitochondrial fragmentation 105
3.3.3 Immunogold labelling of mitochondrial CLIC proteins in HPAECs 106
3.3.4 Protein expression levels of key regulators of mitochondrial dynamics 107
3.3.5 mRNA expression levels of key regulators of mitochondrial dynamics 108
3.3.6 Isolation of mitochondria from HPAECs 108
3.3.7 Immunofluorescent staining of microtubules 108
3.3.8 Manipulation of microtubule polymerization 109
3.4 RESULTS 110
3.4.1 CLIC overexpression in endothelial cells 110
3.4.2 Effect of CLIC overexpression on mitochondrial network in HPAECs 114
3.4.3 Analysis of expression levels of fission and fusion proteins 118
3.4.4 Mitochondrial fraction purity analysis 122
3.4.5 Analysis of pyruvate dehydrogenase protein and kinase expression in HPAECs 129
3.4.6 Effect of CLIC overexpression on cristae architecture in HPAECs 131
3.4.7 Analysis of expression level of mitochondrial proteins 132
3.4.8 Role of actin and microtubule cytoskeleton in CLIC-induced effects 134
3.4.9 Effect of microtubule polymerization on CLIC-induced changes in mitochondrial fragmentation 138
***3.4.10** Effect of CLIC-overexpression on the organization of actin cytoskeleton in HPAECs 142*
3.5 SUMMARY 144
3.6 DISCUSSION 148

CHAPTER 4 RESULTS: THE EFFECT OF CLIC PROTEINS ON MITOCHONDRIAL FUNCTION 155

4.1 INTRODUCTION 155
4.2 EXPERIMENTAL AIMS 157
4.3 EXPERIMENTAL DESIGN 158
4.3.1 Manipulation of CLIC gene expression in HPAECs 159
4.3.2 Western blotting 159
4.3.3 Measurement of mitochondrial fragmentation 160
4.3.4 Measurement of mitochondrial membrane potential (ΔΨm) 160
4.3.5 Measurement of mitochondrial reactive oxygen species (mtROS) 160
4.3.6 Cellular bioenergetics assay 162
4.4 RESULTS 167
4.4.1 CLIC overexpression and silencing in endothelial cells 167
4.4.2 The effect of CLIC proteins on mitochondrial network in HPAECs 169
4.4.3 The effect of CLIC proteins on mitochondrial ΔΨm in HPAECs 170
4.4.4 The effect of CLIC proteins on mitochondrial ROS generation in HPAECs 172
4.4.5 The effect of CLIC proteins on the bioenergetic profile of HPAECs 174
4.5 SUMMARY 181
4.6 DISCUSSION 184

CHAPTER 5 RESULTS: PROTEOMIC ANALYSIS OF CLIC-INDUCED CHANGES IN MITOCHONDRIAL PROTEIN EXPRESSION PROFILE IN HPAECS 190

5.1 INTRODUCTION 190
5.2 EXPERIMENTAL AIMS 191
5.3 EXPERIMENTAL OUTLINE 191
5.3.1 Proteomic analysis 193
5.4 RESULTS 195
5.4.1 Proteomic data analysis 195
5.5 DISCUSSION 211

CHAPTER 6 RESULTS: REVERSAL OF CLIC EFFECTS BY MITOFUSIN-2 214

6.1 INTRODUCTION 214
6.2 EXPERIMENTAL AIMS 215
6.3 EXPERIMENTAL DESIGN 215
6.3.1 Manipulation of MFN2 gene expression in HPAECs 217
6.3.2 Western blotting 217
6.3.3 Immunostaining and mitochondrial fragmentation analysis 217
6.3.4 Measurement of mitochondrial membrane potential (ΔΨm) 218
6.3.5 Measurement of mitochondrial reactive oxygen species (mtROS) 218
6.3.6 Cellular bioenergetics assay 219
6.4 RESULTS 220
6.4.1 MFN2 expression in endothelial cells 220
6.4.2 The effect of MFN2 on CLIC-induced changes in mitochondrial fragmentation in HPAECs 222
6.4.3 Effect of MFN2 on CLIC-induced changes in mitochondrial membrane potential 225
6.4.4 The effect of MFN2 on CLIC-induced changes in mitochondrial ROS production in HPAECs 227
6.4.5 The effect of MFN2 on CLIC-induced changes in the bioenergetic profile of HPAECs 229
6.5 SUMMARY 234
6.6 DISCUSSION 237

CHAPTER 7 RESULTS: CLIC PROTEINS IN MITOCHONDRIAL DYSFUNCTION IN PAH: STUDY IN ECFCS 241

7.1 INTRODUCTION 241

7.2 EXPERIMENTAL AIMS 243
7.3 EXPERIMENTAL DESIGN 243
7.3.1 Cell culture 245
7.3.2 Measurement of CLIC and MFN2 gene expression levels by quantitative PCR in ECFCs 246
7.3.3 Immunofluorescence and confocal microscopy of mitochondrial fragmentation 246
7.3.4 Measurement of mitochondrial membrane potential (ΔΨm) 246
7.3.5 Seahorse bioenergetics assay 247
7.4 RESULTS 248
7.4.1 CLIC and MFN2 expression in ECFCs 248
7.4.2 The effect of MFN2 on mitochondrial fragmentation in ECFCs 249
7.4.3 The effect of MFN2 on mitochondrial ΔΨm in ECFCs 254
7.4.4 The effect of CLIC inhibition and MFN2 overexpression on the bioenergetics profile of ECFCs 257
7.5 SUMMARY 264
7.6 DISCUSSION 267

CHAPTER 8: GENERAL DISCUSSION 270

8.1 CLIC1 AND CLIC4 REGULATE MITOCHONDRIAL STRUCTURE AND DYNAMICS IN PULMONARY ENDOTHELIAL CELLS 270
8.1.1 MFN2 mediates effects of CLIC proteins on mitochondrial membrane potential and ROS generation 274
8.1.2 CLIC-induced reduction in MFN2 contributes to the Warburg effect 276
8.1.3 Contribution of ECFCs to PH pathology 278
8.1.4 Potential therapeutic benefits of targeting CLIC and MFN2 in PH 279
8.2 CONCLUSION 281
8.3 STUDY LIMITATIONS 283
8.4 FUTURE WORK 284

APPENDIX 286

REFERENCES 320

List of Figures

Figure 1.1: Schematic illustration of different areas in the respiratory system. 2

Figure 1.2: Schematic representation of pulmonary arterial wall. 3

Figure 1.3: Diagram illustrating pulmonary vascular remodelling and pathogenesis of pulmonary arterial hypertension. 11

Figure 1.4: Schematic illustration of vascular remodelling in pulmonary arterial hypertension. 14

Figure 1.5: Illustration of vasculogenesis and angiogenesis. 17

Figure 1.6: Illustration of currently approved targeted therapies in pulmonary arterial hypertension. 22

Figure 1.7: Summary of mitochondrial alterations in pulmonary hypertension. 24

Figure 1.8: Warburg effect pathways in pulmonary hypertension. 28

Figure 1.9: Illustration of MFN2 structure. 34
Figure 1.10: Two mitophagy mechanisms in mammalian cells. 38
Figure 1.11: Emerging targets and therapies for PAH. 42
Figure 1.12: Mammalian CLIC family and structural relationship with omega-class GST (GSTO-1). 45
Figure 1.13: Intracellular activities and distribution of CLIC proteins. 47
Figure 1.14: Hypothesized role of CLIC proteins in the regulation of mitochondrial function in PAH endothelium. 56
Figure 2.1: Establishing blood-derived endothelial colony forming cells from peripheral blood samples. 62
Figure 2.2: Illustration of the adenovirus construction process. 66
Figure 2.3: An overview of the Agilent Seahorse XF Cell Mito Stress and Glycolysis Stress assays. 74
Figure 2.4: A summary of mitochondrial isolation process using a Mitochondria Isolation Kit for cultured cells. 80
Figure 2.5: Example of bovine serum albumin (BSA) protein standard curve of BCA Protein Assay. 84
Figure 2.6: Western blotting workflow. 88
Figure 2.7: An example of an amplification plot generated by quantitative Real-Time PCR (qRT-PCR) assay. 95
Figure 3.1: Schematic illustration of localization of mitochondrial proteins examined in this study. 101
Figure 3.2: Experimental outline of Chapter 3. 104
Figure 3.3: Schematic illustration of mitochondrial fragmentation analysis using NIP2 image software. 106
Figure 3.4: Example of optimization of viral infection. 110
Figure 3.5: CLIC1, CLIC4 and CLIC5 protein overexpression in HPAECs. 111
Figure 3.6: Overexpression of recombinant CLIC proteins in HPAECs. 112
Figure 3.7: Immunostaining of CLIC1, CLIC4 and CLIC5 in HPAECs. 113
Figure 3.8: Effect of CLIC overexpression on mitochondrial content and fragmentation in HPAECs. 115
Figure 3.9: Representative images of mitochondrial networks in control HPAECs and HPAECs overexpressing AdCLIC1, AdCLIC4, AdCLIC5sh and AdCLIC5L. 115
Figure 3.10: Mitochondrial fragmentation in CLIC-overexpressing HPAECs. 116

Figure 3.11: Mitochondrial network in control and CLIC-overexpressing HPAECs. 117
Figure 3.12: Expression of mitochondrial fusion proteins in HPAECs whole cell lysates. 119
Figure 3.13: Expression of mitochondrial fission regulators in HPAECs whole cell lysates. 120
Figure 3.14: mRNA expression level of fusion proteins in HPAECs overexpressing CLIC1, CLIC4 and CLIC5. 121
Figure 3.15: mRNA expression level of fission proteins in HPAECs overexpressing CLIC1, CLIC4 and CLIC5. 121
Figure 3.16: Mitochondrial fraction quality analysis. 122
Figure 3.17: Localization of recombinant CLIC proteins to mitochondria. 123
Figure 3.18: CLIC1 and CLIC4 localization in mitochondria. 124
Figure 3.19: Expression of mitochondrial fusion proteins in mitochondrial fractions from HPAECs. 126
Figure 3.20: Expression and phosphorylation of mitochondrial fission proteins in HPAECs. 127
Figure 3.21: Expression and phosphorylation of MFF fission protein in HPAECs. 128
Figure 3.22: Effect of CLIC1 and CLIC4 on expression of mitophagy markers. 129
Figure 3.23: Effect of CLIC overexpression on pyruvate dehydrogenase protein and kinase expression. 130
Figure 3.24: The effect of CLIC1 and CLIC4 on cristae architecture in HPAECs. 131
Figure 3.25: Ultrastructural changes in mitochondrial cristae in HPAECs. 132
Figure 3.26: Expression of key protein regulators of mitochondrial structure and function. 133
Figure 3.27: Expression of key protein regulators of mitochondrial structure and function. 134
Figure 3.28: Magnified images of microtubule cytoskeleton in CLIC-overexpressing HPAECs. 136
Figure 3.29: The effect of CLIC protein overexpression on the organization of microtubules in HPAECs. 136
Figure 3.30: Effect of CLIC proteins on microtubule content, cell spreading area and cell polarity. 137
Figure 3.31: The effect of CLIC-overexpression on tubulin and tubulin acetylation levels in HPAECs. 138
Figure 3.32: The effect of nocodazole and taxol on microtubules in CLIC-overexpressing HPAECs. 139
Figure 3.33: The effect of microtubule disruption and stabilization on mitochondrial network of CLIC-overexpressing HPAECs. 140

Figure 3.34: Alignment of mitochondrial network with microtubules in CLIC-overexpressing HPAECs. 142
Figure 3.35: The effect of CLIC-overexpression on actin polymerization in HPAECs. 143
Figure 3.36: Summary of key results in chapter 3. 145
Figure 4.1: Illustration of energy metabolism in PAH. 156
Figure 4.2: Experimental outline for chapter 4. 158
Figure 4.3: Illustration of MitoSOX-based flow cytometry (FC) for detecting mitochondrial reactive oxygen species. 161
Figure 4.4: Illustration of Seahorse XFp Cell Mito Stress Test modulators. 164
Figure 4.5: Seahorse XFp Cell Mito Stress Test profile of the key parameters of mitochondrial respiration. 164
Figure 4.6: Illustration of Seahorse XFp Glycolysis Stress Test modulators. 166
Figure 4.7: Seahorse XFp Glycolysis Stress Test profile showing the key parameters of glycolytic function. 166
Figure 4.8: Comparison of different adenoviral controls. 168
Figure 4.9: Optimization of CLIC4 inhibition in HPAECs. 168
Figure 4.10: Effect of CLIC inhibition on mitochondrial fragmentation in HPAECs. 169
Figure 4.11: Representative images of mitochondrial networks in HPAECs following the overexpression and silencing of CLIC1 and CLIC4. 170
Figure 4.12: The effect of CLIC1 and CLIC4 overexpression and inhibition on mitochondrial membrane potential in HPAECs. 171
Figure 4.13: Changes in the mitochondrial membrane potential induced by modulation of CLIC expression in HPAECs. 171
Figure 4.14: The effect of CLIC overexpression and silencing on mitochondrial ROS production in HPAECs. 173
Figure 4.15: Example of Oxygen consumption rate (OCR) measurement. 176
Figure 4.16: Effect of CLIC overexpression and inhibition on mitochondrial function in HPAECs. 177
Figure 4.17: Example of extracellular acidification rate (ECAR) measurement. 179
Figure 4.18: Effect of CLIC overexpression and inhibition on acidification rate in HPAECs. 180
Figure 4.19: Summary of key results of Chapter 4. 182
Figure 5.1: Experimental outline for Chapter 5. 192
Figure 5.2: IPA group classification of CLIC1, CLIC4, and Hypoxic-control HPAECs. 196

Figure 5.3: Visualization of protein-to-protein interactions of differentially expressed proteins of group F CLIC1, CLIC4, and Hypoxia control cells using STRING analysis. 199
Figure 6.1: Experimental outline for Chapter 6. 216
Figure 6.2: Optimization of MFN2 overexpression in HPAECs. 220
Figure 6.3: MFN2 overexpression in HPAECs. 221
Figure 6.4: MFN2 overexpression compensates loss of MFN2 in CLIC-overexpressing HPAECs. 221
Figure 6.5: The effect of MFN2 on mitochondrial fragmentation count in CLIC-overexpressing HPAECs. 223
Figure 6.6: The effect of MFN2 overexpression on CLIC-induced mitochondrial fragmentation in HPAECs. 223
Figure 6.7: Mitochondrial network in CLIC-overexpressing HPAECs with MFN2 overexpression. 224
Figure 6.8: The effect of MFN2 overexpression on CLIC-induced changes in mitochondrial membrane potential. 225
Figure 6.9: The effect of MFN2 on mitochondrial membrane potential in CLIC-overexpressing HPAECs. 226
Figure 6.10: The effect of MFN2 overexpression on CLIC-induced changes in mitochondrial ROS. 228
Figure 6.11: Example of Oxygen consumption rate (OCR) measurement. 230
Figure 6.12: Effect of MFN2 overexpression on mitochondrial function in CLIC-overexpressing HPAECs. 231
Figure 6.13: Extracellular acidification rate measured following the serial compound injections of glycolysis modulators. 232
Figure 6.14: Effect of MFN2 overexpression on CLIC-induced changes on acidification rate in HPAECs. 233
Figure 6.15: Summary of key results in Chapter 6. 235
Figure 7.1: Experimental outline for chapter 7. 244
Figure 7.2: Gene expression level of CLIC1 and CLIC4 in healthy and PAH ECFCs. 248
Figure 7.3: MFN2 mRNA expression level in healthy and PAH ECFCs. 249
Figure 7.4: Changes in mitochondrial fragmentation count in ECFCs from healthy volunteers and PAH patients. 250
Figure 7.5: Changes in mitochondrial fragmentation in healthy and PAH ECFCs. 251
Figure 7.6: The effect of MFN2 on mitochondrial fragmentation count in ECFCs. 252

Figure 7.7: The effect of MFN2 overexpression on mitochondrial network in ECFCs. 253
Figure 7.8: Changes in mitochondrial membrane potential in ECFCs from healthy controls and PAH patients. 254
Figure 7.9: Changes in mitochondrial membrane potential in ECFCs. 255
Figure 7.10: The effect of MFN2 on mitochondrial membrane potential in ECFCs. 255
Figure 7.11: The effect of MFN2 on mitochondrial membrane potential in ECFCs from healthy controls and PAH patients. 256
Figure 7.12: Example of Oxygen consumption rate (OCR) measurement in ECFCs from patients and healthy controls. 259
Figure 7.13: Effect of CLIC inhibition and MFN2 overexpression on mitochondrial function in healthy and PAH ECFCs. 260
Figure 7.14: Example of extracellular acidification rate (ECAR) measurement in ECFCs from patients and healthy controls. 262
Figure 7.15: Effect of CLIC inhibition and MFN2 overexpression on acidification rate in healthy and PAH ECFCs. 263
Figure 7.16: Summary of key results in Chapter 7. 265
Figure 8.1: Mechanism of CLIC1- and CLIC4-induced changes in mitochondrial function in PAH. 282

List of Tables

Table 1.1: Latest clinical classification of pulmonary hypertension from the Fifth World Symposium on Pulmonary Hypertension held in Nice, France. 7
Table 1.2: Pulmonary hypertension classification according to haemodynamic parameters: pre-capillary pulmonary hypertension and post-capillary pulmonary hypertension. 8
Table1.3: Approved Drugs for pulmonary hypertension (PAH). 23
Table 1.4: An overview of CLIC proteins family. 53
Table 2.1: Human pulmonary artery endothelial cells used in cell experiments. 59
Table 2.2: Endothelial Cell Growth Medium-2 supplements. 61
Table 2.3: Demographics of IPAH patients and healthy volunteers. 61
Table 2.4: Summary of all primary and secondary antibodies used in immunostaining. 71
Table 2.5: Seahorse assay medium preparation. 76

Table 2.6: Concentrations of compounds used in the Seahorse Mito Stress Test and the Seahorse Glycolysis Stress Test. 77
Table 2.7: A list of primary and secondary antibodies used in western blotting. 87
Table 2.8: Composition of cDNA master mix used in the reverse transcription process gene expression. 91
Table 2.9: Final mixture of reverse transcription for gene expression. 92
Table 2.10: SuperScript II Reverse Transcriptase thermal cycling conditions. 93
Table 2.11: List of genes used in qPCR. 93
Table 2.12: Composition of 1X master mix used in qPCR. 94
Table 2.13: Amplification steps for qPCR reactions. 94
Table 3.1: Localization and function of mitochondrial proteins studied in Chapter 3. 100
Table 3.2: Summary of key findings of the effect of CLIC overexpression proteins on mitochondrial dynamics in HPAECs. 146
Table 4.1: Summary of key findings of the effect of CLIC protein overexpression and inhibition on mitochondrial function in HPAECs. 183
Table 5.1: Differentially expressed proteins in groups E and F. 196
Table 5.2: List of the most significant pathways associated with pathology of PAH. 200
Table 6.1: Summary of key findings on the effect of overexpression of CLIC proteins and MFN2 on mitochondrial function in HPAECs. 236
Table 7.1: Demographics of IPAH patients and healthy volunteers. 245
Table 7.2: Summary of key findings of the effect of CLIC proteins inhibition and overexpression of MFN2 on mitochondrial function in ECFCs from patients and healthy controls. 266

Abbreviations

Abbreviation	*Full name*
Ad	Adenoviral
ALK-1	Activin receptor-like kinase type 1
AMPK	Adenosine monophosphate-activated protein kinase
Ang-1	Angiopoietin-1
NRF1	Activating nuclear respiratory factor 1
AU	Arbitrary unit
ATP	Adenosine triphosphate
BMPR2	Bone morphogenetic protein receptor 2
BSA	Bovine serum albumin
ECAR	Extracellular acidification rate
ECFCs	Endothelial colony-forming cells
EPCs	Progenitor endothelial cells
FADH2	Flavin adeninedinucleotide 2
FATP1/6	Fatty acids tranport protein 1 and 6
cAMP	Cyclic adenosine monophosphate
CTEPH	Chronic thromboembolic pulmonary hypertension
cGMP	Cyclic guanosine monophosphate
CMV	Cytomegalovirus
CLIC	Chloride intracellular channel
COX	Cytochrome c oxidase
DHE	dihydroethidium
DNMT	DNA methyltransferases
DNM1L	dynamin-1-like protein
DPG	Diastolic pulmonary gradient
DRP1	Dynamin-related protein-1
ECM	Extracellular matrix
EDTA	Ethylenediaminetetraacetic acid
EndoMT	Endothelial-to-mesenchymal transition
eNOS	Endothelial nitric oxide synthase
EPCs	Endothelial precursor cells
ET-1	Endothelin-1
FAO	Fatty acid oxidation
FBS	Fetal bovine serum
FGF2	Fibroblast growth factor 2
FCCP	Carbonyl cyanide-4-(trifluoromethoxy) phenylhydrazone
G6P	Glucose-6-phosphate
GDH	Glutamatedehydrogenase
GFP	Green fluorescent protein
HA	Haemagglutinin

HPAECs	Human pulmonary artery endothelial cells
HEK293	Human embryonic kidney cells
HIF-1 α	Hypoxia-inducible factor 1 α
HK	Hexokinase
HPCs	Hematopoietic progenitor cells
HRP	Horseradish peroxidase
HSP60	Heat-shock protein
IMM	Inner membrane of the mitochondria
IPF	Idiopathic pulmonary fibrosis
iPSCs	Induced pluripotent stem cells
KO	Knockout
LDHA	Lactate dehydrogenase
MCT	Monocrotaline
MFC	Mitochondrial fragmentation count
MFN2	Mitofusin2
MIEF1	mitochondrial elongation factor 1
MOI	Multiplicity of infection
mPAP	Mean pulmonary artery pressure
mPAWP	Mean pulmonary artery wedge pressure
MT	Microtubules
NADH	Nicotinamide adenine dinucleotide
NO	Nitric oxide
OCR	Oxygen Consumption Rate
OMM	Outer membrane of the mitochondria
OPA1	Optic atrophy protein-1
PPAR-γ	Peroxisome proliferator-activated receptor-γ (x)
PAH	Pulmonary arterial hypertension
PAECs	Pulmonary artery endothelial cells
PAF	Pulmonary arterial fibroblasts
PASMCs	Pulmonary artery smooth muscle cells
PBS	Phosphate buffered saline
PDE5	Phosphodiesterase type 5
PDGF	Platelet-derived growth factor
PEP	Phosphoenolpyruvate
PGI2	Prostacyclin
PDH	Pyruvate dehydrogenase
PDK	Pyruvate Dehydrogenase kinase
PH	Pulmonary hypertension
PHB1	Prohibition protein 1
PKM2	Pyruvate kinase isoform M2
RIPA	Radioimmunoprecipitation assay buffer
ROS	Reactive oxygen species

SDH	Succinate dehydrogenase
SDS	Sodium dodecyl sulphate
sGC	soluble guanylate cyclase
shRNAs	Small hairpin RNAs
TBST	Tris-buffered saline solution
Tet-off	Tetracycline-off
TGF-β	Transforming growth factor-β
TMRM	Tetramethylrhodamine Methyl Ester
TNF-α	Tumor necrosis factor-α
TRITC	Tetramethylrhodamine
tPA	Tissue-type plasminogen activator
VDAC	Voltage-dependent anion channel
VEGF	Vascular endothelial growth factor
VEGFR	Vascular endothelial growth factor receptor
WHO	The World Health Organization
ΔΨm	Mitochondrial membrane potential

CHAPTER 1:

General Introduction

CHAPTER 1: General Introduction

1.1. Pulmonary vasculature: Structure, function and development

The cardiovascular system comprises the systemic and pulmonary circulation. The systemic circulation moves blood between the heart and the rest of the body, delivering oxygenated blood to cells and deoxygenated blood back to the heart. Meanwhile, the pulmonary circulation transports blood between the heart and lungs. It carries deoxygenated blood from the right ventricle of the heart to the lungs, where it absorbs oxygen and releases carbon dioxide. The lungs then send the oxygenated blood to the left ventricle of the heart (Fishman, 1978).

In the pulmonary loop, the right ventricle of the heart pumps deoxygenated blood into the pulmonary trunk – the main pulmonary artery which branches into the right and left pulmonary arteries. These arteries further sub-divide into muscular pulmonary arteries, arterioles and alveolar capillaries, where gas exchange takes place. The oxygenated blood then travels through a network of pulmonary venules and veins to the left atrium of the heart (Harris & Heath, 1977).

The respiratory airways that run alongside the pulmonary vasculature extend from the respiratory bronchioles to the alveoli, and are made up of respiratory bronchioles, alveolar ducts, alveolar sacs and alveoli. They increase the maximum surface area available for gas-exchange (Kandathil & Chamarthy, 2018; Leslie, Wick, & Smith, 2017) (Figure 1.1).

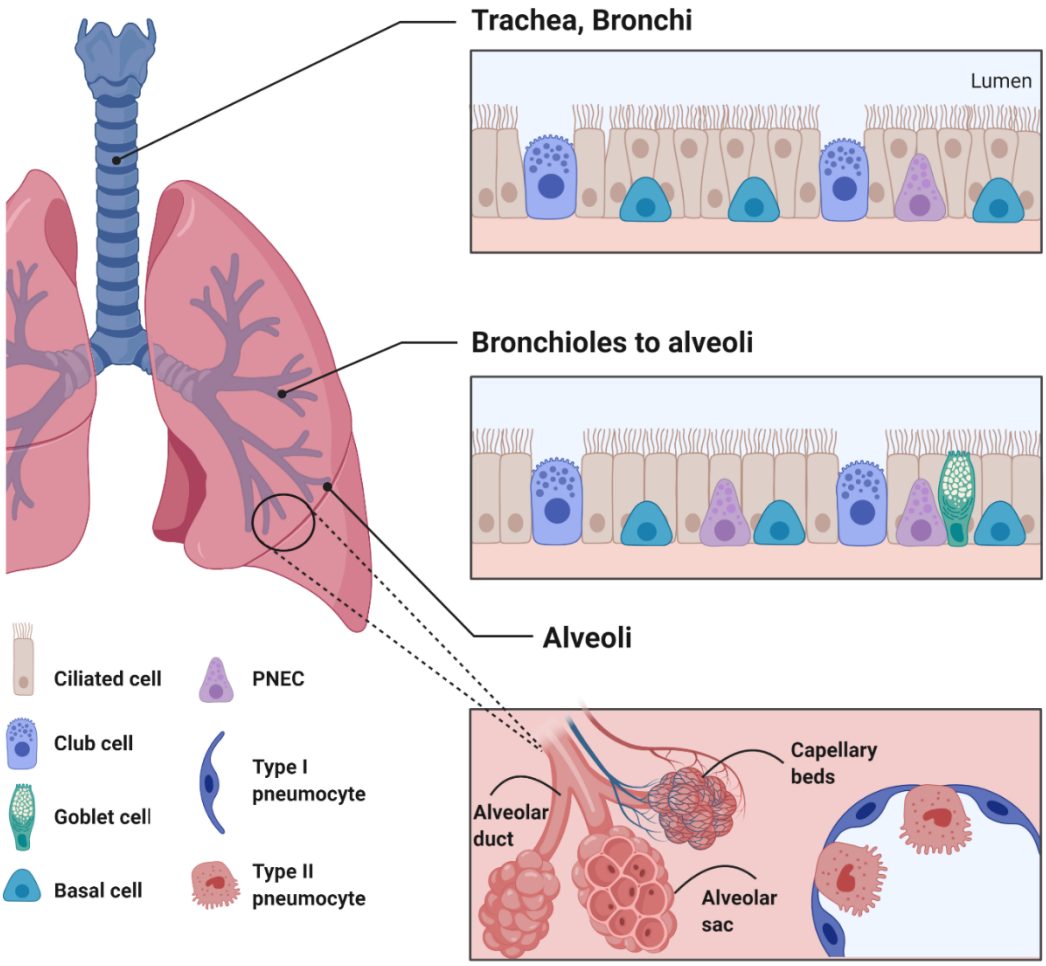


Figure 1.1: Schematic illustration of different areas in the respiratory system. The tracheobronchial vascular tree branches from the trachea to the bronchi, bronchioles and alveoli. The upper panel shows the cell composition of the trachea. The middle panel shows the respiratory bronchioles, which consists of a few alveoli scattered along their walls and the low cuboidal epithelium. The lower panel shows the typical surface area of the lungs, the alveoli. The respiratory bronchiole is divided into between 2 and 11 alveolar ducts that contain smooth muscle fibres in their walls. Along these walls, the alveolar ducts split into single alveoli and groups of alveolar sacs. The epithelium surface of the alveoli contains two distinct cells, known as type I and type II pneumocytes. Abbreviations: PNEC: pulmonary neuroendocrine cell (van der Vaart & Clevers, 2020). Illustration created by the author using BioRender.com

The size and structure of blood vessels in the pulmonary arterial tree change according to their function, from elastic, to muscular and finally to partially muscularised and non-muscularised vessels (Wagenvoort & Wagenvoort, 1979).

The wall of the pulmonary arteries comprises three distinct layers: tunica intima, tunica media, and tunica adventitia (Figure 1.2). The pulmonary arteries have thinner walls than the systemic arteries, which are built to withstand higher blood pressures (Leslie et al., 2017).

The inner layer (tunica intima) is also referred to as the tunica interna, and is made up of a single layer of endothelial cells (ECs), and is supported by the connective tissue of internal elastic lamina. The middle layer (tunica media) consists of elastic fibres, pulmonary artery smooth muscle cells (PASMCs), and extracellular matrix. The outermost layer (tunica externa) is also known as tunica adventitia, and consists of fibroblasts, extracellular matrix rich in collagen fibers, and external elastic lamina (Leslie et al., 2017; Robertson & Watton, 2013).

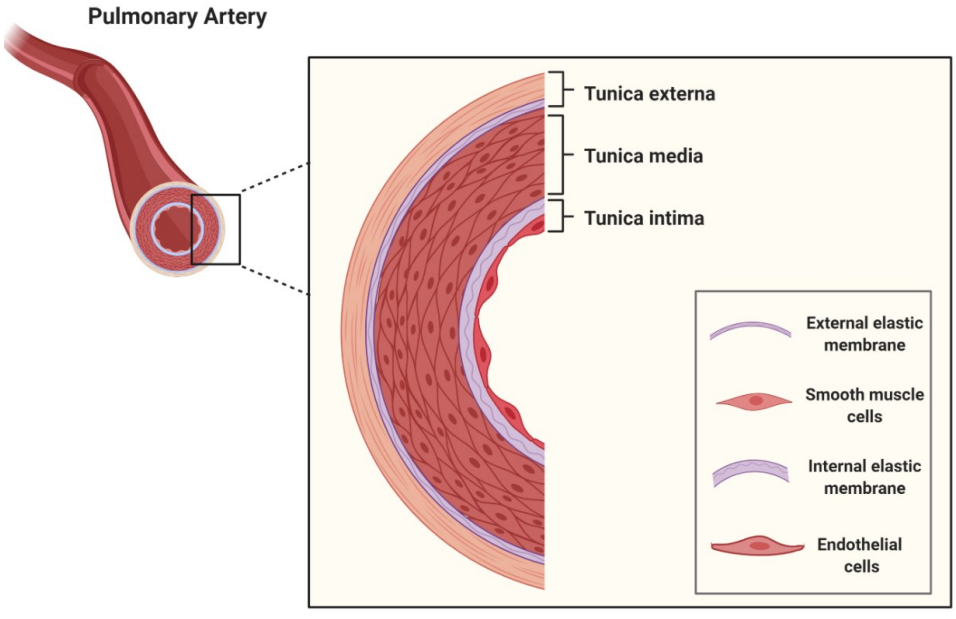


Figure 1.2: Schematic representation of pulmonary arterial wall. Vascular wall consists of three layers: (1) Tunica intima, consisting of an endothelial layer supported by an internal elastic membrane, (2) Tunica media, composed of elastic fibres, smooth muscle cells, and extracellular matrix, and (3) Tunica externa, consisting of connective tissue, fibroblasts, and external elastic membrane (Robertson & Watton, 2013). Illustration created by the author using BioRender.com.

The structure and thickness of the three vascular layers varies among different types of blood vessels. Based on the structure of the medial layer, pulmonary arteries can be divided into two main types: elastic, which contain elastic lamina, and muscular, which contain layers of vascular smooth muscle cells (SMCs). Within the pulmonary vascular tree, arteries are identified as elastic, transitional (with features of both elastic and muscular arteries), muscular, partially-muscular and non-muscular (Rhodin, 2011; Townsley, 2011). In the main pulmonary artery trunk, the tunica media consists of multiple layers of smooth muscle cells separated by elastin fibres for distensibility and collagen fibres for rigidity. In the smaller pulmonary arteries, the muscular layer is often absent, and a single elastic lamina splits the intima from the adventitia (Hall et al., 2000; Townsley, 2011).

The vascular endothelium constitutes a single layer of endothelial cells (ECs) that make up the inner cellular lining of arteries, veins and capillaries and contact the blood components directly. Vasorelaxants, anti-thrombotic and anti-proliferative substances released by endothelial cells are required to maintain pulmonary vascular homeostasis (Yong et al., 1963). An imbalance in the release of these substances, for example high levels of endothelium-derived fibroblast growth factor 2 (FGF2), serotonin or endothelin-1 and low levels of prostacyclin and nitric oxide lead to increased medial SMCs proliferation and migration (Izikki et al., 2009).

New blood vessels are mainly produced by three cellular processes: vasculogenesis, angiogenesis, or arteriogenesis. Vasculogenesis is the differentiation of endothelial precursor cells (EPCs) or angioblasts, into endothelial cells (ECs) and *de novo* formation of primitive blood vessels or endothelial tubes. This is believed to occur very early during the embryonic development (Kubis & Levy, 2003).

The development of pulmonary circulation starts in the first 4-16 weeks of gestation, while the blood gas barrier had begun to form by 24 weeks of gestation (Hislop, 2005). Pulmonary arteries and veins are formed *de novo* as endothelial tubes in the mesenchyme around the airways by the process of vasculogenesis (Hall et al., 2002). The endothelial tubes then join together to form the pulmonary circulation, which develops in parallel with the airways in the lungs. Alveolar capillaries are formed by angiogenesis (Hall et al., 2002; Parera et al., 2005). A number of growth factors such as platelet-derived growth factor (PDGF), vascular endothelial growth factor (VEGF), angiopoietin and fibroblast growth factors (FGF) are involved in the stabilisation and formation of the pulmonary vasculature (Hislop & Pierce, 2000).

1.2. Pulmonary hypertension

1.2.1. Definition and classification

Pulmonary arterial hypertension (PAH) is a progressive disease that affects between 15 and 50 patients per million. It affects 1% of the global population at some stage, and around 10% of sufferers are over 65 years old. PAH prognosis is poor, with estimated median survival time 2.8 years and annual mortality rate of approximately 15%. The median time of survival from the time of diagnosis is about 3 years (Humbert et al., 2010; Thenappan et al., 2010). PAH is defined by a mean pulmonary artery pressure (mPAP) at rest of ≥ 25 mmHg, with a normal (≤15 mmHg) pulmonary artery wedge pressure (PAWP) (Hoeper et al., 2017; Leopold & Maron, 2016; O'Callaghan et al., 2011).

In 1973, the World Health Organisation (WHO) first classified pulmonary hypertension into primary pulmonary hypertension (PPH) and secondary pulmonary hypertension, depending on the presence or absence of recognizable causes or risk factors (Simonneau et al., 2004). The latest classification of PH, which was proposed at the Fifth World Symposium on Pulmonary

Hypertension in Nice, France in 2013, divides PH into five subgroups, summarized in Table 1.1. The five groups are:

- Group (1) Pulmonary Arterial Hypertension (PAH), which is further subdivided into: (1.1) idiopathic PAH due to unrecognized risk factors, (1.2) heritable or familial PAH, (1.3) PAH caused by certain drugs or toxins, and (1.4) PAH associated with other conditions such as connective tissue diseases like scleroderma or lupus, congenital heart problems or high blood pressure.
- Group (2) Pulmonary hypertension due to left heart disease.
- Group (3) Pulmonary hypertension caused by lung disease and/or hypoxia.
- Group (4) Pulmonary hypertension due to thrombotic and embolic obstruction of the lung vasculature, also known as chronic thromboembolic pulmonary hypertension (CTEPH).
- Group (5) Pulmonary hypertension with unclear multifactorial mechanism (Galiè et al., 2016; Simonneau et al., 2004; Simonneau et al., 2013).

According the current clinical classification, PH may also be divided into two categories pre-capillary PH, and post-capillary PH (see Table 1.2) (Galiè et al., 2016).

Table 1.1: Latest clinical classification of pulmonary hypertension from the Fifth World Symposium on Pulmonary Hypertension held in Nice, France. Abbreviations: BMPR2, bone morphogenic protein receptor type 2; ALK-1, activin like receptor kinase-1; ENG, endoglin; SMAD9, S mother against decapentaplegic 9; CAV1, caveolin-1; KCNK3, potassium channel subfamily K member 3; HIV, human immunodeficiency virus inside the same subcategories of pulmonary arterial hypertension. Adapted from Galiè et al., 2016; Simonneau et al., 2013.

Group 1: Pulmonary arterial hypertension (PAH)
1.1. Idiopathic
1.2. Heritable
1.2.1. BMPR2 mutation
1.2.2. ALK-1, ENG, SMAD9, CAV1, KCNK3
1.2.3. Unknown
1.3. Drugs and toxins induced
1.4. Associated with:
1.4.1. Connective tissue disease
1.4.2. Human immunodeficiency virus (HIV) infection
1.4.3. Portal hypertension
1.4.4. Congenital heart disease
1.4.5. Schistosomiasis
Group 1' Pulmonary veno-occlusive disease and/or pulmonary capillary haemangiomatosis*
Group 1'' Persistent pulmonary hypertension of the newborn (PPHN)
Group 2: Pulmonary hypertension due to left heart disease
2.1. Left ventricular systolic dysfunction
2.2. Left ventricular diastolic dysfunction
2.3. Valvular disease
2.4. Congenital/acquired left heart inflow/outflow tract obstruction and congenital cardiomyopathies
2.5. Congenital/acquired pulmonary vein stenosis
Group 3: Pulmonary hypertension due to lung diseases and/or hypoxia
3.1. Chronic obstructive pulmonary disease
3.2. Interstitial lung disease
3.3. Other pulmonary diseases with mixed restrictive and obstructive patterns
3.4. Sleep-disordered breathing
3.5. Alveolar hypoventilation disorders
3.6. Chronic exposure to high altitude
3.7. Developmental lung diseases
Group 4: Chronic thromboembolic pulmonary hypertension (CTEPH) and other pulmonary artery obstructions
4.1. Chronic thromboembolic pulmonary hypertension
4.2. Other pulmonary artery obstructions
4.2.1. Angiosarcoma
4.2.2. Other intravascular tumors
4.2.3. Arteritis
4.2.4. Congenital pulmonary arteries stenoses
4.2.5. Parasites (hydatidosis)
Group 5: Pulmonary hypertension with unclear and/or multifactorial mechanisms
5.1 Haematologic disorders: myeloproliferative disorders, splenectomy
5.2 Systemic disorders: sarcoidosis, pulmonary Langerhans cell histiocytosis: lymphangioleiomyomatosis, neurofibromatosis, vasculitis
5.3 Metabolic disorders: glycogen storage disease, Gaucher disease, thyroid disorders
5.4 Others: tumoral obstruction, fibrosing mediastinitis, chronic renal failure on dialysis

Table 1.2: Pulmonary hypertension classification according to haemodynamic parameters: pre-capillary pulmonary hypertension and post-capillary pulmonary hypertension. Clinical groups according to the latest clinical classification of pulmonary hypertension. Abbreviation: PH, pulmonary hypertension. Adapted from Galiè et al., 2016.

Definition	Characteristics	Clinical group(s)
Pulmonary hypertension (PH)	➢ Mean pulmonary artery pressure (mPAP) ≥ 25mmHg	**ALL**
Pre-capillary PH	➢ Mean pulmonary artery pressure (mPAP) ≥ 25mmHg ➢ Pulmonary artery wedge pressure (PAWP) ≤ 15mmHg	(1) Pulmonary arterial hypertension (3) PH due to lung diseases (4) Chronic thromboembolic PH (5) PH with unclear and/or multifactorial mechanisms
Post-capillary PH	➢ Mean pulmonary artery pressure (mpap) ≥ 25mmhg ➢ Pulmonary artery wedge pressure (pawp) > 15mmhg	(2) PH due to left heart disease (5) PH with unclear and/or multifactorial mechanisms

1.3. Pathobiology of pulmonary arterial hypertension

Pulmonary arterial hypertension is characterised by the progressive remodelling of small intrapulmonary arteries caused by endothelial dysfunction, excessive proliferation of smooth muscle cells, sustained vasoconstriction, inflammation, thrombosis and adventitial fibrosis (O'Callaghan et al., 2011). These changes increase pulmonary vascular resistance, leading to right heart hypertrophy and failure (Leopold & Maron, 2016) (Figure 1.3). The first reference to PAH pathology was provided by German physician Ernst Von Romberg in 1891, who described it as pulmonary vascular sclerosis. Several decades later, the first comprehensive article describing the clinical entity of PAH was published in 1951 by David Dresdale (Dresdale et al.,

1951; Heath & Whitaker, 1956). This opened the way to expanding our understanding of the pre-mortem features of PH (Barst, 2008).

1.3.1. Pulmonary vasoconstriction

Pulmonary arterial vasoconstriction in PAH is induced by endothelial dysfunction, which is observed in the early stages of the disease. The endothelium regulates pulmonary vascular homeostasis and is a key source of vasodilators such as nitric oxide (NO) and prostacyclin (PGI_2), as well as potent vasoconstrictors such as thromboxane A2 (TXA2), endothelin-1 (ET-1), serotonin, and 5-hydroxytryptamine (5-HT) (Schermuly et al., 2011; Wilkins, 2012).

PGI_2 is an effective vasodilator, and reduces vascular tone by increasing cyclic adenosine monophosphate (cAMP) levels and decreasing endothelin-1 levels. This vasodilator also inhibits platelet aggregation and reduces inflammatory response and vascular smooth muscle proliferation, which are implicated in the development of PAH (Clapp et al., 2002; Stitham, Midgett, Martin, & Hwa, 2011).

PGI_2 expression is reduced in pulmonary arteries of PAH patients, while the levels of vasoconstrictor thromboxane A2 are elevated (Christman et al., 1992).

Nitric oxide is a potent vasorelaxant. It is synthesised from oxygen and L-arginine by endothelial nitric oxide synthase (eNOS), its activity is mediated by cyclic guanosine monophosphate (cGMP). cGMP induces the relaxation of vascular smooth muscle cells and is degraded by phosphodiesterases (PDEs) (Corbin, 2004; Corbin & Francis, 1999). PDE5 has been shown to be an abundantly expressed PDE isoform within the pulmonary circulation (Hanson et al., 1998) and its levels are elevated in PAH lungs and heart (Corbin et al., 2005; Murray et al., 2002; Wharton et al., 2005). Nitric oxide prevents platelet aggregation and leukocyte adhesion to

endothelial cells (Gaboury et al., 1993; Nong et al., 1997) and inhibits vascular smooth muscle cell migration and proliferation (Tsihlis et al., 2011).

Endothelin-1 is a potent endothelium-derived vasoconstrictor involved in PAH pathogenesis. PAH patients show elevated ET-1 levels in blood and lung tissues (Said, 2006). ET-1 activity is mediated by two receptors, ET-A and ET-B. Smooth muscle cells express both receptor types and their stimulation induces vasoconstriction. Endothelial cells express ET-B receptors, which can induce vasodilation by releasing nitric oxide and prostacyclin and promoting the clearance of circulating ET-1 (Eddahibi & Adnot, 2001; Hirata et al., 1993).

Thromboxane A2 is another important pulmonary vasoconstrictor, and is produced by the endothelium and platelets. Both ET-1 and TXA2 enhance platelet aggregation, smooth muscle cell proliferation and migration (Budhiraja et al., 2004; Feng et al., 2016; Undem et al., 2012).

1.3.2. Pulmonary vascular remodelling

Alterations in pulmonary vascular structure, termed as pulmonary vascular remodelling, are characterised by the progressive thickening of all three layers of the blood vessel wall (the adventitia, the media, and the intima). Vascular remodelling severely reduces blood supply to the lung and decreases the vasodilation capacity of the vessels (Jeffery & Wanstall, 2001; Tuder et al., 2009). Although the causes of the disease are different in different forms of PAH, the structural abnormalities found in the pulmonary vasculature are remarkably similar (Strange et al., 2002).

The pathological mechanisms underlying this condition remain elusive. PAH is thought to be initiated by endothelial damage due to gene mutations or environmental stresses such as hypoxia, drugs and toxins, DNA damage or inflammation. Endothelial damage is followed by the clonal selection of apoptosis-resistant, highly proliferative endothelial cells, leading to the

formation of obliterative plexiform lesions, which are characteristic of PAH (Masri et al., 2007). Smooth muscle cell proliferation, endothelial-to-mesenchymal transition (EndoMT) and vasoconstriction also play a contributory role to the onset of the disease (Davie et al., 2009; Schermuly et al., 2011) (Figure 1.3).

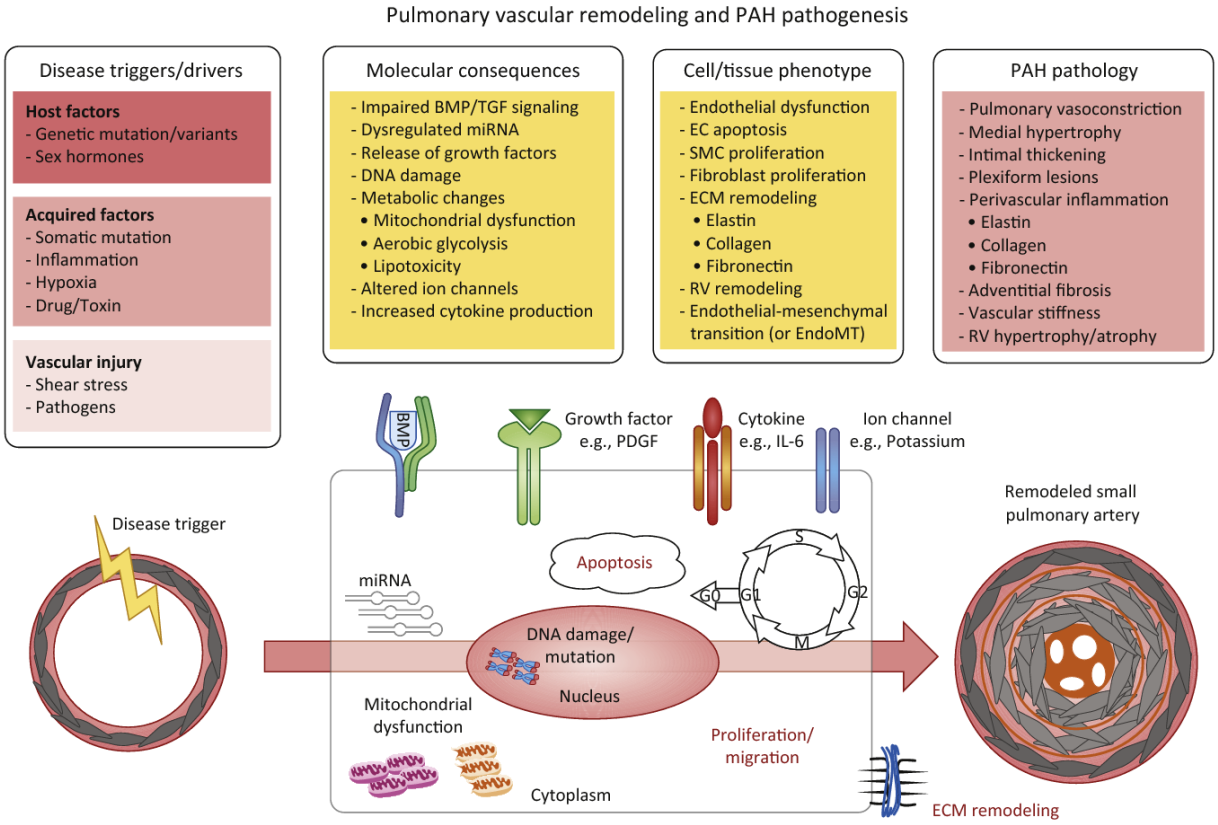


Figure 1.3: Diagram illustrating pulmonary vascular remodelling and pathogenesis of pulmonary arterial hypertension. Risk factors and drivers of the disease pathogenesis include gene mutations in *BMPR2* and other pathways, gender, somatic mutations, DNA damage, exposure to hypoxia or drugs and toxins. These are shown at the top of the diagram. The left image illustrates injury to a healthy vessel resulting in a loss of endothelial cell viability and barrier integrity. The central image shows the most common molecular pathways altered in idiopathic (I) PAH: altered miRNA expression, increased release of growth factors, mitochondrial dysfunction and metabolic changes related to glycolysis. Endothelial cell dysfunction and apoptosis, proliferation of smooth muscle cells and adventitial fibroblasts drive both inward and outward vascular remodelling. The vascular remodelling of resistance pulmonary arteries generates the concentric and plexiform lesions characteristic of PAH (right image). Abbreviations: BMP, bone morphogenetic protein; EC, endothelial cell; ECM, extracellular matrix; PDGF, platelet-derived growth factor; RV, right ventricle; SMC, smooth muscle cell; TGF, transforming growth factor. Adapted from Thompson & Lawrie, 2016.

Pulmonary vascular changes in PAH include the excessive proliferation of endothelial and smooth muscle cells, inflammation, adventitial fibrosis and *in situ* thrombosis. The right ventricle of the heart has to work hard to push blood through the narrowed arteries, leading to right ventricular hypertrophy which can progress to the right heart failure (Leopold & Maron, 2016).

Pulmonary vascular remodelling occurs in all layers of the vascular wall, and is manifested by proliferation and migration of endothelial cells, smooth muscle cells, fibroblasts, inflammatory cells and progenitor cells, as well as platelet aggregation and the increased deposition of extracellular matrix (ECM) components such as collagen, elastin and fibronectin (Tuder et al., 2009; Xu & Shi, 2014).

PAH pulmonary arteries show several abnormalities, including the muscularization of small precapillary arteries, the loss of precapillary arteries, thickening of large pulmonary arteries, neointima formation in small vessels <100-500 μm in diameter and the formation of obliterative plexiform lesions. The abnormalities are characterized by excessive endothelial cell proliferation and abnormal angiogenesis (Jonigk et al., 2011; Rabinovitch, 2012) (Figure.1.4).

The inhibition of bone morphogenetic protein receptor type II (*BMPR2*) function due to genetic mutations, reduced expression or abnormal receptor recycling is one of the key pathological processes associated with PAH. BMPR2 belongs to the transforming growth factor-β (TGF-β) superfamily, and is important for the regulation of vascular development and function (Rol et al., 2018). TGF-β stimulates vascular remodelling and inflammation in the lung as well as hypertrophy and fibrosis in the heart. Mutation in the activin receptor-like kinase type 1 (*AKL-1*) gene, a different member of the TGF-β superfamily, has also been identified in

patients with hereditary haemorrhagic telangiectasia (HHT) who develop severe plexiform pulmonary hypertension (Trembath et al., 2001).

BMPR2 mutations in PAH are associated with increased expression and activity of the platelet-derived growth factor (PDGF) receptor and 5-HT serotonin transporter, as well as the *de novo* expression of the anti-apoptotic protein survivin (Hassoun et al., 2009).

Many other factors have been implicated in the remodelling process, including a higher expression of growth factors such as vascular endothelial growth factor (VEGF), transforming growth factor beta 2 (TGF-β2), fibroblast growth factor (FGF) and epidermal growth factor (EGF) (Hassoun et al., 2009; Humbert et al., 2004). Meanwhile, increased expression of hypoxia-inducible factor-1 (HIF-1), angiopoietin-1 (ANG-1), Tie-2, thrombospondin-1 (THBS1), stem cell growth factor receptor c-kit, angiogenesis regulators (Notch 3 and 4) and matrix metalloproteinase 9 (MMP-9) have also been linked to vascular alterations in PAH (Jonigk et al., 2011).

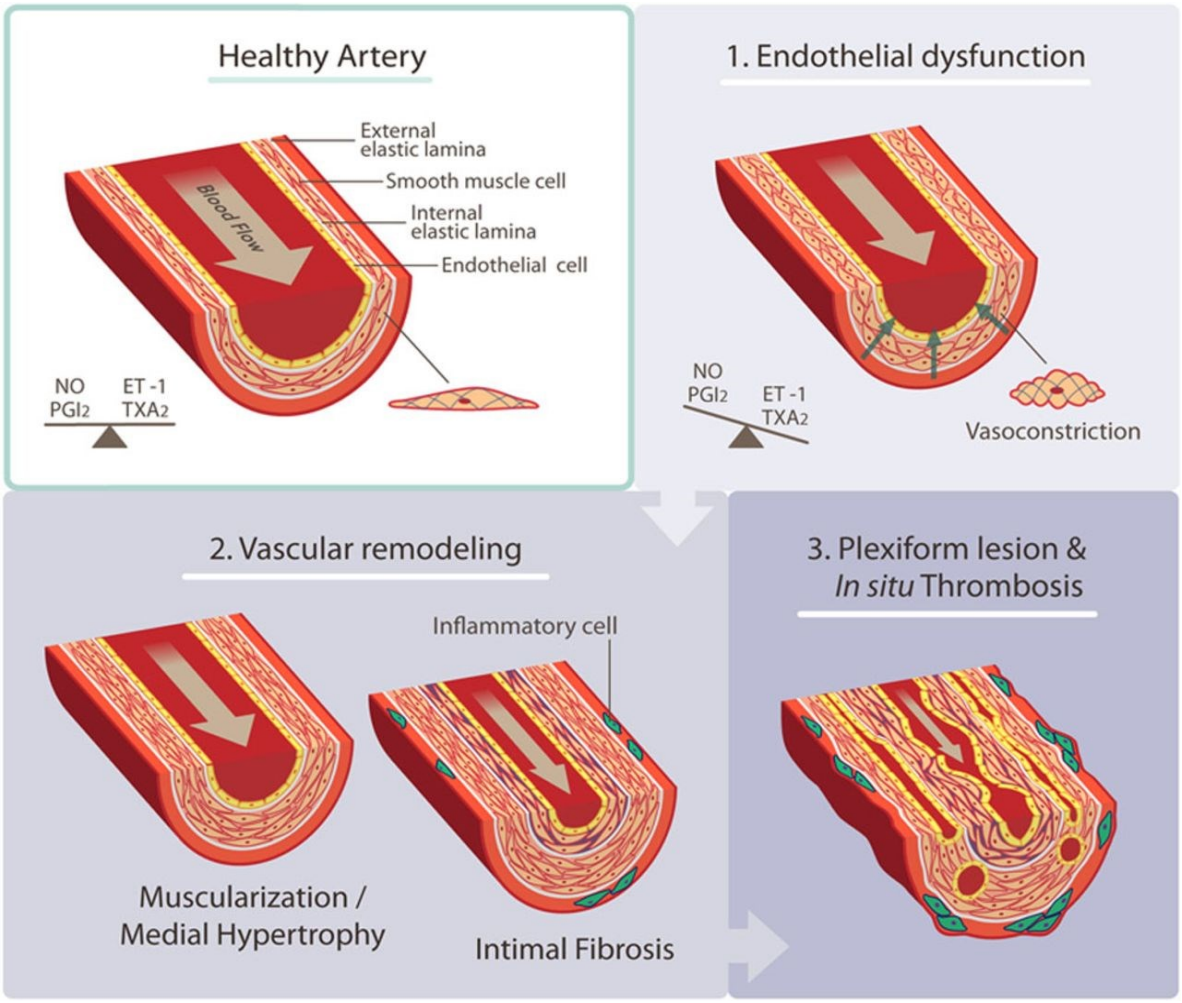


Figure 1.4: Schematic illustration of vascular remodelling in pulmonary arterial hypertension. Healthy endothelial cells regulate the balance between vasodilation and vasoconstriction and inhibits smooth muscle cell proliferation to maintain a low-resistance pulmonary vasculature. 1) In PAH, endothelial dysfunction reduces release of vasodilators (NO and PGI2) and increases release of vasoconstrictors (ET-1 or TXA2). This results in vasoconstriction and reduction in blood flow. 2) Vascular remodelling is a feature of PAH, characterised by excessive smooth muscle cell proliferation and migration, leading to muscularization of peripheral pulmonary arteries and medial hypertrophy. 3) Vascular remodelling results in plexiform lesion formation and in situ thrombosis, which cause occlusions of the vessels in the late stage of disease progression. Abbreviations: NO, nitric oxide; PGI2, prostacyclin; ET-1 endothelin-1; TXA2, thromboxane A2. Adapted from Lai et al., 2014.

1.4. Role of endothelium in pulmonary hypertension

As mentioned in section 1.3, PAH is thought to be initiated by endothelial damage due to inhibition of *BMPR2* function, DNA damage, hypoxia or drugs and toxins. Endothelial dysfunction results in the increased release of growth factors and vasoconstrictions as well as inflammatory cytokines that promote medial and adventitial cell proliferation. Subsequent clonal selection and the activation of highly proliferative, intimal endothelial cells leads to the formation of obliterative plexiform lesions in severe human PAH (Sakao et al. 2009).

1.4.1. Vascular endothelial cells

The pulmonary endothelial layer acts as a barrier between the blood and the underlying tissues, by regulating the exchange of fluids, nutrients, growth factors and cells. Alterations in vascular endothelial permeability allow the access of proliferative mediators to the underlying layers of the vascular wall, resulting in excessive cell proliferation, migration and extracellular matrix production. Changes in the endothelial barrier integrity have been linked to the early pathogenesis of PH both in animal models and patients with PAH (Dejana et al., 2009; Krüger-Genge et al., 2019). Endothelial permeability is regulated by several factors, including hypoxia, flow, growth factors and inflammatory cytokines (McQuaid & Keenan, 1997; van Wetering et al., 2002; Wojciak-Stothard et al., 2005). The endothelium also plays an essential role in regulating blood coagulation. Under normal physiological conditions, the endothelium releases anti-coagulants which exert anti-inflammatory, anti-proliferative and vasodilatory effects. These anticoagulants include nitric oxide, prostacyclin, tissue factor pathway inhibitor, heparan sulphate proteoglycan, thrombomodulin, tissue-type plasminogen activator (tPA) and annexin V (Aytekin et al., 2012; Chen et al., 2005; Liu & Pedersen, 2007). Changes in blood flow and shear stress affect the expression of coagulation regulators and the fibrinolytic pathways. Endothelium-derived pro-coagulants include endothelin-1, tissue factor, von Willebrand Factor

(vWF) and plasminogen activator inhibitor-1. One of the key functions of the pulmonary endothelium under normal conditions is to prevent thrombus formation, but in order to prevent blood loss upon vascular injury, the endothelium can release pro-thrombotic factors and promote the formation of thrombi. Excessive thrombotic responses can be seen in chronic thromboembolic pulmonary hypertension (CTEPH) and other forms of PH (Jeffery & Wanstall, 2001; Matthews & Hemnes, 2016; Yau et al., 2015).

The onset of pulmonary hypertension begins with early apoptosis of the pulmonary endothelial cells (Sakao et al., 2009; Wilkins, 2012), triggering the excessive release of anti-apoptotic, pro-proliferative and pro-angiogenic factors by endothelial and smooth muscle cells. This process is followed by the clonal selection and expansion of apoptosis-resistant, highly proliferative endothelial cells and smooth muscle cells, leading to the formation of occlusive plexiform lesions and thickening of the arterial wall (Sakao et al., 2005; Sakao et al., 2009).

1.4.2. Blood vessel formation and endothelial progenitor cells (EPCs)

Angiogenesis is a process by which new blood vessels form from pre-existing vessels. The process consists of a series of morphogenic events including sprouting, branching, lumen formation, anastomosis (making new connections) and rearrangement. Angiogenesis is regulated by proteases, growth factors and micro-environmental cues (Kubis & Levy, 2003) (Figure 1.5).

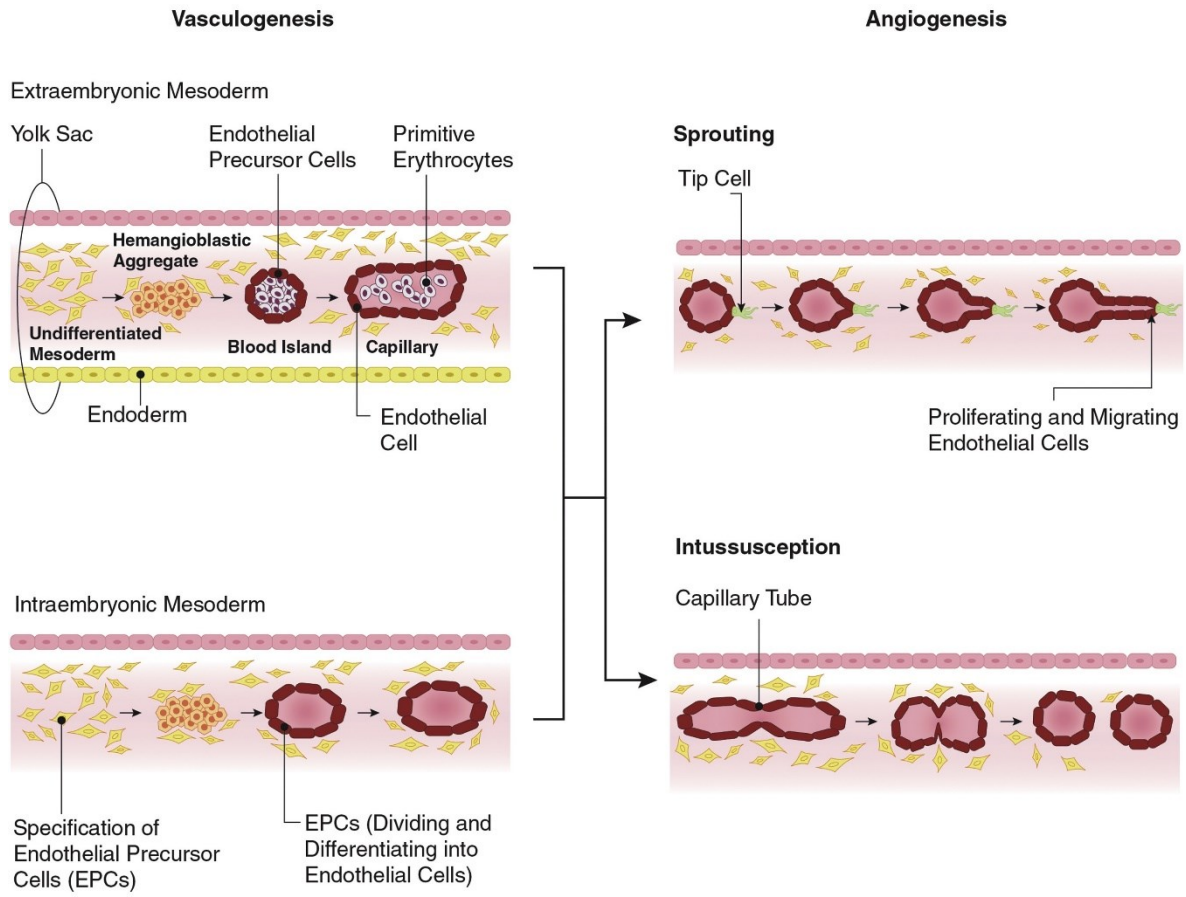


Figure 1.5: Illustration of vasculogenesis and angiogenesis. Vasculogenesis (top left) begins in the wall of the yolk sac in early embryonic development. Cells in the extraembryonic mesoderm form capillary tubes, while cells located in the centre differentiate into hemangioblasts and primitive blood cells. In the intraembryonic mesoderm (lower left), a similar process of aggregation occurs, with mesodermal differentiation into capillary tubes, without the formation of primitive blood cells. The capillary tubes grow contentiously and merge to form a network. The existing vessels of the network can grow by sprouting angiogenesis, as indicated top right. One of the endothelial cells becomes a tip cell, which starts to migrate into the surrounding mesenchyme. The tip cell is followed by adjacent endothelial cells; the following cells maintain a lumen, then a new vessel buds off the existing vessel. Intussusceptive angiogenesis (lower left) occurs in areas where there may be demand for a parallel vessel. The parent vessel splits into two vessels, each with a single lumen. Illustration adapted from DeSesso, 2017.

Arteriogenesis refers to the formation of collateral arterioles through which the blood flow is increased to tissues. Arteriogenesis is also a vital compensation mechanism for restoring tissue perfusion where the key vascular pathway has been obstructed, and the process can occur in response to several stimuli, including alterations in shear stress and tissue hypoxia (Castro et al., 2018). Arteriogenesis, defined by an increase in the diameter of small arterioles, may occur via two distinct mechanisms: *de novo* formation or the remodelling of pre-existing collateral arterioles. The *de novo* formation process comprises the formation and expansion of new vessels from a pre-existing arteriolar network, localised near a blocked artery and reconnecting the distal arterial segment. The remodelling of pre-existing collateral arterioles involves promoting a steady enlargement of arterioles and increasing elasticity and reactivity through the recruitment of smooth muscle cells and other mesenchymal cells that secrete specific ECM components until the arterioles are able to increase blood flow and restore local perfusion (Carmeliet & Jain, 2011; Castro et al., 2018)

Circulating progenitor endothelial cells have a considerable proliferative potential, and can participate in vascular repair and morphogenesis (Robinson et al., 1995; Yoder, 2010). Endothelial progenitor cells, which can be found in adult human peripheral blood, can differentiate into ECs *in vitro* and contribute to postnatal vasculogenesis *in vivo* (Castro et al., 2018). These cells, known as endothelial progenitor cells (EPCs), have become widely recognised as a normal component of the blood. They comprise a heterogeneous group of cells with the potential to form mature ECs and/or participate in angiogenesis. Several studies have attempted to define the circulating levels of EPCs in many clinical disorders, but given the low numbers of circulating true endothelial progenitor cells, an *ex vivo* study is required in order to examine their functional activity and differentiation into endothelium (Hirschi et al., 2008).

1.4.2.1. Endothelial colony-forming cells

Endothelial colony forming cells (ECFCs) are also referred to as blood outgrowth endothelial cells (BOEC), or late outgrowth endothelial cells. Over the last few years, different acronyms has been used by different groups, but it was recently proposed that the term ECFC should be used to harmonize the literature (Medina et al., 2017). ECFCs are proliferative endothelial cells that can be found in the vessel wall but are rarely found in the peripheral blood. ECFCs were originally identified by Ingram et al. using a single cell *in vitro* colony forming assay (Ingram et al., 2004; Duong et al., 2011).

ECFCs display similar properties to original endothelial progenitor cells (EPCs). They show the ability to form *de novo* tubular networks independently *in vitro* (Case et al., 2007; Hur et al., 2004; Sieveking et al., 2008). *In vitro*, cord blood ECFCs exhibit robust human blood vessel formation upon implantation in immunodeficient mice, and also display clonal proliferative potential. Characteristic features of typical endothelial cells were confirmed through the upregulation of activated endothelial cell marker vascular cell adhesion molecule-1 (VCAM-1) on tumour necrosis factor-α (TNF-α) and interleukin-1 (IL-1) stimulation (Ingram et al., 2004; Shepherd et al., 2006). Previous reports have demonstrated that the ability to isolate and culture ECFCs depends largely on the source of their isolation and varies from one animal system to another. For example, ECFCs are abundant in the bloodstream of nonhuman primates, human, pigs, dogs, and cows, but are so rare in mice that the entire blood volume of 5 or more 8-week-old mice was required to identify endothelial colonies in 11% of attempts to isolate at least 1 endothelial colony (Yoder, 2010). Cord blood-derived ECFCs present a higher vasculogenic capacity *in vivo* compared to adult peripheral blood ECFCs (Lin et al., 2000).

ECFCs do not express leukocyte common marker CD45 or monocytic/macrophage markers CD14 and CD115, and do not ingest bacteria or differentiate to hematopoietic progenitor cell (HPC) colonies (Case et al., 2007; Yoder et al., 2007). In order to distinguish ECFCs from early endothelial progenitor cells, many markers have been identified in ECFCs, such as the secretion of high levels of matrix metalloproteinase-2 (MMP-2), low levels of matrix metalloproteinase-9 (MMP-9), and selective expression of bone morphogenetic proteins BMP-2 and BMP-4. These features are considered essential for differentiation and regulation in angiogenesis (Smadja et al., 2008; Yoon et al., 2005). Other factors may affect the survival and proliferation of ECFCs. It has been reported that the activation of thrombin receptor protease-activated receptor 1 induces proliferation, migration, differentiation and interleukin-8 (IL-8) synthesis in these cells, resulting in a pro-angiogenic effect *in vitro* (Smadja et al., 2009; Smadja et al., 2005).

Despite exhibiting features that are consistent with an endothelial lineage, ECFCs may also express specific proteins and have functional characteristics that set them apart from mature endothelial cells (Medina et al., 2010). ECFCs are reported to be highly proliferative and resistant to serum deprivation in comparison with mature endothelial cells, and may also differ in terms of their *in vivo* vasculogenic potential (Finkenzeller et al., 2009; Hur et al., 2004). ECFCs appeared to have a higher rate of spreading and expression of α5β1 (the primary cellular receptor for the extracellular matrix protein fibronectin) than human aortic endothelial cells (Stroncek et al., 2009). ECFCs and mature endothelial cells also display different cellular responses to hypoxia and the deposition of extracellular matrix in culture (Kusuma et al., 2012).

ECFCs have attracted considerable attention because of their multiple potential applications for translational studies, gene therapy and vascular regeneration (Paschalaki & Randi, 2018). They have been used to study endothelial dysfunction in patients with various diseases including

ischemic heart disease (Dauwe et al., 2016; Massa et al., 2009), venous thromboembolic disease (VTD) (Alvarado-Moreno et al., 2016; Hernandez-Lopez et al., 2017), chronic obstructive pulmonary disease (COPD) (Fish et al., 2008; Paschalaki et al., 2013; Paschalaki et al., 2018), idiopathic pulmonary fibrosis (IPF) (Bacha et al., 2018; Smadja et al., 2013), bronchopulmonary dysplasia (BPD) (Baker et al., 2009; Borghesi et al., 2009), and pulmonary arterial hypertension (PAH) (Caruso et al., 2017; Dunmore et al., 2013; Wojciak-Stothard et al., 2014). As well as providing insights into the possible molecular mechanisms that lead to endothelial dysfunction, ECFCs can be used to define new pharmacological targets (Paschalaki & Randi, 2018).

Elevated and dysregulated angiogenesis is a hallmark of many diseases such as cancer, and highly proliferative ECFC is believed to contribute to angiogenesis via cell proliferation and respond to vascular injury and hypoxia by sprouting angiogenesis. The presence of ECFC in the human pulmonary arteries and their role in PAH pathogenesis is poorly understood at present (Duong et al., 2011).

1.5. Current therapies in pulmonary arterial hypertension

Despite extensive pre-clinical investigations and numerous clinical trials, there is currently no cure for pulmonary hypertension, and the existing treatments focus on helping patients cope with the symptoms, which include shortness of breath, fatigue, chest pain or pressure, irregular heartbeat, pain on the upper right side of the abdomen and decreased appetite (O'Callaghan et al., 2011). Patients who suffer from pulmonary hypertension have been treated with conventional therapies such as oral anticoagulants, diuretics, digoxin, oxygen supplements, prostacyclin analogs, phosphodiesterase inhibitors and spirono lactone (Galiè et al., 2016; McLaughlin et al., 2015).

The only therapies available for PAH treatment were those described above until the 1990s. With a better understanding of the pathophysiological mechanisms involved – in particular alterations in the endothelial prostacyclin, endothelin and nitric oxide pathways – several PAH-specific vasodilator therapies have been approved for targeting one of these three key pathways. These include prostacyclin (PGI2), nitric oxide (NO) and endothelin (ET-1) (Humbert et al., 2014; Sitbon et al., 2019) (Figure 1.6). Drugs that are currently approved are listed in Table 1.3 (Kondo et al., 2019).

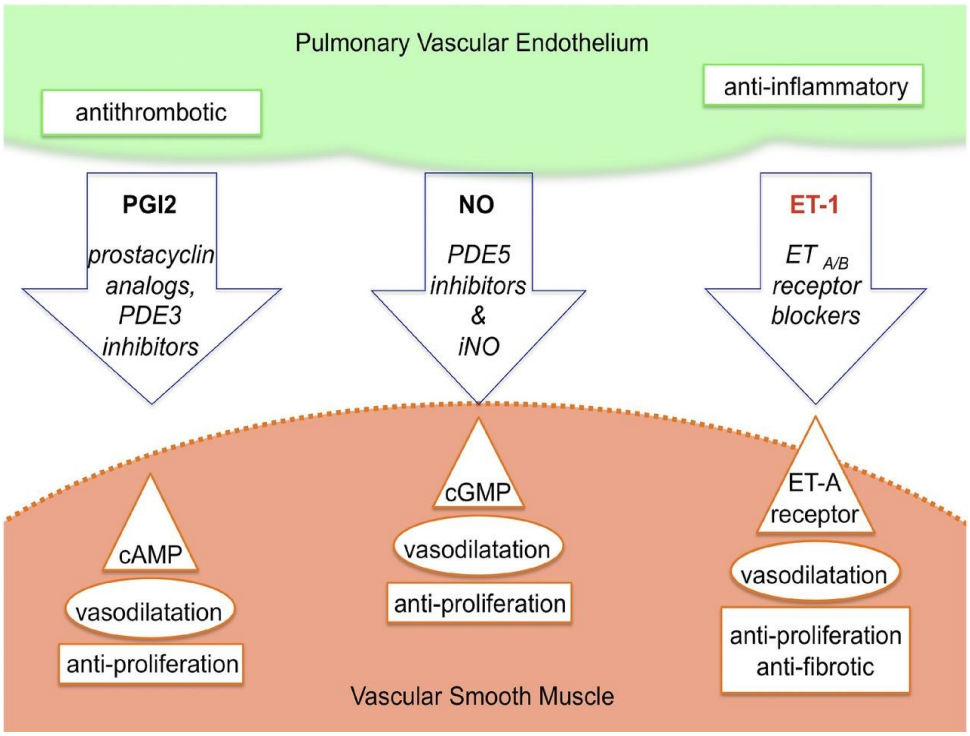


Figure 1.6: Illustration of currently approved targeted therapies in pulmonary arterial hypertension. There are three main vasoreactive pathways (endothelin-1, nitric oxide, and prostacyclin) targeted in PAH. Endothelial dysfunction leads to decreased levels of endogenous vasodilatory mediators (nitric oxide and prostacyclin) and increased endothelin-1 levels, promoting vasoconstriction and smooth muscle cell proliferation. The endothelin-1 pathway can be inhibited either by selective or nonselective endothelin-1 receptor antagonists. The nitric oxide pathway can be manipulated directly by exogenous nitric oxide, the inhibition of phosphodiesterase type-5 to block the downstream degradation of cGMP to GMP or by the stimulation of soluble guanylate cyclase. The prostacyclin signalling can be enhanced by prostanoid analogues or nonprostanoid IP receptor agonists. Abbreviations: NO, nitric oxide; ET-1, endothelin-1; PDE5, phosphodiesterase type-5; PGI2, prostacyclin; cAMP, cyclic adenosine monophosphate; iNO, inhaled nitric oxide; cGMP, cyclic guanosine monophosphate; PAH, pulmonary arterial hypertension. Adapted from Unegbu et al., 2017.

Table1.3: Approved Drugs for pulmonary hypertension (PAH). Modified from Kondo et al., 2019.

Mechanism of Action	Drug Name	Indication	Route
Endothelin-receptor antagonists	Bosentan	PAH	Oral
	Ambrisentan	PAH	Oral
	Macitentan	PAH	Oral
Phosphodiesterase type 5 inhibitors	Sildenafil	PAH	Oral
	Tadalafil	PAH	Oral
Guanylate cyclase stimulators	Riociguat	PAH	Oral
Prostacyclin analogues	Epoprostenol	PAH	Intravenous
	Iloprost	PAH	Inhaled
	Treprostinil	PAH	Subcutaneous Intravenous
Prostaglandin I2 receptor agonists	Beraprost	PAH	Oral
	Selexipag	PAH	Oral

1.6. Role of mitochondria in PAH

Defects in energy metabolism underlie the pathology of many disorders including cancer, diabetes and pulmonary hypertension (Archer et al., 2008; Youle & Van Der Bliek, 2012). Cells from PH arteries and the right ventricle show numerous abnormalities in mitochondrial structure and function, suggesting their role in disease pathogenesis (Freund-Michel et al., 2014). Mitochondrial alterations that are characteristic of PH are summarised in Figure 1.7 (Freund-Michel et al., 2014).

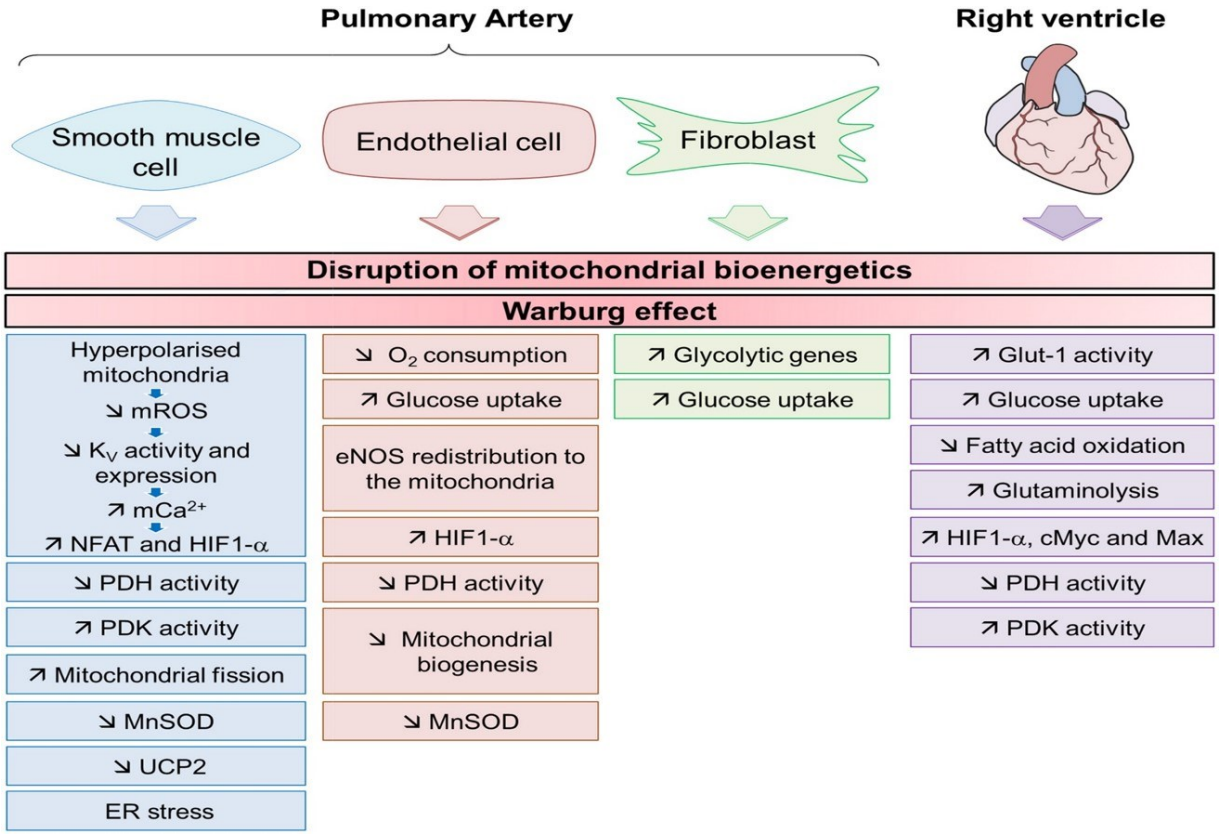


Figure 1.7: Summary of mitochondrial alterations in pulmonary hypertension. Mitochondrial abnormalities occur in pulmonary arterial fibroblasts, smooth muscle and endothelial cells, and the right ventricle. Abbreviations: ER: endoplasmic reticulum; eNOS: endothelial nitric oxide synthase; HIF-1α: hypoxia induced factor-1α; MnSOD: manganese superoxide dismutase; NFAT: nuclear factor of activated T cells; PDH: pyruvate dehydrogenase; PDK: pyruvate dehydrogenase kinase; ROS: reactive oxygen species; UCP2: uncoupling protein 2. Schematic adapted from Freund-Michel et al., 2014.

1.6.1. Mitochondrial alterations in pulmonary arterial endothelial cells

Mitochondrial dysfunction in pulmonary arterial endothelial cells in PH has been less extensively studied compared to pulmonary arterial smooth muscle cells. Mitochondrial numbers are decreased in these cells, with increased glucose uptake, reduced oxygen consumption and reduced mitochondrial pyruvate dehydrogenase (PDH) activity, leading to increased glycolytic metabolism (Xu et al., 2007). Recent studies show that mitochondria compose only 2-6% of the endothelial cell volume, in contrast to 28% in hepatocytes and 32% in cardiac myocytes (Dromparis & Michelakis, 2013; Kluge et al., 2013), indicating that energy metabolism in endothelial cells relies predominantly on glycolysis. Reduction in the number of mitochondria may result from the increased expression of hypoxia induced factor-1α (HIF-1α), seen in PH lungs. Decreased mitochondrial content can also be linked to the reduced expression of manganese superoxide dismutase (MnSOD or SOD2), which results in an increase in ROS levels and endothelial cell damage (Fijalkowska et al., 2010).

Increases in the level of endogenous NOS inhibitor asymmetric dimethylarginine (ADMA) in PH endothelial cells induces the redistribution of eNOS from the plasma membrane to the mitochondria, resulting in an increase in mitochondrial NO levels. This leads to nitric oxide-derived mitochondrial protein nitration and the dysregulation of mitochondrial respiration (Sud et al., 2008; Sun et al., 2013).

1.6.2. Metabolism: general overview

Cellular metabolism is a dynamic process that can change rapidly in a pathophysiological environment. As well as the production of ATP, mitochondria play a central role in the regulation of fatty acid oxidation (FAO), glucose oxidation, and glutaminolysis. Glycolysis occurs in the cell cytosol, converting glucose into pyruvate which is then transported to the mitochondria, where

it participates in glucose oxidation as a substrate for pyruvate dehydrogenase (PDH). Mitochondrial defects result in the uncoupling of glycolysis from glucose oxidation, leading to an increase in intracellular lactate levels when pyruvate dehydrogenase is inhibited (Paulin & Michelakis, 2014). Fatty acid β-oxidation is localised in the mitochondria to generate ATP and acetyl coenzyme A which enters the citric acid cycle (Kennedy & Lehninger, 1949). There is metabolic crosstalk between glycolysis and fatty acid oxidation, so we can conclude that an alteration in the activity of one pathway influences the other (Randle et al., 1963).

1.6.3. Mitochondria and metabolism in PAH

Mitochondrial metabolic defects observed in PAH are similar to the metabolic dysregulations originally defined in cancer by Otto Warburg in 1924, referred to as the Warburg Effect or aerobic glycolysis (Sutendra & Michelakis, 2014; Warburg, 1956). The Warburg effect describes the shift from mitochondrial oxidative phosphorylation (OXPHOS) towards aerobic glycolysis, which is followed by the fermentation of lactic acid instead of pyruvate oxidation in the mitochondria. This metabolic switch usually occurs as a response to the significant inhibition of mitochondrial pyruvate dehydrogenase or an increase in pyruvate dehydrogenase kinase. The advantage of the net gain from this metabolic shift (which was first defined in cancer cells) is the generation of ATP to meet cellular energy requirements and to promote cell growth and survival (Leopold & Maron, 2016; Warburg et al., 1927). Endothelial cells are the first cells to sense low oxygen levels, and they signal this to the surrounding cells, allowing them to make metabolic adaptations. In patients suffering from PH, the Warburg metabolic shift occurs at both higher and normal oxygen levels (Gebb & Stevens, 2004; Marshall et al., 2018).

Pulmonary vascular cells show increased aerobic glycolysis as a result of the normoxic upregulation of HIF-1α and the inhibition of pyruvate dehydrogenase. HIF-1α upregulates

pyruvate dehydrogenase kinase isoforms 1 and 2, which phosphorylate and inhibit pyruvate dehydrogenase (a key OXPHOS enzyme), resulting in the Warburg Effect. Pyruvate dehydrogenase kinase inhibitor improves the structural integrity and function of the mitochondria, decreases pulmonary artery smooth muscle cell proliferation and regresses established pulmonary hypertension (Archer et al., 2008; Bonnet et al., 2006; Guignabert et al., 2009; McMurtry et al., 2004).

The Warburg metabolic shift contributes to disease pathogenesis by inducing hyperproliferation and apoptosis resistance in vascular cells. This effect partially inhibits the transcription of SOD2, reducing hydrogen peroxide (H_2O_2) production and creating a pseudo-hypoxic environment that activates HIF-1α despite normal oxygen availability (Bonnet et al., 2006; Ryan et al., 2015) (Figure 1.8).

Glutaminolysis is a mitochondrial pathway process responsible for producing cellular energy that allows cells to metabolise the amino acid glutamine to enter Krebs' cycle. This rewards cells with amino acid intermediates, which permit rapid cell growth. Glutaminolysis, which was originally identified in cancer cells, has recently been observed in the right ventricle in PH (Ryan & Archer, 2015).

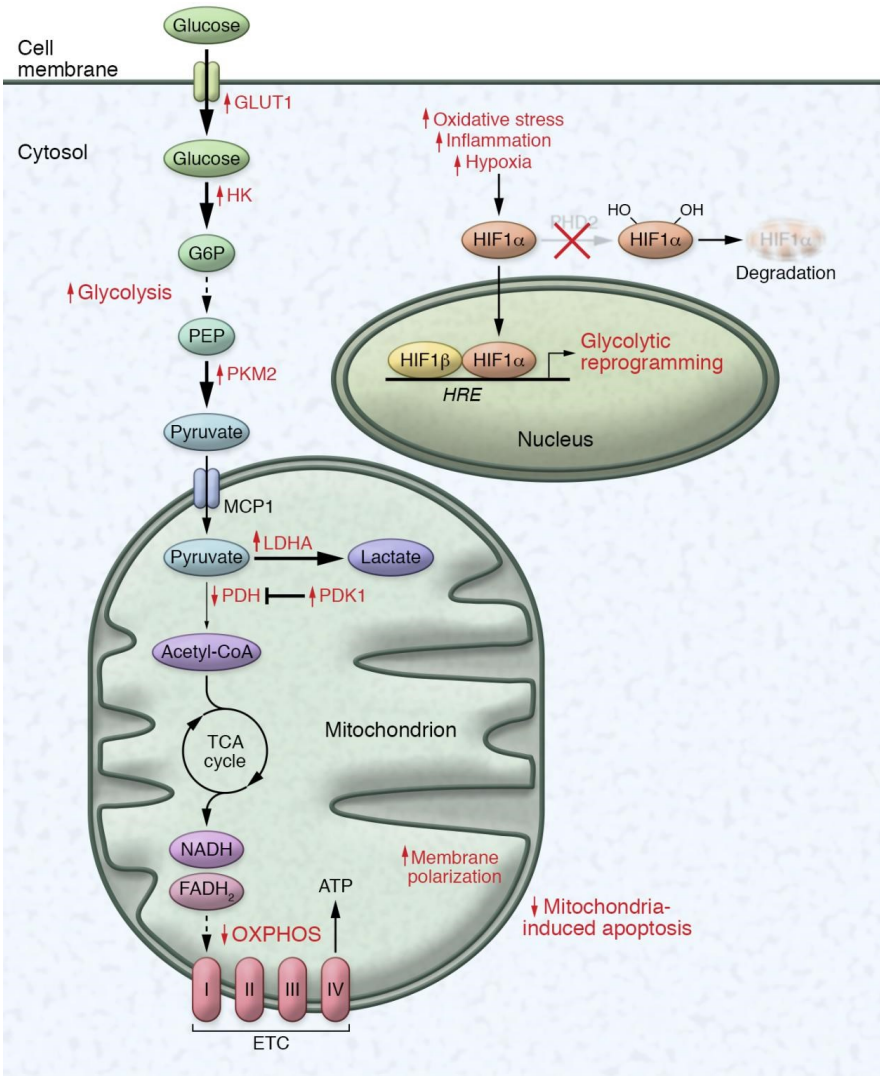


Figure 1.8: Warburg effect pathways in pulmonary hypertension. The illustration shows the disruption of metabolic pathways in PH, exhibiting decreased oxidative phosphorylation and increased glycolysis in mitochondria in pulmonary vascular cells and the right ventricle. This is followed by the stabilization of HIF-1α, which increases the transcription of glycolytic mediators such as glucose transporter 1 (GLUT1) and hexokinase (HK), which traps glucose via conversion to glucose-6-phosphate (G6P), as well as lactate dehydrogenase (LDHA), which converts pyruvate to lactate. The activity of pyruvate kinase isoform M2 (PKM2) is increased, slowing the production of pyruvate from phosphoenolpyruvate (PEP), and reducing pyruvate dehydrogenase (PDH) activity, driven by increased pyruvate dehydrogenase kinase (PDK1/2). The Warburg Effect induces cell survival and proliferation, and the simultaneous hyperpolarization of the mitochondrial membrane potential induces the evasion of mitochondria-dependent apoptosis. This glycolytic switch in pulmonary vascular cells promotes extensive remodelling that results in increasing pulmonary vascular resistance and pulmonary artery pressures. Abbreviations; FADH2: flavin adenine dinucleotide 2; HIF-1α/β: hypoxia inducedfactor-1 alpha and beta; NADH: nicotinamide adenine dinucleotide; PFK: phosphofructokinase. ETC, electron transport chain. Schematic was adapted from Culley & Chan, 2018.

1.6.4. Mitochondrial membrane potential and ROS generation in PAH

Mitochondrial respiration and ATP production represent two critical pathways in cellular metabolism. During respiration, the energy generated from the movement of electrons along multi-subunit enzyme complexes I–IV of the electron transport chain (ETC) is used to pump H^+ protons against their electrochemical gradient across the inner mitochondrial membrane (IMM). The proton gradient across the IMM results in the accumulation of protons within the intermembrane space (Kadenbach et al., 2011; Perry et al., 2011). The electrical potential of the mitochondrial membrane or the electrochemical proton motive force is referred to as the mitochondrial membrane potential (Δψm). Δψm is a key factor that regulates respiratory rate, ATP production and the generation of reactive oxygen species, Δψm is controlled by electron transport and proton leaks (Nicholls, 2004).

Reactive oxygen species (ROS) are free radicals that are naturally produced as by-products of oxygen metabolism, such as hydroxyl (OH•), superoxide ($O_2^{\bullet -}$), peroxyl (RO_2•), and lipid peroxyl (LOO•). ROS includes a group of non-radical species, such as hydrogen peroxide (H_2O_2), hypochloric acid (HOCl), ozone (O_3) and lipid peroxide (LOOH). The group of highly reactive oxygen derivatives includes superoxide anion ($O_2^{\bullet -}$), hydroxyl radical (OH•) and hydrogen peroxide (H_2O_2), which act as key regulators of numerous biological functions and cellular metabolic processes.

Mitochondria are a major source of ROS in most mammalian cells, and are the main sites of ROS generation in the mitochondrial ETC. Mitochondrial ROS are generated during the process of oxidative phosphorylation at ETC complexes I, II, and III, which are localized in the inner mitochondrial membrane (Park et al., 2011). The leakage of electrons at complex I, II and complex III of ETC results in a partial reduction of oxygen to produce superoxide. Under normal

physiological conditions, superoxide is rapidly converted to hydrogen peroxide by superoxide dismutase (SOD) (Turrens, 2003). However, in PAH the function of superoxide dismutase is compromised, leading to the increased synthesis of mitochondrial superoxide.

While base levels of ROS generation are critical for healthy vascular homeostasis, the accumulation of ROS causes oxidative stress and vascular damage (Aggarwal et al., 2013; Chen et al., 2018) and contributes to diseases such as atherosclerosis, diabetes and pulmonary hypertension (Chen et al., 2018; Tang et al., 2014).

The major sites of ROS generation in the lungs are the endothelial cells, neutrophils, eosinophils, alveolar macrophages and alveolar epithelial cells. Pulmonary vasculature ROS can be generated from complexes in the cell membrane or cellular organelles such as, peroxisomes, mitochondria and the cytoplasm. Meanwhile, low levels of L-arginine and tetrahydrobiopterin (BH4) substrates or co-factors, lead to the uncoupling of eNOS, resulting in a shift from NO production to ROS generation. Several enzymatic sources of ROS are now recognized as being associated with elevated ROS generation in PH, including NADPH oxidase, uncoupled NOS, dysfunctional mitochondria and xanthine oxidase.

There is a direct relationship between the Δψm and ROS generation. Even a slight increase of Δψm enhances ROS emission, while a decrease of Δψm attenuates ROS release (Korshunov et al., 1997; Seifert et al., 2010).

In PH, mitochondrial ROS have been shown to promote pulmonary vascular remodelling by increasing intracellular Ca^{2+}, depolarising or hyperpolarising the mitochondrial membrane and contracting and proliferating the pulmonary arterial smooth muscle cells (PASMC) (Jernigan et al., 2008). Treating PASMCs and PAECs with antioxidants such as dimethylthiourea, recombinant human superoxide dismutase (SOD) and N-acetyl-l-cysteine (the precursor to

nonenzymatic antioxidant glutathione) inhibits peroxide-induced mitochondrial iron uptake, oxidative damage and apoptosis, while reducing ΔΨm, showing the critical role of ROS in regulating mitochondrial function (Wedgwood & Black, 2003; Yu & Chan, 2017). In a regulatory feedback mechanism, the hyperpolarization of mitochondrial membrane affects ROS generation so that mitochondria with high ΔΨm generate higher levels of superoxide (Marshall et al., 2018). This also takes place in PAH, where the inhibition of apoptosis in pulmonary vasculature is associated with the hyperpolarization of mitochondrial membrane, leading to increased mitochondrial potential (Suliman and Nozik-Grayck, 2019). ROS regulate the effects of many vasoactive substances, such as thromboxane A2 (TXA2), endothelin-1 (ET-1) peroxisome proliferator-activated receptor-γ (PPAR-γ) and prostacyclin, which can significantly affect vessel tone, resulting in pulmonary vascular remodelling in PH (Aggarwal et al., 2013).

The excessive production of mitochondrial ROS has been linked to increases in the circulating levels of asymmetric dimethylarginine (ADMA) in PH, which induces mitochondrial dysfunction by increasing the expression of uncoupling protein-2 (UCP-2), resulting in the reduction of cellular ATP levels in pulmonary arterial endothelial cells (PAECs) (Sud et al., 2008).

1.6.5. Mitochondrial dynamics

Mitochondrial function relies on structural integrity. Mitochondria are dynamic structures that move about within the cell and constantly undergo division (fission) or fuse together (fusion) to form mitochondrial networks. The connectivity of the mitochondrial networks, the shape of individual mitochondria and the intracellular trafficking of mitochondria reflect processes that are collectively referred to as mitochondrial dynamics (Youle & Van Der Bliek, 2012). Vascular function depends at least in part on the stability of the mitochondrial network in vascular endothelial and smooth muscle cells (Fang et al., 2012; Kluge et al., 2013). Mitochondrial fission

must be coordinated with nuclear division or the cell cycle checkpoint will be disrupted, leading to cell death (Dasgupta et al., 2011).

Mitochondrial dynamics is controlled by several proteins. The fusion of the outer mitochondrial membrane is regulated by the transmembrane GTPases, mitofusin-1 and mitofusin-2 (MFN1 and MFN2), while the fusion of the inner membrane is regulated by optic atrophy protein-1 (OPA1). Fission is regulated by a GTPase dynamin-related protein-1 (DRP1), also known as dynamin-1-like protein (DNM1L) and Fission-1 (FIS1). DRP1 is recruited by FIS1 to the mitochondria to initiate fission (Yoon et al., 2003). Drp1 is mainly localised in the cytoplasm and is recruited to the outer mitochondrial membrane (OMM) by FIS1 in response to different cellular stimuli. Other OMM proteins have recently been reported to promote the recruitment of Drp1 and mitochondrial fission, i.e. mitochondrial dynamics of 51 kDa protein (MiD51), also known as mitochondrial elongation factor 1 (MIEF1), mitochondrial dynamics of 49 kDa protein (MiD49) (Chen et al., 2018; Ma et al., 2019). The phosphorylation of Drp1 on serine-616 (S616) promotes the translocation to OMM and mitochondrial fission, while DRP1 phosphorylation at serine-637 (S637) has an inhibitory effect. The inhibitory phosphorylation of DRP1 is carried out by adenosine monophosphate-activated protein kinase (AMPK), which prevents mitochondrial fission, protecting mitochondria from autophagosomal degradation (Chang & Blackstone, 2007; Cribbs & Strack, 2007; Toyama et al., 2016).

1.6.6. Mitochondrial dynamics in PAH

Mitochondria exist in filamentous networks under normal physiological conditions. However, in PAH the mitochondria are fragmented, showing an imbalance in mitochondrial fission and

fusion. Activation of the fission regulator DRP-1 leads to mitochondrial fragmentation and a decrease in the expression of complex I and superoxide dismutase, resulting in the hyperpolarization of the mitochondrial membrane (Marsboom et al., 2012).

1.6.6.1. Regulation of mitofusin-2 in pulmonary hypertension

Mitochondrial fusion facilitates the diffusion of mitochondrial matrix content within the network, which dilutes harmful substances and minimises mitochondrial damage. This dynamic process also improves mitochondrial communication within the endoplasmic reticulum (ER) to exchange contents between mitochondrial compartments and ER, regulating calcium influx and helping to cope with oxidative damage (Valera-Alberni & Canto, 2018; Westermann, 2012).

Homolog proteins MFN1 and MFN2 were first characterized in *Drosophila melanogaster*. Mammalian MFN1 and MFN2 proteins belong to the large family of highly similar mitochondrial transmembrane GTPases (roughly 80% similar in humans), comprising 737 and 757 amino acids respectively (Figure 1.9) (Filadi, Pendin, & Pizzo, 2018).

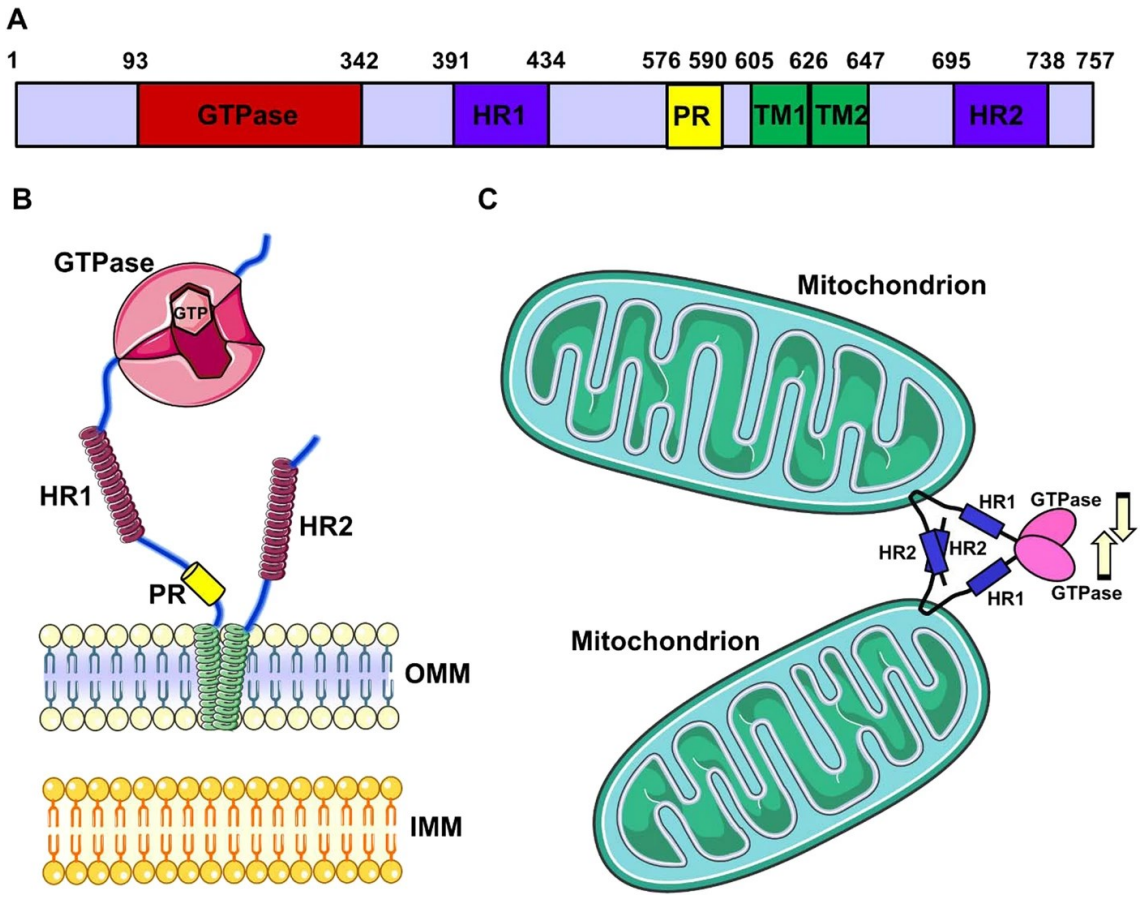


Figure 1.9: Illustration of MFN2 structure. (A) Linear structure of MFN2 consisting of the N-terminal GTPase domain sequentially followed by the HR1-domain, two TM domains (TM1,TM2) and the PR domain with the C-terminal HR2 domain. The numbers above represent the initial and the terminal amino acids of the respective domains. (B) The representation on the left shows MFN2 topology, with two very close TM domains spanning the outer mitochondrial membrane (green helices) and the GTPase domain with two GTP-binding pockets. (C) Shows the structure of the OMM-fusion activity of MFNs. Tethering is regulated by interaction between HR2 domains belonging to MFNs on opposite OMMs. Recent data suggest that the dimerization of the GTPase domains, as well as a power stroke due to GTP hydrolysis, may be essential for fusion. Abbreviations: OMM; outer mitochondrial membrane; IMM; inner mitochondrial membrane; MFN2: mitofusin-2; HR1: heptad-repeat 1; HR2: heptad-repeat 2; TM: transmembrane Illustration adapted from Filadi et al., 2018.

1.6.6.2. Mitofusin-2 function

MFN1- and MFN2-deficient cells show abnormal mitochondrial morphology with clear fragmentation of the mitochondrial network. In human disease and pre-clinical models of PAH, the downregulation of MFN2 expression is thought to contribute to excessive mitochondrial fragmentation and increased rates of PASMC proliferation (Dasgupta et al., 2011; Ryan et al., 2013).

Decreased levels of MFN2 induce apoptosis of endothelial cells in growth factor-reduced media, whereas MFN2 knockdown promotes mitochondrial fragmentation and reduces mitochondrial membrane potential (Lugus et al., 2011). In PAH, the overexpression of MFN2 increases mitochondrial fusion, inhibits cell proliferation and induces PASMC apoptosis, while the inhibition of MFN2 augments glycolysis and proliferation rate in PASMCs (Ryan et al., 2013).

MNF2 is a key regulatory protein that tethers the mitochondria to the endoplasmic reticulum (ER), essential for Ca^{2+} homeostasis, lipid biosynthesis and for the regulation of mitochondrial metabolism and apoptosis (de Brito & Scorrano, 2009). The close interaction between ER and the mitochondria is essential for efficient calcium (Ca^{2+}) transport to mitochondria. Meanwhile, Ca^{2+} uptake by mitochondria is necessary for the activation of intramitochondrial dehydrogenases and the maintenance of mitochondrial energy production (de Brito & Scorrano, 2009). It has been found that mice homozygous deficient in the MFN2 gene die in mid-gestation due to structural and functional abnormalities in the mitochondria. Constitutive or conditional deletions of MFN2 compromise mitochondrial function (Chen et al., 2005). However, the overexpression of MFN2 is beneficial for several components of the respiratory chain (Chandhok et al., 2018). MFN2 is considered to be important for mitochondrial trafficking along axons, and is involved in their attachment to microtubules via interaction with the two key

motor proteins, Miro and Milton. MFN2 also plays a crucial role in modulating other intracellular pathways including cell cycle progression, maintenance of mitochondrial bioenergetics, apoptosis and autophagy (Filadi et al., 2018).

All the factors discussed above indicate that reduced MFN2-mediated mitochondrial fusion is a common pathway in the disease pathogenesis of both human and experimental PAH. MFN2-mediated cell cycle progression is involved in both health and disease (Ryan et al., 2015). However, further studies are needed to determine the specific nature of the relationship between imbalances in fusion and fission and PAH (Boucherat et al., 2017).

1.6.7. Mitophagy changes in pulmonary arterial hypertension

The proper maintenance of the mitochondrial network is key factor in cellular homeostasis, and constant mitochondrial turnover is required to eliminate damaged and dysfunctional mitochondria. Dysregulated or defective mitochondria are selectively removed through a process known as mitophagy (Kotiadis et al., 2014). Networks normally respond to mitochondrial damage through rearrangement and fission, generating different populations of daughter mitochondria in the process of mitochondrial biogenesis. New mitochondria are also provided through the peroxisome proliferator-activated receptor γ coactivator 1-α (PGC-1α)-dependent process, which is triggered by the activation of nuclear respiratory factor 1 (NRF1) and mitochondrial transcription factor A (TFAM). TFAM promotes the transcription of mitochondrial DNA (mtDNA) (Handschin & Spiegelman, 2006; Kluge et al., 2013; Tang et al., 2014). Mitochondrial fusion and fission, mitophagy and biogenesis thus provide a unified mechanism for mitochondrial quality control. There are two distinct principal mechanisms by which mitochondria are marked for clearance, receptor-mediated mitophagy and ubiquitin-

mediated mitophagy (Figure 1.10) (Ashrafi & Schwarz, 2013; Eiyama & Okamoto, 2015; Gregg et al., 2010; Hanna et al., 2012; Yamaguchi et al., 2016).

Mitochondrial biogenesis is downregulated in PAH patients and in experimental PAH. There are several mediators that affect mitochondrial biogenesis in PH patients. It has been reported that the expression of PGC-1α, ETC subunits, and mtDNA copy numbers are reduced in PAH. Another study reported that mice that lacked endothelial BMPR2 developed PH and displayed inhibition in mitochondrial biogenesis (Dasgupta et al., 2011). The proteins that modulate mitochondrial dynamics are usually involved in mitophagy. Fission regulator DRP-1 plays a crucial role in eliminating dysfunctional mitochondria, and fusion regulator MFN2 helps to mitigate mitochondrial stress by redistributing defective DNA, proteins, and lipids within the mitochondrial network. MFN2 is also involved in the removal of dysfunctional mitochondria through selective autophagy (Chen & Dorn, 2013; Filadi et al., 2018; Shirihai et al., 2015).

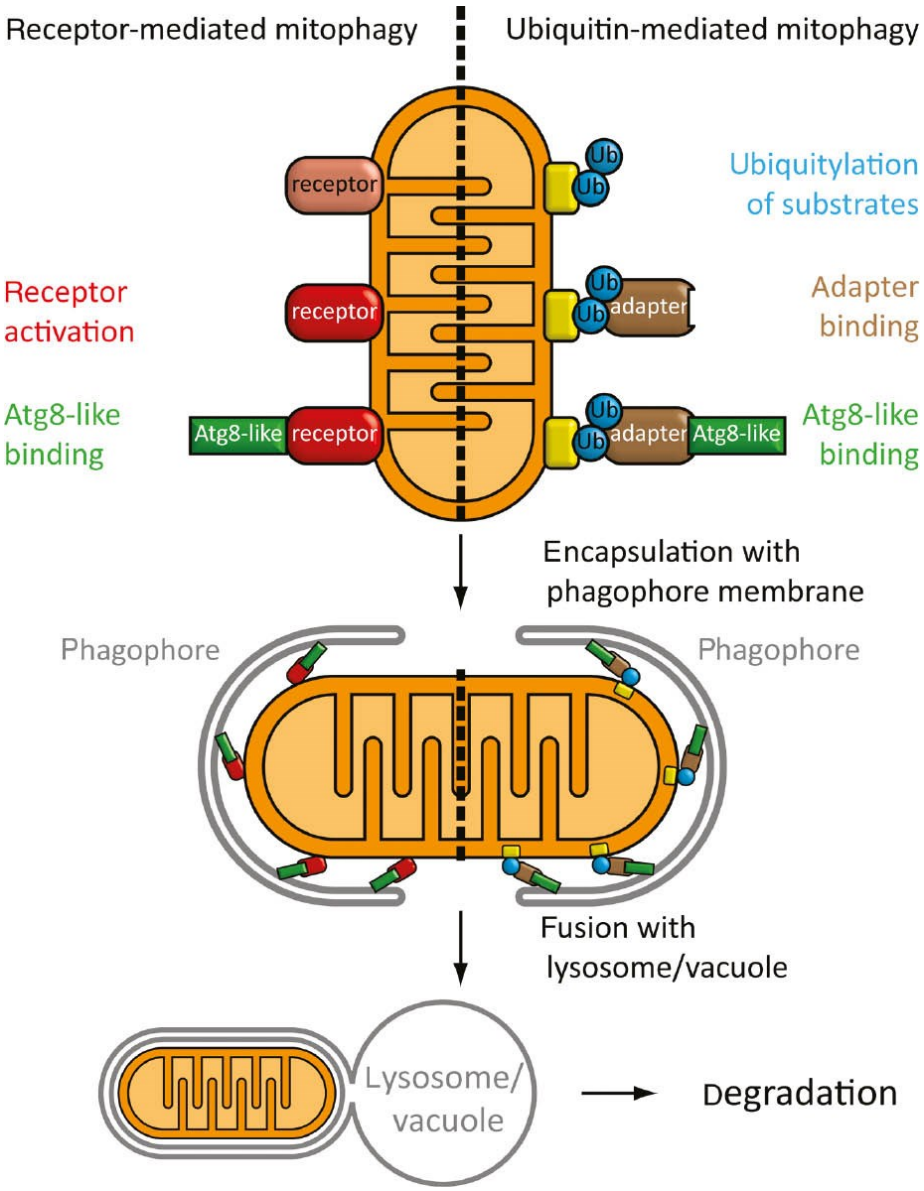


Figure 1.10: Two mitophagy mechanisms in mammalian cells. Left, receptor-regulated mitophagy is localised in the OMM and is activated by receptor phosphorylation, increasing its binding affinity for Atg8-like proteins (LC3s or GABARAPs) which are then recruited to the mitochondria. Right, the ubiquitination pathway. Highly ubiquitylated OMM-proteins recruit bifunctional adapter proteins (e.g. p62) which then recruit Atg8-like proteins. Bottom, the binding of Atg8-like proteins induces the encapsulation of mitochondria into autophagosomes through the expansion of the phagophore membrane; fusion with the lysosome results in the formation of autolysosomes, ensuring the degradation of the selected cargo. OMM: outer mitochondrial membrane. Adapted from Zimmermann & Reichert, 2017.

A large body of evidence suggests that impaired mitophagy contributes to the pathogenesis of vascular diseases, including atherosclerosis and hypertensive heart diseases. A number of studies have examined the involvement of mitophagy in endothelial cells under conditions of oxidative stress and energy deficiency. Oxidative damage induced by the mitochondria-targeted irradiation of endothelial cells induces Parkin translocation to depolarized mitochondria and upregulates LC3-II level and autophagosome formation. Beclin-1/LC3-II-mediated autophagy is also a mechanism for endothelial cells to clear ox-LDL. Taken together, autophagy and mitophagy are important ECs responses to oxidative stress (Mai et al., 2012; Tang et al., 2014; Zhang et al., 2019).

Studies show that LC3B is elevated in the lungs of hypoxic PH mice and in pulmonary artery endothelial cells (PAECs) and pulmonary artery smooth muscle cells (PASMCs) exposed to hypoxia, which is consistent with the observations in human PAH lungs (Aggarwal et al., 2016).

Dysregulated mitophagy promotes PH. In mice exposed to intermittent hypoxia, the loss of endothelial mitochondria uncoupling protein 2 (UCP2) upregulates mitophagy, suppresses mitochondrial biogenesis and increases cell apoptosis (Haslip et al., 2015). Dysfunctional mitochondria undergo DRP1-mediated fission, membrane depolarization, accumulation of phosphatase and tensin homolog-induced putative kinase 1 (PINK1), and encourage the recruitment of E3 ubiquitin ligase PARKIN, which promotes the consumption of mitochondria by autophagosomes (Youle & Narendra, 2011).

1.7. Therapeutic development of metabolic drugs in pulmonary hypertension

Since many metabolic changes in PH share similarities with cancer, metabolic therapies currently being examined for cancer may have a potential for PH. There are no approved metabolic treatments for PH, but the field is promising as the metabolic theory of PH has expanded, placing mitochondria centre stage for our understanding of metabolic dysregulation in disease pathogenesis and for the development of novel therapeutic tools. The development of novel small-molecule inhibitors, therapeutic antibodies or RNA-based therapies for PH continues to grow as new metabolic avenues are opened that extend beyond the original premise constrained by the Warburg effect (Archer et al., 2010; Tuder et al., 2012).

Metabolic dysregulation can be partially improved by inhibiting pyruvate dehydrogenase kinase, the enzyme that phosphorylates and inactivates pyruvate dehydrogenase using dichloroacetate. Pyruvate dehydrogenase activity is then restored, enabling irreversible oxidation by converting pyruvate to acetyl-CoA, which can then enter the Krebs cycle to initiate normal mitochondrial aerobic metabolism. Dichloroacetate has also been shown to prevent and reverse pulmonary hypertension by inducing pulmonary artery smooth muscle cell apoptosis and by upregulating voltage gated potassium channels (Kv1.5) in animal models of PH. Dichloroacetate is currently under investigation in a phase I clinical trial in PAH (NCT01083524) (McMurtry et al., 2004; Michelakis et al., 2002).

Alterations in the Krebs cycle and the electron transport chain are associated with changes in reactive oxygen species (ROS), which are known to control pulmonary vasodilation or vasoconstriction (Archer et al., 1986). The redox-sensitive nuclear factor erythroid 2-related factor 2 (Nrf2), for example, is a transcription factor that reduces ROS production and subsequent inflammation. In pre-clinical PH studies, Nrf2 activation has been shown to improve

mitochondrial dysregulation, reduce ROS and inflammatory signalling, and consequently improve arterial and RV remodelling. A phase II clinical study is currently under way to investigate a chemical inducer of Nrf2, bardoxolone methyl, in PAH patients (NCT02036970) (Eba et al, 2013; Wang et al., 2014).

Currently, the mainstay of investigational metabolic therapies for PH takes the form of repurposing medications already approved by the US-FDA for other diseases. The development or repurposing of metabolic tracers and medications could provide an effective avenue for preventing or reversing disease progression, and further investigation is therefore necessary for accurate diagnostic and therapeutic options for PH (Figure 1.11) (Chan & Rubin, 2017).

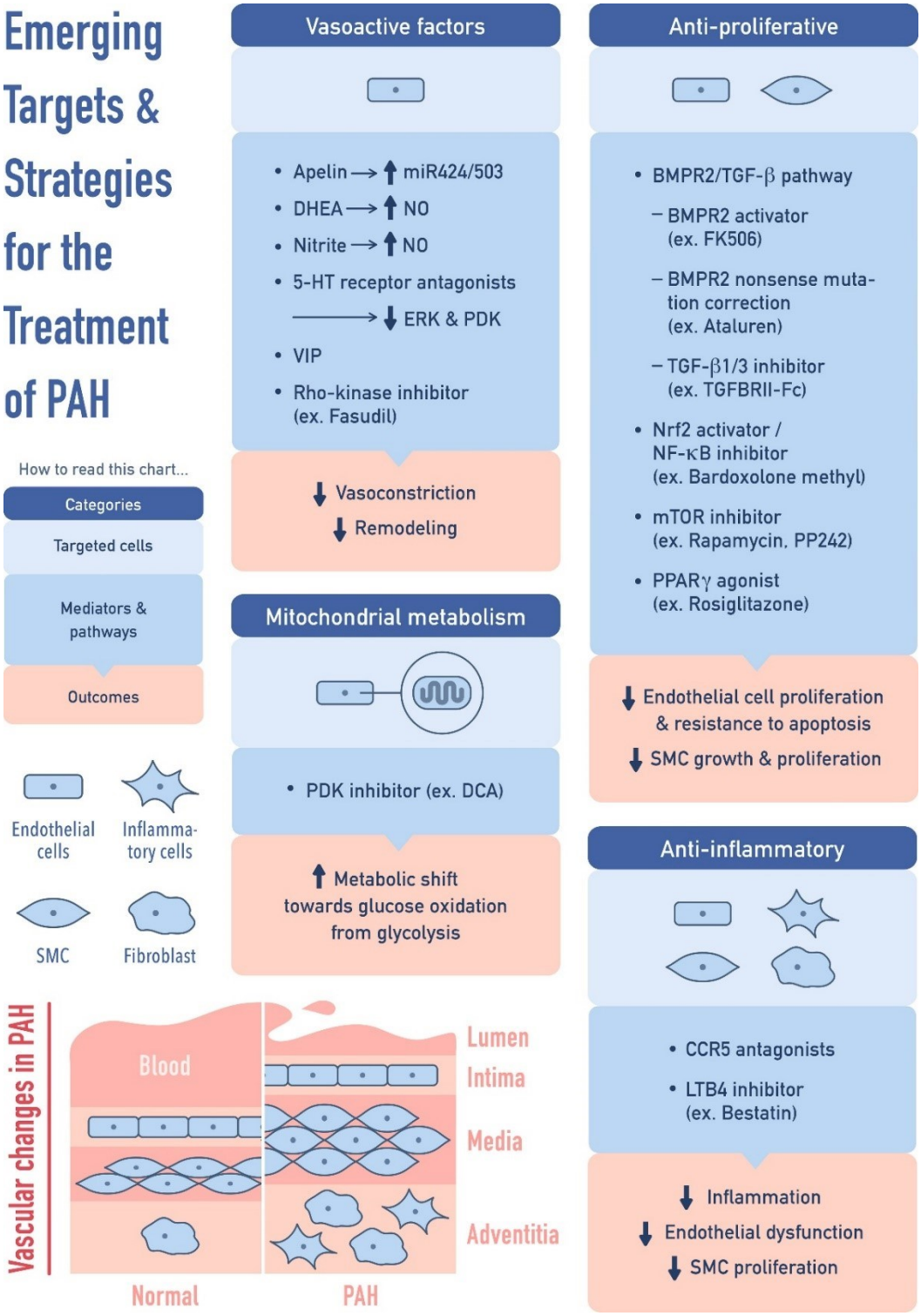


Figure 1.11: Emerging targets and therapies for PAH. The figure summarises various emerging pathways that are amenable to therapeutic manipulation. Abbreviations: TGF-β: transforming growth factor-β; SMC: smooth muscle cells; LTB4: leukotriene B4; mTOR: mammalian target of rapamycin. Adapted from Hensley et al., 2018.

1.8. Chloride intracellular channel proteins

1.8.1. The CLIC protein Family

Chloride intracellular channel proteins are a novel class of widely expressed intracellular ion channels that exist as monomeric, soluble and integral membrane proteins, where they form poorly selective anion channels (Singh et al., 2007). There are six paralogs of the CLICs family that have been identified in mammals up to date, CLIC1 - CLIC6 (Ashley, 2003; Singh, 2010).

CLIC proteins were identified using sequence homology (Chuang et al., 1999; Edwards, 1999; Heiss & Poustka, 1997) or isolating them from macromolecular complexes, as in case of CLIC3 and CLIC5 (Berryman & Bretscher, 2000; Qian et al., 1999). CLIC5 is expressed in two different splice forms: a smaller and more abundant gene product named CLIC5A (CLIC5 short), and larger gene product named CLIC5B (CLIC5 long), along with an additional unique N-terminal region that includes an SH2 domain binding site. This site, at which tyrosine is phosphorylated, can interact with Src family kinases (Edwards & Kapadia, 2000), was identified in a complex alongside cytoskeletal components (Berryman & Bretscher, 2000; Shanks et al., 2002). The best-studied isoform is CLIC5A. However, CLIC6 is the latest protein identified in the CLIC family (Friedli et al., 2003), and its high molecular mass (~72 kDa) makes it an unusual member, the function of which is unknown. Mutations in CLIC2 and CLIC5 have been linked to heart disease and deafness respectively (Seco et al., 2015; Takano et al., 2012).

CLIC proteins have also been implicated in several important cellular functions, such as membrane trafficking, cytoskeletal function (Berryman et al., 2004), apoptosis (Fernández-Salas et al., 2002; Suh et al., 2004), cell cycle control (Valenzuela et al., 2000), tubulogenesis (Berry et al., 2003), the vascular endothelial growth factor (VEGF)-mediated angiogenesis of endothelial cells (Tung et al., mitosis, and differentiation (Suh et al., 2007). Chloride channel

blocker indanyloxyacetic acid 94 (IAA94) is the only current inhibitor used in CLIC research, has a wide spectrum of intracellular targets and was initially used to identify and purify the first CLIC protein, p64/ CLIC5B (Landry et al., 1989).

1.8.2. CLIC structure

CLIC proteins are possible ion channels that belong to the p64 gene family and are members of the glutathione S-transferase (GSTs) fold family of proteins (Harrop et al., 2001). These unique features of CLICs distinguish them from other ion channel proteins.

Structural studies have reported that soluble CLICs are similar to omega-class glutathione-S-transferases (GSTs), which display a three-dimensional fold (Dulhunty et al., 2001), and contain an N-terminal thioredoxinlike domain followed by an all α-helical C-terminal domain.

The N- and C-terminal domains consist of a putative transmembrane region (PTM) and a nuclear localization signal (NLS) respectively. Each member of CLIC family comprises ~241-amino acid protein. Only CLIC5B and CLIC6 contain an additional large hydrophobic N-terminal domain. Like the omega-class of GST proteins, mammalian CLICs consist of a conserved glutaredoxin-like site (Harrop et al., 2001; Dene R Littler et al., 2005), and a reactive cysteine residue (Cys24 and Cys35 in CLIC1 and CLIC4 respectively). These unique features of CLICs suggest that CLIC functions can be controlled by redox-dependent processes (Harrop et al., 2001; D. R. Littler et al., 2004; Singh & Ashley, 2006). CLIC1 and CLIC4 share high structural similarities due to a 67 % sequence homology rate (Dene R Littler et al., 2008) (Figure 1.12).

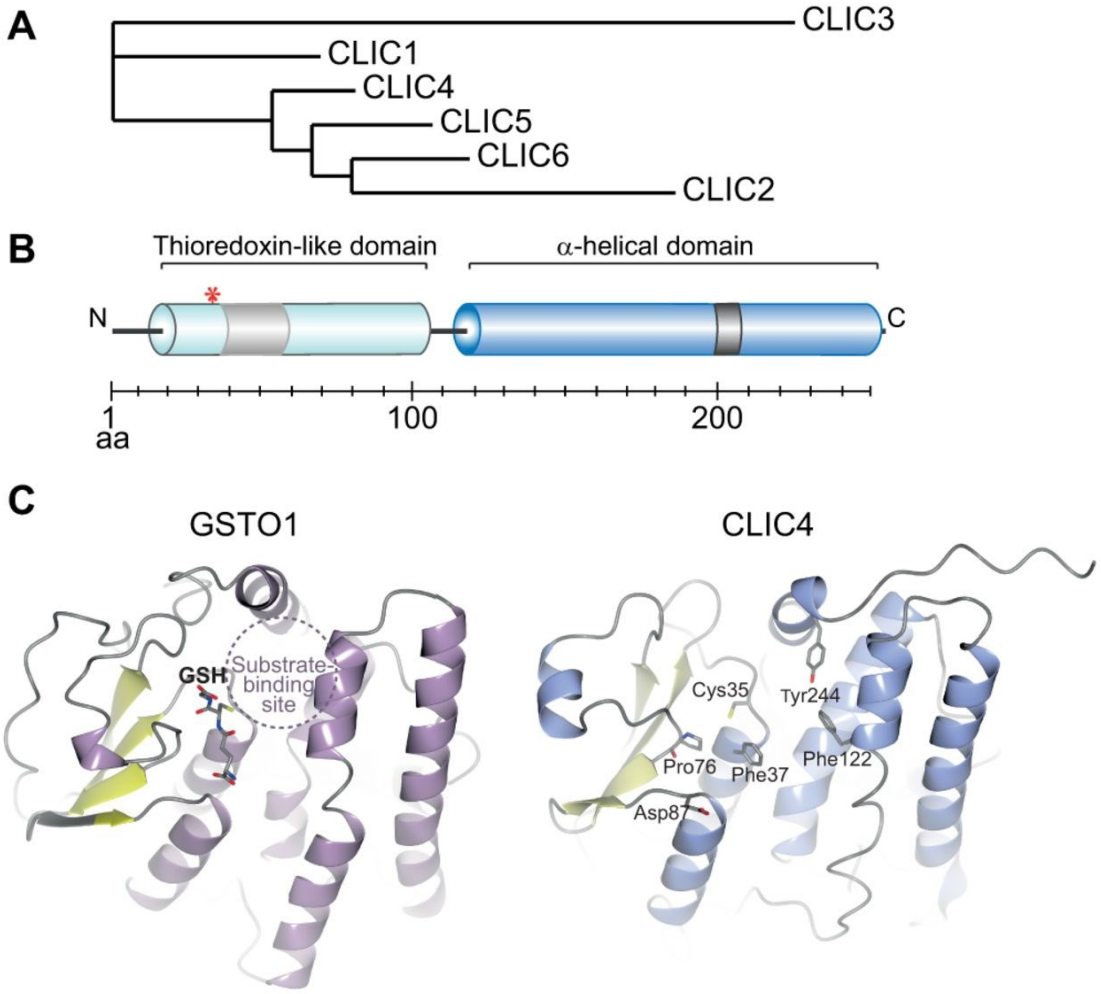


Figure 1.12: Mammalian CLIC family and structural relationship with omega-class GST (GSTO-1). (A) Phylogenetic analysis of mammalian CLIC proteins based on homology screening. CLIC proteins are 236-253 amino acids in length. CLIC5 has two isoforms, A and B, with CLIC5B (410 amino acid) having an extended N-terminal region. CLIC6 is the largest of the CLIC family (704 amino acid), and has a unique extended N-terminal region without sequence similarity to other proteins. (B) CLIC domain structure. Illustration was adapted from Argenzio & Moolenaar, 2016.

1.8.3. CLIC localization

The cellular localization of CLIC proteins has not been systematically explored due to a lack of specific antibodies, although they have been identified as intracellular ion channels. However, some CLIC localization was identified, localized to various intracellular organelles (Ponnalagu & Singh, 2016; Singh, 2010) such as nuclear membranes (Ulmasov et al., 2007; Valenzuela et al., 1997), secretory vesicles (Chuang et al., 1999), caveolae, the *trans*-Golgi network (Edwards & Kapadia, 2000), the endoplasmic reticulum, (Duncan et al., 1997; Ponnalagu et al., 2016b) and mitochondria (Edwards & Kapadia, 2000; Fernández-Salas et al., 1999; Ponnalagu et al., 2016a; Ponnalagu et al., 2016b).

CLIC2 is mainly localized in the endoplasmic reticulum of adult cardiomyocytes (Ponnalagu et al., 2016a; Ponnalagu et al., 2016b), while CLIC3 is present on placental and foetal membranes and its distribution is regulated during trimesters (Money et al., 2007).

Among all the CLIC proteins, only CLIC4 and CLIC1 are reported to be highly expressed in all endothelial cells (Bohman et al., 2005; Ulmasov et al., 2007), while CLIC5 is relatively less abundant (Money et al., 2007; Wegner et al., 2010). CLIC6 is localized in water and hormone secreting cells (Figure 1.13).

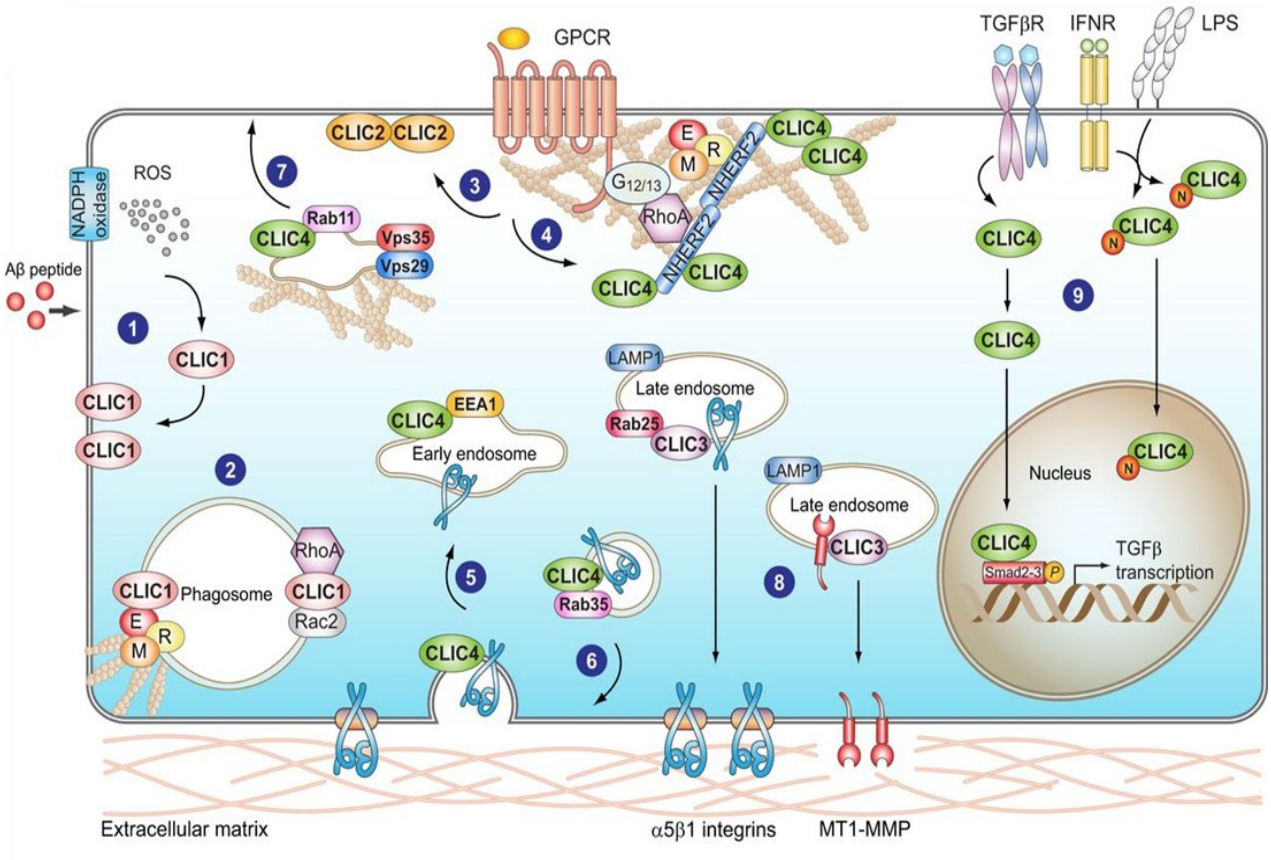


Figure 1.13: Intracellular activities and distribution of CLIC proteins. The illustration shows an overview of the cellular roles of CLIC1 to CLIC4. Aβ peptide promotes CLIC1 translocation and insertion into the plasma membrane, where it contributes to NADPH oxidase-mediated oxygen species (ROS) production. GPCR stimulates the translocation of CLIC2 and CLIC4 to the plasma membrane. TGFβ stimulates the translocation of CLIC4 into the nucleus, where it inhibits the dephosphorylation of SMAD proteins to enhance transcription. Abbreviations: Aβ ,Amyloid β; TGFβ, transforming growth factor β; GPCR, G-protein-coupled receptor. Illustration adapted from Argenzio & Moolenaar, 2016.

1.8.4. CLIC function

CLIC proteins have been implicated in several important cellular functions, including membrane trafficking, cytoskeletal function (Berryman et al., 2004), apoptosis (Fernández-Salas et al., 2002; Suh et al., 2004), cell cycle control (Valenzuela et al., 2000), tubulogenesis (Berry et al., 2003), Vascular endothelial growth factor (VEGF)-mediated angiogenesis of endothelial cells (Tung et al., 2009), mitosis and differentiation (Suh et al., 2007).

Recent studies show that CLIC2 participates in modulating the function of ryanodine receptors (RyR1 and RyR2). Other functional roles of CLIC2 remain unknown (Board et al., 2004; Takano et al., 2012). It has been considered that CLIC3 interacts with extracellular signal-regulated kinase (ERK7), and that it may also play a role in chloride movement and the regulation of cellular processes (Singh, 2010).

A recent study also revealed that the abrogation of CLIC5 increased ROS generation of cardiac mitochondria in mice (Ponnalagu et al., 2016a). Meanwhile, CLIC4 and CLIC5 also interact with filamentous (F)-actin, which can control the activity of ion channels, suggesting that CLIC can be specifically activated when the cell undergoes physiological changes such as cell cycle apoptosis. CLIC6 may play a role in the regulation of water and hormone secretion in cells (Singh, 2010; Singh et al., 2007).

1.8.5. CLIC in PAH

CLICs have been identified as new mediators of vascular dysfunction in PAH (Abdul-Salam et al., 2010; Wojciak-Stothard et al., 2014). CLIC1 and CLIC4 are highly expressed in animal and human PAH lungs and are elevated in plasma and blood-derived endothelial colony-forming cells (ECFCs) from PAH patients. CLIC1 and CLIC4 localise to the vascular endothelium, particularly in plexiform lesions, but can also be found in other vascular layers in the remodelled pulmonary vasculature (Wojciak-Stothard et al., 2014). CLIC5 levels are found to be low in placental endothelial cells (Money et al., 2007) but high in glomerular endothelial cells (Wegner et al., 2010). CLIC1, CLIC4 and CLIC5 are the most abundant CLIC transcripts present in the heart (Singh et al., 2007).

This study focuses predominantly on the role of CLIC1 and CLIC4 in the regulation of mitochondrial function, as increased expression of these proteins has been linked to vascular dysfunction in PAH (Abdul-Salam et al., 2010). CLIC5 has been studied to a more limited extent, and has been identified as a component of cardiac mitochondria. A brief overview of tissue distribution and the function of all CLIC proteins is provided in Table 1.4 at the end of this chapter.

1.8.6. Chloride intracellular channel 1

Chloride intracellular channel 1 (CLIC1), is expressed extensively in epithelial and non-epithelial cells, where it shows tissue-specific distribution and sub-cellular localization. Low levels of CLIC1 expression exist in the skeletal muscle and brain (Singh, 2010). In activated human macrophages, CLIC1 is cloned based on its enhanced expression, and is greatly conserved across several species (Ulmasov et al., 2007; Valenzuela et al., 1997). CLIC1 shows a wide tissue and subcellular distribution in mammalian cells, and is present in the cytoplasm and nucleoplasm in a soluble form under normal conditions. In contrast, under oxidizing conditions, CLIC1 is subjected to structural reorganization, undergoing membrane insertion within the plasma membrane and the nuclear membrane (Edwards & Kapadia, 2000; Fernández-Salas et al., 1999; Littler et al., 2004; Ong et al., 2015; Suh et al., 2005). The expression of CLIC1 vary in different stages of the cell cycle process, suggesting that the protein may contribute to the regulation of cell volumes (Valenzuela et al., 2000). In response to cellular stress, CLIC1 is transferred to the cell membrane and inserted into lipid membranes to form a functional chloride ion channel (Singh & Ashley, 2006; Valenzuela et al., 1997).

CLIC1 is involved in the regulation of diverse cellular pathways, including cell-signalling, cell-cycle regulation, endocytosis, exocytosis, and is known to be involved in the pathogenesis of

pulmonary arterial hypertension (Laudi et al., 2007; Y. Xu et al., 2016). CLIC1 is also involved in the stabilization of cell membrane potential, the maintenance of intracellular pH, and cell proliferation and differentiation (Harrop et al., 2001; Liao & Chang, 2012). CLIC1 overexpression increases cell proliferation, migration, invasion and tumour engraftment (Wojciak-Stothard et al., 2014).

The N-terminal domain of CLIC1 includes a binding site for a reduced form of glutathione (GSH) (Dulhunty et al., 2001). Evidence from several studies shows that CLIC1 acts as a sensor for cell oxidation (Averaimo et al., 2010; Littler et al., 2004; Novarino et al., 2004).

Macrophages exhibit decreased CLIC1 expression which suppressed tumour necrosis factor α (TNF-α) levels (Martínez-Solano et al.,2009). Previous studies have also shown that disruption of the CLIC1 gene in mice leads to mild platelet dysfunction (Qiu et al., 2010) and compromised phagosome acidification in macrophages and dendritic cells (Jiang et al., 2012; Salao et al., 2016). These data indicate the importance of CLIC1 in regulating macrophage function via its ion channel activity, so CLIC1 is considered to be a suitable target for the development of anti-inflammatory drugs (Jiang et al., 2012).

1.8.7. Chloride intracellular channel 4

Chloride intracellular channel 4 (CLIC4) is characterized as a putative mitochondrial ion channel protein, and proved to exist in mitochondria of keratinocytes (Fernández-Salas et al., 2002; Szabo & Zoratti, 2014), where it is involved in the Ca^{2+} induced differentiation of keratinocytes. CLIC4 is also known as mitochondrial CLIC4 (mtCLIC4) (Misak et al., 2013; Suh et al., 2007). Recent studies have confirmed that CLIC4 and CLIC5 are cardiac mitochondrial proteins which are localized to the outer mitochondrial membrane, where they regulate the endothelial function. Furthermore, the overexpression of CLIC4 in keratinocytes induces its mitochondrial

localization and reduces mitochondrial membrane potential, thereby triggering apoptosis (Fernández-Salas et al., 2002). It has also been shown that the suppression of CLIC4 enhances H_2O_2-induced glioma cell apoptosis (Xu et al., 2013). CLIC4 expression is also elevated in breast cancers and in myofibroblasts that form stroma (Rønnov-Jessen et al., 2002).

CLIC4 is most abundantly expressed in endothelial cells, specifically in the plexiform and occlusive lesions that are characteristic of PAH. It is also expressed in macrophages and keratinocytes (Edwards & Kapadia, 2000; Fernández-Salas et al., 1999; Ong et al., 2015; Suh et al., 2005; Tuder & Voelkel, 2002). CLIC4 is localised to endocytotic vesicles, lysosomes, Golgi apparatus and the endoplasmic reticulum (Edwards & Kahl, 2010). CLIC4 induces a pseudo-hypoxic state in HPAECs, which is characterised by the activation of HIF and the increased expression of HIF-dependent proteins, including ET-1, VEGF and glycolytic enzymes (Wojciak-Stothard et al., 2014). CLIC4 expression is influenced by transforming growth factor- β (TGF-β), TNF-α, oxidative stress and DNA damage and cytokines (Suh et al., 2005; Yao et al., 2009).

The depletion of CLIC4 has a protective effect on null mutant mice, which do not develop PH when exposed to hypoxia (Wojciak-Stothard et al., 2014). In patients with PAH, CLIC4 expression levels are raised in the lung tissues, compared with lung tissues from healthy donors (Wojciak-Stothard et al., 2014). High levels of CLIC4 indicate early signs of endothelial dysfunction in PAH (Wojciak-Stothard et al., 2014), while in HPAECs, CLIC4 overexpression induces pro-angiogenic effects (Marshall et al., 2018).

Proteomic analysis has identified numerous CLIC4-interacting proteins that are involved in vesicular transport, including GAP proteins (GIT1 and GIT2), clathrin heavy chain, dynein, actin crosslinking proteins and tubulin. A novel effector of CLIC4 named ADP Ribosylation Factor 6 (Arf6) was proposed as a new therapeutic target in PH (Abdul-Salam et al., 2019). As well as

showing angiogenic defects, CLIC4 has been reported to play a role in the regulation of epithelial cell adhesion and morphology in a rat retinal detachment model. The knockdown of CLIC4 in pigment epithelium cells *in situ* results in a reduction in retinal adhesion, F-actin redistribution, and a loss of apical microvilli and basal infoldings, which is important in epithelial-mesenchymal transition (EMT) phenotype (Chuang et al., 2010). These effects of CLIC4 knockdown are associated with altered transmembrane transport mechanisms, leading to the accumulation of subretinal fluid (Argenzio & Moolenaar, 2016).

CLIC4-null mice are smaller and display more still-births than wild-type animals (Ulmasov et al, 2009). Deficiencies in CLIC4 lead to the impairment of tubulogenesis and vacuole formation in both endothelial and renal epithelial cells (Chou et al., 2016; Ulmasov et al., 2009). CLIC4 was reported as being present in the midbody and centrosome of cultured bovine aortic endothelial cells as well as at the cell-to-cell junctions, suggesting its involvement in establishing or maintaining cell polarization (Berryman & Goldenring, 2003). The discovery of the involvement of CLIC4 in PH is important and strongly supports the role for CLIC4 in lung remodelling (Gururaja Rao et al., 2020).

1.8.8. Chloride intracellular channel 5

Chloride intracellular channel 5 (CLIC5) was the first mitochondrial chloride channel to be identified in the inner mitochondrial membrane in adult cardiomyocytes, although regulatory mechanisms between CLIC5 activity and mitochondrial function are not well understood (Ponnalagu et al., 2016b). CLIC5A is known to interact with cytoskeletal proteins and its channel activity can be regulated by F-actin either through direct blocking of the pore or indirectly by removing the channel from the membrane (Kader et al., 2014). CLIC5B is localized mainly in osteoclasts and bone marrow cells, where it plays a crucial role in the process of acidifying

osteoclast vesicles. Osteoclast bone restoration and chloride conductance plays a major role in the stabilization of the resting membrane potential (Valenzuela et al., 2013).

It has been reported that CLIC5 is associated with a radixin–actin cytoskeletal complex in the inner earstereocilia, where it may play a role in forming or stabilizing connections between the plasma membrane and the actin bundle of the stereocilium (Gagnon et al., 2006). In stereocilia, CLIC5 may be involved in cytoskeletal assembly, protein localization and signal transduction. CLIC5 was involved in cellular ROS generation, which was recently found to contribute to mitochondrial stress and the activation of inflammasome to regulate inflammatory response (Tang et al., 2017). CLIC5B is believed to be present in human orthologue of bovine p64 (Valenzuela et al., 2013).

Table 1.4: An overview of CLIC proteins family. The table lists tissue distribution and the gene knockout phenotype is given along with the known function for human CLICs (Argenzio & Moolenaar, 2016).

CLIC	Expression*	Biological function	Somatic mutation	Gene knockout phenotype	References
***C. elegans* EXC-4**	—	Tubulogenesis	—	Defective formation of excretory canal	Argenzio & Moolenaar, 2016
Mammals CLIC1	Wide (not in brain)	Ion channel activity, phagosomal acidification	—	Mild platelet dysfunction, less phagosomal acidification, resistance to rheumatoid arthritis, reduced autoimmune encephalomyelitis	Argenzio & Moolenaar, 2016; Ashley, 2003; Ponnalagu & Singh, 2016
CLIC2	Heart and liver	Ryanodine receptor (RyR) activity modulation	H101Q Implicated in RyR activity	—	Argenzio & Moolenaar, 2016; Ashley, 2003; Dulhunty et al., 2011

CLIC3	Skeletal muscle, heart, kidney, lung and placenta	Endosomal trafficking	—	Slightly reduced phagosomal acidification in macrophages	Ashley, 2003; Kim et al., 2013; Money et al., 2007
CLIC4	Wide (not in T cells)	Angiogenesis, vacuole formation, vesicle acidification, integrin trafficking	—	Reduced body weight at birth. More stillbirths, impaired endothelial and renal tubulogenesis. Impaired vacuolar acidification and fusion, defective wound healing and cornea. Mice protected from LPS induced death	Ashley, 2003; Duncan et al., 1997; Fernández-Salas et al., 1999; Ponnalagu & Singh, 2016
CLIC5A	Kidney, heart, inner ear, lung, colon and placenta	Membrane-ERM interaction in cilia. Maintenance of podocyte and glomerular architecture. Actin-dependent membrane remodelling	c.96T>A (p.Cys32Ter). Loss of CLIC5 segregates with hearing loss.	Also known as jitterbug mouse. Progressive hearing loss and vestibular dysfunction, altered podocyte morphology, renal dysfunction, proteinuria	Argenzio & Moolenaar, 2016; Ponnalagu & Singh, 2016; Tavasoli et al., 2016
CLIC5B	Kidney, heart, bone morrow and skeletal muscle	Actin-dependent membrane remodelling, osteoclast differentiation	—	—	Edwards & Kahl, 2010; Redhead et al., 1997
CLIC4 and CLIC5	—	—	—	Development of spontaneous proteinuria, glomerular cell proliferation and matrix deposition.	Tavasoli et al., 2016
CLIC6	Bronchial epithelial cells, kidney, brain, gastric mucosa and choroid plexus*	Unknown	—	—	(Ashley, 2003; Nishizawa, Nagao, Iwatsubo, Forte, & Urushidani, 2000)

1.9. Main hypothesis and project aims

1.9.1. Hypothesis

CLIC proteins induce mitochondrial dysfunction in human pulmonary arterial endothelial cells (HPAECs) *in vitro*, consistent with pathological changes seen in PAH (Figure 1.14).

1.9.2. Study aims

- To confirm the mitochondrial localization of CLIC1 and CLIC4 proteins in HPAECs.
- To determine the effect of CLIC overexpression on mitochondrial dynamics, including mitochondrial content, fusion and fission, mitophagy and the organization of actin and microtubule cytoskeleton in control and CLIC-overexpressing human pulmonary artery endothelial cells (HPAECs).
- To study the effect of CLIC overexpression on mitochondrial structure.
- To determine the effect of CLIC proteins on mitochondrial function i.e. mitochondrial membrane potential, and mitochondrial ROS production in HPAECs.
- To study the effect of CLIC proteins on energy metabolism in HPAECs *in vitro*.
- To characterise effects of CLIC1 and CLIC4 on mitochondrial protein expression profile utilising mitochondrial proteomic analysis.
- To identify signalling mediators of CLIC proteins affecting mitochondrial structure and function.
- To establish the role of MFN2 as a mediator of CLIC1/CLIC4-induced changes in mitochondrial dynamics and function.
- To determine changes in CLIC protein expression and mitochondrial distribution/biogenesis/energy metabolism in blood-derived endothelial colony-forming cells from healthy volunteers and PAH patients.

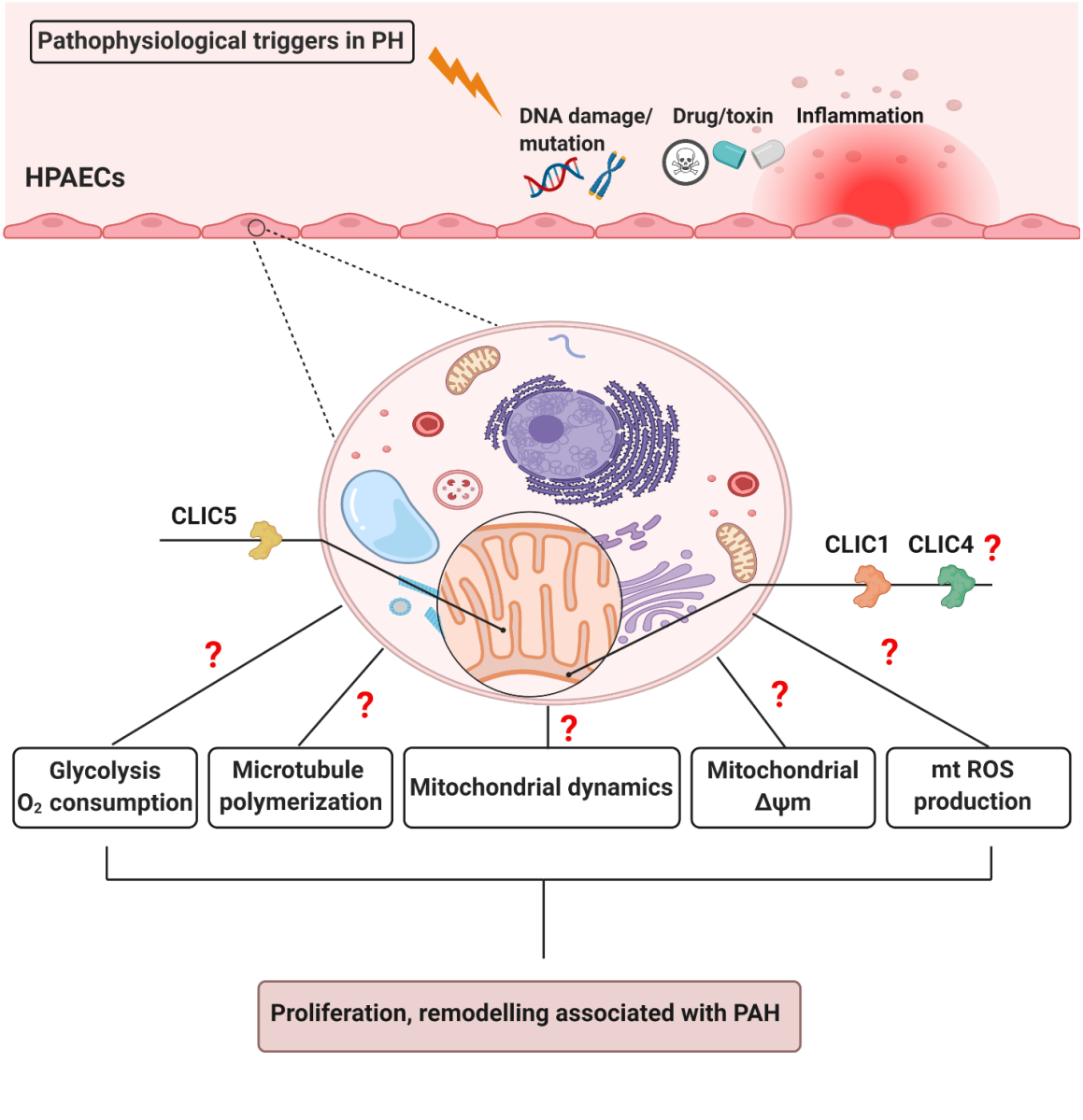


Figure 1.14: Hypothesized role of CLIC proteins in the regulation of mitochondrial function in PAH endothelium. CLIC1 and CLIC4 are highly expressed in PAH endothelium. CLIC1 and CLIC4 overexpression affects glycolysis, O_2 consumption, microtubule polymerization, the levels of proteins regulating mitochondrial dynamics, mitochondrial ROS (mtROS) production and mitochondrial membrane potential: Δψm.

CHAPTER 2

Materials and Methods

CHAPTER 2: Materials and Methods

2.1 Cell culture techniques

2.1.1 Cell culture

All cell culture experiments were carried out under sterile conditions using class II biological safety vertical laminar flow cabinet.

2.1.1.1 Human Pulmonary Artery Endothelial Cells.

Human Pulmonary Artery Endothelial Cells (HPAECs) that had been isolated from the main human pulmonary artery (left and right branches) were purchased from Promocell (Germany, c-12241) at passage 3. See Table 2.1 for more information about HPAEC donors.

The cells were cultured in Endothelial Cell Basal Medium-2 (Promocell, Germany, C-22211) supplemented with Endothelial Cell Growth Medium-2 (EGM2) Supplement Pack (Promocell, Germany, C-39211) (see Table 2.2 for further details), penicillin (100 U/mL) and streptomycin (100 µg/mL; Thermo Fisher Scientific, UK, 15140). The cells were cultured in tissue culture flasks (T75) (Sarstedt, Germany, 83.3911.002) pre-coated with bovine plasma fibronectin (10 µg/mL; Thermo Fisher Scientific, UK, 33010018) and incubated in a humidified incubator (20% O_2 and 5% CO_2, 37°C). Endothelial cell growth medium was replaced with a fresh medium every third day. The cells were used for experiments between passages 4-10, and displayed a cobblestone-like morphology, typical for endothelial cells.

Table 2.1: Human pulmonary artery endothelial cells used in cell experiments. Table indicates HPAECs donors, age, gender, and doubling time in hour.

Lot #	Age	Gender	Doubling Time
431Z031	23	Female	48.3h
433Z034	34	Female	23.6h
433Z034.1	34	Female	55.4h
433Z034.2	34	Female	58.1h
451Z031.14	68	Male	25.4h
458Z016.12	51	Female	28.5h

2.1.1.2 Blood-derived human endothelial cells

All investigations were conducted in accordance with the Declaration of Helsinki ethical principles of research. Venous blood samples were obtained with the approval of the Brompton Harefield & NHLI and Hammersmith Hospitals Research Ethics committees and informed written consent was obtained from healthy volunteers (n=14) and patients with idiopathic PAH (IPAH, n=12) (Table 2.3).

50 mL of peripheral blood samples from each participant were collected in EDTA vacutainers (blood collection tubes). Samples were diluted 1:1 with sterile PBS containing 0.2% EDTA and 2% FBS and layered on top of a Ficoll Plaque PLUS solution (GE Healthcare, Amersham, UK) for density gradient centrifugation. Tubes were centrifuged for 20 minutes at 1000 g and the buffy coat mononuclear cells (MNCs) (the white layer located between the Ficoll solution border and the aqueous phase – see Figure 2.1) was carefully aspirated, washed once with PBS and centrifuged for 7 minutes at 540 x g. The supernatant was discarded and the cellular pellet re-suspended in 5 mL of EGM-2 medium supplemented with growth factors, 20% FBS and 1% antibiotic and antimycotic solution (Gibco, Invitrogen, Paisley, UK). MNCs were seeded in 6-well

plates that had been pre-coated with type 1 rat tail collagen (BD Biosciences, Bedford, MA, USA) at a density of 3-5 × 10^7 in 4 mL of EGM-2 medium per well. The culture medium was replaced daily for the first week to eliminate non-adherent cells, and every 48 hours thereafter.

Most of the colonies appeared between days 14 and 28. However, earlier and later growth was also observed. Individual colonies were collected using an attaching cloning cylinder (8 or 10mm in diameter) (Millipore, Watford, UK) with vacuum grease. Pre-warmed 0.05% Trypsin-EDTA solution was used to remove all the cells from the inside of the cylinder. Detached cells were re-suspended in a fresh EGM-2 medium, seeded at 3000–5000 cells per cm^2 in 1% gelatin pre-coated culture vessels and sub-cultured when 70–80% confluent. Distinct colonies of cells were observed, capable of sequential proliferation for at least 8 serial passages and clonal growth. Cells displayed a stable population doubling time and endothelial phenotype, and were used between passages 4 to 7.

The culture identity of blood-derived endothelial colony-forming cells (ECFCs) was confirmed with a cobblestone-like morphology that is typical of mature endothelial cells. Specific markers were also applied to confirm endothelial cell lineage, FITC-conjugated Ulex europaeus agglutinin-1 (UEA-1) lectin, mouse monoclonal anti-human CD31 (JC/70 A, Dako, Glostrup, Denmark), anti-human VE-Cadherin (sc-9989, Santa Cruz Biotechnology, Santa Cruz, CA) and rabbit polyclonal anti-human von Willebrand factor (A0082, Dako), with Alexa-488 green-conjugated secondary antibodies. A three-colour FACSCalibur flow cytometer and CellQuest Pro software (BD Biosciences, Oxford, UK) were applied to analyse the stained cells by flow cytometry (Martin-Ramirez et al., 2012; Sindi et al., 2020).

Table 2.2: Endothelial Cell Growth Medium-2 supplements.

Media supplement	Final supplement concentration
Fetal Calf Serum	0.02 mL / mL
Epidermal Growth Factor	5 ng / mL
Basic Fibroblast Growth Factor	10 ng / mL
Insulin-like Growth Factor	20 ng / mL
Vascular Endothelial Growth Factor 165	0.5 ng / mL
Ascorbic Acid	1 µg / mL
Heparin	22.5 µg / mL
Hydrocortisone	0.2 µg / mL

Table 2-3: Demographics of IPAH patients and healthy volunteers. Data represented as median (range). mPAP; mean Pulmonary Arterial Pressure; ER, Estrogen-Receptor; PDE5; Phosphodiesterase type 5.

		Control (n=14)	***IPAH (n=12)***
Male/Females		3/11	1/11
Age (years)		30.0 (23.0 - 45.0)	38.33 (27.0 - 67.0)
Time from diagnosis (months)		-	13.0 (0.1 - 60.0)
mPAP (mmHg)		-	65.0 (28.0 - 94.0)
Six minute walk distance (m)		-	396.0 (300.0 – 540.0)
WHO Functional Class	I	-	1
	II	-	3
	III	-	5
	IV	-	3
Treatment Naïve		-	2
Warfarin		-	4
Calcium Antagonists		-	1
ER Antagonists		-	7
PDE5 Inhibitors		-	8
Prostanoids		-	4
Statins		-	0

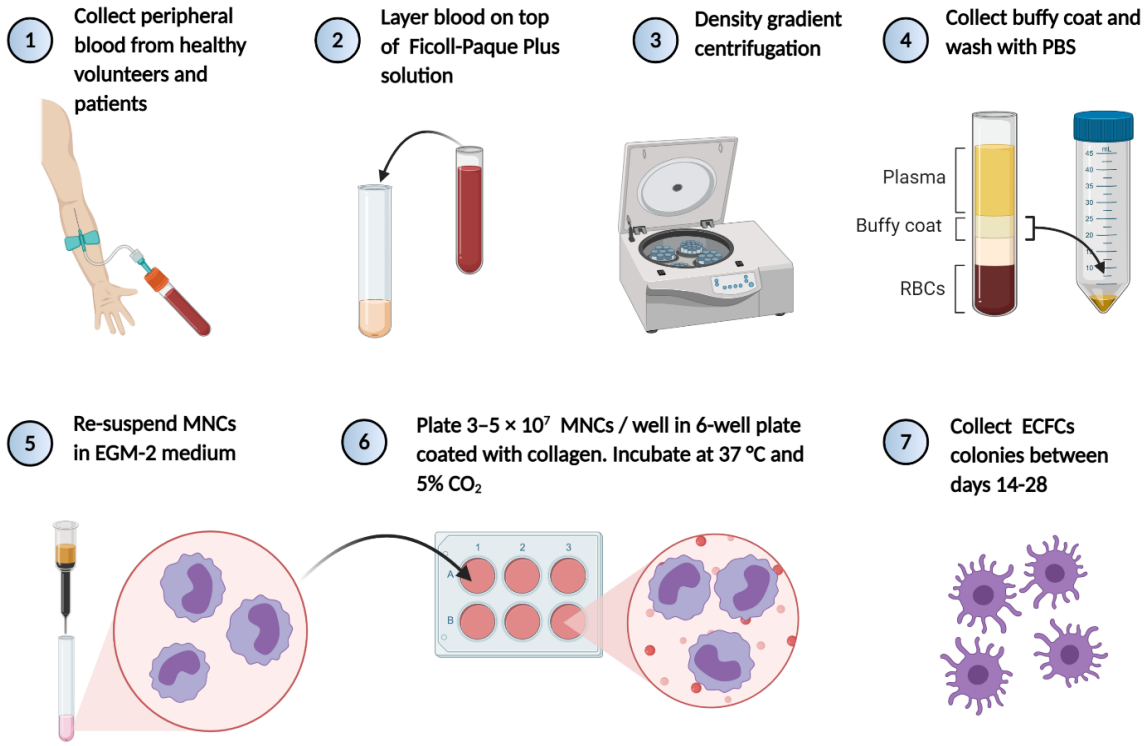


Figure 2.1: Establishing blood-derived endothelial colony forming cells from peripheral blood samples. The illustration shows the process of isolating ECFCs from human blood samples from healthy donors and PAH patients. Abbreviations: MNCs, mononuclear cells; ECFCs, blood-derived endothelial colony forming cells. Illustration created by the author using BioRender.com.

2.1.2 Sub-culturing cells

In order to passage cells, 80% confluent cell cultures growing in T-75 flasks (Sarstedt, Germany) were washed twice in 5 mL of pre-warmed sterile phosphate buffered saline (PBS) (Sigma-Aldrich, UK, D8537-500ml) and were then trypsinised with 5 mL of Trypsin-EDTA solution containing 0.05% trypsin and 0.01% EDTA (Gibco™ Trypsin, 25300104) for 3 minutes at room temperature. The flasks were then tapped gently to dislodge cells and 5 mL of Dulbecco's Modified Eagle's Medium (DMEM; Sigma-Aldrich, UK, D6429) containing 10% foetal bovine serum (FBS; Thermo Fisher Scientific, UK, 10270098) and penicillin-streptomycin was added to

the flask to inactivate trypsin. The cell suspension was collected in 50 mL Falcon tubes and centrifuged at 1500 x g for 5 minutes. The supernatant was discarded and the cell pellet was re-suspended in fresh culture media. The cells were split in a 1:3 ratio. For experiments, cells were seeded either in tissue culture flasks or in 6- or 24-well cell culture plates (Sarstedt, Germany, 83.3920, 83.3922) as required. Further details regarding cell culture conditions in different assays are provided in sections 2.1.1.1 and 2.1.1.2.

2.1.3 Establishment and storage of cells

Thawing procedure- upon removal from -80°C/liquid nitrogen storage, HPAECs/ECFCs were defrosted in a 37°C water bath and carefully poured to 10 mL supplemented culture media. Cell suspension was then transferred to a T75 tissue culture flask and placed in a humidified incubator at 37°C, 5% CO_2. Culture media were changed after 2 hours to allow sufficient cell attachment. Cultures were then maintained and sub-cultured as described in Section 2.1.2.

Freezing procedure - cells were frozen in liquid nitrogen to generate stocks with low passage numbers. Cells of passages 3-4 were grown to 80% confluency, trypsinized and pelleted as described in Section 2.1.2 and then re-suspended in cell freezing medium-DMSO (ThermoFisher Scientific), supplemented with 10% FBS. Cell suspension was aliquoted into 1.5 mL cryotubes (Thermo Fisher Scientific, UK, 5011-0020) and placed in a Nalgene™ Cryo 1°C freezing container overnight at -80°C. Cell stocks were transferred to a liquid nitrogen tank for indefinite storage.

2.2 Manipulation of protein expression in cells by adenoviral gene transfer

Overexpression of human chloride intracellular channel-1, -4, and -5 (CLIC1, CLIC4, CLIC5), mitofusin-2 (MFN2) was achieved by adenoviral gene transfer. AdTet-off was used as an adenoviral control (AdCTRL). The silencing of CLIC expression was achieved by the adenoviral gene transfer of CLIC1 and CLIC4 small hairpin RNA (shRNA), co-expressed with green fluorescent protein (GFP).

2.2.1 Adenoviral constructs

Short (sh) and long (L) isoforms of AdCLIC5, AdCLIC1 and AdMFN2 were purchased from Vector Biolabs (Philadelphia, USA) (please see Supplementary Figures S.1, S.2, and S.3 for adenoviral vectors map), while AdCLIC4 and AdTet-off were a kind gift from Professor Stuart Yuspa (National Cancer Institute, NIH, Bethesda, USA) a detailed procedure of its construction is described in (Suh et al., 2004).

Recombinant human adenoviral (Ad) constructs used in this study were generated using backbone vectors (Ad5 ΔE1/ΔE3) with target protein expression driven by a cytomegalovirus (CMV) promoter. The Tet-off gene expression system was used to achieve the expression of the AdCLIC4 gene.

Since the early three (E3) regions of the adenovirus are not involved in the replication of the virus, the E3 region was deleted to accommodate larger recombinant genes (up to 8 Kb).

AdCLIC1, AdCLIC4, and AdMFN2 were haemagglutinin-tagged (HA), while AdCLIC5 (sh and L) was c-terminally tagged with Myc epitope to ensure the precise localization of the recombinant proteins within cells.

The adenovirus construction process consisted of five steps: (i) cloning the gene of interest (GOI) into appropriate vectors, (ii) transferring the entire expression cassette into the adenoviral vector, (iii) generating the first production of low-titre virus stock, (iv) virus amplification and concentration achieved by transfecting the recombinant adenoviral DNA into packaging cells and (v) virus titration (Figure 2.2).

2.2.2 Adenoviral multiplication and purification

The adenoviruses used in this study were multiplied in human embryonic kidney cells type A (HEK293A; Sigma-Aldrich, UK, 85120602), concentrated by centrifugation in caesium chloride and titrated. Purification was carried out by Dr Beata Wojciak-Stothard (Sindi et al., 2020). The titre of all adenoviruses was established as ~2 x 10^{11} pfu (plaque forming units)/mL.

2.2.3 Cell infection

At 80% confluency, HPAECs grown in 6- or 24-well cell culture plates or Thermanox® Plastic Coverslips (13 mm; Thermo Fisher Scientific, UK, 12-565-88) were infected with AdCLIC1, AdCLIC4, AdCLIC5/AdMFN2 or AdCTRL at a multiplicity of infection (MOI) of 1:100. After 2 hours, the media were changed and cells were then incubated for 24 hours at 37°C, 5% (v/v) CO_2, prior to further experimentation.

For CLIC protein silencing, CLIC1- and CLIC4- specific small hairpin RNAs (shRNAs) were expressed in HPAECs by adenoviral gene transfer 48 hours prior to experimentation. Scrambled (non-targeting) shRNA co-expressed with GFP (AdshRNA-GFP), served as adenoviral infection controls (please see Supplementary Figures S.4 for adenoviral shRNA map). HPAECs were grown in 6-well plates and were infected with AdshCLIC1 and AdshCLIC4 at different dilutions to establish an optimal MOI. Changes in CLIC expression were evaluated by western blotting 48 hours post-infection.

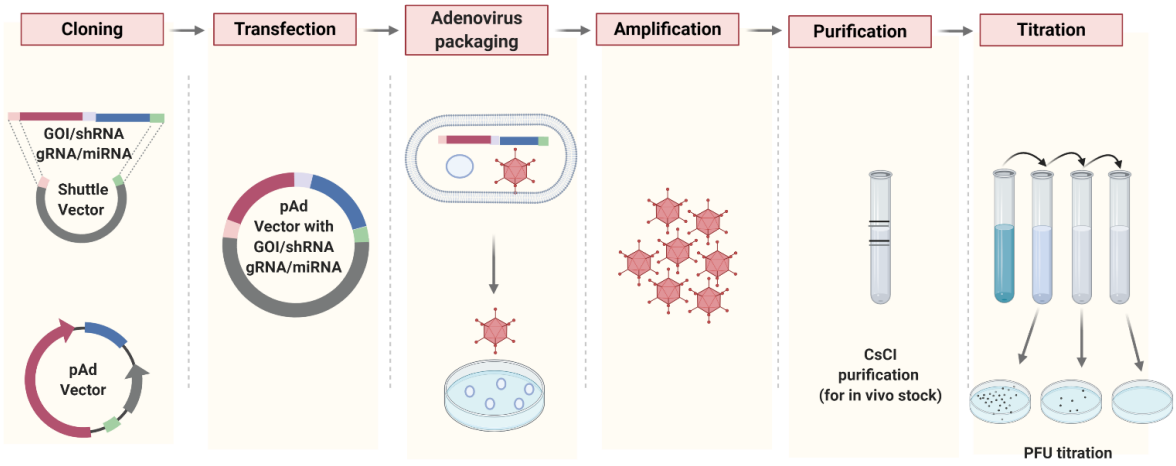


Figure 2.2: Illustration of the adenovirus construction process. The adenovirus construction process goes through five steps: (i) Cloning the gene of interest (GOI) into appropriate vectors. (ii) Transferring the entire expression cassette into the adenovirus genome vector. (iii) Generation of the first production of low-titre virus stock. (iv) Virus amplification and concentration achieved by transfecting the recombinant adenoviral vectors into packaging cells. (v) Virus titration. Illustration created by the author using BioRender.com (Modified from www.vectorbiolabs.com).

2.3 Transmission electron microscopy

2.3.1 Preparation of culture dishes, cell culture and fixation

Solutions and buffers were prepared prior to fixation:

1- To prepare 200 mL of 0.4M PIPES solution (piperazine-N,N'-bis[2-ethanesulfonic acid]), pH 7.2, 24.189g of PIPES (Sigma-Aldrich, UK, P6757) was dissolved in 150 mL of distilled water (dH_2O_2). NaOH solution (5N) (Sigma-Aldrich, UK, 1310-73-2) was added to the solution until the pH reached 7.2 (PIPES starts to dissolve as the pH is increased). The PIPES solution was aliquoted and stored at -20°C.

2- To prepare 2.3 M of sucrose, 78.729g of sucrose (Sigma-Aldrich, UK, S0389) was dissolved in 100 mL distilled H_2O_2, aliquoted and stored at -20°C for future use.

An acetate sheet was cut into circles of about 3cm in diameter using gloves to avoid fingerprints on the acetate sheet. Under a tissue culture hood, acetate circles were placed in a large Petri dish (Thermo Fisher Scientific, UK, 172931) and the dish was filled with 100% ethanol. Acetate sheets were immersed in the ethanol and incubated for 5 minutes. The sheets were then transferred into a sterile Petri dish to allow the ethanol to evaporate, after which they were rinsed 3 times with sterile PBS. The sheets were then incubated with bovine plasma fibronectin (10 µg/mL) and incubated for 2 hours at 37°C. The fbronectin solution was removed and the HPAECs were seeded on acetate sheets. 80% confluent HPAECs were infected with AdCLIC and AdCTRL as described above. 24 hours later, the media were removed and cells were rinsed in PBS and fixative solution containing 0.05% glutaraldehyde (Thermo Fisher Scientific, UK, 340855) and 2% paraformaldehyde (Thermo Fisher Scientific, UK, 28906) in 0.2M PIPES pH 7.2 for 15 minutes at room temperature. Most of the fixative solution was then removed, leaving about 1 mL in the dish. The cells were gently scraped with a plastic cell scraper and the resultant cell suspension was collected in 1.5 mL Eppendorf tubes (Thermo Fisher Scientific, UK, 3448) and centrifuged at 10,000 x g for 10 minutes. The supernatant was discarded and the cell pellet was gently washed 3 times for 5 minutes with 0.2M PIPES pH 7.2. Samples were then immersed in 2.3M sucrose in PBS (1mL) for cryo-protection and kept at 4°C for further processing.

2.3.2 Immunogold labelling of mitochondria in CLIC-overexpressing HPAECs

For immunogold labelling, samples were processed according to the Tokuyasu method for cryo-ultrathin sectioning (Tokuyasu, 1973). Control and CLIC-overexpressing HPAECs were fixed (see Section 2.3.1). To produce ultra-thin sections, small fragments of the cryo-protected cell pellet were mounted onto aluminium stubs and plunge-frozen into liquid nitrogen before sectioning at a nominal thickness of 60nm using an ultra-microtome (LN ultra powertome, RMC Boeckeler,

Tucson, USA) at -100°C. Sections were set in a 1:1 mix of 2% methyl cellulose (Sigma-Aldrich, UK, 9004-67-5)/2.3M sucrose using a wire loop before being defrosted and transferred onto pioloform-coated 100 mesh copper grids (Agar scientific, UK, AGS134-1) in PBS, and were then stored at 4°C until further use. Cell sectioning was carried out by Dr Patricia Lovell (Electron Microscopy Facility, Imperial College London).

Prior to labelling, grids were washed 3 times for 5 minutes by floating the grids upside down in PBS (cooled on ice) to remove sucrose and methyl cellulose. Unspecific binding sites were blocked using 0.5% fish skin gelatin (FSG, Sigma-Aldrich, UK, G7041) in PBS for 10 minutes before incubating sections with a primary antibody (mouse monoclonals anti-CLIC1, anti-CLC4, Santa Cruz, dilutions prepared in FSG) for 30 minutes at room temperature.

After being washed 3 times for 5 minutes in PBS, the sections were incubated using a secondary rabbit anti-mouse antibody (see Table 2.3) (1 in 200 in FSG,) for 20 minutes followed by another set of washes in PBS (3 times for 5 minutes). Sections were then incubated in 10nm protein-A gold (Sigma-Aldrich, UK,P6855) (1 in 60 in FSG) for 20 minutes before being washed 6 times for 5 minutes in PBS followed by 10 minutes in deionised water. Sections were then contrasted in droplets of 2% methyl cellulose/2% uranyl acetate (Thermo Fisher Scientific, UK, 73943, mixed 9:1) on ice for 10 minutes. Grids were picked up using a wire loop and dried in air after removing excess contrasting solution using filter paper. Dried grids were analysed using a JEOL JEM 1400 transmission electron microscope operated at 120 kV, and images were taken with a digital camera (Gatan, ES1000W CCD, Abingdon, UK). The dried grids were analysed using a JEOL JEM 1400 transmission electron microscope operated at 120 kV and images taken with a digital camera (Gatan, ES1000W CCD, Abingdon, UK). Immunogold labelling was carried out by Dr

Christian Hacker, University of Exeter. TEM images were taken with the help of Dr Paul Simpson (Electron Microscopy Facility, Imperial College London).

2.4 Fluorescent labelling of mitochondria and measurement of mitochondrial fragmentation

To evaluate the total mitochondrial area and the mitochondrial fragmentation count (MFC) in cells, mitochondria were labelled by fluorescent immunostaining. Briefly, 80% confluent HPAECs cultured on Thermanox® Plastic Coverslips (13 mm) were washed twice in PBS, fixed in 4% formaldehyde solution in PBS for 15 minutes at room temperature, washed 3 times in PBS and then permeabilised in 0.1% Triton X-100 (Sigma-Aldrich, UK, 234729) in PBS for 10 minutes. The cells were then rinsed with PBS, blocked in 10% normal goat serum to reduce non-specific antibody binding for 1 hour and incubated with anti-mitochondria (Vector Laboratories, S-1000) at a dilution 1:200 in 10% goat serum and 5% BSA in PBS-T (see Table 2.4) for 1 hour in a humidified chamber. The cells were then rinsed with PBS and incubated in 50µL of fluorescently-labelled secondary antibody (for the list of antibodies see Table 2.4) for 1 hour, with or without F-actin dye, tetramethylrhodamine (TRITC)-phalloidin (1µg/mL; Sigma-Aldrich, UK, P1951) in the humidified chamber. The cells were then washed 3 times in PBS and mounted in Vectashield mountant with nuclear dye DAPI (4',6-diamidino-2-phenylindole) (Vector Laboratories, H-1200).

Total mitochondrial coverage area and mitochondrial fragmentation count (MFC) analysis was performed using NIP2 image analysis software (Martinez & Cupitt, 2005). MFC provides an evaluation of the number of small mitochondrial particles, and MFC values reflect the extent of mitochondrial fission. Images were acquired using a Zeiss LSM 780 confocal microscope with 20x/40x lens. The acquired images were filtered (according to median), thresholded, and binarized to identify individual mitochondrial segments (with less than 500-pixel <2 μm^2 cut-off size). This cut-off size was found to be optimal in selecting mitochondria that were not associated

with the mitochondrial network. The normalization of particle counts was performed on the total mitochondrial area (in pixels). This helped us to define the MFC of each individual cell. 20 cells in 3 separate experiments were randomly selected for measurement (Hong et al., 2013).

2.5 Microtubule staining

For the immunofluorescent staining of microtubules, control and CLIC-overexpressing HPAECs grown on Thermanox® Plastic Coverslips (13 mm diameter) were fixed in 4% formaldehyde as described above, and then incubated in 100% methanol for 5 minutes at -20°C and then in acetone for 1 minute at -20°C. The cells were air dried, re-hydrated in PBS, blocked in 5% BSA for 15 minutes and then incubated with primary anti-α tubulin antibodies in PBS (see Table 2.4) for 1 hour in a humidified chamber. The cells were then washed 3 times in PBS and incubated in fluorescently-labelled secondary antibodies for 1 hour. The cells were then rinsed 3 times in PBS and mounted in Vectashield with DAPI. Cell images were acquired using a confocal microscope (Zeiss LSM780) and analysed with Image J software.

To assess microtubule dynamics in CLIC-overexpressing HPAECs, cells were treated with microtubule-stabilising agent taxol (Sigma-Aldrich, UK, PHL89806-10MG) or mirotubule depolymerising agent nocodazole (Sigma-Aldrich, UK, M1404-50MG). 24 hours post-infection, the control (AdCTRL) and CLIC-overexpressing HPAECs were rinsed 3 times in PBS, then incubated with taxol (10 µM) for 30 minutes or nocodazole (20 µM) for 10 minutes (Takesono et al., 2010). After that, the cells were fixed and stained as described above. Images of microtubules and mitochondrial networks were acquired under the confocal microscope (Zeiss LSM780) and analysed with Image J software.

Table 2.4: Summary of all primary and secondary antibodies used in immunostaining.

Antibody	Host Species	Manufacturer	Catalogue No.	Working Dilution
Anti-CLIC1	Mouse mAb	Santa Cruz Biotechnology	sc-271051	1:200
Anti-CLIC4	Mouse mAb	Santa Cruz Biotechnology	sc-135739	:200
Anti-CLIC1-Alexa flour 647	Mouse mAb	Santa Cruz Biotechnology	sc-374202	1:250
Anti-CLIC4-Alexa flour 488	Mouse mAb	Santa Cruz Biotechnology	sc-135739	1:250
Anti-CLIC1	Mouse mAb	Santa Cruz Biotechnology	sc-271051	1:200
Anti-c-Myc	Rabbit pAb	Novus Biologicals	NB600-336SS	1:1000
Anti-HA-Tag	Mouse mAb	Santa Cruz Biotechnology	sc-7392	1:1000
Anti-Mitochondria	Mouse mAb	abcam	ab92824	1:1000
Rhodamine (TRITC) Anti-Rabbit IgG	Goat pAb	Jackson Immuno Research Laboratories	111-025-144	1:300
Cy™5 Anti-Mouse IgG	Goat pAb	Zymed® Laboratories	81-6516	1:300
Anti-Rabbit IgG, Alexa Fluor 488	Goat pAb	Invitrogen	A11008	1:300
Anti-Mouse IgG, Alexa Fluor 647	Goat pAb	Invitrogen	A32728	1:300
Anti-α-tubulin	Mouse mAb	Sigma-Aldrich	T51681	1:200

2.6 Evaluation of mitochondrial function

2.6.1 Measurement of mitochondrial membrane potential by TMRE staining

Mitochondria are the main source of energy, generating adenosine triphosphate (ATP) in a process known as oxidative phosphorylation. This process involves the transfer of positively charged protons across a mitochondrial inner membrane, resulting in a negatively charged transmembrane potential (ΔΨm). This net negative charge can be detected by staining live cells with positively charged dyes such as Tetramethylrhodamine, methyl ester (TMRE), which emit red fluorescence that can be detected by flow cytometry or fluorescence microscopy (Crowley et al., 2016).

To measure ΔΨm, 150 nM TMRE (Life Technologies T669) was added to HPAEC media for 30 minutes, after which the cells were washed twice with PBS. Fresh culture medium was added and the imaging of live cells was performed using a Zeiss confocal microscope with a heated stage (Zeiss LSM780) and analysed using ImageJ (1.46r, NIH, USA).

2.6.2 Measurement of mitochondrial reactive oxygen species (mtROS)

MitoSOX Red (Thermo Fisher Scientific, UK, M36008) is a live-cell dye indicator that at low concentrations of 1µM is highly selective in terms of detecting mitochondrial superoxide/ROS production. MitoSOX is oxidized by superoxide, but not by other ROS, and exhibits red fluorescence (Kauffman et al., 2016). Following the manipulation of CLIC protein or mitofusin 2 expression, HPAECs growing in 6-well plates were trypsinised and pelleted in 5 mL Falcon round-bottom polystyrene tubes (Fisher Scientific, UK, 14-959-5) by centrifugation at 1,500 x g for 5 minutes. The medium was carefully aspirated and the pellet re-suspended in 1 mL PBS, followed by a second centrifugation. 5mM of MitoSOX stock solution was prepared by diluting 50 µg of

MitoSOX Red in 13µL of 100% DMSO. The cells were then re-suspended in 300µL of Live Cell Imaging Solution, supplemented with 1% BSA (Thermo Fisher Scientific, UK, A14291DJ), containing 1µM MitoSOX Red. This was then incubated at 37°C, 5% (v/v) CO_2 for 30 minutes, protected from light. Mitochondrial ROS production was measured by flow cytometry using a BD FACS Canto Flow Cytometer. 10,000 events were recorded for each sample with a selected FL2 channel (EX/Em 510/580 nm).

2.6.3 Mitochondrial bioenergetic profile

To investigate the effects of CLIC proteins on mitochondrial bioenergetic profiles, the Agilent Seahorse XFp (Seahorse Bioscience, Billerica, MA, USA) Cell Mito Stress Test (Agilent, UK, 103010-100) and Glycolysis Stress Test (Agilent, UK, 103017-100) were carried out. Cell-based Oxygen Consumption Rate (OCR) was measured directly according to the Mito Stress Test in response to the serial injection of the compounds involved in the regulation of different components of the electron transport chain (ETC), revealing a comprehensive view on the key parameters of mitochondrial function. Glycolytic function was evaluated by measuring the extracellular acidification rate (ECAR) using the Glycolysis Stress Test in response to the automated drug injections in real time (Figure 2.3).

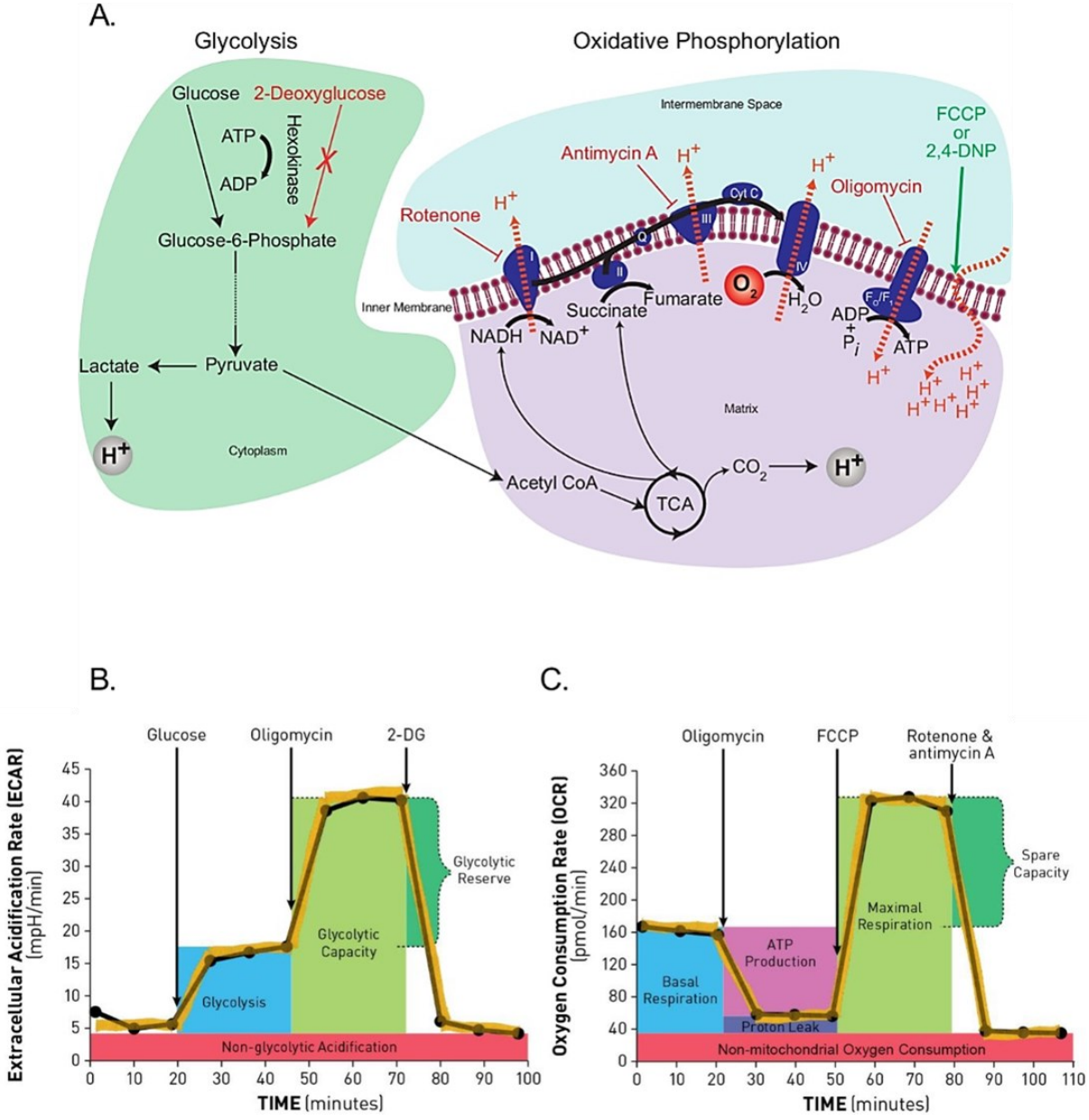


Figure 2.3: An overview of the Agilent Seahorse XF Cell Mito Stress and Glycolysis Stress assays. (A) Illustrations of glycolysis (left) and oxidative phosphorylation (mitochondrial respiration) (right), showing the effect of serial metabolic drug injections used in the Seahorse assays in real time. **(B)** Evaluation of glycolytic function by the measurement of extracellular acidification rate (ECAR) in cells; **(C)** Evaluation of mitochondrial function by measuring the oxygen consumption rate (OCR) in cells. Image **(A)** modified from Traba et al, 2016, and **(B, C)** obtained from the Agilent Seahorse Cell Mito Stress and Glycolysis Stress Test User Guide (Agilent Technologies, 2019).

2.6.3.1 Cell preparation for the assay

Visual assessment was used first in order to approximate optimal cell seeding numbers. The cells should be at 70-90 % confluent, evenly distributed within each individual well and across each well of the plate to ensure data accuracy and precision. HPAECs/ECFCs were plated in Seahorse 96-well plates (Agilent, UK, 102601-100) at the optimized density of $2x10^4$ cells/well. The next day, the cells were infected with AdCLIC and AdCTRL and incubated for a further 24 hours at 37°C, 5% (v/v) CO_2. A Seahorse utility plate, XFe96 Sensor Cartridge (Agilent, UK, 102601-100) was hydrated with Seahorse calibrant solution (200 µL/well) (Agilent, UK, 102601-100) and the sensor cartridge was lowered onto the utility plate, submerging the sensors in the calibrant solution. The Seahorse cartridge was placed in a 37°C incubator that was not supplemented with CO_2, and incubated overnight at 37°C in a CO_2-free incubator.

2.6.3.2 Running the assay

The cells were washed twice with pre-warmed PBS and then once with pre-warmed XF Seahorse DMEM medium (phenol red- and serum- free, pre-adjusted pH to 7.4) (Agilent, UK, 103575-100). The assay medium was supplemented for each assay, according to the manufacture's protocol (Mito Stress Test: Seahorse XF Cell Mito Stress Test Kit User Guide (agilent.com); Glycolysis Stress Test: Seahorse XF Glycolysis Stress Test Kit User Guide (agilent.com) (Table 2.5). The cells were then incubated in the supplemented assay medium (175 µL/well) for 1 hour at 37°C in a CO_2-free incubator.

Table 2.5: Seahorse assay medium preparation. XF seahorse DMEM medium was supplemented with L-Glutamine, pyruvate, and glucose for the Mito Stress Test. L-Glutamine was the only supplement used for the Glycolysis Stress Test, according to the manufacture's guidelines.

Assay	Supplement	Concentration	Supplier/cat.no
Mito Stress Test	L-Glutamine	2 mM	Agilent, 103579-100
	Pyruvate	1 mM	Agilent, 103578-100
	Glucose	10 mM	Sigma-Aldrich, 68769
Glycolysis Stress Test	L-Glutamine	2 mM	Agilent, 103579-100

During cell incubation, the Mito Stress Test compounds (oligomycin, carbonyl cyanide-4 (trifluoromethoxy), phenylhydrazone (FCCP) and a mix of rotenone and antimycin A, included in the assay kit) and/or the Glycolysis Stress Test compounds (oligomycin, glucose, 2-deoxy-glucose (2-DG), provided with the kit) were reconstituted in the prepared assay medium, according to the manufacturer's instructions. The working concentration of each compound was previously optimised with help of Dr Daria Capece (Department of Immunology and Inflammation, Imperial College London) in accordance with the manufacturer's guidelines. Stocks and final working concentrations of each compound are shown in Table 2.6. The compounds were loaded into the appropriate ports of the hydrated sensor cartridge.

Table 2.6: Concentrations of compounds used in the Seahorse Mito Stress Test and the Seahorse Glycolysis Stress Test.

Assay	Compound	Stock concentrations	Working concentrations	Port
Mito Stress Test	Oligomycin	100 µM	1.5 µM	A
	FCCP	100 µM	2 µM	B
	Rotenone/Antimycin A	50 µM	0.5 µM	C
Glycolysis Stress Test	Glucose	100 µM	1.5 µM	A
	Oligomycin	100 mM	15 mM	B
	2-DG	500 mM	65 mM	C

The utility plate with the loaded sensor cartridge was placed onto the Seahorse instrument tray for calibration for 15-30 minutes. Following calibration, the cell culture microplate was placed for the assay run.

2.6.3.3 Seahorse XF data analysis

After the run, the data were exported from Wave software into Excel, and the Mito Stress Test and/or the Glycolysis Stress Test parameters were then automatically calculated using the Seahorse XF Report Generators which were installed directly from the Agilent Cell Analysis website.[1]

[1] https://www.agilent.com/en/products/cell-analysis/cell-analysis-software/data-analysis/seahorse-xf-cell-mito-stress-test-report-generators

2.7 Isolation of mitochondria

The Isolation of mitochondria was performed using the Mitochondria Isolation Kit for cultured cells (Abcam, UK, ab110170), according to the manufacturer's guidelines.[2] The procedure used to isolate mitochondria from cells consists of three key steps. The first step involves rupturing the cell membrane by mechanical and/or chemical means using homogenizers and lysis buffers. The second step involves differential centrifugation at low speed in order to remove cell debris and very large cellular organelles (Spin 1). In the final step, the cells are centrifuged at a higher speed to isolate mitochondrial fractions (Spin 2). The detailed isolation procedure is described in section 2.6.2 below, and a summary of the isolation process is shown in Figure 2.4.

2.7.1 Isolation of mitochondria from HPAECs

HPAECs were cultured in 175 cm^2 culture flasks (Sarstedt, Germany) in endothelial cell growth medium EGM-2 supplemented with growth factors, 20% FBS, and 1% antibiotic/antimycotic solution. At ~80% confluency, HPAECs were infected with AdCLICs, with or without AdCTRL (four 175 cm^2 flasks per treatment). From this point, the assay was carried out according to the manufacturer's instructions. All reagents (A,B and C) provided were kept in the fridge at 4°C. 24 hours after infection, the cells were trypsinised using 0.05% trypsin and pelleted by centrifugation at 1,000 x g. The total protein concentrations of each cell pellet was measured using a Pierce™ BCA Protein Assay Kit. The cell pellet was subjected to 3 freeze-thaw cycles to disrupt cell membranes, and the cell pellet was then re-suspended to provide 5 mg protein/mL in Reagent A (Tris, digitonin, triethanolamine, sucrose and EDTA) in a 2-mL microtube. The tube containing the cell solution was incubated for 10 minutes on ice.

[2] Mitochondria-Isolation-Kit-for-Cultured-Cells-protocol-book-ab110170 (website).pdf (abcam.com).

I. **Rupturing step**. The cells were transferred into a pre-cooled 2.0-mL Dounce Homogenizer and homogenized with 30 strokes using pestle B to rupture the cell membrane.

II. **Spin 1 step**. The homogenate was transferred to a 2-mL centrifuge tube and centrifuged at 1,000 x g for 10 minutes at 4°C. The supernatant (SN) was saved (SN #1) and the pellet was then re-suspended in Reagent B to provide 5 mg/mL protein (Tris, digitonin, sucrose and EDTA). After that, the rupturing and spin 1 steps were repeated. After the final spin, the supernatant was saved (SN#2) and the pellet was discarded. Supernatants (SNs #1 & #2) were combined, mixed thoroughly and transferred to a 2-mL centrifuge tube.

III. **Spin 2 step**. The combined supernatants were centrifuged at 12,000 x g for 15 minutes at 4°C. The pellet was collected and the supernatant was discarded. The pellet containing the mitochondrial fractions was resuspended in 500µL of Reagent C (Tris, sucrose and EDTA), supplemented with protease inhibitors. The mitochondrial fractions were aliquoted and stored at -80°C until they could be used for mitochondrial quality assays or western blotting.

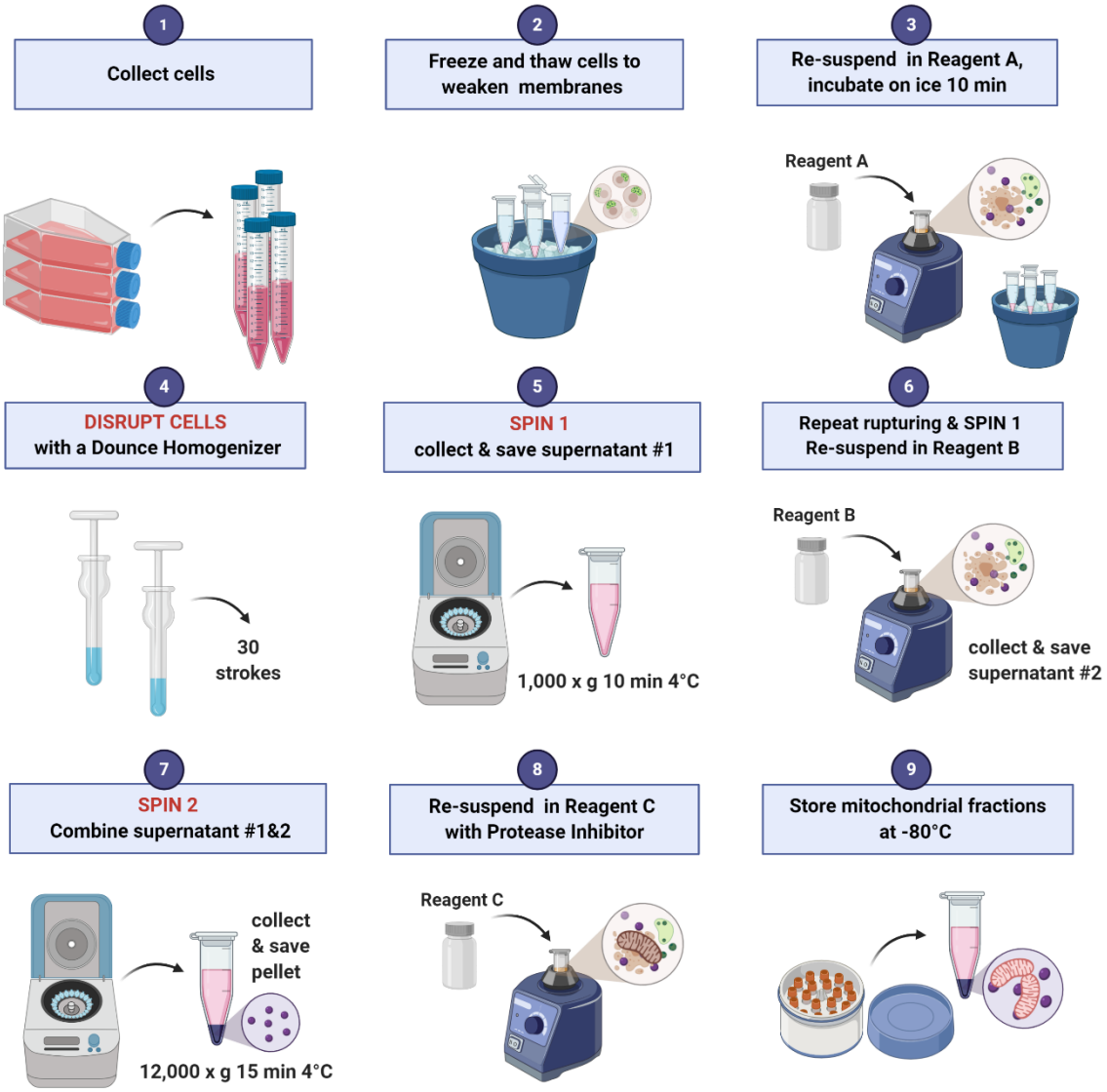


Figure 2.4: A summary of mitochondrial isolation process using a Mitochondria Isolation Kit for cultured cells (Abcam, UK, ab110170). Illustration created by the author using BioRender.com.

2.7.2 Mitochondrial proteomic analysis

2.7.2.1 Preparation of samples for LC-MS/MS analysis

Mitochondrial fractions that were isolated from HPAECs were infected with AdCTRL, AdCLIC1 or AdCLIC4 and incubated under normoxic conditions (5% CO_2,) at 37^{o}C. In order to compare the effects of CLIC proteins with the effects induced by hypoxia, control cells (AdCTRL) were also cultured under hypoxic conditions (2% O_2 for 24 hours) at 37^{o}C.

Mitochondrial fractions were pooled from (n=4/group), and were dissolved in 300 µL of 9 mol/L urea and reduced by the addition of 50 mmol/L of dithiothreitol before being heated at 100°C for 2 minutes and then carbamidomethylated by adding 200 mmol/L iodoacetamide and left in the dark for 30 minutes. SDS-PAGE was performed on 10 µg of each sample using 10% NuPAGE Novex bis-tris gels and reagents (Thermo Fisher Scientific, UK, NP0302BOX). Gels were stained with InstantBlue® (Sigma-Aldrich, UK, ISB1L). The gel lanes for each sample was divided into a series of regions based on the position of molecular weight (MW) markers (Invitrogen, UK,SeaBlue Marker®, LC5925) and the distribution of proteins observed in the gel. Gel pieces were washed with 1 mL water and dehydrated in 1 mL acetonitrile (Sigma-Aldrich, UK, 576956) for 30 minutes. After that, proteins present in the gel pieces were digested in 300 µL of 50 mmol/L ammonium bicarbonate containing 1 ng/mL trypsin (Sigma-Aldrich, UK, A6141) at 37°C overnight. The next day, tryptic peptides from each group were extracted by adding 300 µL 0.1% formic acid (Sigma-Aldrich, UK, 159013) in 2% acetonitrile and mixed for 30 minutes. 420 µL were then removed and dried.

2.7.2.2 LC-MS/MS analysis method

The dried samples were reconstituted in 30 µL of 0.1% trifluoroacetic acid (TFA) (Thermo Fisher Scientific, UK, 85172), and 8 µL of the solution was injected onto a C18 trap-column (ProteCol, 0.3 x 10 mm, Pore size: 300Å; SGE Analytical Science) followed by a high resolution reverse phase separation on a C18 column (PicoFrit, 75µm ID × 10 cm ProteoPrep column, New Objective) using Agilent 1200 LC series (Agilent, UK, Agilent 1200 LC series). The mobile phases comprised 0.1% formic acid in water (buffer A) and 0.1% formic acid in acetonitrile (buffer B). A linear gradient of 0-54% buffer B was introduced at a flow rate of 300 nL/min for 48 minutes. After that, the peptides eluting from the reversed phase column were analysed online using a Thermo LTQ linear ion trap MS equipped with a dynamic nano-spray interface. The MS method consisted of a cycle combining one full MS scan (m/z 400-1600) with three data dependent MS/MS events (35% collision energy at each event) for 70 minutes. Dynamic activation time was set at 30 seconds with scans at every 2 seconds.

2.7.2.3 MS data analysis

MS data was evaluated on the basis of the ion intensity of peptide ions with coincident LC retention time and m/z values. The identity of peptides was determined by exporting the MS/MS output files from the matched analysis into the Turbo SEQUEST search engine (BioWorks Browser 3.3, Thermo Electron Corporation) and interrogating it against the NCBI human RefSeq database Release 51. The search parameters were as follows: peptide tolerance was set to 2 atomic mass unit, MS/MS tolerance was set at 1 atomic mass unit, charge states allowed ranged from +1 to +3 and up to two missed cleavages were allowed. Modifications were set to allow for the detection of S-carbamidomethylated cysteine (+57 Da). Each MS2 spectrum was matched to only a single peptide with the highest scoring SEQUEST peptide hit. Cross-correlating (XCorr) MS data, with values >1.5, >2.0 and >2.5 (for singly, doubly and triply charged ions, respectively) were used to

select peptides of high quality and reduce the possibility of including redundant peptides in subsequent data analysis.

All keratins were excluded from the protein identification list. The current status of each protein, its name and molecular weight was updated by batch processing it on the NCBI protein database website. Where protein names contained the word 'predicted' or 'like protein', the accuracy of the assigned names were tested and if necessary corrected. The matter of redundancy in identified proteins was addressed by comprising all possible assignments in the results table to make the data as transparent as possible. In those cases where an identified protein shared its sequence with other entries in the database, all entries were listed. The uniqueness (or otherwise) of the assignment of peptides to the sequence of one or more proteins was used to determine whether assignment could be made to a specific protein or to a group of related proteins (isoforms).

2.8 Protein identification methods

2.8.1 Western blotting

2.8.1.1 Sample preparation

HPAECs were cultured in 6-well plates (Sarstedt; 200,000 cells/well) and infected with AdCLIC and AdCTRL, as described in section 2.2. 24 hours post infection, the 6-well plates were placed on ice, cell culture medium was aspirated, and the cells were rinsed twice with ice-cold phosphate buffered saline (PBS) (Sigma-Aldrich, UK, D8537-500mL). The PBS was removed and a 180 µL lysis buffer of ice-cold radioimmunoprecipitation (RIPA) (Sigma-Aldrich, UK, R0278) supplemented with Protease and Phosphatase Inhibitor cocktail (100x, Thermo Fisher Scientific, UK, 78444) was added to each well for 5 minutes. Adherent HPAECs were mechanically dislodged using a cell scraper, collected in 1.5 mL Eppendorf tubes, centrifuged at 1200 x g at 4°C for 5 minutes to remove cell debris, and the supernatant was reserved for protein quantification.

2.8.1.2 Protein quantification

Total protein concentrations were measured using the Pierce™ BCA Protein Assay Kit (Thermo Fisher Scientific, UK, 23225), according to the manufacturer's protocol.[3] A bovine serum albumin (BSA) standard curve was prepared by diluting 2 mg/ml BSA standard to obtain concentrations ranging from 0.2 mg/mL to 1 mg/mL.

The working solution was prepared by adding 50 parts of reagent A to 1 part of reagent B. 200 µL of working reagent was then added to 10 µL of protein sample in a clear bottom 96-well plate, which was then protected from light and incubated at 37°C for 15 minutes. Optical densities were measured at 490nm using a Glomax™ luminometer (Promega, E6501). Sample protein concentrations were determined using the curve generated by the protein standard (Figure 2.5).

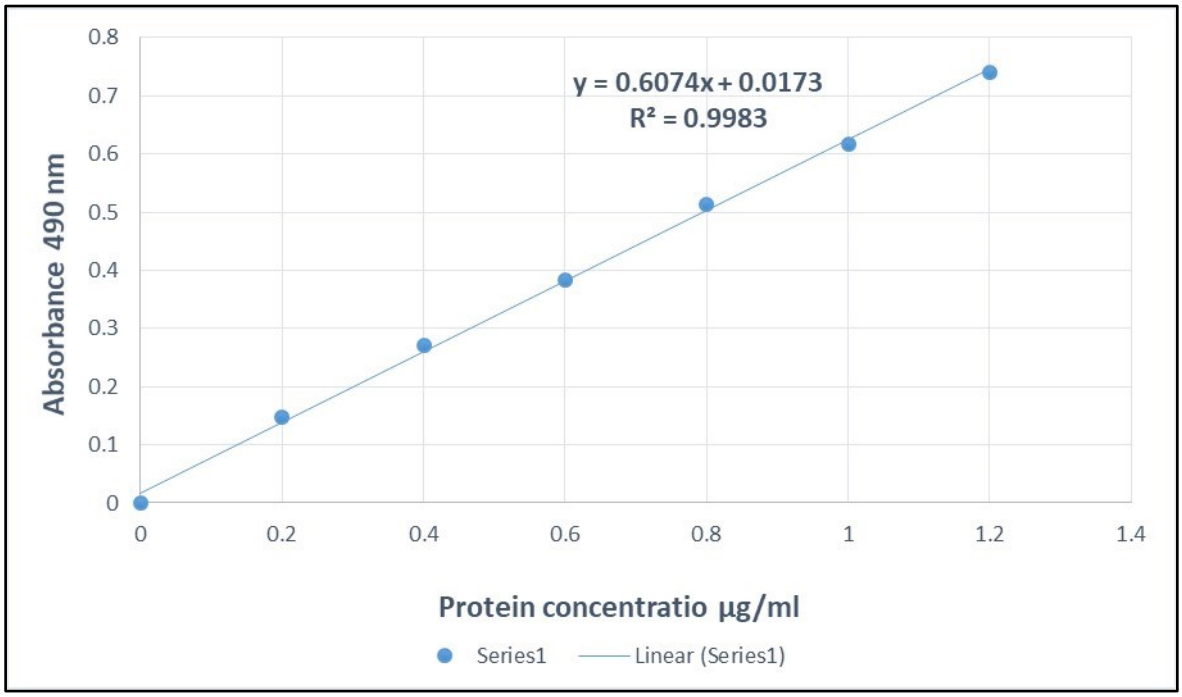


Figure 2.5: Example of bovine serum albumin (BSA) protein standard curve of BCA Protein Assay. A standard curve was generated for each BCA assay using samples of a known concentration of BSA. BSA was diluted in dH_2O_2 at different concentrations ranging from 0.2 mg/mL to 1 mg/mL). The slope of the resulting best fit line was used to measure sample protein concentrations. R^2 = 0.9983 is a statistical calculator of how close the data are to the fitted linear regression.

[3] User Guide: Pierce BCA Protein Assay Kit (thermofisher.com).

2.8.1.3 SDS-polyacrylamide gel electrophoresis (PAGE)

Samples containing equal amounts of protein were denatured in a Laemmli SDS sample buffer containing β-mercaptoethanol (4x) (Alfa Aesar by Thermo Fisher Scientific, UK, J60015) at 95°C for 5 minutes. The samples were then resolved by electrophoresis or were stored at -20°C for further analysis. Approximately 10– 20 µg of protein per well in 1.5mm thick NuPAGE 4-12% Bis-Tris protein gels (Thermo Fisher Scientific, UK, WG1403BOX, NP0336BOX) were separated by electrophoresis in NuPAGE MES SDS Running Buffer (20X) (1X: 50 mM MES, 50 mM Tris Base, 0.1% SDS, 1 mM EDTA, pH 7.3) (Thermo Fisher Scientific, UK, NP000202) at 200 V for 35 minutes. To monitor protein separation during SDS-PAGE and evaluate the size of proteins of interest, 5 µl of pre-stained protein ladder covering a wide range of molecular weights from 10 to 260kDa was added into the first well of each gel (Thermo Fisher Scientific, UK, 26623). Proteins were then transferred onto polyvinylidene fluoride (PVDF) membranes (Bio Rad, UK, 1704156) using the wet transfer method (Bio Rad, UK) or Trans-Blot Turbo Transfer System.

I. **Wet transfer method**. The gel and the membrane were put together in a "sandwich" of layers comprising filter papers, gel, membrane and sponges pre-soaked in transfer buffer (20% methanol, in 1xTris-glycine-SDS (0.025M Tris, 0.192M glycine, 0.1% SDS, pH 8.5)) (Thermo Fisher Scientific, UK, 28362) and locked in a transfer cassette. The transfer cassette was then placed in a transfer tank (BioRad), filled with transfer buffer and subjected to electrophoresis at 100 V for 1 h and 30 minutes with ice packs in order to avoid overheating.

II. **Trans-Blot Turbo Transfer System (semi-dry blotting).** Proteins were transferred in 7 minutes using the Trans-Blot Turbo Transfer System (Bio-Rad, UK) onto PVDF membranes contained within the Trans-Blot Turbo Transfer System (Bio-Rad, UK, 1704158, 1704156). The gel and

membrane were sandwiched as described in the wet transfer method, then placed in the cassette. The cassette was then inserted into the bay and “run” for 7 minutes at 25 V.

Successful protein transfer was confirmed by protein staining on the membrane using Ponceau S (Sigma-Aldrich, UK, P7170).

2.8.1.4 Immunoblotting

Membranes were washed with 1xTris Buffered Saline with Tween®20 (TBST-10X; Cell Signalling, UK, 9997). To avoid non-specific protein binding, membranes were blocked in 4% bovine serum albumin (BSA) in TBS-T for 1 hour at room temperature (RT), followed by overnight incubation with the primary antibodies on a shaker at 4°C. The following day, the membranes were washed 3 times with TBS-T (15 minutes each wash) and incubated with horseradish peroxidase (HRP)-labelled secondary antibodies in TBS-T for 1 hour at room temperature. A list of all primary and secondary antibodies were used in this study is provided in Table 2.7.

Membranes were washed 3 times with TBS-T and then visualised using a chemiluminescent horseradish peroxidase (HRP) substrate, Luminata™ Crescendo (Millipore, UK, WBLUR0500) in the ChemiDoc™ MP System (Bio-Rad, UK). Where appropriate, membranes were stripped with Restore™ PLUS Western Blot Stripping Buffer (Thermo Fisher Scientific, UK, 46430) to remove primary and secondary antibodies from the membranes and re-probe using a new primary antibody. Membranes were incubated with stripping buffer for 30 minutes, washed with PBS, and then blocked for 1 hour at room temperature in 4% BSA in TBS-T, before probing with a different set of antibodies as described above. The measurement of band density was performed using ImageJ software (U.S. National Institutes of Health, Bethesda, MD, USA), protein quantification data were normalised to β-actin, the housekeeping protein control (Figure 2.6).

Table 2.7: A list of primary and secondary antibodies used in western blotting.

Antibody	Host Species	Manufacturer	Catalogue No.	Working Dilution
Anti-CLIC4	Mouse mAb	Santa Cruz Biotechnology	sc-135739	1:1000
Anti-CLIC1	Mouse mAb	Santa Cruz Biotechnology	sc-271051	1:1000
CLIC4/5/6	Mouse mAb	Santa Cruz Biotechnology	sc-271863	1:1000
anti-c-Myc	Rabbit pAb	Novus Biologicals	NB600-336SS	1:1000
Mitofusin2	Mouse mAb	abcam	ab56889	1:1000
Mitofusin1	Mouse mAb	abcam	ab126575	1:1000
VDAC	Rabbit mAb	Cell Signaling	4661	1:1000
SDH	Rabbit mAb	Cell Signaling	11998	1:1000
Pyruvate dehdrogenase	Rabbit mAb	Cell Signaling	3205	1:1000
PHB1	Rabbit mAb	Cell Signaling	2426	1:1000
Cytochrome c	Rabbit mAb	Cell Signaling	4280	1:1000
HSP60	Rabbit mAb	Cell Signaling	12165	1:1000
COX IV	Rabbit mAb	Cell Signaling	4850	1:1000
β-actin	Mouse mAb	Sigma-Aldrich	A1978	1:3000
DRP1	Rabbit mAb	Cell Signaling	8570	1:1000
Phospho-DRP1 (Ser-616)	Rabbit mAb	Cell Signaling	3455	1:1000
Phospho-DRP1 (Ser-637)	Rabbit mAb	Cell Signaling	4867	1:1000
MFF	Rabbit mAb	Cell Signaling	84580	1:1000
Phospho-MFF (Ser-146)	Rabbit mAb	Cell Signaling	49281	1:1000
OPA1	Rabbit mAb	Cell Signaling	80471	1:1000
Tubulin	Rat mAb	abcam	ab6161	1:1000
Pyruvate dehydrogenase E1	Rabbit mAb	abcam	ab168379	1:1000
Anti-VDAC1/ Mitochondrial Loading Control	Rabbit mAb	abcam	ab15895	1:1000

Pyruvate dehydrogenase kinase2	Rabbit mAb	abcam	ab68164	1:1000
Pyruvate dehydrogenase kinase1	Mouse mAb	abcam	ab110025	1:1000
PINK1	Rabbit mAb	Cell Signaling	6946	1:1000
LC3B	Rabbit mAb	Cell Signaling	3868	1:1000
Parkin (Prk8)	Mouse mAb	Cell Signaling	4211	1:1000
Optineurin	Rabbit mAb	Cell Signaling	58981	1:1000
HRP-linked Anti-Rabbit IgG	Goat pAb	Cell Signaling	7076	1:3000
HRP-linked Anti-mouse IgG	Horse pAb	Cell Signaling	7074	1:3000
HRP-linked Anti-rat IgG	Goat pAb	Cell Signaling	7077	1:3000

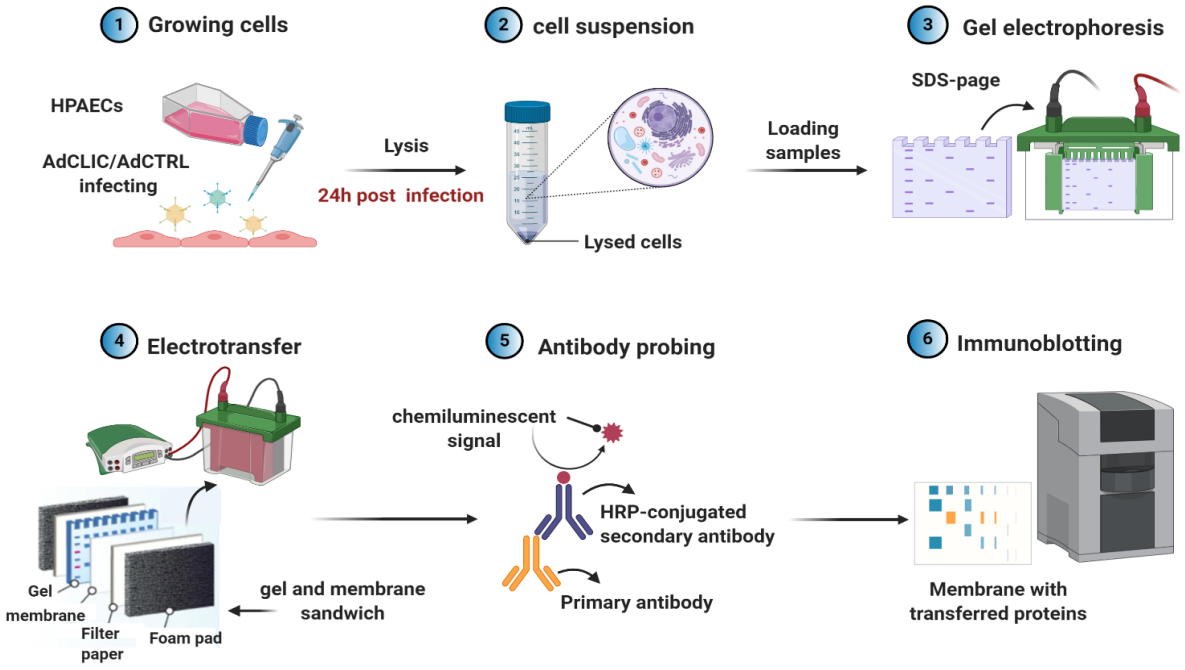


Figure 2.6: Western blotting workflow. Illustration created by the author using BioRender.com.

2.9 RNA extraction, purification and quantification

2.9.1 RNA extraction from cultured cells

Total RNA was extracted from untreated and treated HPAECs (see Section 2.3, Materials and Methods) using Monarch® Total RNA Miniprep Kit (New England Biolabs UK, T2010S), according to the manufacturer's instructions.[4] Before the start of the experiment, RNaseZap solution (Invitrogen, USA, AM9780) was applied to all exposed working surfaces and instruments in order to decontaminate them from RNase on contact. To minimise RNase activity, all steps were performed in a frozen state, unless stated otherwise.

The cell culture medium was aspirated and the cells were rinsed briefly twice with pre-warmed PBS. HPAECs were then trypsinised and pelleted by centrifugation in a falcon 15 mL conical centrifuge tube (Thermo Fisher Scientific, UK, 11507411) at 1,500 x g for 5 minutes. The supernatant was then aspirated and the cell pellet was re-suspended in PBS and re-pelleted again by centrifugation. Following the manufacturer's guidelines, the dry cell pellet was resuspended in 300 µL RNA Lysis buffer by pipetting gently to avoid foaming and incubated for 5 minutes. All subsequent steps were carried out at room temperature to prevent precipitation, and all centrifugations were carried out at 16,000 x g.

The lysate mixture was transferred to a gDNA Removal Column (light blue) (provided with the kit) fitted with a collection tube, and centrifuged for 1 minute to remove most of the gDNA. The flow-through was saved as it contained the RNA, and the gDNA Removal Column was discarded. 300 µL of ethanol (≥ 95%) (not included in the kit) was added to the flowthrough and mixed thoroughly by pipetting to generate favourable conditions for the RNA to bind to the RNA Purification column.

[4] Quick Protocol for Total RNA Extraction (NEB #T2010) | NEB

The mixture was then transferred to an RNA Purification Column (dark blue) (included in the kit), fitted with a collection tube. The mixture was centrifuged for 1 minute and the flow-through was discarded. 500 µL of RNA Wash Buffer (included in the kit) was added to the RNA purification column and centrifuged for 1 minute to remove all salts prior to the addition of DNase I. The flowthrough was then discarded. 5 µL of DNase I was mixed with 75 µL of DNase I Reaction Buffer in an RNase-free microfuge tube (Thermo Fisher Scientific, UK, AM12400). The mixture was pipetted directly to the top of the column matrix and incubated for 15 minutes at room temperature. 500 µL of RNA Priming Buffer (provided with the kit) was added and the mixture was centrifuged for 1 minute, then the flowthrough was discarded. 500 µL of RNA Wash Buffer was added and centrifuged for a further minute, and the flow-through was once again discarded. An additional 500 µL of RNA Wash Buffer was added and subjected to centrifugation for 1 minute, the flow-through was discarded. The column was then placed into a fresh RNase-free microfuge tube to ensure that no ethanol contamination was carried over.

50 µl of Nuclease-free Water (Thermo Fisher Scientific, UK, R0581) was directly pipetted to the centre of the column matrix and centrifuged for 1 minute. For best RNA recovery, a second elution was performed by pipetting the eluted samples back onto the column matrix and re-centrifuging them for a further 2 minutes. The RNA was aliquoted into two 0.5 mL RNase-free microfuge tubes (Thermo Fisher Scientific, UK, AM12300), assessed by nanodrop and stored at -80°C for qPCR step.

2.9.2 RNA quality assessment

The concentration and purification of the extracted RNA were assessed using a NanoDrop™ ND2000 spectrophotometer (Thermo Scientific). The purity of the RNA samples was evaluated by measuring the absorbance ratios A260/280 nm and A230/A260 nm. Acceptable ratios are generally in the range of 1.8-2.0. Higher values than this may indicate contamination with DNA or residual reagents used in the extraction protocol. The RNA was then stored at -80°C for future experiments. Reverse transcriptase polymerase chain reaction (RT-PCR)

RNA samples were equalised at 100 ng/µL using RNase-free water. Input RNA was reverse-transcribed into complimentary DNA (cDNA) by RT-PCR using SuperScrip™ II Reverse Transcriptase (Invitrogen, 18064014). All reagents for the cDNA master mix were placed on ice and prepared for each sample as shown in Table 2.8.

Table 2.8: Composition of cDNA master mix used in the reverse transcription process gene expression.

Reagent	Master mix (X1) (µL)	Supplier/cat.no
DNase/RNase-free distilled water	8	Thermo Fisher Scientific, 10977035
Oligo(dT)$_{12-18}$ 500 µg/mL	1	Thermo Fisher Scientific, 18418012
dNTP Mix (10 mM each)	1	Thermo Fisher Scientific, 10610851
Total	12	

10 µL of the master mix was added to 2 µL RNA in a 96-well PCR plate (Thermo Fisher Scientific, A31728), at a total volume of 12 µL/well. The plate was then sealed with adhesive PCR plate seal (Thermo Fisher Scientific, AB0558) before being vortexed and centrifuged briefly. The PCR plate was incubated for 5 minutes at 65°C in SimpliAmp™ Thermal Cycler (Applied Biosystems) followed by a quick chill on ice before being subjected to centrifugation. Another mix was prepared for each sample, as shown in Table 2.9. 7 µL of the mix was added to each well to a final volume of 19 µL and mixed thoroughly by pipetting.

Table 2.9: Final mixture of reverse transcription for gene expression.

Reagent	Volume (µl)	Supplier/ Catalogue No.
DNase/RNase-free water	1	Thermo Fisher Scientific, 10977035
5X First-Strand Buffer	4	Invitrogen, 18064014
0.1 M DTT	2	Invitrogen, 18064014
Total	**7**	

The plate was sealed as described previously and centrifuged. The samples were incubated for 2 minutes at room temperature and then centrifuged again. This was followed by adding 1 µL of SuperScript II Reverse Transcriptase to each well (a total reaction mixture of 20 µL) and mixed thoroughly by pipetting. The plate then was sealed again, centrifuged, and PCR reactions were performed in a SimpliAmp™ Thermal Cycler (Applied Biosystems, USA) (Table 2.10). A negative RT control was also included in the reaction in order to monitor the presence of DNA contamination. cDNA samples were then stored at -20°C for use in subsequent gene expression analysis.

Table 2.10: SuperScript II Reverse Transcriptase thermal cycling conditions

Temperature	Time (minute)
42°C	50
70°C	15
4°C	∞

2.9.3 Real-time quantitative PCR (qPCR) for gene expression

Gene expression was quantified using real time quantitative PCR (qPCR). In order to perform qPCR, a Luna® Universal qPCR master mix (New England Biolabs, M3003) and a 20X TaqMan® Gene Expression Assay (FAM™ dye-labeled MGB probe) (Thermo Fisher Scientific, 4331182) were used (Table 2.11). Each assay includes a pair of target primers and a sequence-specific TaqMan probe with a reporter fluorescent dye label (FAM) on the 5' end and a quencher dye minor groove binder (MGB) and non-fluorescent quencher (NFQ) on the 3' end.

Table 2.11: List of genes used in qPCR.

Target gene symbol	5' Reporter dye	3' Quencher	Human Assay ID
MFF	FAM	MGB	Hs00697394_g1
DNM1L	FAM	MGB	Hs01552605_m1
FIS1	FAM	MGB	Hs00211420_m1
MFN1	FAM	MGB	Hs00966851_m1
MFN2	FAM	MGB	Hs00208382_m1
OPA1	FAM	MGB	Hs01047013_m1
CLIC1	FAM	MGB	Hs00559461_m1
CLIC4	FAM	MGB	Hs00749895_s1
CLIC5	FAM	MGB	Hs00213494_m1
GAPDH	FAM	MGB	Hs02786624_g1

cDNA samples were first diluted using 1X Tris-EDTA (TE) (Alfa Aesar, J60234) (10 µL cDNA in 90 µL 1X TE). The Master mix for each qPCR reaction was then prepared according to Table 2.12.

Table 2.12: Composition of 1X master mix used in qPCR.

Reagent	Volume (µl)/well
DNase/RNase-free water	2.5
20X TaqMan Gene Expression Assay	0.5
Luna® Universal qPCR master mix	5.0
Total	8

8 µL of the qPCR master mix plus 2 µL of the diluted cDNA (10ng/µL) were pipetted to a 384-well Skirted PCR Plate (StarLab, UK, E1042-3840). Negative controls for each gene of interest were included in the plate containing no cDNA template. The plate was then sealed using a MicroAmp Optical Adhesive Film (Thermo Fisher Scientific, 4311971), inverted several times and centrifuged at 1,000 x g to ensure the plate was free of air bubbles. The qPCR was performed using a QuantStudio 12K Flex Real-Time PCR System (Applied Biosystems, USA). The amplification process involved 2 steps, melting and annealing over 40 cycles according to the manufacturer's instructions (Table 2.13).

Table 2.13: Amplification steps for qPCR reactions.

qPCR step	Temperature	Time	
Pre-incubation (hold)	95°C	10 minutes	
Melting	95°C	15 seconds	X40
Annealing	60°C	60 seconds	

2.9.4 PCR data analysis

Following the amplification curve, data were analysed at individual sample levels, where a single peak represented the amplification of a single product. A fixed fluorescence threshold level of 0.2 was applied to determine cycle threshold (C_T) values for all genes. C_T values represent the number of cycles required for the fluorescent signal to cross the threshold (above background level) and be detectable in real-time PCR, C_T values over 35 cycles were excluded from the analysis and were defined as non-detectable expressions. All reactions were carried out in triplicate. Fluorescence data collection were also performed during the annealing step. An example of amplification plot is shown in Figure 2.7. C_T values for the gene of interest were compared to reference values using housekeeping genes of stable expression (GAPDH), and the relative gene expression was then calculated using the $2^{-\Delta\Delta Ct}$ method, where GAPDH was used as an endogenous normalisation control for messenger RNA (mRNA) expression:

$$\Delta\Delta C_T = \Delta C_{T\ sample} - \Delta C_{T\ control}$$

ΔC_T represents the value of the gene of interest (sample)/housekeeping gene (control).

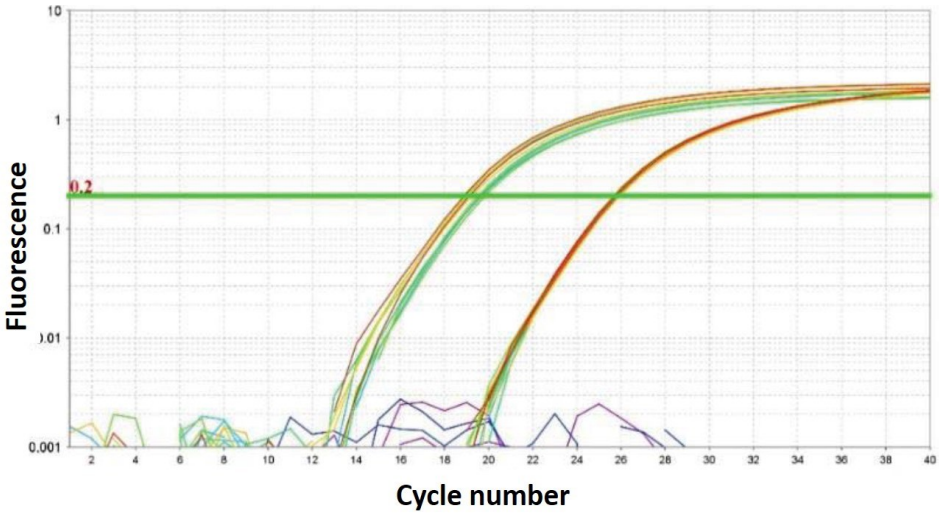


Figure 2.7: An example of an amplification plot generated by quantitative Real-Time PCR (qRT-PCR) assay. Y-Axis = log of the change in fluorescence, X-Axis = Cycle number. Cycle threshold (C_T) is around 0.2 when the reaction exceeds background level and reaches the fluorescent intensity.

2.10 Statistical analysis

Experiments were conducted at least in triplicate, with 3 technical replicates performed per experiment. All data are tested for normal distribution using Shapiro-Wilk test. Statistical analyses were performed by unpaired t-test (for normally distributed data) for two sample groups. For multiple comparisons between various groups with equal variances, a one-way analysis of variance (ANOVA) combined with Tukey's post hoc test to compare every mean with every other mean or Dunnett's post hoc test to compare every mean to a control mean were performed using GraphPad Prism 8 software (GraphPad Software Inc., USA). Data are presented as mean or + standard error of the mean (SEM). Values of $P \leq 0.05$ was considered statistically significant.

CHAPTER 3 RESULTS:

Effects of CLIC protein expression changes on mitochondrial structure and dynamics in HPAECs

CHAPTER 3 RESULTS: Effects of CLIC protein expression changes on mitochondrial structure and dynamics in HPAECs

This chapter focuses on the effects of CLIC proteins on mitochondrial structure and mitochondrial dynamics in the context of pulmonary arterial hypertension.

3.1 Introduction

Intracellular chloride channel proteins (CLIC) have been identified as new mediators of vascular dysfunction in pulmonary arterial hypertension (PAH) (Wojciak-Stothard et al., 2014). Expression levels of CLIC1 and CLIC4 are elevated in PAH plasma, blood-derived late outgrowth endothelial colony forming cells (BOECs or ECFCs) and in animal and human PAH lung tissue (Abdul-Salam et al., 2010; Wojciak-Stothard et al., 2014). While no variations in the expression of CLIC5 were detected in PAH, CLIC5 is expressed in endothelial cells (Edwards & Kapadia, 2000; Money et al., 2007) and cardiac tissue (Ponnalagu et al., 2016), and was therefore included in some experiments described in this study. There are two splice variants of CLIC5: the smaller and more abundant gene product CLIC5A (short CLIC5), and the larger and less abundant gene product CLIC5B (long CLIC5), which has an additional hydrophobic N-terminal sequence (Edwards & Kapadia, 2000).

Mitochondria are cellular power generators that convert oxygen and nutrients into adenosine triphosphate (ATP). They are dynamic structures that move constantly within cells and undergo division (fission) or fusion to form mitochondrial networks. Changes in connectivity within the mitochondrial network, in mitochondrial shape and in intracellular trafficking are collectively referred to as mitochondrial dynamics (Youle & Van Der Bliek, 2012). Defects in mitochondrial dynamics underlie the pathology of many disorders, including cancer, diabetes and pulmonary hypertension (Mathew, 2014; H. Zhang et al., 2017).

Mitochondrial dynamics is controlled by various proteins. Fusion of the outer mitochondrial membrane (OMM) is regulated by the transmembrane GTPases mitofusin-1 and mitofusin-2 (MFN1, MFN2), while fusion of the inner mitochondrial membrane (IMM) is controlled by optic atrophy protein-1 (OPA1). The key regulators of fission are dynamin-related protein-1 (DRP1) and Fission-1 (FIS1). FIS1 recruits DRP1 to the mitochondria to initiate fission (Yoon, Krueger, Oswald, & McNiven, 2003). Phosphorylation at Ser637 inhibits Drp1 (pSer637-DRP1) activity, while phosphorylation at Ser616 activates Drp1 (Cribbs & Strack, 2007; C. Hu, Huang, & Li, 2017).

The activation of DRP-1 in PAH lung vasculature has been shown to reduce the expression of mitochondrial complex I and superoxide dismutase, leading to mitochondrial fragmentation and hyperpolarization of the mitochondrial membrane (Marsboom et al., 2012). In addition, the reduced expression of MFN2 has been shown to induce mitochondrial fragmentation and increased cell proliferation rates in PAH vascular cells (J. J. Ryan et al., 2013).

Mitochondrial dynamics depends on the intracellular organisation and polymerization of microtubules and the actin cytoskeleton (Moore & Holzbaur, 2018). Microtubules allow the transport of mitochondria to metabolically active, energy-demanding regions of the cell, where they act as key regulators of mitochondrial fission and fusion (McCarron et al., 2013). The actin cytoskeleton is a complex network of polarised filaments that regulates cell contraction, motility, vesicle trafficking, intracellular organization, cytokinesis, endocytosis and apoptosis. CLIC proteins associate with cytoskeletal proteins including tubulin, molecular motor protein dynein and actin polymerization regulator, Arp2 and Arp3 (Abdul-Salam et al., 2019; Ackema et al., 2014; Mathur, 2005; Pimkina & Murphy, 2011; Yang et al., 2009) and may therefore indirectly affect mitochondrial dynamics. The depolymerisation of microtubules leads to mitochondrial fragmentation, while changes in actin polymerization can induce apoptosis and encourage the

accumulation of reactive oxygen species (ROS) in cells (Desouza et al., 2012; Jourdain et al., 2009).

The localization and function of mitochondrial proteins studied in this chapter is described in Table 3.1, while the localization of these proteins within the mitochondrion is illustrated in Figure 3.1.

Table 3.1 Localization and function of mitochondrial proteins studied in Chapter 3. Mitochondrial marker antibodies were provided in the mitochondrial marker antibody sampler kit (Cell Signalling, UK, 8674T).

Protein name	Localization	Function	Reference
Cytochrome c oxidase IV (COX IV)	IMM	-Terminal enzyme of the mitochondrial respiratory transport chain. -Transfers electrons from cytochrome *c* to an oxygen molecule.	(Ostermeier et al., 1996)
Heat-shock protein-60 (HSP60)	Mitochondrial matrix	-Member of the 'chaperonin' class of proteins. -Required for folding imported key proteins from the cytoplasm into the mitochondrial matrix.	(Zeilstra-Ryalls et al., 1991)
Prohibition protein 1 (PHB1)	IMM	-Essential for the stabilization of newly synthesized mitochondrial proteins.	(Tatsuta et al., 2005)
Pyruvate dehydrogenase (PDH)	Mitochondrial matrix	-Catalyses oxidative decarboxylation of pyruvate to form acetyl-CoA that participates in the Citric Acid Cycle to carry out the cellular respiration.	(Sutendra et al., 2011)
Succinate dehydrogenase (SDH)	IMM	-Key component of the citric acid cycle as well as the electron transport chain.	(Oyedotun & Lemire, 2004)
Voltage-dependent anion channel (VDAC)	OMM	-Controls the diffusion of metabolites between mitochondria and other cell compartments.	(Ponnalagu & Singh, 2016)

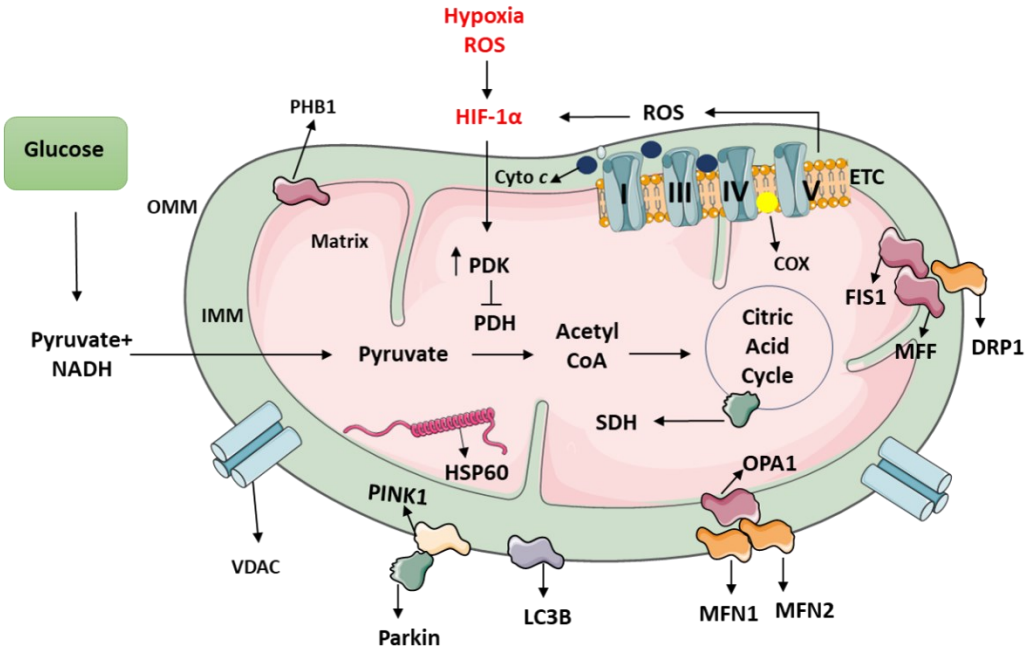


Figure 3.1: Schematic illustration of localization of mitochondrial proteins examined in this study. Abbreviations: COX IV, cytochrome c oxidase IV; HSP60, heat-shock protein-60; PHB1, prohibition protein 1; PDH, pyruvate dehydrogenase; PDK, pyruvate dehydrogenase kinase; SDH, succinate dehydrogenase; MFN1, mitofusin-1; MFN2, mitofusin-2; OPA1, optic atrophy 1; DRP1, dynamin-related protein-1; FIS1, fission-1; MFF, mitochondrial fission factor; LC3B, microtubule-associated protein 1-B light chain-3B; PINK1, PTEN-induced kinase 1; VDAC, voltage-dependent anion channel; NADH, nicotinamide adenine dinucleotide (H = hydrogen); IMM, inner mitochondrial membrane; OMM, outer mitochondrial membrane; ETC, electron transport chain; ROS, reactive oxygen species; HIF-1α, hypoxia-inducible factor 1 α. Illustration created by author using Servier Medical Art.

The selective removal of dysfunctional or defective mitochondria by autophagy is known as mitophagy. Initially, it was believed that mitophagy took place at random, but subsequent studies have shown the selective nature of the process (Chiu et al., 2009; Dasgupta et al., 2011). Clearing defective mitochondria through mitophagy requires two steps: firstly the induction of autophagy, and secondly the priming of dysfunctional mitochondria for selective autophagic recognition. Mitochondrial priming is mediated either by the PTEN-induced kinase 1 (PINK1)-Parkin signalling pathway or the BCL2 interacting protein 3 (BNIP3) pathway (Ding & Yin, 2012). Another autophagic marker that has been investigated in the context of PH is microtubule-

associated protein 1-B light chain-3B, known as LC3B (Aggarwal et al., 2016). Previous studies have shown that LC3B expression is elevated in the lungs of mice that were exposed to hypoxia for 3 weeks, and remains at higher levels in the pulmonary artery endothelial cells (PAECs) and the pulmonary artery smooth muscle cells (PASMCs) for 24 weeks (Lee et al., 2011). LC3B levels are also increased in the lungs of PH patients (Aggarwal et al., 2016). The PINK1/Parkin-mediated mitophagy pathway is also activated under hypoxia, promoting pulmonary vascular remodelling (Linqing et al., 2020).

Changes in the density and morphology of mitochondrial cristae can alter mitochondrial bioenergetics and impair mitochondrial respiration. The structure of the cristae is controlled by a large protein complex located in the IMM comprising OPA1, the mitochondrial contact site and the cristae organizing system (MICOS), which connects the IMM with the OMM (Merkwirth et al., 2008; Quintana-Cabrera et al., 2018). Several studies have also confirmed that the loss of IMM structural proteins such as stomatin-like protein 2 (SLP2), and Prohibitin (PHB) family proteins affects cristae architecture and impairs mitochondrial respiration (Merkwirth et al., 2008; Tondera et al., 2009). Fission and fusion proteins have also been implicated in regulating cristae morphology, including MFN1, MFN2, and DRP1, located in the OMM (Cogliati et al., 2016).

3.2 Experimental aims

The aims of the experiments presented in this chapter were to:

1. Optimize conditions for the adenoviral overexpression of CLIC proteins in HPAECs.
2. Confirm the mitochondrial localization of CLIC1 and CLIC4 proteins in HPAECs.
3. Determine the effect of CLIC overexpression on mitochondrial dynamics, including mitochondrial content, fusion and fission in control and CLIC-overexpressing HPAECs.
4. Investigate the mechanisms involved in CLIC-induced effects by

- studying changes in the expression of fusion and fission proteins in total cell lysates and purified mitochondrial fractions.
- investigating the effect of CLIC overexpression on the organization of actin and the microtubule cytoskeleton.
- verifying the potential role of mitophagy in CLIC-induced changes in mitochondrial dynamics by studying changes in the expression of mitophagy markers.

5. Study the effect of CLIC overexpression on mitochondrial structure.

3.3 Experimental outline

The outline of the experimental process is shown in Figure 3.2, and a brief description of the experimental methods is provided below. For further detail, see Chapter2 - Materials and Methods.

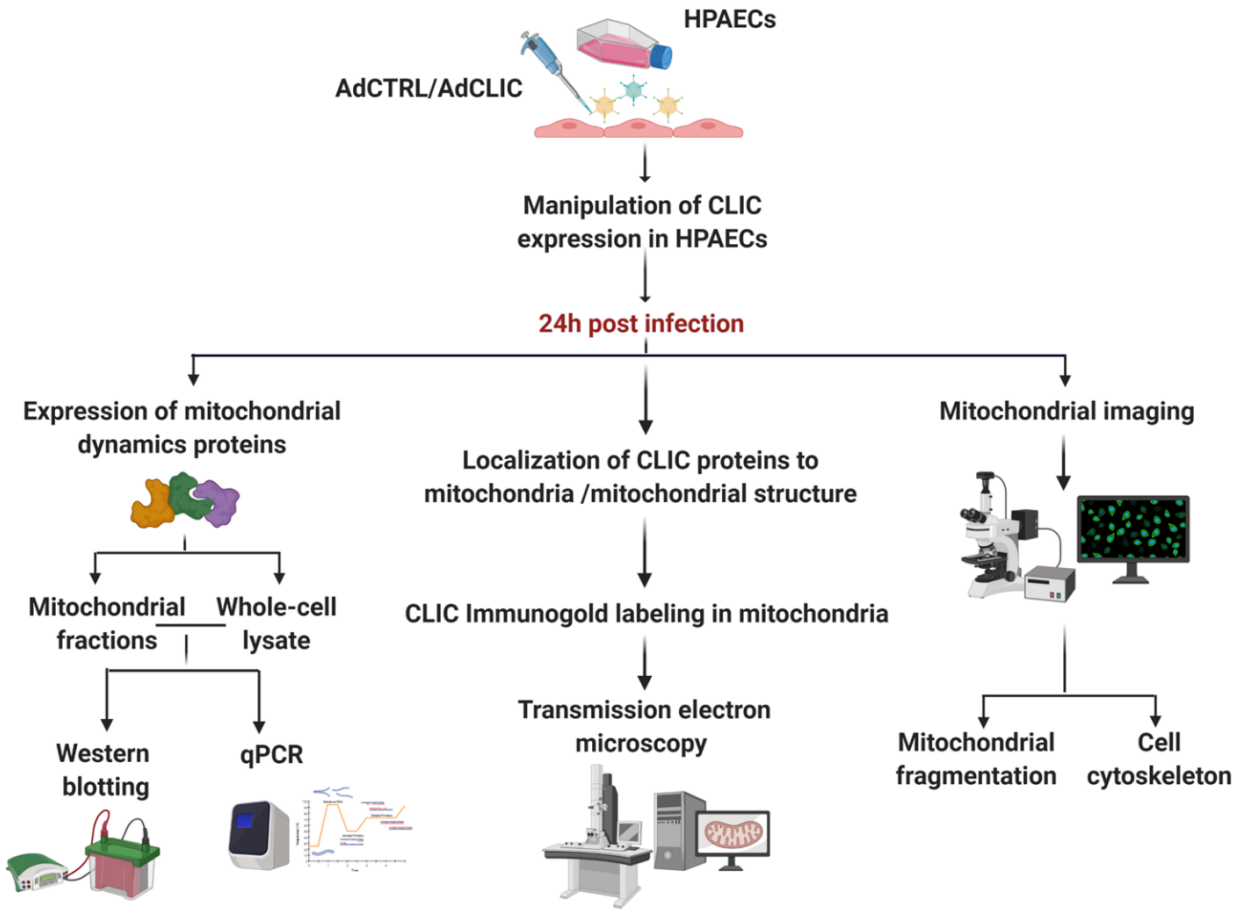


Figure 3.2: Experimental outline of Chapter 3. CLIC overexpression induced by adenoviral gene transfer was confirmed by immunofluorescent staining and western blotting in HPAECs, 24 hours post-infection. The effect of CLIC proteins on mitochondrial structure and dynamics in HPAECs was studied using TEM, immunofluorescence, confocal microscopy, western blotting and qPCR. Illustration created by the author with BioRender.com.

3.3.1 Manipulation of CLIC expression in HPAECs

CLIC proteins were overexpressed in HPAECs via adenoviral gene transfer. AdCLIC1 and AdCLIC4 were c-terminally tagged with the haemagglutinin (HA) tag, while AdCLIC5sh and AdCLIC5L were myc-tagged, allowing the precise localization of recombinant proteins in cells. In this study, I used the most commonly expressed short isoform of CLIC5 (CLIC5sh) (Argenzio & Moolenaar, 2016). AdCLIC4 was expressed under tetracycline-off (Tet-off) gene expression system (Abdul-Salam et al., 2019; Wojciak-Stothard et al., 2014). Briefly, HPAECs growing in 6-well plates were left untreated or were infected with different dilutions of the adenoviral stock in order to modulate the overexpression levels of AdCLIC1, AdCLIC4, and AdCLIC5 (5 µL, 10 µL, and 20 µL of adenoviral stock, corresponding to MOI of 1:100, 1:200, and 1:400). Empty adenovirus or Ad-Tet-off were used as adenoviral controls. The cells were lysed 24 hours post-infection, and the protein lysates were resolved by electrophoresis, after which western blotting was used to confirm mutant protein expression and select an optimal adenoviral MOI for further experiments. An optimal MOI would increase the expression of CLIC proteins to the level seen in PAH. For further details see Chapter 2 - Materials and Methods, Section 2.2.

3.3.2 Measurement of mitochondrial fragmentation

The quantitative assessment of mitochondrial fission follows two main strategies. The first involves the measurement of mitochondrial length to determine the degree of fission, but this approach is impractical for situations in which there are numerous mitochondrial fragments and/or mitochondrial coiling and knotting (Farrand et al., 2013). The other strategy, which was used in this study, involves measuring the number of mitochondrial particles smaller than 2-3 µm in length (Farrand et al., 2013). The cut-off size is typically determined by individual observers to ensure that all mitochondrial particles are taken into account.

The Mitochondrial Fragmentation Count (MFC) determines the number of discrete mitochondrial particles per cell. The mitochondrial coverage area is the total area taken by mitochondria within a cell. Here, the MFC and the total mitochondrial area were determined using NIP2 imaging software (Martinez & Cupitt, 2005). Briefly, images of fluorescently-labelled mitochondria were acquired and filtered (by median), thresholded and binarized to identify individual mitochondrial segments in order to score the total area of the fragmented mitochondria. The combined area of mitochondrial fragments was normalized to the total mitochondrial area (in pixels) in each cell to define the cell's MFC. For each intervention, 20 randomly selected cells were analysed in 3 separate experiments (Hong et al., 2013) (Figure 3.3). For further details see Chapter 2 - Materials and Methods, Section 2.4.

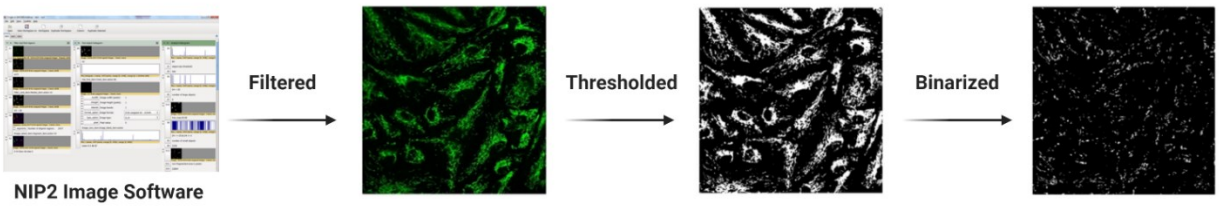


Figure 3.3: Schematic illustration of mitochondrial fragmentation analysis using NIP2 image software.

3.3.3 Immunogold labelling of mitochondrial CLIC proteins in HPAECs

For immunogold labelling, samples were processed according to the Tokuyasu method of cryo-ultrathin sectioning (Tokuyasu, 1973). Control and CLIC-overexpressing HPAECs were fixed with 0.05% glutaraldehyde and 2% paraformaldehyde in 0.2M PIPES pH 7.2 for 15 minutes at room temperature. The cells were scraped off, centrifuged at 400 x g and the cell pellet was then washed gently with PBS. Samples were kept in the PBS at 4°C before further processing. To produce ultra-thin sections, small fragments of the cryo-protected cell pellet were frozen in liquid nitrogen before sectioning, and the sections were then defrosted and transferred onto copper

grids in PBS. Prior to labelling, grids were washed with PBS and blocked in 0.5% fish skin gelatine and PBS for 10 minutes, before incubating sections with a primary antibody (mouse monoclonals anti-CLIC1, anti-CLC4, Santa Cruz, dilutions prepared in FSG) for 30 minutes at room temperature. Afterwards, samples were washed in PBS and incubated with secondary rabbit anti-mouse antibodies (1 in 200 in FSG, Southern Biotech, Birmingham, UK) for 20 minutes, followed by another set of washes in PBS. Sections were then incubated in 10 nm protein-A gold (Sigma-Aldrich, UK, P6855) for 20 minutes and were then washed in PBS and deionised water. Sections were contrasted in droplets for 10 minutes, and the grids were air-dried after removing any excess contrasting solution using filter paper. Dried grids were analysed using a JEOL JEM 1400 transmission electron microscope operated at 120 kV, and images were taken using a digital camera. For further details see Chapter 2 - Materials and Methods, Section 2.3.

3.3.4 Protein expression levels of key regulators of mitochondrial dynamics

Whole cells or isolated mitochondrial fractions from control and CLIC-overexpressing HPAECs were lysed in a RIPA lysis buffer with protease inhibitors, and protein concentrations were then measured using Pierce™ BCA Protein Assay Kit using standard protocols. Samples were resolved with SDS-PAGE (10 µg – 20 µg protein/lane) and analysed by western blotting. Subsequently the membranes were probed with primary antibodies, followed by incubation with horseradish peroxidase (HRP)-labelled secondary antibodies. Bands were visualized using Luminata Crescendo Western HRP Substrate in a ChemiDoc™ Imager. For further details see Chapter 2 - Materials and Methods, Section 2.8.

3.3.5 mRNA expression levels of key regulators of mitochondrial dynamics

HPAECs were harvested by trypsinization, and RNA was purified and reverse transcribed to cDNA. The cDNAs were then subjected to a real time qPCR. For details see Chapter 2- Materials and Methods, Section 2.9.

3.3.6 Isolation of mitochondria from HPAECs

Mitochondrial isolation was carried out using a Mitochondria Isolation Kit for Cultured Cells, according to the manufacturer's guidelines. HPAECs grown in 175 cm^2 culture flasks (4 flasks per condition), were infected with Adcontrol, AdCLIC1, AdCLIC4 or AdCLIC5. The following day the cells were collected and ruptured using a Dounce Homogenizer. Cell homogenates were centrifuged at low speed (1,000 x g) to remove debris and large cellular organelles and were then centrifuged at a higher speed (12,000 x g) to isolate the mitochondria. Mitochondrial fractions were collected and frozen at -80°C to be used later for mitochondrial fraction quality assay and western blotting. For further methodological detail, see Chapter 2- Materials and Methods, Section 2.7.

3.3.7 Immunofluorescent staining of microtubules

HPAECs were grown on coverslips, fixed and incubated in methanol and then in acetone, air dried, re-hydrated in PBS, blocked in 5% BSA and immunostained with primary mouse monoclonal anti-α tubulin antibodies and fluorescently-labelled secondary antibodies. The cells were then washed in PBS and mounted in Vectashield with DAPI. See Chapter 2- Materials and Methods, Section 2.5.

3.3.8 Manipulation of microtubule polymerization

24 hours post-infection, the control (AdCTRL) and CLIC-overexpressing HPAECs were treated with microtubule-stabilising agent taxol (10 µM) for 30 minutes or mirotubule depolymerising agent nocodazole (20 µM) for 10 minutes (Takesono et al., 2010). After that, the cells were fixed and stained as described above. Images of microtubules and mitochondrial networks were acquired under the confocal microscope and processed for further analysis. For details see Chapter 2- Materials and Methods, Section 2.5.

3.4 Results

3.4.1 CLIC overexpression in endothelial cells

In the first set of experiments I optimized the conditions for adenoviral infection so that the expression levels of recombinant proteins corresponded to the ~4-5 fold increase in the expression of CLIC proteins, as seen in PAH lungs (Abdul-Salam et al., 2010). An MOI of 1:100 was found optimal for inducing a 4 to 5-fold increase in the expression levels of recombinant HA-tagged CLIC1 and CLIC4 and myc-tagged CLIC5 in HPAECs 24 hours post-infection (Figures 3.4 and 3.5). The specificity of CLIC1 and CLIC4 antibodies was confirmed by western blotting (see Supplementary Figures S.5).

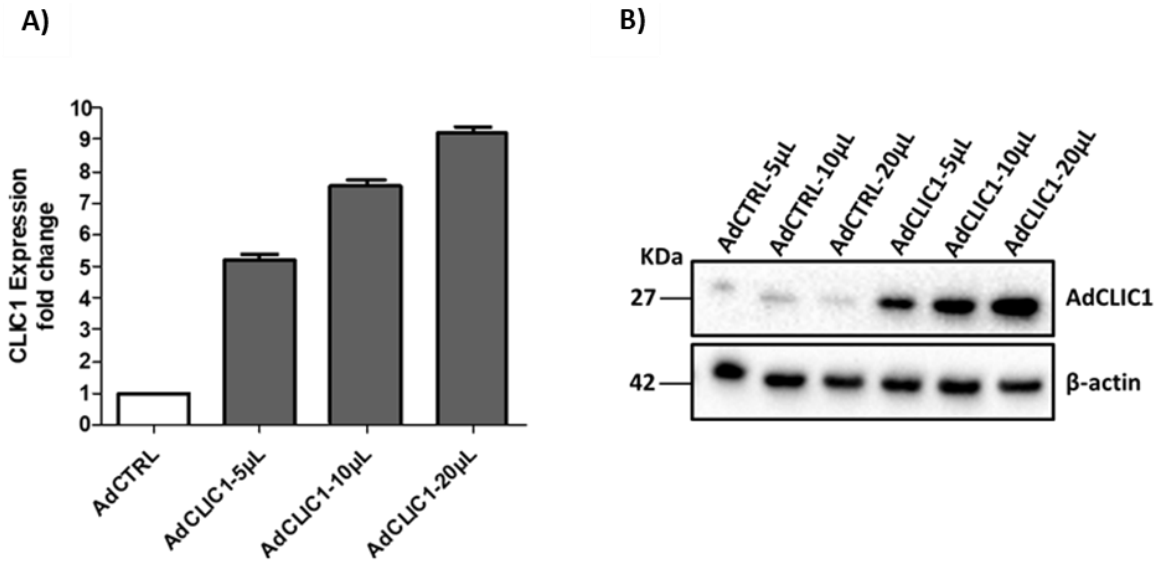


Figure 3.4: Example of optimization of viral infection. (A) Bar graph indicates fold changes in CLIC1 protein levels in HPAECs infected with different dilutions of AdCLIC1 or AdCTRL (Adenoviral control) 24 hours post-infection. 5µL=MOI 1: 100, 10µL=MOI 1: 200, and 20µL=MOI 1: 400. **(B)** Representative western blots corresponding to **(A).** Expression levels were normalised to β-actin. A similar strategy was used to optimise expression levels of recombinant proteins in AdCLIC4- and AdCLIC5-infected cells (not shown).

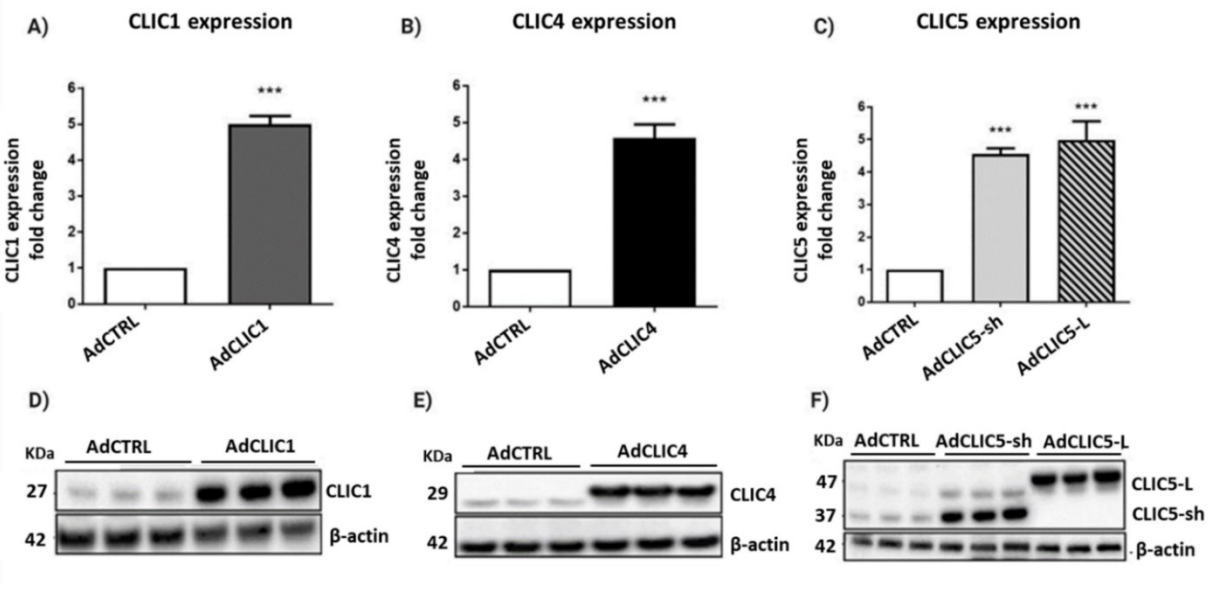


Figure 3.5: CLIC1, CLIC4 and CLIC5 protein overexpression in HPAECs. (A, B, C). Changes in CLIC protein levels in HPAECs infected with AdCLIC1, AdCLIC4, AdCLIC5sh (short) and AdCLIC5L (Long) and AdCTRL, are as shown. 24 hours post-infection at the MOI 1:100, HPAECs showed a ~4 to 5 fold increase in the expression level of recombinant AdCLIC1, AdCLIC4, and AdCLIC5 (sh and L), compared with viral control (AdCTRL) as shown. ***P<0.001 n=3, Student t-test. **(D, E, F)** Corresponding representative western blots show CLIC protein overexpression; β-actin was used as a loading control.

The overexpression of recombinant proteins was also confirmed by the immunofluorescent staining of cells with anti-CLIC, anti-HA and anti-myc-tag antibodies, followed by confocal microscopy analysis. ~95-97% of the cells showed an overexpression of recombinant proteins (Figures 3.6, and 3.7).

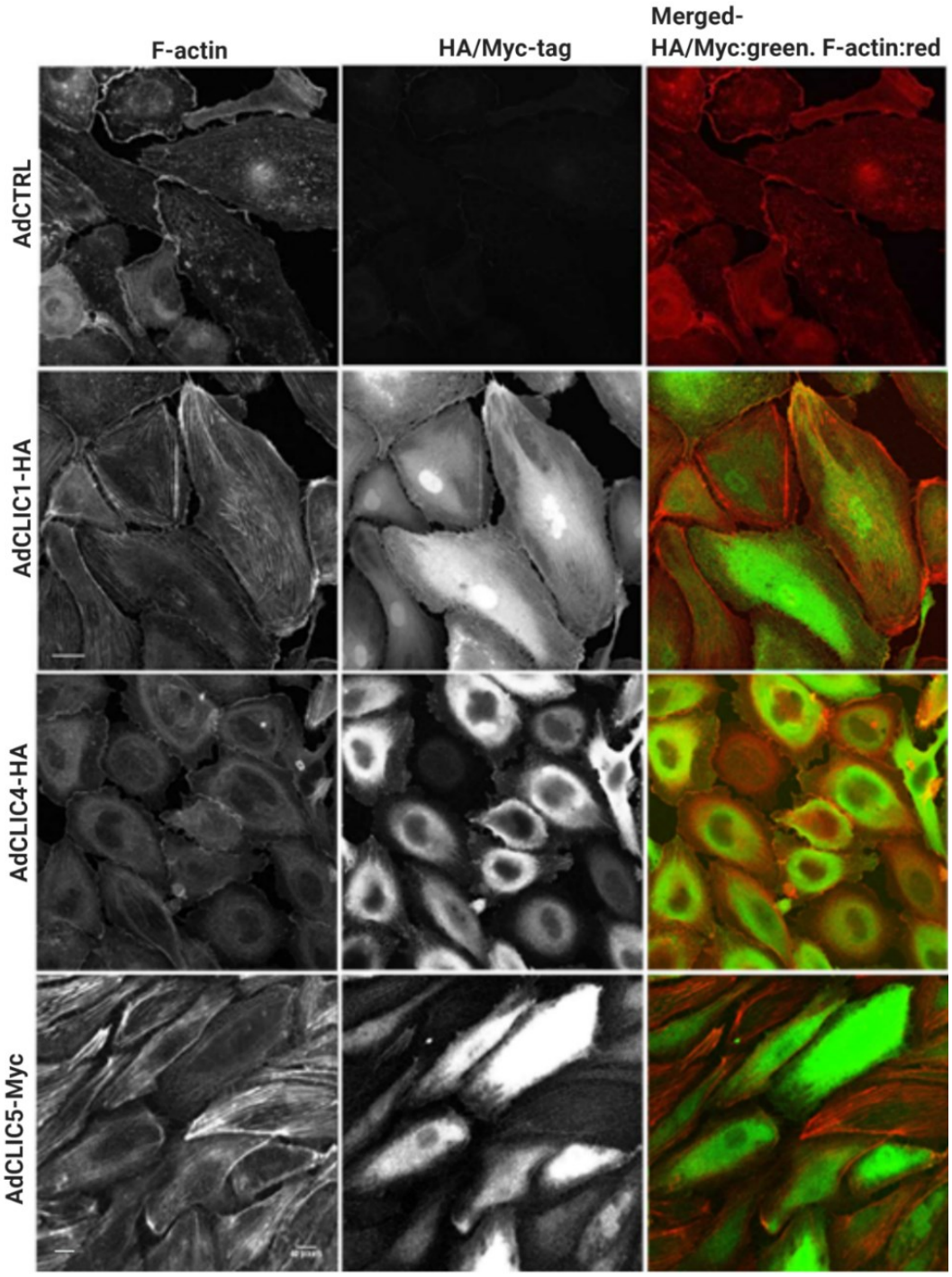


Figure 3.6: Overexpression of recombinant CLIC proteins in HPAECs. Representative confocal images show the immunostaining of recombinant HA-tagged CLIC1 (AdCLIC1), HA-tagged CLIC4 (AdCLIC4) and myc-tagged short isoform CLIC5 (AdCLIC5) 24h post-infection in cells treated as shown. In the merged images, F-actin is red and HA-CLIC1, HA-CLIC4 and Myc-CLIC5 are green. Bar=15 µm in the first top two panels; Bar=10 µm in the bottom two panels. Images were taken using a Zeiss LSM 780 confocal micrseaoscope with 40x objective.

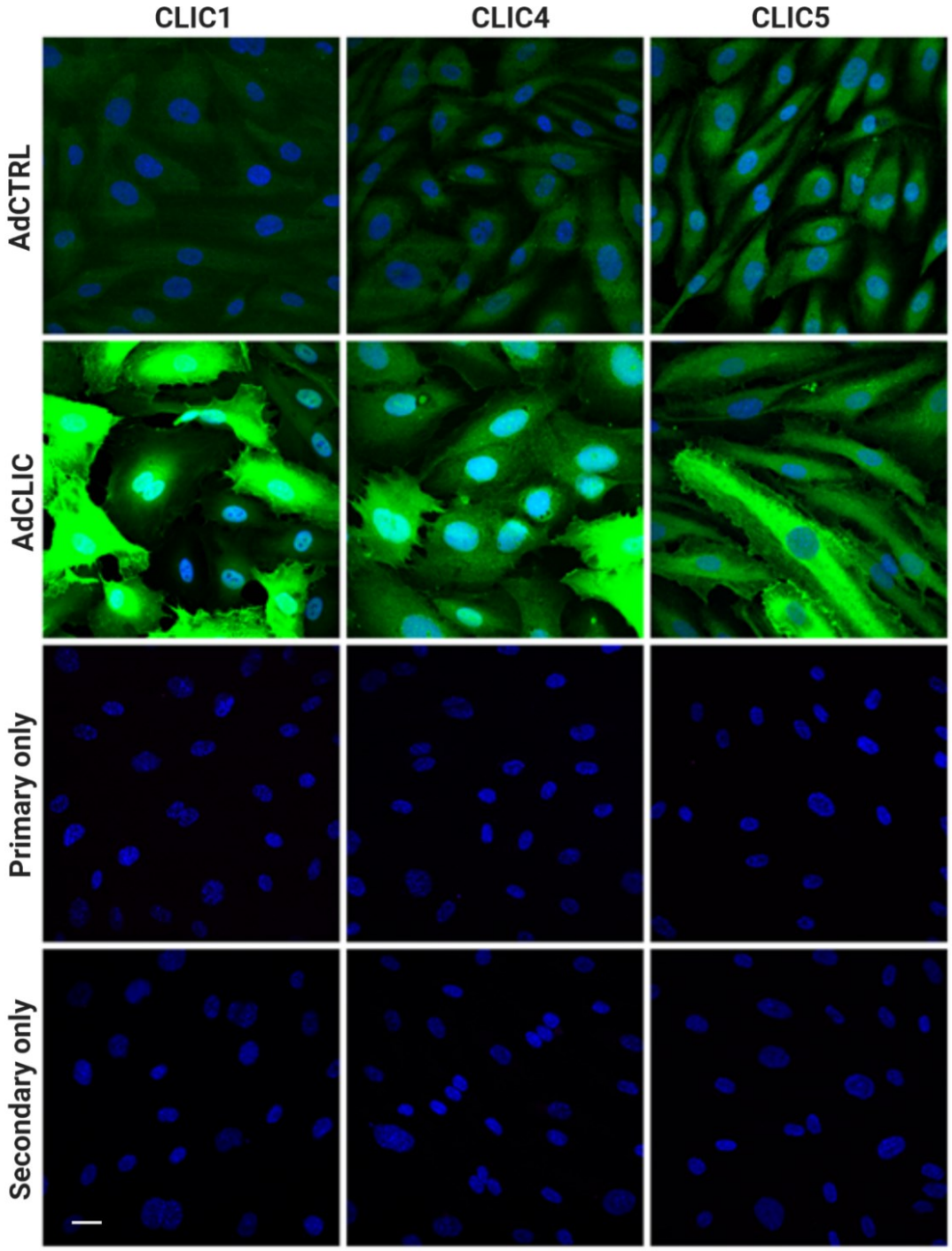


Figure 3.7: Immunostaining of CLIC1, CLIC4 and CLIC5 in HPAECs. Representative images show the expression levels of CLIC1, CLIC4 and CLIC5 in control cells (AdCTRL) and cells treated with AdCLIC1, AdCLIC4 or short AdCLIC5 24 hours post-infection. Nuclei are blue, while CLIC1, CLIC4 and CLIC5 are green. The last two panels are primary and secondary antibody-only controls. Bar=10 µm. Images were obtained using a Zeiss LSM 780 confocal microscope with 40x objective.

3.4.2 Effect of CLIC overexpression on mitochondrial network in HPAECs

Total mitochondrial coverage area was significantly increased in CLIC1- and CLIC4-overexpressing HPAECs, but was decreased in CLIC5-overexpressing HPAECs (Figure 3.8).

The analysis of the mitochondrial fragmentation count (MFC) was carried out by measuring the area occupied by small (< 2µm^2 in diameter) mitochondria, normalised to the total mitochondrial coverage area. CLIC1, CLIC4 and CLIC5-overexpressing cells showed a significant increase in the number of small, fragmented mitochondria compared with adenoviral controls, which is a likely indicator of increased mitochondrial fission or reduced mitochondrial fusion (Figure 3.8). Mitochondrial fragmentation was particularly prominent in CLIC1- and CLIC4-overexpressing cells. Figure 3.9 shows representative enlarged images of the mitochondrial network in different treatment groups, while Figure 3.10 shows the subsequent image analysis steps used to quantify mitochondrial coverage and mitochondrial fragmentation in HPAECs. The overexpression of exogenous HA-tagged CLIC1, HA-tagged CLIC4 and Myc-tagged CLIC5 in cells was confirmed by the immunofluorescent staining of HA-tag and Myc-tag (Figure 3.11).

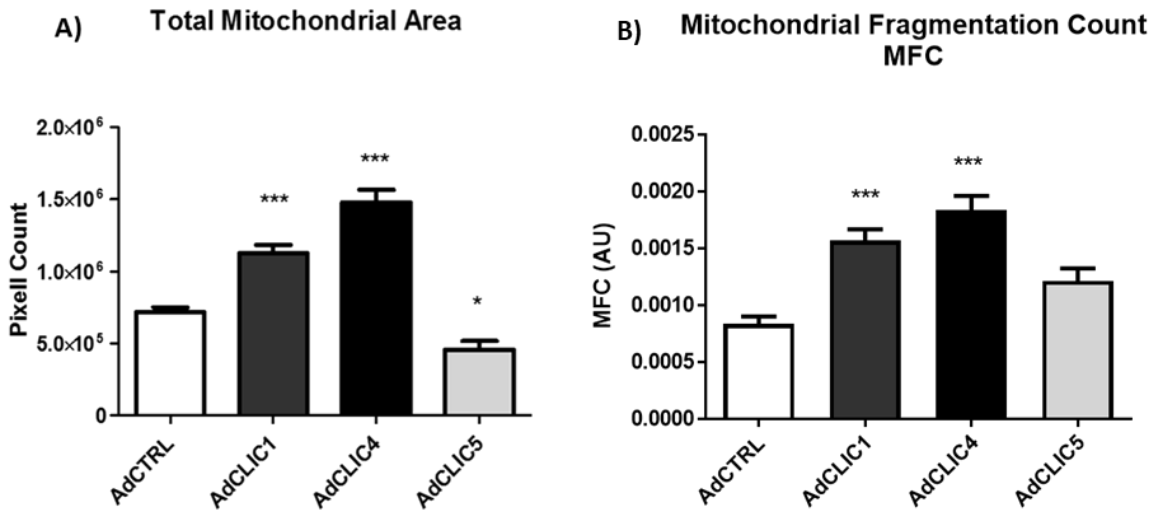


Figure 3.8: Effect of CLIC overexpression on mitochondrial content and fragmentation in HPAECs. (A) Total mitochondrial area per cell and **(B)** Mitochondrial Fragmentation Count (MFC) in HPAECs infected with AdCTRL, AdCLIC1, AdCLIC4 and AdCLIC5 as indicated. Total mitochondrial coverage area (in pixels) and MFC (in arbitrary units) were measured using NIP2 image software. 20 cells per treatment were analysed in in 3 separate experiments. *P < 0.05, **P <0.01 ***P<0.0001, comparison with AdCRTL; One-way ANOVA was used with Dunnett's post hoc test. Data are presented as mean ± SEM.

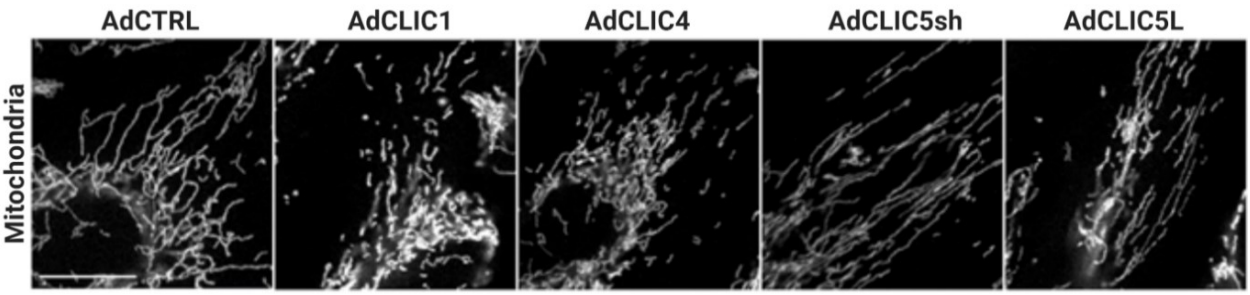


Figure 3.9: Representative images of mitochondrial networks in control HPAECs and HPAECs overexpressing AdCLIC1, AdCLIC4, AdCLIC5sh and AdCLIC5L. CLIC1- and CLIC4-overexpressing HPAECs showed fragmented mitochondria, while the mitochondria of CLIC5 (sh,L)-overexpressing HPAECs are tubular and less fragmented. Images were taken using a Zeiss LSM 780 confocal microscope with 40x objective. Bar=10µm.

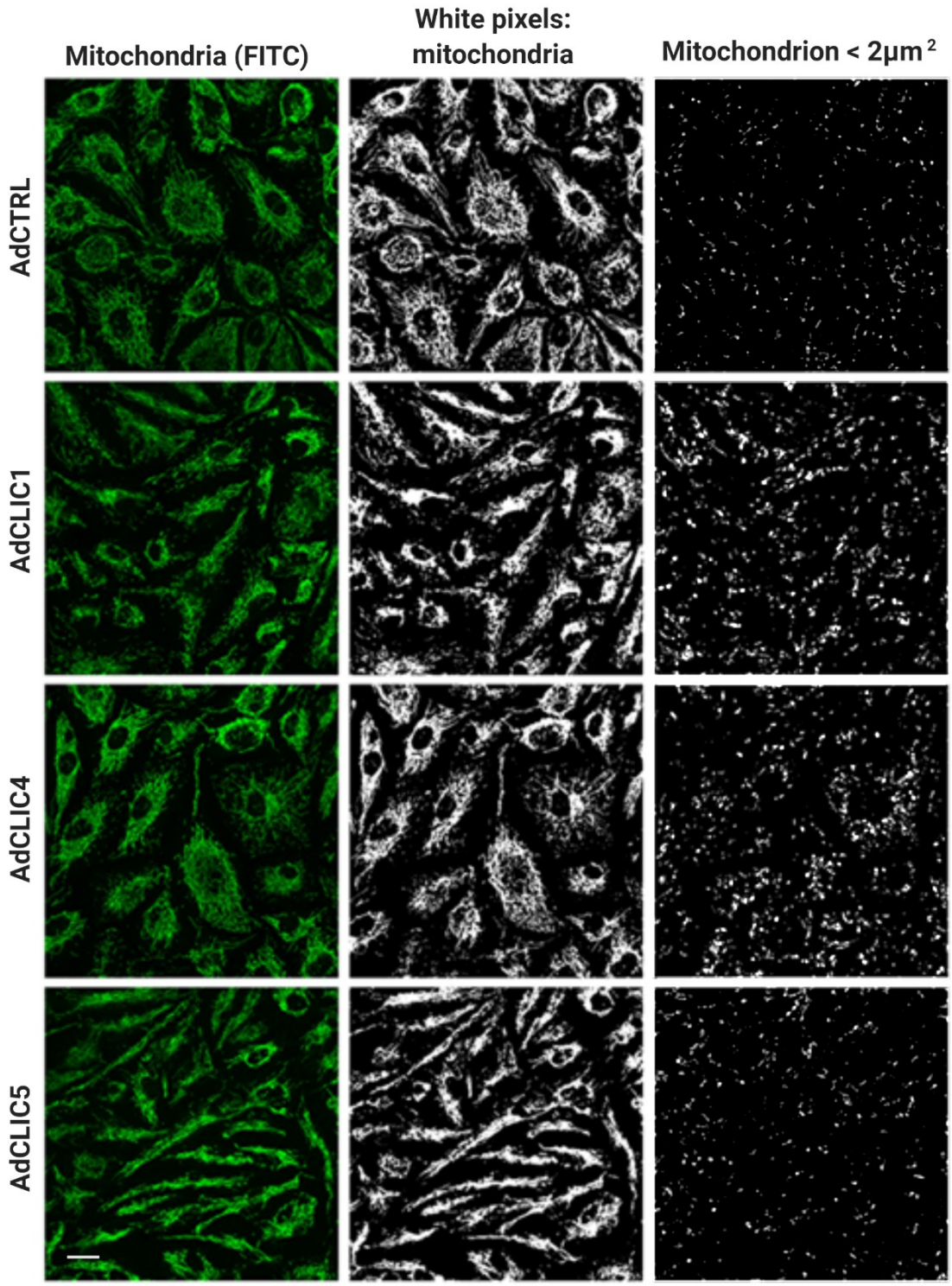


Figure 3.10: Mitochondrial fragmentation in CLIC-overexpressing HPAECs. Representative images of mitochondrial fragmentation analysis show FITC-labelled mitochondria (green; left column), black and white images of mitochondrial network (middle column), mitochondrial fragments identified by image processing with NIP2 image software (small, rod-shaped white particles, size < 2µm^2; right column). The area covered by fragmented mitochondria was normalised to the area of the whole mitochondrial network to provide MFC. Images were taken using a Zeiss LSM 780 confocal microscope with 20x objective. Bar=10µm.

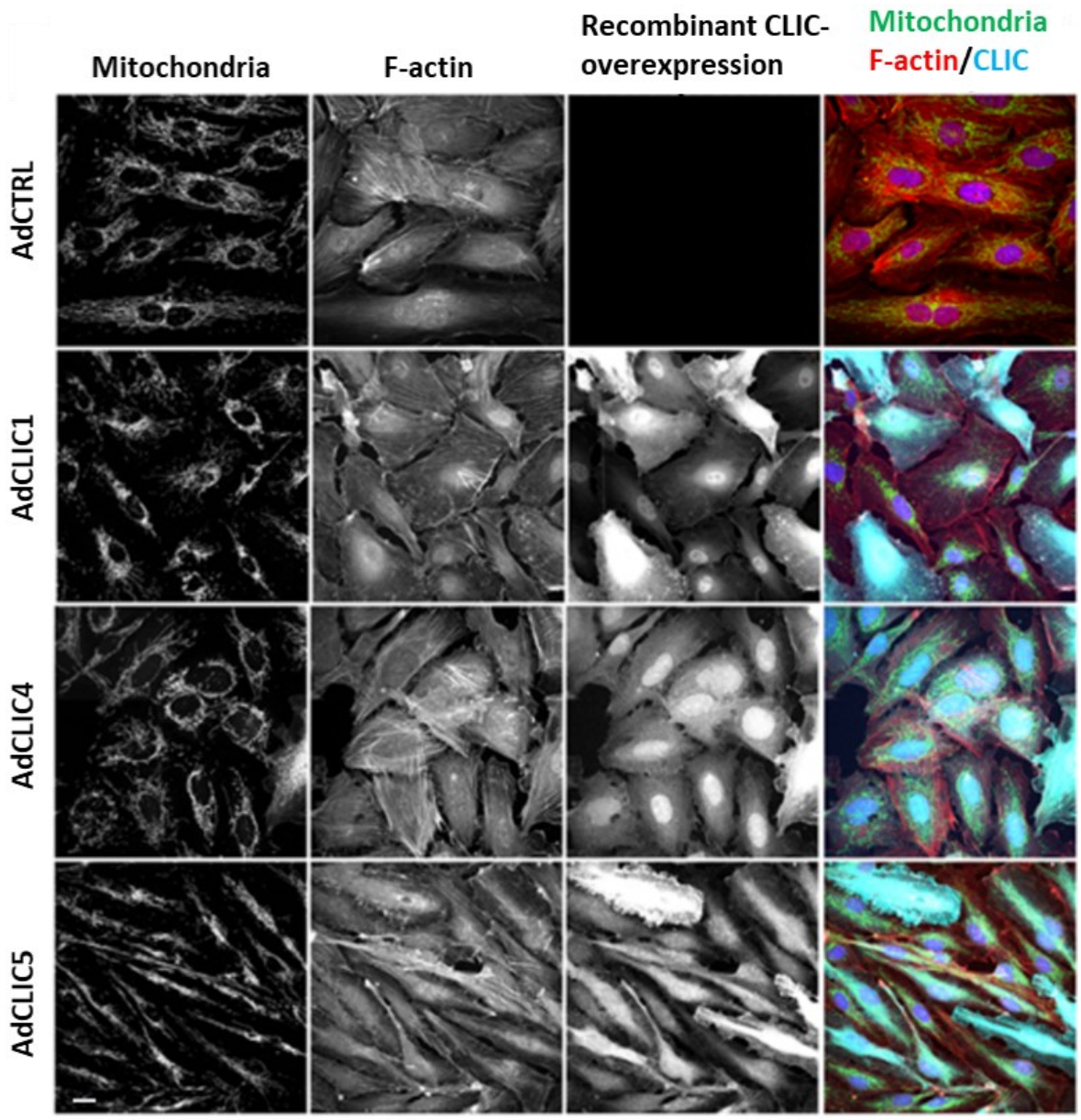


Figure 3.11: Mitochondrial network in control and CLIC-overexpressing HPAECs. Representative confocal images show mitochondrial network, F-actin staining and HA-tag or Myc-tag staining, indicating the expression of HA-tagged recombinant CLIC1, CLIC4 and Myc-tagged CLIC5. In the merged images on the right, mitochondria are in green, F-actin is red and recombinant CLIC1, CLIC4 and CLIC5 are cyan. Bar=10 µm. Images were taken using a Zeiss LSM 780 confocal microscope with 20x objective.

3.4.3 Analysis of expression levels of fission and fusion proteins

Fission and fusion processes are controlled by numerous mitochondrial proteins (Ong et al., 2015). In the subsequent series of experiments, I examined the expression levels of fusion proteins, which are key regulators of mitochondrial dynamics. Mitofusin1 (MFN1), Mitofusin2 (MFN2), and Optic atrophy-1 (OPA1) and fission proteins, Dynamin-related protein 1 (DRP1), Mitochondrial fission protein 1 (FIS1) and mitochondrial fission factor (MFF) were used in total cell lysates and purified mitochondrial fractions from HPAECs under normoxic (20% O_2, 5% CO_2) conditions at 37°C.

3.4.3.1 Western blotting analysis of fission and fusion proteins in whole cell lysates

The expression of fusion proteins MFN1, MFN2, and OPA1, and fission proteins FIS1, DRP1, and MFF were analysed using western blotting in total cell lysates of control HPAECs and HPAECs with overexpressed CLIC proteins. Meanwhile, the levels of pSer616-DRP1, which stimulates fission (Marsboom et al., 2012), pSer637-DRP1, which inhibits fission (Marsboom et al., 2012) and p-Ser146 MFF, which promotes fission (Seabright et al., 2020), were also measured.

Although some reduction in MFN2 protein levels was seen in CLIC1- and CLIC4- overexpressing HPAECs compared with controls, the difference was too small to be statistically significant (Figure 3.12). No significant changes in the expression of fusion proteins MFN1, MFN2, and OPA1 were seen in other experimental groups. CLIC1 and CLIC4 proteins did not significantly affect DRP1 expression, while CLIC5 had an inhibitory effect. CLIC4 significantly increased pSer637-DRP1 levels in HPAECs (Figure 3.13).

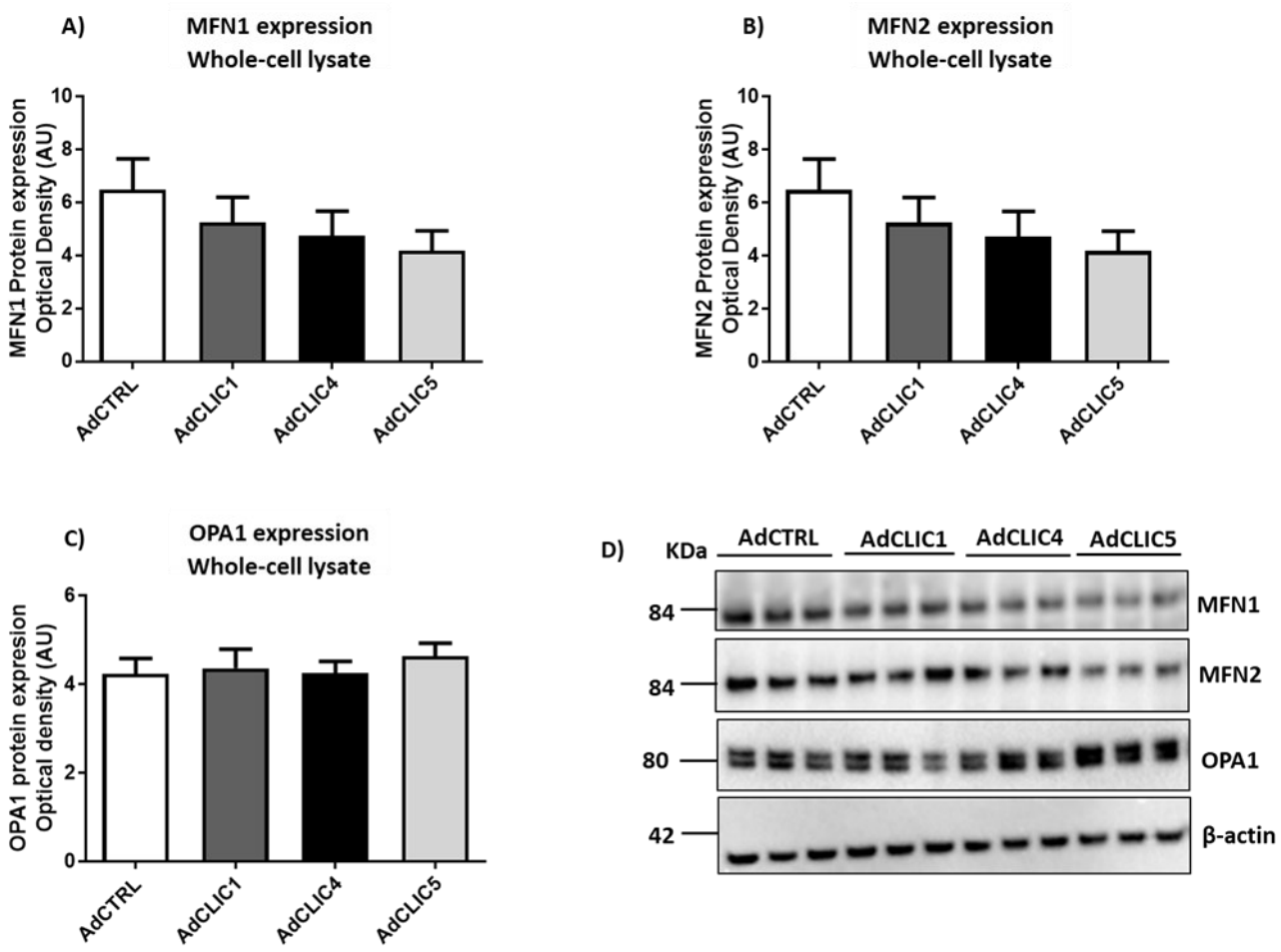


Figure 3.12: Expression of mitochondrial fusion proteins in HPAECs whole cell lysates. Graphs show changes in expression levels of **(A)** Mitofusin 1 (MFN1), **(B)** Mitofusin 2 (MFN2), **(C)** Optic atrophy1 (OPA1) in whole cell lysates from HPAECs treated with AdCTRL, AdCLIC1, AdCLIC4, and AdCLIC5 as indicated, 24 hours post-infection. Expression values were normalised to β-actin. **(D)** Corresponding representative western blots, showing the overexpression of CLIC1, CLIC4 and CLIC5 were confirmed, as shown in Figure 3.5. One-way ANOVA was used, with Dunnett's post hoc test. Data are presented as the mean ± SEM of 3 experiments with 3 technical repeats.

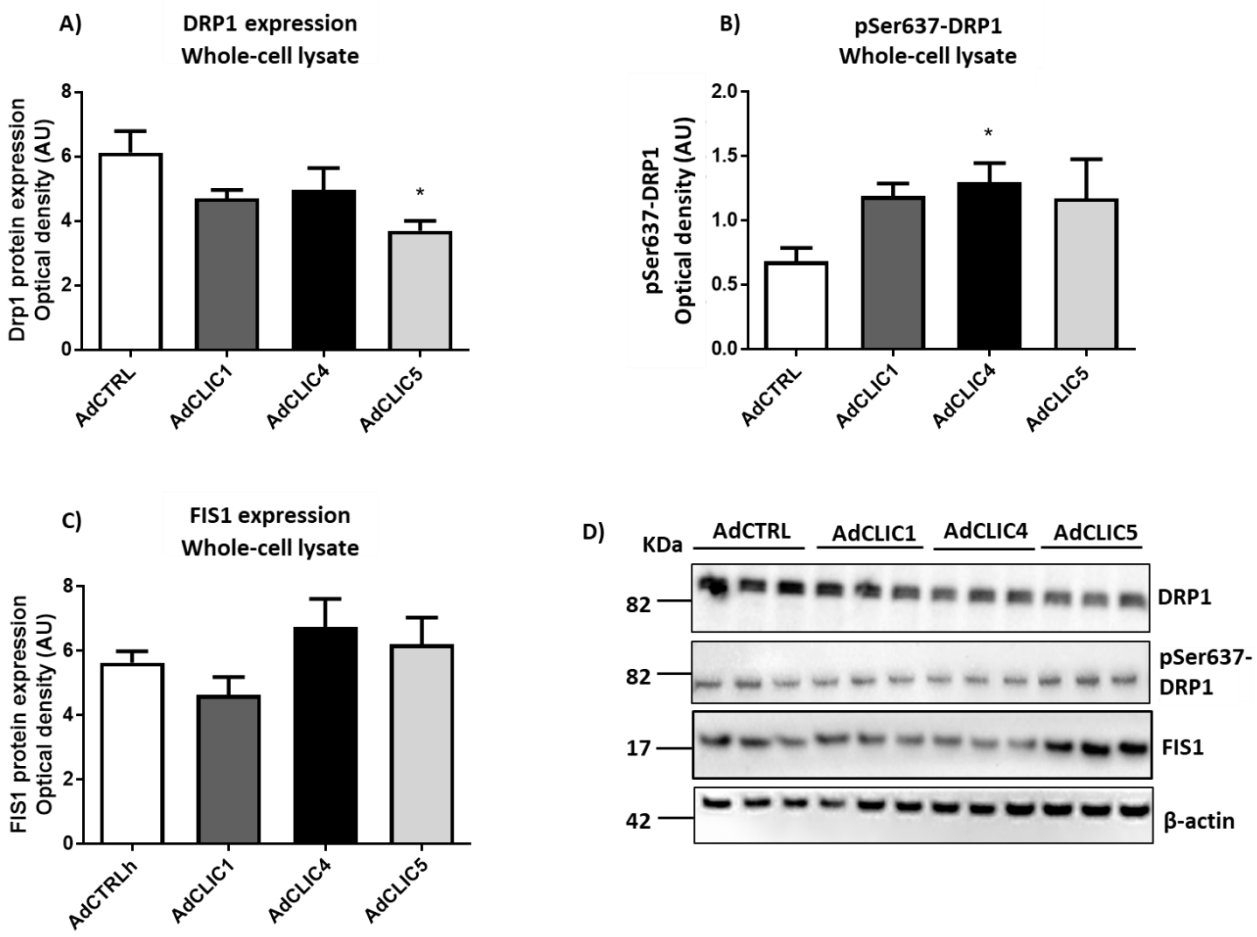


Figure 3.13: Expression of mitochondrial fission regulators in HPAECs whole cell lysates. Graphs show changes in expression of fission proteins in HPAECs treated as indicated. **(A)** Dynamin-related protein 1 (DRP1), **(B)** pSer637-DRP1 levels normalised to total DRP1 expression; **(C)** Mitochondrial fission protein 1 (FIS1), **(D)** Corresponding representative western blots showing the overexpression of CLIC1, CLIC4 and CLIC5 were confirmed as shown in Figure 3.5. *P<0.05, comparison with corresponding controls. One-way ANOVA was used with Dunnett's post hoc test. Data are presented as mean ± SEM of 3 experiments with 3 technical repeats.

3.4.3.2 qPCR analysis of fission and fusion proteins in whole cell lysates

Messenger RNA (mRNA) expression of mitochondrial dynamic proteins was determined by qPCR. Data analysis revealed a trend towards reduced MFN1 mRNA expression in CLIC1-, CLIC4- and CLIC5-overexpressing cells, while MFN2 mRNA levels remained relatively unchanged. There was a significant reduction in OPA1 in CLIC4 and CLIC5-overexpressing HPAECs, while no change was observed in CLIC1-overexpressing cells (Figure 3.14). The gene expression level of mitochondrial

fission protein DRP1 was significantly reduced in all treatment groups. mRNA levels of FIS1 were relatively unaffected by CLIC1, CLIC4 and CLIC5 (Figure 3.15).

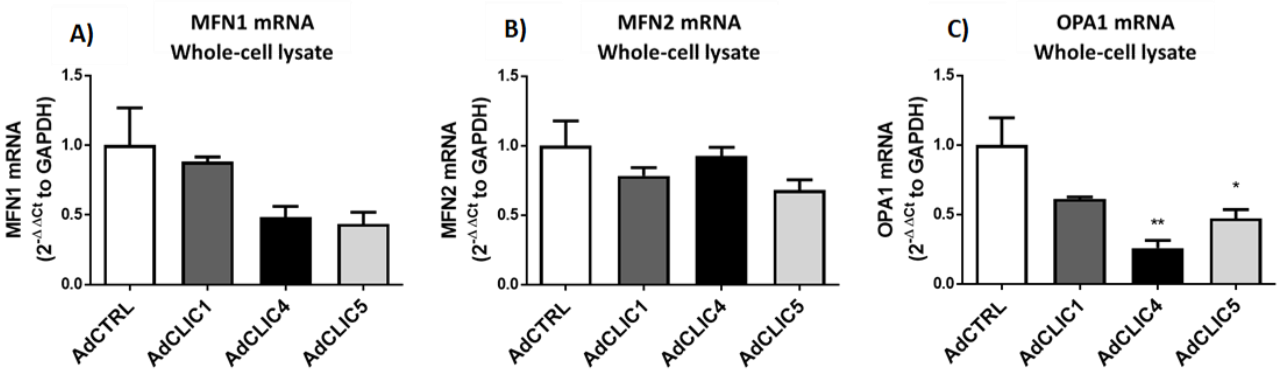


Figure 3.14: mRNA expression level of fusion proteins in HPAECs overexpressing CLIC1, CLIC4 and CLIC5. **(A)** MFN1 mRNA, **(B)** MFN2 mRNA and **(C)** OPA1 mRNA levels in cells treated with AdCTRL, AdCLIC1, AdCLIC4 and AdCLIC5, 24 hours post-infection. One-way ANOVA was used with Dunnett's post-hoc test. *P < 0.05, **P <0.01 ***P<0.0001, comparison with AdCRTL. Data are presented as mean ± SEM. n=3 experiments with 3 technical repeats.

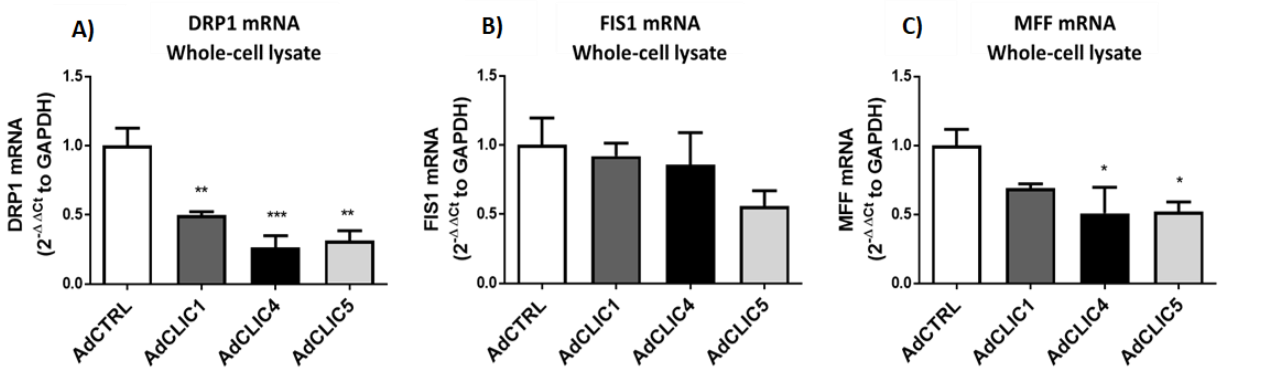


Figure 3.15: mRNA expression level of fission proteins in HPAECs overexpressing CLIC1, CLIC4 and CLIC5. **(A)** DRP1 mRNA, **(B)** FIS1 mRNA and **(C)** MFF mRNA in cells treated with AdCTRL, AdCLIC1, AdCLIC4 and AdCLIC5, 24 hours post-infection. One-way ANOVA was used with Dunnett's post hoc test. *P < 0.05, **P <0.01 ***P<0.0001, in comparison with AdCRTL. Data are presented as mean ± SEM. n=3 experiments with 3 technical repeats.

3.4.4 Mitochondrial fraction purity analysis

Because the analysis of CLIC-induced changes in the expression levels of mitochondrial fission and fusion proteins in total cell lysates did not provide conclusive results, the next set of experiments looked at the expression of these proteins in purified mitochondrial fractions.

Mitochondrial enrichment was assessed by comparing changes in the expression of mitochondrial marker proteins SDH and VDAC in mitochondrial fractions and total cell lysates following cell fractionation. The analysis showed ~6-fold enrichment in mitochondrial content compared with the whole cell extract (Figure 3.16).

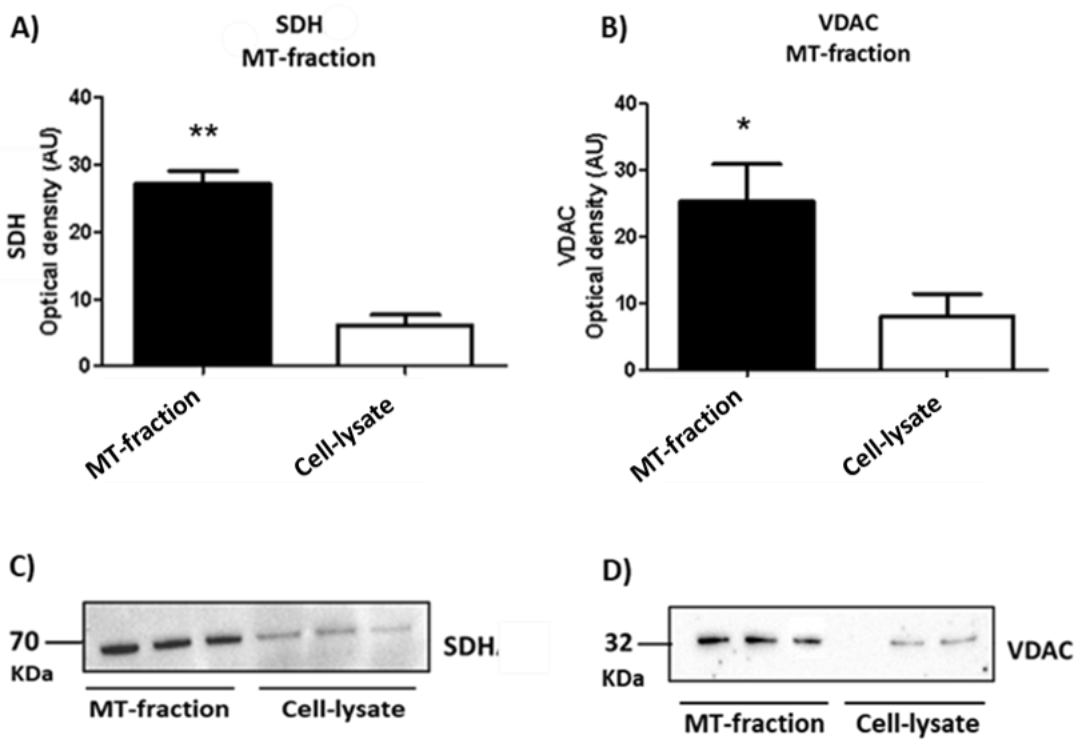


Figure 3.16: Mitochondrial fraction quality analysis. Graphs **(A)** and **(B)** show SDH and VDAC expression, respectively (band optical density, AU). Bars are means +/- SEM. N=3, *P < 0.05 **P <0.01, comparison with whole cell lysates using the Student t-test. **(C, D)** Corresponding representative western blots.

3.4.4.1 Localization of CLIC1 and CLIC4 to mitochondria in HPAECs

The localisation of CLIC proteins to mitochondria was verified using western blotting, showing an increase in HA-CLIC1, HA-CLIC4 and Myc-CLIC5 in mitochondrial fractions of HPAECs infected with recombinant adenoviruses (Figure 3.17).

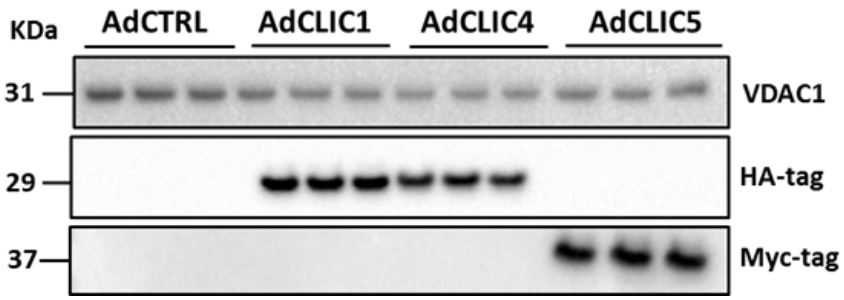


Figure 3.17: Localization of recombinant CLIC proteins to mitochondria. Representative western blots show the expression of VDAC1 and recombinant HA-CLIC1, HA-CLIC4 and Myc-CLIC5 in mitochondrial fractions. VDAC1 was used as a loading control.

Transmission electron microscopy (TEM) was also utilized to determine the localization of immunogold-labelled CLIC1 and CLIC4 within the mitochondrial structure. TEM images revealed the presence of CLIC1 and CLIC4 in the outer and inner mitochondrial membrane and in the mitochondrial cristae, with CLIC1 more frequently seen in the inner membrane and cristae, compared with CLIC4 (Figure 3.18).

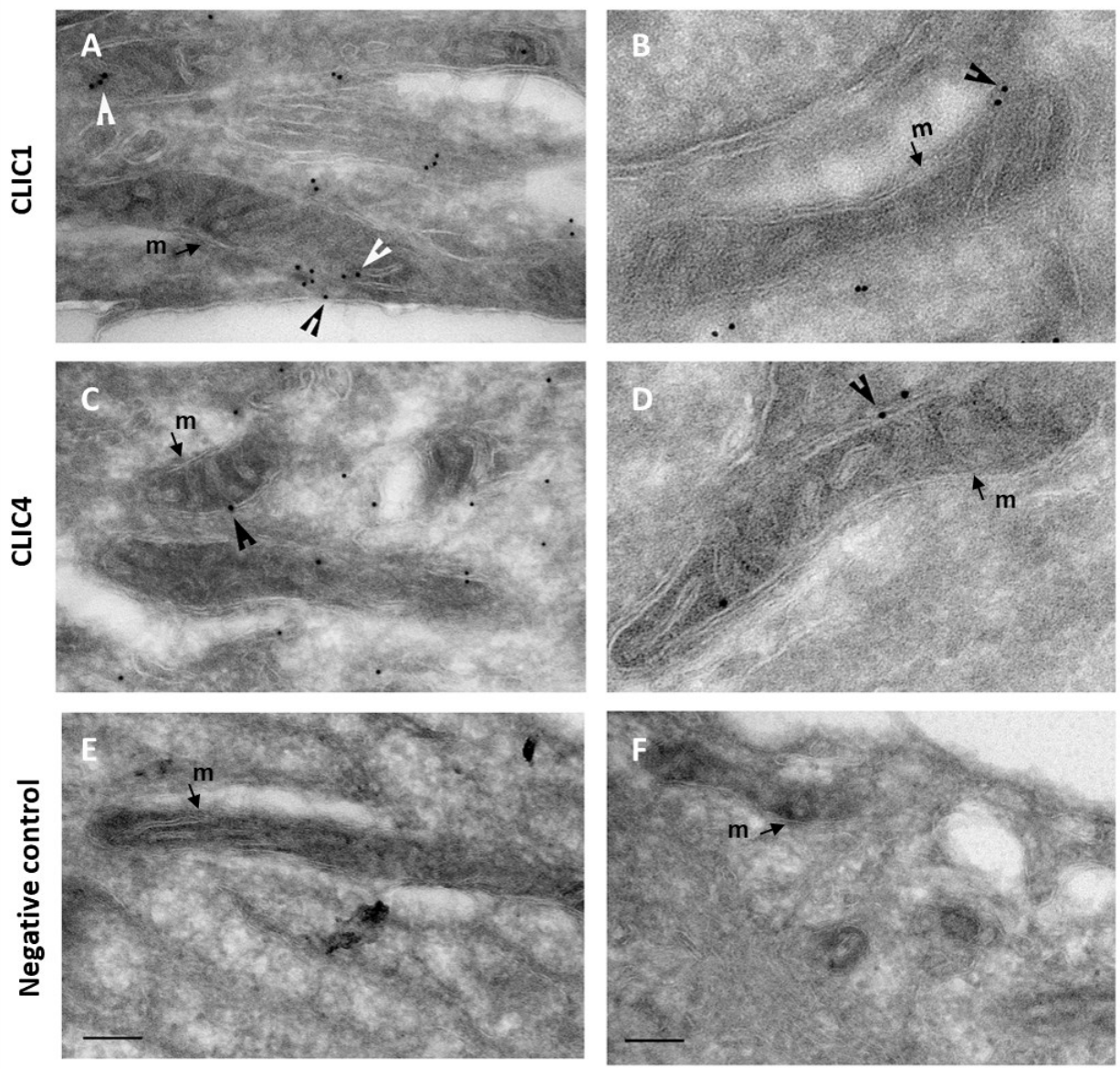


Figure 3.18: CLIC1 and CLIC4 localization in mitochondria. Represetative TEM images of immunogold-labelled CLIC1 and CLIC4 in mitochondria 24 hours post-infection with respective adenoviruses. White arrowheads point to CLIC localization in mitochondrial cristae, while black arrowheads point to CLIC localization in mitochondrial outer and inner membranes; m indicates mitochondria. Scale bar=200 nm.

3.4.4.2 Western blotting analysis of fission and fusion proteins in mitochondrial fractions

In the next set of experiments, I examined changes in the expression of key regulators of mitochondrial dynamics, fusion proteins (MFN1, MFN2, and OPA1) and fission proteins (DRP1, FIS1, and MFF) in mitochondria-enriched fractions from HPAECs, 24 hours after adenoviral infection with AdCtrl, AdCLIC1, AdCLIC4 and AdCLIC5.

CLIC1, CLIC4 and CLIC5-overexpressing cells showed reduced expression of fusion proteins MFN1, MFN2, and OPA1 in mitochondria, with CLIC1 and CLIC4 displaying the most prominent effect (Figure 3.19).

The expression of fission regulator DRP1 was reduced in mitochondrial fractions from HPAECs that overexpressed CLIC1, CLIC4, and CLIC5. The phosphorylation of DRP1 on Ser637 (inhibitory effect) was significantly increased in mitochondria from CLIC1- and CLIC4- overexpressing HPAECs. The levels of pDRP1-S616 (representing the activating effect) were significantly reduced by CLIC1 and increased by CLIC4 in HPAECs. The levels of phosphorylated DRP1 were normalized to the total of DRP1 expression. The mitochondria from CLIC5-overexpressing HPAECs showed an increased level of FIS1 expression compared with the control group, while CLIC1 and CLIC4 showed no significant effect. MFF expression levels were significantly decreased in mitochondrial fractions from HPAECs that overexpressed CLIC4 and CLIC5, while CLIC1, CLIC4, and CLIC5 increased the phosphorylation of MFF on Ser146, which was normalized to the total expression level of MFF (Figures 3.20, 3.21).

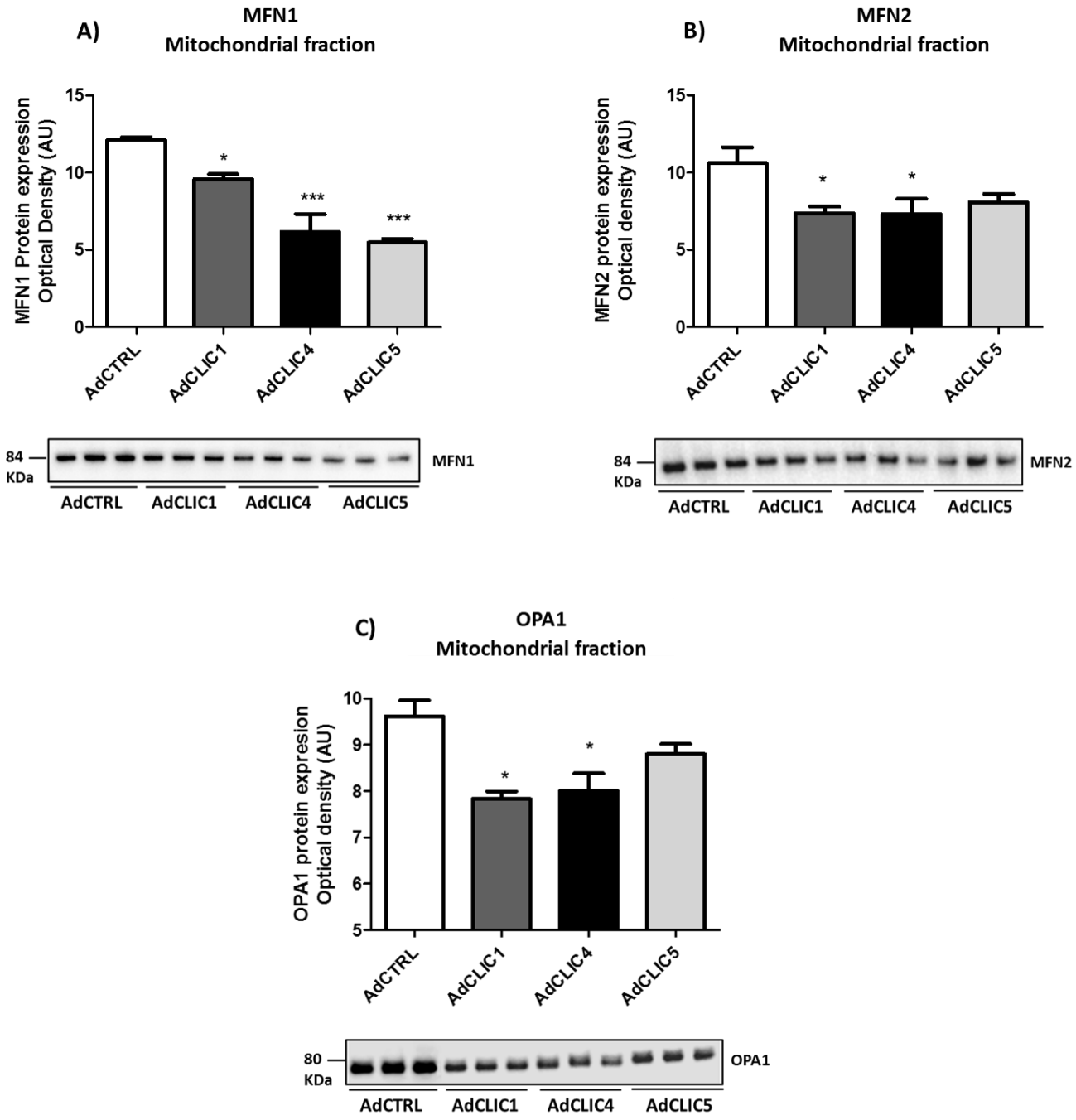


Figure 3.19: Expression of mitochondrial fusion proteins in mitochondrial fractions from HPAECs. (A) MFN1, **(B)** MFN2, **(C)** OPA1 expression in mitochondrial fractions from HPAECs treated with AdCTRL, AdCLIC1, AdCLIC4 and AdCLIC5 as indicated using western blotting. The expression of fusion proteins was normalised to mitochondrial loading protein VDAC1 (see Figure 3.17). *P < 0.05, ***P<0.0001, comparison with AdCRTL; One-way ANOVA was used with Dunnett's post hoc test. Data are presented as mean ± SEM, N=4. Representative examples of western blots are shown underneath the graphs.

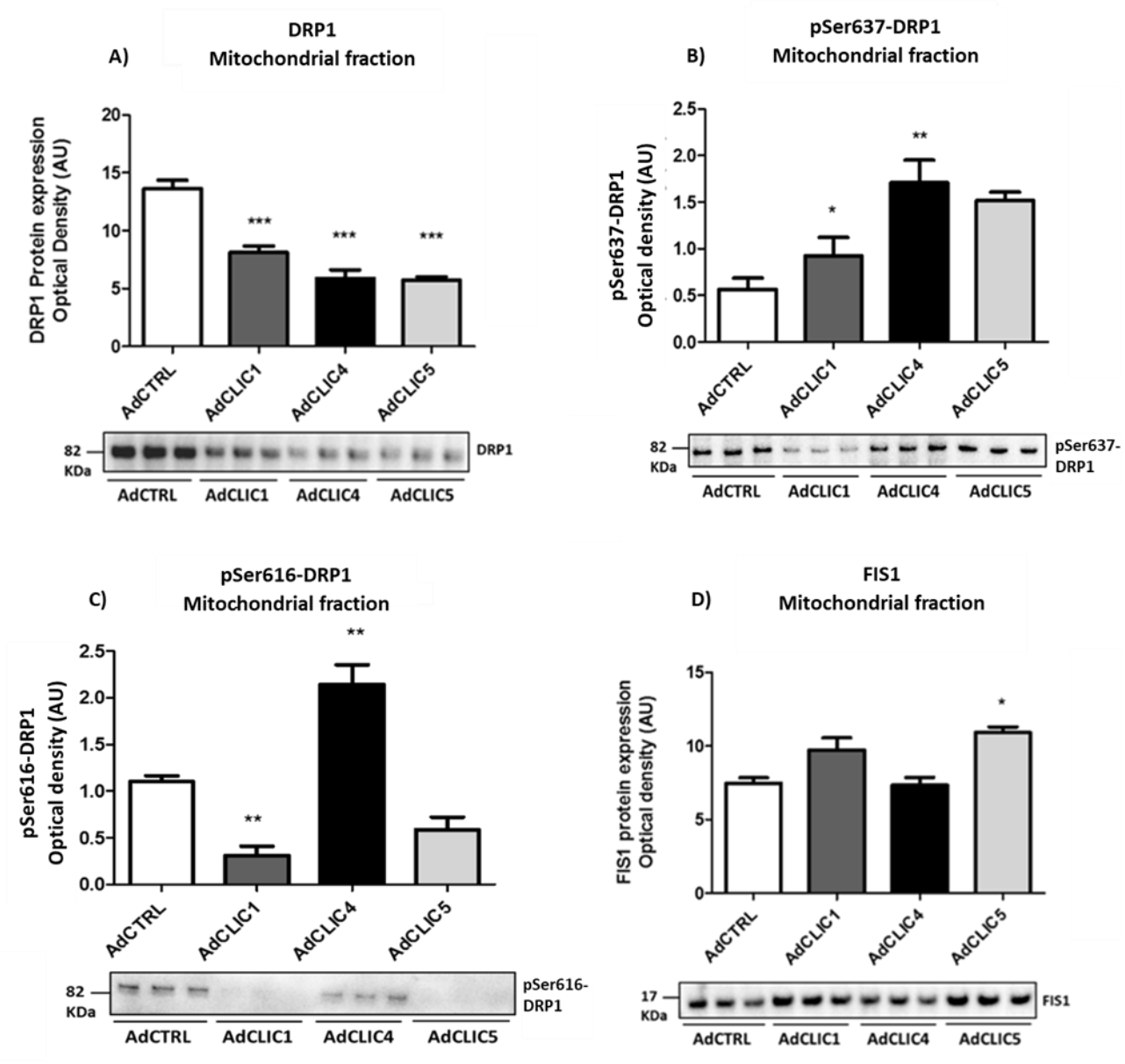


Figure 3.20: Expression and phosphorylation of mitochondrial fission proteins in HPAECs. (A) DRP1 **(B)** pDRP1-S637, **(C)** pDRP1-S616 were normalized to DRP1 total expression level. **(D)** FIS1 expression in mitochondrial fraction from HPAECs treated with AdCTRL, AdCLIC1, AdCLIC4 and AdCLIC5 as indicated. Expression of fission proteins was normalised to VDAC1 expression (see Figure 3.17). Representative western blots are shown under each graph. *P < 0.05, **P <0.01 ***P<0.0001, comparison with AdCRTL; One-way ANOVA was used with Dunnett's post hoc test. Data are presented as mean ± SEM; N=4.

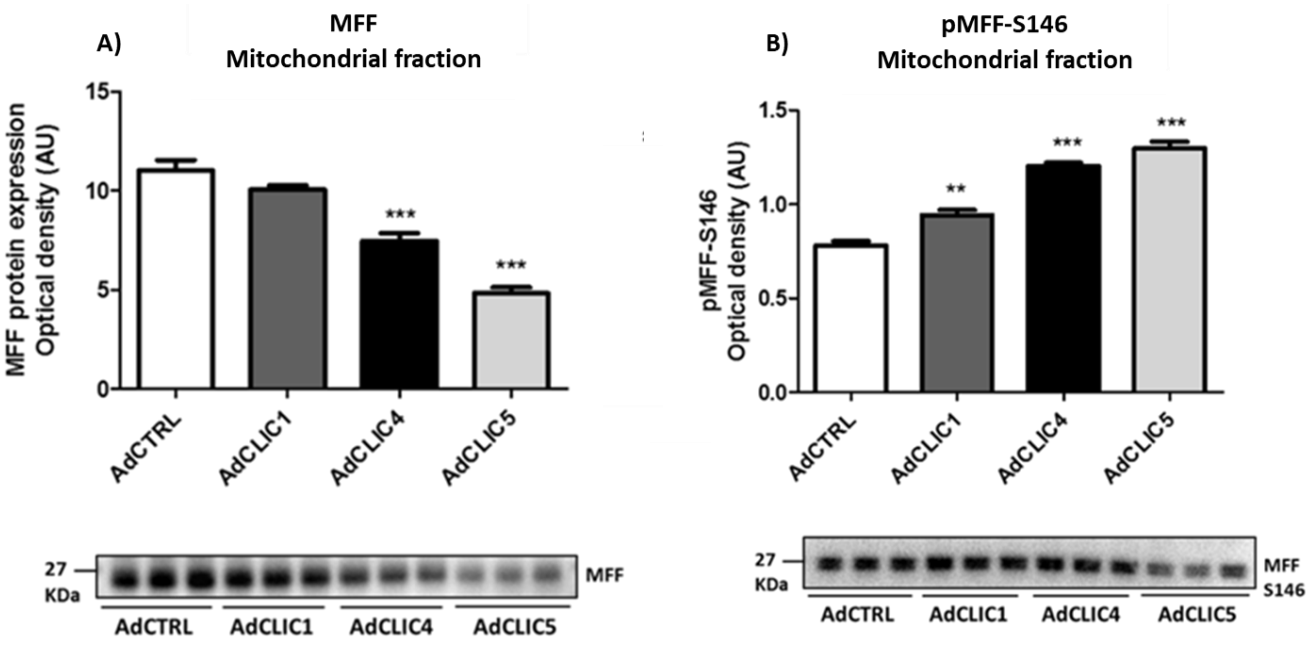


Figure 3.21: Expression and phosphorylation of MFF fission protein in HPAECs. (A) MFF and **(B)** pMFF-S146 expression in mitochondrial fraction from HPAECs treated with AdCTRL, AdCLIC1, AdCLIC4 and AdCLIC5 as indicated. The expression of phosphorylated MFF-S146 was normalised to total MFF expression, and the expression of fission proteins was normalised to mitochondrial loading protein VDAC1 (see Figure 3.17). Representative western blots are shown under each graph. *P < 0.05, **P <0.01 ***P<0.0001, comparison with AdCRTL using one-way ANOVA with Dunnett's post hoc test. Data are presented as mean ± SEM; N=4.

3.4.4.3 Analysis of protein expression of mitophagy regulators in mitochondrial fraction in HPAECs

The effect of CLIC proteins on mitophagy was assessed by examining the expression of Parkin and LC3B, the two key markers of this process in mitochondria-enriched fractions from HPAECs. Parkin is a cytosolic, 52-kDa E3 ubiquitin ligase responsible for targeting specific substrates for proteasomal degradation. In this study, Parkin was detected as multiple bands with molecular weight 50-55 kDa, which may represent different isoforms produced as a result of alternative splicing (Scuderi et al., 2014). Data show that CLIC1 and CLIC4 increased the expression of LC3B and Parkin expression in HPAECs, while CLIC5 had no effect (Figure 3.22).

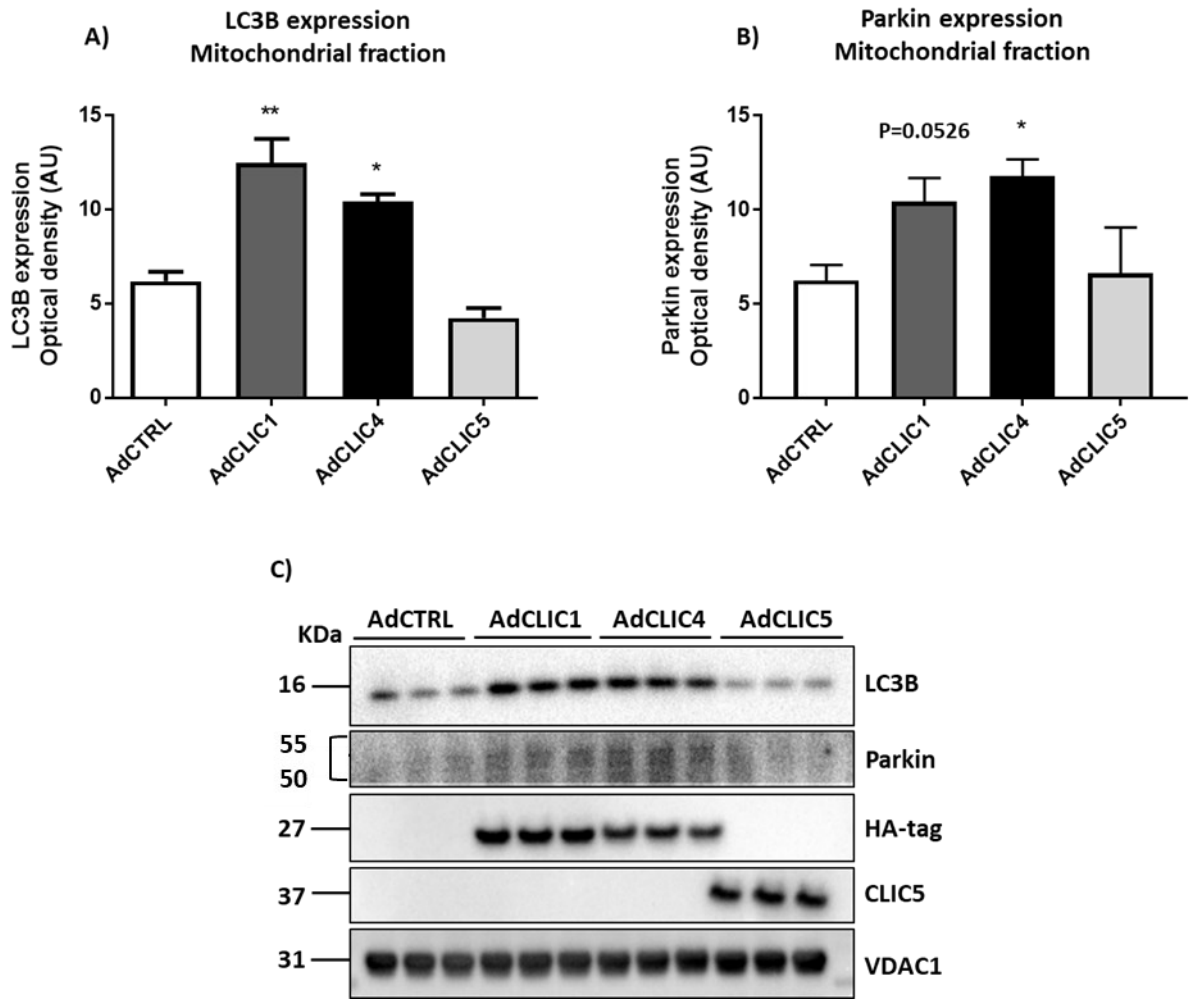


Figure 3.22: Effect of CLIC1 and CLIC4 on expression of mitophagy markers. (A) LC3B and **(B)** Parkin protein expression in CLIC1 and CLIC4 overexpressing cells. Expression of proteins was normalized to VDAC1 **(C)** Representative western blots corresponding to **(A)** LC3B and **(B)** Parkin with multiple bands of molecular weight from ~55-50 KDa. *P < 0.05, **P <0.01 in comparison with AdCRTL; One-way ANOVA was used with Dunnett's post hoc test. Data are presented as mean ± SEM. N=3.

3.4.5 Analysis of pyruvate dehydrogenase protein and kinase expression in HPAECs

I studied the effect of CLIC proteins on pyruvate dehydrogenase (PDH) and pyruvate dehydrogenase kinase 1 and 2 (PDK1 and PDK2), which are key enzymes that regulate cell metabolism. These kinases, phosphorylate and inactivate pyruvate dehydrogenase, thus contributing to the inhibition of mitochondrial respiration seen in PAH (Humbert et al., 2014;

Park et al., 2018). Quantification of pyruvate dehydrogenase expression levels and their activity was done by western blotting in control and CLIC-overexpressing HPAECs.

The analysis revealed a significant reduction in PDH protein levels in CLIC1- and CLIC4-overexpressing cells, while CLIC5 did not have a significant effect. CLIC1 and CLIC4 significantly increased PDK1 and PDK2 expression, while CLIC5 had no effect when compared with the controls (Figure 3.23).

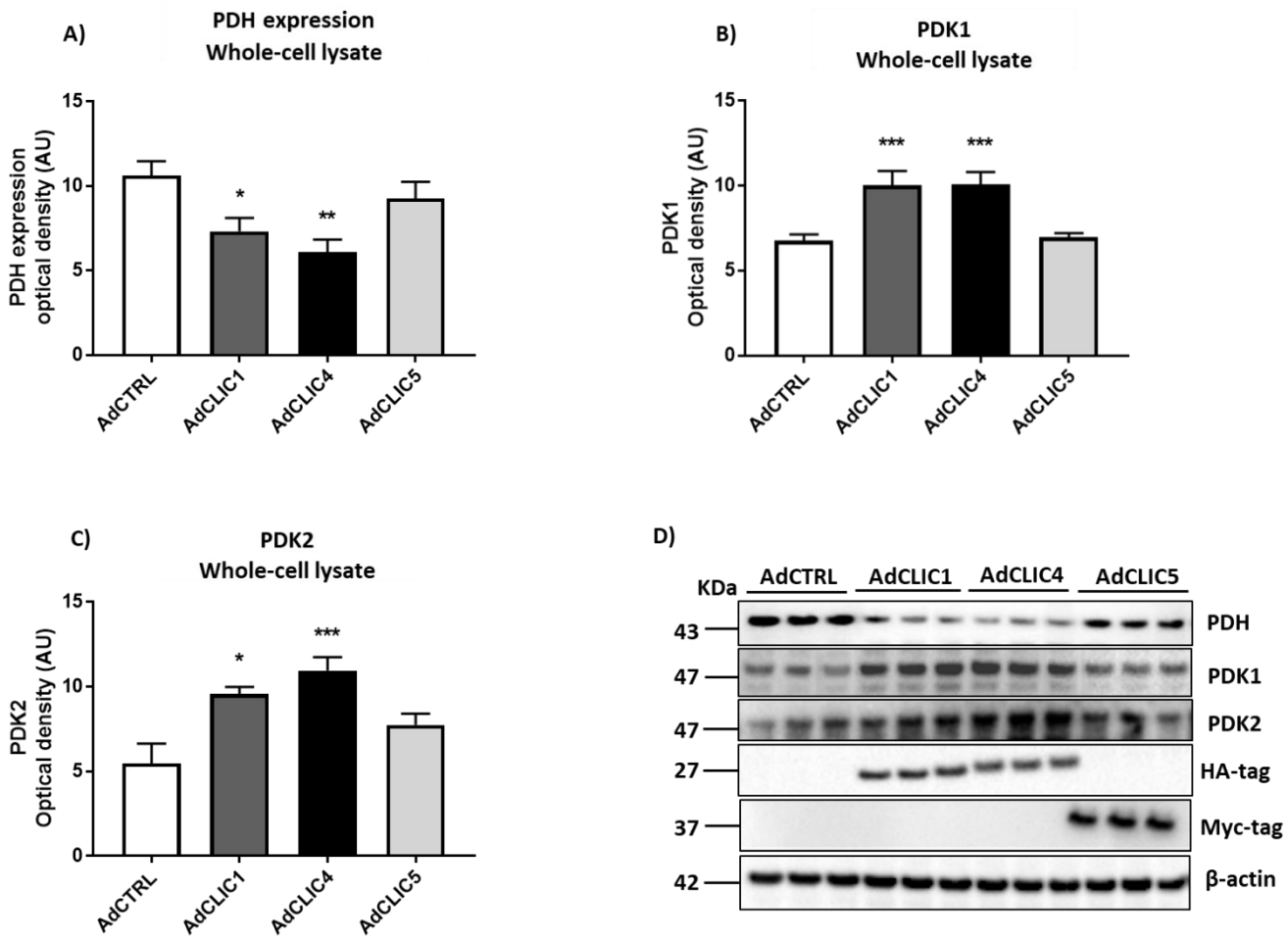


Figure 3.23: Effect of CLIC overexpression on pyruvate dehydrogenase protein and kinase expression. **(A)** PDH expression; **(B)** PDK1 and **(C)** PDK2 expression in whole cell lysates from HPAECs treated with AdCTRL, AdCLIC1, AdCLIC4, and AdCLIC5 as indicated, 24 hours post-infection. Expression values were normalised to β-actin. **(D)** Representative western blots correspond to **(A-C)**.*P < 0.05, **P <0.01, ***P<0.001 comparison with AdCRTL; One-way ANOVA was used with Dunnett's post hoc test. Data are presented as mean ± SEM of 3 experiments with 3 technical repeats.

3.4.6 Effect of CLIC overexpression on cristae architecture in HPAECs

3.4.6.1 Quantification of mitochondrial cristae in CLIC- overexpressing HPAECs

TEM micrographs revealed significant changes in mitochondrial structure induced by CLIC1 and CLIC4. HPAECs overexpressing CLIC1 and CLIC4 showed fragmented mitochondria, with a significant reduction (~2-fold decrease, P<0.0001) in the number of mitochondrial cristae compared with controls (Figures 3.24 and 3.25). The effects of CLIC5 were not studied, as they are not related to the pathology of PAH.

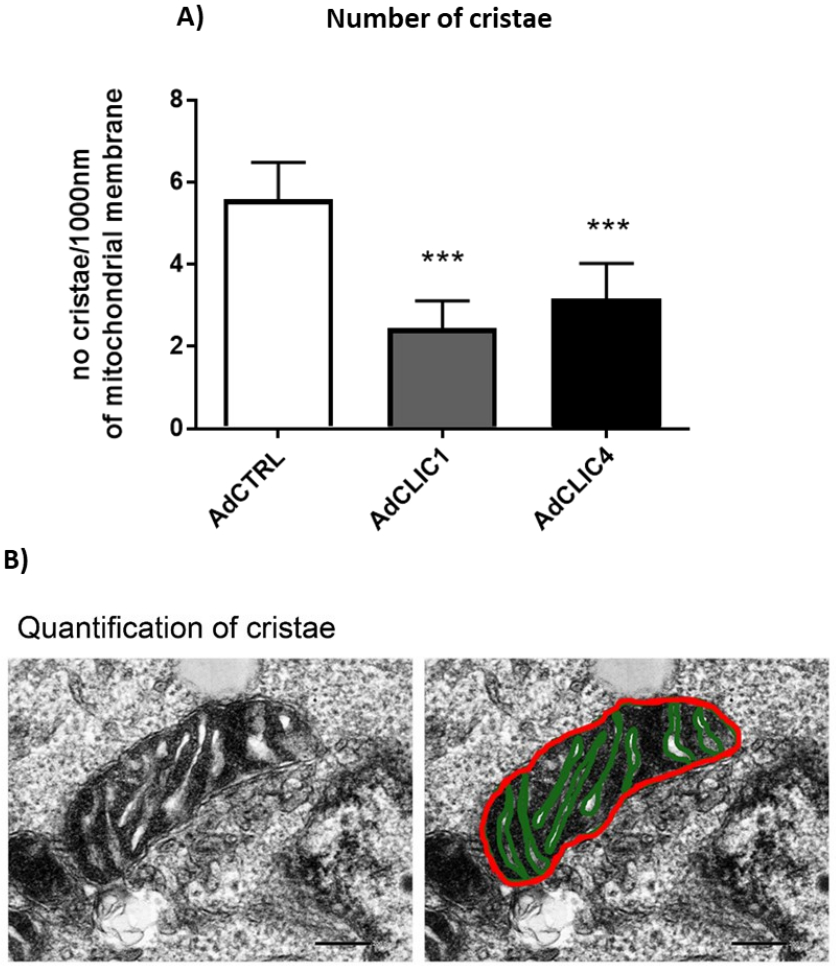


Figure 3.24: The effect of CLIC1 and CLIC4 on cristae architecture in HPAECs. (A) Reduction in cristae number per 1000 nm of mitochondrial outer membrane in CLIC1 and CLIC4 overexpressing cells. **(B)** Example of cristae quantification using Image J software. In **(B)** the mitochondrial perimeter is marked in red and cristae are in green. ***P<0.0001, comparison with AdCRTL; One-way ANOVA was used with Dunnett's post hoc test. Data are presented as mean ± SEM. In **(B)** Bar=50 nm. N=40-60 mitochondria per treatment.

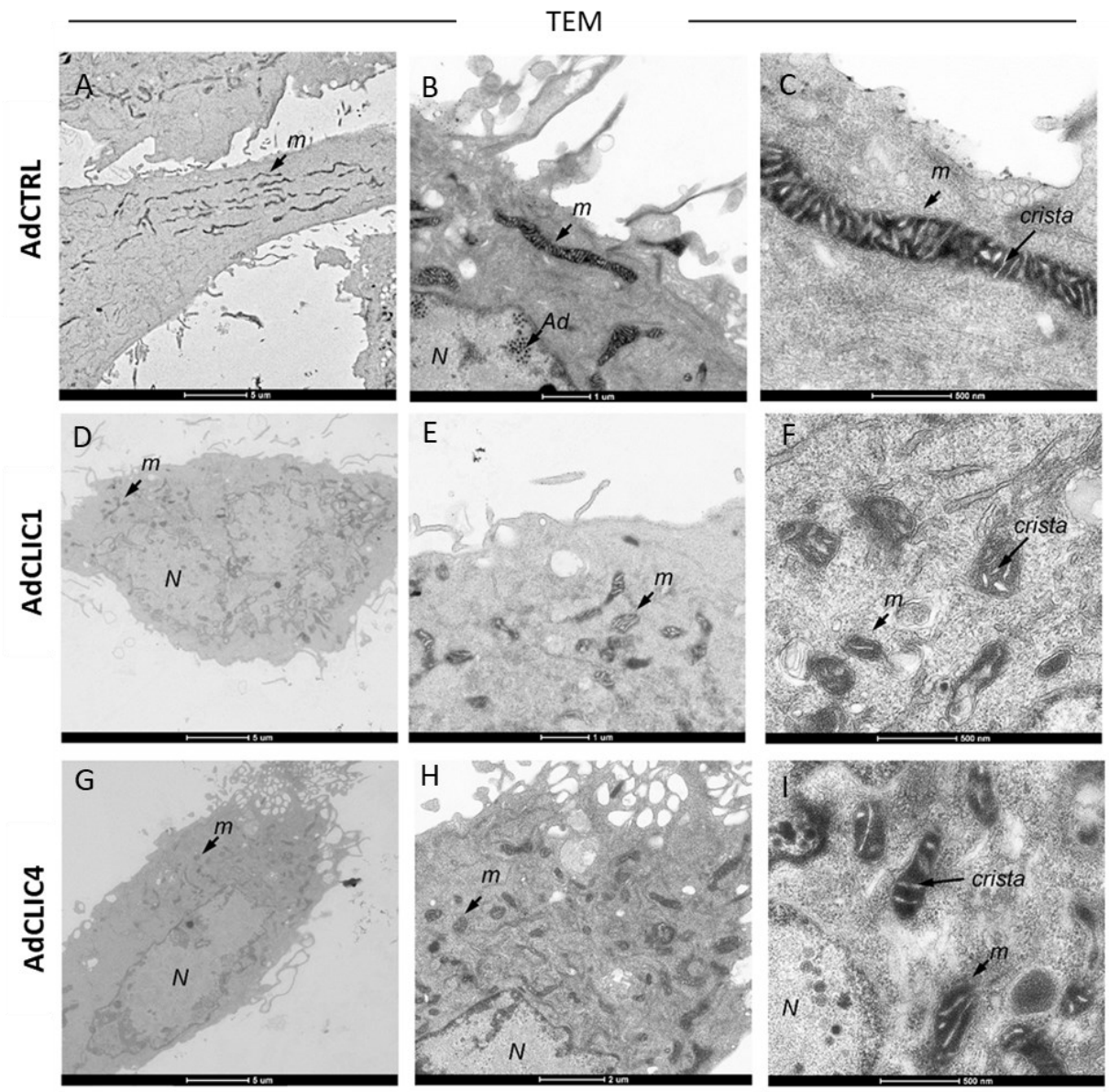


Figure 3.25: Ultrastructural changes in mitochondrial cristae in HPAECs. Representative TEM images of control HPAECs and CLIC-overexpressing HPAECs. CLIC1 and CLIC4 induced changes in cristae structure. Arrows point to mitochondria (m), single crista or adenoviral particles (Ad). N-nucleus. The bar size is indicated at the bottom of each image **(A, D, G**=5µm; B,E=1 µm; **H**=2 µm; **C,F,I**=500µm).

3.4.7 Analysis of expression level of mitochondrial proteins

As well as the fission and fusion proteins (described in Section 3.5.3), I studied the expression levels of other key regulators of mitochondrial structure and function. Table 3.1 shows details of the localisation and function of the proteins studied. A significant decrease in HSP60 protein levels was observed in cells that overexpressed CLIC1 and CLIC5, compared with control cells. No

significant changes in protein levels of COX IV, cytochrome c, PHB1 or VDAC were found in the experimental groups studied (Figures 3.26 and 3.27).

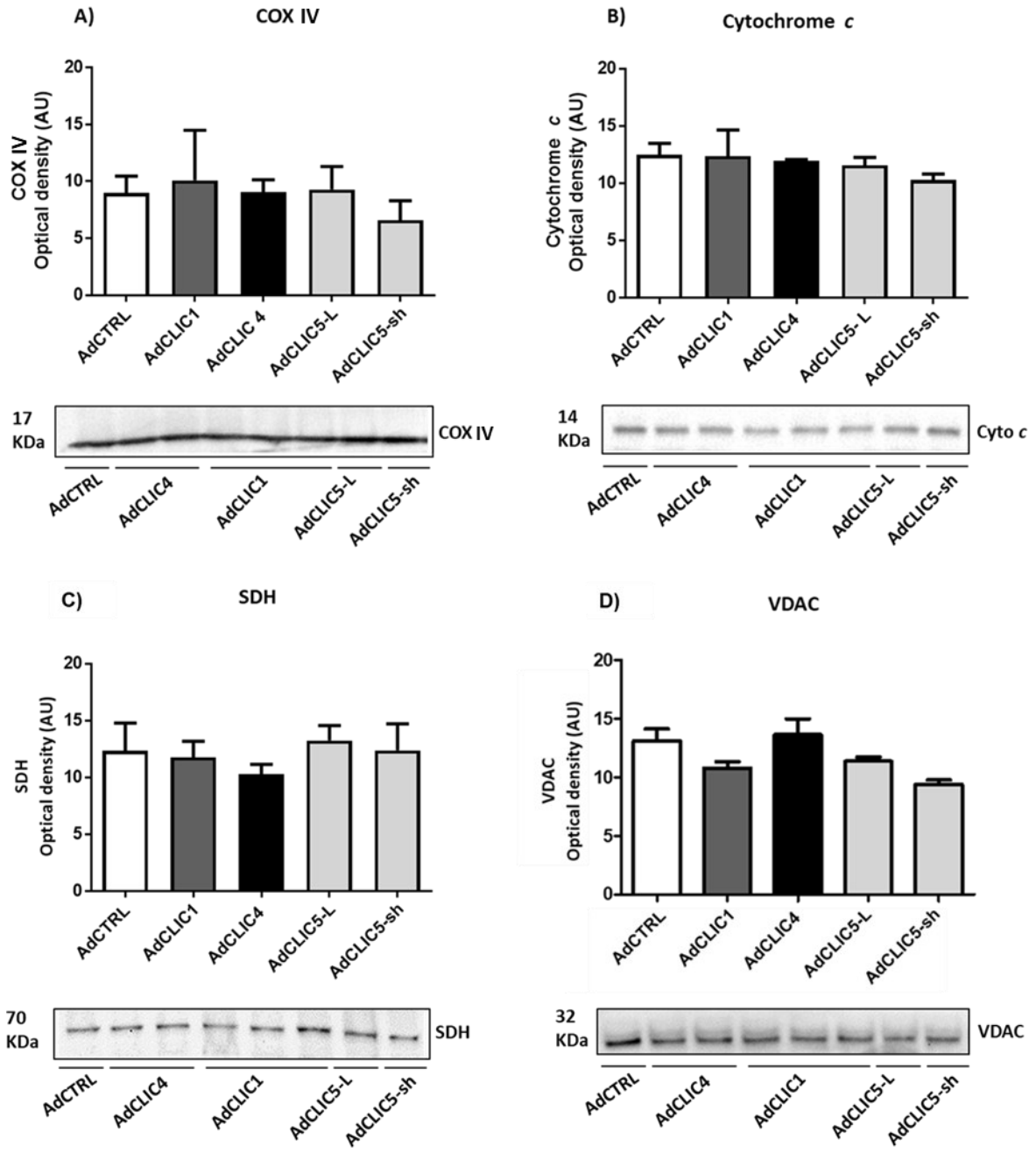


Figure 3.26: Expression of key protein regulators of mitochondrial structure and function. (A-D) Graphs showing mitochondrial protein expression levels of COX IV, cytochrome c, SDH, and VDAC, in CLIC1, CLIC4 and CLIC5 overexpressing cells. Representative western blots are shown below each graph. One-way ANOVA was used with Dunnett's post hoc test. Data are presented as mean ± SEM. N=3 (3 separate experiments were performed with 3 technical repeats).

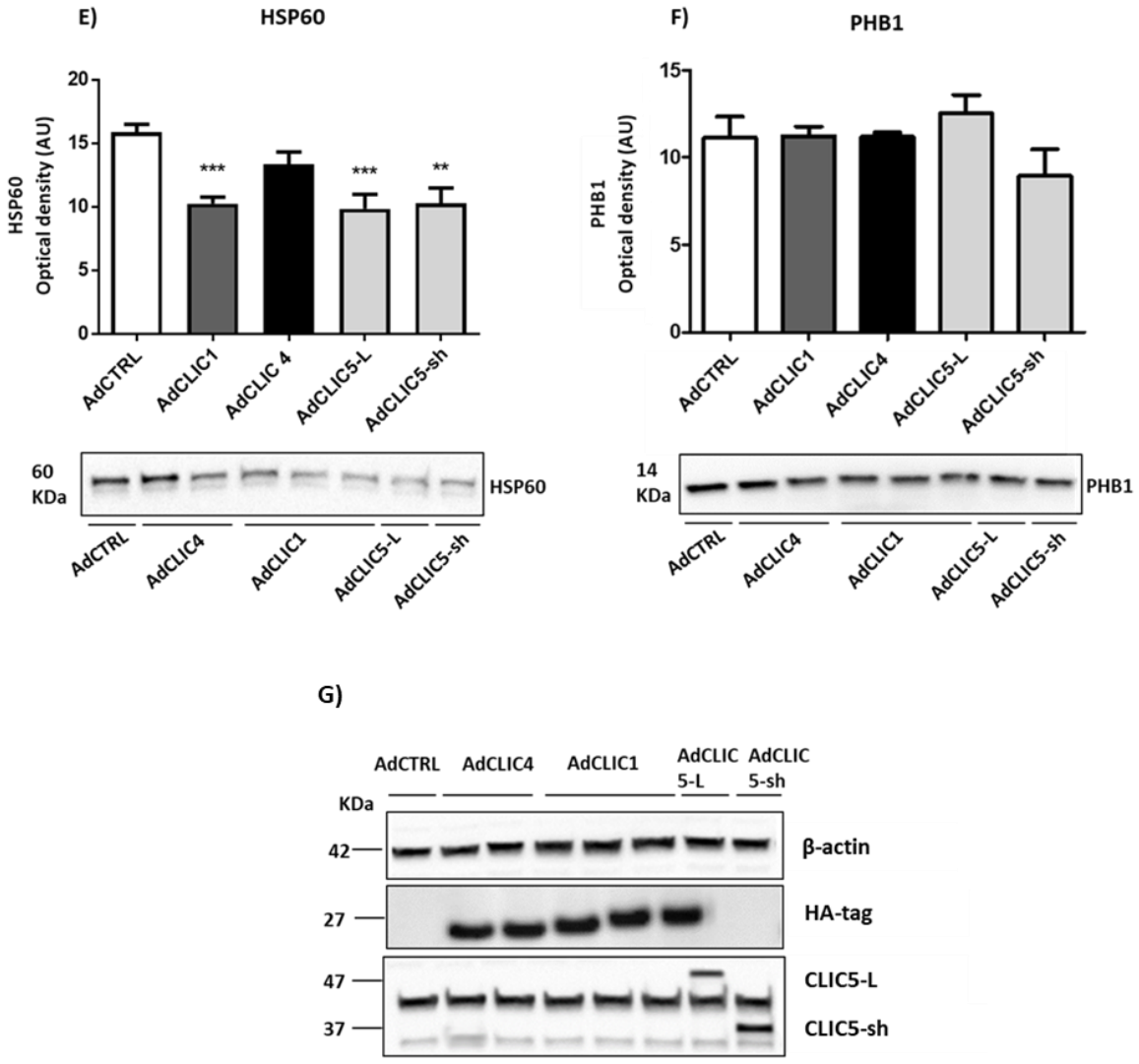


Figure 3.27: Expression of key protein regulators of mitochondrial structure and function. (E) Protein expression of HSP60, **(F)** PHB1 and **(G)** Representative western blots showing the expression of β-actin (loading control) and exogenous CLIC1, CLIC4 and CLIC5. *P < 0.05, **P <0.01, ***P<0.0001 compared with AdCTRL; One-way ANOVA was used with Dunnett's post hoc test. Data are presented as mean ± SEM. N=3 (3 separate experiments were performed with 3 technical repeats).

3.4.8 Role of actin and microtubule cytoskeleton in CLIC-induced effects

CLIC proteins are associated with numerous cytoskeletal proteins, therefore the organization of microtubules (MTs) and actin filaments may affect mitochondrial biogenesis. Microscopic examination revealed that the organization of microtubules in cells that overexpressed CLIC4 and CLIC1 was not very different from the control group. In contrast, CLIC5sh (short isoform)-

overexpressing cells were elongated and showed bundles of aligned microtubules extending to the cell periphery (Figure 3.28). The overexpression of CLIC5L, the less common long isoform of CLIC5, affected cell morphology in a similar way to CLIC5sh (Figure 3.29).

Microtubule content was evaluated by measuring the fluorescence intensity of FITC-immunolabelled microtubules in HPAECs. The organization of the microtubule network determines cell polarity and direction of the intracellular transport of organelles, including mitochondria (Meiring et al., 2020). Here, changes in cell shape and polarity were determined by measuring the cell spreading area and circularity (the ratio between the long axis and the short axis of the cell) with Image J, using confocal images of HPAECs.

CLIC1 and CLIC4 induced a significant increase in the microtubule content of HPAECs, while cell spreading area and circularity remained unchanged. In contrast, CLIC5 induced cell elongation (significantly reduced circularity), but did not affect microtubule content (Figure 3.30).

An increase in microtubule content can result from either increased polymerization or increased microtubule stabilization. Microtubule stabilisation is accompanied by the increased acetylation of tubulin (Maruta et al., 1986; Piperno, LeDizet, & Chang, 1987). While it is not clear whether the effect is causative or correlative (Eshun-Wilson et al., 2019), acetylated tubulin is often used as a marker of microtubule stability.

In this study, expression levels of tubulin and acetylated tubulin were measured by immunoblotting. Data show that protein expression of tubulin remained unchanged in cells that overexpressed CLIC1, CLIC4 and CLIC5, while tubulin acetylation was only reduced in CLIC5-overexpressing cells (Figure 3.31).

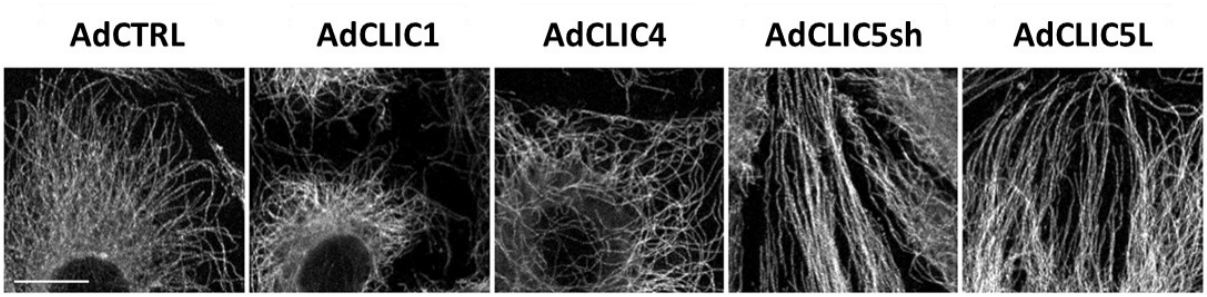


Figure 3.28: Magnified images of microtubule cytoskeleton in CLIC-overexpressing HPAECs. Cells were infected with AdCTRL, AdCLIC1, ADCLIC4 or AdCLIC5, as indicated. Images were taken 24 hours post-infection using a Zeiss LSM 780 confocal microscope with 40x objective. Scale bar =40µm.

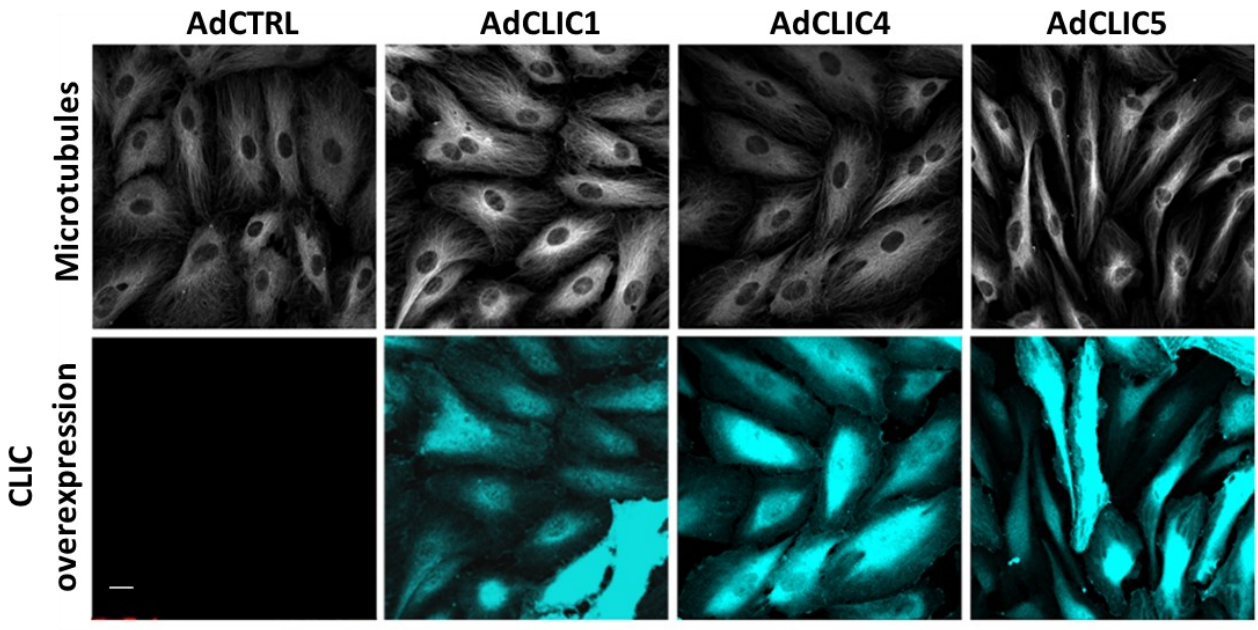


Figure 3.29: The effect of CLIC protein overexpression on the organization of microtubules in HPAECs. HPAECs were infected with AdCTRL, AdCLIC1, ADCLIC4 or AdCLIC5, as indicated. Overexpression of exogenous CLIC1 and CLIC4 was identified by fluorescent immunostaining of HA-tag, while overexpression of CLIC5 was identified by immunostaining of Myc-tag. Images were taken 24 hours post-infection using a Zeiss LSM 780 confocal microscope with 20x objective. Scale bar =10µm.

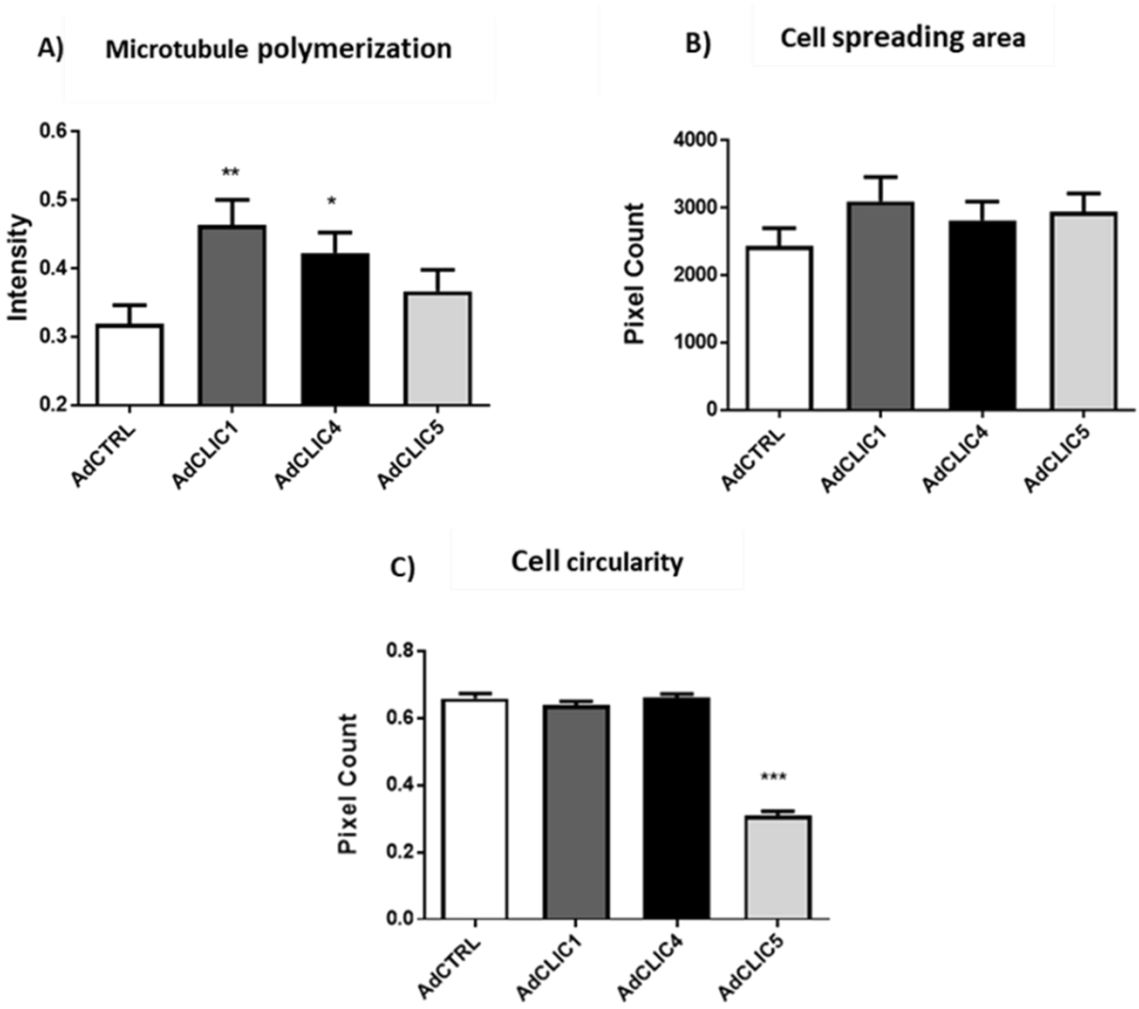


Figure 3.30: Effect of CLIC proteins on microtubule content, cell spreading area and cell polarity. (A) Microtubule polarization in HPAECs treated, as indicated. Polymerised tubulin content per cell was quantified by measuring the intensity of fluorescence of FITC-labelled microtubules in each cell. **(B)** Cell spreading area (in pixels), **(C)** cell circularity. All parameters were quantified from confocal microscopy images using Image J. Data are means (+ SEM).*P < 0.05, **P <0.01, ***P<0.0001 comparison with AdCTRL. One-way ANOVA was used with Dunnett's post hoc test. n=3, ~80 cells/treatment.

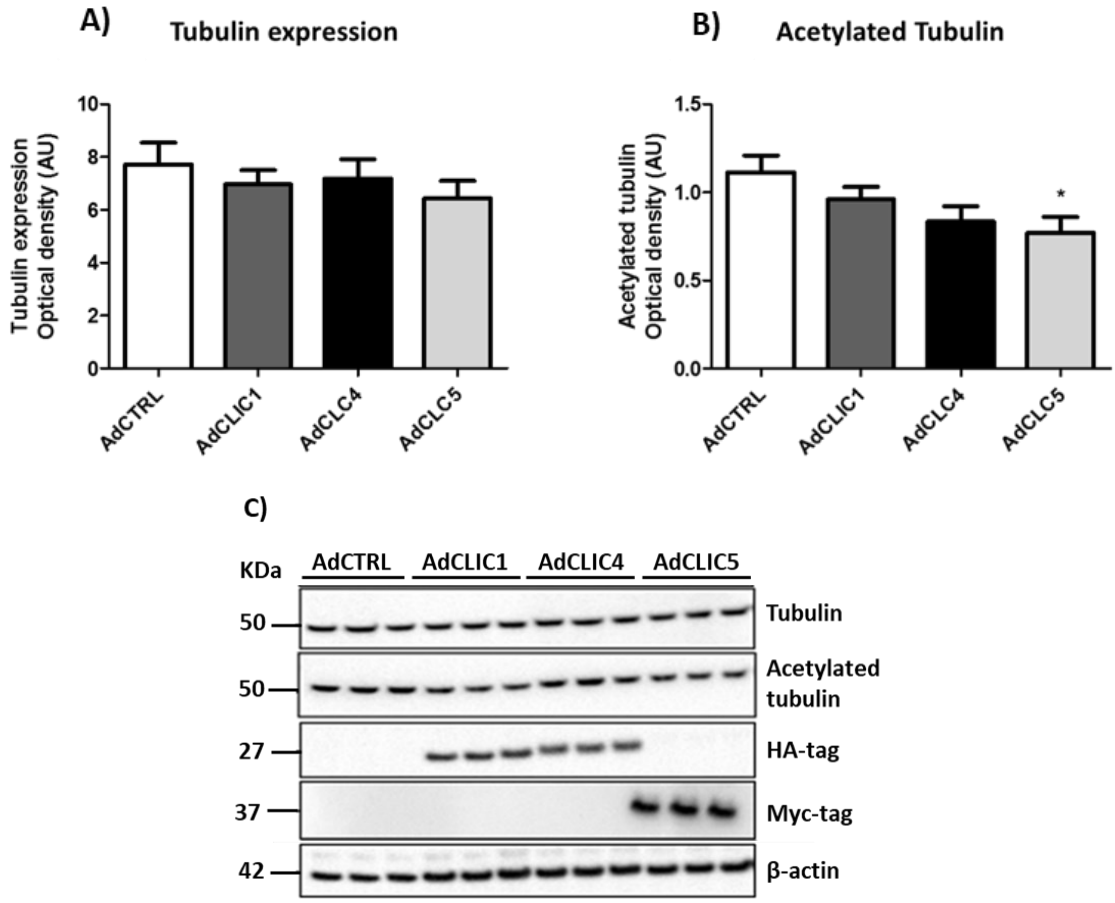


Figure 3.31: The effect of CLIC-overexpression on tubulin and tubulin acetylation levels in HPAECs. (A) Tubulin expression, **(B)** Acetylated tubulin expression in CLIC1-, CLIC4-, and CLIC5-overexpressing HPAECs 24h post-infection. Corresponding representative western blots are shown below each graph. **(C)** Western blots showing the expression of β-actin (loading control), HA-tagged and myc-tagged proteins in the analysed samples. In **(A, B)** Data are means (+ SEM).*P < 0.05 comparison with AdCTRL. One-way ANOVA was used with Dunnett's post hoc test. N=3.

3.4.9 Effect of microtubule polymerization on CLIC-induced changes in mitochondrial fragmentation

The results shown in section 3.7 suggest that CLIC1 and CLIC4 may affect mitochondrial biogenesis by increasing the polymerization of microtubules. To verify this, control HPAECs and HPAECs that overexpressed CLIC1 and CLIC4 were treated with microtubule-stabilising agent (taxol) and microtubule de-polymerizing agent (nocodazole). As expected, taxol increased microtubule content, while nocodazole completely depolymerised the microtubules in all experimental groups, irrespective of changes in CLIC protein expression (Figure 3.32).

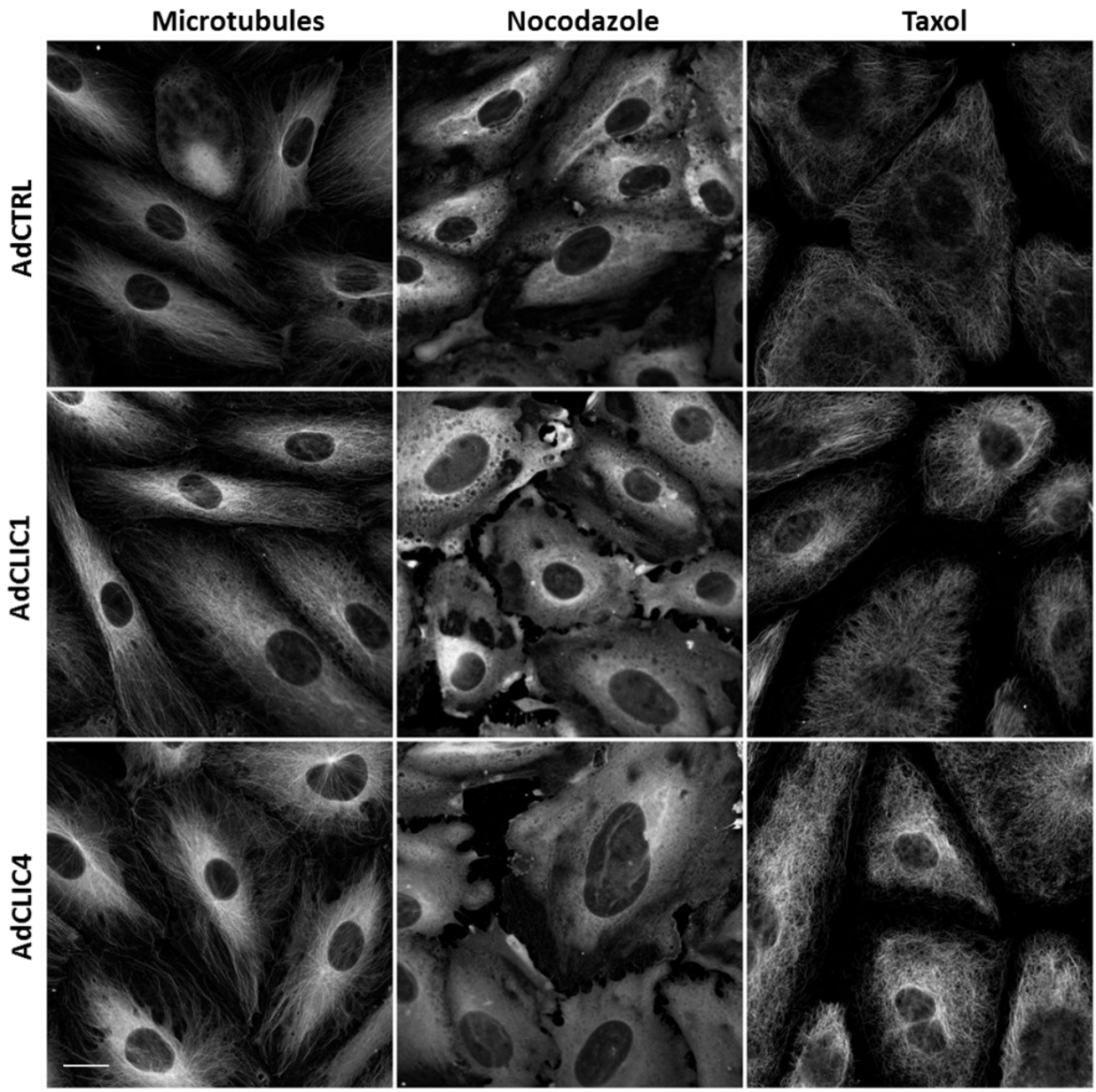


Figure 3.32: The effect of nocodazole and taxol on microtubules in CLIC-overexpressing HPAECs. Control (AdCTRL), CLIC1- and CLIC4-overexpressing cells were treated with nocodazole (20 µM, 10 mins) or taxol (10 µM taxol, 30 mins), fixed and immunostained for tubulin. Images were acquired using a Zeiss LSM 780 confocal microscope with 20x objective. Scale bar= 10µm.

The effect of nocodazole and taxol on mitochondrial fragmentation was examined using the quantification method described in section 4.4.1.1. The results showed that both the polymerization and the depolymerisation of microtubules had a destabilising effect on the mitochondrial network, irrespective of changes in CLIC1 or CLIC4 expression levels. While dynamic interactions between CLIC proteins and microtubules may still affect mitochondrial distribution in cells to some degree, it is unlikely that the level of tubulin polymerization plays a significant role in CLIC1- and CLIC4-induced mitochondrial fragmentation (Figure 3.33).

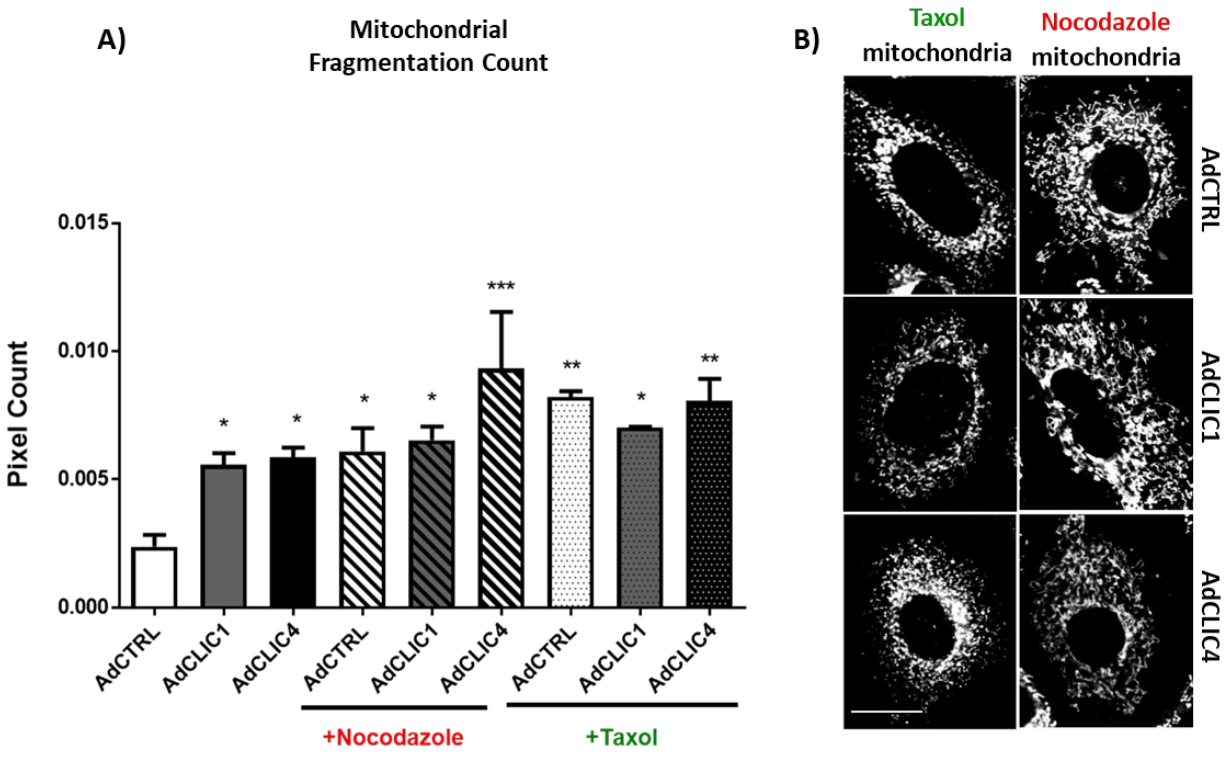


Figure 3.33: The effect of microtubule disruption and stabilization on mitochondrial network of CLIC-overexpressing HPAECs. (A) Mitochondrial fragmentation count (MFC; in pixels) and **(B)** Representative images of mitochondrial network in CLIC1 and CLIC4 overexpressing HPAECs treated with 20 µM nocodazole or 10 µM taxol. In **(A)** Data are means (+ SEM). *P < 0.05, **P <0.01, ***P<0.0001 comparison with untreated AdCTRL. One-way ANOVA was used with Dunnett's post hoc test. N=3, 25 mitochondria/treatment. Confocal images were taken using a Zeiss LSM 780 confocal microscope with 20x objective. Scale bar= 10µm.

3.4.9.1 Alignment of mitochondria with microtubule network

Mitochondrial-cytoskeletal interactions play a well-established role in mitochondrial motility. Mitochondria show close association with microtubules throughout the entire cell cycle, apart from mitosis (Moore & Holzbaur, 2018). The movement of mitochondria along microtubules in control and CLIC-overexpressing HPAECs was evaluated in a preliminary study using time-lapse recording of live cells overexpressing FITC-labelled tubulin (green) and fluorescent protein (RFP)-labelled mitochondria under a confocal microscope (red). The aim of this experiment was to identify any potential dysregulation of the function of the molecular motor proteins that guide mitochondria along microtubule networks.

Mitochondrial dynamics in live cells were monitored for 5 minutes under the confocal microscope. The preliminary analysis of time-lapse recordings revealed that within this time both individual mitochondria and mitochondrial networks showed good alignment with the microtubule filaments in all experimental groups (Figure 3.34). While a more detailed analysis over a longer period of time would be required to detect any subtle differences in mitochondrial motility and alignment between the treatment groups, it seems unlikely that mitochondrial-microtubule interactions could be responsible for significant changes in mitochondrial morphology or the fragmentation observed in CLIC-overexpressing cells.

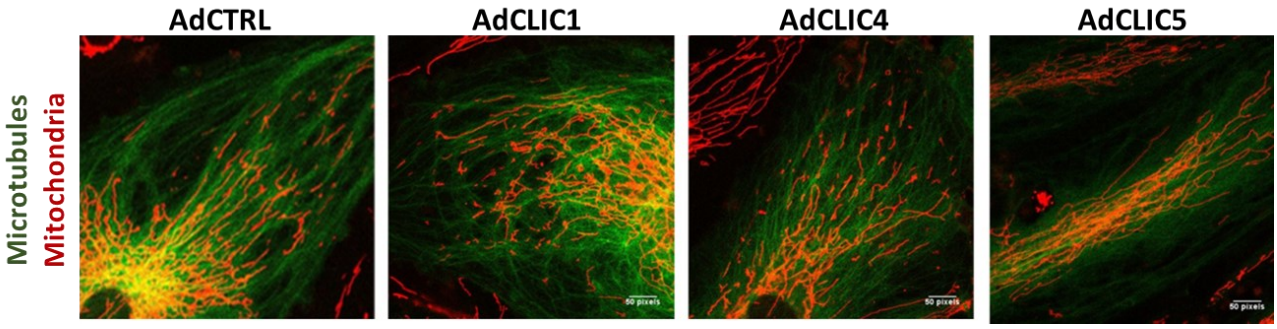


Figure 3.34: Alignment of mitochondrial network with microtubules in CLIC-overexpressing HPAECs. Representative images acquired from time-lapse recordings of live HPAECs overexpressing FITC-labelled tubulin (green) and RFP-labelled mitochondria (red) (Cell Light lentiviral overexpression). Scale bar=5µm.

3.4.10 Effect of CLIC-overexpression on the organization of actin cytoskeleton in HPAECs

Filamentous (F)-actin is thought to play a role in the pre-constriction of mitochondria, prior to the DRP-1-mediated fission (Moore & Holzbaur, 2018). To evaluate the potential effect of CLIC proteins on F-actin polymerization, TRITC-phalloidin affinity binding to F-actin was quantified by measuring the intensity of fluorescence using confocal microscopy images. The results showed no significant changes in F-actin content in any of the experimental groups. The cellular organization of F-actin is shown in Figure 3.35.

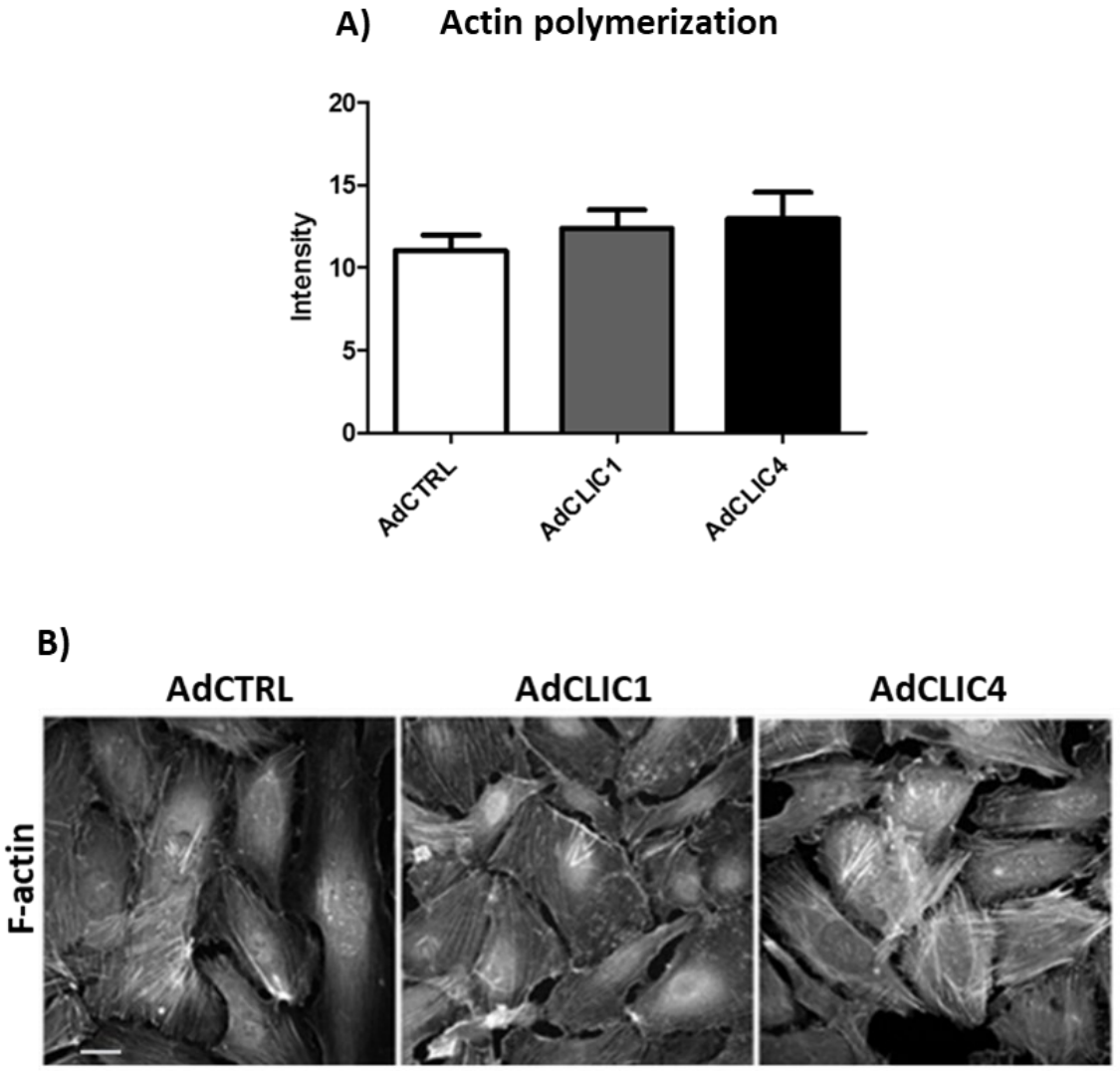


Figure 3.35: The effect of CLIC-overexpression on actin polymerization in HPAECs. F-actin levels were evaluated by measuring the intensity of fluorescence of TRITC-phalloidin-labelled actin in HPAECs treated, as shown in **(A)**. One-way ANOVA was used with Dunnett's post hoc test. Data are presented as mean ± SEM based on 3 experiments with 3 technical repeats, and the total of analysed cells was ~100/treatment. **(B)** Shows the representative confocal images of F-actin in CLIC-overexpressing HPAECs. Scale=10 µm.

3.5 Summary

The key findings presented in this chapter show that:

- Pathological levels of CLIC1 and CLIC4 expression increase mitochondrial fragmentation in HPAECs.
- CLIC1 and CLIC4 localise to outer and inner mitochondrial membrane and mitochondrial cristae.
- CLIC1 and CLIC4 significantly reduce the expression of mitochondrial fusion proteins, MFN1, MFN2 and OPA1, and dysregulate the expression and phosphorylation of fission proteins, FIS1, DRP1 and MFF.
- CLIC1 and CLIC4 do not affect the mRNA expression of mitochondrial fusion proteins, suggesting that regulation may occur at protein translation or stability levels.
- CLIC1 and CLIC4 reduce pyruvate dehydrogenase expression and increase its kinases in HPAECs.
- CLIC1 and CLIC4 greatly increase the expression of mitophagy markers, LC3B and Parkin.
- CLIC1 and CLIC4 reduce the number of mitochondrial cristae.
- CLIC1 significantly reduces levels of HSP60 protein expression in HPAECs.
- CLIC1 and CLIC4 significantly increase microtubule polymerization, but have no effect on F-actin polymerization in HPAECs. The increase in microtubule polymerization by CLIC1 and CLIC4 is unlikely to be directly associated with their effects on mitochondria.

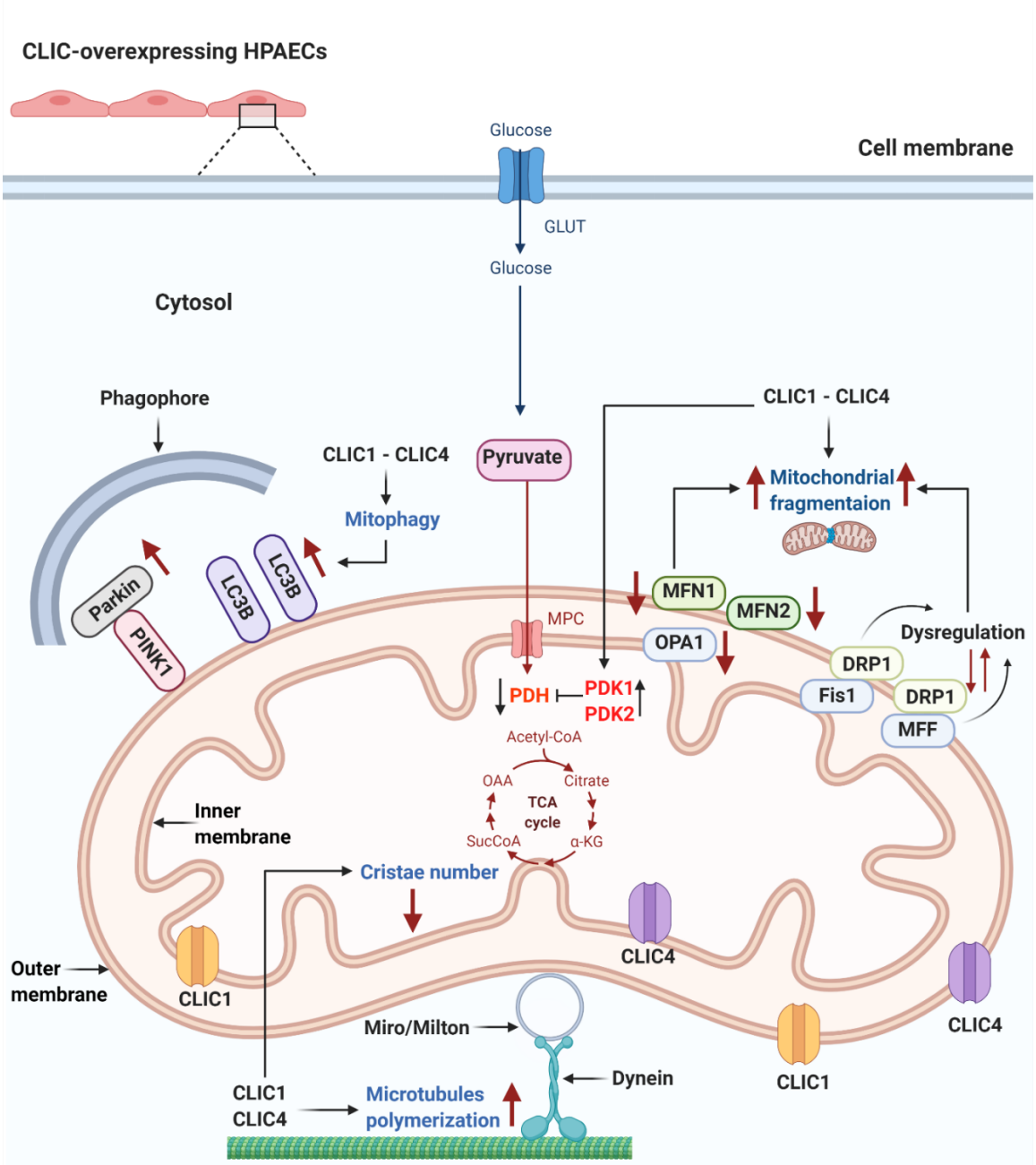


Figure 3.36: Summary of key results in chapter 3. Details of key findings are presented in the table below (Table 3.2). Illustration created by the author using BioRender.com.

Table 3.2: Summary of key findings of the effect of CLIC overexpression proteins on mitochondrial dynamics in HPAECs. Red arrows pointed upwards indicate upregulation, black arrows pointed downwards indicate downregulation. Dash shows no effect, ND (not determined) means the effect was not tested.

	Investigation	CLIC1	CLIC4	CLIC5
	Mitochondrial fragmentation	↑	↑	↑
Fission proteins	**MFN1 expression**	↓	↓	↓
	MFN2 expression	↓	↓	—
	OPA1 expression	↓	↓	—
Fusion proteins	**DRP1 expression**	↓	↓	↓
	pDRP1-S616 expression (Activating phosphorylation)	↓	↑	—
	pDRP1-S367 expression (Inactivating phosphorylation)	↑	↑	—
	FIS1 expression	—	—	↑
	MFF expression	—	↓	↓
	pMFF-Ser146 expression (Activating phosphorylation)	↑	↑	↑

Mitochondrial proteins	**COX IV expression**	—	—	—
	Cytochrome c	—	—	—
	SDH	—	—	—
	VDAC	—	—	—
	HSP60	↓	—	↓
	PHB1	—	—	—
PDH expression		↓	↓	↑
PDK1 expression		↑	↑	—
PDK2 expression		↑	↑	—
Mitophagy proteins	**LC3B expression**	↑	↑	ND
	Parkin expression	↑	↑	ND
Number of cristae		↓	↓	ND
Microtubule polymerization		↑	↑	—
Microtubule coverage area		—	—	—
Cell polarity		—	—	↑
Tubulin expression		—	—	—
Tubulin acetylation		—	—	↓
Actin polymerization		—	—	ND

3.6 Discussion

The key findings presented here show that overexpression of CLIC1, CLIC4 and CLIC5 alters the structure of mitochondria and affects mitochondrial dynamics and function. The increased expression of CLIC proteins is a feature of proliferative disorders characterised by abnormal angiogenesis, increased cell proliferation, oxidative stress and inflammation, such as cancer, PAH and atherosclerosis (Averaimo et al., 2010; Xu et al., 2016).

Changes in mitochondrial structure and distribution are determined by the energy requirements of the cell. Mitochondrial elongation, for example, can be linked with the high ATP supply required to sustain cell duplication (Mitra et al.2009; Schieke, McCoy Jr, & Finkel, 2008), while mitochondrial fission is required to ensure the equal distribution of mitochondria in daughter cells as well as the mitochondrial quality control mechanism (Mitra et al., 2009; Taguchi et al., 2007). Changes in mitochondrial morphology have also been linked to other important cellular functions, such as Ca^{2+} and ROS signalling (McCarron et al., 2013).

Mitochondria in endothelial and vascular smooth muscle cells in the remodelled vasculature in PAH show functional abnormalities, including mitochondrial fragmentation, increases in mitochondrial ROS generation and imbalances in the redox-related enzymes (Marshall et al., 2018). We observed that CLIC1 and CLIC4 induced mitochondrial fission, which is consistent with the postulated role of CLIC1 and CLIC4 in PAH pathogenesis.

Short and long splicing variants of CLIC5 reduced the mitochondrial area but had a lesser effect on mitochondrial fragmentation, which appears to support mitochondrial fusion and the formation of mitochondrial networks in HPAECs.

An imbalance in the expression of fusion and fission regulators is the most likely cause of CLIC-induced mitochondrial fragmentation that was observed. Immunogold staining showed the

localization of CLIC1 and CLIC4 to the outer and inner mitochondrial membranes as well as the mitochondrial cristae. This is consistent with the findings of Fernandez-Salas et al (1999), who identified CLIC proteins in the inner mitochondrial keratinocyte mitochondria of mice. In 2016, Ponnalagu et al showed that CLIC4 is enriched in the outer mitochondrial membrane of adult cardiomyocytes (Ponnalagu et al., 2016). The specific localization of CLIC1 within the mitochondrial structure has not been seen before, though fluorescent immunostaining and western blotting analyses suggested that CLIC1 may be present in mitochondria in osteoblastic cells (Yang et al., 2009).

Fusion and fission proteins, like CLIC proteins, are found in the outer mitochondrial membrane, but specific interactions between these proteins have not been investigated. GTPases MFN1, MFN2 and OPA1 play a fundamental role in the regulation of mitochondrial fusion, while Drp1, MFF and FIS1 control mitochondrial fission (Marsboom et al., 2012). The inhibition of MFN2 function has been implicated in PAH pathogenesis (Dasgupta et al., 2011), along with the activation of DRP1 via increased expression and/or phosphorylation on Serine 616 (pDRP1-Ser616) (Marsboom et al., 2012).

In this study, the most consistent feature observed for CLIC1 and CLIC4 was the downregulation of fusion proteins, MFN1, MFN2 and OPA1. Changes in the expression and phosphorylation of fission proteins indicated an imbalance in the regulation of mitochondrial dynamics. While both CLIC1 and CLIC4 decreased the expression of DRP1 and increased its phosphorylation on Ser637 (inactivating phosphorylation), CLIC4 also increased the Ser616 phosphorylation of DRP1, which is an activating phosphorylation. CLIC1 and CLIC4 also increased the activity of MFF, which is critical for the recruitment of Drp1 to the OMM (Kotiadis et al., 2014). A decrease in the expression of fission regulator DRP1, and an increase in the inhibitory phosphorylation of DRP1

on Serine 637 is counterintuitive, but it may constitute a compensatory response to the significant reduction in the expression of fusion proteins. The fact that these changes were significant in mitochondrial fractions but failed to reach statistical significance in total cell lysates can be explained by the dilution effect, considering that mitochondrial content in endothelial cells is relatively low, compared with other cell types (Tang et al., 2014). A reduction in the expression of fusion proteins is likely to result from CLIC-induced effects on translation or protein stability rather than transcription, as the mRNA levels of these proteins were relatively unaffected. Alterations in the balance between fusion and fission proteins is likely to be the cause of mitochondrial fragmentation seen in CLIC1- and CLIC4-overexpressing cells. The precise mechanisms involved in these responses will require further investigation.

Preliminary data show that CLIC proteins did not significantly affect the expression levels of other mitochondrial proteins, such as COX IV, cytochrome c, VDAC, SDH, and PHB1. However, a significant reduction in the expression of the mitochondrial gate-keeping enzyme pyruvate dehydrogenase (PDH), and an increase in the expression of pyruvate dehydrogenase kinase (PDK1/2), the enzyme that inactivate PDH, was noted in HPAECs expressing high levels of CLIC1 and CLIC4. This is consistent with changes seen in PAH, leading to the inhibition of oxidative phosphorylation and a metabolic switch towards glycolysis and anti-apoptotic environment (Culley & Chan, 2018). PDH inhibition has also been linked to mitochondrial hyperpolarization (Sutendra et al., 2011). The decrease in HSP60 levels seen in CLIC1-overexpressing cells might affect mitochondrial function, as HSP60 is essential for the folding and assembly of newly imported proteins and belongs to the mitochondrial quality control system, which is important in mitochondrial responses to stress conditions (Cheng et al., 1990; Haslip et al., 2015; Sarangi et al., 2013).

The increased expression of autophagy markers such as LC3B and Parkin seen in CLIC1- and CLIC4-overexpressing cells is consistent with changes seen in the lungs of PH patients (Zhai et al., 2018). MFN1 and MFN2 are distributed and then degraded in a PINK1-Parkin dependent pathway (Valera-Alberni & Canto, 2018). In some studies, autophagy is shown to be an adaptive response in the progression of cell proliferation and PH. However, the relationship between autophagy and PH pathogenesis remains incompletely studied (Zhang et al., 2019).

As well as changes in mitochondrial fusion and fission proteins, mitochondrial fragmentation can be mediated by the cell cytoskeleton. We observed that microtubule polymerization was increased (although not significantly) in CLIC1- and CLIC4-overexpressing cells, while F-actin content remained relatively unaffected. The depolymerization and polymerization of microtubules by specific toxins induced further fragmentation of the mitochondrial network regardless of changes in CLIC protein expression, suggesting that CLIC-induced changes in fusion and fission and microtubule polymerization are not directly linked. However, this experiment does not exclude the potential role of CLIC proteins in the regulation of mitochondrial transport and energy distribution within the cell. CLIC1 and CLIC4 interact with microtubule-associated proteins such as dynein, dynamin-related protein 1 (DRP1), Arf (Ackema et al., 2014; Pimkina & Murphy, 2011) and proteins regulating actin dynamics, such as Arp2, 3 complex (Mathur, 2005). The movement of mitochondria along the MT tracks depends on microtubule-associated proteins (MAPs), such as dyneins and kinesins (Anesti & Scorrano, 2006), so the association of CLIC proteins with these proteins may potentially affect the organization of the mitochondrial network. While the alignment of the mitochondrial network and the movement of individual mitochondria along microtubules appeared to be unaffected by CLIC1 or CLIC4, further in-depth analyses involving a higher number of cells analysed over a longer period would be required to

confirm this observation. Experiments described here showed differences in the distribution of mitochondria within cells, with the perinuclear localization of mitochondria in CLIC1- and CLIC4-overexpressing cells and long, extended mitochondrial networks in CLIC5-overexpressing cells. The accumulation of mitochondria in the perinuclear region may suggest the enhancement of dynein function, which propels mitochondria towards the negative end of microtubules in the microtubule organising centre (MTOC), as opposed to kinesin, which moves mitochondria towards the positive end of microtubules in the cell periphery. The interaction of CLIC1 and CLIC4 with dynein (Abdul-Salam et al., 2010; Huang et al., 2014) may facilitate the dynein-mediated retrograde movement of mitochondria towards the nuclei. Meanwhile, the perinuclear clustering of mitochondria is thought to facilitate the delivery of energy to the nucleus, helping to maintain local ATP/ADP and GTP/GDP ratios required for efficient nuclear transport and cell proliferation (Dzeja et al., 2002). The potential contribution of this phenomenon to the hyperproliferative phenotype of pulmonary endothelial and smooth muscle cells in PAH will require further study.

Interestingly, in CLIC5-overexpressing cells, the MTs and mitochondrial networks both extended to the periphery of the cell. CLIC5 is highly expressed in the heart and skeletal muscles, and moderate levels can be detected in the kidney, lung, and placenta (Berryman & Bretscher, 2000). CLIC5 also interacts with the actin-binding ezrin, radixin and moesin (ERM proteins) (Gururaja Rao et al., 2018) that link membrane receptors with the actin cytoskeleton and play a crucial role in cell polarization and movement in response to chemotactic stimuli (Berryman & Bretscher, 2000). Extending mitochondrial networks to the cell periphery are thought to facilitate energy transfer to the ATP-demanding leading edge of the cell (Skulachev, 2001). CLIC5 is also believed

to have a cardioprotective role (Kühlbrandt, 2015; Ponnalagu et al., 2015), but the mechanisms involved are poorly understood.

The expression of CLIC5 in pulmonary endothelial cells and mitochondria was almost undetectable, and its expression in PAH lungs, as opposed to CLIC1 and CLIC4, was unchanged (Gururaja Rao et al., 2018). While the expression of CLIC5 has not been implicated in PAH pathogenesis, CLIC5 is enriched in the mitochondrial membrane of cardiomyocytes (Ponnalagu et al., 2016). In this study, CLIC5 was used as a control in some experiments to identify CLIC1- and CLIC4-specific responses and to study the effects of CLIC5, which may be relevant to changes seen in other cell types.

CLIC1 and CLIC4 overexpression significantly reduced the number of cristae in HPAEC mitochondria. Previous studies have shown that cristae morphology controls mitochondrial respiration and defective organization affects the electron transport chain in the cristae and impairs mitochondrial dynamics and respiration (Norton et al., 2014). This may result in the reduction in MFN2, remodelling the cristae through C-cleavage or the cleavage of OPA1, which is a MFN2-dependent pathway (Sood et al., 2014).

CHAPTER 4 RESULTS:

The effect of CLIC proteins on mitochondrial function

CHAPTER 4 RESULTS: The effect of CLIC proteins on mitochondrial function

This chapter focuses on the effects of activation and inhibition of CLIC protein expression on mitochondrial membrane potential (ΔΨm), mitochondrial reactive oxygen species (mtROS), mitochondrial respiration and glycolysis.

4.1 Introduction

Mitochondria are the major sources of energy, providing adenosine triphosphate (ATP) through oxidative phosphorylation, a process that involves the dynamic transfer of positively charged protons via the mitochondrial inner membrane, resulting in a voltage gradient across that membrane, with the inside negative and the outside positive. The gradient is known as the mitochondrial membrane potential (ΔΨm).

Mitochondria oxidize carbohydrates, fatty acids and amino acids, producing energy and generating reactive oxygen species (ROS) (Crowley et al., 2016). It is thought that mitochondria generate almost 90% of the total number of cellular reactive oxygen species (Balaban & Mitoehondria, 2005).

Mitochondria are thought to play a crucial role in PH pathogenesis through the regulation of calcium homeostasis, mitochondrial ROS generation, the release of pro-apoptotic factors and the alteration of cellular metabolism (Dromparis & Michelakis, 2013; Schermuly et al., 2011).

Glycolysis converts glucose into pyruvate, which is then transported to mitochondria, where it participates in glucose oxidation as a substrate for pyruvate dehydrogenase. The shift in metabolism from oxidative phosphorylation towards glycolysis, which is followed by the fermentation of lactic acid instead of pyruvate oxidation in the mitochondria, is referred to as the Warburg Effect, or aerobic glycolysis. The Warburg effect can occur when pyruvate dehydrogenase (PDH) is inhibited through phosphorylation induced by pyruvate dehydrogenase

kinase (PDK) (Figure 4.1). Such a metabolic shift was identified in pulmonary arteries and the right ventricle (RV) of pulmonary hypertensive patients (Archer et al, 2013; Sutendra & Michelakis, 2014). The advantage of this metabolic shift, which was first defined in cancer cells, is the generation of ATP to meet cellular energy requirements and to promote cell growth and survival in conditions of limited oxygen supply or compromised mitochondrial function (Leopold & Maron, 2016; Warburg et al, 1927).

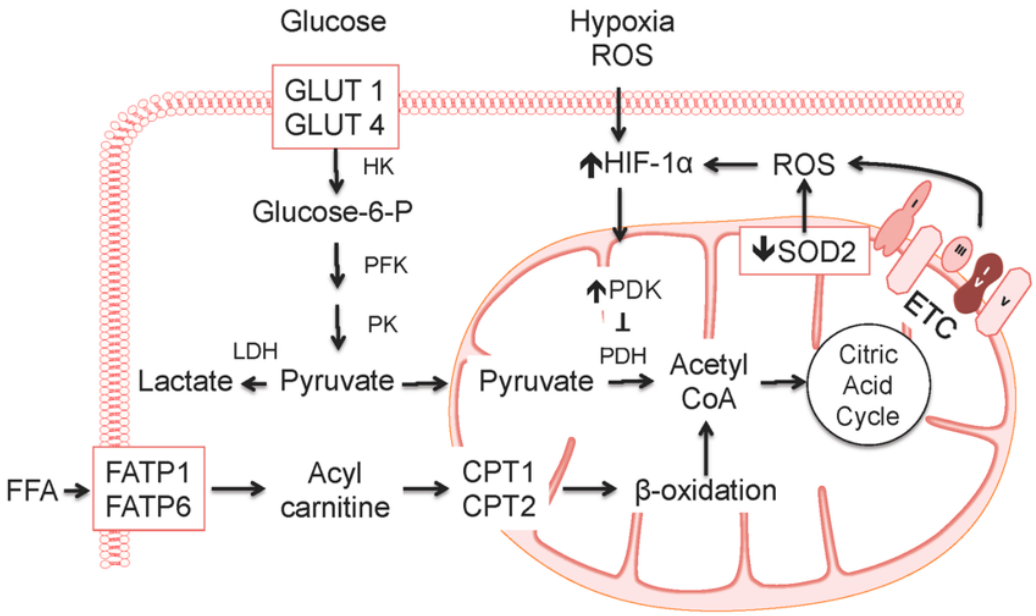


Figure 4.1: Illustration of energy metabolism in PAH. Glycolysis occurs when glucose is taken up by the glucose transporters (GLUT-1&4), becomes phosphorylated by hexokinase (HK), and goes through a chain of reactions to generate pyruvate, which is a substrate for pyruvate dehydrogenase (PDH) in mitochondria to support glucose oxidation. Free fatty acids (FFA) are taken up by fatty acid transport proteins 1 (FATP-1) and 6 (FATP-6), and converted to acyl carnitines that are shuttled across the mitochondrial membrane by carnitine palmitoyltransferase-1 (CPT1) and converted to acyl CoA by carnitine palmitoyltransferase-2 (CPT2). Acyl CoA is transformed to acetyl CoA during β-oxidation. In PAH, aerobic glycolysis increases due to normoxic upregulation of HIF-1α, which upregulates pyruvate dehydrogenase kinase (PDK) to inhibit pyruvate dehydrogenase, and encourages the epigenetic regulation of the superoxide dismutase 2 (*SOD2*) gene. Abbreviations: PFK, phosphofructokinase; PK, pyruvate kinase; LDH, lactate dehydrogenase; ROS. Adapted from Leopold & Maron, 2016.

4.2 Experimental aims

The studies described in this chapter are aimed at:

1. Optimizing conditions for adenoviral gene silencing of CLIC proteins in HPAECs.
2. Determining the effect of CLIC silencing on mitochondrial fragmentation.
3. Verifying the effects of CLIC proteins on mitochondrial membrane potential in human pulmonary artery endothelial cells (HPAECs).
4. Studying the effect of CLIC proteins on mitochondrial ROS production in HPAECs.
5. Investigating the effect of CLIC proteins on energy metabolism in HPAECs.

4.3 Experimental design

A detailed description of specific methods and protocols used in this chapter is provided in Chapter 2, Materials and Methods, and an overview of the experimental outline is presented in Figure 4.2.

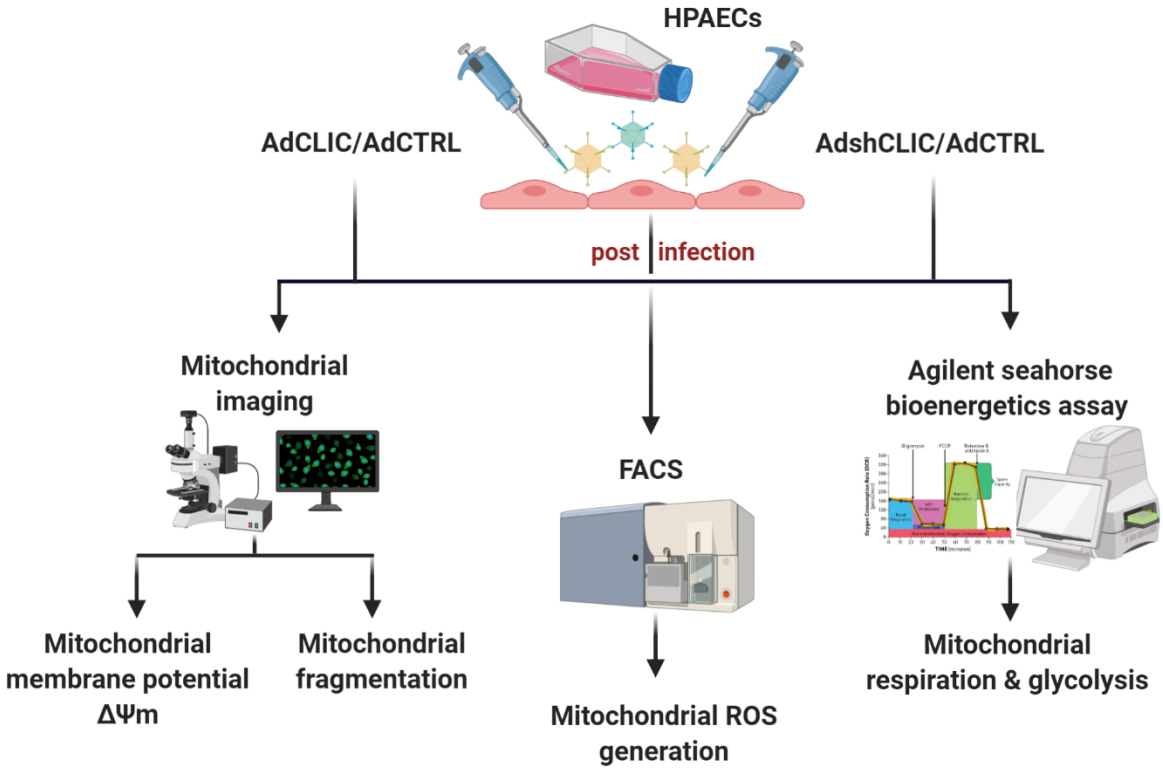


Figure 4.2: Experimental outline for chapter 4. CLIC expression was manipulated by the adenoviral overexpression or shRNA-mediated silencing of CLIC proteins. Changes in mitochondrial membrane potential, mitochondrial fragmentation, mitochondrial ROS generation, glycolysis, and mitochondrial respiration in HPAECs were studied by fluorescent imaging, FACS, and Seahorse bioenergetics assay.

4.3.1 Manipulation of CLIC gene expression in HPAECs

The overexpression of CLIC1 and CLIC4 was induced by adenoviral gene transfer with AdCLIC1 and AdCLIC4, as previously described (see Chapter 2- Section 2.2). The effects of CLIC1 and CLIC4 overexpression were studied in greater detail because they are implicated in the disease pathogenesis. In order to learn more about the role of these proteins in the regulation of mitochondrial function under basal conditions, the expression of CLIC1 and CLIC4 were inhibited by the overexpression of specific small hairpin RNAs (shRNAs), co-expressed with green fluorescent protein (GFP) by adenoviral gene transfer. Adenoviruses overexpressing GFP (AdCTRL; AdGFP) or scrambled (non-targeting) shRNA co-expressed with GFP (AdshCTRL) served as adenoviral infection controls. HPAECs grown in 6-well plates were infected with AdshCTRL, AdCLIC1-shRNA or AdCLIC4-shRNA at different dilutions to establish an optimal MOI. Changes in CLIC expression were evaluated by western blotting 24 hours post-infection with AdCLIC1 and AdCLIC4, while CLIC silencing was evaluated 48 hours post-infection.

4.3.2 Western blotting

HPAECs were lysed using modified RIPA buffer supplemented with protease/phosphatase inhibitors. The protein concentrations of individual samples were measured using a Pierce™ BCA Protein Assay Kit following standard protocols. Samples were resolved using SDS PAGE (10 µg – 20 µg protein/lane) and analysed by western blotting. The membranes were blocked using BSA (5%) for an hour, then probed with primary antibodies, followed by incubation with secondary HRP-linked antibodies. Bands were visualized using a Luminata Crescendo Western HRP Substrate in ChemiDoc™ Imager. ImageJ software was used to perform a densitometric quantification of western blot bands. For further details see Chapter 2- Materials and Methods, Section 2.8.1.

4.3.3 Measurement of mitochondrial fragmentation

The effect of CLIC proteins on mitochondrial fragmentation was verified as previously described (see Chapter 3, Section 3.4.2). Mitochondria were fluorescently stained and cells were examined under a confocal microscope. The mitochondrial fragmentation count (MFC) and the total mitochondrial area were determined using NIP2 image analysis software (Martinez & Cupitt, 2005), with mitochondrial particles having a 500 pixel cut-off size. For further details see Chapter 2- Materials and Methods, Section 2.4.

4.3.4 Measurement of mitochondrial membrane potential (ΔΨm)

In order to measure the mitochondrial membrane potential (ΔΨm), HPAECs cultured on Thermanox® Plastic Coverslips (13 mm) were infected with recombinant adenoviruses to induce CLIC overexpression or silencing. 24 hours (for AdCLIC) or 48 hours (for AdCLICshRNA) post-infection, 100 nM Tetramethylrhodamine, methyl Ester (TMRM) was added to the culture medium and the cells were incubated for 30 min at 37 ˚C. The cells were then washed twice with PBS and new medium was added to the cells. Live imaging was performed using a Zeiss confocal microscope (Zeiss LSM780) and the acquired images were analysed using ImageJ software. For further details see Chapter 2- Materials and Methods, Section 2.6.1.

4.3.5 Measurement of mitochondrial reactive oxygen species (mtROS)

The term “mitochondrial reactive oxygen species” (mtROS) refers predominantly to superoxide anion radical ($^{\bullet}O_2^-$). Mitochondrial $^{\bullet}O_2^-$ is released in control cells and cells overexpressing AdCLIC1, AdCLIC4, AdCLIC1 shRNA or AdCLIC4. shRNA was detected with MitoSOX. Cells were trypsinised and pelleted by centrifugation in 5 mL Falcon round-bottom polystyrene tubes. The medium was carefully aspirated and the pellet was re-suspended in 1 mL PBS followed by another centrifugation. 1µM MitoSOX Red, a highly selective dye used in the detection of mitochondrial

ROS (Kauffman et al., 2016), was added to the cells at 37°C, 5% (v/v) CO_2 for 30 minutes, protected from light. MitoSOX Red accumulates in mitochondria and becomes fluorescent upon oxidation by $^{\bullet}O_2^-$. MtROS production was measured by flow cytometry at an excitation of 510 nm and an emission of 580 nm using a BD FACS Canto Flow Cytometer, where 10,000 events were recorded for each sample with a selected FL2 channel (Figure 4.3). For more details see Chapter 2- Materials and Methods, Section 2.6.2.

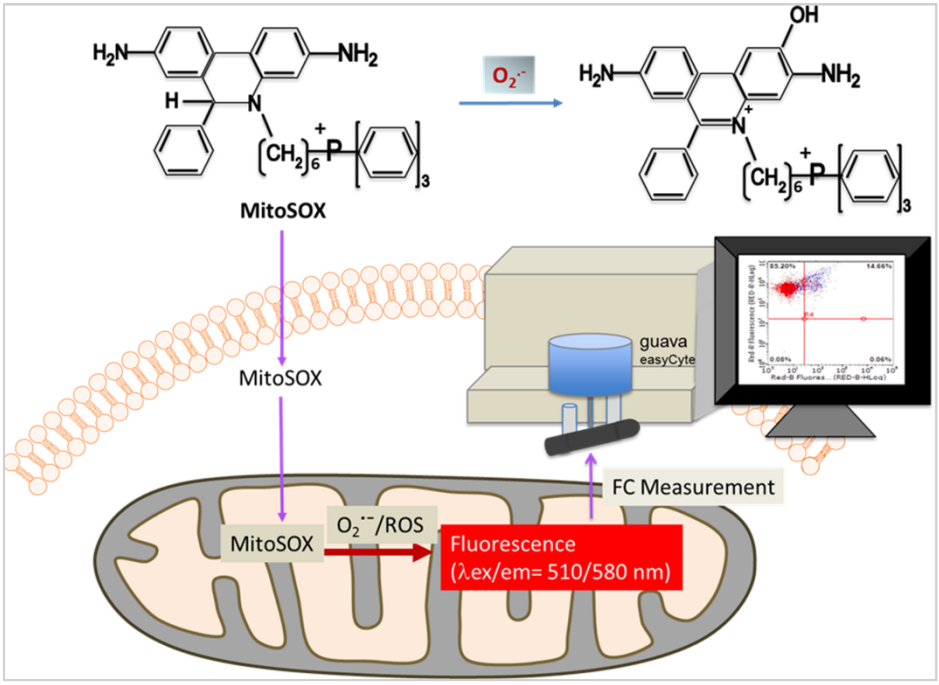


Figure 4.3: Illustration of MitoSOX-based flow cytometry (FC) for detecting mitochondrial reactive oxygen species. Measurement of mitochondrial superoxide $^{\bullet}O_2^-$ release was detected with MitoSOX. Adapted from Kauffman et al., 2016.

4.3.6 Cellular bioenergetics assay

To assess cellular metabolism and mitochondrial function in intact endothelial cells, a Cell Mito Stress Test and a Glycolysis Stress Test were carried out using an Agilent Seahorse XFp Extracellular Flux Analyzer. This technology enabled the measurement of oxygen consumption rate (OCR) and the extracellular acidification rate (ECAR) in response to sequential compound injections of respiratory and glycolysis modulators (Figures 4.4 and 4.5).

In the first series of experiments, the optimal number of HPAECs needed to obtain measurable OCR and ECAR was established. A seeding density of $2x10^4$/well was selected to allow for the optimal detection of any changes in OCR and ECAR.

HPAECs were seeded at the density of $2x10^4$/well in Seahorse 96-well plates designed for the Seahorse XFp instrument. The following day, the cells were infected with AdCTRL, AdshCTRL, AdCLIC or AdCLIC-shRNA and incubated for 24 or 48 hours respectively. Cells were equilibrated with Agilent Seahorse XF DMEM Medium pH 7.4 supplemented with 2mM L-Glutamine, 1mM pyruvate, and 10 mM glucose for Mito Stress Test. According to the manufacture's guidelines, 2mM L-Glutamine was the only supplement used in the Glycolysis Stress Test. The plates were then incubated in a CO_2-free XF prep station at 37°C for 40 minutes to allow temperature and pH calibration.

The Seahorse XFp Cell Mito Stress Test measures oxygen consumption rate (OCR) in response to the serial injection of oligomycin (1.5 µM) at 15 minutes, carbonyl cyanide 4-(trifluoromethoxy) phenylhydrazone (FCCP, 2 µM) at 34 minutes, and rotenone/antimycin A (Rot/Ant, 0.5 µM) at 54 minutes, as illustrated in Figure 4.4.

The Mito Stress Test begins with a basal respiration measurement of the OCR in adherent HPAECs prior to the injection of compounds, which reflects the energy demand of the cells under baseline

conditions. This is followed by the injection of ATP synthase inhibitor (oligomycin), resulting in a decrease in OCR that reflects ATP produced by the mitochondria. The inhibition of ATP production rapidly hyperpolarizes the mitochondrial membrane, preventing further proton pumping through respiratory complexes, meaning that the respiratory rate decreases. The remaining respiration is known as proton leak, and this reflects the flow of protons through lipids or other channels. Proton leaks can be a sign of mitochondrial damage, or can be used as a mechanism to control mitochondrial ATP generation. The maximal oxygen consumption rate was measured following the injection of the uncoupler agent (FCCP). FCCP allows for uninhibited movement of protons across the inner mitochondrial membrane, stimulating the electron transport chain (ETC) to operate at maximum capacity, which leads to rapid oxidation of substrates (sugars, fats, and amino acids) to meet this metabolic challenge. This in turn increases the OCR, and through the deduction of basal respiration, spare respiratory capacity is calculated, an important parameter that indicates the capability of the cell to respond to energy demand. Finally, with the additional injection of two ETC inhibitors (rotenone/antimycin A) (Rot/Ant), mitochondrial respiration is completely inhibited and OCR decreases to its lowest rate. At this point the oxygen consumption is not due to mitochondrial activity. Instead it indicates non-mitochondrial respiration (Tan et al., 2015; Traba et al., 2016) (Figure 4.5).

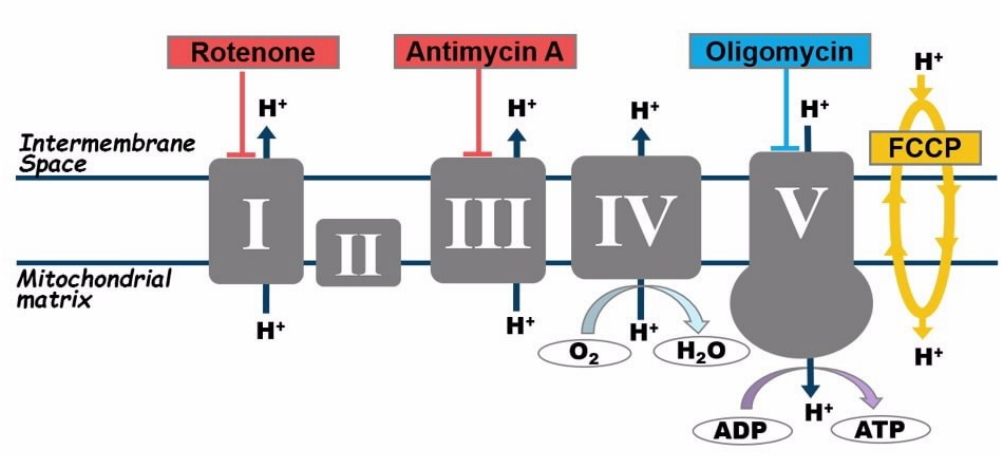


Figure 4.4: Illustration of Seahorse XFp Cell Mito Stress Test modulators. Diagram shows the specific components targeting electron transport chain (ETC). Oligomycin inhibits ATP synthase by targeting complex V, while FCCP is an uncoupler that targets the inner mitochondrial membrane, causing collapse of the proton gradient and disruption of the mitochondrial membrane potential. As a result, complex IV consumes large amounts of oxygen. Rotenone is a complex I inhibitor, while antimycin A is a complex III inhibitor, causing a shutdown of mitochondrial respiration system. Image obtained from the Agilent Seahorse Cell Mito Stress Test User Guide (Agilent Technologies, 2019).

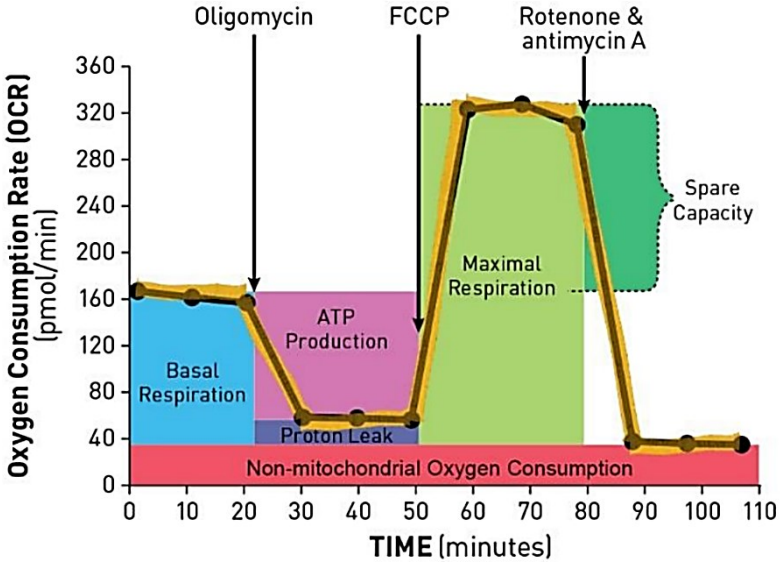


Figure 4.5: Seahorse XFp Cell Mito Stress Test profile of the key parameters of mitochondrial respiration. OCR is measured in response to sequential injections of respiratory modulators oligomycin, FCCP and rotenone/antimycin A. The assay allows the determination of basal respiration, ATP production, maximal respiration, spare respiratory capacity, proton leak and non-mitochondrial respiration. Abbreviations: OCR, oxygen consumption rate; FCCP, carbonyl cyanide-4 (trifluoromethoxy) phenylhydrazone. Image obtained from the Agilent Seahorse Cell Mito Stress Test User Guide (Agilent Technologies, 2019).

The Seahorse XFp Glycolysis Stress Test measures the extracellular acidification rate (ECAR) following the serial injection of glucose (1.5 µM) at 15 minutes, oligomycin (34 µM) at 34 minutes, and 2-Deoxy-glucose (2-DG, 65 µM) at 54 minutes, as shown in Figure 4.6.

The Glycolysis Stress Test starts with a baseline measurement of the ECAR of HPAECs prior to the injection of the assay components, which identifies any other sources of extracellular acidification that are not attributed to glycolysis. This is referred to as the non-glycolytic acidification rate, which likely corresponds to the respiratory CO_2 produced in the TCA cycle being converted to HCO^{3-} and H^+. This is followed by a glucose injection to activate glycolysis, which results in an increase in extracellular acidification due to lactate formation, and is referred to as the normal rate of glycolysis. The cells are then challenged by the injection of oligomycin, which inhibits ATP production. As a result of this dramatic decrease in ATP production, cells activate glycolysis to its maximum level, which leads to a secondary increase in the ECAR level (called the glycolytic reserve). Glycolysis is then totally inhibited following the injection of the glucose analogue (2-DG), which brings the ECAR back down to its non-glycolytic level (Figure 4.7) (Tan et al., 2015; Traba et al., 2016).

After the run, (OCR/ECAR) data were exported from the Wave controller software 2.6 to Microsoft Excel format and the Mito Stress Test and/or the Glycolysis Stress Test parameters were then automatically calculated using the Seahorse XF Report Generators as described in Chapter 2- Materials and Methods, Section 2.6.3.

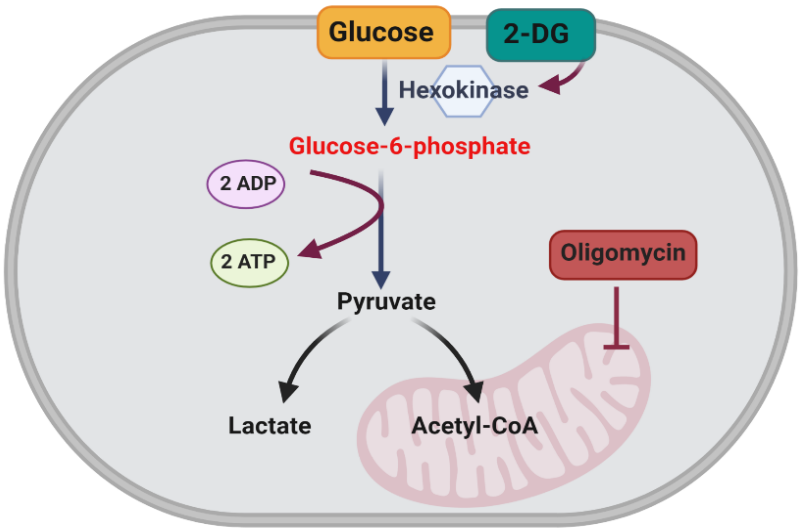


Figure 4.6: Illustration of Seahorse XFp Glycolysis Stress Test modulators. Diagram shows the sites of action of the assay components. Cells convert glucose to pyruvate through the glycolytic pathway producing ATP, NADH, H_2O, and protons. Oligomycin inhibits mitochondrial ATP synthesis causing a shift in energy production to glycolysis. 2-DG is a glycolysis inhibitor that competitively inhibits hexokinase, leading to decreased ATP production. Illustration created by the author using Biorender.

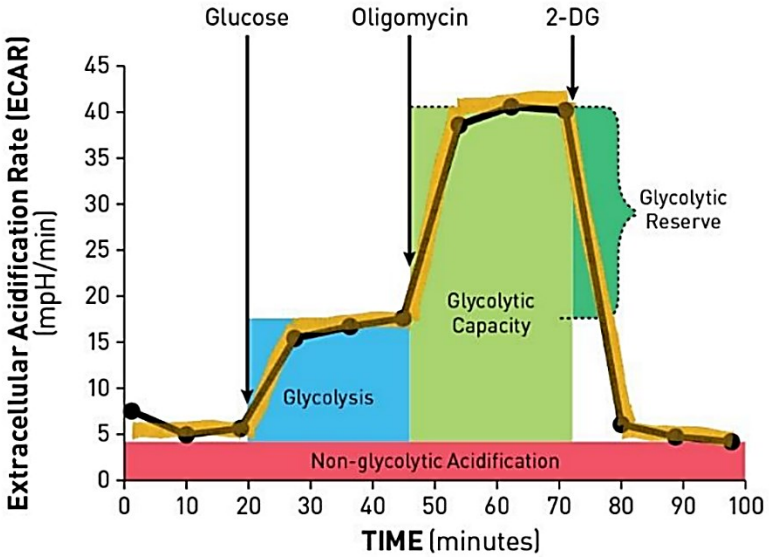


Figure 4.7: Seahorse XFp Glycolysis Stress Test profile showing the key parameters of glycolytic function. ECAR is measured during serial injections of glycolysis modulators: glucose, oligomycin and 2-DG, thus allowing the calculation of glycolysis, glycolytic capacity, glycolytic reserve and non-glycolytic acidification. Abbreviations: ECAR, extracellular acidification rate; 2-DG, 2-deoxy-glucose. Image obtained from the Agilent Seahorse Glycolysis Stress Test User Guide (Agilent Technologies, 2019).

4.4 Results

4.4.1 CLIC overexpression and silencing in endothelial cells

The MOI for CLIC1 and CLIC4 overexpression was optimised in order to achieve a 4 to 5-fold increase in the levels of these proteins, which is consistent with the increase in PAH-affected lungs (Abdul-Salam et al., 2010). The optimization process was described in detail in Chapter3, Section 3.5.1.

Experiments described in this part of the study aimed to test whether the presence of CLIC proteins is required to support mitochondrial biogenesis under basal conditions. In order to determine this, HPAECs were infected with AsdshCLIC1 and AdshCLIC4. Approximately 70% reduction in the expression of respective proteins was achieved in cells infected with AdCLICshRNA at the multiplicity of infection (MOI) of 1:200, 48 hours post-infection. As no differences in CLIC1 (data not shown) and CLIC4 expression between the two adenoviral controls (AdCTRL and AdshRNA-GFP) were noted (Figure 4.8), AdCTRL was chosen as the adenoviral control in further experiments. Figure 4.9 shows an example of the optimisation of adenoviral MOI for AdshCLIC4. Similar optimization was carried out for AdshCLIC1 (data not shown).

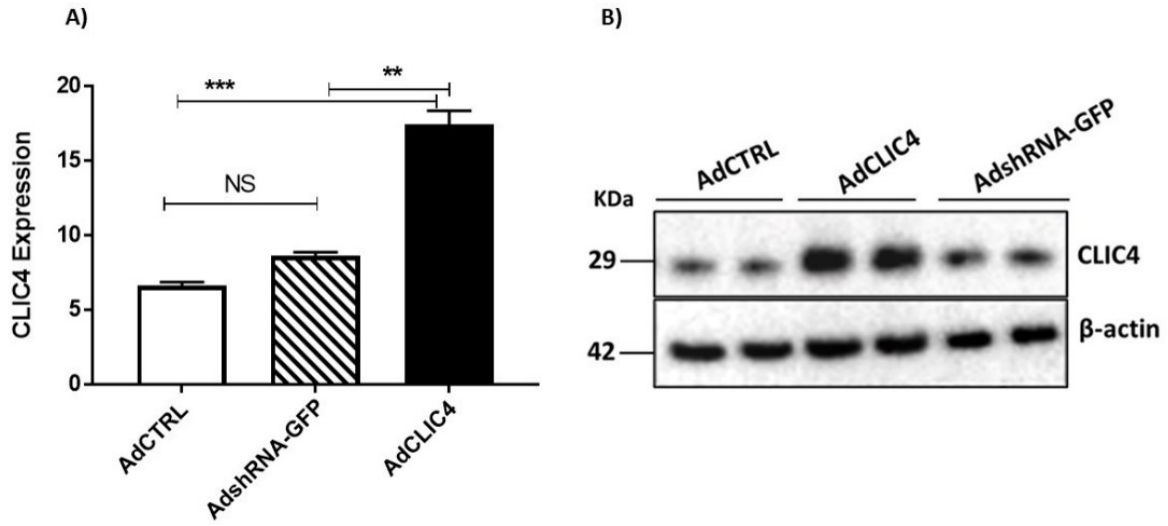


Figure 4.8: Comparison of different adenoviral controls. (A) Graph shows no statistically significant differences between adenoviral control AdCTRL (AdTet-off) and shRNA control (AdshRNA-GFP), while AdCLIC4 induced a significant, ~3-fold increase in CLIC4 expression **(B)** Representative western blots corresponding to **(A)**. **P <0.01, comparison with AdshRNA-GFP; ***P<0.0001, comparison with AdCTRL using one-way ANOVA with Tukey's multiple comparison test. Data are presented as mean ± SEM of three independent experiments with 3 technical repeats. Protein expression was normalised to β-actin.

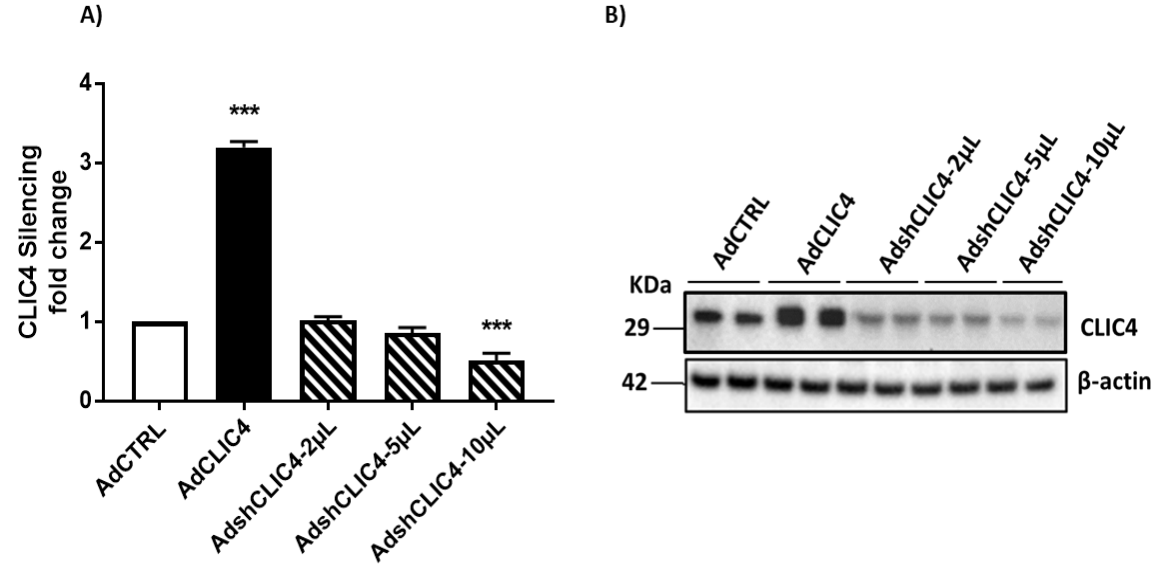


Figure 4.9: Optimization of CLIC4 inhibition in HPAECs. **(A)** The bar-graph shows fold change in CLIC4 protein levels in HPAECs infected with different dilutions of AdshCLIC4 or AdCTRL (Adenoviral control) 48 hours post-infection, as indicated. 2μL=MOI 1: 50, 5μL=MOI 1: 100, and 10μL=MOI 1: 200. **(B)** Representative western blots corresponding to (A). Expression levels were normalised to β-actin. Similar optimization strategies were used for AdshCLIC1 infection (not shown). ***P<0.0001, comparison with AdCTRL, using one-way ANOVA with Tukey's multiple comparison test. Data are presented as mean ± SEM of three independent experiments with 3 technical repeats.

4.4.2 The effect of CLIC proteins on mitochondrial network in HPAECs

CLIC1 and CLIC4 protein overexpression increased mitochondrial fragmentation in HPAECs. The cells showed increased numbers of small and fragmented mitochondria, indicative of increased mitochondrial fission and reduced fusion, as previously described in Chapter 3, Section 3.4.2. Inhibition of CLIC and CLIC4 expression significantly reduced mitochondrial fragmentation in cells, compared with controls (Figure 4.10). This suggests that the optimal expression levels of these proteins are important for the maintenance of mitochondrial homeostasis.

Representative confocal images of changes in the mitochondrial network induced by overexpression and silencing of CLIC proteins are shown in Figure 4.11.

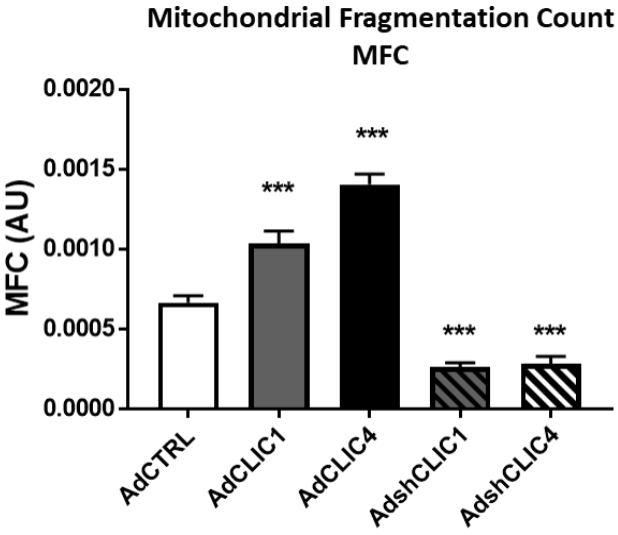


Figure 4.10: Effect of CLIC inhibition on mitochondrial fragmentation in HPAECs. Mitochondrial Fragmentation Count (MFC) in HPAECs infected with AdCTRL, AdCLIC1, AdCLIC4, AdshCLIC1, and AdshCLIC4, as indicated. MFC (arbitrary units) were measured using NIP2 image software. N=20 cells/treatment were analysed in in 3 separate experiments. ***P<0.0001, comparison with AdCRTL using One-way ANOVA with Dunnett's post hoc test. Data are presented as mean ± SEM.

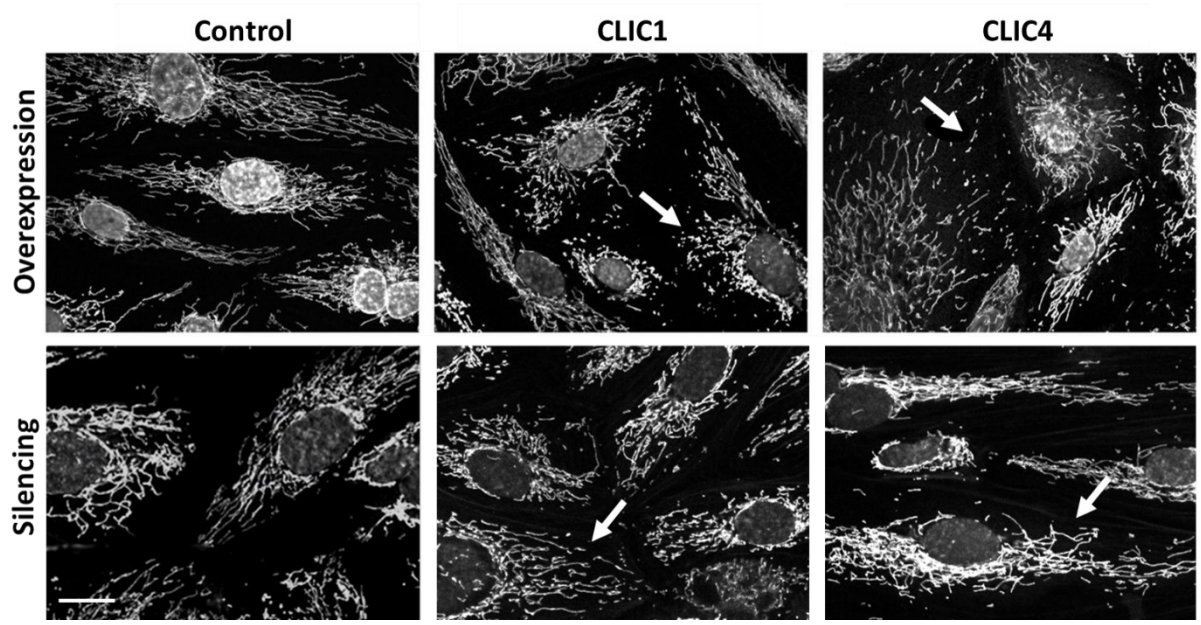


Figure 4.11: Representative images of mitochondrial networks in HPAECs following the overexpression and silencing of CLIC1 and CLIC4. AdCLIC1 and AdCLIC4-overexpressing HPAECs showed fragmented mitochondria, while AdshCLIC1 and AdshCLIC4-silenced HPAECs reduced mitochondrial fragmentation. Mitochondria were immunostained with anti-mitochondria antibodies. Images were captured using a Zeiss LSM 780 confocal microscope at 40x objective. Arrows point to mitochondria. Bar=10µm.

4.4.3 The effect of CLIC proteins on mitochondrial ΔΨm in HPAECs

Changes in the mitochondrial membrane potential were evaluated using a fluorescent indicator, Tetramethylrhodamine, methyl ester (TMRM). TMRM is a cell permeant, positively-charged, red-orange dye that readily accumulates in active mitochondria due to their relative negative charge. Depolarized or inactive mitochondria have decreased membrane potential and fail to sequester TMRM (Crowley et al., 2016).

The effect of CLIC protein overexpression and silencing on ΔΨm was assessed 24 or 48 hours post-adenoviral infection using AdCLIC1/AdCLIC4 and AdshCLIC1/AdshCLIC4 respectively. The mitochondrial potential was significantly elevated in CLIC1 and CLIC4-overexpressing HPAECs, while inhibition of CLIC proteins significantly decreased ΔΨm, compared with controls (Figure 4.12). Representative confocal images of changes in mitochondrial membrane potential induced by overexpression and silencing of CLIC proteins are shown in Figure 4.13.

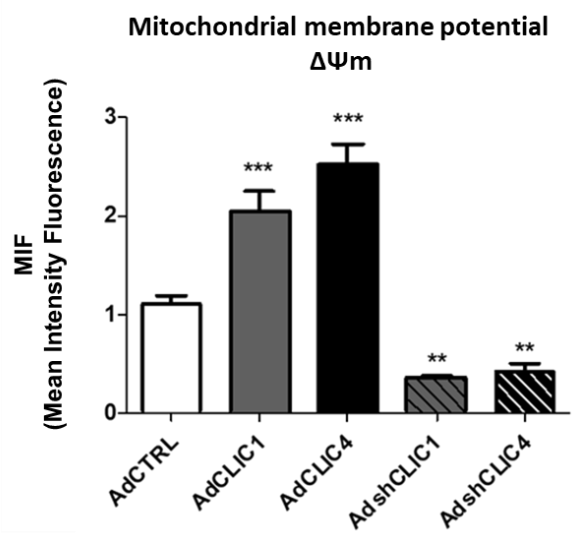


Figure 4.12: The effect of CLIC1 and CLIC4 overexpression and inhibition on mitochondrial membrane potential in HPAECs. Δψm was evaluated by measuring TMRM fluorescence intensity in HPAECs overexpressing/silencing CLIC1, and CLIC4. *P < 0.05, **P <0.01 ***P<0.0001, comparison with AdCRTL using one-way ANOVA with Tukey's multiple comparison test. Data are presented as mean ± SEM of 3 independent experiments with 3 technical repeats.

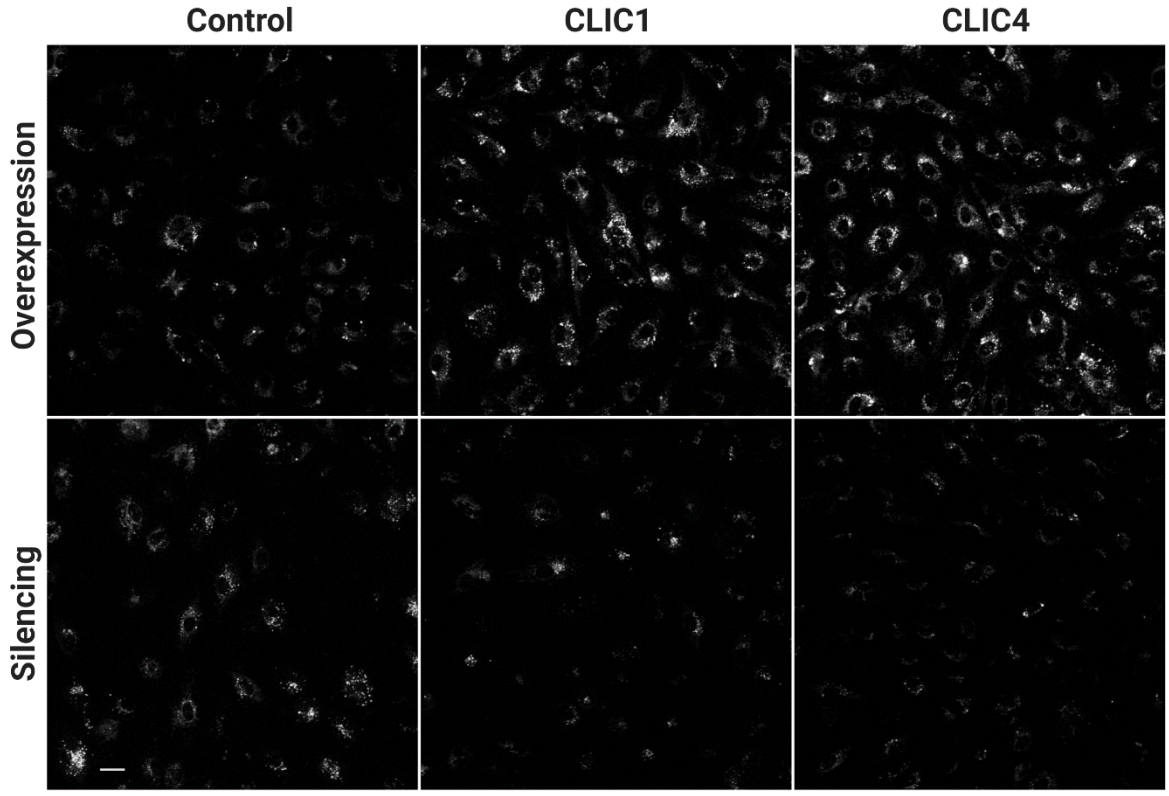


Figure 4.13: Changes in the mitochondrial membrane potential induced by modulation of CLIC expression in HPAECs. Representative images of TMRM-labelled mitochondria in HPAECs, following overexpression or silencing of CLIC1 or CLIC4, with AdCTRL serving as control. Images were captured using a Zeiss LSM 780 confocal microscope at 20x objective. Scale Bar=10 µM.

4.4.4 The effect of CLIC proteins on mitochondrial ROS generation in HPAECs

In order to evaluate the production of mitochondrial ROS (mtROS), HPAECs treated with recombinant adenoviruses were stained with MitoSOX, a fluorescent dye used in detection of mitochondrial reactive oxygen species (ROS), predominantly a superoxide anion radical (Kauffman et al., 2016). FACS data revealed a significant increase in ROS generation (~2-fold increase) in CLIC1- and CLIC4-overexpressing HPAECs, compared with control cells. The inhibition of CLIC proteins had no effect on basal mtROS generation (Figure 4.14).

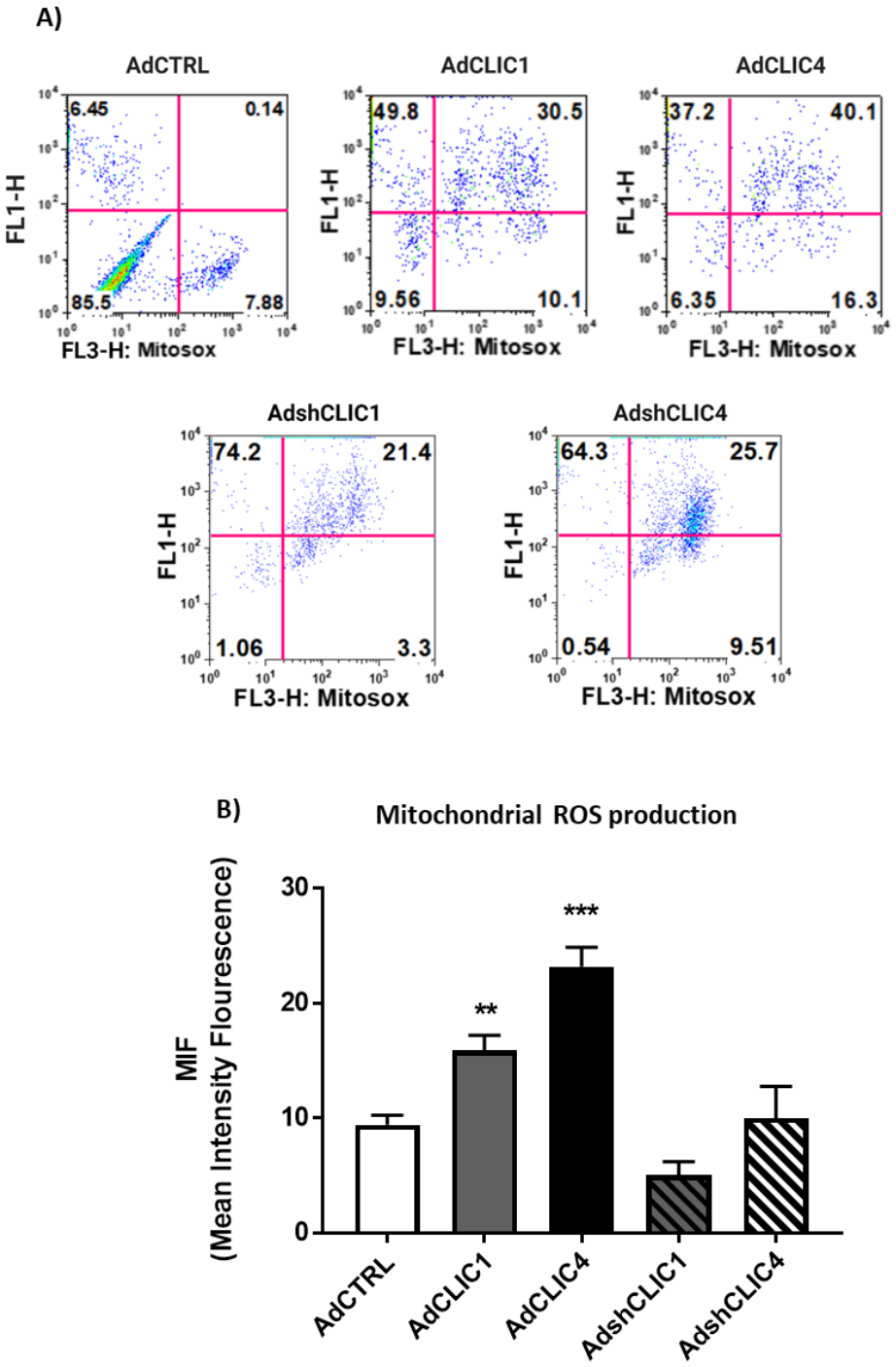


Figure 4.14: The effect of CLIC overexpression and silencing on mitochondrial ROS production in HPAECs. (A) Examples of mean fluorescent intensity histograms showing the ratio of MitoSox red (FL3-H) to Mitotracker green (FL1-H) (labelling all mitochondria) measured by Fluorescence Activated Cell Sorting (FACS). **(B)** The effect of CLIC expression changes on ROS production, measured as mean intensity of fluorescence (arbitrary units: AU) in HPAECs treated, as indicated. *P < 0.05, ***P<0.0001, comparison with AdCRTL using One-way ANOVA with Dunnett's post hoc test. Data are presented as mean ± SEM of 3 experiments with 3 technical repeats.

4.4.5 The effect of CLIC proteins on the bioenergetic profile of HPAECs

The effect of CLIC proteins on the mitochondrial bioenergetic profile of HPAECs was evaluated using the Agilent Seahorse Mito Stress Test and Glycolysis Stress Test. The Oxygen Consumption Rate (OCR) was assessed in response to the sequential addition of respiratory modulators: oligomycin at 15 minutes, FCCP at 34 minutes, and rotenone/antimycin (Rot/Ant) at 54 minutes. All the OCR values were expressed in pmoles/min of oxygen consumed. The extracellular Acidification Rate (ECAR) was detected under basal conditions followed by the serial injection of glycolysis modulators: glucose, oligomycin, and 2-DG at 15, 34, and 54 minutes respectively, with the data represented as mpH/min. A consistent protein concentration for each experiment was confirmed across all cells in each well. OCR and ECAR data were automatically calculated using Wave software then exported to Excel and used to determine the effect of CLIC proteins on key mitochondrial respiration and glycolysis parameters.

The analysis revealed the following changes in OCR parameters:

- Basal respiration: CLIC1 and CLIC4 overexpression decreased basal mitochondrial respiration in HPAECs compared with AdCTRL, while their inhibition had no significant effect (Figure 4.16 A).
- A significant decrease in ATP production was observed in CLIC1 and CLIC4 overexpressing HPAECs. CLIC1 and CLIC4 gene silencing did not significantly alter basal ATP production in cells, though an upward trend was noted (Figure 4.16 B).
- CLIC-overexpressing HPAECs showed a significant decrease in maximal respiration compared with control cells. In contrast, inhibition of CLIC1 and CLIC4 expression resulted in a small increase in the maximal respiration level, compared with AdCTRL (Figure 4.16 C).

- CLIC1- and CLIC4-overexpressing cells showed a significant increase in proton leak, compared with control HPAECs, while the inhibition of CLIC1 and CLIC4 had no effect (Figure 4.16 D).
- A significant reduction in the spare respiratory capacity was induced by CLIC1 and CLIC4 overexpressing HPAECs, while no significant change was induced by CLIC1 and CLIC4 gene silencing (Figure 4.16 E).
- CLIC1- and CLIC4-overexpressing HPAECs induced a significant increase in non-mitochondrial respiration, while CLIC1 and CLIC4 gene silencing had no significant effect (Figure 4.16 F).

An example of OCR data generated by the XF Mito Stress Test report generator is shown in Figure 4.15, and changes in various parameters of bioenergetics profile in HPAECs are shown in Figure 4.16.

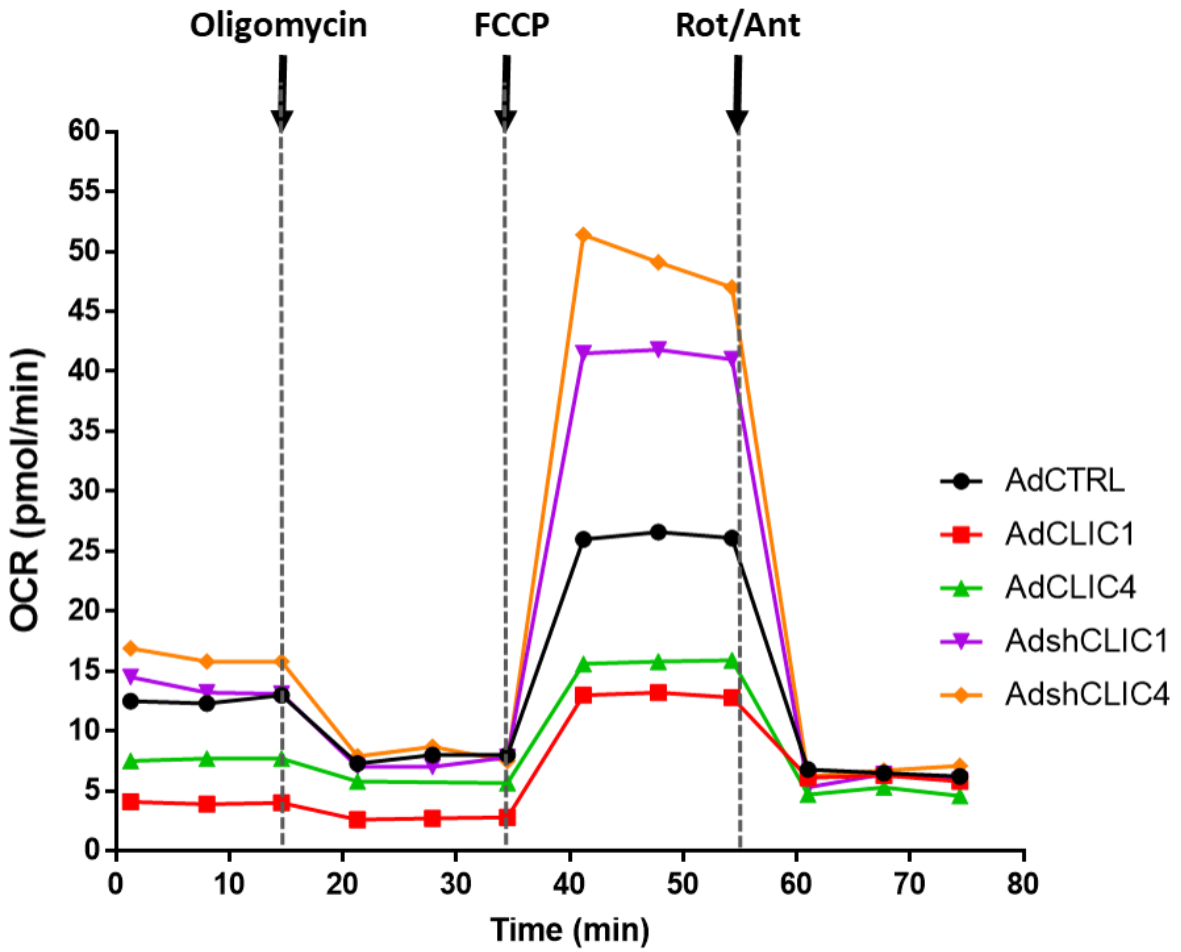


Figure 4.15: Example of Oxygen consumption rate (OCR) measurement. HPAECs were infected with either AdCTRL and/or AdCLIC1, AdCLIC4, AdshCLIC1, AdshCLIC4 and OCR was measured at various time intervals following the injection of oligomycin, FCCP, and Rot/Ant at 15, 34, 54 minutes respectively. Black circle: AdCTRL; red square: AdCLIC1; green triangle: AdCLIC4; purple triangle: AdshCLIC1; orange diamond: AdshCLIC4. Abbreviations: FCCP, carbonyl cyanide-4 (trifluoromethoxy) phenylhydrazone; Rot/Ant, Rotenone plus antimycin A; OCR, oxygen consumption rate. Representative trace from four independent experiments.

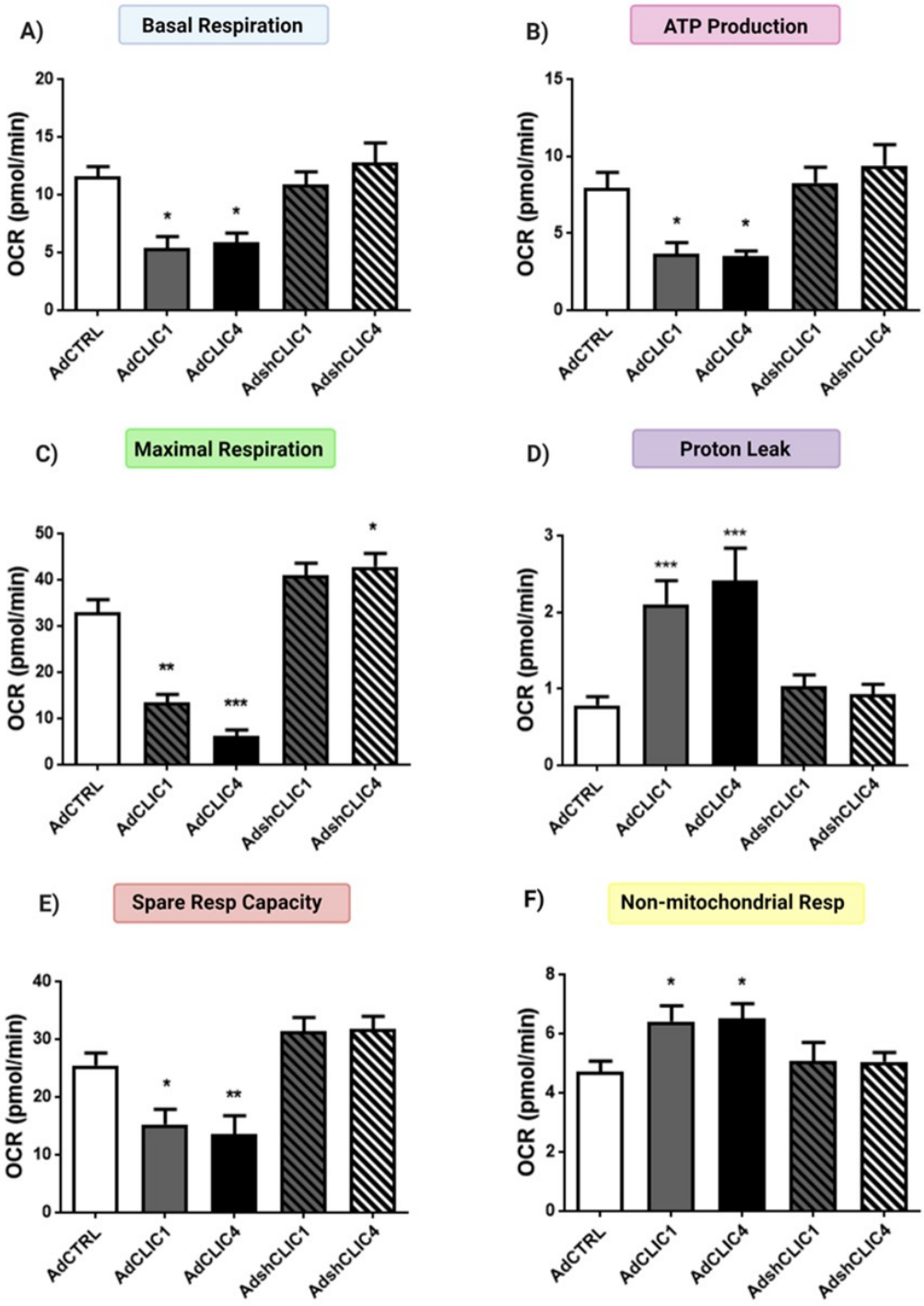


Figure 4.16: Effect of CLIC overexpression and inhibition on mitochondrial function in HPAECs. Cells were infected with either AdCTRL and/or AdCLIC, AdshCLIC and key parameters of mitochondrial respiration were measured using the Seahorse XFp Cell Mito Stress Test. *P < 0.05, **P <0.01 ***P<0.0001, comparison with AdCRTL, using One-way ANOVA with Tukey's multiple comparison test. Data are presented as mean ± SEM of 4 independent experiments with 4 to 8 replicate wells in the Seahorse XF analyser. Data were normalised to protein concentration for each experiment across all cells in each well.

The analysis revealed the following changes in ECAR parameters

- Glycolysis: overexpression of CLIC1 and CLIC4 induced a strong upregulation of glycolysis in HPAECs, while CLIC1 and CLIC4 gene silencing had no significant effect (Figure 4.18 A).
- A significant increase in glycolytic capacity was noted in CLIC1- and CLIC4-overexpressing cells, while CLIC1 and CLIC4 gene silencing had no significant effect (Figure 4.18 B).
- Glycolytic reserve: no significant differences were noted among the groups (Figure 4.18 C).
- A significant reduction in non-glycolytic acidification was induced by AdCLIC1 and AdCLIC4 in HPAECs, while CLIC1 and CLIC4 silencing increased non-glycolytic acidification to the control level (Figure 4.18 D).

An example of ECAR data generated by the XF Glycolysis Stress Test report generator is shown in Figure 4.17. The effects of CLIC1 and CLIC4 overexpression and silencing on various ECAR parameters are shown in Figure 4.18.

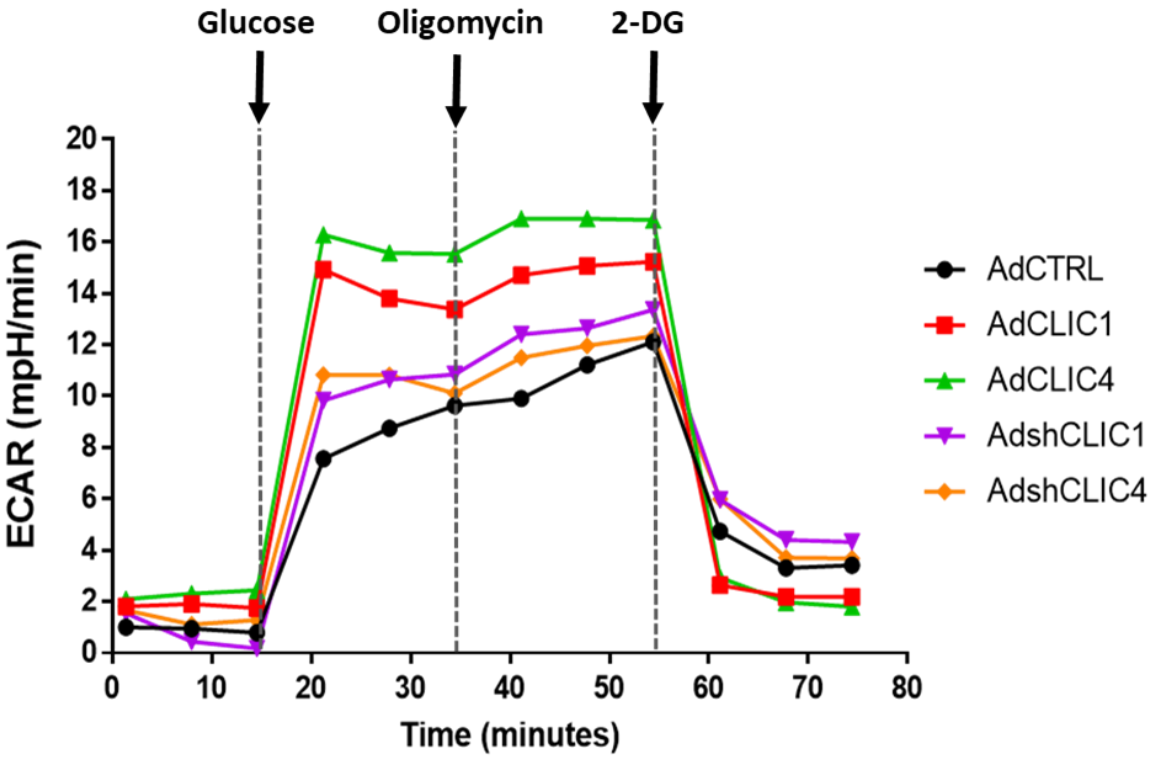


Figure 4.17: Example of extracellular acidification rate (ECAR) measurement. HPAECs were infected with AdCLIC1, AdCLIC4, AdshCLIC1 or AdCLIC4 and ECAR was measured at various time intervals following the injection of glucose at 15 minutes, oligomycin at 34 minutes, and 2-DG at 54 minutes. Black circle: AdCTRL; red square: AdCLIC1; green triangle: AdCLIC4; purple triangle: AdshCLIC1; orange diamond: AdshCLIC4. Abbreviations: 2-DG, 2-Deoxy-glucose; ECAR, extracellular acidification rate. Representative trace from four independent experiments.

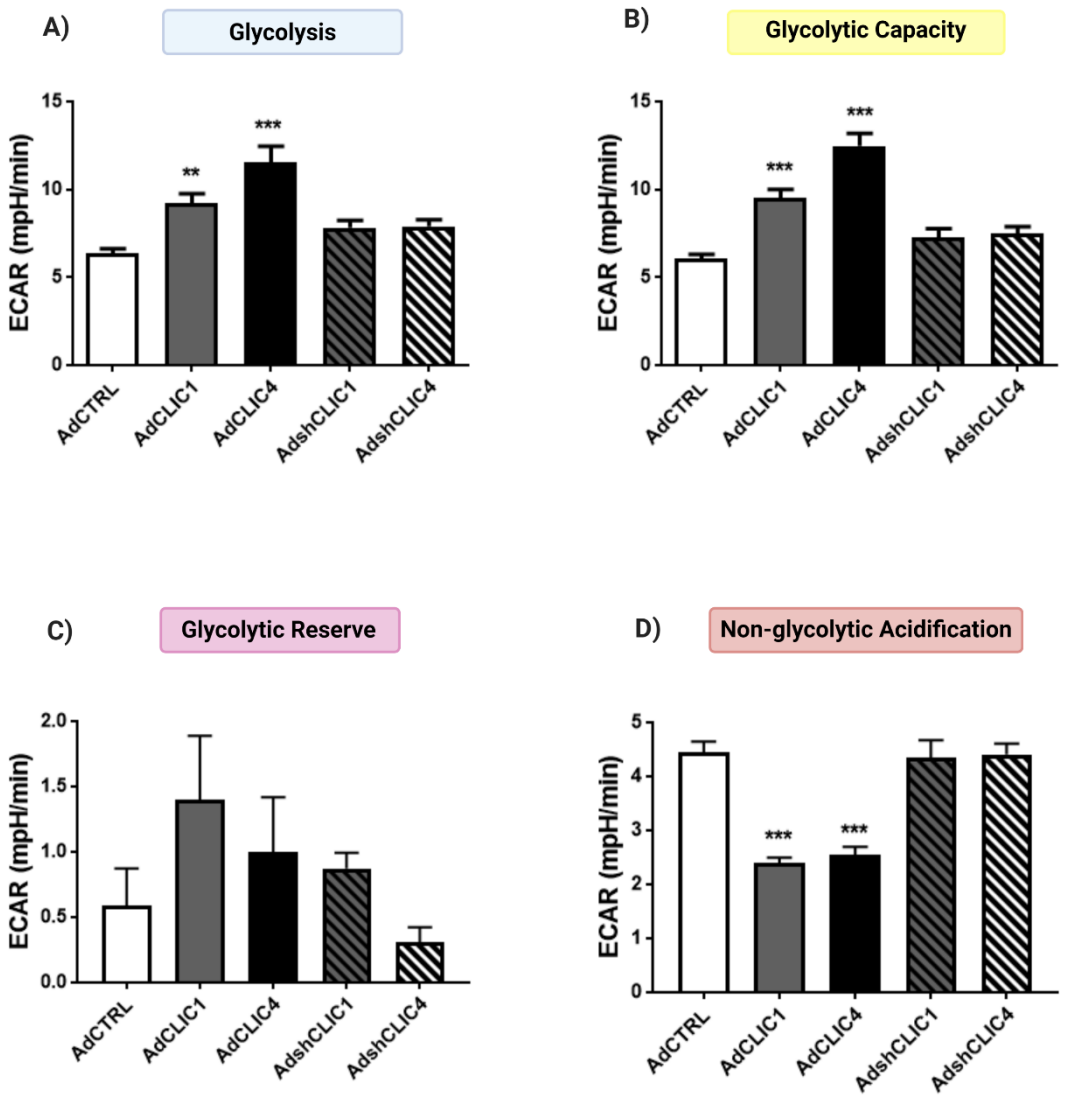


Figure 4.18: Effect of CLIC overexpression and inhibition on acidification rate in HPAECs. Cells were infected with either AdCTRL and/or AdCLIC, AdshCLIC and key parameters of glycolytic function were measured using the Seahorse XFp Cell Glycolysis Stress Test. *P <0.05, **P <0.01 ***P<0.0001, comparison with AdCRTL using One-way ANOVA with Tukey's multiple comparison test. Data are presented as mean ± SEM of four independent experiments with 4 to 8 replicate wells/treatment. Data were normalised to protein concentration for each experiment across all cells in each well.

4.5 Summary

The key findings presented in this chapter show that:

- CLIC1 and CLIC4 overexpression increased mitochondrial fragmentation and mitochondrial membrane potential ΔΨm, while the silencing of these proteins significantly reduced mitochondrial fragmentation and ΔΨm.
- CLIC1 and CLIC4 increased mitochondrial ROS production in HPAECs, while inhibition of these proteins had no impact on mitochondrial ROS.
- Overexpression of CLIC1 and CLIC4 significantly reduced the rate of oxygen consumption and the production of ATP in HPAECs, while inhibition of CLIC1, and CLIC4 expression had no effect.
- CLIC-overexpressing HPAECs showed an increase in proton leak, while CLIC1 and CLIC4 silencing had no effect.
- A significant decrease in basal respiration, maximal respiration and spare respiratory capacity was observed in CLIC1- and CLIC4-overexpressing HPAECs. These cells also showed and an increase in non-mitochondrial respiration.
- CLIC1 and CLIC4 induced a metabolic shift towards glycolysis, which was manifested by increased glycolysis and glycolytic capacity. The inhibition of CLIC proteins had no major impact on glycolysis.

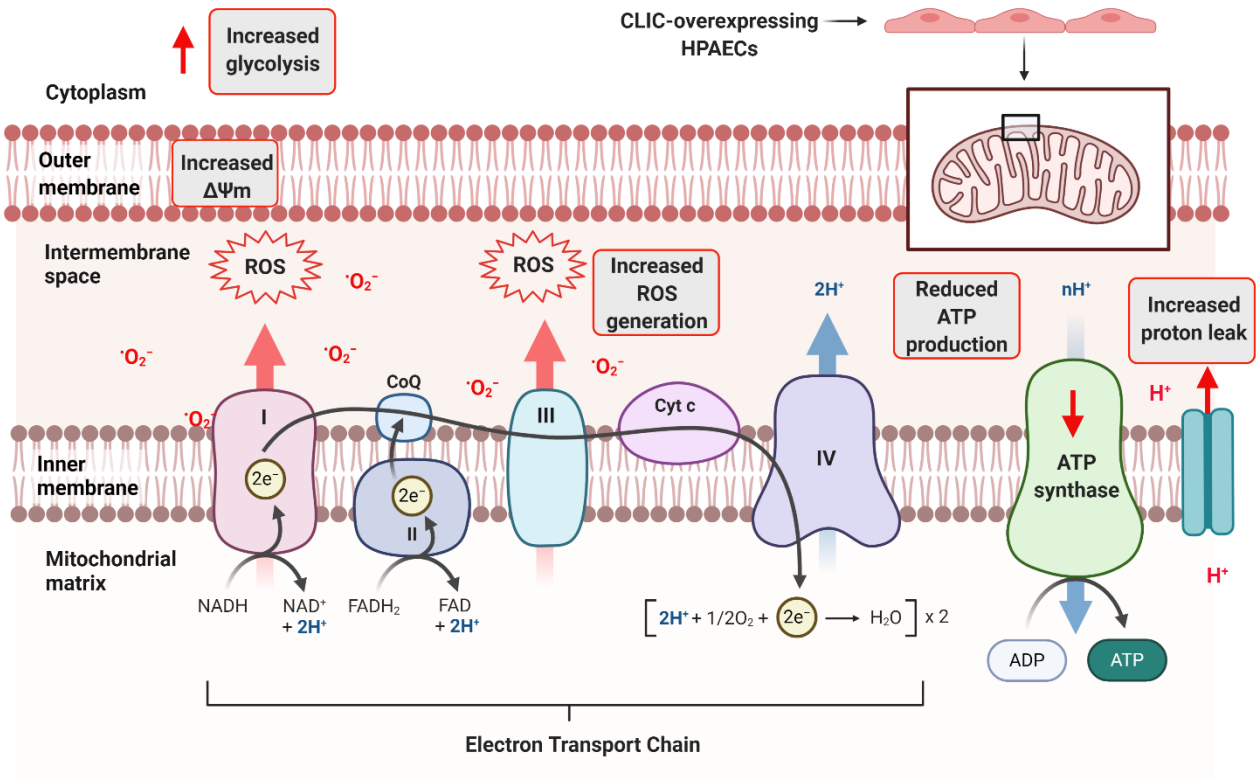


Figure 4.19: Summary of key results of Chapter 4. Key findings are summarised in Table 4.1. Abbreviations: ROS; reactive oxygen species, ΔΨm; mitochondrial membrane potential. Illustration created by the author using with BioRender.com.

Table 4.1: Summary of key findings of the effect of CLIC protein overexpression and inhibition on mitochondrial function in HPAECs. Red arrows pointed up indicate increase, black arrows pointed down indicate decrease, and dashes (–) indicate no change.

Investigation	CLIC1	CLIC4	shRNA-CLIC1	shRNA-CLIC4
Mitochondrial fragmentation	↑	↑	↓	↓
Mitochondrial membrane potential	↑	↑	↓	↓
Mitochondrial ROS production	↑	↑	—	—
Basal respiration	↓	↓	—	—
ATP production	↓	↓	—	—
Maximal respiration	↓	↓	—	↑
Proton leak	↑	↑	—	—
Spare respiratory capacity	↓	↓	—	—
Non-mitochondrial respiration	↑	↑	—	—
Glycolysis	↑	↑	—	—
Glycolytic capacity	↑	↑	—	—
Non-glycolytic acidification	↑	↑	—	—
Glycolytic reserve	—	—	—	—

4.6 Discussion

The experiments discussed in this chapter investigated the role of CLIC proteins in the regulation of mitochondrial function to identify potential links between pathological overexpression of these proteins and mitochondrial dysfunction in PAH. The silencing of CLIC1 and CLIC4 was carried out to find out whether the basal expression of these proteins is required for the maintenance of mitochondrial structure and function. The role of CLIC5, which is not associated with PAH pathology, has not been studied.

In PAH, vascular remodelling is characterized by proliferative smooth muscle and endothelial cell dysfunction. Endothelial dysfunction is associated with a decline in mitochondrial function that is reflected in reduced mitochondrial ATP synthesis, increased mitochondrial ROS production, hyperpolarized mitochondrial membrane potential, and imbalance in the redox-related enzymes (Marshall et al., 2018). Hyperpolarization of mitochondrial membrane has been linked with resistance to apoptosis in vascular smooth muscle cells from rats with pulmonary hypertension (McMurtry et al., 2004; Pak et al., 2013; Rafikov et al., 2015). Expression of CLIC proteins in endothelial cells is increased in response to oxidative stress, DNA damage or inflammatory cytokines and is thought to activate repair mechanisms, cell proliferation and angiogenesis (Ponnalagu & Singh, 2016). Here, a significant increase in mitochondrial membrane potential was observed in CLIC1- and CLIC4-overexpressing cells, which would therefore be consistent with the role of CLIC proteins as the mediators of cellular stress response. Meanwhile, CLIC abundance in plexiform lesions is likely to reflect the demand for larger energy supply in response to pro-angiogenic stimuli and local hypoxia.

Mitochondrial membrane hyperpolarization leads to higher ROS production (Kluge et al., 2013; Marshall et al., 2018).

The main sources of ROS in the pulmonary vasculature are nicotinamide adenine dinucleotide phosphate (NADPH) oxidases, uncoupled endothelial nitric oxide synthase (eNOS), xanthine oxidase (XO) and the mitochondrial electron transport chain (ETC) (Freund-Michel et al., 2013). The ETC is the main producer of mtROS, and superoxide generation is attributed to Complexes I and III. Any defects in mitochondrial electron transport can lead to the generation of reactive oxygen species as well as proton leak (Lenaz & Genova, 2010).

The data in my study show an increase in mitochondrial ROS production and proton leak in CLIC1- and CLIC4-overexpressing cells, which is consistent with previous observations linking CLIC overexpression with oxidative stress and excessive repair mechanisms (Ponnalagu & Singh, 2016; Rafikov et al., 2015). HIF is a master-regulator of the hypoxia-induced expression of genes that are involved in glycolysis and angiogenesis. CLIC4 stabilises HIF under normoxic conditions through the activation of NF-κB (Wojciak-Stothard et al., 2014) so it is likely that the CLIC1- and CLIC4-induced upregulation of glycolysis is mediated, at least in part, by HIF. The stabilization of HIF under hypoxic conditions is independent of mitochondrial ROS generation (Chua et al., 2010), so CLIC-induced ROS are unlikely to play a role in the process. Further investigation is necessary to establish whether CLIC-induced ROS mediate the pro-angiogenic effects of these proteins.

Defects in the energy metabolism underlie the pathology of many disorders, including cancer, diabetes and pulmonary hypertension. Pulmonary vascular cells in PH show a metabolic shift towards glycolysis, and this switch is known to give a proliferative advantage to cancer cells (Leopold & Maron, 2016; Rafikov et al., 2015). To assess the possible contribution of CLIC proteins to this glycolytic switch, mitochondrial respiration (OCR) and glycolysis rate (ECAR) were evaluated in CLCI1- and CLiC4- overexpressing cells using Seahorse XF Analyser (Rafikov et al., 2015).

HPAECs overexpressing CLIC1 and CLIC4 showed a significant increase in ECAR and a reduction in mitochondrial ATP generation and OCR, indicating the upregulation of glycolysis. This shift from mitochondrial oxidative phosphorylation to glycolysis has also been attributed to the activation of HIF, which activates pyruvate dehydrogenase kinase (PHK) that then inhibits pyruvate dehydrogenase (PDH), resulting in the suppression of mitochondrial oxidative phosphorylation due to the failure to produce acetyl-CoA for the Krebs cycle (Papandreou et al., 2006). The observation concurs with the results shown in Chapter3, Section 3.5.5, that CLIC1 and CLIC4 increase PDK expression and reduce PDH expressing levels in CLIC-overexpressing HPAECs. Currently, PDH inhibition is considered as the primary mechanism for the suppression of mitochondrial respiration, pulmonary vasoconstriction and remodelling in PH (Rounds & McMurtry, 1981; Ten & Ratner, 2020).

Alterations to the mitochondrial structure and biogenesis have also been implicated in the metabolic changes seen in PH. Previous studies have demonstrated that imbalances in the expression levels of proteins regulating fission and fusion processes contribute to the metabolic shift (Chan, 2007; Marsboom et al., 2012; Ryan et al., 2013; Westermann, 2010). Previous evidence also shows that the architecture of the cristae regulates mitochondrial respiration, while changes in cristae organization alter the electron transport chain, mitochondrial dynamics and respiration (Norton et al., 2014). These findings support the results of our experiments described in Chapter 3, Sections 3.5.6 and 3.5.4.6, where CLIC1 and CLIC4 overexpression significantly decreased MFN2 expression levels and the number of cristae in HPAEC mitochondria. This might be linked to the reduction in MFN2, as the remodelling of the cristae is a MFN2-dependent process. The reduction seen in MFN2 may also contribute to a mitochondrial respiration shift towards glycolysis (Sood et al., 2014).

shRNA treatment significantly reduced but did not completely inhibit CLIC1 and CLIC4 expression, so any remaining CLIC activity may have been sufficient for the maintenance of mitochondrial respiration. Our data show that mitochondrial fragmentation and membrane potential were significantly reduced in CLIC1-, and CLIC4-silenced cells. Mitochondrial ROS production was reduced in shRNACLIC1- and shRNACLIC4- treated HPAECs, while ATP production was enhanced and glycolysis levels were reduced. Strong evidence indicates that CLIC1 acts as a sensor of cell oxidation and responds to metabolic and oxidative stress challenges (Averaimo et al., 2010; Littler et al., 2004). Consistent with our findings, results from other laboratories have shown that CLIC1 and CLIC4 inhibition significantly reduces ROS generation and expression of pro-inflammatory cytokines in endothelial cells (Xu et al., 2016).

Considering that alterations in mitochondrial morphology can also be linked to ROS signalling (McCarron et al., 2013), reduction in mitochondrial fragmentation in CLIC-silencing cells may be contributed to reduced mtROS in CLICshRNA-treated cells. Emerging evidence reveals a direct relationship between mitochondrial membrane potential and mtROS generation (Korshunov et al., 1997; Seifert et al., 2010), suggesting that the observed reduction in mitochondrial membrane potential in CLIC1, and CLIC4-silenced HPAECs can also be linked to reduced mtROS production. In addition, reduced ROS production has been reported to improve mitochondrial respiration (Marshall et al., 2018). This is consistent with our data, which showed that CLIC silencing may enhance mitochondrial respiration.

In conclusion, our data suggests that overexpression of CLIC1 and CLIC4 in HPAECs dysregulates mitochondrial complexes in the ETC. This imbalance appears to have a major impact on the activity of downstream respiratory chain complexes as well as mitochondrial ROS production and membrane potential, driving cells towards adaptational changes to low oxygen levels that are linked to increased glycolysis, ROS production and membrane potential (Archer et al., 2013). Based on our data, CLIC inhibitors may be considered in potential therapies aiming to improve mitochondrial function in PAH.

The results reported here suggests the existence of functional redundancy between CLIC1 and CLIC4. Previous studies have documented phenotypical similarities between CLIC1 and CLIC4 cell knockdowns, including reduced cell growth, increased cell viability and inhibited angiogenic network formation. However, there were also few differences - CLIC1 (but not CLIC4) knockdown inhibited cell migration, while CLIC4 (but not CLIC1) knockdown reduced vascular lumen formation (Tung et al., 2009; Tung & Kitajewski, 2010).

CHAPTER 5 RESULTS:

Proteomic analysis of CLIC-induced changes in mitochondrial protein expression profile in HPAECs

CHAPTER 5 RESULTS: Proteomic analysis of CLIC-induced changes in mitochondrial protein expression profile in HPAECs

This chapter focuses on proteomic analysis of mitochondrial proteins from CLIC1- and CLIC4-overexpressing HPAECs. This analysis was carried out to identify potential mediators of CLIC-induced effects on endothelial cells.

5.1 Introduction

Intracellular chloride channel proteins (CLICs) have been identified as mediators of vascular dysfunction in PAH (Wojciak-Stothard et al., 2014). CLIC 1 and CLIC4 are highly expressed in animal and human PAH lungs and are elevated in plasma and blood-derived late outgrowth endothelial cells from PAH patients. CLIC1 and CLIC4 are localised to the vascular endothelium, particularly in plexiform lesions, but can also be found in other layers of the remodelled pulmonary vasculature (Abdul-Salam et al., 2010; Wojciak-Stothard et al., 2014). Recent evidence shows that these proteins form some of the components of the mitochondrial membrane. The role of CLIC proteins in the regulation of mitochondrial function and dynamics is at present poorly understood (Singh, 2010).

Mass spectrometry (MS)-based proteomics has become an indispensable tool in cellular and molecular biology, and has been widely used for protein identification and quantification. MS-based proteomics has been extensively applied to the study of protein-to-protein interactions, the mapping of various organelles, and generation of quantitative protein profiles (Aebersold & Mann, 2003).

5.2 Experimental aims

The aim of the experiments presented in this chapter was to characterise the effects of CLIC1 and CLIC4 on mitochondrial protein expression profiles to gain new insights into the mechanisms and actions of these proteins.

5.3 Experimental outline

An experimental outline (Figure 5.1) and a brief description of methodology is provided below. Further experimental details can be found in Chapter2- Materials and Methods, Section 2.7.2. The proteomic analysis was conducted by Dr. Vahitha B. Abdul-Salam.

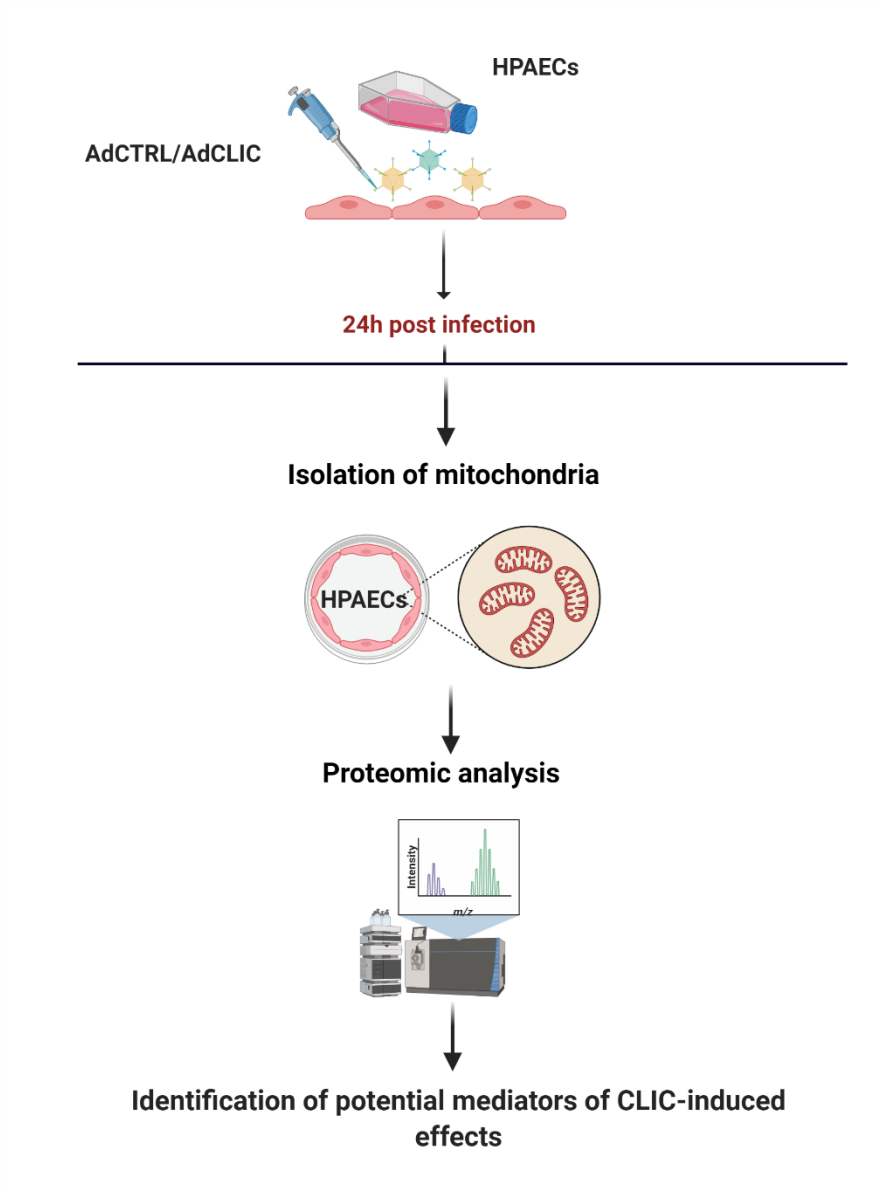


Figure 5.1: Experimental outline for Chapter 5. CLIC overexpression was induced by adenoviral gene transfer in HPAECs. 24 hours post-infection, mitochondria were isolated from CLIC-overexpressing HPAECs. Proteomic analysis was performed to identify mitochondrial protein expression profile induced by CLIC overexpression in HPAECs. Illustration created by the author using BioRender.com.

5.3.1 Proteomic analysis

80% confluent HPAECs were infected with AdCTRL, AdCLIC1 or AdCLIC4 and incubated under normoxic conditions (5% CO_2,) at 37^{o}C. To compare the effects of CLIC proteins with the effects induced by hypoxia, control cells (AdCTRL) were also cultured under hypoxic conditions (2% O_2 for 24 hours) at 37^{o}C. 24 hours post-infection, mitochondrial fractions were isolated (see Chapter 2- Materials and Methods, Section 2.7.2). Fractions were pooled from four groups, and were then lysed and subjected to SDS-PAGE. After in-gel digestion, the resultant tryptic peptides from each experiment were separated and analysed using a nano-liquid chromatography-tandem mass spectrometry (nano LC-MS/MS) for identification. Data analysis was performed by applying various criteria to ensure certainty in the assignment of protein identifications. A detailed description of the methods is provided in Chapter2- Section 2.6.2., Materials and Methods.

To identify the potential mechanisms affecting mitochondrial function, samples were subjected to proteomic analysis. MS data were evaluated on the basis of the intensity of peptide ions with coincident LC retention time and m/z values. Peptides were identified by exporting the MS/MS output files from the matched analysis into the Turbo SEQUEST search engine (BioWorks Browser 3.3, Thermo Electron Corporation) and interrogating them against the NCBI human RefSeq database release 51. The search parameters were as follows: peptide tolerance was set to 2 atomic mass units, MS/MS tolerance was set at 1 atomic mass unit, charge states allowed is from +1 to +3, and up to two missed cleavages were allowed. Changes were set to allow for the detection of S-carbamidomethylated cysteine (+57 Da). Each MS2 spectrum was matched to only a single peptide with the highest scoring SEQUEST peptide hit. Cross-correlating (XCorr) MS data, with values >1.5, >2.0 and >2.5 for singly, doubly and triply charged ions respectively were used to select peptides of high quality and reduce the possibility of including redundant peptides in

subsequent data analysis. The differentially expressed peptides were detected with high confidence in each group, and were compared and subjected to pathway analysis using Ingenuity Pathway Analysis (IPA; Ingenuity Systems, USA), and Search Tools for the Retrieval of Interacting Gene (STRING, version 11.0) to identify enriched signalling pathways or networks.

IPA is a powerful tool used to model, analyse and understand complex biological systems, and is especially useful in revealing differentially regulated signalling networks and biological processes (Nagaprashantha et al., 2013). IPA analysis workflow was performed on the differentially expressed proteins using the default settings. The Protein-to-protein interactions were constructed using the online STRING database (https://string-db.org) (Falquet et al., 2013). STRING analysis was based on the evidential mode, and the parameters were applied were species (homo sapiens) and confidence (medium confidence (0.400)).

5.4 Results

5.4.1 Proteomic data analysis

A total of 483 proteins were identified by IPA analysis. Proteins detected with high quality peptides were classified as follows: group **(A)** included proteins found in CLIC1-overexpressing HPAECs only, group **(B)** included common proteins found in CLIC1-overexpressing HPAECs and hypoxic-control cells, group **(C)** included proteins found in CLIC4-overexpressing cells only, group **(D)** included common proteins found in CLIC4-overexpressing cells and hypoxic-control HPAECs, group **(E)** included proteins found in both CLIC1- and CLIC4-overexpressing HPAECs, and group **(F)** included proteins found in CLIC1- and CLIC4-overexpressing cells and hypoxic-control HPAECs, and **(G)** included proteins found in hypoxic-control HPAECs only (Figure 5.2). Groups **E** and **F** are shown in Table 5.1, and lists of proteins in other groups (**A**, **B**, **C**, **D**, and **G**) are provided in Supplementary Table S.1. In silico protein-to-protein interaction for the detected proteins group (**F**: proteins found in CLIC1-, CLIC4-overexpressing cells and hypoxic-control HPAECs) were also visualised using STRING analysis to obtain an interactive cluster. STRING analysis revealed links between CLIC-regulated proteins and pathway involved in PH pathogenesis, including inflammatory response to antigenic stimulus, endothelial cell migration, endothelial cell development, tissue remodelling, mitochondria transport, actin filament capping and metabolic and other biological processes (Table 5.2).

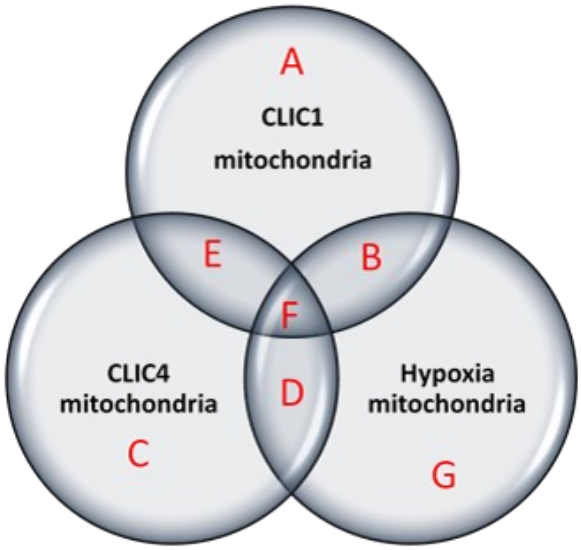


Figure 5.2: IPA group classification of CLIC1, CLIC4, and Hypoxic-control HPAECs.

Table 5.1: Differentially expressed proteins in groups E and F. Proteins found in group E (CLIC1- and CLIC4-overexpressing HPAECs), and group F (CLIC1- and CLIC4-overexpressing HPAECs, and hypoxic cells).

Proteins found in both CLIC1 and CLIC4 overexpression group [E]
calcium-binding mitochondrial carrier protein Aralar2 isoform 1
endothelin-converting enzyme 1 isoform 3
ephrin type-A receptor 2 isoform 2
grpE protein homolog 1, mitochondrial precursor
intercellular adhesion molecule 1 precursor
intercellular adhesion molecule 2 precursor
lactotransferrin isoform 2
lysosome-associated membrane glycoprotein 1 precursor
microtubule-associated protein 1B isoform 2
microtubule-associated protein 4 isoform 4
peroxiredoxin-1
peroxiredoxin-4 precursor
peroxiredoxin-5, mitochondrial isoform d precursor

peroxiredoxin-5, mitochondrial isoform S
plasminogen activator inhibitor 1 RNA-binding protein isoform 1
plexin-D1 precursor
protein LYRIC
ras-related C3 botulinum toxin substrate 2
Rho-related GTP-binding protein RhoC precursor
Rho-related GTP-binding protein RhoG precursor
Talin-1
Transferrin receptor protein 1 isoform 1
Proteins found in CLIC1, CLIC4 & Hypoxic-control group [F]
Aminopeptidase N precursor
Chloride intracellular channel protein 1
Clathrin heavy chain 1 isoform 2
Dysferlin isoform 2
Extended synaptotagmin-1 isoform 1
Fermitin family homolog 3 short form
Fibrous sheath-interacting protein 2
High mobility group protein B1
High mobility group protein HMG-I/HMG-Y isoform a
High mobility group protein HMG-I/HMG-Y isoform b
Histone H1.2
Hypoxia up-regulated protein 1 precursor
Integrin alpha-2 precursor
Kinectin isoform a
Leucine-rich PPR motif-containing protein, mitochondrial precursor
Multimerin-1 precursor
Nitric oxide synthase, endothelial isoform 1
Nodal modulator 2 isoform 1 precursor
Ribosome-binding protein 1

Spectrin alpha chain, Non-erythrocytic 1 isoform 1
Spectrin beta chain, Non-erythrocytic 1 isoform 1
Ubiquitin-60S ribosomal protein L40 isoform 1 precursor
Dynamin-related protein-1 (DRP1)
Mitochondrial fission factor (MFF)
Mitofusin-1 (MFN1)
Mitofusin-2 (MFN2)
Optic atrophy protein-1 (OPA1)
Parkin
PINK1

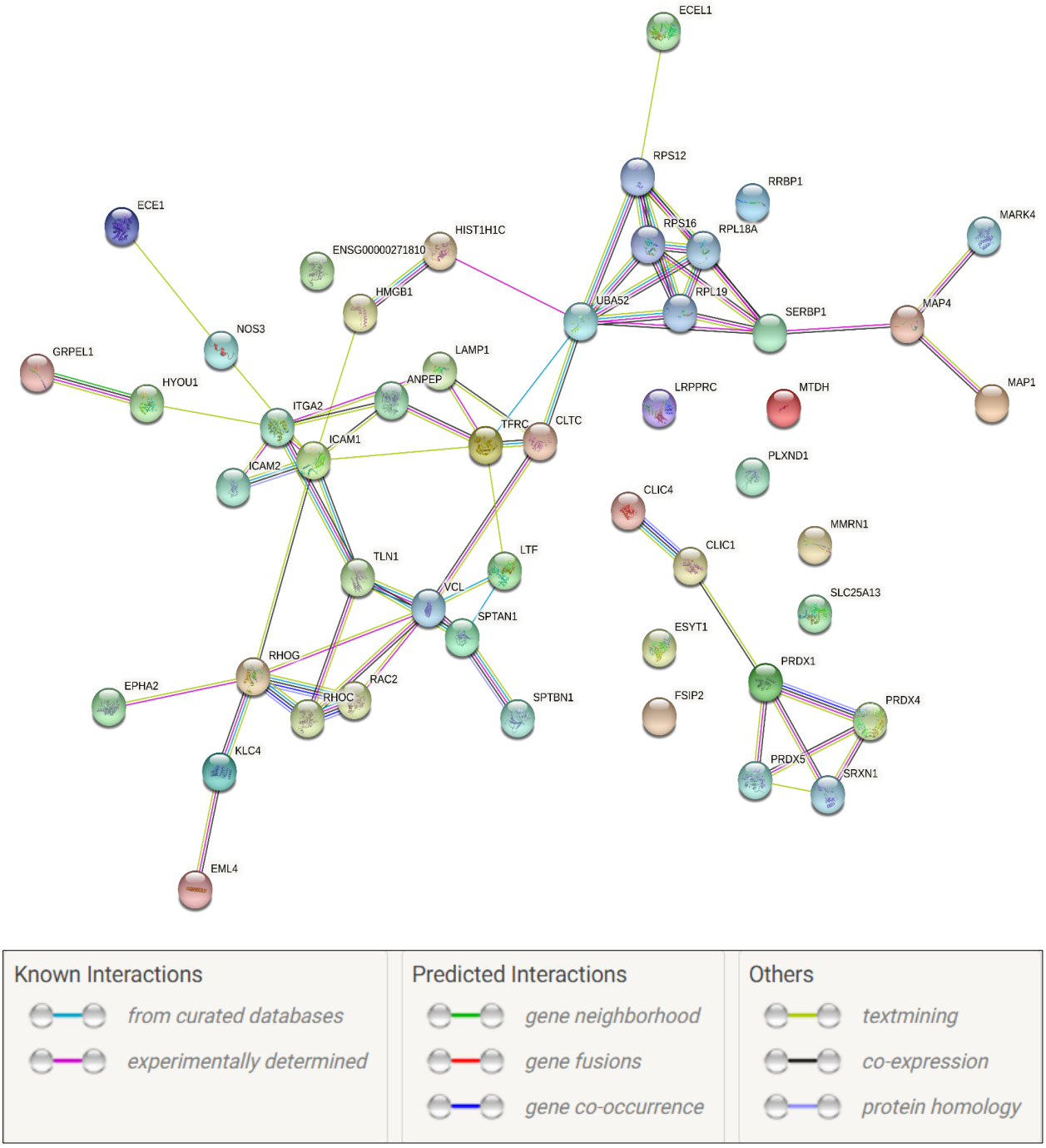


Figure 5.3: Visualization of protein-to-protein interactions of differentially expressed proteins of group F CLIC1, CLIC4, and Hypoxia control cells using STRING analysis. Number of nodes: 49; number of edges: 68, expected number of edges: 40, PPI enrichment p-value: 3.46e-05. Coloured lines between the proteins indicate the various types of interactions evidenced.

Table 5.2: List of the most significant pathways associated with pathology of PAH. Biological processes, gene names, protein's full name, protein's location, protein's function, and presence in hypoxic conditions as indicated. Data was generated using STRING.

Gene	Protein name	Location	Function	Hypoxia
Regulation of systemic arterial blood pressure by endothelin				
1- *ECE1*	Endothelin-converting enzyme 1	Cell membrane, nucleus	• Converts big endothelin-1 to endothelin-1; Belongs to the peptidase M13 family.	**No**
2- *NOS3*	Nitric oxide synthase, endothelial	Cell membrane, cytoskeleton, Golgi apparatus	• Produces nitric oxide (NO) which is implicated in vascular smooth muscle relaxation through a cGMP-mediated signal transduction pathway. • NO mediates vascular endothelial growth factor (VEGF)-induced angiogenesis in coronary vessels and promotes blood clotting through the activation of platelets.	**Yes**
Removal of superoxide radicals				
1- *PRDX1*	Peroxiredoxin-1	Cytoplasm	• Thiol-specific peroxidase that catalyzes the reduction of hydrogen peroxide and organic hydroperoxides to water and alcohols, respectively. • Plays a role in cell protection against oxidative stress by detoxifying peroxides and as sensor of hydrogen peroxide-mediated signalling events. • Might participate in the signalling cascades of growth factors and tumor necrosis factor-alpha by regulating the intracellular concentrations of H_2O_2. • Reduces an intramolecular disulfide bond in GDPD5 that gates the ability to GDPD5 to drive postmitotic motor neuron differentiation.	**No**
2- *NOS3*	Nitric oxide synthase, endothelial	Cell membrane, cytoskeleton, Golgi apparatus	Please see function in **Regulation of systemic arterial blood pressure by endothelin.**	**Yes**

Mitochondrial transport along microtubules				
1- *MAP1B*	Microtubule-associated protein 1B	Cytoskeleton	• Facilitates tyrosination of alpha-tubulin in neuronal microtubules (by similarity). Phosphorylated MAP1B may play a role in the cytoskeletal changes that accompany neurite extension. • Possibly MAP1B binds to at least two tubulin subunits in the polymer, and this bridging of subunits might be involved in nucleating microtubule polymerization and in stabilizing microtubules. • Acts as a positive cofactor in DAPK1-mediated autophagic vesicle formation and membrane blebbing; Protein phosphatase 1 regulatory subunits.	**No**
2- *LRPPRC*	Leucine-rich PPR motif-containing protein, mitochondrial	Mitochondria, nucleoplasm, nucleus inner membrane, nucleus outer membrane	• May play a role in RNA metabolism in both nuclei and mitochondria. In the nucleus binds to HNRPA1-associated poly(A) mRNAs and is part of nmRNP complexes at late stages of mRNA maturation which are possibly associated with nuclear mRNA export. • May bind mature mRNA in the nucleus outer membrane. In mitochondria binds to poly(A) mRNA. • Plays a role in translation or stability of mitochondrially encoded cytochrome c oxidase (COX) subunits. • May be involved in transcription regulation. Cooperates with PPARGC1A to regulate certain mitochondrially encoded genes and gluconeogenic genes and may regulate docking of PPARGC1A to transcription factors. Seems to be involved in the transcription regulation of the multidrug-related genes MDR1 and MVP.	**Yes**

Inflammatory response to antigenic stimulus				
1- *ICAM1*	Intercellular adhesion molecule 1	Cell membrane	• ICAM proteins are ligands for the leukocyte adhesion protein LFA-1 (integrin alpha-L/beta-2). During leukocyte *trans*- endothelial migration. • ICAM1 engagement promotes the assembly of endothelial apical cups through ARHGEF26/SGEF and RHOG activation; CD molecules.	**No**
2- *HMGB1*	High mobility group protein B1	Cell membrane, nucleus, endosome	• Multifunctional redox sensitive protein with various roles in different cellular compartments. • Proposed to be involved in mitochondrial quality control and autophagy in a transcription-dependent fashion implicating HSPB1. • May be involved in platelet activation.	**Yes**
Lipopolysaccharide-mediated signalling pathway				
1- *MTDH*	Protein LYRIC	Endoplasmic reticulum membrane, nucleolus	• Downregulates SLC1A2/EAAT2 promoter activity when expressed ectopically. • Activates the nuclear factor kappa-B (NF- kappa-B) transcription factor. • Promotes anchorage-independent growth of immortalized melanocytes and astrocytes which is a key component in tumor cell expansion. • Promotes lung metastasis and also has an effect on bone and brain metastasis, possibly by enhancing the seeding of tumor cells to the target organ endothelium.	**No**
2- *NOS3*	Nitric oxide synthase, endothelial	Cell membrane, cytoskeleton, Golgi apparatus	Please see function in **Regulation of systemic arterial blood pressure by endothelin.**	**Yes**

Actin filament capping				
3- *SPTBN1*	Spectrin beta chain, Non-erythrocytic 1	Cytoskeleton	• Fodrin, which seems to be involved in secretion, interacts with calmodulin in a calcium-dependent manner and is thus candidate for the calcium-dependent movement of the cytoskeleton at the membrane.	**Yes**
Endothelial cell migration				
1- *PLXND1*	Plexin-D1	Cell membrane	• Cell surface receptor for SEMA4A and for class 3 semaphorins, such as SEMA3A, SEMA3C and SEMA3E. • Plays an important role in cell-cell signalling, and in regulating the migration of a wide spectrum of cell types. • Regulates the migration of thymocytes in the medulla. Regulates endothelial cell migration. • Plays an important role in ensuring the specificity of synapse formation. • Required for Normal development of the heart and vasculature (by similarity). • Mediates anti-angiogenic signalling in response to SEMA3E; Belongs to the plexin family.	**No**
2- *NOS3*	Nitric oxide synthase, endothelial	Cell membrane, cytoskeleton, Golgi apparatus	Please see function in **Regulation of systemic arterial blood pressure by endothelin.**	**Yes**
3- *HMGB1*	High mobility group protein B1	Cell membrane, Nucleus, Endosome	Please see function in **Inflammatory response to antigenic stimulus.**	**No**

Endothelial cell development				
1- *Clic4*	Intercellular chloride channel protein 4	Mitochondria, nucleus matrix, cell membrane, centrosome	• Can insert into membranes and form poorly selective ion channels that may also transport chloride ions. • Channel activity depends on the pH. Membrane insertion seems to be redox-regulated and may occur only under oxydizing conditions. • Promotes cell- surface expression of HRH3. Has alternate cellular functions like a potential role in angiogenesis or in maintaining apical- basolateral membrane polarity during mitosis and cytokinesis. • Could also promote endothelial cell proliferation and regulate endothelial morphogenesis (tubulogenesis).	**Yes**
2- *ICAM1*	Intercellular adhesion molecule 1	Cell membrane	Please see function in **Inflammatory response to antigenic stimulus.**	**No**
Regulation of protein localization to plasma membrane				
1- *EPHA2*	Ephrin type-A receptor 2	Cell membrane	• Binds promiscuously membrane-bound ephrin-A family ligands residing on adjacent cells, leading to contact-dependent bidirectional signalling into neighboring cells. • The signalling pathway downstream of the receptor is referred to as forward signalling while the signalling pathway downstream of the ephrin ligand is referred to as reverse signalling. Activated by the ligand ephrin-A1/EFNA1 regulates migration, integrin-mediated adhesion, proliferation and differentiation of cells. Regulates cell adhesion and differentiation through DSG1/desmoglein-1 and inhibition of the ERK1/ERK2	**No**

			(MAPK3/MAPK1, respectively) signalling pathway. • May also participate in UV radiation-induced apoptosis and have a ligand-independent stimulatory effect on chemotactic cell migration. • During development, may function in distinctive aspects of pattern formation and subsequently in development of several fetal tissues. • Involved for instance in angiogenesis, in early hindbrain development and epithelial proliferation and branching morphogenesis during mammary gland development. • Engaged by the ligand ephrin-A5/EFNA5 may regulate lens fiber cells shape and interactions and be important for lens transparency development and maintenance. • With ephrin-A2/EFNA2 may play a role in bone remodelling through regulation of osteoclastogenesis. • Osteoblastogenes.	
2- *RHOG*	Rho-related GTP-binding protein RhoG	Cell membrane	• Required for the formation of membrane ruffles during micropinocytosis. • Plays a role in cell migration and is required for the formation of cup-like structures during *trans*-endothelial migration of leukocytes. • In case of *Salmonella enterica* infection, activated by SopB and ARHGEF26/SGEF, which induces cytoskeleton rearrangements and promotes bacterial entry.	**No**

3- *SPTBN1*	Spectrin beta chain, Non-erythrocytic 1	Cytoskeleton	Please see function in **Actin filament capping.**	**No**
Tissue remodelling				
1- *RAC2*	Ras-related C3 botulinum toxin substrate 2	Cytoplasm	• Plasma membrane-associated small GTPase which cycles between an active GTP-bound and inactive GDP-bound state. • In active state binds to a variety of effector proteins to regulate cellular responses, such as secretory processes, phagocytosis of apoptotic cells and epithelial cell polarization. • Augments the production of reactive oxygen species (ROS) by NADPH oxidase.	**No**
2- *EPHA2*	Ephrin type-A receptor 2	Cell membrane	Please see function in **Regulation of protein localization to plasma membrane.**	**No**
3- *HMGB1*	High mobility group protein B1	Cell membrane, Nucleus, Endosome	Please see function in **Inflammatory response to antigenic stimulus.**	**No**
4- *NOS3*	Nitric oxide synthase, endothelial	Cell membrane, cytoskeleton, Golgi apparatus	Please see function in **Regulation of systemic arterial blood pressure by endothelin.**	**Yes**

Iron ion transport				
1- *CLTC*	Clathrin heavy chain 1	Cytoskeleton	• Two different adapter protein complexes link the clathrin lattice either to the plasma membrane or to the *trans*-Golgi network. • Acts as component of the TACC3/ch- TOG/clathrin complex proposed to contribute to stabilization of kinetochore fibers of the mitotic spindle by acting as inter- microtubule bridge. • The TACC3/ch-TOG/clathrin complex is required for the maintenance of kinetochore fiber tension. • Plays a role in early autophagosome formation.	**Yes**
2- *TFRC*	Transferrin receptor protein 1	Cell membrane	• Cellular uptake of iron occurs via receptor-mediated endocytosis of ligand-occupied transferrin receptor into specialized endosomes. • Endosomal acidification leads to iron release. The apotransferrin-receptor complex is then recycled to the cell surface with a return to neutral pH and the concomitant loss of affinity of apotransferrin for its receptor. • Transferrin receptor is necessary for development of erythrocytes and the nervous system.	**Yes**
3- *LTF*	Lactotransferrin	Nucleus	• Lactoferroxins A, B and C have opioid antagonist activity. • Lactoferroxin A shows preference for mu-receptors, while lactoferroxin B and C have somewhat higher degrees of preference for kappa-receptors than for mu-receptors; Transferrins	**No**

Reactive oxygen species metabolic process				
1- *PRDX4*	Peroxiredoxin-4	Endoplasmic reticulum	• Thiol-specific peroxidase that catalyzes the reduction of hydrogen peroxide and organic hydroperoxides to water and alcohols, respectively. • Plays a role in cell protection against oxidative stress by detoxifying peroxides and as sensor of hydrogen peroxide-mediated signalling events. • Regulates the activation of NF-kappa-B in the cytosol by a modulation of I- kappa-B-alpha phosphorylation; Peroxiredoxins.	**No**
2- *PRDX1*	Peroxiredoxin-1	Cytoplasm	• Please see function in **Endothelial cell migration.**	**No**
3- *PRDX5*	Peroxiredoxin-5, mitochondrial	Mitochondria	• Thiol-specific peroxidase that catalyzes the reduction of hydrogen peroxide and organic hydroperoxides to water and alcohols, respectively. • Plays a role in cell protection against oxidative stress by detoxifying peroxides and as sensor of hydrogen peroxide-mediated signalling events.	**No**
Regulation of blood vessel endothelial cell migration				
1- HMGB1	High mobility group protein B1	Cell membrane, nucleus, endosome	Please see function in **Inflammatory response to antigenic stimulus.**	**No**
2- NOS3	Nitric oxide synthase, endothelial	Cell membrane, cytoskeleton, Golgi apparatus	Please see function in **Regulation of systemic arterial blood pressure by endothelin.**	**Yes**
3- EPHA2	Ephrin type-A receptor 2	Cell membrane	Please see function in **Regulation of protein localization to plasma membrane.**	**No**

Regulation of angiogenesis				
1- HMGB1	High mobility group protein B1	Cell membrane, nucleus, endosome	Please see function in **Inflammatory response to antigenic stimulus.**	**No**
1- EPHA2	Ephrin type-A receptor 2	Cell membrane	Please see function in **Regulation of systemic arterial blood pressure by endothelin.**	**No**
2- NOS3	Nitric oxide synthase, endothelial	Cell membrane, cytoskeleton, Golgi apparatus	Please see function in **Regulation of systemic arterial blood pressure by endothelin.**	**Yes**
3- MTDH	Protein LYRIC	Endoplasmic reticulum membrane, Nucleus membrane	Please see function in **Lipopolysaccharide-mediated signalling pathway.**	**No**
4- PLXND1	Plexin-D1	Cell membrane	Please see function in **Endothelial ell migration.**	**No**
Angiogenesis				
1- *ANPEP*	Aminopeptidase N	Cell membrane	• Plays a role in the final digestion of peptides generated from hydrolysis of proteins by gastric and pancreatic proteases. • Also involved in the processing of various peptides including peptide hormones, such as angiotensin III and IV, neuropeptides, and chemokines. • May also be involved in the cleavage of peptides bound to major histocompatibility complex class II molecules of antigen presenting cells. • May have a role in angiogenesis and promote cholesterol crystallization. • May have a role in amino acid transport by acting as binding partner of amino acid transporter SLC6A19 and regulating its activity.	**Yes**

2- *Clic4*	Chloride intracellular channel protein 4	Mitochondria, Nucleus matrix, Cell membrane, centrosome	Please see function in **Endothelial cell development.**	**Yes**
3- *PLXND1*	Plexin-D1	Cell membrane	Please see function in **Endothelial ell migration.**	
4- *EPHA2*	Ephrin type-A receptor 2	Cell membrane	Please see function in **Regulation of systemic arterial blood pressure by endothelin.**	**No**
5- *NOS3*	Nitric oxide synthase, endothelial	Cell membrane, cytoskeleton, Golgi apparatus	Please see function in **Regulation of systemic arterial blood pressure by endothelin.**	**Yes**

5.5 Discussion

Proteomic analysis is used for identification and quantification of proteins in complex biological samples, to improve our understanding of disease mechanisms (Zhao et al., 2015). Here, qualitative proteomic profiling was carried out on mitochondria-enriched fractions from CLIC1- and CLIC4-overexpressing HPAECs.

Data presented in this chapter represent a preliminary evaluation of protein expression in different treatment groups. Mitochondria-enriched fractions are likely to contain some contaminants of mitochondria-associated cytoplasmic proteins (here, each group represented pooled samples from n=4 fractions). Mitochondrial enrichment was confirmed by western blotting (data shown in Chapter 3, Section 3.4.4).

CLIC proteins have been implicated in the regulation of several important cellular processes such as, membrane trafficking, cytoskeletal function (Berryman et al., 2004), apoptosis (Fernández-Salas et al., 2002; Suh et al., 2004), cell cycle control (Valenzuela et al., 2000), tubulogenesis (Berry et al., 2003), vascular endothelial growth factor (VEGF)-mediated angiogenesis of endothelial cells (Tung et al., 2009), mitosis and differentiation (Suh et al., 2007).

Expression levels of specific proteins vary widely within the cell proteome. Many transcription factors show low abundance and are difficult to detect (Garbis et al., 2005).

Proteomics offer a snapshot of proteome at any given time and the detection is dependent upon the relative abundance of protein in the overall proteome. In this preliminary study we were able to detect a number of mitochondrial proteins, including those that are involved in fusion and fission events (listed in Table 5.1). We also detected proteins that localise to other organelles

such as ER, and nucleus, suggesting the presence of cytoplasmic contaminants. Some fission/fusion or mitophagy proteins were below detection level.

Pathway analysis of CLIC1- and CLIC4-regulated mitochondrial and mitochondria-associated proteins revealed numerous links with PAH pathogenesis, involving endothelial development, migration, angiogenesis, cell-cycle regulation, endocytosis and exocytosis (Laudi et al., 2007; Marshall et al., 2018). The analysis also revealed links of CLIC proteins with reactive oxygen species metabolic processes, iron ion transport, mitochondrion transport along microtubules, actin filament capping, and removal of superoxide radicals (Gururaja Rao et al., 2018; Wojciak-Stothard et al., 2014). A number of other pathways associated with CLIC proteins, such as regulation of blood vessel endothelial cell migration, angiogenesis, tissue remodelling, and inflammatory response to antigenic stimulus, have been reported in other studies (Boucherat et al., 2017; Jeffery & Wanstall, 2001). These data reaffirm the importance of CLIC signalling in the pathogenesis of PAH.

CLIC proteins may affect mitochondrial function directly, by their interaction with mitochondrial membrane proteins. Identification of binding partners of CLIC proteins will require further investigation. CLIC proteins can also act indirectly, by increasing mitochondrial redox potential. Purified soluble CLIC1 and CLIC4 show glutaredoxin (glutathione-dependent oxidoreductase) activity in *ex-vivo* assays (Al Khamici et al., 2015). Another indirect way involves HIF-induced mitochondrial fission and inhibition of oxidative phosphorylation (Ong et al., 2015). Our group have shown that CLIC4 activates HIF in cultured cells and animal models of PAH (Wojciak-Stothard et al., 2014). CLIC4 also associates with a number of cytoskeletal and cytoskeleton-associated proteins that may affect mitochondrial transport and fission, i.e. dynein, tubulin and Arp2/3 complex (Tavasoli et al., 2016).

CHAPTER 6 RESULTS:

Reversal of CLIC effects by mitofusin-2

CHAPTER 6 RESULTS: Reversal of CLIC effects by mitofusin-2

PAH vascular cells display reduced mitochondrial content, increased mitochondrial fragmentation, membrane potential, glycolysis, and reduced oxidative phosphorylation (Ranchoux et al., 2016; Russomanno et al., 2020; Tang et al., 2014). Our data show that similar effects are induced by the overexpression of CLIC1 and CLIC4.

The overall aim of the studies presented in this chapter was to investigate whether the overexpression of MFN2 can reverse CLIC-induced mitochondrial dysfunction, including changes in mitochondrial fragmentation, mitochondrial membrane potential ($\Delta\Psi m$), mitochondrial reactive oxygen species (mtROS), and mitochondrial respiration.

6.1 Introduction

Mitochondria are remarkably dynamic organelles, and mitochondrial dynamics – which involves mitochondrial fission, fusion, movement and mitophagy – plays an essential role in mitochondrial function. In addition to the regulation of mitochondrial fusion, MNF2 plays a crucial role in mitochondrial communication with the endoplasmic reticulum (ER), which is essential for calcium (Ca^{2+}) homeostasis, lipid biosynthesis and thus for the regulation of mitochondrial metabolism and apoptosis (de Brito & Scorrano, 2009). The knockdown of MFN2 in endothelial cells causes mitochondrial fragmentation, diminished mitochondrial membrane potential and apoptosis in growth factor-reduced media (Lugus et al., 2011).

Endothelial and smooth muscle cells from the remodelled vasculature in PAH share multiple pathophysiological and molecular similarities with cancer cells, including increased glycolysis, apoptosis resistance, increased proliferation and mitochondrial fragmentation, all of which are associated with the upregulation of fission protein DRP-1 and the downregulation of MFN2 (de Brito & Scorrano, 2009) (Ryan et al., 2013).

6.2 Experimental aims

The studies described in this chapter aimed at:

1. Optimising the conditions for MFN2 gene expression in control and CLIC–overexpressing HPAECs.
2. Determining the effect of MFN2 overexpression on mitochondrial dynamics (fusion and fission) in control and CLIC-overexpressing HPAECs.
3. Exploring the role of MFN2 as a mediator of CLIC1/CLIC4-induced changes in mitochondrial membrane potential and ROS production.
4. Investigating the effect of MFN2 overexpression on energy metabolism in control and CLIC-overexpressing HPAECs.

6.3 Experimental design

Detailed methods on specific methods and protocols for each investigation in this chapter are described in Chapter 2, and an overview of the experimental outline is presented in Figure 6.1.

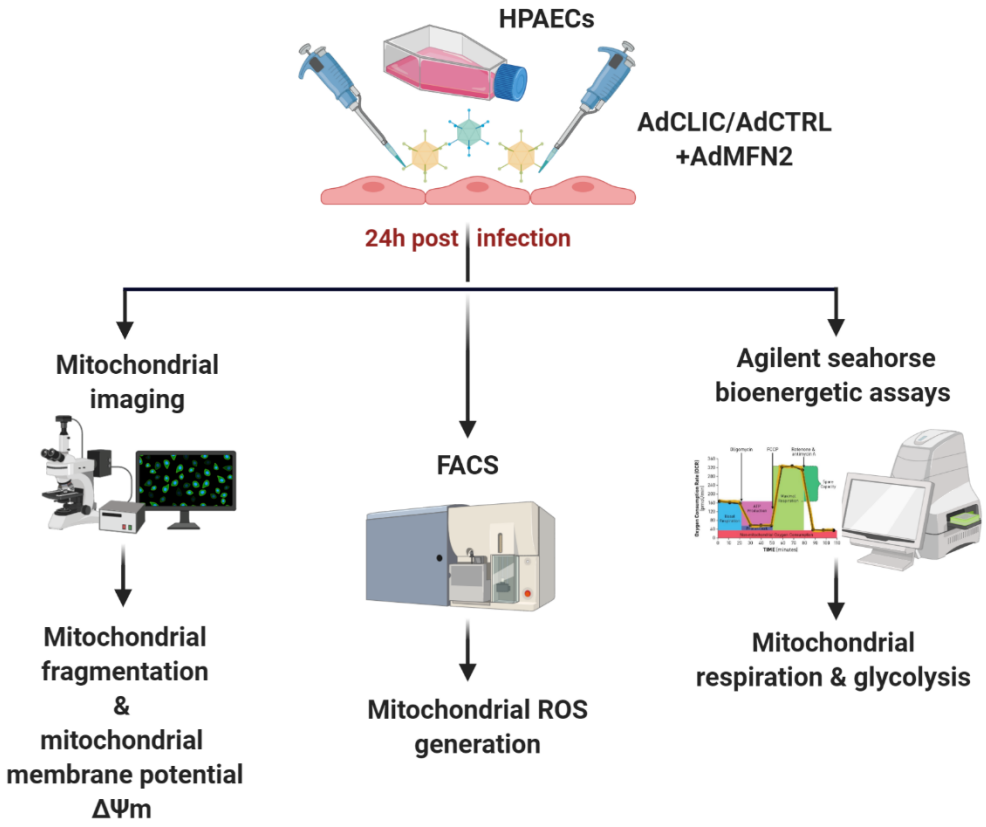


Figure 6.1: Experimental outline for Chapter 6. MFN2 expression was manipulated by the adenoviral overexpression of human MFN2 protein in control HPAECs and HPAECs overexpressing AdCLIC1 or AdCLIC4. Changes in mitochondrial fragmentation, mitochondrial membrane potential, ROS generation, glycolysis and mitochondrial respiration in CLIC-overexpressing HPAECs were studied using fluorescent imaging, FACS and Seahorse bioenergetics assay, as appropriate. Illustration created by the author using BioRender.com.

6.3.1 Manipulation of MFN2 gene expression in HPAECs

Overexpression of CLIC1, CLIC4, and MFN2 was induced by adenoviral gene transfer, as described in Chapter 3, Section 3.4.1.

The titre of the AdMFN2 stock was estimated at ~2 x 10^{11} pfu (plaque forming units) per mL. 70-80% confluent HPAECs growing in 24-well plates were infected with adenoviruses at the multiplicity of infection (MOI 1:100). The expression of CLIC1, CLIC4, and MFN2 proteins was confirmed by western blotting and immunofluorescence 24 hours post-infection.

6.3.2 Western blotting

24 hours post-infection, control and adenovirus-treated HPAECs were lysed using a modified RIPA buffer supplemented with protease/phosphatase inhibitors. The protein concentrations of individual samples were measured using a Pierce™ BCA Protein Assay Kit following standard protocols. Samples were resolved with SDS PAGE (10µg – 20µg protein/lane) and analysed using western blotting. The membranes were blocked using BSA (5%) for an hour, then probed with goat polyclonal anti-CLIC1, CLIC4, and MFN2 (1:1000 dilution) for a minimum of 1-2 hours, before being washed in TBST and probed with secondary mouse anti-goat IgG HRP-linked antibodies (1:3000) for 1 hour. Bands were visualized using a Luminata Crescendo Western HRP Substrate in ChemiDoc™ Imager. ImageJ software was used to perform a densitometric quantification of western blot bands. Further methodological details can be found in Chapter2, Materials and Methods, Section 2.8.1.

6.3.3 Immunostaining and mitochondrial fragmentation analysis

Control, CLIC-overexpressing and MFN2-overexpressing endothelial cells were cultured in 8-well chambered coverslips, washed with PBS and fixed. HPAECs were then permeabilised, blocked

and incubated overnight with the primary antibodies. The cells were subsequently incubated with fluorescently-labelled secondary antibodies, then mounted and examined under the confocal microscope (Zeiss LSM780). The acquired images were analysed using ImageJ software and NIP2 image software to determine the number of mitochondria and the total mitochondrial area. Images were filtered by median, thresholded, and binarized to identify individual mitochondrial segments (with a 500 pixel =2 μm^2 cut-off size). The ratio of the total number of mitochondria to total mitochondrial area in each cell provided the mitochondrial fragmentation count (MFC).

6.3.4 Measurement of mitochondrial membrane potential (ΔΨm)

HPAECs cultured on Thermanox® Plastic Coverslips (13 mm) were infected with adenoviruses (AdCLIC1, AdCLIC4, and AdMFN2) to induce CLIC and MFN2 overexpression. 24 hours post-infection, 100 nM of Tetramethylrhodamine, methyl ester (TMRM) was added to the culture medium and the cells were incubated for 30 minutes at 37˚C. The cells were then washed twice with PBS and new media was added to the cells. Live imaging was performed using a Zeiss confocal microscope (Zeiss LSM780) and the acquired images were then analysed using ImageJ.

6.3.5 Measurement of mitochondrial reactive oxygen species (mtROS)

HPAECs infected with AdCTRL, AdCLIC1 or AdCLIC4, with or without AdMFN2, were seeded in 6-well plates. 24 hours post infection, the cells were trypsinised and pelleted by centrifugation in 5 mL Falcon round-bottom polystyrene tubes. The medium was carefully aspirated, and the pellet was re-suspended in 1 mL PBS then subjected to a second centrifugation. 1µM MitoSOX Red was added to HPAECs at 37°C, 5% (v/v) CO_2 for 30 minutes, protected from light. MitoSOX Red accumulates in mitochondria and becomes fluorescent upon oxidation by $^{\bullet}O_2^-$. MtROS

production was measured by flow cytometry at an excitation of 510 nm and an emission of 580 nm using a BD FACS Canto Flow Cytometer, where 10,000 events were recorded for each sample with a selected FL2 channel. For more details see Chapter 2- Materials and Methods, Section 2.6.2.

6.3.6 Cellular bioenergetics assay

HPAECs were seeded at a density of $2x10^4$/well in Seahorse 96-well plates designed for use with the Seahorse XFp instrument. The following day the cells were infected with AdCLIC1, AdCLIC4, and AdMFN2 and incubated for 24 hours. Cells were then equilibrated with an XF assay medium containing 2mM L-Glutamine, 1mM pyruvate, and 10 mM glucose for the Mito Stress Test. 2mM L-Glutamine was the only supplement used in the Glycolysis Stress Test, according to the manufacture's guidelines. Baseline rates of oxygen consumption were measured in adherent HPAECs. Prior to the Mitostress assay, all wells were serially injected with 1.5 µM oligomycin, 2 µM carbonyl cyanide 4-(trifluoromethoxy) phenylhydrazone (FCCP), and 0.5 µM rotenone/antimycin A (Rot/Ant). Extracellular acidification rates (ECAR) were measured in response to the serial injections of 1.5 µM glucose, 15 µM oligomycin and 65 µM 2-Deoxy-glucose (2-DG). Afterwards, the total protein in each well was measured using the BCA protein assay kit and OCR and ECAR were normalized to the protein levels before the data were analysed. For further details see Chapter 2- Materials and Methods, Section 2.6.3.

6.4 Results

6.4.1 MFN2 expression in endothelial cells

Results in previous chapters have shown that the pathological overexpression of CLIC1 and CLIC4 induce roughly a 3-fold decrease in mitochondrial MFN2 expression. Therefore, the optimal MOI of AdMFN2 (1:200) was set to achieve a compensatory increase in the expression of MFN2 in CLIC1- and CLIC4-overexpressing HPAECs (Figures 6.2, 6.3, and 6.4).

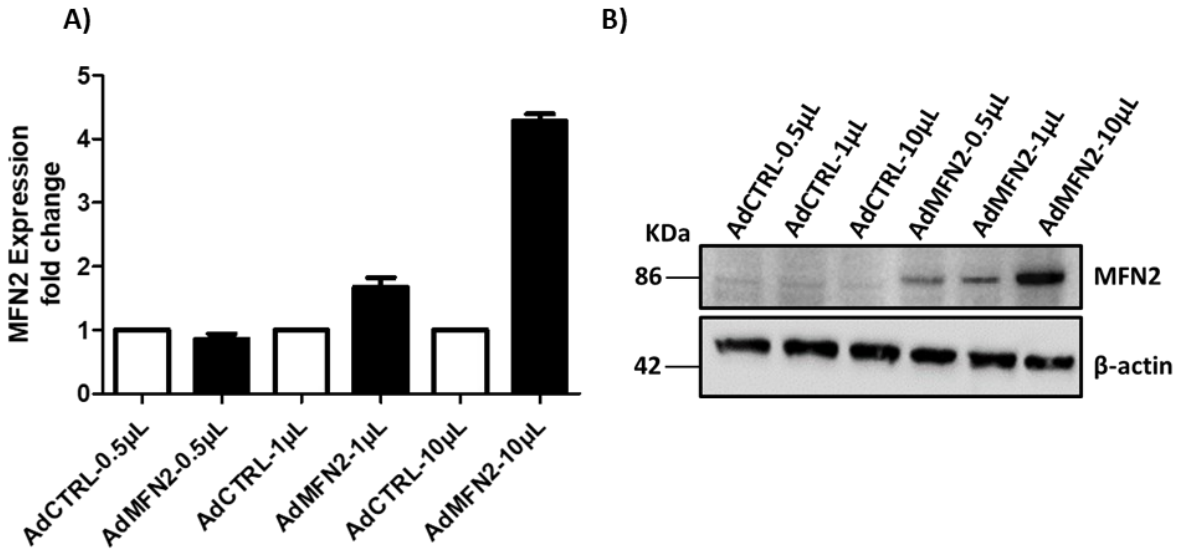


Figure 6.2: Optimization of MFN2 overexpression in HPAECs. (A) The bar-graph indicates fold-change in MFN2 protein levels in HPAECs grown in 6-well dishes and infected with different dilutions of AdMFN2 or AdCTRL (Adenoviral control) stocks 24 hours post-infection. Under these experimental conditions, 0.5µL=MOI 1: 20, 1µL=MOI 1: 40, and 10µL=MOI 1: 400. **(B)** Representative western blots correspond to (A). Expression levels were normalised to β-actin. N=3

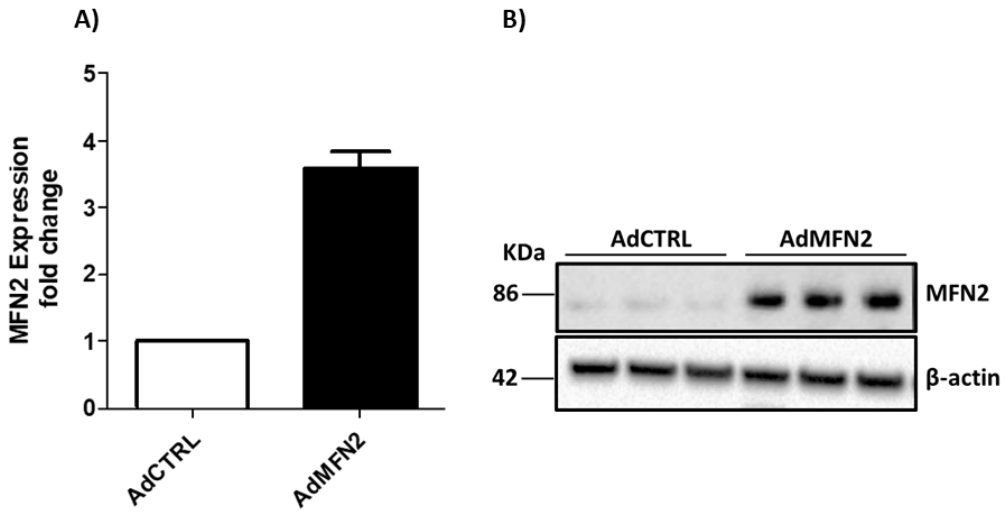


Figure 6.3: MFN2 overexpression in HPAECs. (A) The bar-graph shows a ~3-fold increase in MFN2 protein expression levels in HPAECs infected with 5µL (MOI 1:200) of AdMFN2, compared with cells infected with AdCTRL (MOI 1:200) 24 hours post-infection. **(B)** Representative western blots correspond to **(A)**. Expression levels were normalised to β-actin. N=3

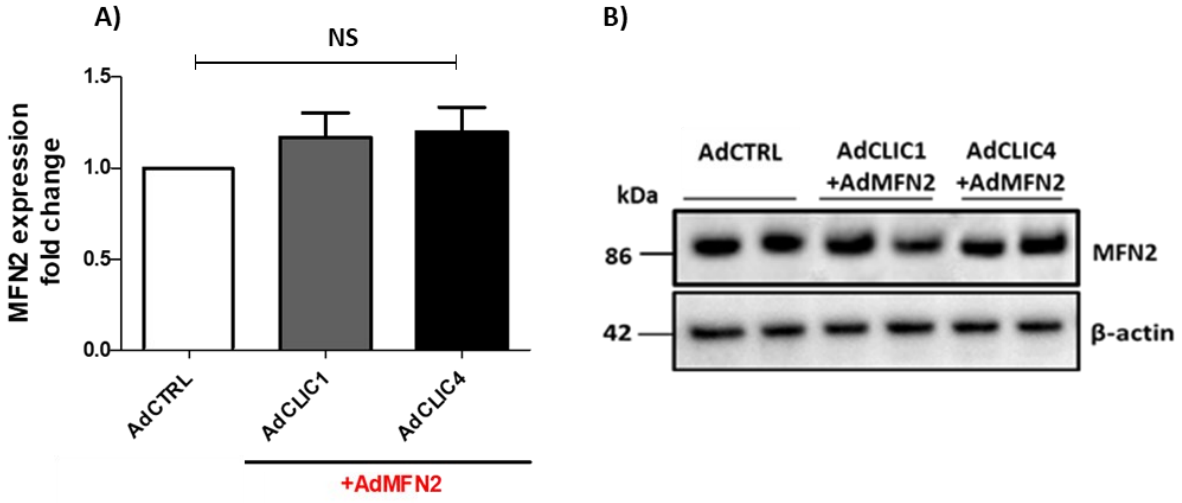


Figure 6.4: MFN2 overexpression compensates loss of MFN2 in CLIC-overexpressing HPAECs. (A) The bar-graph shows fold change in MFN2 protein expression levels in CLIC-overexpressing HPAECs infected with AdMFN2, with or without AdCLIC1, AdCLIC4 or AdCTRL (Adenoviral control) 24 hours post-infection to obtain a ~3-fold increase of MFN2, as indicated. **(B)** Representative western blots correspond to **(A)**. Expression levels were normalised to β-actin, NS (non-significant). One-way ANOVA was used with Tukey's multiple comparison test. Data are presented as mean ± SEM. N=3

6.4.2 The effect of MFN2 on CLIC-induced changes in mitochondrial fragmentation in HPAECs

In order to investigate the effects of MFN2 protein overexpression on mitochondrial fragmentation in CLIC-overexpressing endothelial cells, mitochondria were fluorescently-labelled and visualised using confocal microscopy, and mitochondrial fragmentation count (MFC) was then evaluated.

Overexpression of MFN2 prevented any CLIC1- and CLIC4-induced increase in mitochondrial fragmentation in HPAECs (Figure 6.5). A decrease in mitochondrial fragmentation was also noted in MFN2-overexpressing control cells, but the change was too small to be statistically significant (Figure 6.5). Representative fluorescent images of mitochondrial fragmentation in cells overexpressing CLIC1 or CLIC4, with and without MFN2, are shown in Figures 6.6 and 6.7.

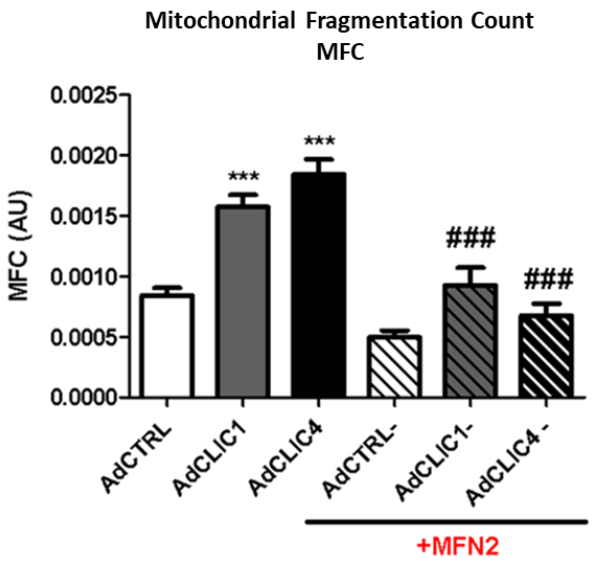


Figure 6.5: The effect of MFN2 on mitochondrial fragmentation count in CLIC-overexpressing HPAECs. MFC (arbitrary units) was measured in endothelial cells infected with AdCTRL, AdCLIC1, and AdCLIC4, with and without MFN2, using NIP2 image software. The bar-graph shows a significant decrease in MFC caused by MFN2 in CLIC1, and CLIC4-overexpressing HPAECs, compared to CLIC1- or CLIC4-overexpressing HPAECs, as appropriate. Control data (AdCTRL) were acquired in the previous series of experiments (shown in Figure 3.8 on page 115). N=20 cells/treatment were analysed in 3 separate experiments. ***P<0.0001, comparison with AdCRTL, ###P<0.0001, comparisons between AdCLIC1+MFN2 or AdCLIC4+MFN2 and corresponding AdCLIC1 or AdCLIC4 controls. One-way ANOVA was used with Tukey's multiple comparison test. Data are presented as mean ± SEM.

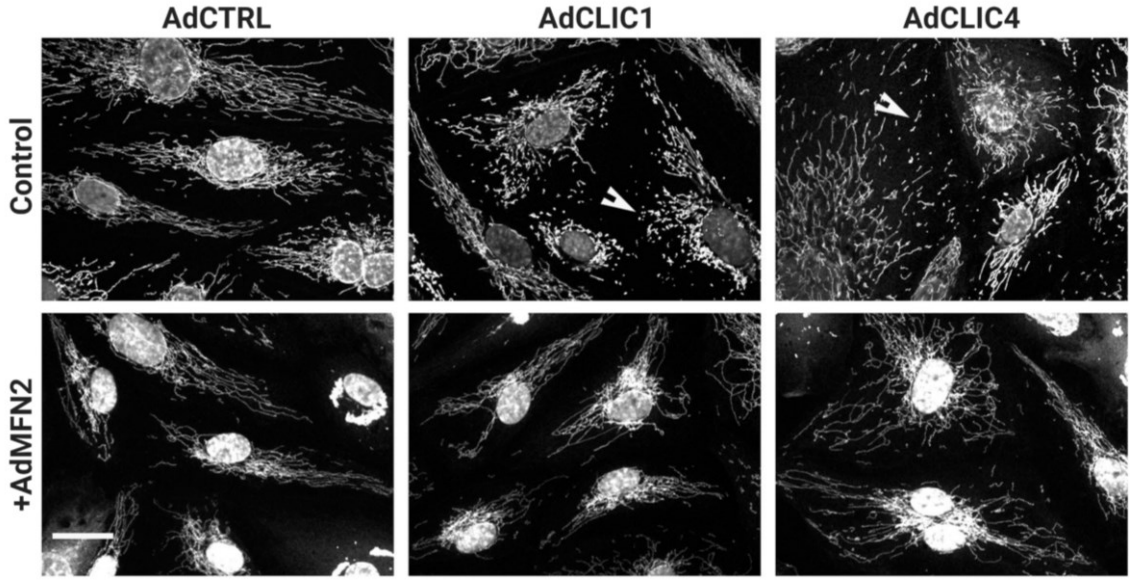


Figure 6.6: The effect of MFN2 overexpression on CLIC-induced mitochondrial fragmentation in HPAECs. Representative fluorescent confocal images of mitochondrial network in HPAECs were treated with AdCTRL, AdCLIC1 and AdCLIC4, with and without MFN2, 24 hours post-infection. AdCTRL served as controls. Arrowheads point to small, fragmented mitochondria in CLIC1-, and CLIC4-overexpressing cells. Images were obtained using Zeiss LSM 780 confocal microscope with 20x objective. Bar=10µm.

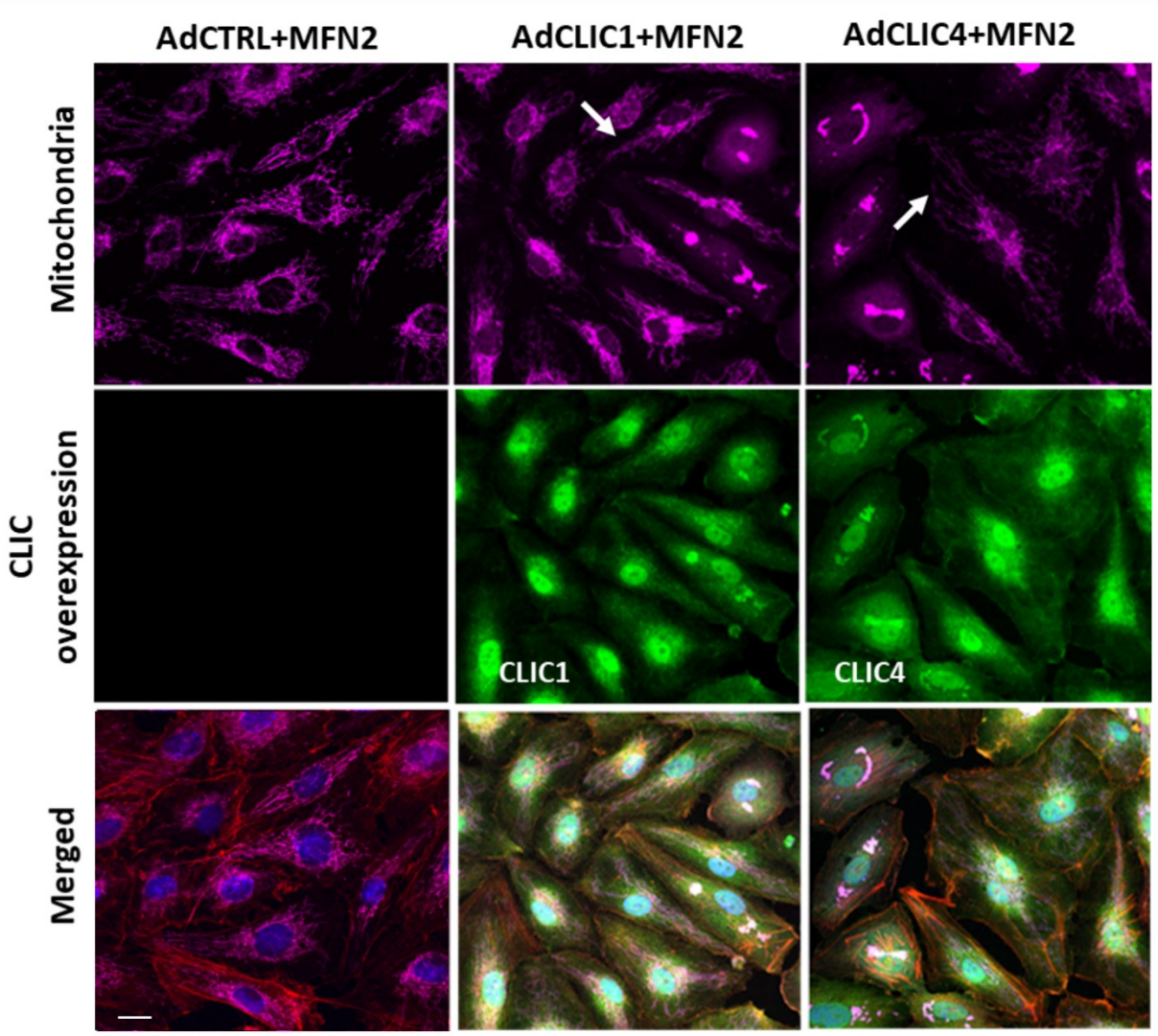


Figure 6.7: Mitochondrial network in CLIC-overexpressing HPAECs with MFN2 overexpression. Representative confocal images indicate mitochondrial network in control (AdCTRL), CLIC1, and CLIC4-overexpressing endothelial cells with MFN2 overexpression 24 hours post-infection. Mitochondria are magenta (Alexa Fluor 647), nuclei are blue (DAPI), F-actin is red (TRITC-phalloidin) and CLIC1, CLIC4 protein is green (anti-HA-tag Alexa Fluor 488). Arrowheads point to mitochondrial network in CLIC1-, and CLIC4-overexpressing cells plus MFN2 overexpression. Images were acquired using a Zeiss LSM 780 confocal microscope with 20x objective. Bar=50µm.

6.4.3 Effect of MFN2 on CLIC-induced changes in mitochondrial membrane potential

In order to investigate the effect of MFN2 on CLIC1- and CLIC4-induced changes in mitochondrial membrane potential (ΔΨm), cells were stained with fluorescent ΔΨm indicator, Tetramethylrhodamine, methyl ester (TMRM). ΔΨm was evaluated 24 hours post- infection using recombinant adenoviruses. Overexpression of MFN2 completely prevented an increase in mitochondrial ΔΨm induced by CLIC1 and CLIC4 in HPACEs (Figure 6.8 and 6.9). Base levels of ΔΨm in control cells were relatively unaffected by MFN2 overexpression (Fig. 6.8).

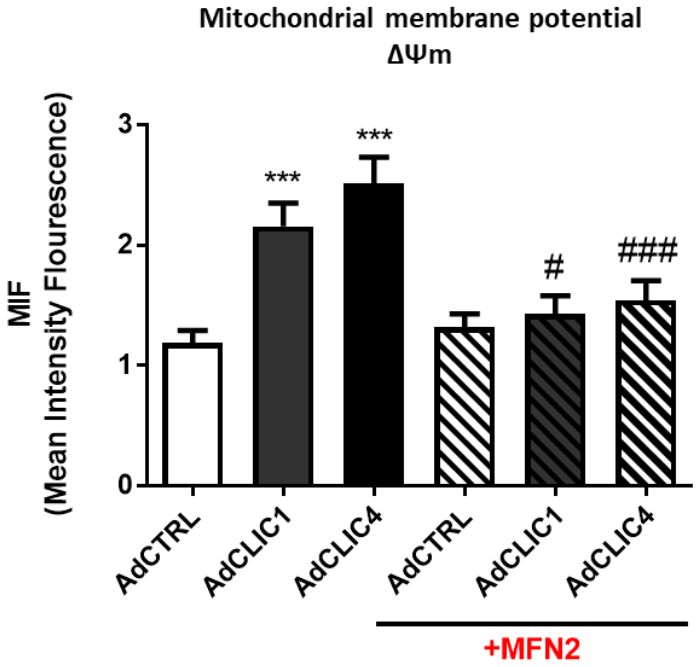


Figure 6.8: The effect of MFN2 overexpression on CLIC-induced changes in mitochondrial membrane potential. The bar-graph indicates mean mitochondrial membrane potential, assessed by the measurement of TMRM fluorescence intensity (+SEM) in HPAECs overexpressing CLIC1 and CLIC4, with or without AdMFN2, 24 hours post-infection. AdCTRL, and AdCTRL+MNF2 served as controls. ***P <0.0001, comparison with AdCRTL; #P<0.05, comparison with AdCLIC1+AdMFN2; ###P<0.0001, comparison with AdCLIC4+AdMFN2. One-way ANOVA was used, with Tukey's multiple comparison test. Data are presented as mean ± SEM of 3 experiments with 3 technical repeats.

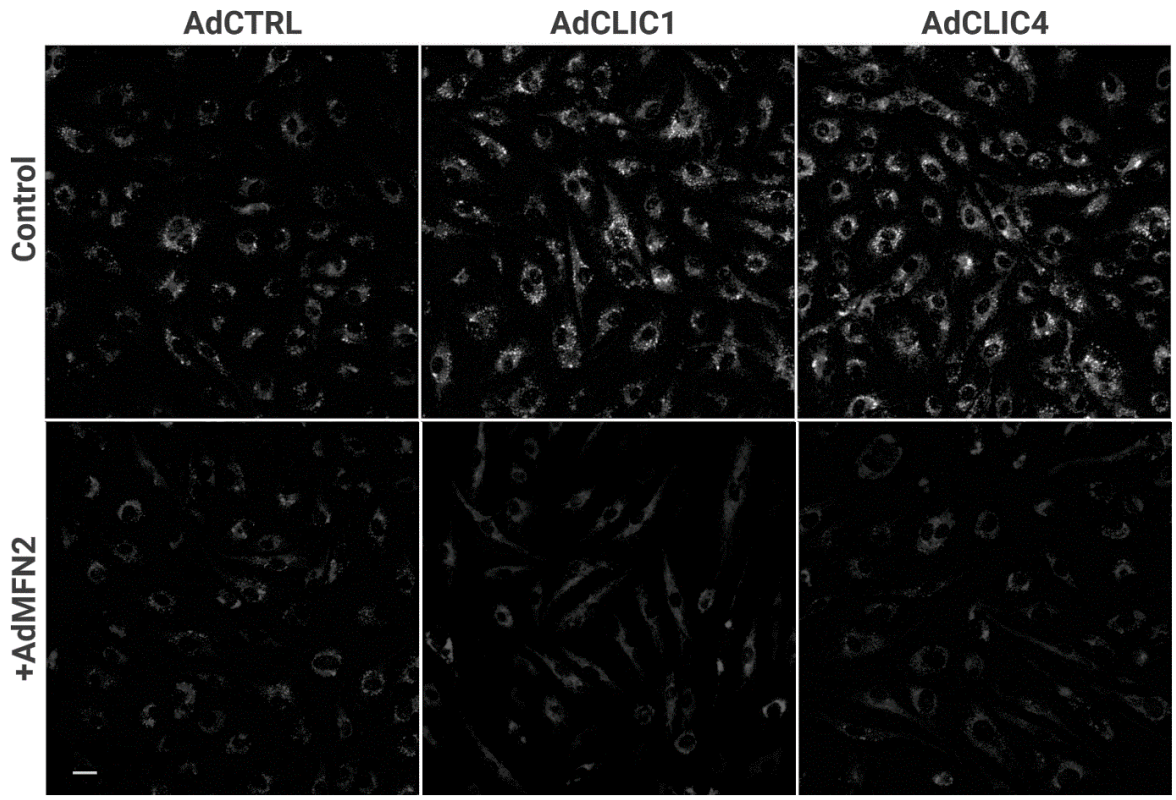


Figure 6.9: The effect of MFN2 on mitochondrial membrane potential in CLIC-overexpressing HPAECs. Representative confocal images of live control HPAECs (AdCTRL, AdCLIC1, and AdCLIC4) and HPAECs overexpressing CLIC1, CLIC4 and MFN2 24 hours post-infection, as shown. Live endothelial cells were incubated with 100nM TMRM for 30 minutes at 37°C and the cells were then imaged using confocal microscopy. Images were obtained using a Zeiss LSM 780 confocal microscope with 20x objective. Bar=10µm.

6.4.4 The effect of MFN2 on CLIC-induced changes in mitochondrial ROS production in HPAECs

To evaluate the production of mitochondrial reactive oxygen species (mtROS) in cells, MitoSOX™ Red Mitochondrial Superoxide indicator was added to live HPAECs overexpressing CLIC1 and CLIC4, with or without MFN2, and mtROS generation in different cell populations was assessed by Fluorescence-activated cell sorting (FACS).

The analysis revealed that MFN2 overexpression prevented an increase in CLIC1- and CLIC4-induced mitochondrial ROS production in HPAECs (Figure 6.10). ROS production in control cells overexpressing MFN2 was also reduced, compared with adenoviral controls, although this change was too small to be statistically significant (Figure 6.10).

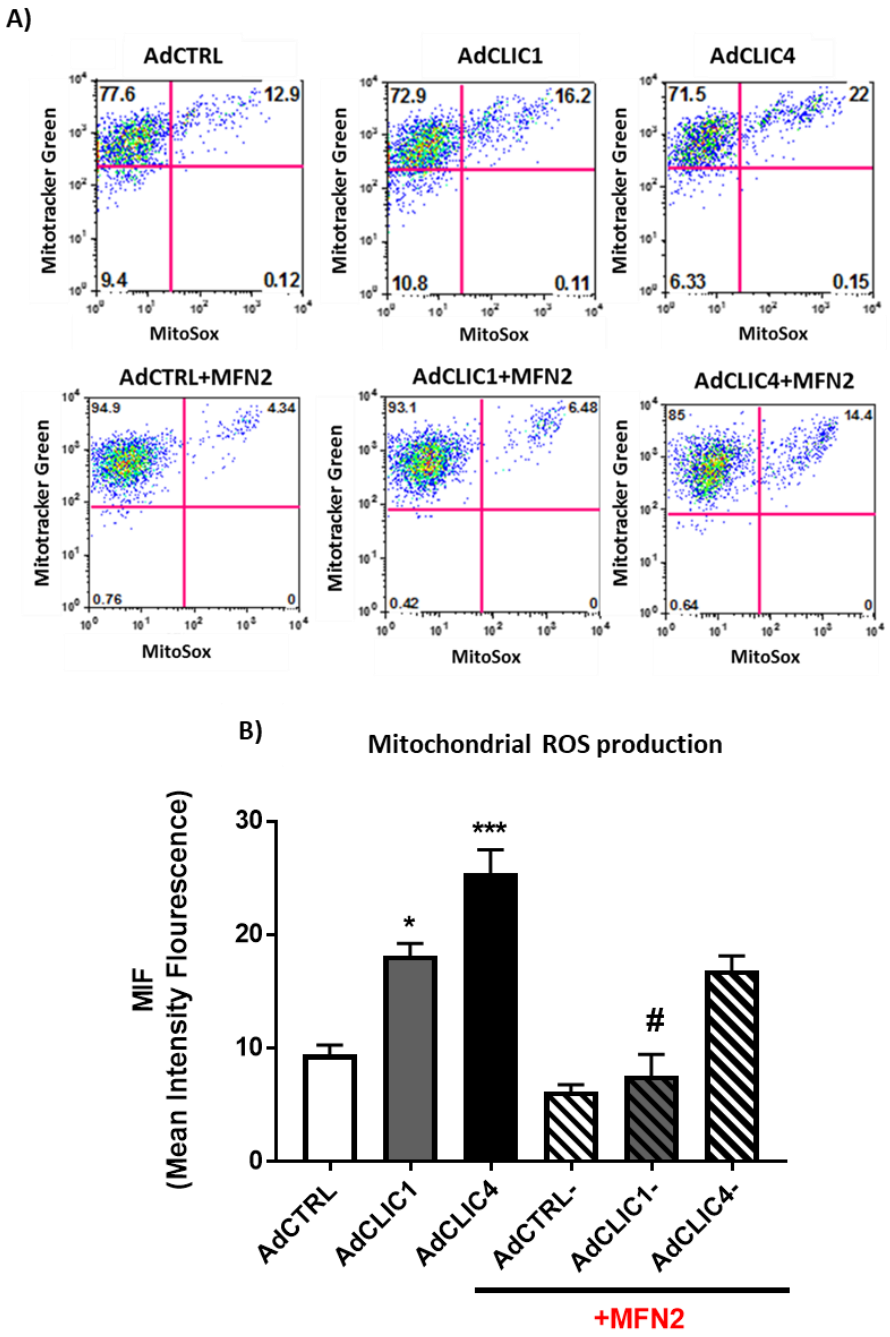


Figure 6.10: The effect of MFN2 overexpression on CLIC-induced changes in mitochondrial ROS. (A) Examples of mean fluorescent intensity histograms showing the ratio of MitoSox red (FL3-H) to Mitotracker green (FL1-H) (labelling all mitochondria), measured by Fluorescence Activated Cell Sorting (FACS). **(B)** The effect of MFN2 overexpression on CLIC1 and CLIC4-induced changes on mtROS production, measured as mean intensity of fluorescence (arbitrary units: AU) in HPAECs. AdCTRL, and AdCTRL+MNF2 served as controls. *P<0.05, ***P <0.0001, comparison with AdCRTL; #P<0.05, comparison with AdCLIC1+AdMFN2. One-way (ANOVA) was used with Tukey's multiple comparison test. Data are presented as mean ± SEM of 3 experiments with 3 technical repeats.

6.4.5 The effect of MFN2 on CLIC-induced changes in the bioenergetic profile of HPAECs

The effect of MFN2 protein on mitochondrial respiration and glycolysis in HPAECs overexpressing CLIC1 and CLIC4 was assessed using the Agilent Seahorse Mito Stress Test and the Glycolysis Stress Test. OCR was measured in response to the serial injection of respiratory modulators oligomycin, FCCP, and rotenone/antimycin (Rot/Ant). ECAR was evaluated under basal conditions, followed by the sequential injection of glycolysis modulators glucose, oligomycin, and 2-DG. A consistent protein concentration for each experiment was confirmed across all HPAECs treated in each well. OCR and ECAR data were automatically calculated using Wave software then exported to Excel to determine the effect of CLIC proteins on key mitochondrial respiration and glycolysis parameters. The results are summarized below.

Changes in OCR parameters:

- Basal respiration, which measures the energy demand of cells at baseline conditions, was markedly reduced by CLIC1 and CLIC4 overexpression (~2-fold decrease compared to controls). MFN2 induced a significant increase in basal respiration in CLIC-overexpressing cells (Figure 6.12 A).
- MFN2 overexpression significantly increased mitochondrial ATP production in CLIC-overexpressing cells (~2-3-fold increase compared with CLIC-overexpressing HPAECs) and restored normal mitochondrial ATP production to control levels (Figure 6.12 B)
- The overexpression of MFN2 restored optimal respiration in CLIC1- and CLIC4-overexpressing cells to control levels (Figure 6.12 C).
- Proton leak was markedly increased in CLIC1 and CLIC4-overexpressing HPAECs. This response was reduced to control levels by MFN2 overexpression (Figure 6.12 D)

- The overexpression of MFN2 prevented a decrease in spare respiratory capacity induced by CLIC1 and CLIC4 (~2-3-fold increase compared with CLIC-overexpressing HPAECs) (Figure 6.12 E).
- MFN2 overexpression reduced non-mitochondrial respiration in all study groups (Figure 6.12 F).

OCR data generated by the XF Mito Stress Test report generator are presented in Figures 6.11, and 6.12.

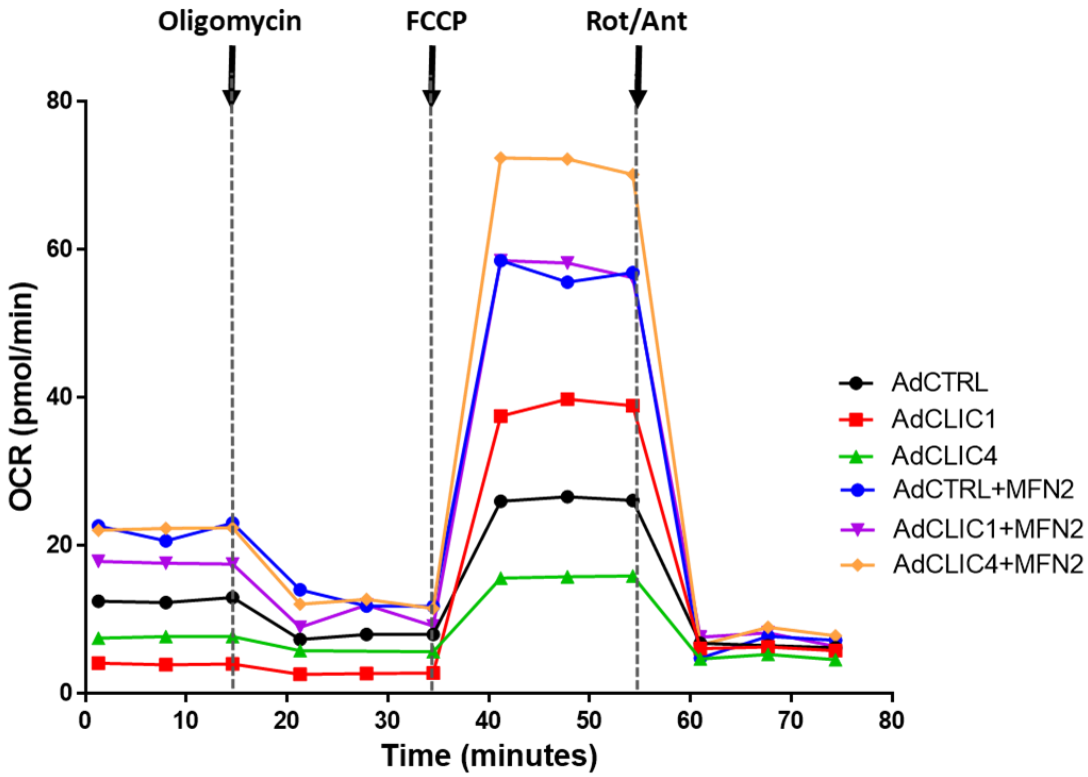


Figure 6.11: Example of Oxygen consumption rate (OCR) measurement. HPAECs were infected with either AdCTRL and/or AdCLIC1, AdCLIC4, AdMFN2, and OCR was measured following the injection of oligomycin, FCCP, and Rot/Ant at 15, 34 and 54 minutes respectively. Black circle = AdCTRL; red square = AdCLIC1; green triangle: AdCLIC4; purple triangle: AdCTRL+MFN2; orange diamond: AdCLIC4+MFN2; blue diamond: AdCLIC1+MFN2. Data are presented as mean ± SEM of three independent experiments. Abbreviations: FCCP, carbonyl cyanide-4 (trifluoromethoxy) phenylhydrazone; Rot/Ant, Rotenone plus antimycin A; OCR, oxygen consumption rate. Representative trace from four independent experiments.

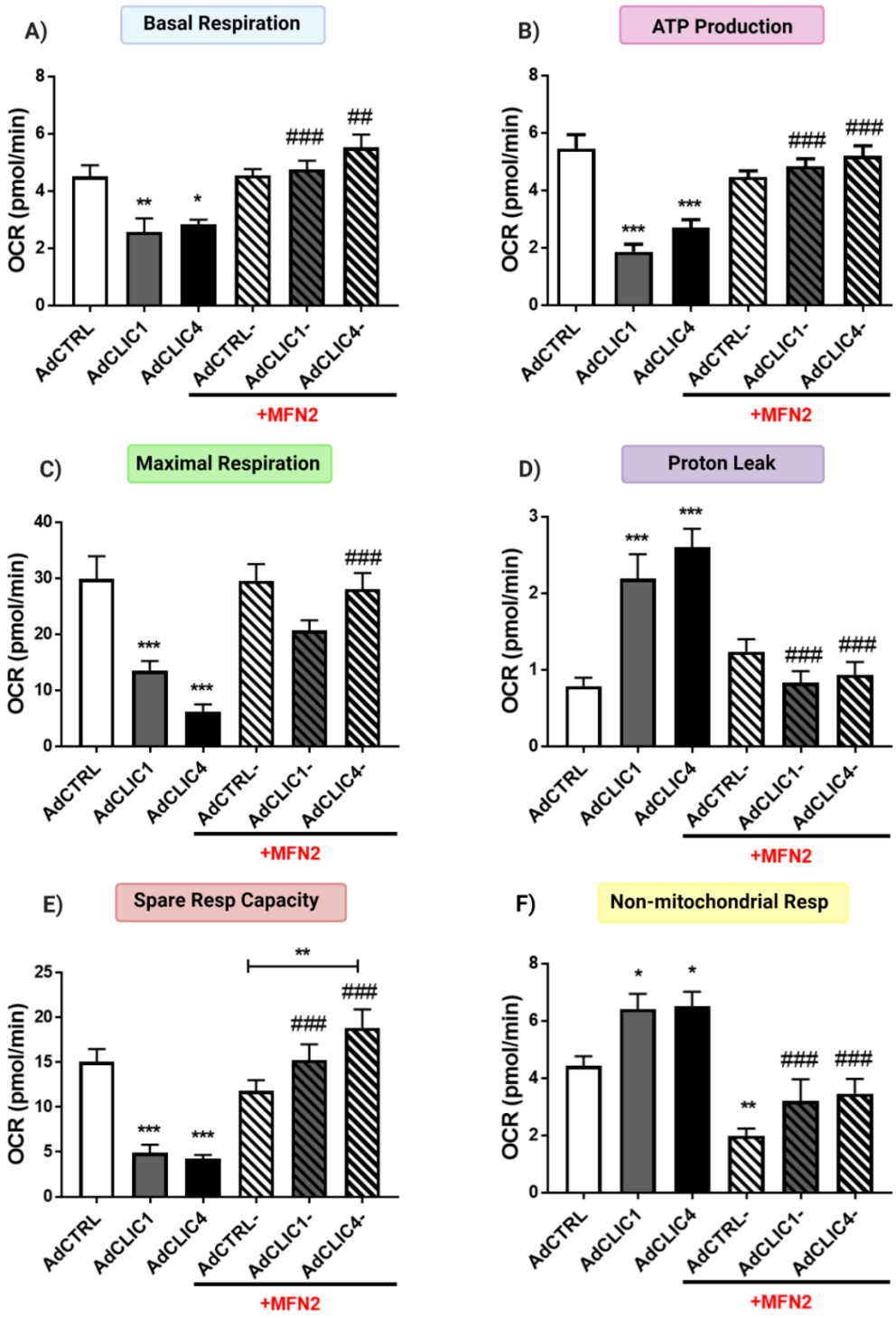


Figure 6.12: Effect of MFN2 overexpression on mitochondrial function in CLIC-overexpressing HPAECs. Cells were infected with either AdCTRL and/or AdCLIC, AdMFN2, and key parameters of mitochondrial respiration were measured using the Seahorse XFp Cell Mito Stress Test 24 hours post-infection. *P <0.05, **P <0.01 ***P<0.0001, comparison with AdCRTL; #P<0.05, comparison with AdCLIC; One-way ANOVA was used with Tukey's multiple comparison test. Data are presented as mean ± SEM of four independent experiments with 4 to 8 replicate wells in the Seahorse XF analyzer.* comparisons with AdCTRL, comparisons between CLIC1+MFN2- and CLIC4+MFN2 groups and CLIC1- and cLIC4-overexpressing groups, as required. Data were normalised to protein concentration for each experiment across all cells in each well.

Changes in ECAR parameters:

- MFN2 prevented CLIC1- and CLIC4-induced increases in glycolysis and glycolytic capacity (Figure 6.14 A and B).
- All treatment groups showed a noticeable, albeit not statistically significant elevation in glycolytic reserve, compared with untreated controls (Figure 6.14 C).
- MFN2 overexpression prevented a decrease in non-glycolytic acidification in CLIC1- and CLIC4-overexpressing HPAECs (Figure 6.14 D).

ECAR data generated by the XF Glycolysis Stress Test report generator are shown in Figures 6.13, and 6.14.

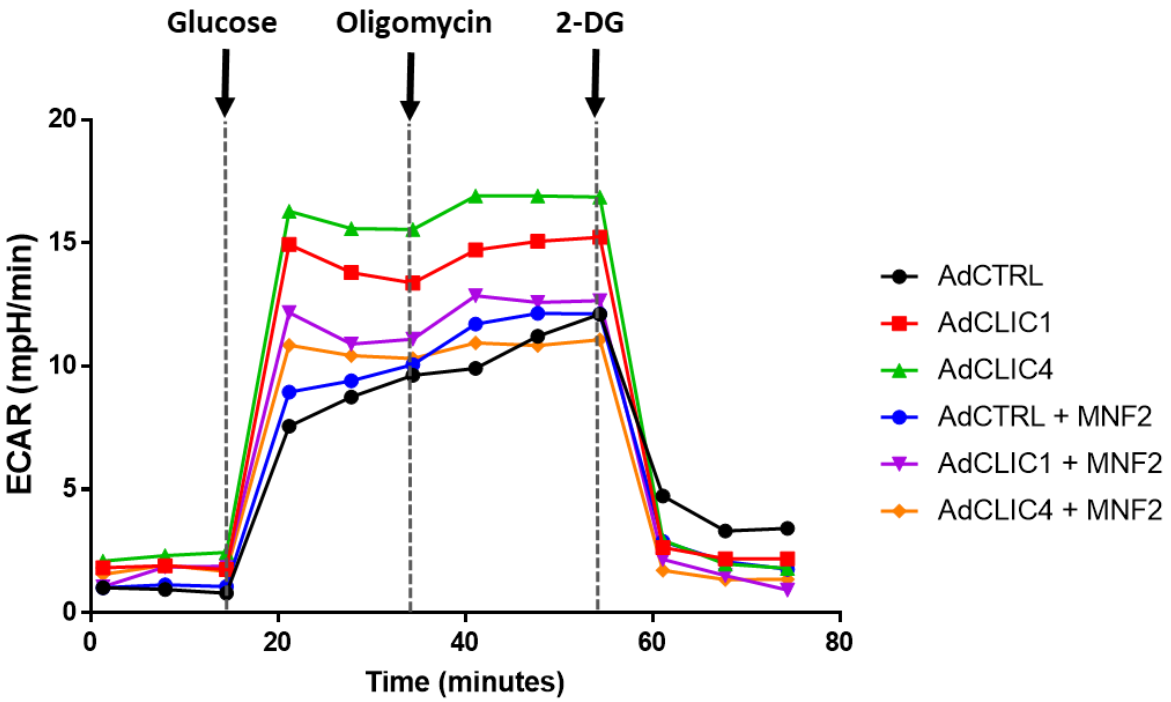


Figure 6.13: Extracellular acidification rate measured following the serial compound injections of glycolysis modulators. HPAECs were infected with AdCLIC1, AdCLIC4, AdshCLIC1, AdCLIC4 and ECAR measured at intervals following the injection of glucose at 15 minutes, oligomycin at 34 minutes, and 2-DG at 54 minutes. Black circle: CTRL (untreated HPAECs); red square: AdCLIC1; green triangle: AdCLIC4; purple triangle: CTRL+MFN2; orange diamond: AdCLIC4+MFN2; blue diamond: AdCLIC1+MFN2. Data are presented as mean ± SEM of three independent experiments. Abbreviations: 2-DG, 2-Deoxy-glucose; ECAR, extracellular acidification rate. Representative trace from four independent experiments.

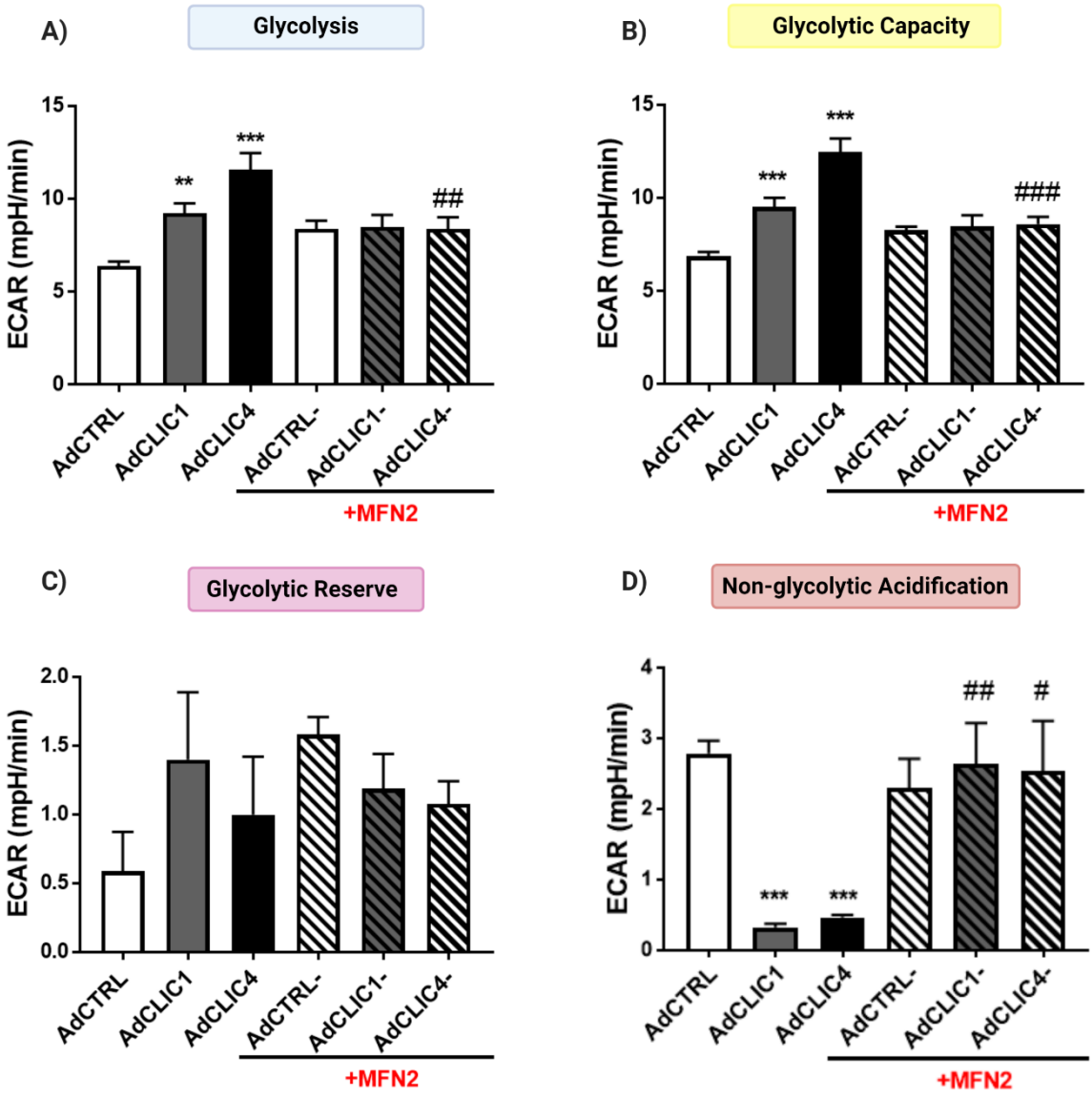


Figure 6.14: Effect of MFN2 overexpression on CLIC-induced changes on acidification rate in HPAECs. Cells were infected with either AdCTRL and/or AdCLIC, AdMFN2, and key parameters of mitochondrial respiration were measured using the Seahorse XFp Cell Glyco Stress Test. *P <0.05, **P <0.01 ***P<0.0001, comparison with AdCRTL; ##P<0.01, comparison with AdCLIC; # P<0.05, comparison between AdCLIC and AdCLIC+MFN2. One-way ANOVA was used with Tukey's multiple comparison test. Data are presented as mean ± SEM of four independent experiments with 4 to 8 replicate wells in the Seahorse XF analyser. Data were normalised to protein concentration for each experiment across all cells in each well.

6.5 Summary

The key findings presented in this chapter show that:

- MFN2 overexpression had little effect on mitochondrial fragmentation or mitochondrial function in untreated HPAECs under basal conditions.
- MFN2 overexpression prevented CLIC1- and CLIC4-induced mitochondrial fragmentation and a rise in mitochondrial membrane potential in HPAECs.
- MFN2 also prevented CLIC1- and CLIC4- induced increase in mitochondrial ROS generation.
- MFN2 overexpression prevented CLIC1- and CLIC4- induced reduction in basal respiration, mitochondrial ATP generation, maximal respiration, and spare respiratory capacity.
- MFN2 prevented CLIC1- and CLIC4-induced increase proton leak and non-mitochondrial respiration.
- MFN2 prevented CLIC1- and CLIC4-increase in glycolysis and glycolytic capacity and reduction in non-glycolytic acidification.
- CLIC1, CLIC4, and MFN2 have no significant impact on glycolytic reserve.

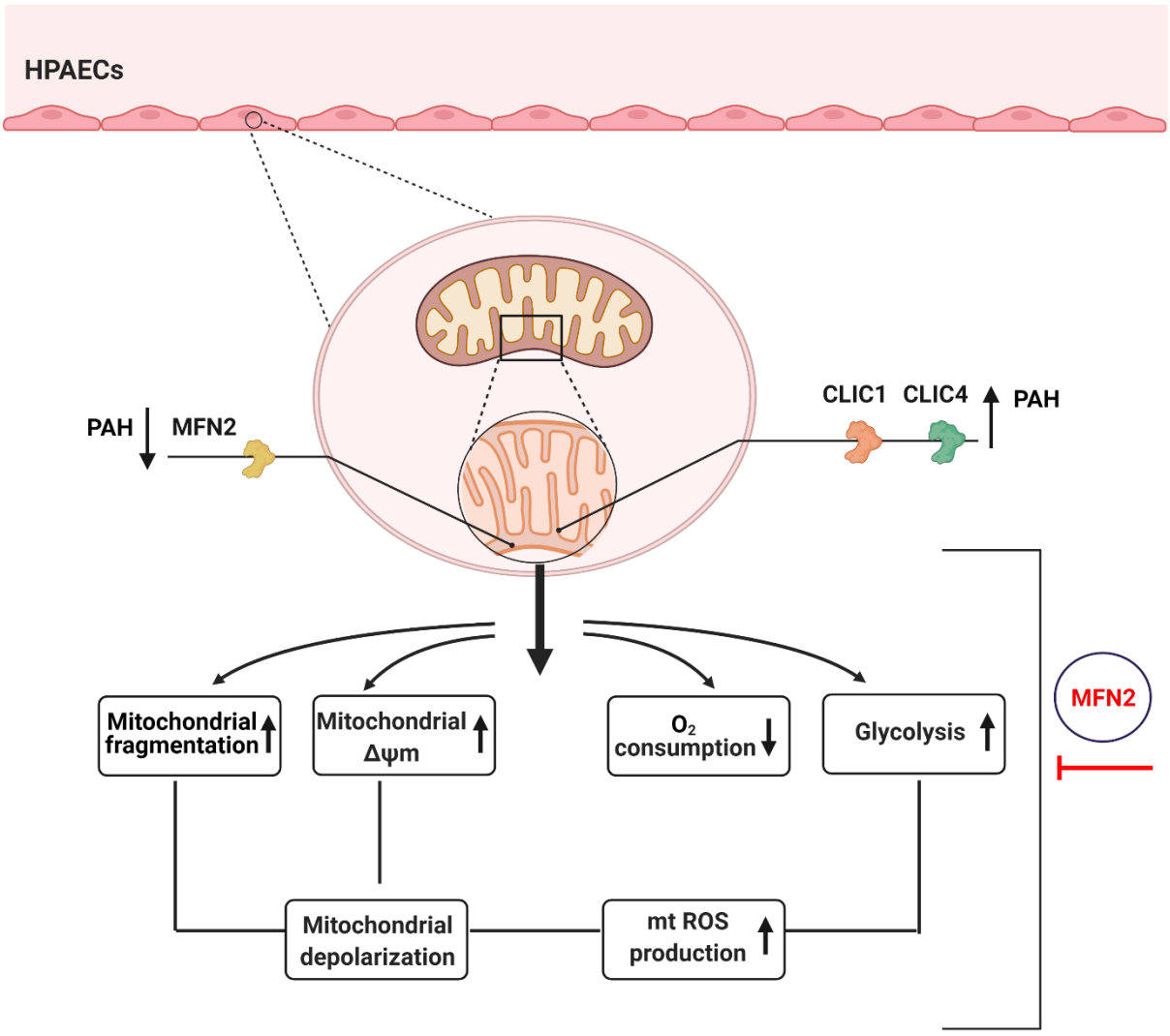


Figure 6.15: Summary of key results in Chapter 6. Key findings are summarised in Table 6.1. Illustration created by the author using BioRender.com.

Table 6.1: Summary of key findings on the effect of overexpression of CLIC proteins and MFN2 on mitochondrial function in HPAECs. Red arrows pointed upwards indicate increase, black arrows pointed downwards indicate decrease, and dashes indicate no change.

Investigation	CLIC1	CLIC4	CLIC1+MFN2	CLIC4+MFN2
Mitochondrial fragmentation	↑	↑	↓	↓
Mitochondrial membrane potential	↑	↑	↓	↓
Mitochondrial ROS production	↑	↑	↓	↓
Basal respiration	↓	↓	↑	↑
ATP production	↓	↓	↑	↑
Maximal respiration	↓	↓	↑	↑
Proton leak	↑	↑	↓	↓
Spare respiratory capacity	↓	↓	↑	↑
Non-mitochondrial respiration	↑	↑	↓	↓
Glycolysis	↑	↑	↓	↓
Glycolytic capacity	↑	↑	↓	↓
Non-glycolytic acidification	↓	↓	↑	↑
Glycolytic reserve	—	—	—	—

6.6 Discussion

Data from this study show that CLIC1 and CLIC4 proteins are components of the mitochondrial membrane in HPAECs, which is consistent with previous findings in cardiomyocytes (Singh, 2010). CLIC1- and CLIC4-overexpression reduces the expression of MFN2 in HPAECs, similar to the changes seen in remodelled vasculature cells in PAH (Ryan et al., 2013). MFN2 is a large GTPase located in the outer mitochondrial membrane which acts as a crucial regulator of mitochondrial network integrity (Chandhok et al., 2018). GTP binding and hydrolysis on MFN2 tethers the opposing membranes of multiple mitochondria, causing mitochondrial fusion and branching of the mitochondrial network (Van der Bliek et al., 2013). The interaction of MFN2 with MFN1 and optic atrophy 1 (OPA1) is necessary for the regulation of normal mitochondrial shape, distribution and quality control (Zhao et al., 2013). The suppression of MFN2 induces metabolic changes in cell lines of different origins and is characterized by reduced cellular oxygen consumption and a metabolic shift towards glycolysis. A reduction in mitochondrial membrane potential was also reported (Gouriou et al., 2020), which is characteristic of changes seen in PAH (Yu & Chan, 2017). Our findings suggest that the increased expression of CLIC1 and CLIC4 is likely to contribute to a decrease in MFN2 expression, leading to a reduction in mitochondrial respiration and an increase in the rate of glycolysis in vascular endothelial cells. An increase in CLIC1 and CLIC4 expression in PAH was seen predominantly in the vascular endothelium, but some less pronounced changes were also seen in smooth vascular muscle cells, so these results may to some extent also apply to other cell types. Considering that mitochondria constitute almost 40% of the volume of cardiac tissue (Barth et al., 1992), establishing the role of CLIC proteins in the regulation of energy

metabolism in the heart may be of particular importance in the context of PAH. This will need to be addressed in future studies.

MFN2 overexpression prevented abnormal increases in the mitochondrial membrane potential (Δψm) in CLIC-overexpressing HPAECs. The hyperpolarization of the mitochondrial membrane has been linked to an increase in ROS generation as well as increased sensitivity to apoptosis (Martínez-Reyes et al., 2016). Normal levels of Δψm are required to sustain ATP production and maintain a healthy balance between mitochondrial fusion and fission as well as proliferation and apoptosis and to regulate protein import and metabolite exchange with the cytosol. Mitochondrial membrane potential can therefore be considered as a key functional readout of mitochondrial health (Forkink et al., 2014). PAH carries many of the hallmarks of cancer, including apoptosis resistance, increased cell proliferation and mitochondrial dysfunction – which is characterised by dysmorphic, hyperpolarized mitochondria in vascular endothelial and smooth muscle cells (Ranchoux et al., 2016). As the reduction in mitochondrial membrane potential is associated with cell cycle arrest (Ryan et al., 2015), the overexpression of MFN2 may be beneficial to the inhibition of proliferative activation of pulmonary vascular cells in PAH.

The leak of electrons from the electron transport chain is the major cause of generating mitochondrial superoxide, which is known to play a key role in pulmonary hypertension (Russomanno et al., 2020). Elevated levels of mitochondrial ROS are linked to cellular response to stress or inflammation, and are likely to act as upstream activators of CLIC proteins in the pulmonary endothelial vasculature. Proton leak reflects the protons that migrate into the matrix without producing ATP, so a reduction in proton leak is indicative of an improvement in the

coupling of substrate oxygen and ATP generation (Cheng et al., 2017). Consistent with this, we observed an increase in mitochondrial ATP generation in MFN2-overexpressing cells.

CLIC4 activates HIF (Wojciak-Stothard et al., 2014), and HIF stabilization is known to promote ROS production, thus provoking oxidative stress, which plays an important role in endothelial dysfunction and the development of vascular remodelling in PH (Aggarwal et al., 2013). Our results show that MFN2 restores the control levels of mitochondrial membrane potential and reduces mitochondrial ROS generation in CLIC1- and CLIC4-overexpressing endothelial cells, and this is consistent with other reports showing the effectiveness of MFN2 in reducing oxidative stress in diabetic cardiomyopathy (Hu et al., 2019). The reduction in mitochondrial proton leak by MFN2 can therefore be linked to the reduction in mitochondrial ROS generation and the reduction in mitochondrial membrane potential.

CHAPTER 7 RESULTS:

CLIC proteins in mitochondrial dysfunction in PAH: study in ECFCs

CHAPTER 7 RESULTS: CLIC proteins in mitochondrial dysfunction in PAH: study in ECFCs

The aim of the studies presented in this chapter was to determine the changes in CLIC protein expression, mitochondrial distribution, biogenesis, and energy metabolism in blood-derived late outgrowth endothelial colony forming cells (ECFCs) from healthy volunteers and pulmonary arterial hypertension (PAH) patients.

7.1 Introduction

Endothelial colony forming cells (ECFC) are endothelial progenitor cells that circulate in peripheral blood that can become mature endothelial cells and form vascular networks (Toshner et al. 2009). Circulating ECFCs have been used as biomarkers in various cardiovascular diseases, but their role in PAH remains relatively unexplored (Asosingh et al. 2008). PAH ECFCs display highly proliferative, pro-angiogenic phenotypes, and may play a role in the formation of pulmonary vascular obstruction (Toshner et al. 2009). Mature ECFCs express endothelial cell markers, such as vascular endothelial cadherin (VE-cadherin), and exhibit a cobblestone morphology typical of endothelial cells (ECs) (Lin et al. 2000, Minami and Aird 2005).

Proteomic analysis of ECFC from hereditary pulmonary arterial hypertension (HPAH) patients with BMPRII mutations reveals an increased expression of the key mediators of cell survival and proliferation (Lavoie et al. 2014). Metabolic abnormalities, such as a switch from oxidative phosphorylation to aerobic glycolysis have also been observed in IPAH and HPAH ECFCs (Caruso et al. 2017). The expression of CLIC4 is increased in IPAH ECFCs, reflecting the changes seen in PAH vasculature (Wojciak-Stothard et al. 2014). CLIC4 was shown to activate the nuclear factor-nuclear factor kappa-light-chain-enhancer of activated B (NFκB) and stabilize HIF-1α, leading to increased release of VEGF and endothelin-1 (Wojciak-Stothard et al. 2014).

Considering the difficulties involved in obtaining pulmonary endothelial cells, non-invasive methods of isolating endothelial cells from patient blood have been extensively recognized as key tools for studying endothelial dysfunction in lung diseases. *Ex vivo* expansion of blood-derived ECFCs has been used as an accessible surrogate to study endothelial cells in PAH (Toshner et al. 2009) and other diseases, including systemic sclerosis (Avouac et al. 2008), von Willebrand disease (Starke et al. 2011), macular degeneration (Thill et al. 2008), diabetes (Ingram et al. 2008, Tan et al. 2010) and coronary artery diseases (Wang et al. 2011).

This study aimed to investigate whether or not ECFCs display CLIC-related mitochondrial and metabolic dysfunction, which are key features of mature lung endothelial cells in PAH.

7.2 Experimental aims

The overall aim of studies presented in this chapter was to

1. Evaluate the differences in CLIC (CLIC1 and CLIC4) and MFN2 expression between ECFCs from healthy individuals and PAH patients.
2. Study the effects of compensatory changes in MFN2 expression on mitochondrial network formation and mitochondrial membrane potential in PAH ECFCs.
3. Investigate the effects of compensatory changes in CLIC1, CLIC4 and MFN2 expression on energy metabolism in ECFCs.

7.3 Experimental design

An overview of the experimental outline is presented in Figure 7.1. A detailed description on specific methods and protocols can be found in Chapter 2, Materials and methods.

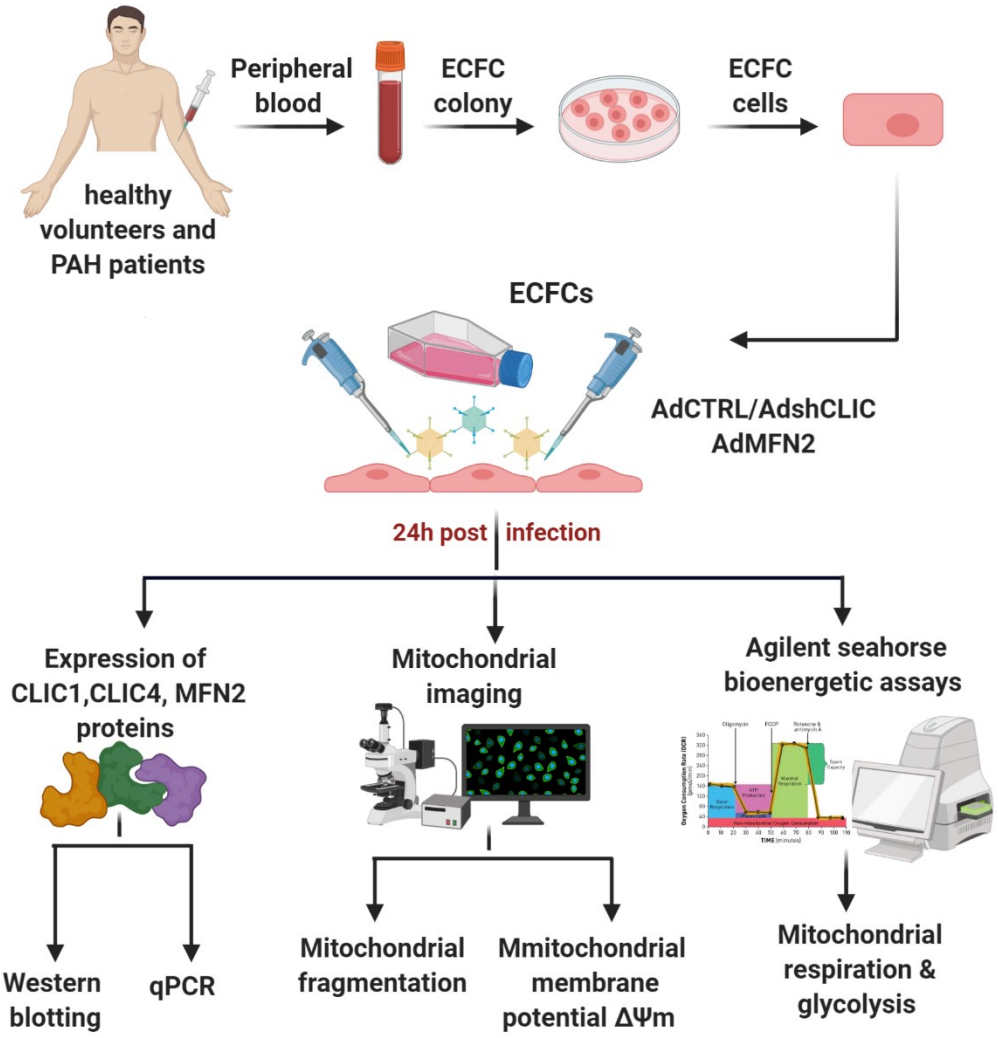


Figure 7.1: Experimental outline for chapter 7. Blood-derived endothelial colony forming cells (ECFCs), were obtained from Imperial College London's PH biobank (see Chapter 2, Materials and Methods, Section 2.1.1.2) and cultured for further investigation. The inhibition of CLIC expression and overexpression of MFN2 were achieved by adenoviral gene transfer of AdshCLIC or AdMFN2, as appropriate. AdCTRL and non-targeting (scrambled) AdshRNA were used as treatment controls. Changes in mitochondrial fragmentation, mitochondrial membrane potential (ΔΨm), glycolysis and mitochondrial respiration in MFN2-overexpressing ECFCs were studied using fluorescent imaging and the Seahorse bioenergetics assay. The effects of CLIC inhibition on respiratory metabolism were also evaluated using the Seahorse bioenergetics assay. Illustration created by the author using BioRender.com.

7.3.1 Cell culture

7.3.1.1 Blood-derived human endothelial cells

Blood-derived endothelial colony forming cells (ECFCs) were isolated, as described in Chapter 2-Materials and Methods, Section 2.1.1.2. Peripheral blood samples were collected with the approval of the local ethics committee and informed written consent from healthy volunteers (n=14) and from patients with idiopathic PAH (IPAH, n=12). Patient demographics is shown in Table 7-1. ECFCs were cultured in an EGM-2 medium supplemented with growth factors, 20% FBS and 1% antibiotic/antimycotic solution. The inhibition of CLIC expression and the overexpression of MFN2 were achieved by adenoviral gene transfer (AdshCLIC, AdMFN2), as described in Chapter 4, Section 4.4.1 and Chapter 6, Section 6.4.1 respectively). 70-80% confluent passage 5 ECFCs growing in 24-well plates were infected with adenoviruses at a MOI of 1:100. After 24 hours' incubation, the cells were used for further investigations.

Table 7.1: Demographics of IPAH patients and healthy volunteers. Data are represented as median (range). Abbreviations: mPAP, mean Pulmonary Arterial Pressure; ER, Estrogen-Receptor; PDE5, Phosphodiesterase type 5 (Russomanno, Jo et al. 2020).

		Control (n=14)	***IPAH (n=12)***
Male/Females		3/11	1/11
Age (years)		30.0 (23.0 - 45.0)	38.33 (27.0 - 67.0)
Time from diagnosis (months)		-	13.0 (0.1 - 60.0)
mPAP (mmHg)		-	65.0 (28.0 - 94.0)
Six minute walk distance (m)		-	396.0 (300.0 – 540.0)
WHO Functional Class	I	-	1
	II	-	3
	III	-	5
	IV	-	3
Treatment Naïve		-	2
Warfarin		-	4
Calcium Antagonists		-	1
ER Antagonists		-	7
PDE5 Inhibitors		-	8
Prostanoids		-	4
Statins		-	0

7.3.2 Measurement of CLIC and MFN2 gene expression levels by quantitative PCR in ECFCs

70-80% confluent ECFCs were harvested by trypsinization, and RNA was purified and reverse transcribed to the cDNA, which was then subjected to a real time qPCR. For details see Chapter 2- Section 2.8, Materials and Methods.

7.3.3 Immunofluorescence and confocal microscopy of mitochondrial fragmentation

ECFCs (from healthy controls and PAH patients) cultured on 8-well chambered coverslips were left untreated or were infected with AdCRTL or AdMFN2. 24 hours post-infection, the cells were immunostained with anti-mitochondrial antibodies, and mitochondrial fragmentation was evaluated as described in Chapter 2- Section 2.4.1, Materials and Methods.

7.3.4 Measurement of mitochondrial membrane potential (ΔΨm)

ECFCs cultured on Thermanox® Plastic Coverslips (13 mm) were infected with AdCLIC1 shRNA, AdCLIC4 shRNA, AdCTRL or AdMFN2. 24 hours post-infection, 100 nM Tetramethylrhodamine, methyl ester (TMRM) was added to the culture medium and the cells were incubated for 30 minutes at 37 ˚C. The ECFCs were then washed twice with PBS, and new medium was added to the cells. Live imaging was performed using a Zeiss confocal microscope (Zeiss LSM780) and the acquired images were then analysed with ImageJ. For details see Chapter 2- Section 2.5.1, Materials and Methods.

7.3.5 Seahorse bioenergetics assay

The mitochondrial respiration (OCR) and glycolytic function (ECAR) were measured in ECFCs using Agilent Seahorse XFp. ECFCs were seeded at the density of $2x10^4$/well in Seahorse 96-well plates designed for the Seahorse XFp instrument. The following day, cells were infected with AdCTRL, AdshCLIC1, AdshCLIC4, and AdMFN2 and incubated for 24 hours before being equilibrated with XF assay medium containing 2mM L-Glutamine, 1mM pyruvate, and 10 mM glucose for the Mito Stress Test. 2mM L-Glutamine was the only supplement used in the Glycolysis Stress Test, according to the manufacturer's guidelines. In the Mitostress test, baseline rates of oxygen consumption were measured in ECFCs. Prior to the assay, all wells were serially injected with 1.5 µM oligomycin, 2 µM carbonyl cyanide 4-(trifluoromethoxy) phenylhydrazone (FCCP), and 0.5 µM rotenone/antimycin A (Rot/Ant). The extracellular Acidification Rate (ECAR) was measured in response to the serial injections of 1.5 µM glucose, 15 µM oligomycin, and 65 µM 2-Deoxy-glucose (2-DG). After the run, the total protein levels in each well were measured using the BCA protein assay kit and OCR/ECAR were normalized to the protein levels. Further methodological details are provided in Chapter 2- Section 2.5.3, Materials and Methods.

7.4 Results

7.4.1 CLIC and MFN2 expression in ECFCs

CLIC1 and CLIC4 mRNA expression levels in PAH ECFCs were significantly increased compared to healthy controls (Figure 7.2 A and B). Gene expression of MFN2 was significantly reduced in PAH ECFCs. (Figure 7-3).

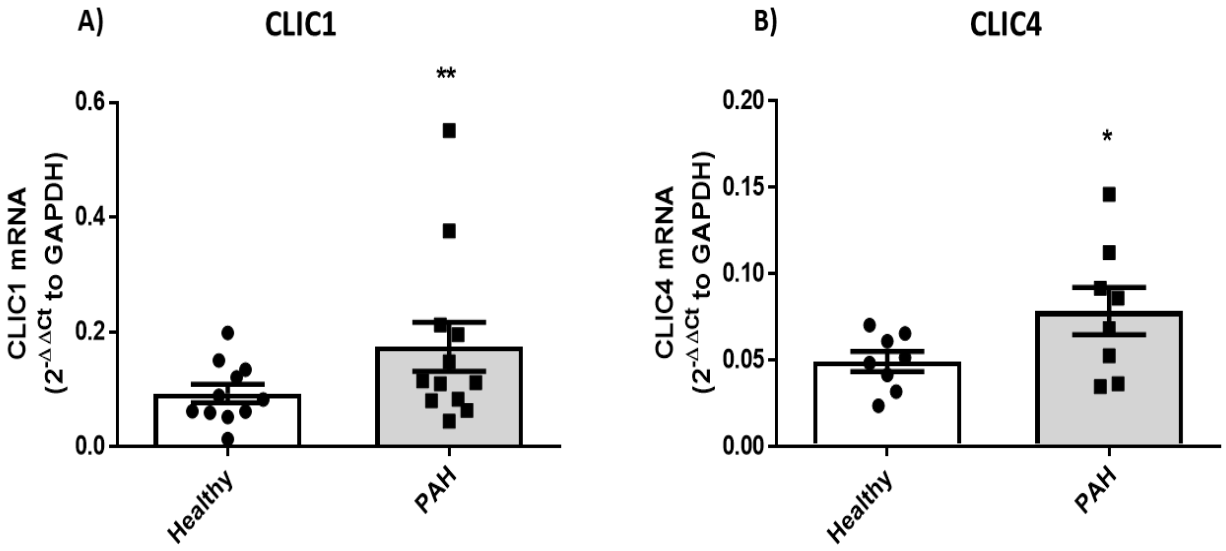


Figure 7.2: Gene expression level of CLIC1 and CLIC4 in healthy and PAH ECFCs. Bar-graphs (**A**) and (**B**) show changes in mRNA expression of CLIC1, and CLIC4 in healthy and PAH cells, as indicated. Expression levels were normalised to GAPDH. *P <0.05, **P <0.01 in comparison with healthy control cells. Data are presented as mean ±SEM of 3 independent experiments with 3 technical repeats. The Statistical analysis was performed using unpaired t-test. N=8-healthy and 12-patient samples.

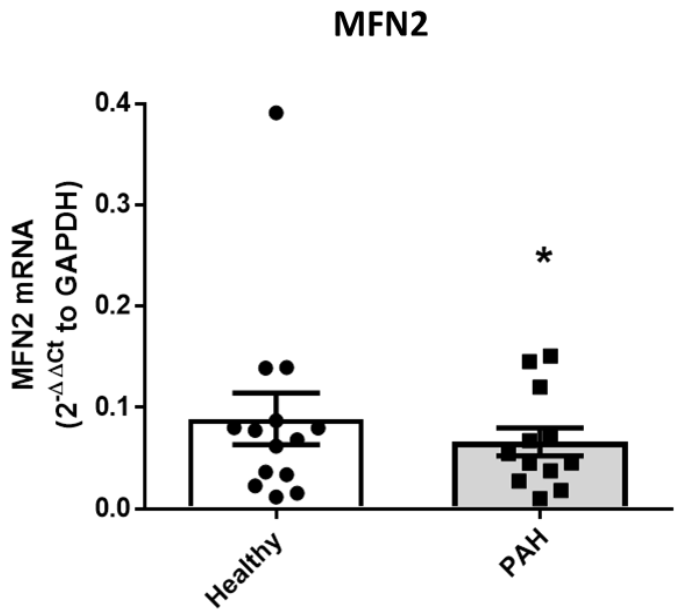


Figure 7.3: MFN2 mRNA expression level in healthy and PAH ECFCs. Expression levels were normalised to GAPDH. *P <0.05, in comparison with healthy control cells. Data are presented as mean ±SEM based on 3 independent experiments with 3 technical repeats, and the statistical analysis was performed using the unpaired t-test. N=12 healthy and 14 patient samples.

7.4.2 The effect of MFN2 on mitochondrial fragmentation in ECFCs

PAH ECFCs showed a significant increase in the number of small, fragmented mitochondria in ECFCs compared with healthy controls (P = 0.0045) (Figure 7.4 and 7.5).

Since the compensatory overexpression of MFN2 significantly decreased mitochondrial fragmentation in CLIC1- and CLIC4-overexpressing HPAECs (Chapter 6, Section 6.5.2), the effect of MFN2 overexpression was subsequently studied in PAH ECFCs. Image analysis revealed that MFN2 overexpression significantly reduced MFC in PAH cells to the levels seen in healthy controls (Figure 7.6). Representative images of mitochondrial fragmentation in healthy and PAH ECFCs with and without MFN2 are shown in Figure 7.7.

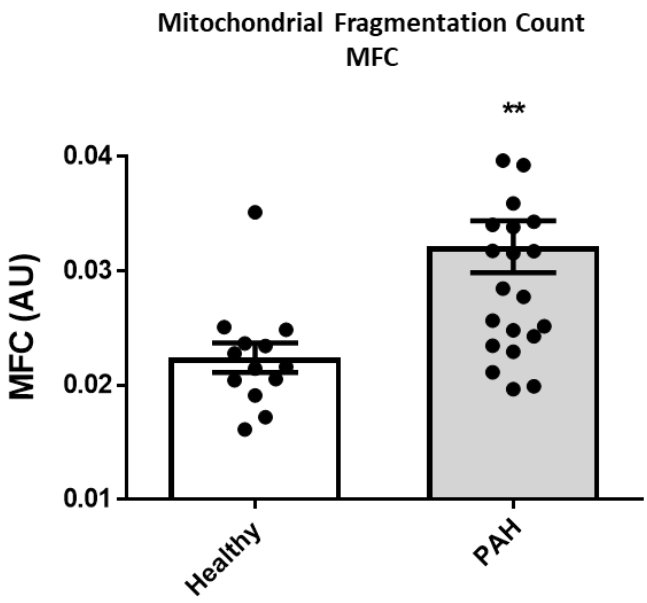


Figure 7.4: Changes in mitochondrial fragmentation count in ECFCs from healthy volunteers and PAH patients. MFC (AU: arbitrary units) was measured in ECFCs from healthy individuals and PAH patients using NIP2 image software. The bar-graph shows the significant increase in MFC in PAH ECFCs, compared to healthy volunteers. N=25 cells/group in total 12 healthy controls, and 14 patients were analysed in 3 separate experiments. **P <0.01, in comparison with the healthy group; unpaired t-test. Data are presented as mean ± SEM.

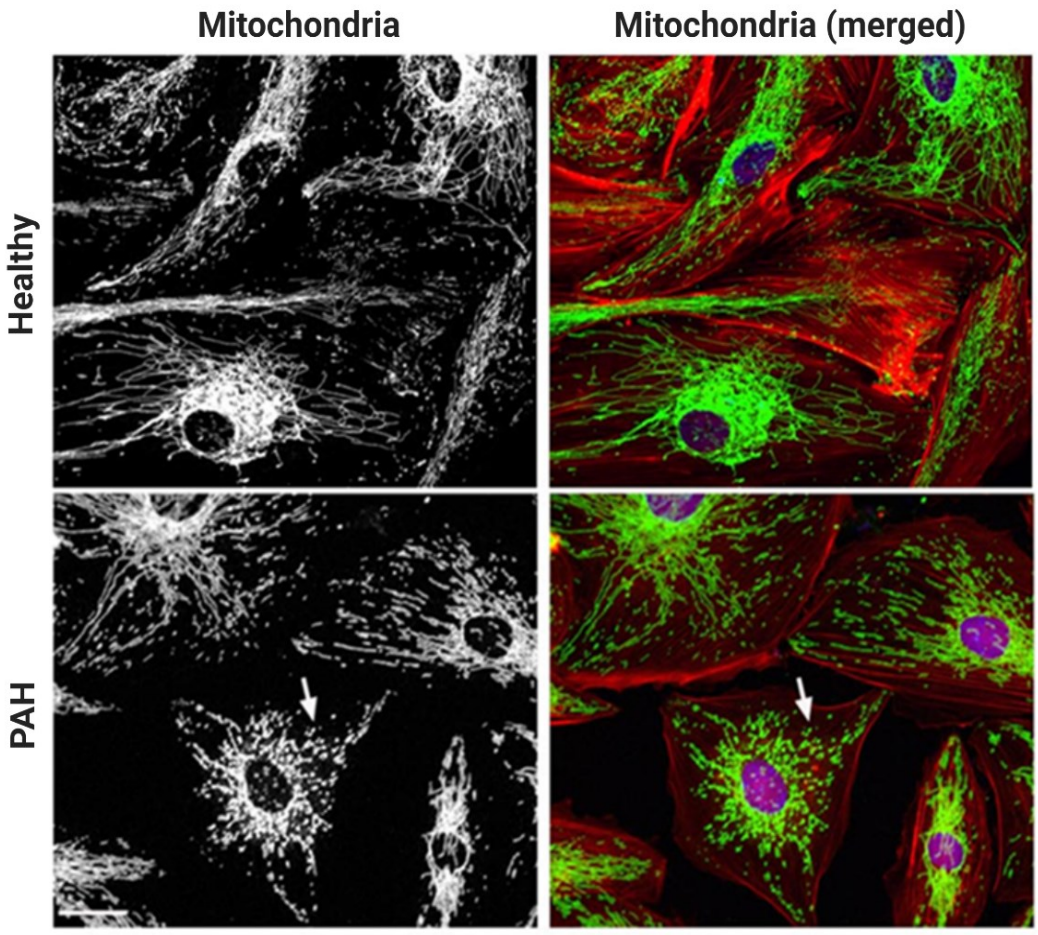


Figure 7.5: Changes in mitochondrial fragmentation in healthy and PAH ECFCs. Representative confocal images of mitochondria (immunofluorescence) in ECFCs from healthy controls and PAH patients. Corresponding merged images show mitochondria (green), F-actin (red) and nuclei (blue). Arrows point to fragmented mitochondria. Images were obtained using a Zeiss LSM 780 confocal microscope with 20x objective. Bar=10µm.

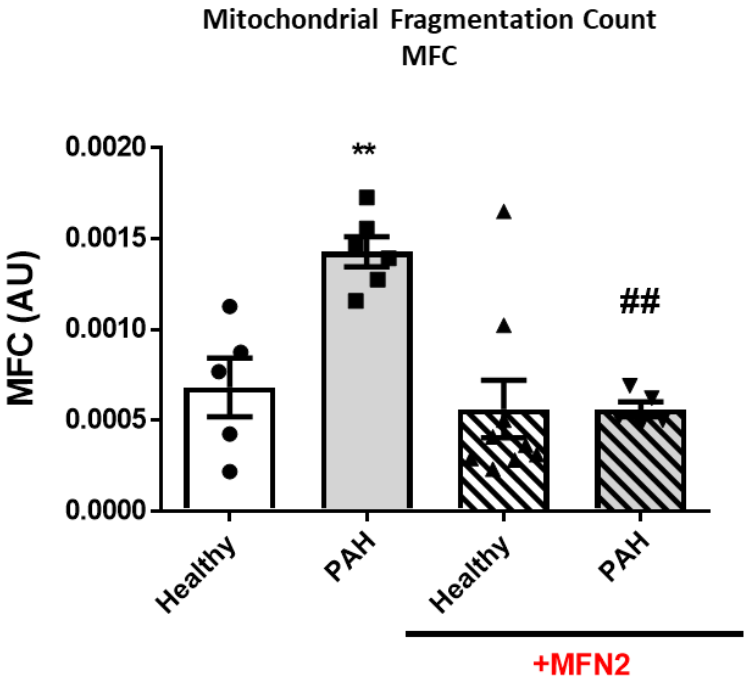


Figure 7.6: The effect of MFN2 on mitochondrial fragmentation count in ECFCs. MFC (AU: arbitrary units) was assessed in ECFCs infected with AdCTRL, with and without AdMFN2 using NIP2 image software. The bar-graph shows a significant decrease in MFC caused by MFN2 in PAH ECFCs overexpressing MFN2 compared PAH. N=25 cells/group in 5 healthy controls. 6 patients were analysed in 3 separate experiments. **P <0.01, comparison with healthy ECFCs infected with AdCTRL, ##P <0.01, comparison with PAH ECFCs infected with AdCTRL using One-way ANOVA with Tukey's multiple comparison test. Data are presented as mean ± SEM.

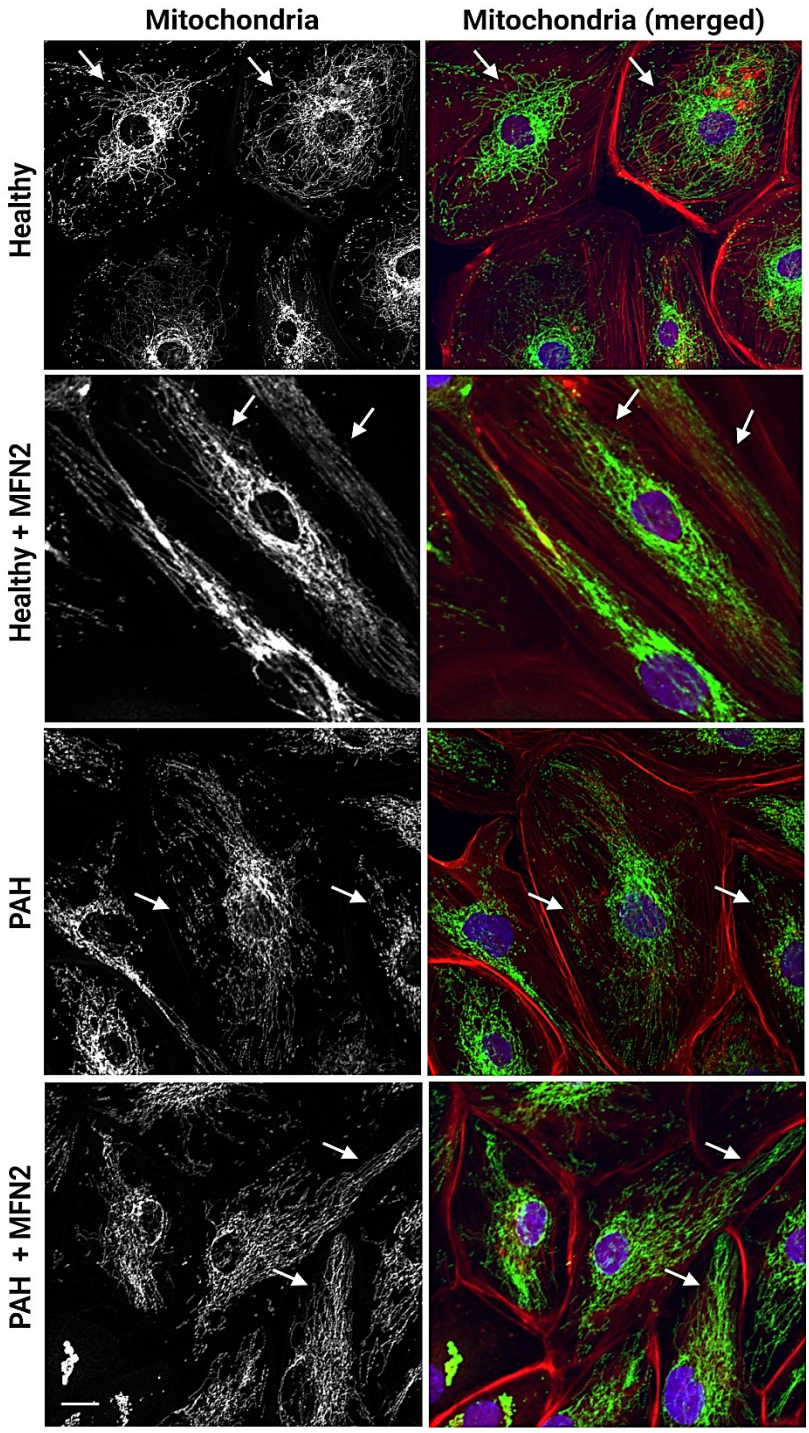


Figure 7.7: The effect of MFN2 overexpression on mitochondrial network in ECFCs. Representative fluorescent confocal images of mitochondrial network in healthy volunteers and PAH patients ECFCs treated with AdCTRL, with and without MFN2, 24 hours post-infection, healthy ECFCs infected with AdCTRL served as respective controls. Corresponding merged images show mitochondria (green), F-actin (red) and nuclei (blue). Arrows point to mitochondrial network in healthy, healthy+MFN2, PAH+MFN2, and mitochondrial fragmentation in PAH. Images were obtained using a Zeiss LSM 780 confocal microscope with 20x objective. Bar=10 µm.

7.4.3 The effect of MFN2 on mitochondrial ΔΨm in ECFCs

Mitochondrial ΔΨm was measured using TMRM, which allows us to determine mitochondrial permeability transition and membrane de-polarization in cells. Microscopic analysis showed a significant increase in the mitochondrial membrane potential of PAH cells, compared with healthy ECFCs (Figures 7.8 and 7.9).

The effect of MFN2 overexpression on ΔΨm in ECFCs infected with AdCTRL or AdMFN2 was evaluated 24 hours post-infection. The overexpression of MFN2 significantly reduced ΔΨm in PAH ECFCs, compared with PAH control (AdCTRL). TMRM fluorescence levels in MFN2-overexpressing ECFCs were comparable with TMRM fluorescence levels observed in healthy controls, as shown in Figures 7.10 and 7.11.

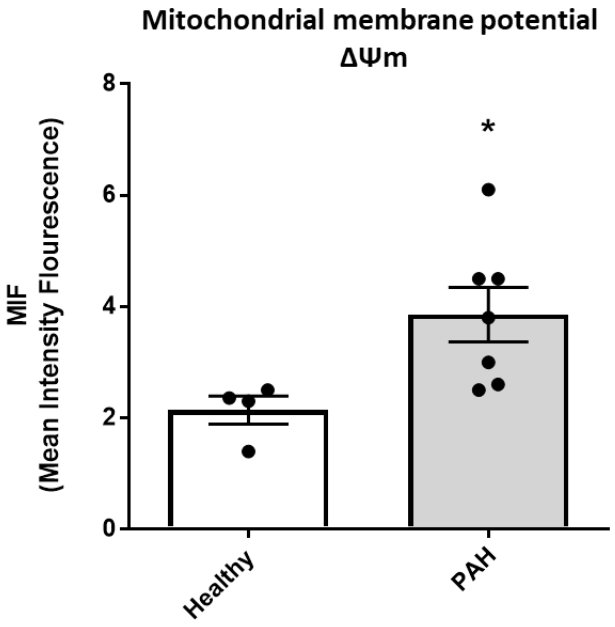


Figure 7.8: Changes in mitochondrial membrane potential in ECFCs from healthy controls and PAH patients. Bar-graph shows mean ΔΨm, evaluated by the measurement of TMRM fluorescence intensity (+SEM) in ECFCs from 7 PAH patients and 4 healthy volunteers: *P <0.05, in comparison to healthy controls using one-way ANOVA with Tukey's multiple comparison test. Data are presented as mean ± SEM, obtained from 3 experiments with 3 technical repeats/group.

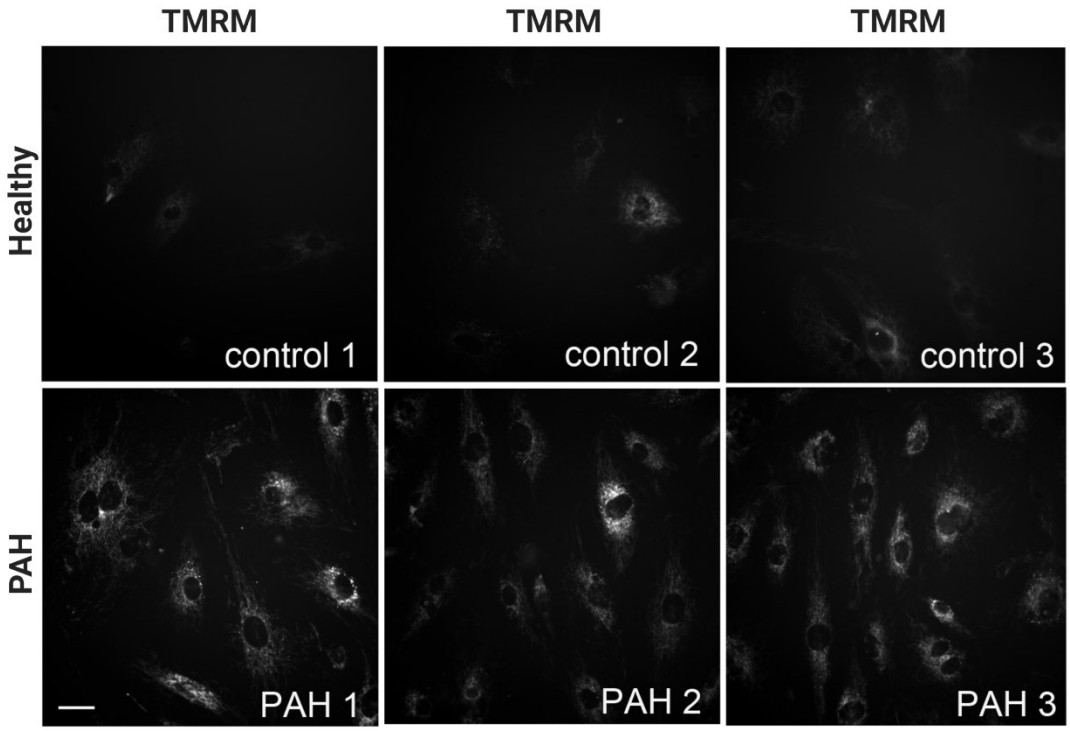


Figure 7.9: Changes in mitochondrial membrane potential in ECFCs. Representative images of ECFCs from healthy individuals and PAH patients. Live endothelial cells were incubated with 100 nM TMRM for 30 minutes at 37 ˚C and were then imaged using a Zeiss LSM 780 fluorescent confocal microscope with 20x objective. Bar=10 µm.

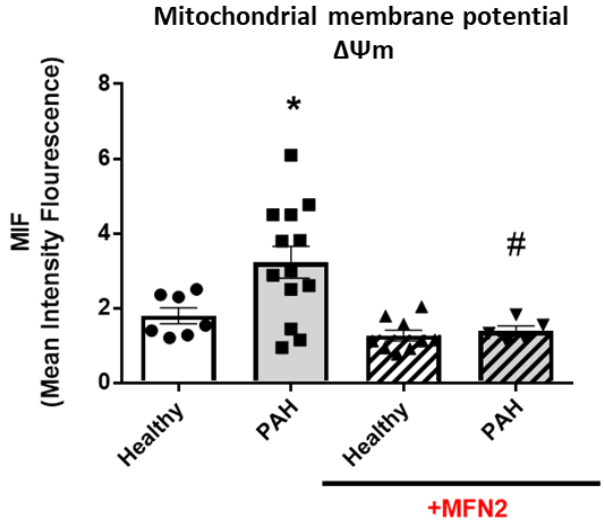


Figure 7.10: The effect of MFN2 on mitochondrial membrane potential in ECFCs. Mitochondrial membrane potential was assessed in ECFCs infected with AdCTRL or AdMFN2 by the measurement of TMRM fluorescence intensity (+/-SEM). The bar graph shows a significant decrease in MFC caused by MFN2 in PAH ECFCs overexpressing MFN2, compared PAH+AdCTRL. N=7-12 (images analysed from different patients with ~20 cells/image). *P <0.05 in comparison to healthy, #P <0.05, comparison with PAH. One-way ANOVA was used with Tukey's multiple comparison test. Data are presented as mean ± SEM.

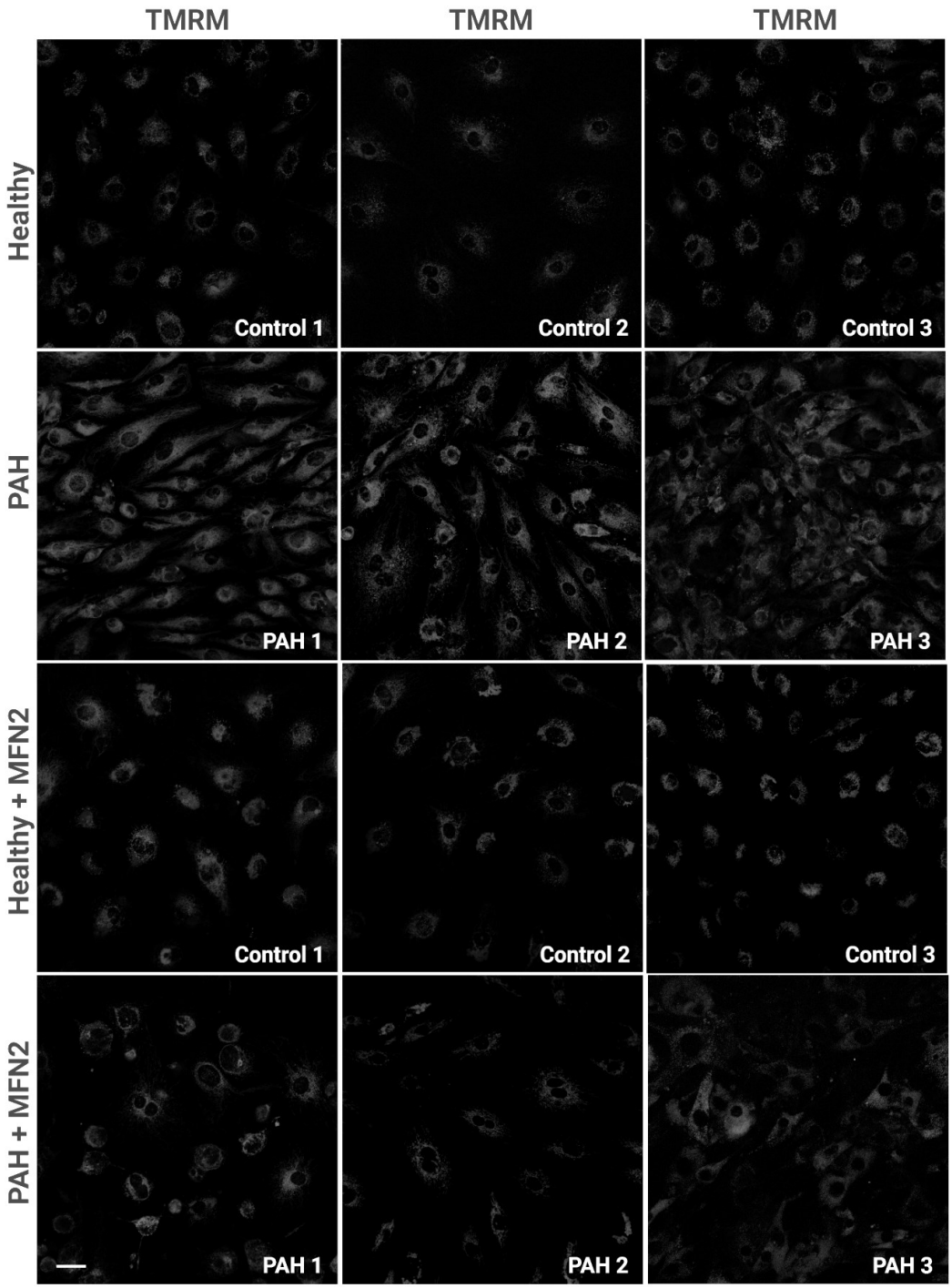


Figure 7.11: The effect of MFN2 on mitochondrial membrane potential in ECFCs from healthy controls and PAH patients. Representative confocal images of live healthy control and PAH ECFCs with or without AdMFN2 24 hours post-infection, as indicated. Live ECFCs were incubated with 100 nM TMRM for 30 minutes at 37 °C and the cells were then imaged using a Zeiss LSM 780 confocal microscope with 20x objective. Bar=10 µm.

7.4.4 The effect of CLIC inhibition and MFN2 overexpression on the bioenergetics profile of ECFCs

In order to determine whether CLIC inhibition and MFN2 overexpression affects mitochondrial function in ECFCs from healthy controls and PAH patients, the Agilent Seahorse Mito Stress Test and the Glycolysis Stress Test were used. Oxygen consumption rates (OCR) were measured in response to the sequential injection of respiratory modulators: oligomycin, FCCP, and rotenone/antimycin. Extracellular acidification rate (ECAR) was calculated at base conditions followed by the serial injection of glycolysis modulators: glucose, oligomycin, and 2-DG. A consistent protein concentration for each experiment was confirmed across all treated ECFCs in each well. OCR and ECAR data were automatically calculated from Wave software, then exported to Excel and used to determine the key mitochondrial respiration and glycolysis parameters. This provided the following results:

Mito Stress Test - changes in OCR parameters:

- The basal respiration of ECFCs from PAH patients was significantly reduced in comparison to ECFCs from healthy controls. CLIC1 and CLIC4 silencing and MFN2 overexpression increased basal respiration levels in PAH ECFCs (Figure 7.13; A).
- A significant decrease in ATP production was observed in PAH cells compared with healthy controls. MFN2 overexpressing PAH ECFCs showed a significant increase in ATP production. CLIC1 and CLIC4 inhibition also enhanced ATP levels in PAH ECFCs, compared with PAH patients' cells (Figure 7.13; B).
- Maximal respiratory capacities in healthy ECFCs following inhibition of CLIC1 and CLIC4 or overexpression of MFN2 were not significantly different from untreated healthy controls.

However, the silencing of CLIC1, CLIC4 and MFN2 overexpression significantly increased maximal respiration levels of PAH ECFCs (Figure 7.13; C).

- PAH ECFCs showed high proton leak rates compared to healthy controls. CLIC1, CLIC4 silencing and overexpression of MFN2 significantly reduced proton leak rates in PAH ECFCs. (Figure 7.13; D).
- Spare respiratory capacity: a significant reduction was observed in PAH ECFCs compared with healthy individuals. The inhibition of CLIC1, CLIC4 and the overexpression of MFN2 significantly increased spare respiratory capacity in PAH ECFCs (Figure 7.13; E).
- PAH ECFCs showed a high rate of non-mitochondrial respiration. The silencing of CLIC1, CLIC4, and the overexpression of MFN2 resulted in a significant increase in non-mitochondrial respiration levels compared to healthy ECFCs (Figure 7.13; F).

OCR data generated by the XF Mito Stress Test report generator are presented in Figures 7.12, and 7.13.

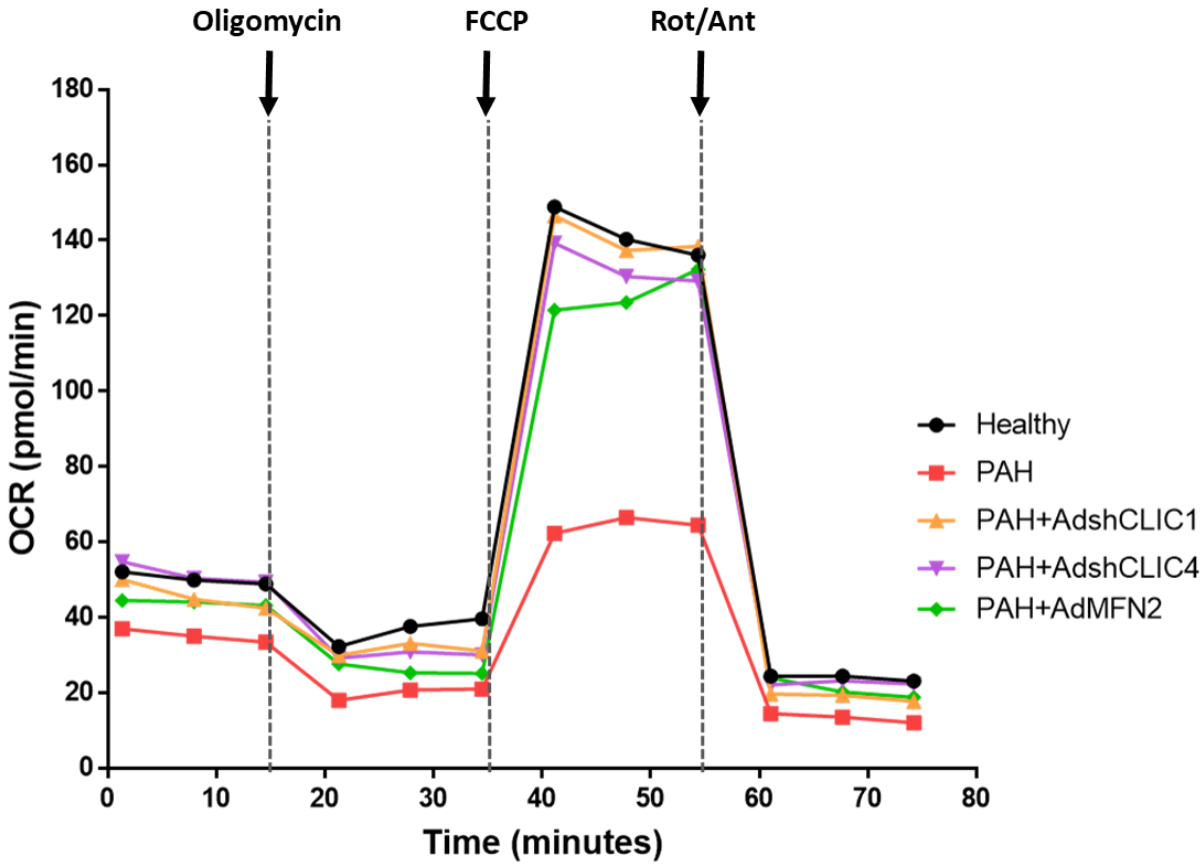


Figure 7.12: Example of Oxygen consumption rate (OCR) measurement in ECFCs from patients and healthy controls. ECFCs were infected with AdCTRL, AdshCLIC1, AdshCLIC4, AdMFN2 and OCR was measured at various time intervals following the injection of oligomycin, FCCP, and Rot/Ant at 15, 34 and 54 minutes respectively. Black circle: Healthy+AdCTRL; red square: PAH+AdCTRL; orange triangle: PAH+AdshCLIC1; purple triangle: PAH+AdshCLIC4; green diamond: PAH+AdMFN2. Abbreviations: FCCP, carbonyl cyanide-4 (trifluoromethoxy) phenylhydrazone; Rot/Ant, Rotenone plus antimycin A; OCR, oxygen consumption rate; PAH, pulmonary arterial hypertension. Representative trace from four independent experiments.

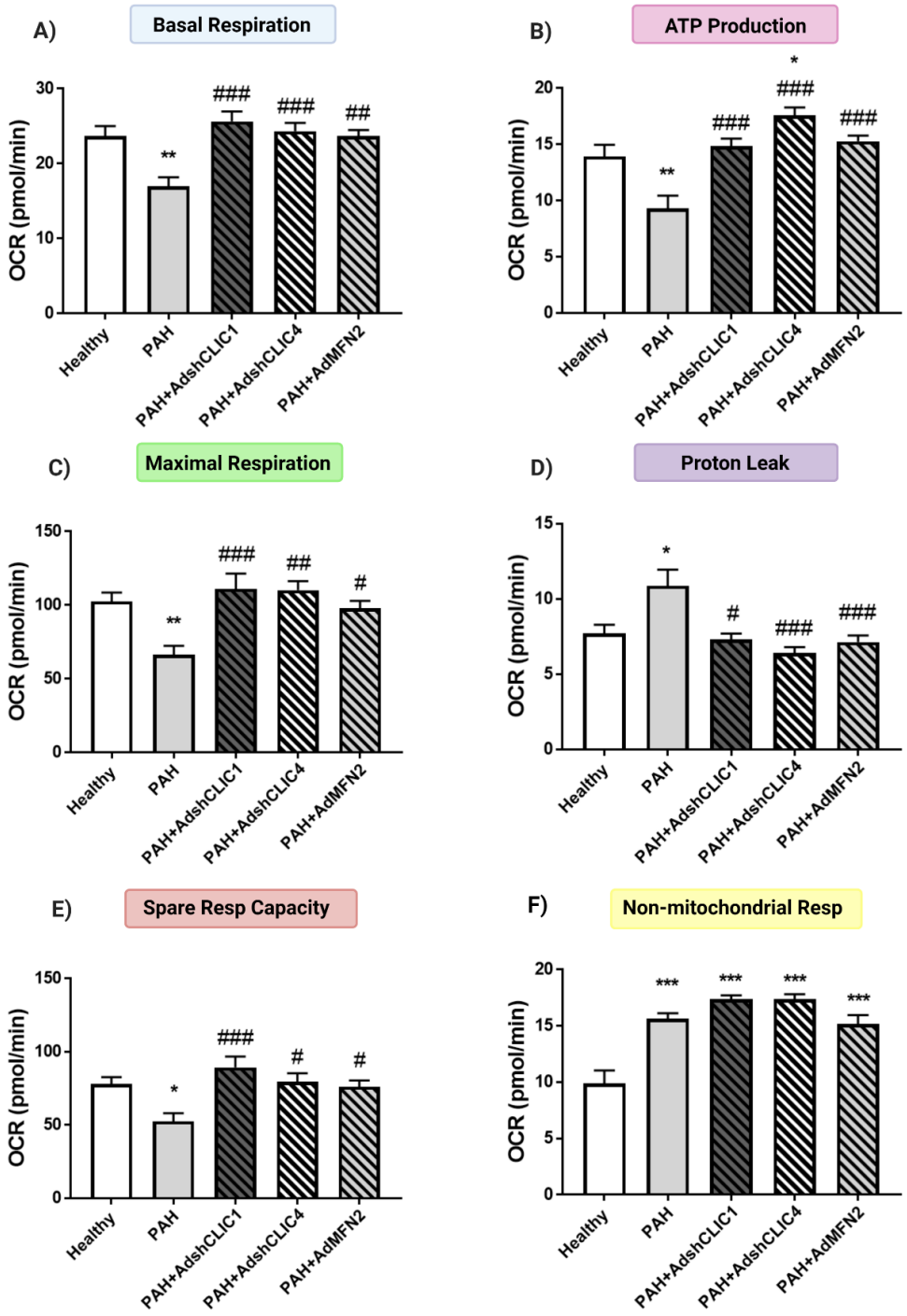


Figure 7.13: Effect of CLIC inhibition and MFN2 overexpression on mitochondrial function in healthy and PAH ECFCs. Cells were infected with AdCTRL (Healthy, PAH) and/or AdshCLIC, AdMFN2 as indicated, and the key parameters of mitochondrial respiration were assessed using the Seahorse XFp Cell Mito Stress Test. *P <0.05, **P <0.01 ***P<0.0001, in comparison with (Healthy+AdCTRL); #P<0.05, ##P <0.01 ###P<0.0001 comparison with PAH infected with AdCTRL using One-way ANOVA with Tukey's multiple comparison test. Data are presented as mean ± SEM of 4 independent experiments with 4 to 8 replicate wells of 4 healthy controls, and 4 PAH patients in the Seahorse XF analyzer. Data were normalised to protein concentration for each experiment across all cells in each well.

Glycolysis Stress Test - changes in ECAR parameters:

- Glucose was injected to evaluate the normal rate of glycolysis in the cells. PAH cells showed a significant increase in glycolysis. The silencing of CLIC and the overexpression of MFN2 significantly reduced glycolysis in PAH ECFCs (Figure 7.15; A).
- Glycolytic capacity: the final injection of 2-DG returned ECAR to its base level, confirming that the ECAR produced in the experiment was due to glycolysis. PAH ECFCs showed a significant increase in glycolytic capacity compared to healthy ECFCs. The silencing of CLIC1, CLIC4 and the overexpression of MFN2 reduced glycolytic capacity of PAH ECFCs (Figure 7.15; B).
- The glycolytic reserve indicates the capability of ECFCs to respond to increased energy demand and shows how close the glycolytic function is to the cell's theoretical maximum. The glycolytic reserve was not significantly changed in all groups (Figure 7.15; C).
- Non-glycolytic acidification measures other sources of extracellular acidification that are not attributed to glycolysis. Non-glycolytic acidification was significantly reduced in PAH ECFCs compared with healthy controls, and was not affected by compensatory changes in CLIC1, CLIC4 and MFN2 expression (Figure 7.15; D).

Representative examples of ECAR data provided by the XF Glycolysis Stress Test report generator are shown in Figure 7.14.

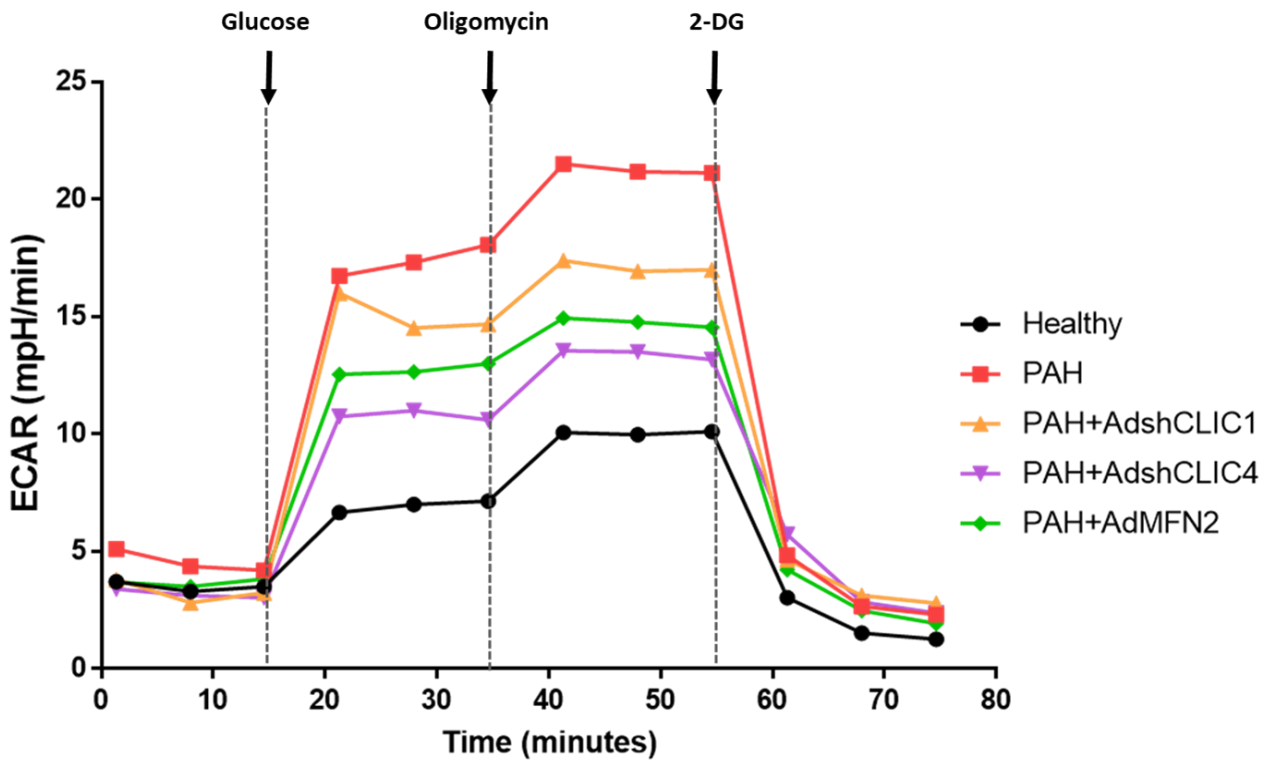


Figure 7.14: Example of extracellular acidification rate (ECAR) measurement in ECFCs from patients and healthy controls. ECFCs were infected with AdCTRL (Healthy and PAH groups), AdshCLIC1, AdshCLIC4, AdMFN2 as indicated, and ECAR was measured at various time intervals following the injection of glucose at 15 minutes, oligomycin at 34 minutes, and 2-DG at 54 minutes Black circle=Healthy+AdCTRL; red square=PAH+AdCTRL; orange triangle=PAH+AdshCLIC1; purple triangle=PAH+AdshCLIC4; green diamond=PAH+AdMFN2. Abbreviations: 2-DG, 2-Deoxy-glucose; ECAR, extracellular acidification rate. ; PAH, pulmonary arterial hypertension. Representative trace from four independent experiments.

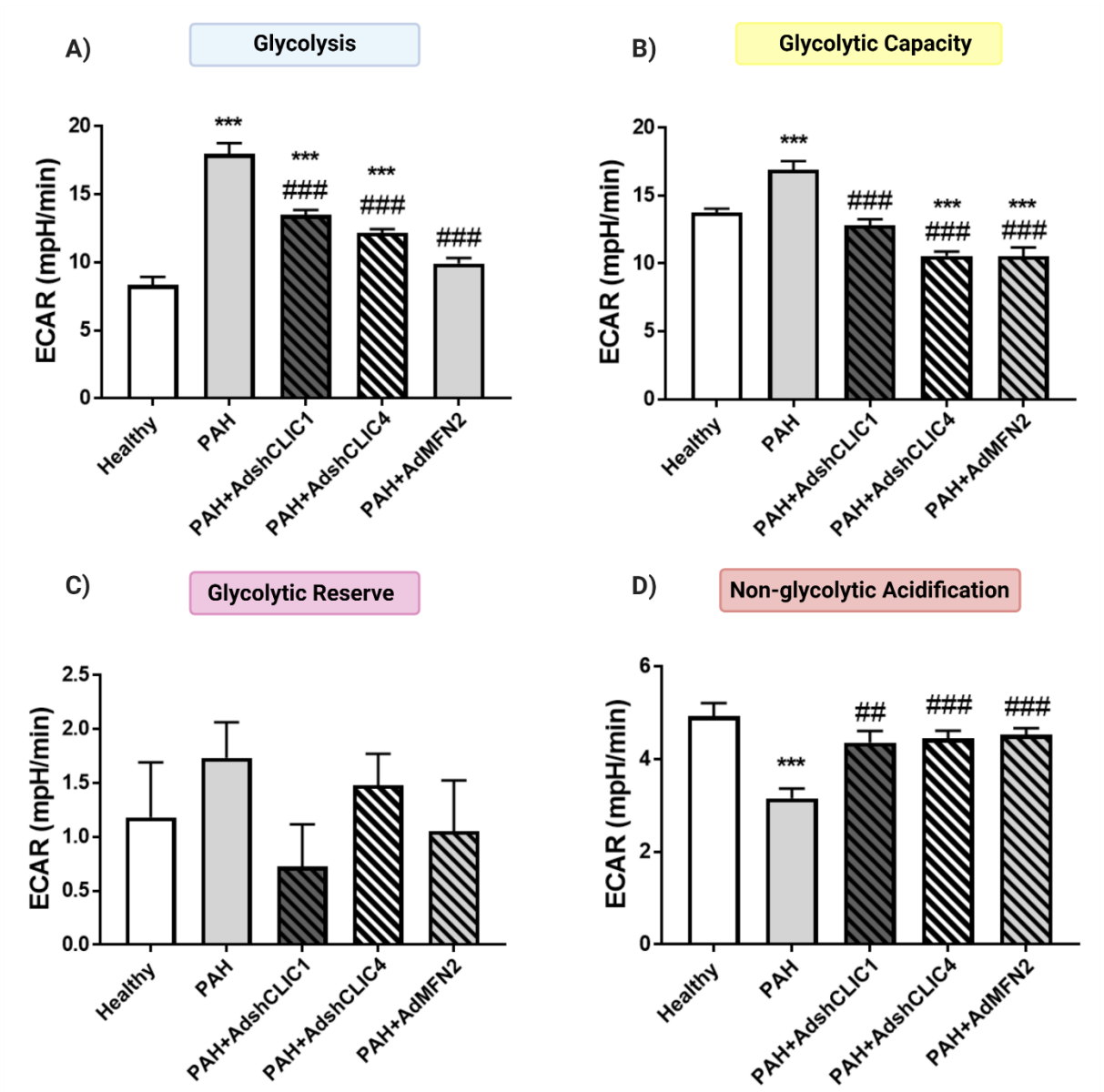


Figure 7.15: Effect of CLIC inhibition and MFN2 overexpression on acidification rate in healthy and PAH ECFCs. Cells were infected with either AdCTRL (Healthy and PAH), AdshCLIC or AdMFN2 and key parameters of glycolytic function were measured using the Seahorse XFp Cell Glyco Stress Test. *P <0.05, **P <0.01 ***P<0.0001, comparison with the healthy group (healthy ECFCs infected with AdCTRL); #P<0.05, ##P <0.01 ###P<0.000, comparison with PAH group (PAH ECFCs infected with AdCTRL) using One-way ANOVA with Tukey's multiple comparison test. Data are presented as mean ± SEM of 4 independent experiments with 4 to 8 replicate wells of 4 healthy controls, and 4 PAH patients in the Seahorse XF analyser. Data were normalised to protein concentration for each experiment across all cells in each well.

7.5 Summary

The key findings presented in this chapter show that:

- Mitochondrial fragmentation was highly increased in PAH ECFCs, but was reduced by overexpression of MFN2.
- Mitochondrial membrane potential was significantly increased in PAH ECFCs, and MFN2 reduced this effect.
- Basal respiration, ATP production, maximal respiration, and spare respiratory capacity were significantly reduced in ECFCs from PAH patients. The inhibition of CLIC1, CLIC4 and the overexpression of MFN2 brought all mentioned parameters to the levels seen in healthy controls.
- PAH ECFCs showed increased proton leak compared with healthy controls. CLIC1, CLIC4 silencing and MFN2 overexpression decreased proton leak in PAH ECFCs to control levels.
- The inhibition of CLIC1, CLIC4 and the overexpression of MFN2 in patient ECFCs inhibited glycolysis and glycolytic capacity.

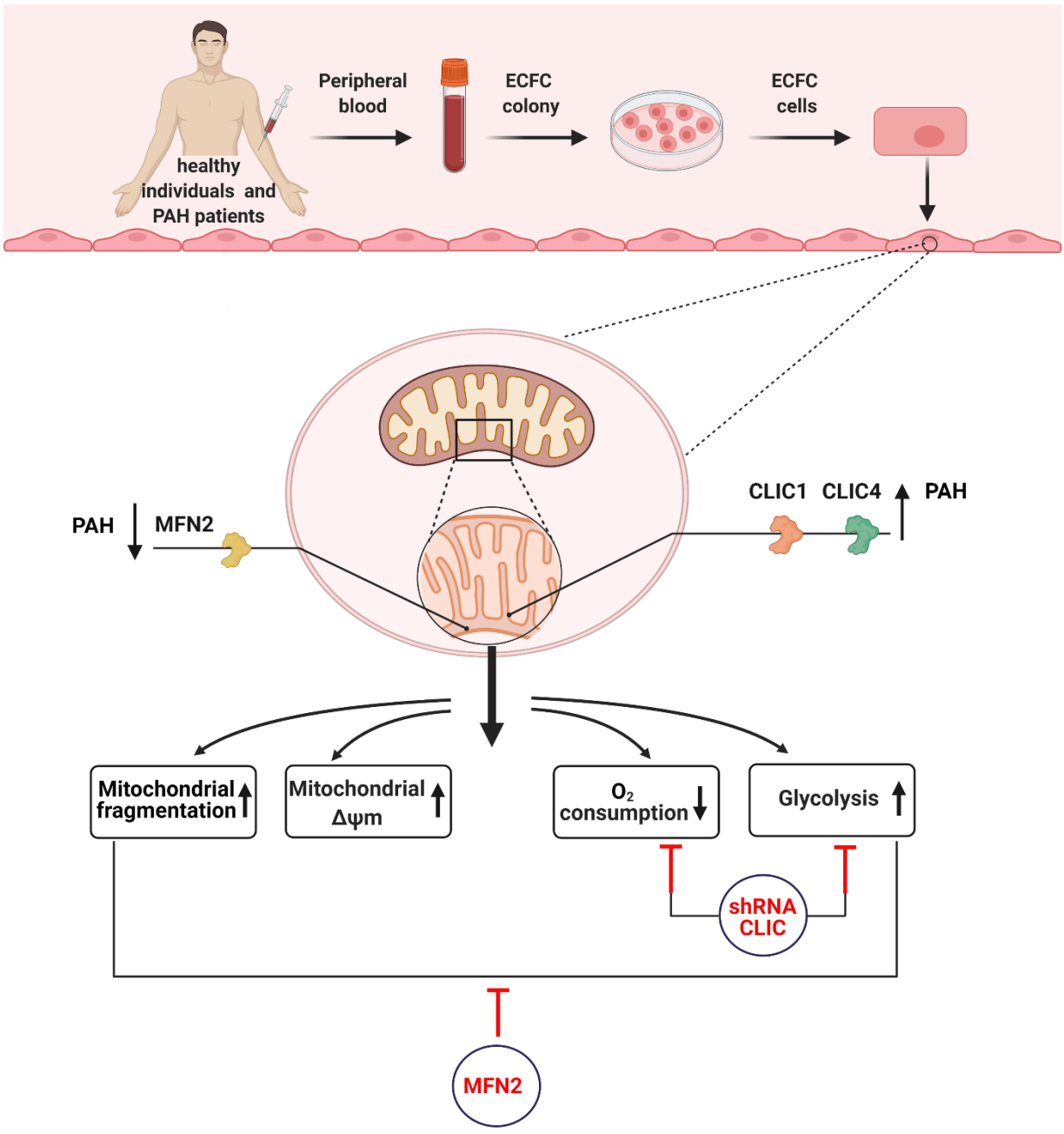


Figure 7.16: Summary of key results in Chapter 7. Details of key findings are presented in Table 7.2. Abbreviations: ECFCs; endothelial colony forming cells, PAH; pulmonary arterial hypertension, MFN2; mitofusin 2, CLIC; chloride intracellular channel, ΔΨm; mitochondrial membrane potential. Illustration created by the author using BioRender.com.

Table 7.2: Summary of key findings of the effect of CLIC proteins inhibition and overexpression of MFN2 on mitochondrial function in ECFCs from patients and healthy controls. Red arrows pointed upwards indicate increase, black arrows pointed downwards indicate decrease, ND; not determined, and the dash (–) indicates no change.

Investigation	Healthy	PAH	shRNA-CLIC1	shRNA-CLIC4	AdMFN2
Mitochondrial fragmentation	—	↑	ND	ND	↓
Mitochondrial membrane potential	—	↑	ND	ND	↓
Basal respiration	—	↓	↑	↑	↑
ATP production	—	↓	↑	↑	↑
Maximal respiration	—	↓	↑	↑	↑
Proton leak	—	↑	↓	↓	↓
Spare respiratory capacity	—	↓	↑	↑	↑
Non-mitochondrial respiration	—	↑	↑	↑	↑
Glycolysis	—	↑	↓	↓	↓
Glycolytic capacity	—	↑	↓	↓	↓
Non-glycolytic acidification	—	↓	↑	↑	↑
Glycolytic reserve	—	—	—	—	—

7.6 Discussion

ECFCs have been widely used to investigate the pathogenesis of PAH (Paschalaki and Randi 2018). They are a powerful tool for studying the molecular mechanisms of endothelial dysfunction in disease in a non-invasive way (Medina, O'Neill et al. 2012). This study therefore investigated the contribution of CLIC1 and CLIC4 to mitochondrial dysfunction in PAH ECFCs. The results showed that CLIC1 and CLIC4 levels are elevated in PAH ECFCs, which is consistent with previously reported increases in CLIC1 and CLIC4 expression in the endothelium of the remodelled pulmonary vasculature (Abdul-Salam et al. 2010, Singh 2010, Wojciak-Stothard et al. 2014). MFN2 downregulation was also observed in PAH ECFCs, reflecting the trend seen in PAH vasculature (Ryan et al. 2013). The reduction of MFN2 expression in PAH has been linked to increased mitochondrial fragmentation and endothelial apoptosis (Lugus et al. 2011). We consistently observed increased mitochondrial fragmentation in ECFCs from PAH patients compared to healthy controls, which was reversed by MFN2 overexpression. Increased mitochondrial fragmentation can also be associated with pro-survival and pro-proliferative effects and this is more likely to be the case for CLIC1- and CLIC4-induced signalling. CLIC1 and CLIC4 overexpression improves PAEC survival and induces angiogenesis, so the observed changes in mitochondrial function and dynamics are likely to facilitate endothelial repair under stress conditions.

We noted that the mitochondria from PAH ECFCs were hyperpolarized, which is a feature of mitochondria from PAH vasculature (Sutendra and Michelakis 2014). Our results suggest that most of the observed CLIC1- and CLIC4-induced effects on mitochondrial structure and function are likely to be the consequence of reduced expression of MFN2. MFN2 has multiple regulatory

functions, which include the regulation of mitochondrial membrane potential, fuel oxidation and the OXPHOS system (Schrepfer and Scorrano 2016). Consistent with this, we observed that the overexpression of MFN2 restored mitochondrial membrane potential, mitochondrial respiration and glycolysis in PAH ECFCs to the levels seen in healthy cells. PAH ECFCs showed reduced mitochondrial ATP production resulting from a metabolic shift from oxidative phosphorylation towards glycolysis, a phenomenon also known as the Warburg effect which has been reported in PAH (Chan and Rubin 2017). Studies in human, rodent, avian and lamb PH have demonstrated that endothelial cells generate energy mainly from glycolysis (Bonnet et al., 2006). The inhibition of MFN2 increases glycolysis and glucose uptake, while inhibiting mitochondrial respiration, increasing proliferation and inhibiting apoptosis in *in vitro* and *in vivo* (Peng et al., 2015, Schrepfer & Scorrano 2016), and this agrees with our observations. High levels of proton leak in ECFCs from PAH patients was reduced by CLIC1 and CLIC4 silencing as well as the overexpression of MFN2. Increased proton leak level suppresses ATP synthesis in cardiovascular disease, cancer and age-related disease caused by oxidative stress (Cheng et al., 2017), so a reduction is likely to improve mitochondrial ATP generation in diseased cells. Understanding the role of ECFCs in PAH may ultimately lead to the discovery of new biomarkers of PAH or to the use of ECFCs in potential therapies (Smits et al., 2018).

In conclusion, this study demonstrated a major mitochondrial dysfunction in PAH ECFCs which is likely to reflect the changes seen in PAH endothelium, including increased mitochondrial fragmentation, mitochondrial membrane potential ($\Delta\Psi m$), glycolysis and the inhibition of mitochondrial respiration. These changes are likely to be mediated, at least in part, by CLIC1- and CLIC4-induced reduction in MFN expression.

CHAPTER 8

General Discussion

CHAPTER 8: General Discussion

Endothelial and vascular smooth muscle cells in PAH vasculature display alterations in mitochondrial dynamics and function, including mitochondrial fragmentation (fission), the hyperpolarization of mitochondrial membrane, increased mitochondrial ROS generation, imbalance in mitochondrial biogenesis and mitophagy and a metabolic switch from mitochondrial oxidative phosphorylation towards cytoplasmic glycolysis (Marshall et al., 2018; Ranchoux et al., 2016).

In this study, I hypothesized that CLIC1 and CLIC4 proteins, which are highly expressed in PAH endothelium (Wojciak-Stothard et al., 2014) act as regulators of mitochondrial biogenesis and mitochondrial function.

8.1 CLIC1 and CLIC4 regulate mitochondrial structure and dynamics in pulmonary endothelial cells

The data in this study show that CLIC1 and CLIC4 overexpression induces mitochondrial fragmentation and the accumulation of mitochondrial networks in the perinuclear region of HPAECs. Mitochondrial fragmentation facilitates the transport of mitochondria to high-energy demanding sites within the cell (Youle & Van Der Bliek, 2012) and is essential for supplying mitochondria into daughter cells during cell division (Taguchi et al, 2007). Pathological rates of mitochondrial fission are therefore likely to facilitate cell proliferation and vascular remodelling in PAH (Marsboom et al., 2012). The fact that increased mitochondrial fragmentation coincides with heightened proliferative and angiogenic responses in PAH ECFCs (Joo et al., 2015; Yoder et al., 2007) corroborates this hypothesis. The increase in mitotic fission in PAH favours rapid cell cycle progression as well as apoptosis resistance. Comparable changes in mitotic fission have been reported as a result of similar mechanisms in cancer (Rey-Parra et al., 2008). Mitochondrial

fragmentation has also been linked to apoptosis and the permeabilization of the mitochondrial outer membrane (Ryan et al., 2015). However, previous findings have shown that CLIC1 and CLIC4 trigger anti-apoptotic and pro-proliferative responses in endothelial cells, which suggests that mitochondrial fragmentation is more likely to be linked with endothelial regeneration in response to stress conditions than with endothelial apoptosis.

The mitochondrial fragmentation mechanism in PAH is caused by an imbalance in mitochondrial fusion, fission and mitophagy. This imbalance has been linked with the reduced expression of fusion regulator MFN2 (Ryan et al., 2013), the activation of fission regulator Drp1 (Marsboom et al., 2012) and the epigenetic upregulation of expression of DRP1 (Chen et al., 2014) or its binding partners (MiD49 and MiD51) (Chen et al., 2018).

Observations reported in this study suggest that MFN2 is a key mediator of the CLIC1-and CLIC4-induced effects on mitochondrial fragmentation and function in HPAECs. MFN2 expression was reduced by CLIC1 and CLIC4 in HPAECs, along with other fusion regulators OPA1, MFN1, and these changes are known to cause fragmentation of the mitochondrial network and induce mitochondrial dysfunction (Dasgupta et al., 2011; Ishihara et al., 2004). However, we cannot exclude the role of MFN1 in this process, as MFN1 and MFN2 have both redundant and distinct functions and can act in three separate molecular complexes to promote mitochondrial fusion (Chen et al., 2003). Preliminary data from proteomic analysis of mitochondria from CLIC1- and CLIC4-overexpressing HPAECs confirmed the differential expression of several proteins involved in the regulation of mitochondrial fission, fusion and mitophagy. However, these data were obtained from pooled samples and will need further validation.

The mechanisms of CLIC1-and CLIC4-induced reduction in the expression of MFN2, MFN1 and OPA1 will require further study. It is possible that this regulation occurs indirectly, and is mediated by CLIC1- and CLIC4 interactions with other regulatory proteins. For example, CLIC4 activates HIF-1α (Wojciak-Stothard et al., 2014) and HIF stabilization promotes mitochondrial fission in PAH (Wolin, 2012). Meanwhile, HIF-1 suppresses the expression of peroxisome proliferator-activated receptor gamma coactivator 1-alpha (PGC-1α), which acts as a transcriptional activator of MFN2, leading to reduced MFN2 expression and resulting in mitochondrial fragmentation, increased cell proliferation and decreased apoptosis, which are the characteristics of PAH (Ryan et al., 2013). The activity of fission mediator DRP-1 may also be suppressed by MFN2, resulting in fragmented mitochondria (Van der Bliek et al., 2013).

The localization of CLIC1 and CLIC4 to the outer and inner mitochondrial membrane, as well as mitochondrial cristae, was confirmed by immunogold staining. CLIC4 has previously been identified in the inner mitochondrial membrane of mouse keratinocytes (Fernández-Salas et al., 1999) and in the outer mitochondrial membrane of adult cardiomyocytes (Ponnalagu et al., 2016a), and this study is the first to document its presence in the inner and outer mitochondrial membranes of endothelial cells. This study is also the first to demonstrate the localization of CLIC1 within the mitochondrial structure, as previous findings have only documented its presence by western blotting in subcellular fractions of osteoblastic cells (Yang et al., 2009).

CLIC1 and CLIC4 induced a significant decrease in the number of mitochondrial cristae in HPAEC mitochondria. The modulation of cristae structure affects the electron transport chain and impairs mitochondrial dynamics and respiration (Norton et al., 2014). This effect may be directly

linked to a reduction in MFN2 expression, as the remodelling of cristae involves the MFN2-dependent cleavage of OPA1 (Sood et al., 2014).

The results showed no direct associations between the polymerization status of actin and microtubules and CLIC-induced effects on mitochondrial fragmentation. However, CLIC1 and CLIC4 interact with microtubule-associated proteins such as dynein, dynamin-related protein 1 (DRP1) or ADP-ribosylation factor (Arf) (Ackema et al., 2014; Pimkina & Murphy, 2011), as well as proteins regulating actin dynamics, such as Arp2,3 complex (Mathur, 2005). The movement of mitochondria along microtubules depends on microtubule-associated proteins (MAPs) such as dyneins and kinesins (Anesti & Scorrano, 2006), so it is likely that the association of CLIC proteins with these proteins will have an impact on the intracellular distribution of mitochondria.

The mitochondrial network and microtubules of hyperproliferating cells tend to show perinuclear organization that is consistent with the phenotype observed in CLIC1- and CLIC4-overexpressing cells. In contrast, CLIC5 overexpressing cells are elongated, with microtubules and mitochondrial networks that extend to the cell periphery. CLIC5 affects cell movement, swelling or cell division, vesicular transport and apoptosis through its relationship with F-actin (Singh et al., 2007b). The role of CLIC5, likely to impact the function of cardiomyocytes, will require further investigation.

Mitophagy was previously thought to take place at random, but studies involving mitochondrial damage and hypoxia have proved the selective nature of this process (Chiu et al., 2009). Evidence from several cohort studies suggests that the process of mitochondrial autophagy depends upon both the activation of fission and an increase in mitochondrial oxidant production (Zhong et al., 2012). It has been reported that mitophagy regulators such as LC3B and Parkin are elevated in the lungs of PH patients (Zhai et al., 2018), representing changes that were also seen in CLIC1-

and CLIC4-overexpressing HPAECs. Hypoxia increases the expression of CLIC1 and CLIC4 in PH lungs (Abdul-Salam et al., 2019) and promotes mitochondrial fragmentation and mitophagy (Liu et al., 2012). Consistent with this, we observed that CLIC1 and CLIC4 promoted mitochondrial fragmentation and stimulated mitophagy in HPAECs. The role of mitophagy is poorly understood, and can be associated with apoptosis (Zhong et al., 2012) or enhanced cell proliferation (Marshall et al., 2018). The exact role of mitophagy in PH is also unclear, with some studies reporting an increase (Zhai et al., 2018) and some a decrease in mitophagy (Deng et al., 2016). Ultimately, a dynamic balance between mitochondrial biogenesis and mitophagy regulates the size and function of the mitochondrial network. Given that there are over 40 regulatory proteins involved in this process, defining the exact mechanism accurately constitutes a challenge (Aggarwal et al., 2016).

8.1.1 MFN2 mediates effects of CLIC proteins on mitochondrial membrane potential and ROS generation

Mitochondria-derived reactive oxygen species (mtROS) are key mediators of cellular stress responses, and are considered to be risk factors in many cardiovascular diseases (Tang et al., 2014). We observed that the overexpression of CLIC1 and CLIC4 increased mitochondrial membrane potential and promoted ROS generation in HPAECs. Alterations in mitochondrial membrane potential can trigger excessive mtROS generation in response to stress conditions associated with aging, hypercholesterolemia, hyperglycaemia, smoking, infection and hypoxia (Dromparis & Michelakis, 2013). Mitochondria are the main source of ROS generation in the pulmonary vasculature, with superoxide and hydrogen peroxide acting as mediators of pulmonary vascular cell proliferation (Freund-Michel et al., 2013; Wedgwood et al., 2001). The primary sites of ROS production in the mitochondrial electron transport chain are Complex I,

Complex II, and Complex III (Dromparis & Michelakis, 2013). Meanwhile, mitochondrial ROS production is directly coupled to mitochondrial membrane potential (Korshunov et al., 1997; Lambert & Brand, 2004). Membrane potential is not only essential for ATP generation, but is also important for mitochondrial fusion, the import and export of proteins across the mitochondrial membrane and the exchange of metabolites with cytosol and apoptosis induction. Δψm is therefore thought to play a central role in mitochondrial health (Forkink et al., 2014; Zorova et al., 2018). Mitochondrial hyperpolarization seen in CLIC-overexpressing endothelial cells and PAH ECFCs is a feature shared with many forms of cancer (Sutendra & Michelakis, 2014).

Mitochondria with higher Δψm tend to generate higher levels of mitochondrial superoxide (Marshall et al., 2018) and increases in Δψm also contribute to the elevation of reactive oxygen intermediates (ROI) generation, reduction in ATP production and inflammation (Gergely et al., 2002). Mitochondria-derived ROS mediate pro-thrombotic and pro-inflammatory responses in the vascular endothelium in PH (Marshall et al., 2018). Mitochondrial ROS generation has been linked to HIF-1α stabilisation (Aggarwal et al., 2013). CLIC4 induces a pseudo-hypoxic state in HPAECs which is characterised by the activation of HIF and the increased expression of HIF-dependent proteins, including ET-1, VEGF and glycolytic enzymes (Wojciak-Stothard et al., 2014). It is therefore likely that CLIC4-induced changes in Δψm and mtROS production are mediated by HIF.

CLIC1 has also been shown to use ROS as secondary messengers. Silencing CLIC1 expression reduces the phosphorylation of extracellular signal related kinase (p-ERK1/2) and matrix metalloproteinase 2 and 9 (MMP 2, 9) (Tian et al., 2014), which are both downstream targets of oxidative stress pathways in cancer (Gan et al., 2014; Lehner et al., 2011).

The mechanism by which mitochondrial ROS increase during PH development is not clear (Lambert & Brand, 2004). According to our results, the CLIC-induced inhibition of MFN2 is likely to play a role in this process, as compensatory MFN2 overexpression was able to restore Δψm and mtROS in CLIC1- and CLIC4-overexpressing HPAECs to the levels seen in healthy controls. In accordance with the hypothesised role of MFN2 in our study, MFN2 was shown to reduce oxidative stress in diabetic cardiomyopathy (Hu et al., 2019). Mitofusin 2 mutations in fibroblasts were shown to affect mitochondrial function by mitochondrial DNA depletion, suggesting that other regulatory pathways (Vielhaber et al., 2013) might be involved in CLIC1/CLIC4-MFN2-induced mitochondrial dysfunction.

Interestingly, increased mtROS generation also increase the expression of CLIC proteins in pulmonary endothelial vasculature, suggesting the existence of a positive regulatory feedback loop (Wojciak-Stothard et al., 2014).

8.1.2 CLIC-induced reduction in MFN2 contributes to the Warburg effect

Metabolic shift from mitochondrial oxidative phosphorylation to aerobic glycolysis, known as the Warburg Effect, is a key feature of PAH (Ranchoux et al., 2016). The Warburg effect is associated with the hyperproliferation of vascular endothelial and smooth muscle cells and increased apoptosis resistance (Marshall et al., 2018). The main site of oxygen consumption in mitochondria is cytochrome c oxidase (complex IV) (Kluge et al., 2013), and alterations in mitochondrial metabolism are associated with changes in mitochondria-derived ROS generation, mitochondrial membrane potential and mitochondrial morphology (Dasgupta et al., 2011).

The high expression levels of CLIC1 and CLIC4 seen in PAH endothelium are likely to contribute to the Warburg effect. Our data showed that CLIC proteins induced a significant metabolic shift

toward glycolysis. The oxygen consumption rate (OCR) was decreased in endothelial cells that overexpressed CLIC1 and CLIC4, resulting in a significant reduction in ATP production and increased proton leak. These observations conform with published data showing that mitochondrial ROS generation is directly proportional to the extent of the proton leak (Tabassum et al., 2020). Proton leak is also a sign of poor mitochondrial health and reduced ATP generation. ATP is generated during the re-entry of protons into the mitochondrial matrix via complex V, so an increased proton leak would depict the protons that migrate into the matrix without producing ATP (Lassègue et al., 2012).

The compensatory metabolic switch to glycolysis was also confirmed by elevated extracellular acidification rates (ECARs) in CLIC1- and CLIC4-overexpressing HPAECs and PAH ECFCs. These effects are likely to be mediated by the activation of HIF, a known inducer of glycolysis.

CLIC4 induces HIF-1α activity in normoxic HPAECs as a result of NFκB activation (Wojciak-Stothard et al., 2014). The normoxic stabilization of HIF by CLIC proteins is likely to drive vascular remodelling fuelled by glycolysis, increasing the availability of non-oxidized lipids, amino acids and essential sugars for rapid cell proliferation (Paulin & Michelakis, 2014). HIF-1α was shown to compromise mitochondrial function and oxygen consumption in some tumour cells by inactivating the pyruvate dehydrogenase complex (Marshall et al., 2018).

Increased aerobic glycolysis in PAH has been linked to the activation of HIF-1α, which activates pyruvate dehydrogenase kinase (PDK). This leads to the inhibition of pyruvate dehydrogenase and the epigenetic regulation of superoxide dismutase 2 (*SOD2*) gene (Leopold & Maron, 2016). Consistent with the observations in PAH tissues, our data showed an upregulation of PDK 1 and

2 in CLIC1 and CLIC4-overexpressing HPAECs, which is likely to lead to phosphorylation and inhibition of pyruvate dehydrogenase.

Increased experimental evidence supports a critical role of MFN2 in the regulation of cell metabolism. Cells with low MFN2 activity appear to rely on anaerobic glycolysis to generate energy (Bach et al., 2003; Chandhok et al., 2018). In line with this, our data show that CLIC-overexpressing HPAECs and PAH ECFCs tend to have low expression levels of MFN2 and display higher aerobic glycolysis levels and reduced ATP production compared with control cells. This effect was reversed by compensatory overexpression of MFN2.

8.1.3 Contribution of ECFCs to PH pathology

A deeper understanding of the functional phenotype of ECFCs is required to establish them as an endothelial cell model for PAH. This study and others have demonstrated that ECFCs derived from PAH patients exhibit numerous characteristics that are similar to those shown by endothelial cells in the pulmonary vasculature of PAH patients, including increased mitochondrial fragmentation, elevated mitochondrial membrane potential and compromised endothelial function (Abdul-Salam et al., 2019; Paschalaki & Randi, 2018; Russomanno et al., 2020; Sindi et al., 2020; Smits et al., 2018). The origin of ECFCs and their role in the pathogenesis of the disease is not yet fully understood.

ECFCs might provide a valuable surrogate source of patient-specific endothelial-like cells that could be used to test potential therapeutic approaches and reduce the need to use animal models of PH (Faris et al., 2020). The phenotype of PAH ECFCs suggests that they are highly proliferative and angiogenic cells that are primed to facilitate endothelial repair, but can also potentially contribute to the formation of plexiform lesions (Smits et al., 2018). However, the

clinical potential of targeting ECFCs or using them to repair vascular damage in human disease will require further investigation and careful consideration (Faris et al., 2020; O'Neill et al., 2018).

8.1.4 Potential therapeutic benefits of targeting CLIC and MFN2 in PH

Despite the extensive research, there is currently no cure for pulmonary hypertension, and the existing treatments provide only a symptomatic relief (Leopold & Maron, 2016). Several regulators of mitochondrial function in PAH have been identified, but the strategies of therapeutic targeting are still under development (Marshall et al., 2018). The role of mitochondria in the complexity of lung biology is gaining more attention, and acquired mitochondrial dysfunction is now broadly accepted as a contributary mechanism to many pathological features of pulmonary vascular disease in PAH.

CLIC proteins may represent potential targets for reducing metabolic dysfunction and, arising from this, cell hyperproliferation and plexiform lesion formation in PAH. However, an additional difficulty may arise from the fact that CLIC family members often show overlapping and redundant functionalities, therefore confusing the interpretation of the findings of single-gene targeting (Argenzio & Moolenaar, 2016). Our results confirm the existence of functional redundancy between CLIC1 and CLIC4, previously reported by others (Tung et al., 2009; Tung & Kitajewski, 2010). Overexpression of either protein had similar effects in HPAECs, while single knockdowns of either CLIC1 or CLIC4 did not have a significant impact on mitochondrial function under basal conditions, suggesting the existence of compensatory mechanisms.

These proteins have overlapping functions, but it is likely that they are differentially regulated. CLIC4 but not CLIC1 is induced by tumour necrosis factor α (TNF-α), c-myc, p53 and Gram-negative bacterial lipopolysaccharide (LPS) (Domingo-Fernández et al., 2017; Fernández-Salas et

al., 2002; He et al., 2011; Shiio et al., 2006). CLIC1, but not CLIC4 is induced by phorbol-12-myristate-13 acetate (PMA), amyloid β activation of microglia, and oxidative stress H_2O_2 (Averaimo et al., 2010; Kanno & Takishima, 1990; Littler et al., 2004; Novarino et al., 2004; Xu et al., 2016).

The results reported here suggest that MFN2 may partially reverse the effect of CLIC-induced mitochondrial dysfunction in PAH vasculature. New strategies of therapeutic supplementation of MFN2 through the actions of regulatory microRNAs or via viral vectors *in vivo* will need to be established. As mitochondrial function necessitates a balance between fission and fusion, a prolonged overexpression of MFN2 may also have adverse effects on vascular function (Dasgupta et al., 2011). The delivery of therapeutic agents would have to be lung-specific to ensure targeting of pulmonary but not systemic vasculature. At present, identifying CLIC effectors and evaluating strategies that specifically target CLIC signalling in pulmonary hypertension might play a critical role in disease pathogenesis. Recently, our group has identified a novel strategy of blocking CLIC4 signalling in PAH using endothelium- targeted liposomal (DACC) siRNA delivery system in Sugen/hypoxia mice. This treatment reduced restored BMPRII expression and attenuated the development of PH in Sugen/hypoxia mice (Abdul-Salam et al., 2019), illustrating potential of CLIC proteins as therapeutic targets in PAH.

8.2 Conclusion

To summarize, this study is first to demonstrate the critical role of CLIC proteins in the regulation of mitochondrial function in pulmonary endothelial cells and to establish a link between CLIC-MFN2 signalling and mitochondrial dysfunction in PAH. The results of the study suggest that CLIC proteins modulate pulmonary vascular adaptation to environmental stress conditions by changing mitochondrial dynamics and increasing endothelial repair mechanisms. The dysregulated and prolonged overexpression of CLIC proteins may contribute to pulmonary vascular remodelling by enhancing glycolysis and mitochondrial superoxide production, further augmenting inflammatory, pro-proliferative and pro-angiogenic responses in vascular endothelial cells.

This study also demonstrates the potential therapeutic effects of MFN2 supplementation in CLIC-induced mitochondrial dysfunction. Further studies are needed in order to fully understand the nature of CLIC-MFN2 interaction within the mitochondrial membrane and address the mechanisms behind the observed alterations in mitochondrial function and energy metabolism as well as their role in pulmonary vascular remodelling in PAH. The hypothesized mechanism of CLIC signalling is shown in Figure 8.1.

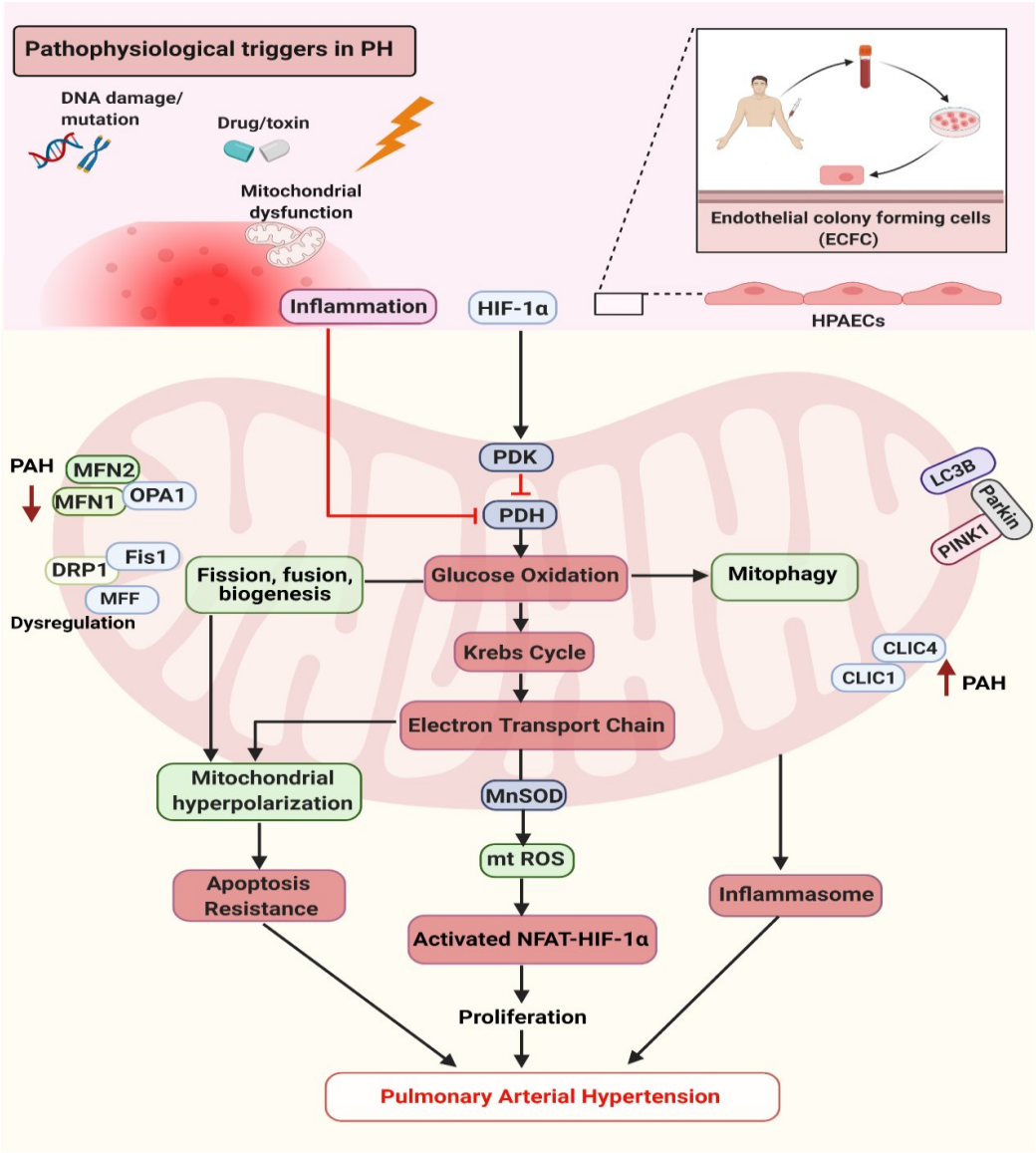


Figure 8.1: Mechanism of CLIC1- and CLIC4-induced changes in mitochondrial function in PAH. DNA mutations/damage, exposure to drugs, environmental toxins, or inflammation increase expression of CLIC1 and CLIC4 in pulmonary endothelium. CLIC1 and CLIC4 increase mitochondrial fragmentation, mitochondrial ROS generation, mitochondrial membrane potential, mitophagy, and induce a metabolic switch from oxidative phosphorylation towards glycolysis. These alterations are associated with increased HIF-1α, reduced expression of mitochondrial fusion regulators, MNF2, MFN1, and OPA-1, dysregulation in fission modulators, DRP1, MFF, and FIS1, increased mitophagy markers LC3B, and Parkin, likely to lead to apoptosis-resistance, excessive proliferation, mitochondrial hyperpolarization, and increased inflammation in pulmonary arterial hypertension. Red arrows indicate changes seen in PAH. Abbreviations: HIF-1α, hypoxia-inducible factor; MnSOD, manganese superoxide dismutase; mtROS, mitochondria-derived reactive oxygen species; NFκB, nuclear factor; PDH, pyruvate dehydrogenase; PDK, pyruvate dehydrogenase kinase; CLIC, chloride intracellular channel protein; LC3B, microtubule-associated protein 1-B light chain-3B; MFN1 &MFN2, mitofusin 1 &2; OPA1, optic. Illustration created by author using BioRender.

8.3 Study limitations

- In this study, we chose the adenoviral-mediated overexpression of CLIC proteins and MFN2 because of their high transduction efficiency. However, adenoviral overexpression models may not reflect transient physiological alterations in the expression levels of studied proteins.
- The study focused only on the effects of CLIC1 and CLIC4, as these two proteins were found to be overexpressed in PAH endothelial cells. However, the potential contributions of other CLIC proteins cannot be excluded. This will require further investigation.
- Due to the time limitations, we did not investigate the effect of CLIC silencing on mitochondrial ROS generation in cells derived from PAH patients. Such investigation would help us gain a deeper understanding of the role of CLIC proteins in mitochondrial function in PAH. However, MFN2 overexpression effect was determined in ECFCs mitochondrial function.
- Due to time limitations, the control for MFN2 overexoression effect on CLIC-induced mitochondrial fragmentation was not assessed on the same day, the effect of MFN2 was compared to CLIC-overexpressing HPAECs from previous experiments.
- Proteomic analysis was performed on pooled samples from 4 mitochondrial isolations, so the results will have to be validated further by a larger number of experimental repeats.
- The study focused on the investigation of CLIC-induced effects in cultured endothelial cells *in vitro*. The full evaluation of the role of CLIC-MFN2 signalling in pathological changes in

PAH vasculature needs to be addressed experimentally using pre-clinical models of PAH and tissues from PAH patients.

- The sample size for patient ECFCs represented the shortage of accessible ECFC populations available for our study.
- To date no selective CLIC inhibitor is available to explore the functional significance of inhibiting CLIC expression in PH animal modules.

8.4 Future Work

Future studies should evaluate the effect of CLIC overexpression on the activity of electron transport chain complexes I–IV in HPAECs in order to improve our understanding of the mechanisms of change in mitochondrial ROS generation and membrane potential. In addition, it would be valuable to investigate the role of MFN2 and CLIC proteins in smooth muscle cells (PASMCs). PASMCs possess more mitochondria than endothelial cells, and the effect of CLIC-MFN signalling on PASMC hyperproliferative phenotype may be substantially greater than the one seen in endothelial cells.

Perhaps more importantly, MFN2 has the ability to tether the mitochondrial membrane to the endoplasmic reticulum, so its overexpression (or silencing) may alter the interaction between these two organelles. Since we have established that CLIC1 and CLIC4 overexpression affects mitochondrial dynamics, it would be interesting to explore alterations in the interaction between mitochondria and the endoplasmic reticulum induced by CLIC proteins. This interaction regulates intra-mitochondrial calcium levels, mitochondrial membrane potential and mitochondria-dependent apoptosis in pulmonary arterial cells of PAH patients (Sutendra et al., 2011). Finally,

future work on proteomic analysis should explore the quantitative differences and the contribution of the detected proteins to CLIC-induced mitochondrial function.

Appendix

Appendix 1: Supplementary data and tables

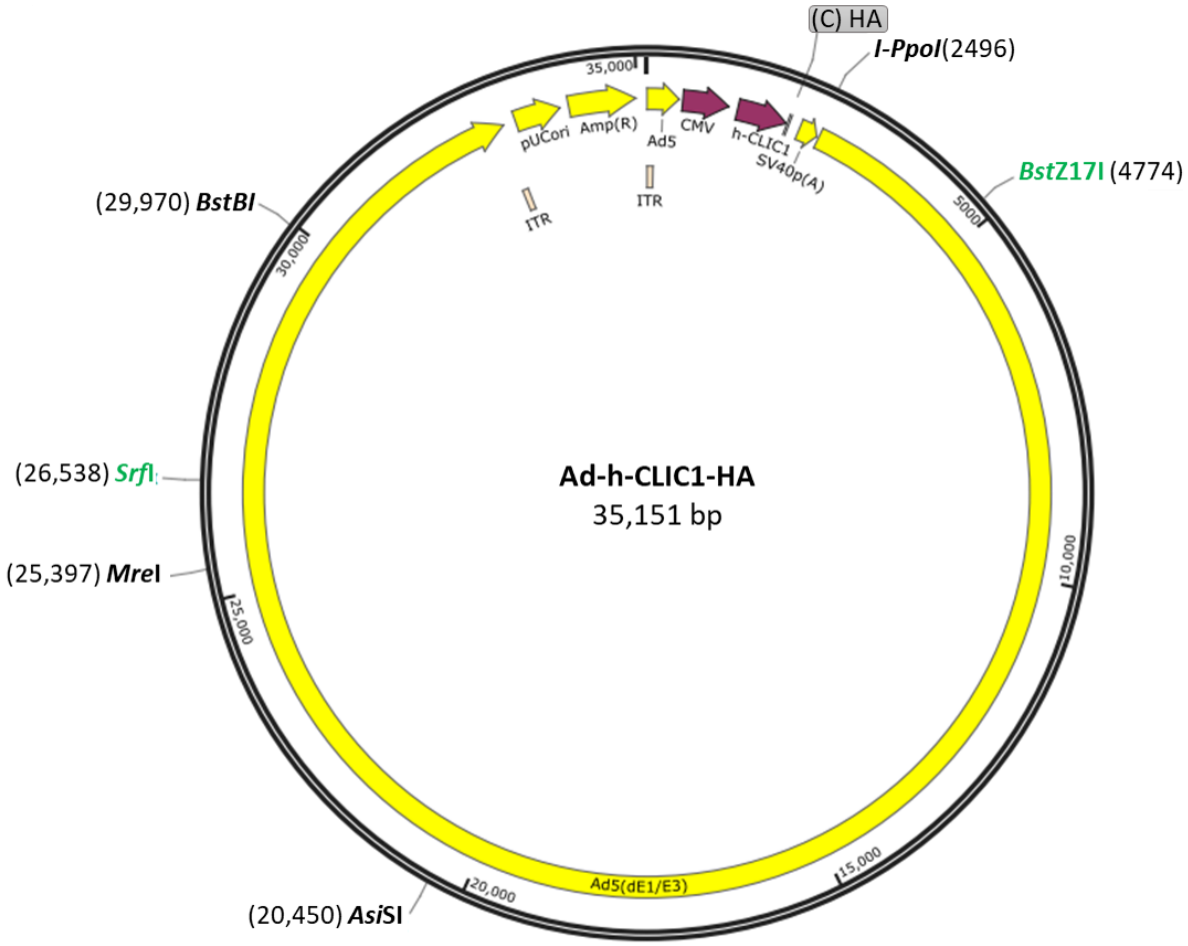


Figure S.1: Adenoviral vector map human CLIC1-HA. Backbone: human adenovirus Type 5; promoter: CMV; transgene: human CLIC1; marker/tag: HA (fused to C-terminal of GOI); RefSeq# BC095469. Map obtained from (Vector Biolabs, ADV-205450).

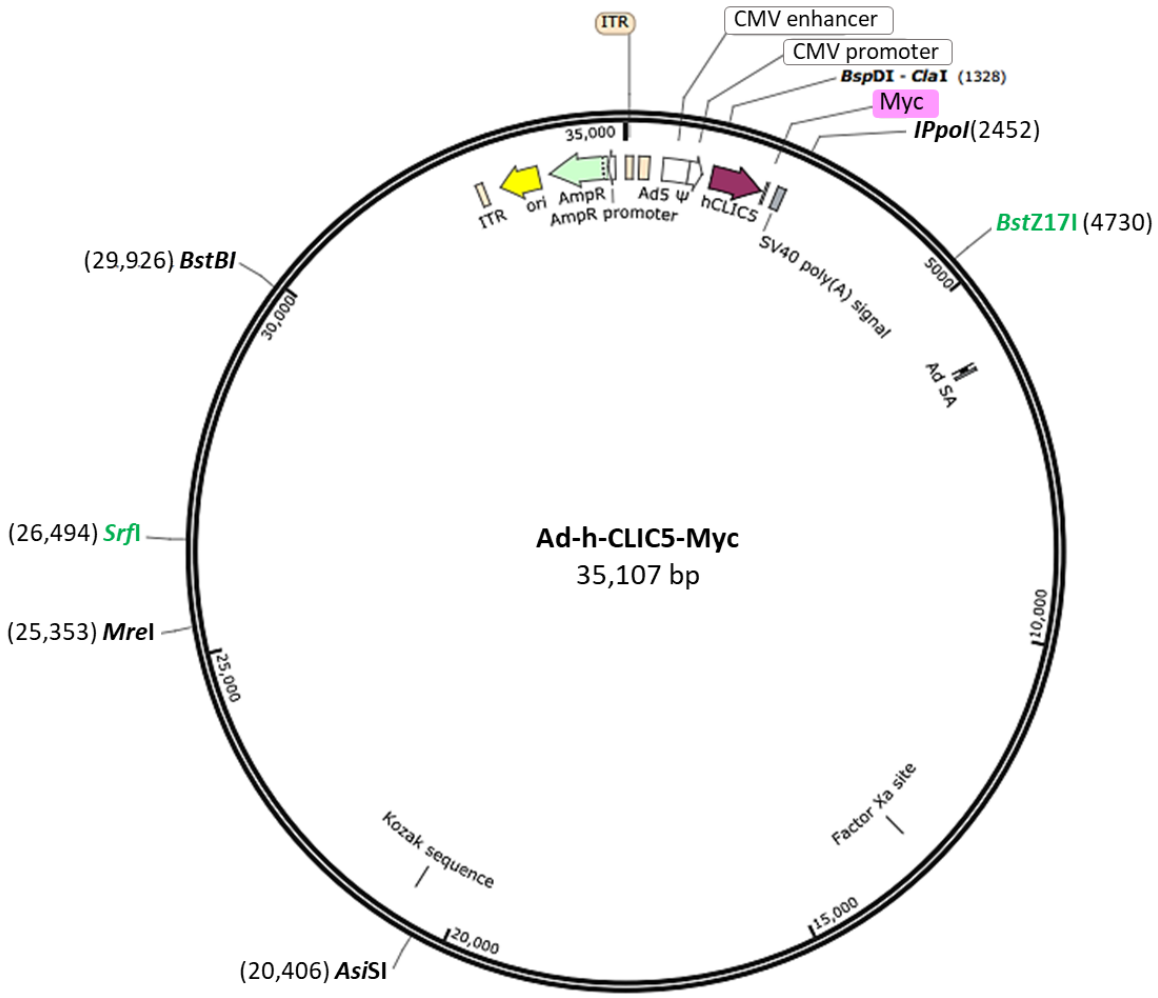


Figure S.2: Adenoviral vector map human CLIC5-Myc. Backbone: human adenovirus Type 5 (dE1/E3); promoter: CMV; transgene: human CLIC5; marker/tag: Myc (fused to C-terminal of GOI); RefSeq# BC035968. Map obtained from (Vector Biolabs, ADV-205455).

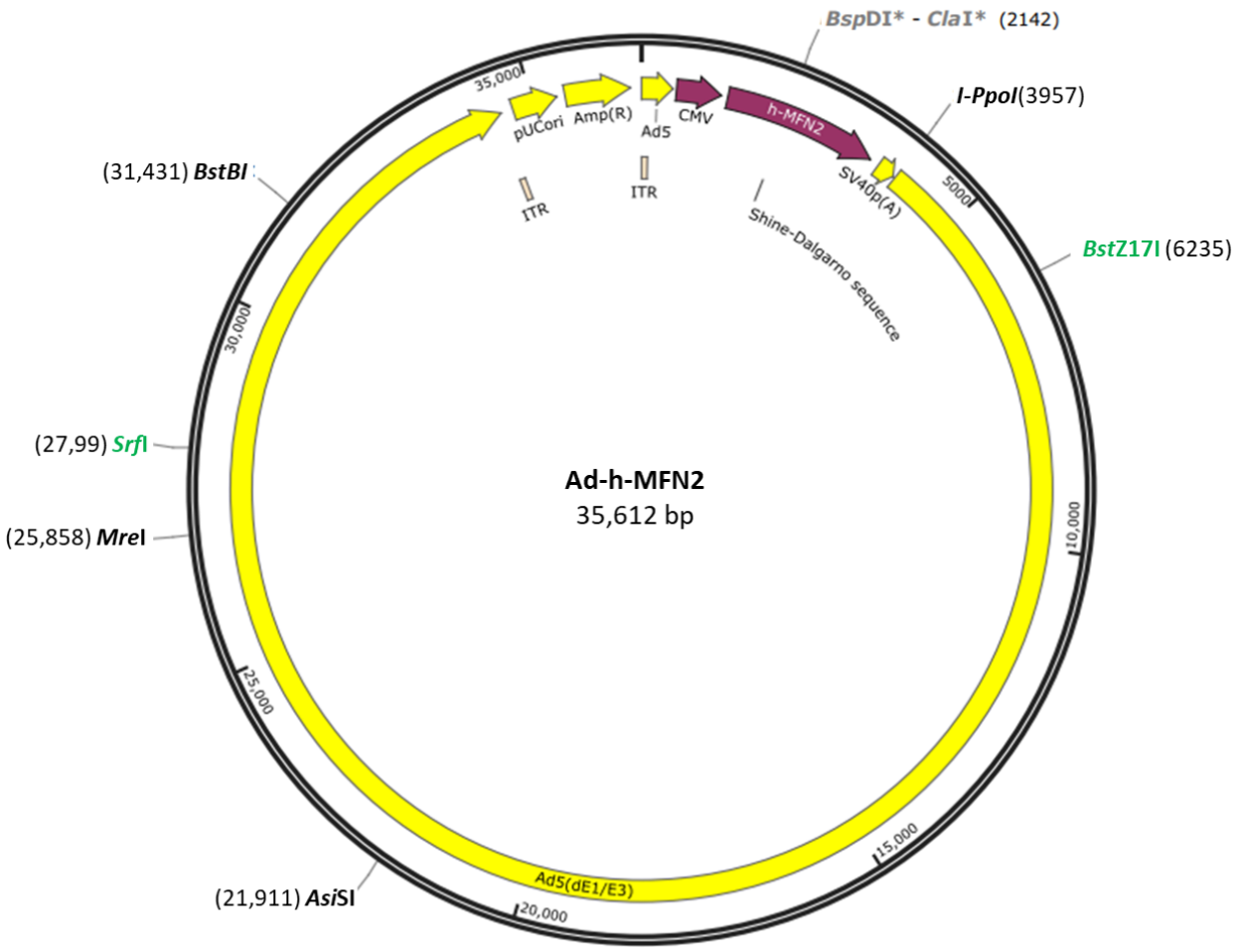


Figure S.3: Adenoviral vector map human MFN2. Backbone: human Adenovirus Type5 (dE1/E3); promoter: CMV; transgene: human MFN2; RefSeq# BC017061. Map obtained from (Vector Biolabs, ADV-215368).

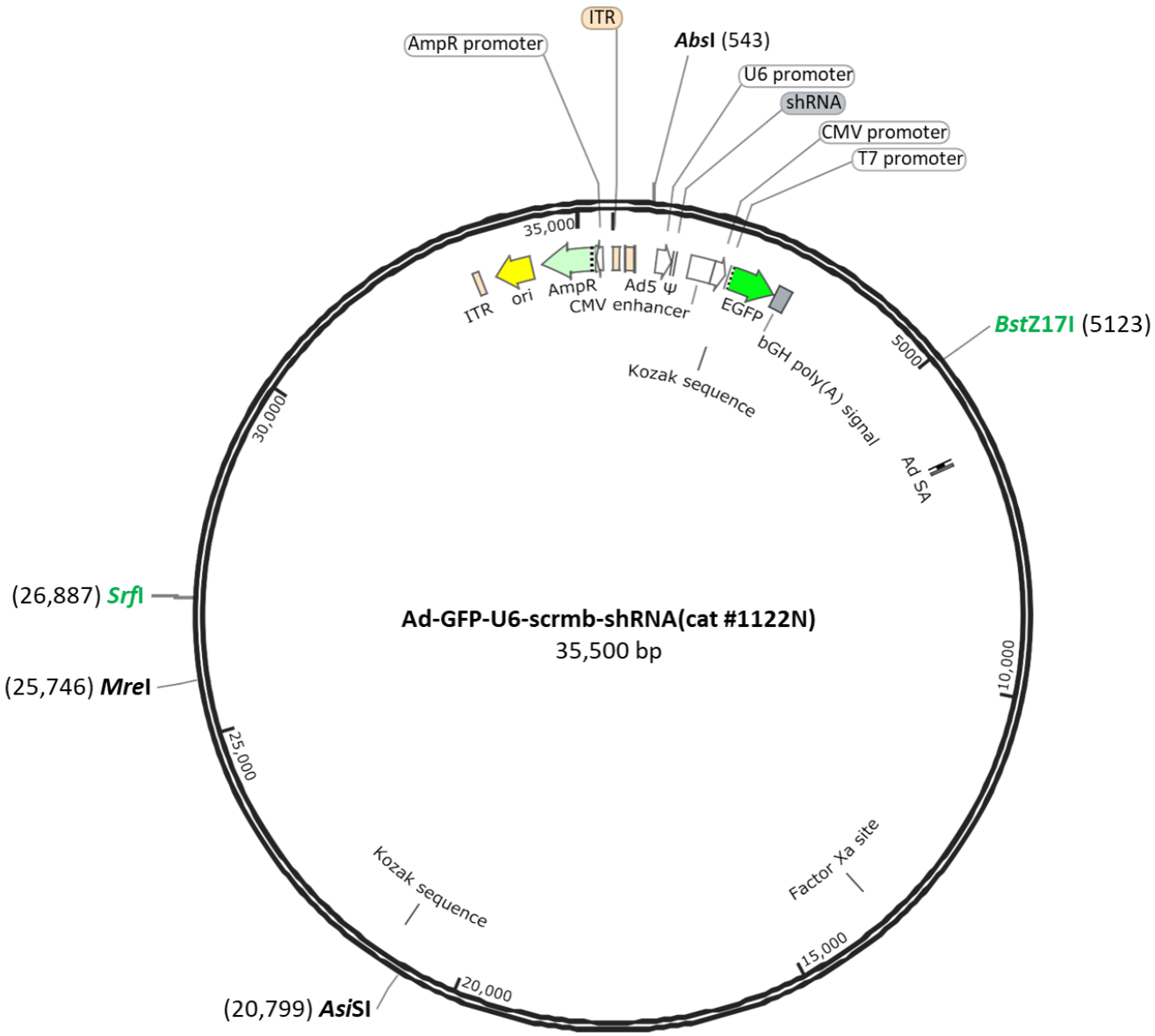


Figure S.4: Adenoviral vector map GFP-shRNA. Vector maps of other shRNA constructs differ only in the sequence of shRNA insert. Backbone: Adenoviral - Type 5 (dE1/E3); Promoter: U6; marker/tag: eGFP (under a CMV promoter); Ad-h-GFP-CLIC1-shRNA RefSeq# NM_001288; and Ad-h-GFP-CLIC4-shRNA RefSeq# NM_013943. Map obtained from (Vector Biolabs, shADV-205450, and shADV-205454).

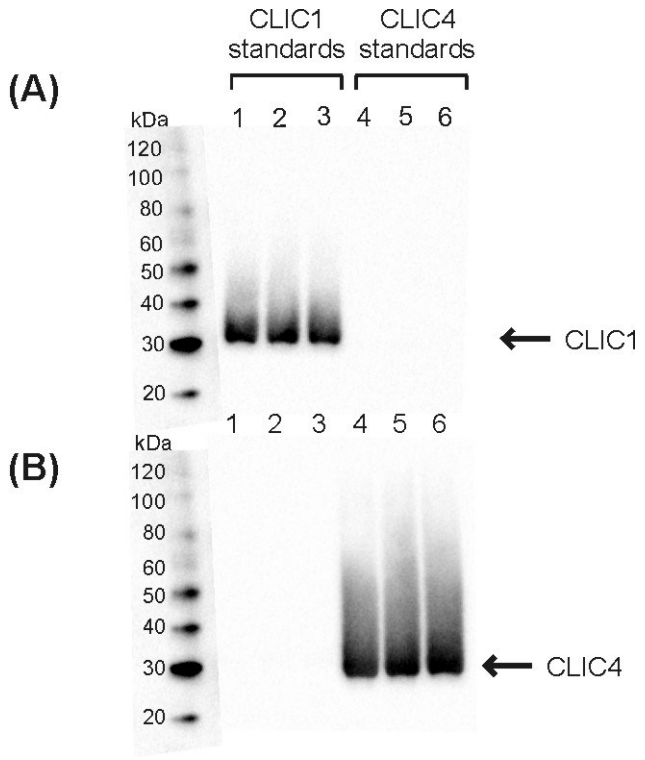


Figure S.5: Specificity of CLIC1 and CLIC4 antibodies. Equal amounts of protein standards of CLIC1 and CLIC4 (5µg) were used for western blot analysis using antibodies against CLIC1 and CLIC4. The antibodies were specific to the proteins probed and did not cross-react

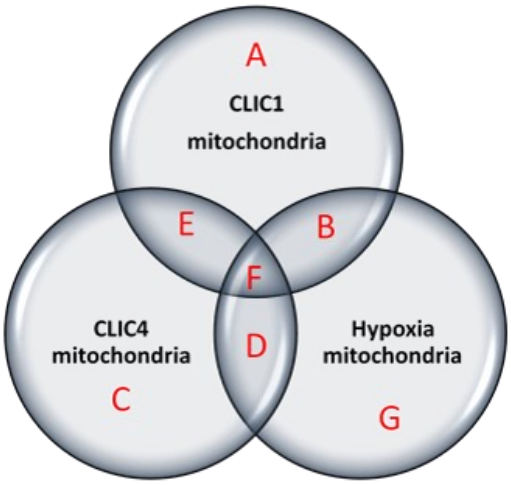


Figure S.6: IPA group classification of mitochondrial proteomic analysis of CLIC1, CLIC4, and Hypoxic-control HPAECs.

Table S.1: **Differentially expressed proteins in group A,B,C,D and G**. A list of proteins found in group A (CLIC1-overexpressing HPAECs only), group B (CLIC1-overexpressing HPAECs, and hypoxic-control cells) group C (CLIC4-overexpressing HPAECs only), group D (CLIC4-overexpressing HPAECs, and hypoxic cells) and group G (Hypoxic-control only).

MITOCHONDRIAL PROTEINS
Proteins found with CLIC1 overexpression [A]
10 kDa heat shock protein, mitochondrial
14-3-3 protein zeta/delta
2',3'-cyclic-nucleotide 3'-phosphodiesterase isoform 2
abnormal spindle-like microcephaly-associated protein isoform 1
acyl-CoA dehydrogenase family member 9, mitochondrial
adenomatous polyposis coli protein isoform b
adenylate kinase 2, mitochondrial isoform c
adenylate kinase 9 isoform 1
AFG3-like protein 2
alpha-aminoadipic semialdehyde dehydrogenase isoform 1 precursor
aspartyl/asparaginyl beta-hydroxylase isoform f
ATP synthase F(0) complex subunit B1, mitochondrial precursor
calcineurin B homologous protein 1
chloride intracellular channel protein 5 isoform a
cytochrome c1, heme protein, mitochondrial precursor
cytosolic acyl coenzyme A thioester hydrolase isoform hBACHa
delta(3,5)-Delta(2,4)-dienoyl-CoA isomerase, mitochondrial precursor
elongation factor G, mitochondrial isoform 1
erythrocyte band 7 integral membrane protein isoform a
erythrocyte band 7 integral membrane protein isoform c
evolutionarily conserved signalling intermediate in Toll pathway, mitochondrial isoform 2 precursor
girdin isoform 1
glutathione peroxidase 1 isoform 1
GTP:AMP phosphotransferase AK3, mitochondrial isoform b
HBS1-like protein isoform 2
heat shock protein beta-1

heme oxygenase 1
hydroxyacyl-coenzyme A dehydrogenase, mitochondrial isoform 1 precursor
immunoglobulin-like and fibronectin type III domain-containing protein 1
laminin subunit beta-1 precursor
membrane-associated progesterone receptor component 2
mitochondrial carrier homolog 2 isoform 1x
nestin
pentatricopeptide repeat domain-containing protein 3, mitochondrial precursor
phosphate carrier protein, mitochondrial isoform b precursor
phosphoenolpyruvate carboxykinase
protocadherin-17 precursor
raftlin
ras-related protein Rab-11A isoform 2
ras-related protein Rab-14
ras-related protein Rab-2A isoform b
ras-related protein Rab-5C isoform b
ras-related protein Ral-A precursor
ras-related protein Ral-B
receptor of activated protein C kinase 1
redox-regulatory protein FAM213A isoform 1 precursor
rho GDP-dissociation inhibitor 1 isoform a
sorting and assembly machinery component 50 homolog
sphingosine-1-phosphate lyase 1
succinate--CoA ligase
tricarboxylate transport protein, mitochondrial isoform b
utrophin
vacuolar protein sorting-associated protein 35
vesicle-trafficking protein SEC22b precursor
vinculin isoform VCL
CLIC1 and hypoxia [B]
2,4-dienoyl-CoA reductase, mitochondrial isoform 2
acyl-coenzyme A thioesterase 9, mitochondrial isoform b precursor
alpha-mannosidase 2

amine oxidase
B-cell receptor-associated protein 31 isoform b
CD166 antigen isoform 2 precursor
histone H1.5
inositol 1,4,5-trisphosphate receptor type 1 isoform 1
inositol 1,4,5-trisphosphate receptor type 3
leucine-rich repeat-containing protein 59
myoferlin isoform a
ras-interacting protein 1
ras-related protein Rab-7a
transmembrane emp24 domain-containing protein 10 precursor
transmembrane emp24 domain-containing protein 9 precursor
thiosulfate sulfurtransferase
Found with CLIC4 overexpression [C]
26S proteasome non-ATPase regulatory subunit 1 isoform 2
calpastatin isoform f
caspase recruitment domain-containing protein 6
contactin-associated protein 1 precursor
DNA excision repair protein ERCC-6 isoform 2
E3 ubiquitin-protein ligase UHRF1 isoform 1
erlin-2 isoform 1
FACT complex subunit SPT16
lysosome membrane protein 2 isoform 2 precursor
manganese-transporting ATPase 13A1
metal transporter CNNM1 isoform 2
peroxidasin homolog precursor
poliovirus receptor isoform beta precursor
poly [ADP-ribose] polymerase 1
protein AHNAK2 isoform 2
thymopoietin isoform beta
transcription elongation regulator 1-like protein
xin actin-binding repeat-containing protein 2 isoform 4
YP_003024029.1 cytochrome c oxidase subunit II (mitochondrion)

zinc finger protein 577 isoform b
CLIC4 and hypoxia [D]
CD9 antigen isoform 2
plasma membrane calcium-transporting ATPase 1 isoform 1a
plasma membrane calcium-transporting ATPase 4 isoform 4a
podocalyxin isoform 1 precursor
ras GTPase-activating-like protein IQGAP1
transgelin-2 isoform b
UDP-GalNAc:beta-1,3-N-acetylgalactosaminyltransferase 1 isoform b
UDP-glucose:glycoprotein glucosyltransferase 1 precursor
found in hypoxic control only [G]
MORC family CW-type zinc finger protein 4 isoform b
calmodulin-2 isoform 1
caskin-1
chromobox protein homolog 2 isoform 1
cofilin-1
DNA-(apurinic or apyrimidinic site) lyase
interferon-induced helicase C domain-containing protein 1
mesencephalic astrocyte-derived neurotrophic factor precursor
microsomal glutathione S-transferase 1 isoform a
nebulin-related-anchoring protein isoform 3
neuron navigator 2 isoform 3
PDZ domain-containing protein 8
periostin isoform 2 precursor
protein ERGIC-53 precursor
protein piccolo isoform 2
transmembrane protein 43
dystonin isoform X3
X-ray repair cross-complementing protein 6 isoform 1
Found in control normoxia only and disappears in other groups
CD99 antigen isoform b precursor
centromere protein I isoform 2

centromere-associated protein E isoform 2
disintegrin and metalloproteinase domain-containing protein 30 preproprotein
galectin-1
inter-alpha-trypsin inhibitor heavy chain H2 precursor
interleukin enhancer-binding factor 3 isoform e
myristoylated alanine-rich C-kinase substrate
programmed cell death 6-interacting protein isoform 2
prolyl 3-hydroxylase 1 isoform 2 precursor
protein disulfide-isomerase TMX3 isoform 4 precursor
saccharopine dehydrogenase-like oxidoreductase
signal peptidase complex subunit 3
splicing factor 3B subunit 3
aminopeptidase N precursor
common proteins found in all samples
basement membrane-specific heparan sulfate proteoglycan core protein isoform a precursor
3-ketoacyl-CoA thiolase, mitochondrial
28S ribosomal protein S22, mitochondrial
28S ribosomal protein S23, mitochondrial
28S ribosomal protein S29, mitochondrial isoform 1
28S ribosomal protein S9, mitochondrial
2-oxoglutarate dehydrogenase, mitochondrial isoform 2 precursor
2-oxoglutarate dehydrogenase, mitochondrial isoform 3 precursor
2-oxoglutarate dehydrogenase-like, mitochondrial isoform b
39S ribosomal protein L12, mitochondrial
39S ribosomal protein L39, mitochondrial isoform a
39S ribosomal protein L49, mitochondrial
3-hydroxyacyl-CoA dehydrogenase type-2 isoform 2
40S ribosomal protein S14
40S ribosomal protein S3 isoform 1
4F2 cell-surface antigen heavy chain isoform b
5'-nucleotidase isoform 2 preproprotein
60 kDa heat shock protein, mitochondrial

60S acidic ribosomal protein P0
60S acidic ribosomal protein P2
60S ribosomal protein L11 isoform 1
60S ribosomal protein L12
60S ribosomal protein L14
60S ribosomal protein L18 isoform 1
60S ribosomal protein L22
60S ribosomal protein L27
60S ribosomal protein L30
60S ribosomal protein L4
60S ribosomal protein L7
60S ribosomal protein L7a
78 kDa glucose-regulated protein precursor
acetyl-CoA acetyltransferase, mitochondrial precursor
aconitate hydratase, mitochondrial precursor
actin, alpha skeletal muscle
actin, cytoplasmic 1
actin-related protein 2/3 complex subunit 1B
actin-related protein 2/3 complex subunit 4 isoform c
actin-related protein 3 isoform 2
adipocyte plasma membrane-associated protein
ADP/ATP translocase 1
ADP/ATP translocase 2
aldehyde dehydrogenase, mitochondrial isoform 1 precursor
alkyldihydroxyacetonephosphate synthase, peroxisomal precursor
alpha-actinin-1 isoform b
annexin A1
annexin A2 isoform 2
annexin A5
AP-1 complex subunit beta-1 isoform a
AP-2 complex subunit alpha-1 isoform 1
AP-2 complex subunit alpha-2 isoform 1
AP-2 complex subunit beta isoform a

aspartate aminotransferase, mitochondrial isoform 1 precursor
aspartate aminotransferase, mitochondrial isoform 2 precursor
ATP synthase subunit alpha, mitochondrial isoform c
ATP synthase subunit beta, mitochondrial precursor
ATP synthase subunit delta, mitochondrial precursor
ATP synthase subunit gamma, mitochondrial isoform L (liver) precursor
ATP synthase subunit O, mitochondrial precursor
ATP-binding cassette sub-family A member 13
ATP-binding cassette sub-family B member 5 isoform 1
ATP-dependent DNA helicase Q1
basigin isoform 2 precursor
beta-actin-like protein 2
biorientation of chromosomes in cell division protein 1-like 1
brain acid soluble protein 1
calnexin precursor
calreticulin precursor
carnitine O-palmitoyltransferase 1, liver isoform isoform 2
catenin alpha-1 isoform 2
catenin alpha-2 isoform 2
catenin beta-1 isoform 1
catenin delta-1 isoform 1ABC
caveolae-associated protein 1
caveolin-1 isoform alpha
CD44 antigen isoform 1 precursor
CD59 glycoprotein preproprotein
cell surface glycoprotein MUC18 precursor
citrate synthase, mitochondrial precursor
c-myc promoter-binding protein-1 isoform MBP-1
collagen alpha-1(I) chain preproprotein
collagen alpha-5(VI) chain isoform 1 precursor
complement component 1 Q subcomponent-binding protein, mitochondrial precursor
cytochrome b-c1 complex subunit 1, mitochondrial precursor

cytochrome b-c1 complex subunit 2, mitochondrial precursor
cytochrome b-c1 complex subunit 7 isoform 2
cytochrome b-c1 complex subunit Rieske, mitochondrial
cytochrome c
cytochrome c oxidase subunit 4 isoform 1, mitochondrial isoform 1 precursor
cytochrome c oxidase subunit 5B, mitochondrial precursor
cytoplasmic dynein 1 heavy chain 1
cytoplasmic dynein 1 intermediate chain 2 isoform 1
cytoskeleton-associated protein 4
delta-1-pyrroline-5-carboxylate synthase isoform 2
desmin
dihydrolipoyl dehydrogenase, mitochondrial isoform 1 precursor
dihydrolipoyllysine-residue acetyltransferase component of pyruvate dehydrogenase complex, mitochondrial precursor
dihydrolipoyllysine-residue succinyltransferase component of 2-oxoglutarate dehydrogenase complex, mitochondrial isoform 1 precursor
dihydrolipoyllysine-residue succinyltransferase component of 2-oxoglutarate dehydrogenase complex, mitochondrial isoform 2 precursor
DNA-dependent protein kinase catalytic subunit isoform 2
dolichyl-diphosphooligosaccharide--protein glycosyltransferase 48 kDa subunit precursor
dolichyl-diphosphooligosaccharide--protein glycosyltransferase subunit 1 precursor
dolichyl-diphosphooligosaccharide--protein glycosyltransferase subunit 2 isoform 2 precursor
dolichyl-diphosphooligosaccharide--protein glycosyltransferase subunit STT3A isoform a
EH domain-containing protein 2
EH domain-containing protein 4
electron transfer flavoprotein subunit alpha, mitochondrial isoform a
electron transfer flavoprotein subunit beta isoform 2
elongation factor 1-alpha 1
elongation factor 1-beta
elongation factor 1-delta isoform 1
elongation factor 1-gamma

elongation factor 2
elongation factor Tu, mitochondrial precursor
endoglin isoform 2 precursor
endoplasmic reticulum aminopeptidase 1 isoform b precursor
endoplasmic reticulum resident protein 44 precursor
endoplasmin precursor
enoyl-CoA delta isomerase 1, mitochondrial isoform 2 precursor
enoyl-CoA delta isomerase 2, mitochondrial isoform 1
enoyl-CoA hydratase, mitochondrial
ER membrane protein complex subunit 1 isoform 2 precursor
eukaryotic initiation factor 4A-I isoform 1
eukaryotic initiation factor 4A-I isoform 2
eukaryotic translation initiation factor 5A-1 isoform A
ezrin
filamin-A isoform 2
filamin-B isoform 1
filamin-C isoform b
fructose-bisphosphate aldolase A isoform 1
fructose-bisphosphate aldolase C
fumarate hydratase, mitochondrial
glucosidase 2 subunit beta isoform 2 precursor
glutamate dehydrogenase 1, mitochondrial isoform a precursor
glutamate dehydrogenase 1, mitochondrial isoform b
glutaminase kidney isoform, mitochondrial isoform 2
glyceraldehyde-3-phosphate dehydrogenase isoform 2
glyceraldehyde-3-phosphate dehydrogenase, testis-specific
glycerol-3-phosphate dehydrogenase, mitochondrial precursor
guanine nucleotide-binding protein G(i) subunit alpha-2 isoform 2
guanine nucleotide-binding protein G(I)/G(S)/G(T) subunit beta-1 isoform 1
guanine nucleotide-binding protein G(I)/G(S)/G(T) subunit beta-1 isoform 2
guanine nucleotide-binding protein G(I)/G(S)/G(T) subunit beta-2
guanine nucleotide-binding protein G(k) subunit alpha
guanine nucleotide-binding protein G(q) subunit alpha

heat shock 70 kDa protein 1A
heat shock 70 kDa protein 6
heat shock cognate 71 kDa protein isoform 1
heat shock protein 75 kDa, mitochondrial isoform 2
heat shock protein HSP 90-alpha isoform 1
heat shock protein HSP 90-beta isoform a
heterogeneous nuclear ribonucleoprotein C-like 1
heterogeneous nuclear ribonucleoprotein K isoform c
heterogeneous nuclear ribonucleoprotein U isoform b
heterogeneous nuclear ribonucleoproteins A2/B1 isoform A2
hexokinase-1 isoform HKI
high mobility group protein HMGI-C isoform c
histone H2A type 2-A
histone H2B type 1-O
histone H2B type 2-F isoform a
histone H3.2
histone H4
HLA class I histocompatibility antigen, A-1 alpha chain A*01:01:01:01 precursor
HLA class I histocompatibility antigen, Cw-1 alpha chain precursor
importin subunit beta-1 isoform 1
integrin alpha-5 precursor
integrin alpha-V isoform 2 precursor
integrin beta-1 isoform 1A precursor
integrin beta-3 precursor
integrin beta-4 isoform 1 precursor
isocitrate dehydrogenase
isocitrate dehydrogenase
isoleucine--tRNA ligase, mitochondrial precursor
lamin isoform C
lamin isoform D
lamin-B1 isoform 1
lamin-B1 isoform 2
lamin-B2

L-lactate dehydrogenase A chain isoform 2
lon protease homolog, mitochondrial isoform 2
long-chain-fatty-acid--CoA ligase 3
long-chain-fatty-acid--CoA ligase 4 isoform 2
lysophospholipid acyltransferase 7 isoform 2
major vault protein isoform 2
malate dehydrogenase, mitochondrial isoform 2 precursor
mannosyl-oligosaccharide glucosidase isoform 2
MICOS complex subunit MIC19 isoform 1
MICOS complex subunit MIC60 isoform 2
MICOS complex subunit MIC60 isoform 3
mitochondrial import inner membrane translocase subunit TIM44
mitochondrial import inner membrane translocase subunit TIM50 isoform 1
mitochondrial import receptor subunit TOM40 homolog
mitochondrial import receptor subunit TOM70
mitochondrial proton/calcium exchanger protein precursor
moesin
monofunctional C1-tetrahydrofolate synthase, mitochondrial isoform 1 precursor
myosin light chain 6B
myosin light polypeptide 6 isoform 1
myosin regulatory light chain 12B
myosin-10 isoform 1
myosin-11 isoform SM2B
myosin-15 precursor
myosin-7B
myosin-9
NAD(P) transhydrogenase, mitochondrial isoform 1
NAD(P) transhydrogenase, mitochondrial isoform 2
NADH dehydrogenase
NADH dehydrogenase
NADH dehydrogenase
NADH dehydrogenase

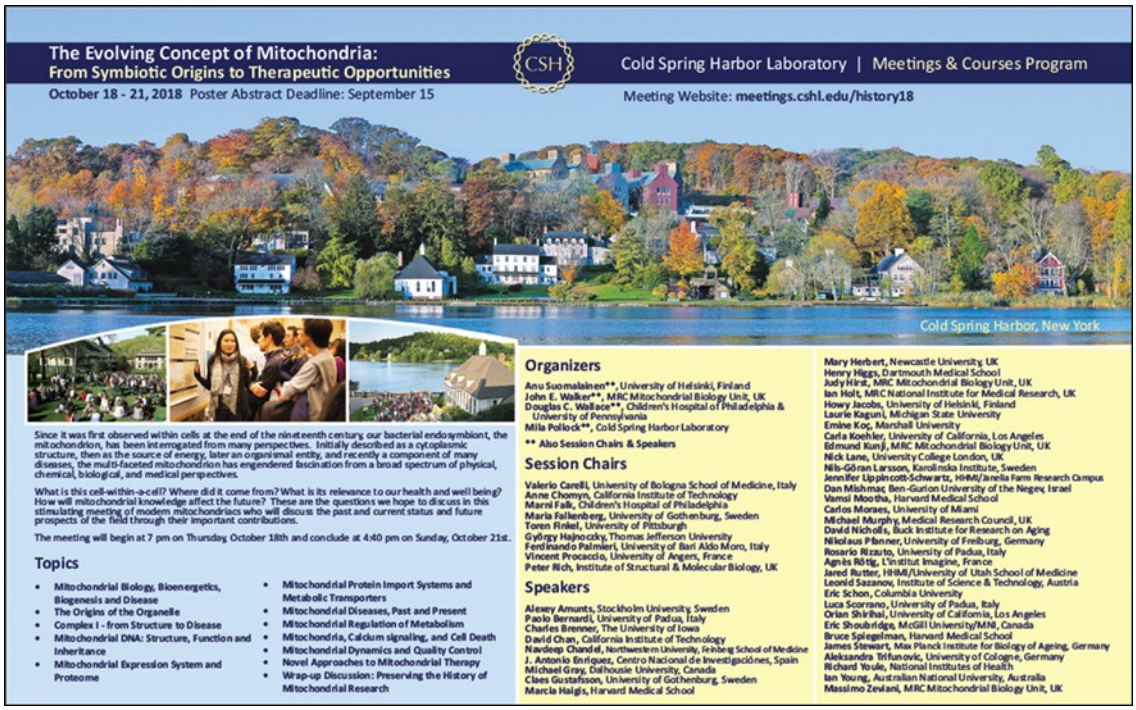
NADH dehydrogenase
NADH dehydrogenase
NADH dehydrogenase
NADH dehydrogenase
NADH dehydrogenase
NADH-cytochrome b5 reductase 1
NADH-cytochrome b5 reductase 3 isoform 1
neuroblast differentiation-associated protein AHNAK isoform 1
neurofibromin isoform 2
neutral alpha-glucosidase AB isoform 4
neutral alpha-glucosidase AB isoform 6
neutral cholesterol ester hydrolase 1 isoform a
nucleolar RNA helicase 2 isoform 2
nucleolin
ornithine aminotransferase, mitochondrial isoform 1 precursor
peptidyl-prolyl cis-trans isomerase A isoform 1
peptidyl-prolyl cis-trans isomerase A isoform 2
peptidyl-prolyl cis-trans isomerase B precursor
peptidyl-prolyl cis-trans isomerase FKBP8 isoform 2
peroxisomal multifunctional enzyme type 2 isoform 2
phosphoglycerate kinase 1
platelet endothelial cell adhesion molecule precursor
plectin isoform 1c
poly(rC)-binding protein 1
poly(rC)-binding protein 2 isoform c
POTE ankyrin domain family member E
presequence protease, mitochondrial isoform 1 precursor
procollagen-lysine,2-oxoglutarate 5-dioxygenase 1 isoform 2 precursor
procollagen-lysine,2-oxoglutarate 5-dioxygenase 2 isoform 2 precursor
procollagen-lysine,2-oxoglutarate 5-dioxygenase 3 precursor
profilin-1
prohibitin isoform 1
prohibitin-2 isoform 1

protein disulfide-isomerase A3 precursor
protein disulfide-isomerase A4 precursor
protein disulfide-isomerase A6 isoform a
protein disulfide-isomerase precursor
protein transport protein Sec61 subunit alpha isoform 1
protein-glutamine gamma-glutamyltransferase 2 isoform a
pyruvate dehydrogenase E1 component subunit alpha, somatic form, mitochondrial isoform 1 precursor
pyruvate dehydrogenase E1 component subunit beta, mitochondrial isoform 1 precursor
pyruvate kinase PKM isoform c
reticulocalbin-1 precursor
reticulocalbin-2 isoform b precursor
reticulon-4 isoform A
reticulon-4 isoform E
sarcoplasmic/endoplasmic reticulum calcium ATPase 1 isoform c
sarcoplasmic/endoplasmic reticulum calcium ATPase 2 isoform a
septin-11 isoform 1
septin-2 isoform a
serine hydroxymethyltransferase, mitochondrial isoform 2 precursor
serine/threonine-protein kinase SMG1
serine/threonine-protein phosphatase PGAM5, mitochondrial isoform 1
serpin H1 precursor
serum albumin preproprotein
sideroflexin-1 isoform 1
sideroflexin-3
signal recognition particle receptor subunit alpha isoform 2
signal recognition particle receptor subunit beta
sodium/potassium-transporting ATPase subunit alpha-1 isoform a
sodium/potassium-transporting ATPase subunit beta-3
solute carrier family 12 member 2 isoform 1
staphylococcal nuclease domain-containing protein 1
stomatin-like protein 2, mitochondrial isoform b

stress-70 protein, mitochondrial precursor
succinate dehydrogenase
succinate dehydrogenase
sulfide:quinone oxidoreductase, mitochondrial
SWI/SNF complex subunit SMARCC2 isoform c
SWI/SNF-related matrix-associated actin-dependent regulator of chromatin subfamily A member 5
synaptic vesicle membrane protein VAT-1 homolog
thioredoxin domain-containing protein 5 isoform 3
titin isoform N2BA
transcriptional adapter 2-beta
transitional endoplasmic reticulum ATPase isoform 2
transketolase isoform 1
translocon-associated protein subunit alpha isoform 1 precursor
translocon-associated protein subunit delta isoform 1 precursor
trifunctional enzyme subunit alpha, mitochondrial precursor
trifunctional enzyme subunit beta, mitochondrial isoform 1 precursor
tubulin alpha chain-like 3 isoform 2
tubulin alpha-1A chain isoform 1
tubulin alpha-8 chain isoform 2
tubulin beta chain isoform a
tubulin beta-2A chain isoform 1
tubulin beta-3 chain isoform 2
tubulin beta-4A chain isoform 1
tubulin beta-6 chain isoform 1
unconventional myosin-Ic isoform a
unconventional myosin-Id isoform 2
very long-chain specific acyl-CoA dehydrogenase, mitochondrial isoform 1 precursor
vimentin
voltage-dependent anion-selective channel protein 1
voltage-dependent anion-selective channel protein 2 isoform 1
voltage-dependent anion-selective channel protein 3 isoform 2

Appendix 2: Achievements

- PhD Travel Award, Department of Medicine, Imperial College London, 2018.
- The first-place winner of £5,000 credit in the Immunofluorescence imaging competition across Europe by abcam, 2017.



The Evolving Concept of Mitochondria:
From Symbiotic Origins to Therapeutic Opportunities

October 18 - 21, 2018 Poster Abstract Deadline: September 15

Cold Spring Harbor Laboratory | Meetings & Courses Program

Meeting Website: meetings.cshl.edu/history18

Cold Spring Harbor, New York

Since it was first observed within cells at the end of the nineteenth century, our bacterial endosymbiont, the mitochondrion, has been interrogated from many perspectives. Initially described as a cytoplasmic structure, then as the source of energy, later an organismal entity, and recently a component of many diseases, the multi-faceted mitochondrion has engendered fascination from a broad spectrum of physical, chemical, biological, and medical perspectives.

What is this cell-within-a-cell? Where did it come from? What is its relevance to our health and well being? How will mitochondrial knowledge affect the future? These are the questions we hope to discuss in this stimulating meeting of modern mitochondriacs who will discuss the past and current status and future prospects of the field through their important contributions.

The meeting will begin at 7 pm on Thursday, October 18th and conclude at 4:40 pm on Sunday, October 21st.

Topics

- Mitochondrial Biology, Bioenergetics, Biogenesis and Disease
- The Origins of the Organelle
- Complex I - from Structure to Disease
- Mitochondrial DNA: Structure, Function and Inheritance
- Mitochondrial Expression System and Proteome
- Mitochondrial Protein Import Systems and Metabolic Transporters
- Mitochondrial Diseases, Past and Present
- Mitochondrial Regulation of Metabolism
- Mitochondria, Calcium signaling, and Cell Death
- Mitochondrial Dynamics and Quality Control
- Novel Approaches to Mitochondrial Therapy
- Wrap-up Discussion: Preserving the History of Mitochondrial Research

Organizers

Anu Suomalainen**, University of Helsinki, Finland
John E. Walker**, MRC Mitochondrial Biology Unit, UK
Douglas C. Wallace**, Children's Hospital of Philadelphia & University of Pennsylvania
Mila Pollock**, Cold Spring Harbor Laboratory

** Also Session Chairs & Speakers

Session Chairs

Valerio Carelli, University of Bologna School of Medicine, Italy
Anne Chomyn, California Institute of Technology
Marni Falk, Children's Hospital of Philadelphia
Maria Falkenberg, University of Gothenburg, Sweden
Toren Finkel, University of Pittsburgh
György Hajnoczky, Thomas Jefferson University
Ferdinando Palmieri, University of Bari Aldo Moro, Italy
Vincent Procaccio, University of Angers, France
Peter Rich, Institute of Structural & Molecular Biology, UK

Speakers

Alexey Amunts, Stockholm University, Sweden
Paolo Bernardi, University of Padua, Italy
Charles Brenner, The University of Iowa
David Chan, California Institute of Technology
Navdeep Chandel, Northwestern University, Feinberg School of Medicine
J. Antonio Enriquez, Centro Nacional de Investigaciónes, Spain
Michael Gray, Dalhousie University, Canada
Claes Gustafsson, University of Gothenburg, Sweden
Marcia Haigis, Harvard Medical School
Mary Herbert, Newcastle University, UK
Henry Higgs, Dartmouth Medical School
Judy Hirst, MRC Mitochondrial Biology Unit, UK
Ian Holt, MRC National Institute for Medical Research, UK
Howy Jacobs, University of Helsinki, Finland
Laurie Kaguni, Michigan State University
Emine Koc, Marshall University
Carla Koehler, University of California, Los Angeles
Edmund Kunji, MRC Mitochondrial Biology Unit, UK
Nick Lane, University College London, UK
Nils-Göran Larsson, Karolinska Institute, Sweden
Jennifer Lippincott-Schwartz, HHMI/Janelia Farm Research Campus
Dan Mishmar, Ben-Gurion University of the Negev, Israel
Vamsi Mootha, Harvard Medical School
Carlos Moraes, University of Miami
Michael Murphy, Medical Research Council, UK
David Nicholls, Buck Institute for Research on Aging
Nikolaus Pfanner, University of Freiburg, Germany
Rosario Rizzuto, University of Padua, Italy
Agnès Rötig, L'institut Imagine, France
Jared Rutter, HHMI/University of Utah School of Medicine
Leonid Sazanov, Institute of Science & Technology, Austria
Eric Schon, Columbia University
Luca Scorrano, University of Padua, Italy
Orian Shirihai, University of California, Los Angeles
Eric Shoubridge, McGill University/MNI, Canada
Bruce Spiegelman, Harvard Medical School
James Stewart, Max Planck Institute for Biology of Ageing, Germany
Aleksandra Trifunovic, University of Cologne, Germany
Richard Youle, National Institutes of Health
Ian Young, Australian National University, Australia
Massimo Zeviani, MRC Mitochondrial Biology Unit, UK



Appendix 3: Publications

- **miR-150-PTPMT1-cardiolipin signaling in pulmonary arterial hypertension.**

Russomanno G, Jo KB, Abdul-Salam VB, Morgan C, Endruschat J, Schaeper U, Osman AH, **Alzaydi MM**, Wilkins MR, Wojciak-Stothard B.Mol Ther Nucleic Acids. 2020 Nov 4;23:142-153. doi: 10.1016/j.omtn.2020.10.042. eCollection 2021 Mar 5.PMID: 33335799.

- **Therapeutic potential of KLF2-induced exosomal microRNAs in pulmonary hypertension.**

Sindi HA, Russomanno G, Satta S, Abdul-Salam VB, Jo KB, Qazi-Chaudhry B, Ainscough AJ, Szulcek R, Jan Bogaard H, Morgan CC, Pullamsetti SS, **Alzaydi MM**, Rhodes CJ, Piva R, Eichstaedt CA, Grünig E, Wilkins MR, Wojciak-Stothard B.Nat Commun. 2020 Mar 4;11(1):1185. doi: 10.1038/s41467-020-14966-x.PMID: 32132543.

Appendix 4: Conferences

- **13th PVRI Annual World Congress on PVD, Barcelona, Spain, 2019**

Mai Alzaydi[1,2], Vahitha Abdul-Salam[1] and Beata Wojciak-Stothard[1]. CLIC Proteins induce mitochondrial dysfunction in pulmonary arterial hypertension (poster).

1.Department of Medicine, Imperial College London, London, UK

2.King Abdulaziz City for Science and Technology (KACST), Saudi Arabia

- **Evolving Concept of Mitochondria: From Symbiotic Origins to Therapeutic Opportunities, Cold Spring Harbor, New York, USA,2018**

Mai M. Alzaydi, Angelos Glynos, Vahitha Abdul-Salam, Beata Wojciak-Stothard. Intracellular chloride channel proteins induce mitochondrial dysfunction in pulmonary arterial hypertension (poster).

- **Mitochondria: Form and Function, UCL, London, UK, 2017**

Mai Alzaydi, Vahitha Abdul-Salam and Beata Wojciak-Stothard. Role of CLIC proteins in the regulation of mitochondrial function in pulmonary hypertension (poster).

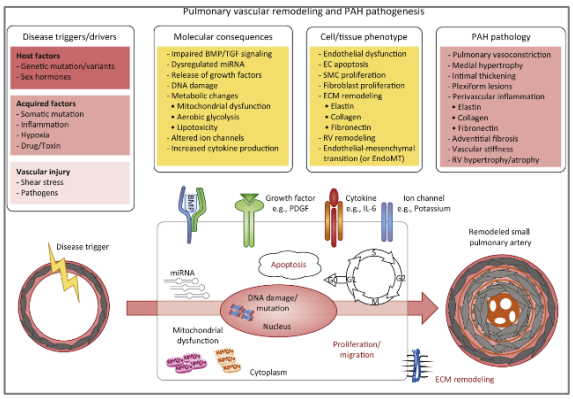
- **Mitochondria: Form and Function workshop, UCL, London, UK, 2017**

Mai Alzaydi, Vahitha Abdul-Salam and Beata Wojciak-Stothard. Role of CLIC proteins in the regulation of mitochondrial function in pulmonary hypertension (presentation).

Appendix 5: Figure permissions

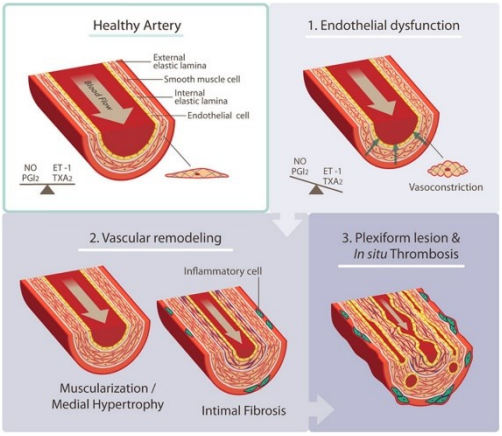
This Agreement between Imperial College London -- Mai Alzaydi ("You") and Elsevier ("Elsevier") consists of your license details and the terms and conditions provided by Elsevier and Copyright Clearance Center.

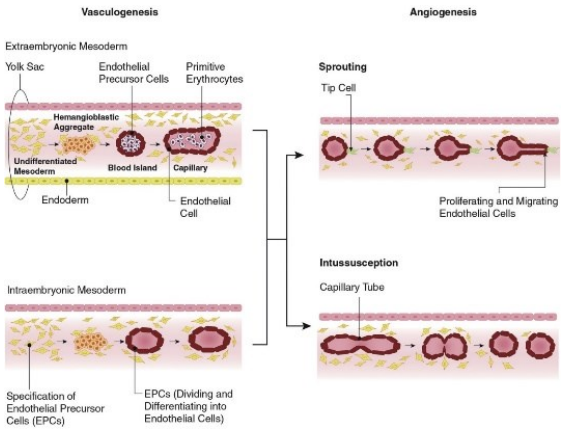
License Number	5024411375979
License date	Mar 08, 2021
Licensed Content Publisher	Elsevier
Licensed Content Publication	Trends in Molecular Medicine
Licensed Content Title	Targeting Vascular Remodeling to Treat Pulmonary Arterial Hypertension
Licensed Content Author	A.A. Roger Thompson,Allan Lawrie
Licensed Content Date	Jan 1, 2017
Licensed Content Volume	23
Licensed Content Issue	1
Licensed Content Pages	15
Start Page	31
End Page	45
Type of Use	reuse in a thesis/dissertation
Portion	figures/tables/illustrations
Number of figures/tables/illustrations	1
Format	electronic
Are you the author of this Elsevier article?	No
Will you be translating?	No
Title	Mrs Mai Alzaydi
Institution name	Imperial College London
Expected presentation date	Mar 2021
Portions	Figure 2. Pulmonary Vascular Remodeling and Pulmonary Arterial Hypertension (PAH) Pathogenesis
Requestor Location	Imperial College London



This Agreement between Imperial College London -- Mai Alzaydi ("You") and Wolters Kluwer Health, Inc. ("Wolters Kluwer Health, Inc.") consists of your license details and the terms and conditions provided by Wolters Kluwer Health, Inc. and Copyright Clearance Center.

License Number	5033310048513
License date	Mar 20, 2021
Licensed Content Publisher	Wolters Kluwer Health, Inc.
Licensed Content Publication	Circulation Research
Licensed Content Title	Pulmonary Arterial Hypertension
Licensed Content Author	Yen-Chun Lai, Karin C. Potoka, Hunter C. Champion, et al
Licensed Content Date	Jun 20, 2014
Licensed Content Volume	115
Licensed Content Issue	1
Type of Use	Dissertation/Thesis
Requestor type	University/College
Sponsorship	No Sponsorship
Format	Electronic
Will this be posted online?	Yes, on a secure website
Portion	Figures/tables/illustrations
Number of figures/tables/illustrations	1
Author of this Wolters Kluwer article	No
Will you be translating?	No
Intend to modify/change the content	No
Title	Mrs Mai Alzaydi
Institution name	Imperial College London
Expected presentation date	Mar 2021
Portions	Figure 8 Cellular changes in pulmonary arterial hypertension (PAH)







Vascular ontogeny within selected thoracoabdominal organs and the limbs

Author: John M. DeSesso

Publication: Reproductive Toxicology

Publisher: Elsevier

Date: June 2017

© 2016 The Author. Published by Elsevier Inc.

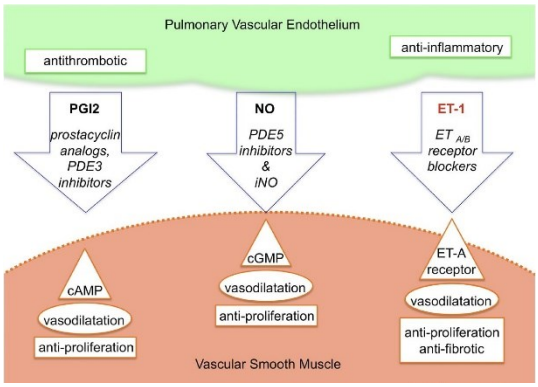
Creative Commons Attribution-NonCommercial-No Derivatives License (CC BY NC ND)

This article is published under the terms of the Creative Commons Attribution-NonCommercial-No Derivatives License (CC BY NC ND).
For non-commercial purposes you may copy and distribute the article, use portions or extracts from the article in other works, and text or data mine the article, provided you do not alter or modify the article without permission from Elsevier. You may also create adaptations of the article for your own personal use only, but not distribute these to others. You must give appropriate credit to the original work, together with a link to the formal publication through the relevant DOI, and a link to the Creative Commons user license above. If changes are permitted, you must indicate if any changes are made but not in any way that suggests the licensor endorses you or your use of the work.

Permission is not required for this non-commercial use. For commercial use please continue to request permission via Rightslink.

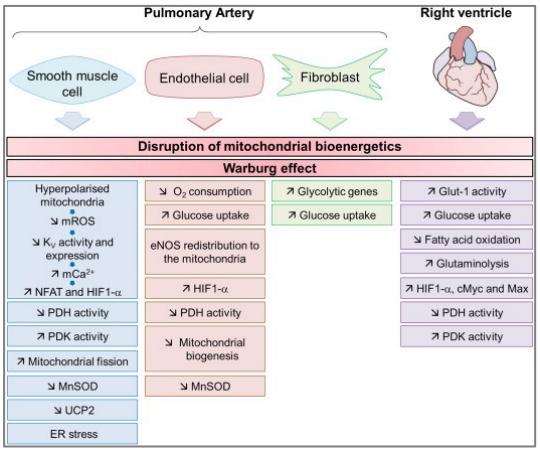
This Agreement between Imperial College London -- Mai Alzaydi ("You") and American Academy of Pediatrics ("American Academy of Pediatrics") consists of your license details and the terms and conditions provided by American Academy of Pediatrics and Copyright Clearance Center.

License Number	5033290821458
License date	Mar 20, 2021
Licensed Content Publisher	American Academy of Pediatrics
Licensed Content Publication	Pediatrics
Licensed Content Title	Pulmonary Hypertension Therapy and a Systematic Review of Efficacy and Safety of PDE-5 Inhibitors
Licensed Content Author	Chinwe Unegbu,Corina Noje,John D. Coulson,Jodi B. Segal,Lewis Romer
Licensed Content Date	Mar 1, 2017
Licensed Content Volume	139
Licensed Content Issue	3
Licensed Content Pages	1
Type of Use	Dissertation/Thesis
Requestor type	Individual Account
Format	Electronic
Portion	Figures/tables/images
Number of figures/tables/images	1
Use of a photo?	No
Title	Mrs Mai Alzaydi
Institution name	Imperial College London
Expected presentation date	Mar 2021
Portions	Figure 1



This Agreement between Imperial College London -- Mai Alzaydi ("You") and Elsevier ("Elsevier") consists of your license details and the terms and conditions provided by Elsevier and Copyright Clearance Center.

License Number	5024430132429
License date	Mar 08, 2021
Licensed Content Publisher	Elsevier
Licensed Content Publication	The International Journal of Biochemistry & Cell Biology
Licensed Content Title	Mitochondria: Roles in pulmonary hypertension
Licensed Content Author	Véronique Freund-Michel,Nafiisha Khoyrattee,Jean-Pierre Savineau,Bernard Muller,Christelle Guibert
Licensed Content Date	Oct 1, 2014
Licensed Content Volume	55
Licensed Content Issue	n/a
Licensed Content Pages	5
Start Page	93
End Page	97
Type of Use	reuse in a thesis/dissertation
Portion	figures/tables/illustrations
Number of figures/tables/illustrations	1
Format	electronic
Are you the author of this Elsevier article?	No
Will you be translating?	No
Title	Mrs Mai Alzaydi
Institution name	Imperial College London
Expected presentation date	Mar 2021
Portions	Fig. 1.
Requestor Location	Imperial College London



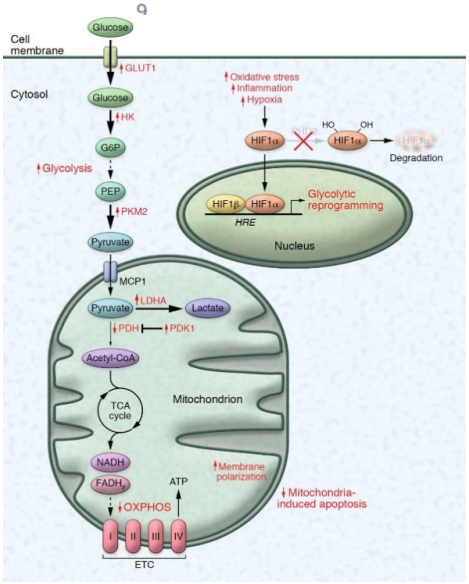
This is a License Agreement between Mai Alzaydi ("You") and American Society for Clinical Investigation ("Publisher") provided by Copyright Clearance Center ("CCC"). The license consists of your order details, the terms and conditions provided by American Society for Clinical Investigation, and the CCC terms and conditions.

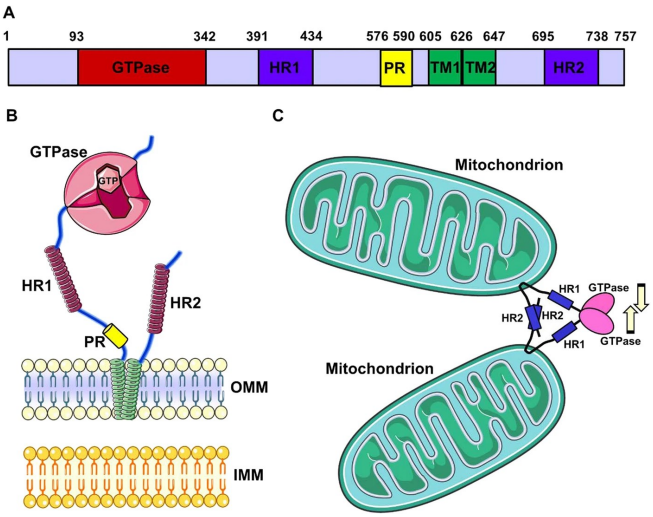
All payments must be made in full to CCC.

Order Date	23-Mar-2021	**Type of Use**	Republish in a thesis/dissertation
Order license ID	1106520-1		
ISSN	0021-9738	**Publisher**	AMERICAN SOCIETY FOR CLINICAL INVESTIGATION
		Portion	Chart/graph/table/figure

LICENSED CONTENT

Publication Title	The journal of clinical investigation	**Rightsholder**	American Society for Clinical Investigation
Article Title	Mitochondrial metabolism in pulmonary hypertension: beyond mountains there are mountains.	**Publication Type**	Journal
		Start Page	3704
		End Page	3715
		Issue	9
Author/Editor	AMERICAN SOCIETY FOR CLINICAL INVESTIGATION., Robinson, George Canby	**Volume**	
Date	01/01/1924		
Language	English		
Country	United States of America		





Mitofusin 2: from functions to disease

Author: Riccardo Filadi et al

Publication: Cell Death & Disease

Publisher: Springer Nature

Date: Feb 28, 2018

Copyright © 2018, The Author(s)

Creative Commons

This is an open access article distributed under the terms of the Creative Commons CC BY license, which permits unrestricted use, distribution, and reproduction in any medium, provided the original work is properly cited.

You are not required to obtain permission to reuse this article.

To request permission for a type of use not listed, please contact Springer Nature

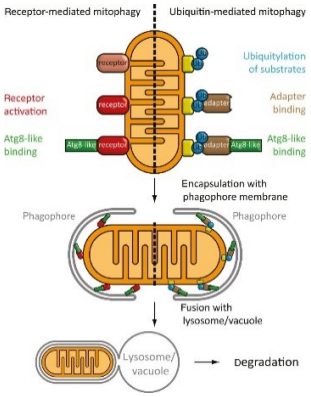
This is a License Agreement between Mai Alzaydi ("You") and Walter de Gruyter and Company ("Publisher") provided by Copyright Clearance Center ("CCC"). The license consists of your order details, the terms and conditions provided by Walter de Gruyter and Company, and the CCC terms and conditions.

All payments must be made in full to CCC.

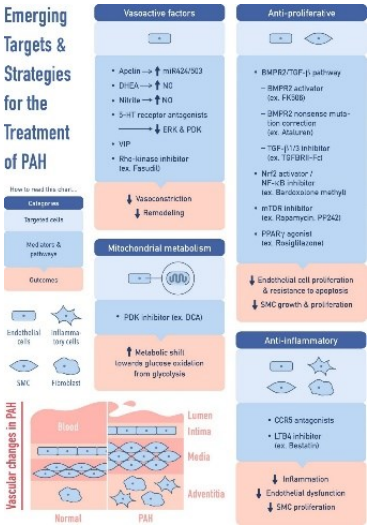
Order Date	23-Mar-2021	**Type of Use**	Republish in a thesis/dissertation
Order license ID	1106522-1		
ISSN	1431-6730	**Publisher**	WALTER/DE GRUYTER GMBH & CO. KG
		Portion	Chart/graph/table/figure

LICENSED CONTENT

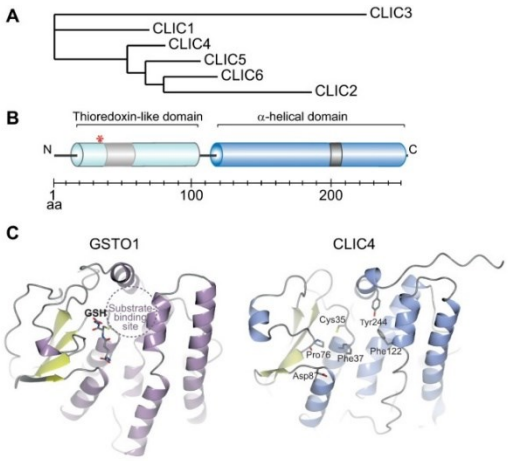
Publication Title	Biological chemistry	**Rightsholder**	Walter de Gruyter and Company
Article Title	How to get rid of mitochondria: crosstalk and regulation of multiple mitophagy pathways.	**Publication Type**	Journal
		Start Page	29
Author/Editor	Gesellschaft für Biochemie und Molekularbiologie.	**End Page**	45
		Issue	1
Date	01/01/1996	**Volume**	399
Language	English		
Country	Germany		

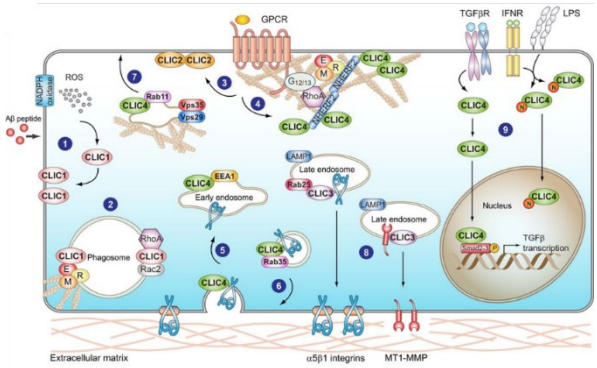


Order Number	501638405
Order date	Mar 08, 2021
Licensed Content Publisher	The American Physiological Society
Licensed Content Publication	Am J Physiol-Lung, Cellular, and Molecular Physiology
Licensed Content Title	Emerging therapeutics in pulmonary hypertension
Licensed Content Author	Matthew K. Hensley, Andrea Levine, Mark T. Gladwin, et al
Licensed Content Date	May 1, 2018
Licensed Content Volume	314
Licensed Content Issue	5
Type of use	Thesis/Dissertation
Requestor type	non-profit academic/educational
Readers being charged a fee for this work	No
Format	electronic
Portion	figures/tables/images
Number of figures/tables/images	1
Will you be translating?	no
World Rights	no
Order reference number	
Title	Mrs Mai Alzaydi
Institution name	Imperial College London
Expected presentation date	Mar 2021
Portions	Fig. 3.
Requestor Location	Imperial College London



Order Number	501638405
Order date	Mar 08, 2021
Licensed Content Publisher	The American Physiological Society
Licensed Content Publication	Am J Physiol-Lung, Cellular, and Molecular Physiology
Licensed Content Title	Emerging therapeutics in pulmonary hypertension
Licensed Content Author	Matthew K. Hensley, Andrea Levine, Mark T. Gladwin, et al
Licensed Content Date	May 1, 2018
Licensed Content Volume	314
Licensed Content Issue	5
Type of use	Thesis/Dissertation
Requestor type	non-profit academic/educational
Readers being charged a fee for this work	No
Format	electronic
Portion	figures/tables/images
Number of figures/tables/images	1
Will you be translating?	no
World Rights	no
Order reference number	
Title	Mrs Mai Alzaydi
Institution name	Imperial College London
Expected presentation date	Mar 2021
Portions	Fig. 3.





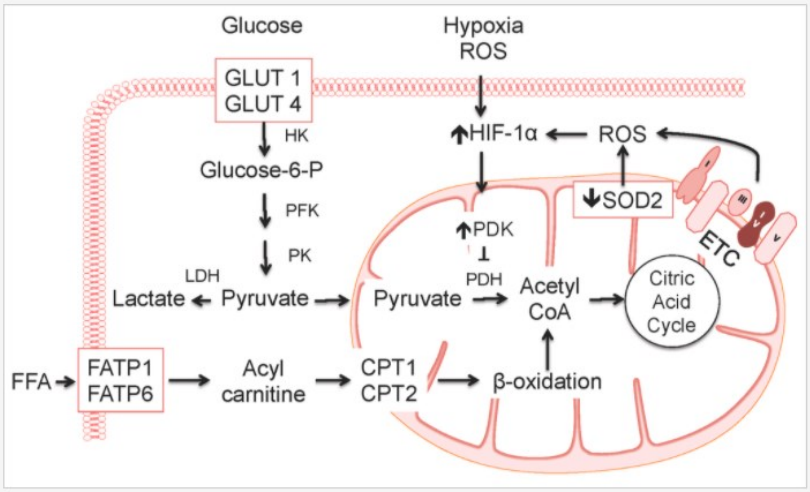


Figure 1

© This is an open access article distributed under the **Creative Commons Attribution License** which permits unrestricted use, distribution, and reproduction in any medium, provided the original work is properly cited

REFERENCES

References

Abdul-Salam, V. B., Russomanno, G., Chien-Nien, C., Mahomed, A. S., Yates, L. A., Wilkins, M. R., Schaeper, U. (2019). CLIC4/Arf6 pathway: a new lead in BMPRII inhibition in pulmonary hypertension. *Circ Res, 124*(1), 52-65.

Abdul-Salam, V. B., Wharton, J., Cupitt, J., Berryman, M., Edwards, R. J., & Wilkins, M. R. (2010). Proteomic Analysis of Lung Tissues from Patients with Pulmonary Arterial Hypertension: A Clinical Perspective. *Circulation, 122*(20), 2058-2067.

Ackema, K. B., Hench, J., Böckler, S., Wang, S. C., Sauder, U., Mergentaler, H., Spang, A. (2014). The small GTPase Arf1 modulates mitochondrial morphology and function. *The EMBO Journal*, e201489039.

Aebersold, R., & Mann, M. (2003). Mass spectrometry-based proteomics. *Nature, 422*(6928), 198-207.

Aggarwal, S., Gross, C. M., Sharma, S., Fineman, J. R., & Black, S. M. (2013). Reactive oxygen species in pulmonary vascular remodeling. *Comprehensive Physiology, 3*(3), 1011-1034.

Aggarwal, S., Mannam, P., & Zhang, J. (2016). Differential regulation of autophagy and mitophagy in pulmonary diseases. *American Journal of Physiology-Lung Cellular and Molecular Physiology, 311*(2), L433-L452.

Al Khamici, H., Brown, L. J., Hossain, K. R., Hudson, A. L., Sinclair-Burton, A. A., Ng, J. P. M., Curmi, P. M. (2015). Members of the chloride intracellular ion channel protein family demonstrate glutaredoxin-like enzymatic activity. *PloS One, 10* (1), e115699.

Alvarado-Moreno, J. A., Hernandez-Lopez, R., Chavez-Gonzalez, A., Yoder, M. C., Rangel-Corona, R., Isordia-Salas, I., Majluf-Cruz, A. (2016). Endothelial colony-forming cells: Biological and functional abnormalities in patients with recurrent, unprovoked venous thromboembolic disease. *Thromb Res, 137*, 157-168. doi:10.1016/j.thromres.2015.11.005

Anesti, V., & Scorrano, L. (2006). The relationship between mitochondrial shape and function and the cytoskeleton. *Biochimica et Biophysica Acta (BBA)-Bioenergetics, 1757*(5), 692-699.

Archer, S., Will, J., & Weir, E. (1986). Redox status in the control of pulmonary vascular tone. *Herz, 11*(3), 127-141.

Archer, S. L., Fang, Y.-H., Ryan, J. J., & Piao, L. (2013). Metabolism and bioenergetics in the right ventricle and pulmonary vasculature in pulmonary hypertension. *Pulmonary Circulation, 3*(1), 144-152.

Archer, S. L., Gomberg-Maitland, M., Maitland, M. L., Rich, S., Garcia, J. G., & Weir, E. K. (2008). Mitochondrial metabolism, redox signaling, and fusion: a mitochondria-ROS-HIF-1α-Kv1. 5 O2-sensing pathway at the intersection of pulmonary hypertension and cancer. *American Journal of Physiology-Heart and Circulatory Physiology, 294*(2), H570-H578.

Archer, S. L., Weir, E. K., & Wilkins, M. R. (2010). Basic science of pulmonary arterial hypertension for clinicians: new concepts and experimental therapies. *Circulation, 121*(18), 2045-2066. doi:10.1161/circulationaha.108.847707

Argenzio, E., & Moolenaar, W. H. (2016). Emerging biological roles of Cl− intracellular channel proteins. *Journal of cell science, 129*(22), 4165-4174.

Ashley, R. (2003). Challenging accepted ion channel biology: p64 and the CLIC family of putative intracellular anion channel proteins (Review). *Molecular Membrane Biology, 20*(1), 1-11.

Ashrafi, G., & Schwarz, T. (2013). The pathways of mitophagy for quality control and clearance of mitochondria. *Cell Death & Differentiation, 20*(1), 31-42.

Asosingh, K., et al. (2008). Circulating angiogenic precursors in idiopathic pulmonary arterial hypertension. *The American Journal of Pathology* **172**(3): 615-627.

Atrih, A., Mudaliar, M., Zakikhani, P., Lamont, D., Huang, J. T., Bray, S., Nabi, G. (2014). Quantitative proteomics in resected renal cancer tissue for biomarker discovery and profiling. *British journal of Cancer, 110*(6), 1622-1633.

Averaimo, S., Milton, R. H., Duchen, M. R., & Mazzanti, M. (2010). Chloride intracellular channel 1 (CLIC1): Sensor and effector during oxidative stress. *FEBS Lett, 584*(10), 2076-2084. doi:10.1016/j.febslet.2010.02.073

Avouac, J., et al. (2008). Angiogenesis in systemic sclerosis: impaired expression of vascular endothelial growth factor receptor 1 in endothelial progenitor–derived cells under hypoxic conditions. *Arthritis & Rheumatism: Official Journal of the American College of Rheumatology* **58**(11): 3550-3561.

Aytekin, M., Aulak, K. S., Haserodt, S., Chakravarti, R., Cody, J., Minai, O. A., & Dweik, R. A. (2012). Abnormal platelet aggregation in idiopathic pulmonary arterial hypertension: role of nitric oxide. *American Journal of Physiology-Lung Cellular and Molecular Physiology, 302*(6), L512-L520.

Bacha, N. C., Blandinieres, A., Rossi, E., Gendron, N., Nevo, N., Lecourt, S., Smadja, D. M. (2018). Endothelial Microparticles are Associated to Pathogenesis of Idiopathic Pulmonary Fibrosis. *Stem Cell Reviews and Reports, 14*(2), 223-235. doi:10.1007/s12015-017-9778-5

Baker, C. D., Ryan, S. L., Ingram, D. A., Seedorf, G. J., Abman, S. H., & Balasubramaniam, V. (2009). Endothelial colony-forming cells from preterm infants are increased and more susceptible to hyperoxia. *Am J Respir Crit Care Med, 180*(5), 454-461. doi:10.1164/rccm.200901-0115OC

Balaban, R., & Mitoehondria, N. S. F. T. (2005). Mitochondria, oxidants and aginngJ. *Cel1, 120*(4), 483-495. doi:10.1016/j.cell.2005.02.001

Barst, R. J. (2008). Pulmonary hypertension: past, present and future. *Annals of Thoracic Medicine, 3*(1), 1.

Barth, E., et al. (1992). Ultrastructural quantitation of mitochondria and myofilaments in cardiac muscle from 10 different animal species including man. *Journal of molecular and cellular cardiology* **24**(7): 669-681.

Berry, K. L., Bülow, H. E., Hall, D. H., & Hobert, O. (2003). A C. elegans CLIC-like protein required for intracellular tube formation and maintenance. *Science, 302*(5653), 2134-2137.

Berryman, M., Bruno, J., Price, J., & Edwards, J. C. (2004). CLIC-5A functions as a chloride channel in vitro and associates with the cortical actin cytoskeleton in vitro and in vivo. *Journal of Biological Chemistry, 279*(33), 34794-34801.

Berryman, M., & Bretscher, A. (2000). Identification of a novel member of the chloride intracellular channel gene family (CLIC5) that associates with the actin cytoskeleton of placental microvilli. *Molecular Biology of the Cell, 11*(5), 1509-1521.

Berryman, M. A., & Goldenring, J. R. (2003). CLIC4 is enriched at cell-cell junctions and colocalizes with AKAP350 at the centrosome and midbody of cultured mammalian cells. *Cell Motility and the Cytoskeleton, 56*(3), 159-172.

Board, P. G., Coggan, M., Watson, S., Gage, P. W., & Dulhunty, A. F. (2004). CLIC-2 modulates cardiac ryanodine receptor Ca 2+ release channels. *The International Journal of Biochemistry & Cell Biology, 36*(8), 1599-1612.

Bohman, S., Matsumoto, T., Suh, K., Dimberg, A., Jakobsson, L., Yuspa, S., & Claesson-Welsh, L. (2005). Proteomic analysis of vascular endothelial growth factor-induced endothelial cell differentiation reveals a role for chloride intracellular channel 4 (CLIC4) in tubular morphogenesis. *Journal of Biological Chemistry, 280*(51), 42397-42404.

Bonnet, S., Michelakis, E. D., Porter, C. J., Andrade-Navarro, M. A., Thébaud, B., Bonnet, S., . . . McMurtry, M. S. (2006). An Abnormal Mitochondrial–Hypoxia Inducible Factor-1α–Kv Channel Pathway Disrupts Oxygen Sensing and Triggers Pulmonary Arterial Hypertension in Fawn Hooded Rats. *Circulation, 113*(22), 2630-2641.

Borghesi, A., Massa, M., Campanelli, R., Bollani, L., Tzialla, C., Figar, T. A., Stronati, M. (2009). Circulating endothelial progenitor cells in preterm infants with bronchopulmonary dysplasia. *Am J Respir Crit Care Med, 180*(6), 540-546. doi:10.1164/rccm.200812-1949OC

Boucherat, O., Vitry, G., Trinh, I., Paulin, R., Provencher, S., & Bonnet, S. (2017). The cancer theory of pulmonary arterial hypertension. *Pulmonary circulation, 7*(2), 285-299.

Budhiraja, R., Tuder, R. M., & Hassoun, P. M. (2004). Endothelial dysfunction in pulmonary hypertension. *Circulation, 109*(2), 159-165.

Carmeliet, P., & Jain, R. K. (2011). Molecular mechanisms and clinical applications of angiogenesis. *Nature, 473*(7347), 298-307. doi:10.1038/nature10144

Caruso, P., Dunmore, B. J., Schlosser, K., Schoors, S., Dos Santos, C., Perez-Iratxeta, C., Morrell, N. W. (2017). Identification of MicroRNA-124 as a Major Regulator of Enhanced Endothelial Cell Glycolysis in Pulmonary Arterial Hypertension via PTBP1 (Polypyrimidine Tract Binding Protein) and Pyruvate Kinase M2. *Circulation, 136*(25), 2451-2467. doi:10.1161/circulationaha.117.028034

Case, J., Mead, L. E., Bessler, W. K., Prater, D., White, H. A., Saadatzadeh, M. R., Ingram, D. A. (2007). Human CD34+ AC133+ VEGFR-2+ cells are not endothelial progenitor cells but distinct, primitive hematopoietic progenitors. *Experimental Hematology, 35*(7), 1109-1118.

Castro, P. R., Barbosa, A. S., Pereira, J. M., Ranfley, H., Felipetto, M., Gonçalves, C. A. X., Barcelos, L. S. (2018). Cellular and Molecular Heterogeneity Associated with Vessel Formation Processes. *Biomed Res Int, 2018*, 6740408. doi:10.1155/2018/6740408

Chan, D. C. (2007). Mitochondrial dynamics in disease. *N Engl J Med, 356*(17), 1707-1709. doi:10.1056/NEJMp078040

Chan, S. Y., & Rubin, L. J. (2017). Metabolic dysfunction in pulmonary hypertension: from basic science to clinical practice. *European Respiratory Review, 26*(146).

Chandhok, G., Lazarou, M., & Neumann, B. (2018). Structure, function, and regulation of mitofusin-2 in health and disease. *Biological Reviews, 93*(2), 933-949.

Chang, C.-R., & Blackstone, C. (2007). Cyclic AMP-dependent protein kinase phosphorylation of Drp1 regulates its GTPase activity and mitochondrial morphology. *Journal of Biological Chemistry, 282*(30), 21583-21587.

Chen, H.-H., Vicente, C. P., He, L., Tollefsen, D. M., & Wun, T.-C. (2005). Fusion proteins comprising annexin V and Kunitz protease inhibitors are highly potent thrombogenic site-directed anticoagulants. *Blood, 105*(10), 3902-3909.

Chen, K., Dasgupta, A., Lin, J., Potus, F., Bonnet, S., & Iremonger, J. (2018). Epigenetic dysregulation of the Drp1 binding partners MiD49 and MiD51 increases mitotic mitochondrial fission and promotes

pulmonary arterial hypertension: mechanistic and therapeutic implications. *Circulation, 138*, 287-304.

Chen, Q., Wang, Q., Zhu, J., Xiao, Q., & Zhang, L. (2018). Reactive oxygen species: key regulators in vascular health and diseases. *British Journal of Pharmacology, 175*(8), 1279-1292. doi:10.1111/bph.13828

Chen, Y., & Dorn, G. W., 2nd. (2013). PINK1-phosphorylated mitofusin 2 is a Parkin receptor for culling damaged mitochondria. *Science, 340*(6131), 471-475. doi:10.1126/science.1231031

Cheng, J., et al. (2017). Mitochondrial proton leak plays a critical role in pathogenesis of cardiovascular diseases. *Mitochondrial Dynamics in Cardiovascular Medicine*: 359-370.

Cheng, M. Y., Hartl, F. U., & Horwich, A. L. (1990). The mitochondrial chaperonin hsp60 is required for its own assembly. *Nature, 348*(6300), 455-458. doi:10.1038/348455a0

Chiu, H.-W., Ho, S.-Y., Guo, H.-R., & Wang, Y.-J. (2009). Combination treatment with arsenic trioxide and irradiation enhances autophagic effects in U118-MG cells through increased mitotic arrest and regulation of PI3K/Akt and ERK1/2 signaling pathways. *Autophagy, 5*(4), 472-483.

Chou, S. Y., Hsu, K. S., Otsu, W., Hsu, Y. C., Luo, Y. C., Yeh, C., Sung, C. H. (2016). CLIC4 regulates apical exocytosis and renal tube luminogenesis through retromer- and actin-mediated endocytic trafficking. *Nat Commun, 7*, 10412. doi:10.1038/ncomms10412

Christman, B. W., McPherson, C. D., Newman, J. H., King, G. A., Bernard, G. R., Groves, B. M., & Loyd, J. E. (1992). An imbalance between the excretion of thromboxane and prostacyclin metabolites in pulmonary hypertension. *New England Journal of Medicine, 327*(2), 70-75.

Chua, Y. L., Dufour, E., Dassa, E. P., Rustin, P., Jacobs, H. T., Taylor, C. T., & Hagen, T. (2010). Stabilization of hypoxia-inducible factor-1alpha protein in hypoxia occurs independently of mitochondrial reactive oxygen species production. *J Biol Chem, 285*(41), 31277-31284. doi:10.1074/jbc.M110.158485

Chuang, J.-Z., Milner, T. A., Zhu, M., & Sung, C.-H. (1999). A 29 kDa intracellular chloride channel p64H1 is associated with large dense-core vesicles in rat hippocampal neurons. *Journal of Neuroscience, 19*(8), 2919-2928.

Chuang, J. Z., Chou, S. Y., & Sung, C. H. (2010). Chloride intracellular channel 4 is critical for the epithelial morphogenesis of RPE cells and retinal attachment. *Mol Biol Cell, 21*(17), 3017-3028. doi:10.1091/mbc.E09-10-0907

Clapp, L. H., Finney, P., Turcato, S., Tran, S., Rubin, L. J., & Tinker, A. (2002). Differential effects of stable prostacyclin analogs on smooth muscle proliferation and cyclic AMP generation in human pulmonary artery. *American Journal of Respiratory Cell and Molecular Biology, 26*(2), 194-201.

Cogliati, S., Enriquez, J. A., & Scorrano, L. (2016). Mitochondrial cristae: where beauty meets functionality. *Trends in Biochemical Sciences, 41*(3), 261-273.

Corbin, J. (2004). Mechanisms of action of PDE5 inhibition in erectile dysfunction. *International Journal of Impotence Research, 16*(1), S4-S7.

Corbin, J. D., Beasley, A., Blount, M. A., & Francis, S. H. (2005). High lung PDE5: a strong basis for treating pulmonary hypertension with PDE5 inhibitors. *Biochemical and Biophysical Research Communications, 334*(3), 930-938.

Corbin, J. D., & Francis, S. H. (1999). Cyclic GMP phosphodiesterase-5: target of sildenafil. *Journal of Biological Chemistry, 274*(20), 13729-13732.

Cribbs, J. T., & Strack, S. (2007). Reversible phosphorylation of Drp1 by cyclic AMP-dependent protein kinase and calcineurin regulates mitochondrial fission and cell death. *EMBO Reports, 8*(10), 939-944.

Crowley, L. C., Christensen, M. E., & Waterhouse, N. J. (2016). Measuring mitochondrial transmembrane potential by TMRE staining. *Cold Spring Harbor Protocols, 2016*(12), pdb. prot087361.

Culley, M. K., & Chan, S. Y. (2018). Mitochondrial metabolism in pulmonary hypertension: beyond mountains there are mountains. *The Journal of Clinical Investigation, 128*(9), 3704-3715.

Dasgupta, A., Wu, D., Tian, L., Xiong, P. Y., Dunham-Snary, K. J., Chen, K. H., Hindmarch, C. C. (2011). Mitochondria in the Pulmonary Vasculature in Health and Disease: Oxygen-Sensing, Metabolism, and Dynamics. *Comprehensive Physiology, 10*(2), 713-765.

Dauwe, D., Pelacho, B., Wibowo, A., Walravens, A. S., Verdonck, K., Gillijns, H., Janssens, S. (2016). Neovascularization Potential of Blood Outgrowth Endothelial Cells from Patients with Stable Ischemic Heart Failure Is Preserved. *J Am Heart Assoc, 5*(4), e002288. doi:10.1161/jaha.115.002288

Davie, N., Schermuly, R., Weissmann, N., Grimminger, F., & Ghofrani, H. (2009). The science of endothelin-1 and endothelin receptor antagonists in the management of pulmonary arterial hypertension: current understanding and future studies. *European Journal of Clinical Investigation, 39*, 38-49.

de Brito, O. M., & Scorrano, L. (2009). Mitofusin-2 regulates mitochondrial and endoplasmic reticulum morphology and tethering: the role of Ras. *Mitochondrion, 9*(3), 222-226.

Dejana, E., Tournier-Lasserve, E., & Weinstein, B. M. (2009). The control of vascular integrity by endothelial cell junctions: molecular basis and pathological implications. *Developmental Cell, 16*(2), 209-221.

DeSesso, J. M. (2017). Vascular ontogeny within selected thoracoabdominal organs and the limbs. *Reprod Toxicol, 70*, 3-20. doi:10.1016/j.reprotox.2016.10.007

Desouza, M., Gunning, P. W., & Stehn, J. R. (2012). The actin cytoskeleton as a sensor and mediator of apoptosis. *Bioarchitecture, 2*(3), 75-87.

Ding, W.-X., & Yin, X.-M. (2012). Mitophagy: mechanisms, pathophysiological roles, and analysis. *Biological Chemistry, 393*(7), 547-564.

Dresdale, D. T., Schultz, M., & Michtom, R. J. (1951). Primary pulmonary hypertension: I. Clinical and hemodynamic study. *The American Journal of Medicine, 11*(6), 686-705.

Dromparis, P., & Michelakis, E. D. (2013). Mitochondria in vascular health and disease. *Annual Review of Physiology, 75*, 95-126.

Dulhunty, A., Gage, P., Curtis, S., Chelvanayagam, G., & Board, P. (2001). The glutathione transferase structural family includes a nuclear chloride channel and a ryanodine receptor calcium release channel modulator. *J Biol Chem, 276*(5), 3319-3323. doi:10.1074/jbc.M007874200

Dulhunty, A. F., Hewawasam, R., Liu, D., Casarotto, M. G., & Board, P. G. (2011). Regulation of the cardiac muscle ryanodine receptor by glutathione transferases. *Drug Metabolism Reviews, 43*(2), 236-252.

Duncan, R. R., Westwood, P. K., Boyd, A., & Ashley, R. H. (1997). Rat brain p64H1, expression of a new member of the p64 chloride channel protein family in endoplasmic reticulum. *Journal of Biological Chemistry, 272*(38), 23880-23886.

Dunmore, B. J., Drake, K. M., Upton, P. D., Toshner, M. R., Aldred, M. A., & Morrell, N. W. (2013). The lysosomal inhibitor, chloroquine, increases cell surface BMPR-II levels and restores BMP9 signalling in endothelial cells harbouring BMPR-II mutations. *Human Molecular Genetics, 22*(18), 3667-3679. doi:10.1093/hmg/ddt216

Duong, H. T., Comhair, S. A., Aldred, M. A., Mavrakis, L., Savasky, B. M., Erzurum, S. C., & Asosingh, K. (2011). Pulmonary artery endothelium resident endothelial colony-forming cells in pulmonary arterial hypertension. *Pulmonary Circulation, 1*(4), 475-486.

Dzeja, P. P., Bortolon, R., Perez-Terzic, C., Holmuhamedov, E. L., & Terzic, A. (2002). Energetic communication between mitochondria and nucleus directed by catalyzed phosphotransfer. *Proceedings of the National Academy of Sciences, 99*(15), 10156-10161.

Eba, S., Hoshikawa, Y., Moriguchi, T., Mitsuishi, Y., Satoh, H., Ishida, K., Okada, Y. (2013). The Nuclear Factor Erythroid 2–Related Factor 2 Activator Oltipraz Attenuates Chronic Hypoxia–Induced Cardiopulmonary Alterations in Mice. *American Journal of Respiratory Cell and Molecular Biology, 49*(2), 324-333.

Eddahibi, S., & Adnot, S. (2001). Endothelins and pulmonary hypertension, what directions for the near future? *The European Respiratory Journal*, 18(1), 1-4. doi:10.1183/09031936.01.00002401

Edwards, J. C. (1999). A novel p64-related Cl− channel: subcellular distribution and nephron segment-specific expression. *American Journal of Physiology-Renal Physiology, 276*(3), F398-F408.

Edwards, J. C., & Kahl, C. R. (2010). Chloride channels of intracellular membranes. *FEBS Lett, 584*(10), 2102-2111.

Edwards, J. C., & Kapadia, S. (2000). Regulation of the Bovine Kidney Microsomal Chloride Channel p64 by p59 fyn, a Src Family Tyrosine Kinase. *Journal of Biological Chemistry, 275*(41), 31826-31832.

Eiyama, A., & Okamoto, K. (2015). PINK1/Parkin-mediated mitophagy in mammalian cells. *Current Opinion in Cell Biology, 33*, 95-101.

Eshun-Wilson, L., Zhang, R., Portran, D., Nachury, M. V., Toso, D. B., Löhr, T., Nogales, E. (2019). Effects of α-tubulin acetylation on microtubule structure and stability. *Proceedings of the National Academy of Sciences, 116*(21), 10366-10371.

Falquet, L., Calderon-Copete, S. P., & Frey, J. (2013). Draft geNome sequence of the virulent Clostridium chauvoei reference strain JF4335. *GeNome anNouncements, 1*(4).

Fang, Y.-H., Piao, L., Hong, Z., Toth, P. T., Marsboom, G., Bache-Wiig, P., Archer, S. L. (2012). Therapeutic inhibition of fatty acid oxidation in right ventricular hypertrophy: exploiting Randle's cycle. *Journal of Molecular Medicine, 90*(1), 31-43.

Farrand, L., Kim, J. Y., Im-Aram, A., Suh, J.-Y., Lee, H. J., & Tsang, B. K. (2013). An improved quantitative approach for the assessment of mitochondrial fragmentation in chemoresistant ovarian cancer cells. *PloS One, 8*(9), e74008.

Feng, X., Liu, P., Zhou, X., Li, M.-T., Li, F.-L., Wang, Z., Xiong, Y. (2016). Thromboxane A2 activates YAP/TAZ protein to induce vascular smooth muscle cell proliferation and migration. *Journal of Biological Chemistry, 291*(36), 18947-18958.

Fernández-Salas, E., Sagar, M., Cheng, C., Yuspa, S. H., & Weinberg, W. C. (1999). p53 and tumor necrosis factor α regulate the expression of a mitochondrial chloride channel protein. *Journal of Biological Chemistry, 274*(51), 36488-36497.

Fernández-Salas, E., Suh, K. S., Speransky, V. V., Bowers, W. L., Levy, J. M., Adams, T., Cheng, C. (2002). mtCLIC/CLIC4, an organellular chloride channel protein, is increased by DNA damage and participates in the apoptotic response to p53. *Molecular and Cellular Biology, 22*(11), 3610-3620.

Fijalkowska, I., Xu, W., Comhair, S. A., Janocha, A. J., Mavrakis, L. A., Krishnamachary, B., Tuder, R. M. (2010). Hypoxia inducible-factor1alpha regulates the metabolic shift of pulmonary hypertensive endothelial cells. *Am J Pathol, 176*(3), 1130-1138. doi:10.2353/ajpath.2010.090832

Filadi, R., Pendin, D., & Pizzo, P. (2018). Mitofusin 2: from functions to disease. *Cell Death & Disease, 9*(3), 1-13.

Finkenzeller, G., Graner, S., Kirkpatrick, C., Fuchs, S., & Stark, G. (2009). Impaired in vivo vasculogenic potential of endothelial progenitor cells in comparison to human umbilical vein endothelial cells in a spheroid-based implantation model. *Cell Proliferation, 42*(4), 498-505.

Fish, J. E., Santoro, M. M., Morton, S. U., Yu, S., Yeh, R. F., Wythe, J. D., Srivastava, D. (2008). miR-126 regulates angiogenic signaling and vascular integrity. *Dev Cell, 15*(2), 272-284. doi:10.1016/j.devcel.2008.07.008

Fishman, A. P. (1978). The pulmonary circulation. *JAMA, 239*(13), 1299-1301.

Forkink, M., et al. (2014). Mitochondrial hyperpolarization during chronic complex I inhibition is sustained by low activity of complex II, III, IV and V. *Biochimica et Biophysica Acta (BBA)-Bioenergetics* **1837**(8): 1247-1256.

Freund-Michel, V., Guibert, C., Dubois, M., Courtois, A., Marthan, R., Savineau, J.-P., & Muller, B. (2013). Reactive oxygen species as therapeutic targets in pulmonary hypertension. *Therapeutic Advances in Respiratory Disease, 7*(3), 175-200.

Freund-Michel, V., Khoyrattee, N., Savineau, J.-P., Muller, B., & Guibert, C. (2014). Mitochondria: roles in pulmonary hypertension. *The international Journal of Biochemistry & Cell Biology, 55*, 93-97.

Gaboury, J., Woodman, R. C., Granger, D. N., Reinhardt, P., & Kubes, P. (1993). Nitric oxide prevents leukocyte adherence: role of superoxide. *American Journal of Physiology-Heart and Circulatory Physiology, 265*(3), H862-H867.

Gagnon, L. H., Longo-Guess, C. M., Berryman, M., Shin, J.-B., Saylor, K. W., Yu, H., Johnson, K. R. (2006). The chloride intracellular channel protein CLIC5 is expressed at high levels in hair cell stereocilia and is essential for normal inner ear function. *Journal of Neuroscience, 26*(40), 10188-10198.

Galiè, N., Humbert, M., Vachiery, J.-L., Gibbs, S., Lang, I., Torbicki, A., Beghetti, M. (2016). 2015 ESC/ERS guidelines for the diagnosis and treatment of pulmonary hypertension: The Joint Task Force for the Diagnosis and Treatment of Pulmonary Hypertension of the European Society of Cardiology (ESC) and the European Respiratory Society (ERS): endorsed by: Association for European Paediatric and Congenital Cardiology (AEPC), International Society for Heart and Lung Transplantation (ISHLT). *European Heart Journal, 37*(1), 67-119.

Gebb, S., & Stevens, T. (2004). On lung endothelial cell heterogeneity. *Microvascular Research, 68*(1), 1-12.

Gegg, M. E., Cooper, J. M., Chau, K.-Y., Rojo, M., Schapira, A. H., & Taanman, J.-W. (2010). Mitofusin 1 and mitofusin 2 are ubiquitinated in a PINK1/parkin-dependent manner upon induction of mitophagy. *Human Molecular Genetics, 19*(24), 4861-4870.

Gouriou, Y., et al. (2020). ANT2-Mediated ATP Import into Mitochondria Protects against Hypoxia Lethal Injury. *Cells* **9**(12): 2542.

Guignabert, C., Tu, L., Izikki, M., Dewachter, L., Zadigue, P., Humbert, M., Eddahibi, S. (2009). Dichloroacetate treatment partially regresses established pulmonary hypertension in mice with SM22α-targeted overexpression of the serotonin transporter. *The FASEB Journal, 23*(12), 4135-4147.

Gururaja Rao, S., Patel, N. J., & Singh, H. (2020). Intracellular Chloride Channels: Novel Biomarkers in Diseases. *Front Physiol, 11*, 96. doi:10.3389/fphys.2020.00096

Gururaja Rao, S., Ponnalagu, D., Patel, N. J., & Singh, H. (2018). Three decades of chloride intracellular channel proteins: from organelle to organ physiology. *Current Protocols in Pharmacology, 80*(1), 11.21. 11-11.21. 17.

Hall, S. M., Hislop, A. A., & Haworth, S. G. (2002). Origin, differentiation, and maturation of human pulmonary veins. *Am J Respir Cell Mol Biol, 26*(3), 333-340.

Hall, S. M., Hislop, A. A., Pierce, C. M., & Haworth, S. G. (2000). Prenatal origins of human intrapulmonary arteries: formation and smooth muscle maturation. *Am J Respir Cell Mol Biol, 23*(2), 194-203.

Handschin, C., & Spiegelman, B. M. (2006). Peroxisome proliferator-activated receptor γ coactivator 1 coactivators, energy homeostasis, and metabolism. *Endocrine Reviews, 27*(7), 728-735.

Hanna, R. A., Quinsay, M. N., Orogo, A. M., Giang, K., Rikka, S., & Gustafsson, Å. B. (2012). Microtubule-associated protein 1 light chain 3 (LC3) interacts with Bnip3 protein to selectively remove endoplasmic reticulum and mitochondria via autophagy. *Journal of Biological Chemistry, 287*(23), 19094-19104.

Hanson, K. A., Burns, F., Rybalkin, S. D., Miller, J. W., Beavo, J., & Clarke, W. R. (1998). Developmental changes in lung cGMP phosphodiesterase-5 activity, protein, and message. *American Journal of Respiratory and Critical Care Medicine, 158*(1), 279-288.

Harris, P., & Heath, D. (1977). The human pulmonary circulation: its form and function in health and disease *The human pulmonary circulation: its form and function in health and disease* (pp. 712-712).

Harrop, S. J., DeMaere, M. Z., Fairlie, W. D., Reztsova, T., Valenzuela, S. M., Mazzanti, M., Warton, K. (2001). Crystal structure of a soluble form of the intracellular chloride ion channel CLIC1 (NCC27) at 1.4-Å resolution. *Journal of Biological Chemistry, 276*(48), 44993-45000.

Haslip, M., Dostanic, I., Huang, Y., Zhang, Y., Russell, K. S., Jurczak, M. J., Lee, P. J. (2015). Endothelial uncoupling protein 2 regulates mitophagy and pulmonary hypertension during intermittent hypoxia. *Arterioscler Thromb Vasc Biol*, ATVBAHA. 114.304865.

Hassoun, P. M., Mouthon, L., Barberà, J. A., Eddahibi, S., Flores, S. C., Grimminger, F., Morrell, N. W. (2009). Inflammation, growth factors, and pulmonary vascular remodeling. *Journal of the American College of Cardiology, 54*(1 Supplement), S10-S19.

Heath, D., & Whitaker, W. (1956). Hypertensive pulmonary vascular disease. *Circulation, 14*(3), 323-343.

Heiss, N. S., & Poustka, A. (1997). Genomic Structure of a Novel Chloride Channel Gene, CLIC2, in Xq28. *Genomics, 45*(1), 224-228. doi:https://doi.org/10.1006/geno.1997.4922

Hensley, M. K., Levine, A., Gladwin, M. T., & Lai, Y. C. (2018). Emerging therapeutics in pulmonary hypertension. *Am J Physiol Lung Cell Mol Physiol, 314*(5), L769-l781. doi:10.1152/ajplung.00259.2017

Hernandez-Lopez, R., Chavez-Gonzalez, A., Torres-Barrera, P., Moreno-Lorenzana, D., Lopez-DiazGuerrero, N., Santiago-German, D., Alvarado-Moreno, J. A. (2017). Reduced proliferation of endothelial colony-forming cells in unprovoked venous thromboembolic disease as a consequence of endothelial dysfunction. *PLoS One, 12*(9), e0183827. doi:10.1371/journal.pone.0183827

Hirata, Y., Emori, T., Eguchi, S., Kanno, K., Imai, T., Ohta, K., & Marumo, F. (1993). Endothelin receptor subtype B mediates synthesis of nitric oxide by cultured bovine endothelial cells. *The Journal of Clinical Investigation, 91*(4), 1367-1373.

Hirschi, K. K., Ingram, D. A., & Yoder, M. C. (2008). Assessing identity, phenotype, and fate of endothelial progenitor cells. *Arterioscler Thromb Vasc Biol, 28*(9), 1584-1595. doi:10.1161/atvbaha.107.155960

Hislop, A. (2005). Developmental biology of the pulmonary circulation. *Paediatr Respir Rev, 6*(1), 35-43.

Hislop, A., & Pierce, C. (2000). Growth of the vascular tree. *Paediatr Respir Rev, 1*(4), 321-328.

Hoeper, M. M., Ghofrani, H.-A., Grünig, E., Klose, H., Olschewski, H., & Rosenkranz, S. (2017). Pulmonary hypertension. *Deutsches Ärzteblatt International, 114*(5), 73.

Hong, Z., Kutty, S., Toth, P. T., Marsboom, G., Hammel, J. M., Chamberlain, C., Morrow, E. (2013). Role of Dynamin-Related Protein 1 (Drp1)-Mediated Mitochondrial Fission in Oxygen Sensing and Constriction of the Ductus ArteriosusNovelty and Significance. *Circulation Research, 112*(5), 802-815.

Hu, C., Huang, Y., & Li, L. (2017). Drp1-dependent mitochondrial fission plays critical roles in physiological and pathological progresses in mammals. *International Journal of Molecular Sciences, 18*(1), 144.

Hu, L., et al. (2019). Targeting mitochondrial dynamics by regulating Mfn2 for therapeutic intervention in diabetic cardiomyopathy. *Theranostics* **9**(13): 3687.

Huang, H.-L., Yao, H.-S., Wang, Y., Wang, W.-J., Hu, Z.-Q., & Jin, K.-Z. (2014). Proteomic identification of tumor biomarkers associated with primary gallbladder cancer. *World Journal of Gastroenterology: WJG, 20*(18), 5511.

Humbert, M., Lau, E. M., Montani, D., Jaïs, X., Sitbon, O., & Simonneau, G. (2014). Advances in therapeutic interventions for patients with pulmonary arterial hypertension. *Circulation, 130*(24), 2189-2208.

Humbert, M., Morrell, N. W., Archer, S. L., Stenmark, K. R., MacLean, M. R., Lang, I. M., . . . Rabinovitch, M. (2004). Cellular and molecular pathobiology of pulmonary arterial hypertension. *J Am Coll Cardiol, 43*(12 Suppl S), 13s-24s. doi:10.1016/j.jacc.2004.02.029

Humbert, M., Sitbon, O., Chaouat, A., Bertocchi, M., Habib, G., Gressin, V., Simonneau, G. (2010). Survival in patients with idiopathic, familial, and anorexigen-associated pulmonary arterial hypertension in the modern management era. *Circulation, 122*(2), 156-163. doi:10.1161/circulationaha.109.911818

Hur, J., Yoon, C.-H., Kim, H.-S., Choi, J.-H., Kang, H.-J., Hwang, K.-K., Park, Y.-B. (2004). Characterization of two types of endothelial progenitor cells and their different contributions to neovasculogenesis. *Arteriosclerosis, Thrombosis, and Vascular Biology, 24*(2), 288-293.

Ingram, D. A., Mead, L. E., Tanaka, H., Meade, V., Fenoglio, A., Mortell, K., Yoder, M. C. (2004). Identification of a novel hierarchy of endothelial progenitor cells using human peripheral and umbilical cord blood. *Blood, 104*(9), 2752-2760.

Ingram, D. A., et al. (2008). In vitro hyperglycemia or a diabetic intrauterine environment reduces neonatal endothelial colony-forming cell numbers and function. *Diabetes* **57**(3): 724-731.

Izikki, M., Guignabert, C., Fadel, E., Humbert, M., Tu, L., Zadigue, P., Maitre, B. (2009). Endothelial-derived FGF2 contributes to the progression of pulmonary hypertension in humans and rodents. *The Journal of Clinical Investigation, 119*(3), 512-523.

Jeffery, T. K., & Wanstall, J. C. (2001). Pulmonary vascular remodeling: a target for therapeutic intervention in pulmonary hypertension. *Pharmacology & Therapeutics, 92*(1), 1-20.

Jernigan, N. L., Walker, B. R., & Resta, T. C. (2008). Reactive oxygen species mediate RhoA/Rho kinase-induced Ca2+ sensitization in pulmonary vascular smooth muscle following chronic hypoxia. *Am J Physiol Lung Cell Mol Physiol, 295*(3), L515-529. doi:10.1152/ajplung.00355.2007

Jiang, L., Salao, K., Li, H., Rybicka, J. M., Yates, R. M., Luo, X. W., Breit, S. N. (2012). Intracellular chloride channel protein CLIC1 regulates macrophage function through modulation of phagosomal acidification. *J Cell Sci, 125*(Pt 22), 5479-5488. doi:10.1242/jcs.110072

Jonigk, D., Golpon, H., Bockmeyer, C. L., Maegel, L., Hoeper, M. M., Gottlieb, J., Lehmann, U. (2011). Plexiform lesions in pulmonary arterial hypertension: composition, architecture, and microenvironment. *The American Journal of Pathology, 179*(1), 167-179.

Jourdain, I., Gachet, Y., & Hyams, J. S. (2009). The dynamin related protein Dnm1 fragments mitochondria in a microtubule-dependent manner during the fission yeast cell cycle. *Cell Motility and the Cytoskeleton, 66*(8), 509-523.

Kadenbach, B., Ramzan, R., Moosdorf, R., & Vogt, S. (2011). The role of mitochondrial membrane potential in ischemic heart failure. *Mitochondrion, 11*(5), 700-706.

Kader, T., Porteous, C. M., Williams, M. J., Gieseg, S. P., & McCormick, S. P. (2014). Ribose-cysteine increases glutathione-based antioxidant status and reduces LDL in human lipoprotein (a) mice. *Atherosclerosis, 237*(2), 725-733.

Kandathil, A., & Chamarthy, M. (2018). Pulmonary vascular anatomy & anatomical variants. *Cardiovascular Diagnosis and Therapy, 8*(3), 201.

Kauffman, M. E., Kauffman, M. K., Traore, K., Zhu, H., Trush, M. A., Jia, Z., & Li, Y. R. (2016). MitoSOX-based flow cytometry for detecting mitochondrial ROS. *Reactive oxygen species (Apex, NC), 2*(5), 361.

Kennedy, E. P., & Lehninger, A. L. (1949). Oxidation of fatty acids and tricarboxylic acid cycle intermediates by isolated rat liver mitochondria. *Journal of Biological Chemistry, 179*(2), 957-972.

Kim, K. H., Choi, B. K., Song, K. M., Cha, K. W., Kim, Y. H., Lee, H., Kwon, B. S. (2013). CRIg signals induce anti-intracellular bacterial phagosome activity in a chloride intracellular channel 3-dependent manner. *European Journal of Immunology, 43*(3), 667-678.

Kluge, M. A., Fetterman, J. L., & Vita, J. A. (2013). Mitochondria and endothelial function. *Circ Res, 112*(8), 1171-1188.

Kondo, T., Okumura, N., Adachi, S., & Murohara, T. (2019). Pulmonary Hypertension: Diagnosis, Management, and Treatment. *Nagoya J Med Sci, 81*(1), 19-30. doi:10.18999/nagjms.81.1.19

Korshunov, S. S., Skulachev, V. P., & Starkov, A. A. (1997). High protonic potential actuates a mechanism of production of reactive oxygen species in mitochondria. *FEBS Letters, 416*(1), 15-18.

Kotiadis, V. N., Duchen, M. R., & Osellame, L. D. (2014). Mitochondrial quality control and communications with the nucleus are important in maintaining mitochondrial function and cell health. *Biochimica et Biophysica Acta (BBA)-General Subjects, 1840*(4), 1254-1265.

Krüger-Genge, A., Blocki, A., Franke, R.-P., & Jung, F. (2019). Vascular Endothelial Cell Biology: An Update. *International Journal of Molecular Sciences, 20*(18), 4411. doi:10.3390/ijms20184411

Kubis, N., & Levy, B. I. (2003). Vasculogenesis and angiogenesis: molecular and cellular controls. Part 1: growth factors. *Interventional neuroradiology: journal of Peritherapeutic Neuroradiology, Surgical Procedures and Related Neurosciences, 9*(3), 227-237. doi:10.1177/159101990300900301

Kühlbrandt, W. (2015). Structure and function of mitochondrial membrane protein complexes. *BMC Biology, 13*(1), 89.

Kusuma, S., Zhao, S., & Gerecht, S. (2012). The extracellular matrix is a novel attribute of endothelial progenitors and of hypoxic mature endothelial cells. *The FASEB Journal, 26*(12), 4925-4936.

Lai, Y. C., Potoka, K. C., Champion, H. C., Mora, A. L., & Gladwin, M. T. (2014). Pulmonary arterial hypertension: the clinical syndrome. *Circ Res, 115*(1), 115-130. doi:10.1161/circresaha.115.301146

Landry, D. W., Akabas, M. H., Redhead, C., Edelman, A., Cragoe, E. J., & Al-Awqati, Q. (1989). Purification and reconstitution of chloride channels from kidney and trachea. *Science, 244*(4911), 1469-1472.

Laudi, S., Steudel, W., Jonscher, K., Schöning, W., Schniedewind, B., Kaisers, U., Trump, S. (2007). Comparison of lung proteome profiles in two rodent models of pulmonary arterial hypertension. *Proteomics, 7*(14), 2469-2478.

Lavoie, J. R., et al. (2014). Proteomic analysis implicates translationally controlled tumor protein as a novel mediator of occlusive vascular remodeling in pulmonary arterial hypertension. *Circulation* **129**(21): 2125-2135.

Lee, S.-J., Smith, A., Guo, L., Alastalo, T.-P., Li, M., Sawada, H., Jin, Y. (2011). Autophagic protein LC3B confers resistance against hypoxia-induced pulmonary hypertension. *American Journal of Respiratory and Critical Care Medicine, 183*(5), 649-658.

Lenaz, G., & Genova, M. L. (2010). Structure and organization of mitochondrial respiratory complexes: a new understanding of an old subject. *Antioxidants & Redox Signaling, 12*(8), 961-1008.

Leopold, J. A., & Maron, B. A. (2016). Molecular mechanisms of pulmonary vascular remodeling in pulmonary arterial hypertension. *International Journal of Molecular Sciences, 17*(5), 761.

Leslie, K. O., Wick, M. R., & Smith, M. L. (2017). *Practical Pulmonary Pathology: A Diagnostic Approach E-Book: A Volume in the Pattern Recognition Series*: Elsevier Health Sciences.

Liao, P.-C., & Chang, Y.-H. (2012). CLIC1 (chloride intracellular channel 1). *http://AtlasGeneticsOncology. org*, 266.

Lin, Y., Weisdorf, D. J., Solovey, A., & Hebbel, R. P. (2000). Origins of circulating endothelial cells and endothelial outgrowth from blood. *The Journal of Clinical Investigation, 105*(1), 71-77.

Linqing, L., Yuhan, Q., Erfei, L., Yong, Q., Dong, W., Chengchun, T., Bo, L. (2020). Hypoxia-induced PINK1/Parkin-mediated mitophagy promotes pulmonary vascular remodeling. *Biochemical and Biophysical Research Communications*.

Littler, D. R., Harrop, S. J., Fairlie, W. D., Brown, L. J., Pankhurst, G. J., Pankhurst, S., Curmi, P. M. (2004). The intracellular chloride ion channel protein CLIC1 undergoes a redox-controlled structural transition. *J Biol Chem, 279*(10), 9298-9305. doi:10.1074/jbc.M308444200

Liu, J., & Pedersen, L. C. (2007). Anticoagulant heparan sulfate: structural specificity and biosynthesis. *Applied Microbiology and Biotechnology, 74*(2), 263-272.

Lugus, J. J., Ngoh, G. A., Bachschmid, M. M., & Walsh, K. (2011). Mitofusins are required for angiogenic function and modulate different signaling pathways in cultured endothelial cells. *Journal of Molecular and Cellular Cardiology, 51*(6), 885-893.

Ma, J., Zhai, Y., Chen, M., Zhang, K., Chen, Q., Pang, X., & Sun, F. (2019). New interfaces on MiD51 for Drp1 recruitment and regulation. *PloS One, 14*(1), e0211459.

Mai, S., Muster, B., Bereiter-Hahn, J., & Jendrach, M. (2012). Autophagy proteins LC3B, ATG5 and ATG12 participate in quality control after mitochondrial damage and influence lifespan. *Autophagy, 8*(1), 47-62. doi:10.4161/auto.8.1.18174

Marsboom, G., Toth, P. T., Ryan, J. J., Hong, Z., Wu, X., Fang, Y.-H., Pogoriler, J. (2012). Dynamin-Related Protein 1–Mediated Mitochondrial Mitotic Fission Permits Hyperproliferation of Vascular Smooth Muscle Cells and Offers a Novel Therapeutic Target in Pulmonary HypertensionNovelty and Significance. *Circ Res, 110*(11), 1484-1497.

Marshall, J. D., Bazan, I., Zhang, Y., Fares, W. H., & Lee, P. J. (2018). Mitochondrial dysfunction and pulmonary hypertension: cause, effect, or both. *American Journal of Physiology-Lung Cellular and Molecular Physiology, 314*(5), L782-L796.

Martin-Ramirez, J., Hofman, M., Van Den Biggelaar, M., Hebbel, R. P., & Voorberg, J. (2012). Establishment of outgrowth endothelial cells from peripheral blood. *Nature Protocols, 7*(9), 1709-1715.

Martinez, K., & Cupitt, J. (2005). *VIPS-a highly tuned image processing software architecture.* Paper presented at the Image Processing, 2005. ICIP 2005. IEEE International Conference on IEEE.

Martínez-Reyes, I., et al. (2016). TCA cycle and mitochondrial membrane potential are necessary for diverse biological functions. *Molecular Cell* **61**(2): 199-209.

Martínez-Solano, L., Reales-Calderón, J. A., Nombela, C., Molero, G., & Gil, C. (2009). Proteomics of RAW 264.7 macrophages upon interaction with heat-inactivated Candida albicans cells unravel an anti-inflammatory response. *Proteomics, 9*(11), 2995-3010. doi:10.1002/pmic.200800016

Maruta, H., Greer, K., & Rosenbaum, J. L. (1986). The acetylation of alpha-tubulin and its relationship to the assembly and disassembly of microtubules. *The Journal of cell biology, 103*(2), 571-579.

Masri, F. A., Xu, W., Comhair, S. A., Asosingh, K., Koo, M., Vasanji, A., Erzurum, S. C. (2007). Hyperproliferative apoptosis-resistant endothelial cells in idiopathic pulmonary arterial hypertension. *American Journal of Physiology-Lung Cellular and Molecular Physiology, 293*(3), L548-L554.

Massa, M., Campanelli, R., Bonetti, E., Ferrario, M., Marinoni, B., & Rosti, V. (2009). Rapid and large increase of the frequency of circulating endothelial colony-forming cells (ECFCs) generating late outgrowth endothelial cells in patients with acute myocardial infarction. *Exp Hematol, 37*(1), 8-9. doi:10.1016/j.exphem.2008.09.007

Mathew, R. (2014). Pulmonary hypertension and metabolic syndrome: Possible connection, PPARγ and Caveolin-1. *World Journal of Cardiology, 6*(8), 692.

Mathur, J. (2005). The ARP2/3 complex: giving plant cells a leading edge. *Bioessays, 27*(4), 377-387.

Matthews, D. T., & Hemnes, A. R. (2016). Current concepts in the pathogenesis of chronic thromboembolic pulmonary hypertension. *Pulmonary Circulation, 6*(2), 145-154.

McCarron, J. G., Wilson, C., Sandison, M. E., Olson, M. L., Girkin, J. M., Saunter, C., & Chalmers, S. (2013). From structure to function: mitochondrial morphology, motion and shaping in vascular smooth muscle. *Journal of vascular research, 50*(5), 357-371.

McLaughlin, V. V., Shah, S. J., Souza, R., & Humbert, M. (2015). Management of Pulmonary Arterial Hypertension. *Journal of the American College of Cardiology, 65*(18), 1976-1997. doi:https://doi.org/10.1016/j.jacc.2015.03.540

McMurtry, M. S., Bonnet, S., Wu, X., Dyck, J. R., Haromy, A., Hashimoto, K., & Michelakis, E. D. (2004). Dichloroacetate prevents and reverses pulmonary hypertension by inducing pulmonary artery smooth muscle cell apoptosis. *Circ Res, 95*(8), 830-840.

McQUAID, K. E., & Keenan, A. K. (1997). Endothelial barrier dysfunction and oxidative stress: roles for nitric oxide? *Experimental Physiology: Translation and Integration, 82*(2), 369-376.

Medina, R. J., Barber, C. L., Sabatier, F., Dignat-George, F., Melero-Martin, J. M., Khosrotehrani, K., Stitt, A. W. (2017). Endothelial Progenitors: A Consensus Statement on Nomenclature. *Stem Cells Transl Med, 6*(5), 1316-1320. doi:10.1002/sctm.16-0360

Medina, R. J., O'Neill, C. L., Sweeney, M., Guduric-Fuchs, J., Gardiner, T. A., Simpson, D. A., & Stitt, A. W. (2010). Molecular analysis of endothelial progenitor cell (EPC) subtypes reveals two distinct cell populations with different identities. *BMC Medical Genomics, 3*(1), 1-13.

Meiring, J. C., Shneyer, B. I., & Akhmanova, A. (2020). Generation and regulation of microtubule network asymmetry to drive cell polarity. *Current Opinion in Cell Biology, 62*, 86-95.

Merkwirth, C., Dargazanli, S., Tatsuta, T., Geimer, S., Löwer, B., Wunderlich, F. T., Langer, T. (2008). Prohibitins control cell proliferation and apoptosis by regulating OPA1-dependent cristae morphogenesis in mitochondria. *Genes & Development, 22*(4), 476-488.

Michelakis, E. D., McMurtry, M. S., Wu, X.-C., Dyck, J. R., Moudgil, R., Hopkins, T. A., Archer, S. L. (2002). Dichloroacetate, a metabolic modulator, prevents and reverses chronic hypoxic pulmonary hypertension in rats: role of increased expression and activity of voltage-gated potassium channels. *Circulation, 105*(2), 244-250.

Minami, T. and W. C. Aird (2005). Endothelial cell gene regulation. *Trends in Cardiovascular Medicine* **15**(5): 174. e171-174. e124.

Misak, A., Grman, M., Malekova, L., Novotova, M., Markova, J., Krizanova, O., Tomaskova, Z. (2013). Mitochondrial chloride channels: electrophysiological characterization and pH induction of channel pore dilation. *European Biophysics Journal, 42*(9), 709-720.

Mitra, K., Wunder, C., Roysam, B., Lin, G., & Lippincott-Schwartz, J. (2009). A hyperfused mitochondrial state achieved at G1–S regulates cyclin E buildup and entry into S phase. *Proceedings of the National Academy of Sciences, 106*(29), 11960-11965.

Money, T., King, R., Wong, M., Stevenson, J., Kalionis, B., Erwich, J., Desoye, G. (2007). Expression and cellular localisation of chloride intracellular channel 3 in human placenta and fetal membranes. *Placenta, 28*(5), 429-436.

Moore, A. S., & Holzbaur, E. L. (2018). Mitochondrial-cytoskeletal interactions: dynamic associations that facilitate network function and remodeling. *Current Opinion in Physiology, 3*, 94-100.

Murray, F., MacLean, M. R., & Pyne, N. J. (2002). Increased expression of the cGMP-inhibited cAMP-specific (PDE3) and cGMP binding cGMP-specific (PDE5) phosphodiesterases in models of pulmonary hypertension. *British Journal of Pharmacology, 137*(8), 1187-1194.

Nagaprashantha, L. D., Talamantes, T., Singhal, J., Guo, J., Vatsyayan, R., Rauniyar, N., Prokai, L. (2013). Proteomic analysis of signaling network regulation in renal cell carciNomas with differential hypoxia-inducible factor-2α expression. *PloS One, 8*(8), e71654.

Nicholls, D. G. (2004). Mitochondrial membrane potential and aging. *Aging Cell, 3*(1), 35-40.

Nishizawa, T., Nagao, T., Iwatsubo, T., Forte, J. G., & Urushidani, T. (2000). Molecular cloning and characterization of a novel chloride intracellular channel-related protein, parchorin, expressed in water-secreting cells. *Journal of Biological Chemistry, 275*(15), 11164-11173.

Nong, Z., Hoylaerts, M., Van Pelt, N., Collen, D. s., & Janssens, S. (1997). Nitric oxide inhalation inhibits platelet aggregation and platelet-mediated pulmonary thrombosis in rats. *Circulation Research, 81*(5), 865-869.

Norton, M., Ng, A. C.-H., Baird, S., Dumoulin, A., Shutt, T., Mah, N., Screaton, R. A. (2014). ROMO1 is an essential redox-dependent regulator of mitochondrial dynamics. *Science Signaling, 7*(310), ra10-ra10.

Novarino, G., Fabrizi, C., Tonini, R., Denti, M. A., Malchiodi-Albedi, F., Lauro, G. M., Mazzanti, M. (2004). Involvement of the intracellular ion channel CLIC1 in microglia-mediated beta-amyloid-induced neurotoxicity. *J Neurosci, 24*(23), 5322-5330. doi:10.1523/jneurosci.1170-04.2004

O'callaghan, D. S., Savale, L., Montani, D., Jaïs, X., Sitbon, O., Simonneau, G., & Humbert, M. (2011). Treatment of pulmonary arterial hypertension with targeted therapies. *Nature Reviews. Cardiology, 8*(9), 526.

Ong, S.-B., Kalkhoran, S. B., Cabrera-Fuentes, H. A., & Hausenloy, D. J. (2015). Mitochondrial fusion and fission proteins as novel therapeutic targets for treating cardiovascular disease. *European Journal of Pharmacology, 763*, 104-114.

Ostermeier, C., Iwata, S., & Michel, H. (1996). Cytochrome c oxidase. *Current Opinion in Structural Biology, 6*(4), 460-466.

Oyedotun, K. S., & Lemire, B. D. (2004). The quaternary structure of the saccharomyces cerevisiae succinate dehydrogenase Homology Modeling, Cofactor Docking, and Molecular Dynamics Simulation Studies. *Journal of Biological Chemistry, 279*(10), 9424-9431.

Pak, O., Sommer, N., Hoeres, T., Bakr, A., Waisbrod, S., Sydykov, A., Weissmann, N. (2013). Mitochondrial hyperpolarization in pulmonary vascular remodeling. Mitochondrial uncoupling protein deficiency as disease model. *Am J Respir Cell Mol Biol, 49*(3), 358-367. doi:10.1165/rcmb.2012-0361OC

Papandreou, I., Cairns, R. A., Fontana, L., Lim, A. L., & Denko, N. C. (2006). HIF-1 mediates adaptation to hypoxia by actively downregulating mitochondrial oxygen consumption. *Cell Metabolism, 3*(3), 187-197. doi:https://doi.org/10.1016/j.cmet.2006.01.012

Parera, M. C., Van Dooren, M., Van Kempen, M., De Krijger, R., Grosveld, F., Tibboel, D., & Rottier, R. (2005). Distal angiogenesis: a new concept for lung vascular morphogenesis. *American Journal of Physiology-Lung Cellular and Molecular Physiology, 288*(1), L141-L149.

Park, S., Jeon, J.-H., Min, B.-K., Ha, C.-M., Thoudam, T., Park, B.-Y., & Lee, I.-K. (2018). Role of the pyruvate dehydrogenase complex in metabolic remodeling: differential pyruvate dehydrogenase complex functions in metabolism. *Diabetes & Metabolism Journal, 42*(4), 270-281.

Paschalaki, K. E., & Randi, A. M. (2018). Recent Advances in Endothelial Colony Forming Cells Toward Their Use in Clinical Translation. *Front Med (Lausanne), 5*, 295. doi:10.3389/fmed.2018.00295

Paschalaki, K. E., Starke, R. D., Hu, Y., Mercado, N., Margariti, A., Gorgoulis, V. G., Barnes, P. J. (2013). Dysfunction of endothelial progenitor cells from smokers and chronic obstructive pulmonary disease patients due to increased DNA damage and senescence. *Stem Cells, 31*(12), 2813-2826. doi:10.1002/stem.1488

Paschalaki, K. E., Zampetaki, A., Baker, J. R., Birrell, M. A., Starke, R. D., Belvisi, M. G., Barnes, P. J. (2018). Downregulation of MicroRNA-126 Augments DNA Damage Response in Cigarette Smokers and Patients with Chronic Obstructive Pulmonary Disease. *Am J Respir Crit Care Med, 197*(5), 665-668. doi:10.1164/rccm.201706-1304LE

Paulin, R., & Michelakis, E. D. (2014). The metabolic theory of pulmonary arterial hypertension. *Circulation Research, 115*(1), 148-164.

Peng, C., et al. (2015). Mitofusin 2 ameliorates hypoxia-induced apoptosis via mitochondrial function and signaling pathways. *The international Journal of Biochemistry & Cell Biology* **69**: 29-40.

Perry, S. W., Norman, J. P., Barbieri, J., Brown, E. B., & Gelbard, H. A. (2011). Mitochondrial membrane potential probes and the proton gradient: a practical usage guide. *Biotechniques, 50*(2), 98-115.

Pimkina, J., & Murphy, M. E. (2011). Interaction of the ARF tumor suppressor with cytosolic HSP70 contributes to its autophagy function. *Cancer Biology & Therapy, 12*(6), 503-509.

Piperno, G., LeDizet, M., & Chang, X. (1987). Microtubules containing acetylated alpha-tubulin in mammalian cells in culture. *The Journal of Cell Biology, 104*(2), 289-302.

Ponnalagu, D., Gururaja Rao, S., & Singh, H. (2015). Molecular Identity of Cardiac Mitochondrial Chloride Intracellular Channel Proteins and Their Role in Mitochondrial Function. *Circulation Research, 117*(suppl_1), A238-A238.

Ponnalagu, D., & Singh, H. (2016b). Anion Channels of Mitochondria. *Pharmacology of Mitochondria* (pp. 71-101): Springer.

Ponnalagu, D., Rao, S. G., Farber, J., Xin, W., Hussain, A. T., Shah, K., Singh, H. (2016a). Molecular identity of cardiac mitochondrial chloride intracellular channel proteins. *Mitochondrion, 27*, 6-14.

Ponnalagu, D., Rao, S. G., Farber, J., Xin, W., Hussain, A. T., Shah, K., Singh, H. (2016b). Data supporting characterization of CLIC1, CLIC4, CLIC5 and DmCLIC antibodies and localization of CLICs in endoplasmic reticulum of cardiomyocytes. *Data in Brief, 7*, 1038-1044.

Qiu, M. R., Jiang, L., Matthaei, K. I., Schoenwaelder, S. M., Kuffner, T., Mangin, P., Valenzuela, S. M. (2010). Generation and characterization of mice with null mutation of the chloride intracellular channel 1 gene. *Genesis, 48*(2), 127-136.

Quintana-Cabrera, R., Mehrotra, A., Rigoni, G., & Soriano, M. (2018). Who and how in the regulation of mitochondrial cristae shape and function. *Biochemical and Biophysical Research Communications, 500*(1), 94-101.

Rabinovitch, M. (2012). Molecular pathogenesis of pulmonary arterial hypertension. *The Journal of Clinical Investigation, 122*(12), 4306-4313.

Rafikov, R., Sun, X., Rafikova, O., Meadows, M. L., Desai, A. A., Khalpey, Z., Black, S. M. (2015). Complex I dysfunction underlies the glycolytic switch in pulmonary hypertensive smooth muscle cells. *Redox Biology, 6*, 278-286.

Ranchoux, B., Meloche, J., Paulin, R., Boucherat, O., Provencher, S., & Bonnet, S. (2016). DNA Damage and Pulmonary Hypertension. *International Journal of Molecular Sciences, 17*(6), 990.

Randle, P., Garland, P., Hales, C., & Newsholme, E. (1963). The glucose fatty-acid cycle its role in insulin sensitivity and the metabolic disturbances of diabetes mellitus. *The Lancet, 281*(7285), 785-789.

Redhead, C., Sullivan, S. K., Koseki, C., Fujiwara, K., & Edwards, J. C. (1997). Subcellular distribution and targeting of the intracellular chloride channel p64. *Mol Biol Cell, 8*(4), 691-704.

Rhodin, J. A. (2011). Architecture of the vessel wall. *Comprehensive Physiology*, 1-31.

Robertson, A. M., & Watton, P. N. (2013). Mechanobiology of the arterial wall. *Transport in Biological Media, 2013*, 275-347.

Robinson, K. A., Candal, F. J., Scott, N. A., & Ades, E. W. (1995). Seeding of vascular grafts with an immortalized human dermal microvascular endothelial cell line. *Angiology, 46*(2), 107-113. doi:10.1177/000331979504600203

Rol, N., Kurakula, K. B., Happé, C., Bogaard, H. J., & Goumans, M.-J. (2018). TGF-β and BMPR2 signaling in PAH: two black sheep in one family. *International Journal of Molecular Sciences, 19*(9), 2585.

Rønnov-Jessen, L., Villadsen, R., Edwards, J. C., & Petersen, O. W. (2002). Differential expression of a chloride intracellular channel gene, CLIC4, in transforming growth factor-β1-mediated conversion of fibroblasts to myofibroblasts. *The American Journal of Pathology, 161*(2), 471-480.

Rounds, S., & McMurtry, I. F. (1981). Inhibitors of oxidative ATP production cause transient vasoconstriction and block subsequent pressor responses in rat lungs. *Circ Res, 48*(3), 393-400. doi:10.1161/01.res.48.3.393

Russomanno, G., Jo, K. B., Abdul-Salam, V. B., Morgan, C., Endruschat, J., Schaeper, U., Wojciak-Stothard, B. (2020). miR-150-PTPMT1-cardiolipin signaling in pulmonary arterial hypertension. *Molecular Therapy-Nucleic Acids*.

Ryan, J., Dasgupta, A., Huston, J., Chen, K.-H., & Archer, S. L. (2015). Mitochondrial dynamics in pulmonary arterial hypertension. *Journal of Molecular Medicine, 93*(3), 229-242.

Ryan, J. J., & Archer, S. L. (2015). Emerging concepts in the molecular basis of pulmonary arterial hypertension: part I: metabolic plasticity and mitochondrial dynamics in the pulmonary circulation and right ventricle in pulmonary arterial hypertension. *Circulation, 131*(19), 1691-1702.

Ryan, J. J., Marsboom, G., Fang, Y.-H., Toth, P. T., Morrow, E., Luo, N., Zhang, H. J. (2013). PGC1α-mediated mitofusin-2 deficiency in female rats and humans with pulmonary arterial hypertension. *Am J Respir Crit Care Med, 187*(8), 865-878.

Said, S. I. (2006). Mediators and modulators of pulmonary arterial hypertension. *American Journal of Physiology-Lung Cellular and Molecular Physiology, 291*(4), L547-L558.

Sakao, S., Taraseviciene-Stewart, L., Lee, J. D., Wood, K., Cool, C. D., & Voelkel, N. F. (2005). Initial apoptosis is followed by increased proliferation of apoptosis-resistant endothelial cells. *The FASEB Journal, 19*(9), 1178-1180.

Sakao, S., Tatsumi, K., & Voelkel, N. F. (2009). Endothelial cells and pulmonary arterial hypertension: apoptosis, proliferation, interaction and transdifferentiation. *Respiratory Research, 10*(1), 95-95. doi:10.1186/1465-9921-10-95

Salao, K., Jiang, L., Li, H., Tsai, V. W.-W., Husaini, Y., Curmi, P. M., Breit, S. N. (2016). CLIC1 regulates dendritic cell antigen processing and presentation by modulating phagosome acidification and proteolysis. *Biology Open, 5*(5), 620-630.

Sarangi, U., Singh, M. K., Abhijnya, K. V. V., Reddy, L. P. A., Prasad, B. S., Pitke, V. V., Sreedhar, A. S. (2013). Hsp60 chaperonin acts as barrier to pharmacologically induced oxidative stress mediated apoptosis in tumor cells with differential stress response. *Drug Target Insights, 7*, 35.

Schermuly, R. T., Ghofrani, H. A., Wilkins, M. R., & Grimminger, F. (2011). Mechanisms of disease: pulmonary arterial hypertension. *Nature Reviews Cardiology, 8*(8), 443.

Schieke, S. M., McCoy Jr, J. P., & Finkel, T. (2008). Coordination of mitochondrial bioenergetics with G1 phase cell cycle progression. *Cell Cycle, 7*(12), 1782-1787.

Scuderi, S., La Cognata, V., Drago, F., Cavallaro, S., & D'Agata, V. (2014). Alternative Splicing Generates Different Parkin Protein Isoforms: Evidences in Human, Rat, and Mouse Brain. *BioMed Research International, 2014*, 690796. doi:10.1155/2014/690796.

Seabright, A. P., Fine, N. H., Barlow, J. P., Lord, S. O., Musa, I., Gray, A., Hardie, D. G. (2020). AMPK activation induces mitophagy and promotes mitochondrial fission while activating TBK1 in a PINK1-Parkin independent manner. *The FASEB Journal, 34*(5), 6284-6301.

Schrepfer, E. and L. Scorrano (2016). Mitofusins, from mitochondria to metabolism. *Molecular Cell* **61**(5): 683-694.

Seifert, E. L., Estey, C., Xuan, J. Y., & Harper, M.-E. (2010). Electron transport chain-dependent and-independent mechanisms of mitochondrial H2O2 emission during long-chain fatty acid oxidation. *Journal of Biological Chemistry, 285*(8), 5748-5758.

Shepherd, B. R., Enis, D. R., Wang, F., Suarez, Y., Pober, J. S., Schechner, J. S., Suarez, Y. (2006). Vascularization and engraftment of a human skin substitute using circulating progenitor cell-derived endothelial cells. *The FASEB Journal, 20*(10), 1739-1741.

Shirihai, O. S., Song, M., & Dorn, G. W., 2nd. (2015). How mitochondrial dynamism orchestrates mitophagy. *Circ Res, 116*(11), 1835-1849. doi:10.1161/circresaha.116.306374

Sieveking, D. P., Buckle, A., Celermajer, D. S., & Ng, M. K. (2008). Strikingly different angiogenic properties of endothelial progenitor cell subpopulations: insights from a novel human angiogenesis assay. *Journal of the American College of Cardiology, 51*(6), 660-668.

Simonneau, G., Galie, N., Rubin, L. J., Langleben, D., Seeger, W., Domenighetti, G., Beghetti, M. (2004). Clinical classification of pulmonary hypertension. *Journal of the American College of Cardiology, 43*(12 Supplement), S5-S12.

Simonneau, G., Gatzoulis, M. A., Adatia, I., Celermajer, D., Denton, C., Ghofrani, A., Machado, R. F. (2013). Updated clinical classification of pulmonary hypertension. *Journal of the American College of Cardiology, 62*(25 Supplement), D34-D41.

Sindi, H. A., Russomanno, G., Satta, S., Abdul-Salam, V. B., Jo, K. B., Qazi-Chaudhry, B., . . . Morgan, C. C. (2020). Therapeutic potential of KLF2-induced exosomal microRNAs in pulmonary hypertension. *Nature Communications, 11*(1), 1-17.

Singh, H. (2010). Two decades with dimorphic chloride intracellular channels (CLICs). *FEBS Lett, 584*(10), 2112-2121.

Singh, H., & Ashley, R. H. (2006). Redox regulation of CLIC1 by cysteine residues associated with the putative channel pore. *Biophys J, 90*(5), 1628-1638. doi:10.1529/biophysj.105.072678

Singh, H., Cousin, M., & Ashley, R. (2007). Functional reconstitution of mammalian 'chloride intracellular channels' CLIC1, CLIC4 and CLIC5 reveals differential regulation by cytoskeletal actin. *FEBS Journal, 274*(24), 6306-6316.

Sitbon, O., Gomberg-Maitland, M., Granton, J., Lewis, M. I., Mathai, S. C., Rainisio, M., Rubin, L. J. (2019). Clinical trial design and new therapies for pulmonary arterial hypertension. *The European Respiratory Journal, 53*(1), 1801908. doi:10.1183/13993003.01908-2018

Skulachev, V. P. (2001). Mitochondrial filaments and clusters as intracellular power-transmitting cables. *Trends in Biochemical Sciences, 26*(1), 23-29.

Smadja, D. M., Bièche, I., Silvestre, J.-S., Germain, S., Cornet, A., Laurendeau, I., Aiach, M. (2008). Bone morphogenetic proteins 2 and 4 are selectively expressed by late outgrowth endothelial progenitor cells and promote neoangiogenesis. *Arteriosclerosis, Thrombosis, and Vascular Biology, 28*(12), 2137-2143.

Smadja, D. M., Bièche, I., Susen, S., Mauge, L., Laurendeau, I., d'Audigier, C., Gaussem, P. (2009). Interleukin 8 is differently expressed and modulated by PAR-1 activation in early and late endothelial progenitor cells. *J Cell Mol Med, 13*(8b), 2534-2546. doi:10.1111/j.1582-4934.2008.00429.x

Smadja, D. M., Bieche, I., Uzan, G., Bompais, H., Muller, L., Boisson-Vidal, C., Gaussem, P. (2005). PAR-1 activation on human late endothelial progenitor cells enhances angiogenesis in vitro with upregulation of the SDF-1/CXCR4 system. *Arteriosclerosis, Thrombosis, and Vascular Biology, 25*(11), 2321-2327.

Smadja, D. M., Mauge, L., Nunes, H., d'Audigier, C., Juvin, K., Borie, R., Israel-Biet, D. (2013). Imbalance of circulating endothelial cells and progenitors in idiopathic pulmonary fibrosis. *Angiogenesis, 16*(1), 147-157. doi:10.1007/s10456-012-9306-9

Smits, J., et al. (2018). Blood outgrowth and proliferation of endothelial colony forming cells are related to markers of disease severity in patients with pulmonary arterial hypertension. *International journal of Molecular Sciences* **19**(12): 3763.

Sood, A., Jeyaraju, D. V., Prudent, J., Caron, A., Lemieux, P., McBride, H. M., . . . Pellegrini, L. (2014). A Mitofusin-2-dependent inactivating cleavage of Opa1 links changes in mitochondria cristae and ER contacts in the postprandial liver. *Proc Natl Acad Sci U S A, 111*(45), 16017-16022. doi:10.1073/pnas.1408061111

Starke, R. D., et al. (2011). Endothelial von Willebrand factor regulates angiogenesis. *Blood* **117**(3): 1071-1080.

Stitham, J., Midgett, C., Martin, K., & Hwa, J. (2011). Prostacyclin: an inflammatory paradox. *Frontiers in Pharmacology, 2*, 24.

Strange, J. W., Wharton, J., Phillips, P. G., & Wilkins, M. R. (2002). Recent insights into the pathogenesis and therapeutics of pulmonary hypertension. *Clin Sci (Lond), 102*(3), 253-268.

Stroncek, J. D., Grant, B. S., Brown, M. A., Povsic, T. J., Truskey, G. A., & Reichert, W. M. (2009). Comparison of endothelial cell phenotypic markers of late-outgrowth endothelial progenitor cells isolated from patients with coronary artery disease and healthy volunteers. *Tissue Engineering Part A, 15*(11), 3473-3486.

Sud, N., Wells, S. M., Sharma, S., Wiseman, D. A., Wilham, J., & Black, S. M. (2008). Asymmetric dimethylarginine inhibits HSP90 activity in pulmonary arterial endothelial cells: role of mitochondrial dysfunction. *American Journal of Physiology-Cell Physiology, 294*(6), C1407-C1418.

Suh, K. S., Mutoh, M., Gerdes, M., & Yuspa, S. H. (2005). *CLIC4, an intracellular chloride channel protein, is a novel molecular target for cancer therapy.* Paper presented at the Journal of Investigative Dermatology Symposium Proceedings.

Suh, K. S., Mutoh, M., Mutoh, T., Li, L., Ryscavage, A., Crutchley, J. M., Yuspa, S. H. (2007). CLIC4 mediates and is required for Ca2+-induced keratinocyte differentiation. *J Cell Sci, 120*(15), 2631-2640.

Suh, K. S., Mutoh, M., Nagashima, K., Fernandez-Salas, E., Edwards, L. E., Hayes, D. D., . . . Levy, J. M. (2004). The organellular chloride channel protein CLIC4/mtCLIC translocates to the nucleus in response to cellular stress and accelerates apoptosis. *Journal of Biological Chemistry, 279*(6), 4632-4641.

Sun, X., Sharma, S., Fratz, S., Kumar, S., Rafikov, R., Aggarwal, S., Dasarathy, S. (2013). Disruption of endothelial cell mitochondrial bioenergetics in lambs with increased pulmonary blood flow. *Antioxidants & Redox Signaling, 18*(14), 1739-1752.

Sutendra, G., & Michelakis, E. D. (2014). The metabolic basis of pulmonary arterial hypertension. *Cell Metabolism, 19*(4), 558-573.

Sutendra, G., Dromparis, P., Wright, P., Bonnet, S., Haromy, A., Hao, Z., Sessa, W. C. (2011). The role of Nogo and the mitochondria–endoplasmic reticulum unit in pulmonary hypertension. *Science Translational Medicine, 3*(88), 88ra55-88ra55.

Szabo, I., & Zoratti, M. (2014). Mitochondrial channels: ion fluxes and more. *Physiological Reviews, 94*(2), 519-608.

Taguchi, N., Ishihara, N., Jofuku, A., Oka, T., & Mihara, K. (2007). Mitotic phosphorylation of dynamin-related GTPase Drp1 participates in mitochondrial fission. *Journal of Biological Chemistry, 282*(15), 11521-11529.

Takano, K., Liu, D., Tarpey, P., Gallant, E., Lam, A., Witham, S., Schwartz, C. E. (2012). An X-linked channelopathy with cardiomegaly due to a CLIC2 mutation enhancing ryanodine receptor channel activity. *Human Molecular Genetics*, dds292.

Takesono, A., Heasman, S. J., Wojciak-Stothard, B., Garg, R., & Ridley, A. J. (2010). Microtubules regulate migratory polarity through Rho/ROCK signaling in T cells. *PloS One, 5*(1), e8774.

Tan, B., Xiao, H., Li, F., Zeng, L., & Yin, Y. (2015). The profiles of mitochondrial respiration and glycolysis using extracellular flux analysis in porcine enterocyte IPEC-J2. *Animal Nutrition, 1*(3), 239-243.

Tan, K., et al. (2010). Impaired function of circulating CD34+ CD45− cells in patients with proliferative diabetic retinopathy. *Experimental Eye Research* **91**(2): 229-237.

Tang, T., Lang, X., Xu, C., Wang, X., Gong, T., Yang, Y., . . . Zhou, R. (2017). CLICs-dependent chloride efflux is an essential and proximal upstream event for NLRP3 inflammasome activation. *Nat Commun, 8*(1), 202. doi:10.1038/s41467-017-00227-x

Tang, X., Luo, Y.-X., Chen, H.-Z., & Liu, D.-P. (2014). Mitochondria, endothelial cell function, and vascular diseases. *Front Physiol, 5*, 175.

Tatsuta, T., Model, K., & Langer, T. (2005). Formation of membrane-bound ring complexes by prohibitins in mitochondria. *Molecular Biology of the Cell, 16*(1), 248-259.

Tavasoli, M., Al-Momany, A., Wang, X., Li, L., Edwards, J. C., & Ballermann, B. J. (2016). Both CLIC4 and CLIC5A activate ERM proteins in glomerular endothelium. *American Journal of Physiology-Renal Physiology, 311*(5), F945-F957.

Ten, V. S., & Ratner, V. (2020). Mitochondrial bioenergetics and pulmonary dysfunction: Current progress and future directions. *Paediatr Respir Rev, 34*, 37-45. doi:10.1016/j.prrv.2019.04.001

Thenappan, T., Shah, S., Rich, S., Tian, L., Archer, S., & Gomberg-Maitland, M. (2010). Survival in pulmonary arterial hypertension: a reappraisal of the NIH risk stratification equation. *European Respiratory Journal, 35*(5), 1079-1087.

Thill, M., et al. (2008). Late outgrowth endothelial progenitor cells in patients with age-related macular degeneration. *Investigative Ophthalmology & Visual Science* **49**(6): 2696-2708.

Thompson, A. R., & Lawrie, A. (2016). Targeting Vascular Remodeling to Treat Pulmonary Arterial Hypertension. *Trends in Molecular Medicine*, *23*(1), 31-45.

Townsley, M. I. (2011). Structure and composition of pulmonary arteries, capillaries, and veins. *Comprehensive Physiology, 2*(1), 675-709.

Tokuyasu, K. (1973). A technique for ultracryotomy of cell suspensions and tissues. *The Journal of Cell Biology, 57*(2), 551-565.

Tondera, D., Grandemange, S., Jourdain, A., Karbowski, M., Mattenberger, Y., Herzig, S., Merkwirth, C. (2009). SLP-2 is required for stress-induced mitochondrial hyperfusion. *The EMBO Journal, 28*(11), 1589-1600.

Toshner, M., et al. (2009). Evidence of dysfunction of endothelial progenitors in pulmonary arterial hypertension. *American Journal of Respiratory and Critical Care Medicine* **180**(8): 780-787.

Toyama, E. Q., Herzig, S., Courchet, J., Lewis, T. L., Losón, O. C., Hellberg, K., Chan, D. C. (2016). AMP-activated protein kinase mediates mitochondrial fission in response to energy stress. *Science, 351*(6270), 275-281.

Traba, J., Miozzo, P., Akkaya, B., Pierce, S. K., & Akkaya, M. (2016). An optimized protocol to analyze glycolysis and mitochondrial respiration in lymphocytes. *Journal of Visualized Experiments: JoVE*(117).

Trembath, R. C., Thomson, J. R., Machado, R. D., Morgan, N. V., Atkinson, C., Winship, I., Humbert, M. (2001). Clinical and molecular genetic features of pulmonary hypertension in patients with hereditary hemorrhagic telangiectasia. *New England Journal of Medicine, 345*(5), 325-334.

Tsihlis, N. D., Oustwani, C. S., Vavra, A. K., Jiang, Q., Keefer, L. K., & Kibbe, M. R. (2011). Nitric oxide inhibits vascular smooth muscle cell proliferation and neointimal hyperplasia by increasing the ubiquitination and degradation of UbcH10. *Cell Biochemistry and Biophysics, 60*(1-2), 89-97.

Tuder, R. M., Abman, S. H., Braun, T., Capron, F., Stevens, T., Thistlethwaite, P. A., & Haworth, S. G. (2009). Development and pathology of pulmonary hypertension. *Journal of the American College of Cardiology, 54*(1 Supplement), S3-S9.

Tuder, R. M., Archer, S. L., Dorfmüller, P., Erzurum, S. C., Guignabert, C., Michelakis, E., Morrell, N. W. (2013). Relevant issues in the pathology and pathobiology of pulmonary hypertension. *Journal of the American College of Cardiology, 62*(25S), D4-D12.

Tuder, R. M., Davis, L. A., & Graham, B. B. (2012). Targeting energetic metabolism: a new frontier in the pathogenesis and treatment of pulmonary hypertension. *Am J Respir Crit Care Med, 185*(3), 260-266. doi:10.1164/rccm.201108-1536PP

Tuder, R. M., & Voelkel, N. F. (2002). Angiogenesis and pulmonary hypertension: a unique process in a unique disease. *Antioxidants and Redox Signaling, 4*(5), 833-843.

Tung, J. J., & Kitajewski, J. (2010). Chloride intracellular channel 1 functions in endothelial cell growth and migration. *Journal of Angiogenesis Research, 2*(1), 1-13.

Tung, J. J., Hobert, O., Berryman, M., & Kitajewski, J. (2009). Chloride intracellular channel 4 is involved in endothelial proliferation and morphogenesis in vitro. *Angiogenesis, 12*(3), 209-220.

Ulmasov, B., Bruno, J., Gordon, N., Hartnett, M. E., & Edwards, J. C. (2009). Chloride intracellular channel protein-4 functions in angiogenesis by supporting acidification of vacuoles along the intracellular tubulogenic pathway. *Am J Pathol, 174*(3), 1084-1096. doi:10.2353/ajpath.2009.080625

Ulmasov, B., Bruno, J., Woost, P. G., & Edwards, J. C. (2007). Tissue and subcellular distribution of CLIC1. *BMC Cell Biol, 8*(1), 8.

Undem, C., Rios, E. J., Maylor, J., & Shimoda, L. A. (2012). Endothelin-1 augments Na+/H+ exchange activity in murine pulmonary arterial smooth muscle cells via Rho kinase. *PloS one, 7*(9), e46303.

Unegbu, C., Noje, C., Coulson, J. D., Segal, J. B., & Romer, L. (2017). Pulmonary hypertension therapy and a systematic review of efficacy and safety of PDE-5 inhibitors. *Pediatrics, 139*(3).

Valenzuela, S. M., Alkhamici, H., Brown, L. J., Almond, O. C., Goodchild, S. C., Carne, S., Cornell, B. A. (2013). Regulation of the membrane insertion and conductance activity of the metamorphic chloride intracellular channel protein CLIC1 by cholesterol. *PLoS One, 8*(2), e56948.

Valenzuela, S. M., Martin, D. K., Por, S. B., Robbins, J. M., Warton, K., Bootcov, M. R., Breit, S. N. (1997). Molecular cloning and expression of a chloride ion channel of cell nuclei. *Journal of Biological Chemistry, 272*(19), 12575-12582.

Valenzuela, S. M., Mazzanti, M., Tonini, R., Qiu, M. R., Warton, K., Musgrove, E. A., Breit, S. N. (2000). The nuclear chloride ion channel NCC27 is involved in regulation of the cell cycle. *The Journal of Physiology, 529*(3), 541-552.

Valera-Alberni, M., & Canto, C. (2018). Mitochondrial stress management: a dynamic journey. *Cell Stress, 2*(10), 253.

van der Bliek, A. M., et al. (2013). Mechanisms of mitochondrial fission and fusion. *Cold Spring Harbor perspectives in biology* **5**(6): a011072.

van der Vaart, J., & Clevers, H. (2020). Airway organoids as models of human disease. *Journal of Internal Medicine*.

van Wetering, S., van Buul, J. D., Quik, S., Mul, F. P., Anthony, E. C., ten Klooster, J.-P., Hordijk, P. L. (2002). Reactive oxygen species mediate Rac-induced loss of cell-cell adhesion in primary human endothelial cells. *Journal of Cell Science, 115*(9), 1837-1846.

Wagenvoort, C., & Wagenvoort, N. (1979). Pulmonary vascular bed: normal anatomy and responses to disease. *Pulmonary Vascular Disease. New York, US: Marcel Dekker*, 1-109.

Wang, C.-H., et al. (2011). Factors associated with purity, biological function, and activation potential of endothelial colony-forming cells. *American Journal of Physiology-Regulatory, Integrative and Comparative Physiology* **300**(3): R586-R594.

Wang, Y.-Y., Yang, Y.-X., Zhe, H., He, Z.-X., & Zhou, S.-F. (2014). Bardoxolone methyl (CDDO-Me) as a therapeutic agent: an update on its pharmacokinetic and pharmacodynamic properties. *Drug Design, Development and Therapy, 8*, 2075.

Warburg, O. (1956). On the origin of cancer cells. *Science, 123*(3191), 309-314.

Warburg, O., Wind, F., & Negelein, E. (1927). The metabolism of tumors in the body. *The Journal of General Physiology, 8*(6), 519.

Wedgwood, S., & Black, S. M. (2003). Induction of apoptosis in fetal pulmonary arterial smooth muscle cells by a combined superoxide dismutase/catalase mimetic. *Am J Physiol Lung Cell Mol Physiol, 285*(2), L305-312. doi:10.1152/ajplung.00382.2002

Wegner, B., Al-Momany, A., Kulak, S. C., Kozlowski, K., Obeidat, M., Jahroudi, N., Ballermann, B. J. (2010). CLIC5A, a component of the ezrin-podocalyxin complex in glomeruli, is a determinant of podocyte integrity. *American Journal of Physiology-Renal Physiology, 298*(6), F1492-F1503.

Westermann, B. (2010). Mitochondrial fusion and fission in cell life and death. *Nat Rev Mol Cell Biol, 11*(12), 872-884. doi:10.1038/nrm3013

Westermann, B. (2012). Bioenergetic role of mitochondrial fusion and fission. *Biochimica et Biophysica Acta (BBA)-Bioenergetics, 1817*(10), 1833-1838.

Wharton, J., Strange, J. W., Møller, G. M., Growcott, E. J., Ren, X., Franklyn, A. P., Wilkins, M. R. (2005). Antiproliferative effects of phosphodiesterase type 5 inhibition in human pulmonary artery cells. *American Journal of Respiratory and Critical Care Medicine, 172*(1), 105-113.

Wilkins, M. (2012). Pulmonary hypertension: the science behind the disease spectrum. *European Respiratory Review, 21*(123), 19-26.

Wojciak-Stothard, B., Abdul-Salam, V. B., Lao, K. H., Tsang, H., Irwin, D. C., Lisk, C., Yuspa, S. H. (2014). Aberrant Chloride Intracellular Channel 4 Expression Contributes to Endothelial Dysfunction in Pulmonary Arterial Hypertension: a clinical perspective. *Circulation, 129*(17), 1770-1780.

Wojciak-Stothard, B., Tsang, L. Y. F., & Haworth, S. G. (2005). Rac and Rho play opposing roles in the regulation of hypoxia/reoxygenation-induced permeability changes in pulmonary artery endothelial cells. *American Journal of Physiology-Lung Cellular and Molecular Physiology, 288*(4), L749-L760.

Xu, J., & Shi, G.-P. (2014). Vascular wall extracellular matrix proteins and vascular diseases. *Biochimica et Biophysica Acta (BBA)-Molecular Basis of Disease, 1842*(11), 2106-2119.

Xu, W., Koeck, T., Lara, A. R., Neumann, D., DiFilippo, F. P., Koo, M., Jennings, C. (2007). Alterations of cellular bioenergetics in pulmonary artery endothelial cells. *Proceedings of the National Academy of Sciences, 104*(4), 1342-1347.

Xu, Y., Kang, J., Yuan, Z., Li, H., Su, J., Li, Y., Sun, L. (2013). Suppression of CLIC4/mtCLIC enhances hydrogen peroxide-induced apoptosis in C6 glioma cells. *Oncology Reports, 29*(4), 1483-1491.

Xu, Y., Zhu, J., Hu, X., Wang, C., Lu, D., Gong, C., Zong, L. (2016). CLIC1 Inhibition Attenuates Vascular Inflammation, Oxidative Stress, and Endothelial Injury. *PLoS One, 11*(11), e0166790. doi:10.1371/journal.pone.0166790

Yamaguchi, O., Murakawa, T., Nishida, K., & Otsu, K. (2016). Receptor-mediated mitophagy. *J Mol Cell Cardiol, 95*, 50-56. doi:10.1016/j.yjmcc.2016.03.010

Yang, J.-Y., Jung, J. Y., Cho, S. W., Choi, H. J., Kim, S. W., Kim, S. Y., Han, J. (2009). Chloride intracellular channel 1 regulates osteoblast differentiation. *Bone, 45*(6), 1175-1185.

Yao, Q., Qu, X., Yang, Q., Wei, M., & Kong, B. (2009). CLIC4 mediates TGF-β1-induced fibroblast-to-myofibroblast transdifferentiation in ovarian cancer. *Oncology reports, 22*(3), 541-548.

Yau, J. W., Teoh, H., & Verma, S. (2015). Endothelial cell control of thrombosis. *BMC Cardiovascular Disorders, 15*(1), 1-11.

Yoder, M. C. (2010). Is endothelium the origin of endothelial progenitor cells? *Arteriosclerosis, Thrombosis, and Vascular Biology, 30*(6), 1094-1103.

Yoder, M. C. (2010). Is endothelium the origin of endothelial progenitor cells? *Arterioscler Thromb Vasc Biol, 30*(6), 1094-1103. doi:10.1161/atvbaha.109.191635

Yoder, M. C., Mead, L. E., Prater, D., Krier, T. R., Mroueh, K. N., Li, F., Ingram, D. A. (2007). Redefining endothelial progenitor cells via clonal analysis and hematopoietic stem/progenitor cell principals. *Blood, 109*(5), 1801-1809.

Yong, N. K., Kinmonth, J. B., & Taylor, G. W. (1963). The Endothelial Lining of Vascular Grafts. *Surg Gynecol Obstet, 117*, 305-310.

Yoon, C. H., Hur, J., Park, K. W., Kim, J. H., Lee, C. S., Oh, I. Y., Kim, H. S. (2005). Synergistic neovascularization by mixed transplantation of early endothelial progenitor cells and late outgrowth endothelial cells: the role of angiogenic cytokines and matrix metalloproteinases. *Circulation, 112*(11), 1618-1627. doi:10.1161/circulationaha.104.503433

Yoon, Y., Krueger, E. W., Oswald, B. J., & McNiven, M. A. (2003). The mitochondrial protein hFis1 regulates mitochondrial fission in mammalian cells through an interaction with the dynamin-like protein DLP1. *Molecular and Cellular Biology, 23*(15), 5409-5420.

Youle, R. J., & Narendra, D. P. (2011). Mechanisms of mitophagy. *Nature Reviews Molecular Cell Biology, 12*(1), 9-14.

Youle, R. J., & Van Der Bliek, A. M. (2012). Mitochondrial fission, fusion, and stress. *Science, 337*(6098), 1062-1065.

Yu, Q., & Chan, S. Y. (2017). Mitochondrial and Metabolic Drivers of Pulmonary Vascular Endothelial Dysfunction in Pulmonary Hypertension. *Advances in Experimental Medicine and Biology, 967*, 373-383. doi:10.1007/978-3-319-63245-2_24

Zeilstra-Ryalls, J., Fayet, O., & Georgopoulos, C. (1991). The universally conserved GroE (Hsp60) chaperonins. *Annual Reviews in Microbiology, 45*(1), 301-325.

Zhai, C., Shi, W., Feng, W., Zhu, Y., Wang, J., Li, S., . . . Chai, L. (2018). Activation of AMPK prevents monocrotaline-induced pulmonary arterial hypertension by suppression of NF-κB-mediated autophagy activation. *Life Sciences, 208*, 87-95.

Zhang, C. F., Zhao, F. Y., Xu, S. L., Liu, J., Xing, X. Q., & Yang, J. (2019). Autophagy in pulmonary hypertension: emerging roles and therapeutic implications. *Journal of Cellular Physiology, 234*(10), 16755-16767.

Zhang, H., Wang, D., Li, M., Plecitá-Hlavatá, L., D'Alessandro, A., Tauber, J., . . . McKeon, B. A. (2017). Metabolic and proliferative state of vascular adventitial fibroblasts in pulmonary hypertension is regulated through a microRNA-124/PTBP1 (polypyrimidine tract binding protein 1)/pyruvate kinase muscle axis. *Circulation, 136*(25), 2468-2485.

Zhao, J., et al. (2013). Regulation of mitochondrial dynamics: convergences and divergences between yeast and vertebrates. *Cellular and Molecular Life Sciences* **70**(6): 951-976.

Zhao, Z., Wu, F., Ding, S., Sun, L., Liu, Z., Ding, K., & Lu, J. (2015). Label-free quantitative proteomic analysis reveals potential biomarkers and pathways in renal cell carciNoma. *Tumor Biology, 36*(2), 939-951.

Zimmermann, M., & Reichert, A. S. (2017). How to get rid of mitochondria: crosstalk and regulation of multiple mitophagy pathways. *Biological Chemistry, 399*(1), 29-45.